SOVIET PHYSICS

JETP

A translation of Zhurnal Éksperimental'noĭ i Teoreticheskoĭ Fiziki.

Vol. 12, No. 6, pp. 1035-1316 (Russ. orig. Vol. 39, No. 6, pp. 1489-1886, Dec., 1960) June, 1961

ELASTIC SCATTERING OF 13.6-Mev DEUTERONS. I

Yu. V. GOFMAN and O. F. NEMETS

Submitted to JETP editor April 9, 1960; resubmitted August 29, 1960

J. Exptl. Theoret. Phys. (U.S.S.R.) **39**, 1489-1491 (December, 1960)

The angular distributions of 13.6-Mev deuterons scattered elastically by Pb, Au, Pt, Sn, Ag, Ni, Cu, and Fe are studied.

REACTIONS between deuterons and nuclei, particularly elastic scattering, exhibit characteristics that result specifically from the small binding energy of the deuteron and from the fact that its center of mass does not coincide with its center of charge distribution.

Because of the experimental difficulties associated with the necessity of using selective spectrometers, very few investigations of elastic deuteron scattering have been published, especially for scattering from medium-weight and heavy nuclei. However, the available literature shows that the angular distributions of elastically scattered deuterons depart considerably from Rutherford scattering, and that the character of the departure is different from that of protons.

As in the case of alpha particles, it is characteristic that, beginning at a specific angle,[1,2] the scattering cross section decreases rapidly compared with the Rutherford cross section. In order to account for this effect, Porter[3] considered the absorption of alpha particles and deuterons having Coulomb orbits in classical approximation. Porter fitted the data by assuming that the deuteron mean free path near the center of a nucleus is longer than that of an alpha particle; this assumption cannot be accepted unconditionally. Nishida[4] calculated the electric breakup of the deuteron, and showed that since deuteron breakup requires the acquisition of energy at least equal to the binding energy, the departure from the Rutherford cross section will occur at a constant angle for nuclei with different charges and will depend only on the deuteron energy. Nishida's calculation of $\sigma(\theta)$ is in good agreement with experiment[1] for 15.2-Mev deuterons scattered from Pb and Bi. Slaus and Alford[5] used 4-Mev deuterons, and interpreted their results by means of the optical model. They fitted data by introducing a very large imaginary part in the potential (~ 15 Mev), but were unable to obtain agreement for lighter nuclei (Mg and Al).

The mechanism responsible for the non-Rutherford elastic scattering cross section has thus far remained undecided. We have sought further information by measuring angular distributions of 13.6-Mev deuterons scattered elastically by Fe, Ni, Cu, Ag, Sn, Pt, Au, and Pb at intervals of 2.5 — 5° in the angle range 10 — 140°.

Our measurements were performed on a deuteron beam extracted from the cyclotron of the Institute of Physics of the Academy of Sciences of the Ukrainian S.S.R. The experimental technique has been described in an earlier paper.[6] The targets were self-supporting metal foils that had been rolled, or that had been deposited on a subsequently dissolved organic film. Target thickness did not exceed 2.5 — 3 mg/cm^2 except in the case of lead (4.7 mg/cm^2). The zero angle was fixed by taking a few spectra on both sides of the zero position. Angles were accurate to within at least 0.2°. The half-widths of peaks were 2.5-3% in the range 20 — 90°, and $\sim 5\%$ above 90°. Statistical errors did not usually exceed 3%. Figure 1 gives the angular distributions of $(\sigma/\sigma_{\mathrm{Ruth}})$ normalized to unity for 10 — 25°.

It is noted, first of all, that in the case of heavy nuclei (Pb, Au, Pt) the departure from Coulomb

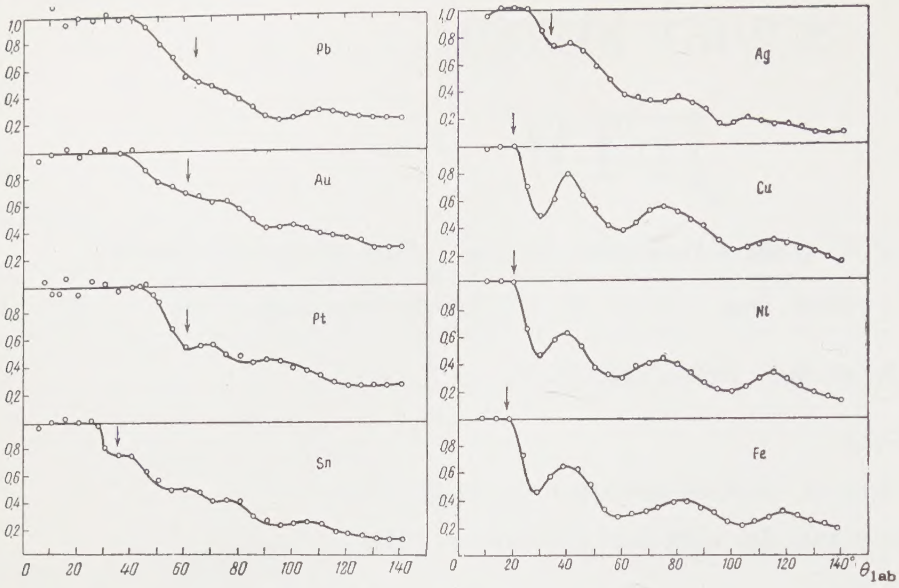

FIG. 1

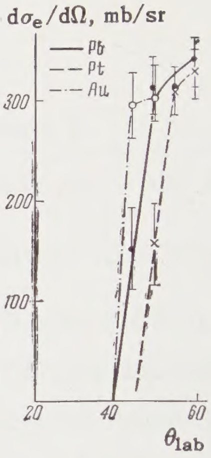

FIG. 2

scattering occurs at angles 35 — 40°. Our account of the mechanism involved in this effect is based on the importance of nuclear interactions at deuteron-nucleus distances $q \leq R_n + R_d + \bar{\lambda}$, while the electric interaction plays the principal role at larger distances. If q is taken to be the impact parameter for Coulomb scattering, the corresponding angle θ_c is determined from*

$$\sin(\theta_c/2) = Ze^2/(2M_p v^2 q - Ze^2). \quad (1)$$

The arrows in Fig. 1 indicate the calculated values of θ_c for $R_d = 4.31$ f and $R_n = 1.25\ A^{1/3}$ f. Thus at the given energy the departure from Rutherford scattering which results from nuclear interaction should be observed beginning at 60 — 64° in the case of heavy nuclei.

According to Nishida,[4] the distance b at which deuteron breakup begins to take place is given by

$$b = Ze^2/v\sqrt{ME_b},$$

where E_b is the deuteron binding energy. For our deuteron energy 30° was the corresponding calculated angle at which electric breakup begins to be effective. The somewhat larger observed angle for the departure can be associated with the fact that breakup becomes appreciable when the interaction energy somewhat exceeds E_b. This can possibly explain why no departure from Rutherford scattering was observed for $E_d = 4$ Mev.[5]

For Pb, Au, and Pt, cross sections smaller than the Rutherford values at angles up to 60° therefore result from electric breakup of the deuteron. Figure 2 shows the absolute electric breakup cross sections for these nuclei.

In the case of lighter nuclei the departure from Rutherford scattering is observed at angles smaller than 40°; the angle decreases with smaller Z. The distribution exhibits a number of peaks. Since in the cases of Fe, Ni, Cu, Ag, and Sn the departure occurs at angles in good agreement with θ_c, nuclear interaction is the most likely cause.

In conclusion we wish to thank Yu. A. Bin'kovskiĭ for preparing the targets, V. N. Dobrikov and N. I. Zaika for assistance with the measurements, and the entire staff of the cyclotron laboratory.

---

*The quasi-classical approximation, which furnishes an adequate general description of scattering on heavy nuclei, is justified in our case by the fact that $Ze^2/\hbar v$ exceeds unity even for Fe. Therefore Eq. (1) can be regarded as suitable for an approximate evaluation of θ_c.

[1] H. E. Gove, Phys. Rev. **99**, 1353 (1955).

[2] J. R. Rees and M. B. Sampson, Phys. Rev. **108**, 1289 (1957).

[3] C. E. Porter, Phys. Rev. **99**, 1400 (1955).

[4] Y. Nishida, Progr. Theoret. Phys. (Kyoto) **19**, 389 (1958).

[5] I. Slaus and W. Parker Alford, Phys. Rev. **114**, 1054 (1959).

[6] N. I. Zaika and O. F. Nemets, Izv. Akad. Nauk SSSR, Ser. Fiz. **23**, 1460 (1959), Columbia Tech. Transl. p. 1447.

Translated by I. Emin
274

SOVIET PHYSICS JETP VOLUME 12, NUMBER 6 JUNE, 1961

INVESTIGATION OF μ^+-MESON DEPOLARIZATION IN NUCLEAR EMULSIONS

Yu. M. IVANOV and A. I. FESENKO

Moscow Engineering-Physics Institute

Submitted to JETP editor April 23, 1960; resubmitted July 28, 1960

J. Exptl. Theoret. Phys. (U.S.S.R.) **39**, 1492-1496 (December, 1960)

The influence of the relative AgBr content in nuclear emulsions on the magnitude of the asymmetry coefficient for the $\mu^+ \rightarrow e^+$ decay was studied experimentally. Values of the μ^+-meson depolarization were obtained separately for AgBr and for gelatin.

INTRODUCTION

THE asymmetry coefficient of the $\mu^+ \rightarrow e^+$ decay for μ^+ mesons stopping in various substances has been investigated in a number of experiments.[1-5] According to the theory of the universal four-fermion interaction,[6,7] the angular distribution of the decay electrons, integrated over the spectrum, is given by $1 - \frac{1}{3}\cos\theta$, where θ is the angle between the electron momentum and the μ^+-meson spin. The experimentally-observed distribution is of the form $1 - \alpha\cos\vartheta$, where ϑ is the angle between the momenta of the μ^+ meson and of the electron, and $\alpha < \frac{1}{3}$. The latter fact is due to the incomplete polarization of μ^+ mesons at the time they are produced, and to additional depolarization during the last stages of their slowing down, which include the period between their stopping and decay.

In experiments with nuclear emulsions and bubble chambers, the $\pi^+ \rightarrow \mu^+$ decay occurs after the μ^+ mesons have stopped completely, and the μ^+ mesons are therefore completely polarized in the beginning. In such experiments, the magnitude of the μ^+-meson depolarization D is determined during the last stages of slowing down and stopping of the μ^+ meson.

Thus, the experimental value of α determines the residual polarization of the μ^+ meson, $P = 1 - D$, according to

$$P = 3\alpha. \tag{1}$$

It is usually assumed[8-12] that the μ^+-meson depolarization in matter is mainly due to the production of mesonium. In the $^3S_1$ mesonium state with $m = 1$, there is no depolarization of the μ^+ meson. In the state with $m = 0$, which is a superposition of the states $^3S_1$ and $^1S_0$, total depolarization occurs. Therefore, in the absence of a strong magnetic field which would decouple the spins of the electrons and the μ^+ mesons in the mesonium, half of the μ^+ mesons become depolarized. For a multiple electron exchange, total depolarization of μ^+ mesons is possible.

The present investigation deals with the depolarization of μ^+ mesons in nuclear emulsions with different relative AgBr content.

EXPERIMENTAL METHOD

An emulsion chamber consisting of stripped layers of NIKFI-R emulsion of four types, differing from each other in their AgBr content, was placed into the 350-Mev π^+-meson beam of the synchrocyclotron at the Joint Institute for Nuclear Research. A copper absorber, whose thickness was chosen in such a way that π^+ mesons stopped in the middle of the chamber, was placed in the path of the particles. The emulsion chamber was surrounded by a double iron screen, which attenuated the intensity of the scattered field of the accelerator and of the earth's magnetic field to 0.04 oersted.

The particle flux density during the irradiation amounted to 5×10^4 particles per cm^2.

The NIKFI emulsion was used in its regular form, or with double, triple, or quadruple gelatin dilution.

The agreement between our data on the density and shrinking of the emulsion with the data supplied by the Research Institute of the Motion Picture Industry and the Physics Institute of the Academy of Science (see Table I) indicates that we can use the values of the relative AgBr content in the emulsion shown in the table.

RESULTS OF SCANNING

In the scanning of the emulsion we measured the points at which the π^+ mesons stopped, and also the direction of the projection on the plane of

TABLE I

Degree of dilution	Supplied by Mot. Pict. Inst.[13] weight content	volume content	density	Supplied by Phys. Inst.[14] shrinkage factor	density	Our data shrinkage factor	density
1	0.82	0.49	3.88	2.8	3,9	3.0±0.1	3.9±0.2
2	0.726	0.36	3,22	2,2	2.84	2.1±0.1	3.2±0.2
3	0.657	0,29	2.86	1.9	2.64	1.9±0.1	2.9±0.2
4	0,598	0,24	2,55	1,63	2.1	1.7±0.1	2.2±0.2

scanning of the μ^+-meson emission line. In addition, the depth of the end of the μ^+-meson track and the direction of emission of the positron were measured. The plane perpendicular to the direction of the projection of the μ^+-meson line of emission and to the plane of the emulsion separates, on the average, the positrons emitted forwards and backwards. In order to exclude redundant detection of the same event, a contact mounted on the microscope table produced a signal when the investigated μ^+ meson left the scanned strip, and also upon its return to the strip for further scanning.

A total of 45 457 events of $\pi^+ \to \mu^+ \to e^+$ decays was found in the emulsions with the four different concentrations. In the reduction of the data obtained, those events were selected in which the μ^+ mesons stopped at a distance $> 50\,\mu$ from the surface of the undeveloped emulsion. As a result of such a selection, the total number of the $\pi^+ \to \mu^+ \to e^+$ decay events was reduced to 38 192.

Data on each type of emulsion are given in Table II.

TABLE II

Degree of dilution	Total number of events	N_f	N_b	α_1	Percentage of unobserved positrons
1	14.184	5.561	6,081	0.089	0.34
2	9.902	3,931	4,420	0,117	0.59
3	11,547	4.514	5.102	0,122	1.73
4	9,824	3,697	4.299	0.151	3,9

CORRECTIONS

The distribution of the μ^+-meson decay positrons is given by the expression

$$dN = \text{const} \cdot (1 - \alpha \cos \vartheta)\, d\Omega,$$

where ϑ is the angle between the momenta of the μ^+ meson and of the positron, and where the positrons emitted in all directions with respect to the primary particles are detected.

For the "forward-backward" positron distribution, the asymmetry coefficient is

$$\alpha = 2(N_b - N_f)/(N_b + N_f).$$

However, in connection with the fact that the μ^+-meson momenta are distributed within the angles 0 — 30° or 0 — 24° with respect to the emulsion plane (depending on the thickness of the emulsion layer), the measured asymmetry coefficient should be divided by the correction coefficient $K_1 = \overline{\cos^2 \varphi} / \overline{\cos \varphi}$, where φ is the angle of dip of the μ^+ meson. Such a correction takes into account the fact that the direction of emission of the μ^+ meson is not horizontal, but inclined by 3 — 4%, depending on the type of emulsion.

A second correction was determined from the double scanning of those events of $\pi^+ \to \mu^+ \to e^+$ decay that can result in the transfer of positrons from group N_b to group N_f and vice-versa. This can be explained by observer errors, bad visibility of the positron because of lowered grain density along the particle track in the diluted emulsion, incorrect detection of the positron direction, etc. The factor obtained is $K_2 = 1 - 2\rho$, where ρ is the relative number of cases of incorrectly-recorded positron direction. With increasing dilution of the emulsion, this factor, averaged over the results of different scanners, varies from 0.94 to 0.9.

The low density of grains along the positron tracks in emulsions with fourfold dilution, and the strong inhomogeneity of the emulsion, lead to a relatively high percentage of omitted positrons at the end of the μ-meson tracks (see Table II). We have attempted to establish the distribution of the positron directions for three cases in which they were not observed, using the method of random tries from the statistics already accumulated for the given dilution. For these tries, a 6% overestimate of the forward-backward asymmetry coefficient was obtained. This was done based on statistics which made it possible to consider such an overestimate as agreeing with the measured value of the asymmetry coefficient for the given dilution.

Taking into account the two corrections and also the fact that the omitted positrons do not affect the result, we obtained the following asymmetry coefficients for the various dilutions of the emulsion:

$$\alpha_{2\times 1} = 0.100 \pm 0.018, \qquad \alpha_{2\times 2} = 0.133 \pm 0.022,$$
$$\alpha_{2\times 3} = 0.153 \pm 0.020, \qquad \alpha_{2\times 4} = 0.170 \pm 0.022^{*},$$

---

*We also studied the asymmetry of positrons in the quadruple-dilution emulsion which had previously been treated with TÉA hypersensitizer [$(C_2H_4OH)_3N$]. Taking the correction factors into account, it was found that $\alpha = 0.148 \pm 0.028$. Thus, the use of TÉA does not lead to a marked depolarization of the μ^+ mesons.

DISCUSSION OF RESULTS

From our experimental results we can, using Eq. (1), estimate the residual polarization of μ^+ mesons in AgBr and in gelatin.

It was assumed that the depolarization occurs during the time after the μ^+ mesons have stopped either in the AgBr or in the gelatin.

In that case, the polarization of the μ^+ mesons decaying in the emulsion can be written in the following manner:

$$P = P_1\gamma + P_2(1-\gamma), \qquad (2)$$

where P_1 and P_2 are the polarizations of the μ^+ mesons decaying in gelatin and AgBr respectively, and $\gamma = xS/(1 + xS)$ is the relative number of μ^+ mesons stopping in gelatin (where x is the ratio of the volume of gelatin to the volume of AgBr, and S is the stopping power of gelatin relative to the stopping power of AgBr). For a known value of γ, one could obtain the values of P_1 and P_2 that best approximate the data obtained according to Eq. (2).

However, γ is related to S, which is not known in our case, so that the problem is to determine the three parameters P_1, P_2, and S. In general, a simultaneous determination of these parameters appearing in Eq. (2) is possible only for very large statistics where, for a unique S, we can obtain a linear variation of P with γ. Moreover, x and S should be interdependent. In the case where the value of P is subject to statistical errors, the linear variation of P with γ is maintained for various values of S, so that the unique correlation of the parameters disappears. Using the least-squares method, we have constructed a family of straight lines with various values of S (see figure). The analysis of these curves by the χ^2 test excludes the possibility of discriminating in favor of one of them.

We therefore have a number of equally-probable values of S with corresponding values of P_1 and P_2. From additional data we can, however, find a lower limit for S.

The measurement of the range of 4.12-Mev μ^+ mesons (originating in the decay of the stopped π^+ mesons) in emulsions with various gelatin contents makes it possible to determine directly the ratio of the stopping power of gelatin and of AgBr, the most reliable value of which is equal to 0.34. It is known that, with decreasing energy of charged particles, the stopping powers of light and heavy elements become comparable, and their ratio tends to unity. Assuming that depolarization occurs in the stopping, or, at any rate, at the end of the μ^+-meson range, where the energy is of the order of several times ten kev, we can assume that, in our case, S lies in the 0.34 — 1 range. P_2 can then vary from 0.09 to 0.12 (i.e., ~ 0), and P_1 from 0.9 to 0.7.

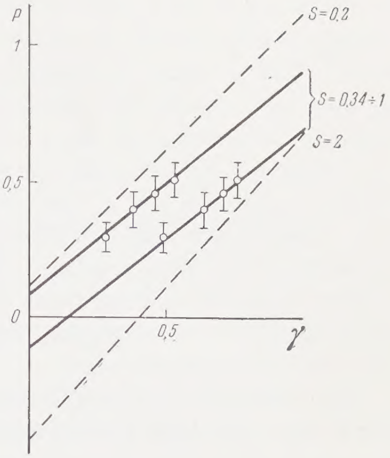

Polarization of μ^+ mesons as a function of the relative number of μ^+ mesons stopping in gelatin (γ) for various values of S. The experimental points correspond to the assumed values S = 0.34 and 1.0.

Data given in the literature make it possible to choose a better value of S. It is first necessary to estimate the energy of μ^+ mesons for which the particles stop in each of the emulsion components (i.e., the energy for which a μ^+ meson incident upon an AgBr grain stops in it).

In a very approximate way, using the tabulated data of Fay, Gottstein, and Hain,[15] or using the empirical formula for small ranges, $E\,[\text{kev}] = 84\,R^{0.655}\,[\mu]$, it was found that the μ^+ meson loses ~ 40 kev in the last AgBr grain. This does not contradict another calculation based on the determination of the residual range in AgBr for 133-kev μ^+ mesons from the formula for ionization losses in the Born approximation.[16]

From the data of Warshau,[17] the ratio of the stopping power of light and heavy substances (Be and Ag) for 0.1-Mev protons or ~ 0.015-Mev μ^+ mesons amounts to 0.8. The ratio of the stopping powers of gelatin and AgBr[18,19] for 0.52-Mev protons (~ 0.06-Mev μ^+ mesons) amounts to 0.81.

Comparing all the various data, it is reasonable to choose S = 0.8.

From a further analysis of the data obtained for S = 0.8 we find $P_1 = 0.72 \pm 0.22$ and $P_2 = 0 + 0.11$ (taking into account that polarization cannot be negative).

A strong depolarization of μ^+ mesons in AgBr, in spite of the multiple exchange with an electron, can evidently be explained by the action of an additional process connected with the production of mesonium. If we regard mesonium as similar to positronium, we can assume that, for certain substances, there is a finite probability of preponderance of the system's orthostate. Thus, the cross section for orthopositronium in halides is $\sim 10^{-16}$ cm^2.[20] This is possibly due to production of the μ^+Br^- molecule, as a result of which the original orientation of the μ^+-meson spin is "forgotten." On the other hand, a relatively small depolarization of the μ^+ meson is observed in gelatin. This means that apparently not all μ^+ mesons produce mesonium in gelatin, and other mechanisms of depolarization being absent, the μ^+ mesons conserve their original spin orientation up to the very moment of decay.

The authors express their deep gratitude to Prof. I. I. Gurevich for his advice and interest in the work. We would like also to thank Prof. V. I. Gol'danskiĭ and B. A. Nikol'skiĭ for their discussion of the results, and Z. S. Galkin, G. I. Polosin, and A. V. Smelyanskaya for help in scanning the emulsion.

---

[1] Gurevich, Kutukova, Mishakova, Nikol'skiĭ, and Surkova, JETP **34**, 280 (1958), Soviet Phys. JETP **7**, 195 (1958).

[2] Alikhanyan, Kirillov-Ugryumov, Kotenko, Kuznetsov, and Popov, JETP **34**, 1101 (1958), Soviet Phys. JETP **7**, 763 (1958).

[3] Chadwick, Durrani, Eisberg, Jones, Wignall, and Wilkinson, Phil. Mag. **2**, 684 (1957).

[4] Garwin, Lederman, and Weinrich, Phys. Rev. **105**, 1415 (1957).

[5] R. A. Swanson, Phys. Rev. **112**, 580 (1958).

[6] R. Feynman and M. Gell-Mann, Phys. Rev. **109**, 193 (1958).

[7] E. Sudarshan and R. Marshak, Phys. Rev. **106**, 1290 (1957).

[8] J. Friedman and V. Telegdi, Phys. Rev. **106**, 1290 (1957).

[9] Sens, Swanson, Telegdi, and Jovanovitch, Phys. Rev. **107**, 1465 (1957).

[10] Lynch, Orear, and Rosendorff, Preprint, 1959.

[11] Vaĭsenberg, Rabin, and Smirnit-skiĭ, JETP **36**, 1680 (1959), Soviet Phys. JETP **9**, 1197 (1959).

[12] Ali-Zade, Gurevich, Dobretsov, Nikol'skiĭ, and Surkova, JETP **36**, 1327 (1959), Soviet Phys. JETP **9**, 940 (1959).

[13] M. F. Rodicheva, NIKFI Reports, Issue 32, pp. 29-34, Moscow, 1959.

[14] G. A. Pomanova, Приборы и техника эксперимента (Instruments and Exptl. Techniques) **4**, 93 (1958).

[15] Fay, Gottstein, and Hain, Nuovo cimento **12**, Suppl. 2, 234 (1954).

[16] E. Segrè, Experimental Nuclear Physics (John Wiley and Sons, Inc., New York, 1953) Vol. I (Russ. Transl. IIL, 1955, p. 144).

[17] S. D. Warshau, Phys. Rev. **76**, 1759 (1949).

[18] M. S. Livingston and H. Bethe, Rev. Mod. Phys. **9**, 245 (1937).

[19] J. H. Webb, Phys. Rev. **74**, 511 (1948).

[20] S. De Benedetti, Nuovo cimento **4**, Suppl. 3, 1209 (1956).

Translated by H. Kasha
275

SOVIET PHYSICS JETP VOLUME 12, NUMBER 6 JUNE, 1961

INVESTIGATION OF MAGNETOACOUSTIC RESONANCE IN A PLASMA WITH AID OF DOUBLE ELECTRIC PROBES

V. D. RUSANOV, B. I. PATRUSHEV, I. A. KOVAN, V. I. GARKUSHA, D. A. FRANK-KAMENETSKIĬ

Submitted to JETP editor April, 1960

J. Exptl. Theoret. Phys. (U.S.S.R.) **39**, 1497-1502 (December, 1960)

The concentration of a plasma in a magnetoacoustic wave is measured. It is shown that the ionization increases considerably and rapidly in magnetoacoustic resonance. The radial concentration distribution in the plasma is almost uniform.

INTRODUCTION

A study of magnetoacoustic resonance is of considerable interest in problems connected with the development of methods of high-frequency ionization and heating of plasma. It was shown by Frank-Kamenetskiĭ[1] that resonant phenomena due to propagation of magnetoacoustic oscillations are possible in a plasma-filled infinite cylinder located in a magnetic field. Magnetoacoustic resonance was actually observed and investigated experimentally.[2] However, comparison of the observed resonant frequencies with the calculated ones is made difficult by lack of exact data on the concentration of the plasma and on its distribution in space. The purpose of the present investigation was to measure the concentration of plasma during the process of magnetoacoustic resonance.

The method of high-frequency probing, used in the earlier experiments,[2] yields only the lower limit of plasma concentration. The microwave-interferometer method gives the average value of the concentration along the line of sight. The advantage of these methods is that they are absolute and do not disturb the plasma. Since we were interested in the measurement of the plasma concentration in space and in time, we chose the method of double electric probes for the relative measurements. The absolute calibration was against a microwave sounding signal. It is well known[3-4] that absolute measurements with electric probes become insufficiently reliable in the presence of a magnetic field, because the magnetic field affects differently the motion of the particles that arrive at the probe at different angles. For this reason the probe measurements were regarded in the present investigation as relative only.

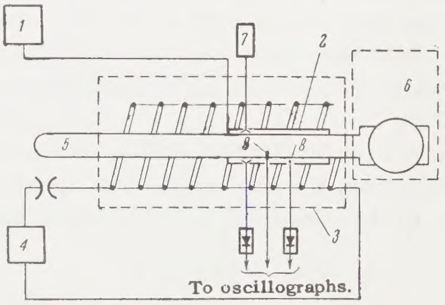

FIG. 1. Diagram of the apparatus: 1 – generator (f = 42–50 Mc/sec, P_{max} = 150 kw, t_s = 10 milliseconds (decrease 67 percent)); 2 – tank circuit coupled to the plasma, in the form of a cylindrical loop with f_{res} = 45 Mc/sec, L = 40 cm, D = 12.5 cm; 3 – coil for longitudinal magnetic field (L = 90 cm, D = 30 cm, H_{max} = 16 koe, T/2 = 4 millisec); 4 – capacitor bank to supply the coil; 5 – cylindrical vacuum chamber of glass, 7 cm i.d. and 150 cm long; 6 – vacuum system; 7 – microwave sounding generator with λ = 3 cm; 8 – magnetic probe; 9 – double electric probes.

1. DESCRIPTION OF THE APPARATUS

The experiments were carried out with the apparatus illustrated in Fig. 1.

A cylindrical plasma column was produced in a longitudinal homogeneous quasi-static magnetic field; the direction of the applied high-frequency magnetic field coincided with that of the quasi-

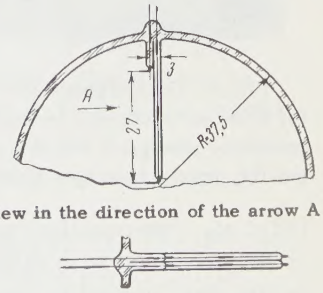

FIG. 2. Arrangement of probes in the chamber.

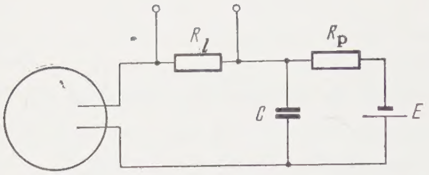

FIG. 3. Connection diagram of the probes.

static one. The experiments were carried out with hydrogen. To estimate the concentration of the charged particles, double probes were sealed into the tube in which the plasma was produced; in addition, soundings were made with pulses from a 3-cm klystron oscillator. The double probes were made of molybdenum wire 0.5 mm in diameter and were sealed into the wall of the vacuum chamber (Fig. 2). One pair was placed along the axis of the chamber, while the other was placed 8 mm away from the wall. The probes were connected as shown in Fig. 3.

To obtain a probe current that is linear with the concentration, the equipment was operated saturated. In this case the Bohm formula holds,[4]

$$i_p = 0.4 n_{\sim} \sqrt{2kT_e/m_i}\, S,$$

where i_p is the probe current, m_i and n_i are the mass and concentration of the ions, T_e is the electron temperature, and S is the collecting area of the probe.

2. PROCESSING OF THE EXPERIMENTAL DATA

Oscillograms were taken of the probe currents with and without voltage applied to the probes (Fig. 4). The oscillograms of Fig. 5 show the currents produced with different probes. The first probe was located at the wall, the second on the chamber axis. Figure 6 shows the oscillograms of the current flowing in a probe located at the chamber walls and the sounding microwave signal with rapid sweep.

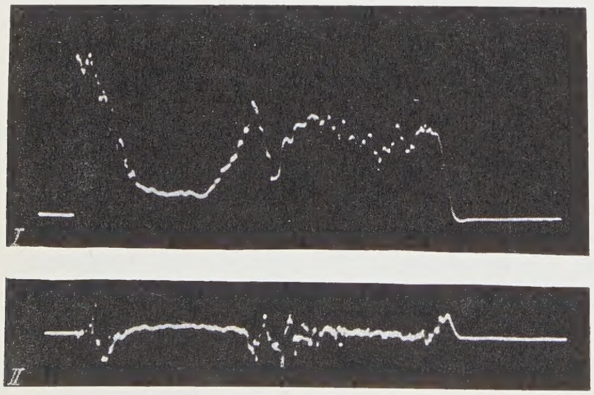

FIG. 4. Oscillograms of signals from one pair of probes for different voltages: I – for $U_p = 300$ v, II – for $U_p = 0$ at a generator voltage $E = 6$ kev and $H_0 = 5.8$ koe; $p = 8 \times 10^{-4}$ mm Hg; sweep time $t_s = 10$ milliseconds.

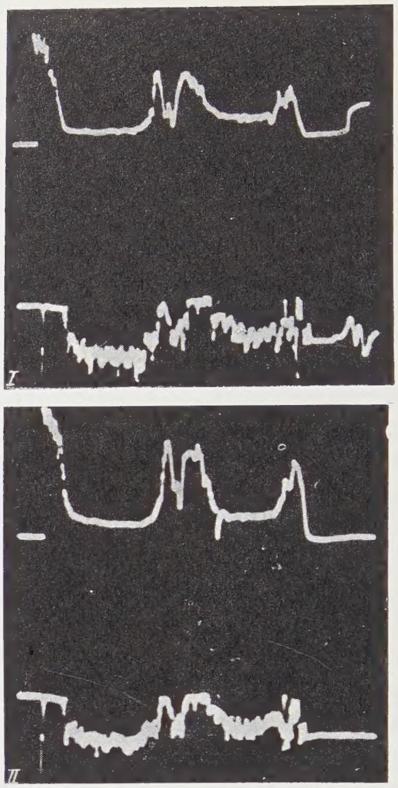

FIG. 5. Oscillograms of probe currents for different pairs of probes (upper beam) and signals of microwave sounding generator (lower beam): I – probes located at the wall, II – along the chamber axis. Values of E, H_0, p, and t_s are the same as in Fig. 4, $U_p = 300$ v.

The oscillograms in Figs. 7 and 8 illustrate the variation dependence of the probe current with the voltage E of the ionizing generator at a constant magnetic field H_0, and of the field intensity H_0 at constant ionizing-generator voltage.

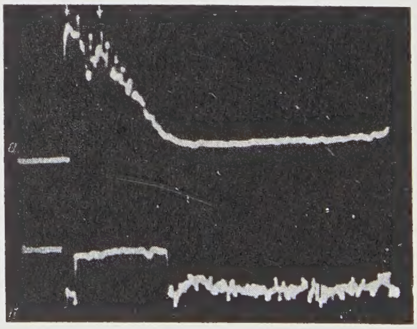

FIG. 6. Oscillogram of the probe current and the signal of the sounding microwave generator with fast oscillogram sweep ($t_s = 3$ milliseconds); the arrows indicate the maxima of concentration, the values of E, H_0, p, and U_p are the same as for Fig. 5.

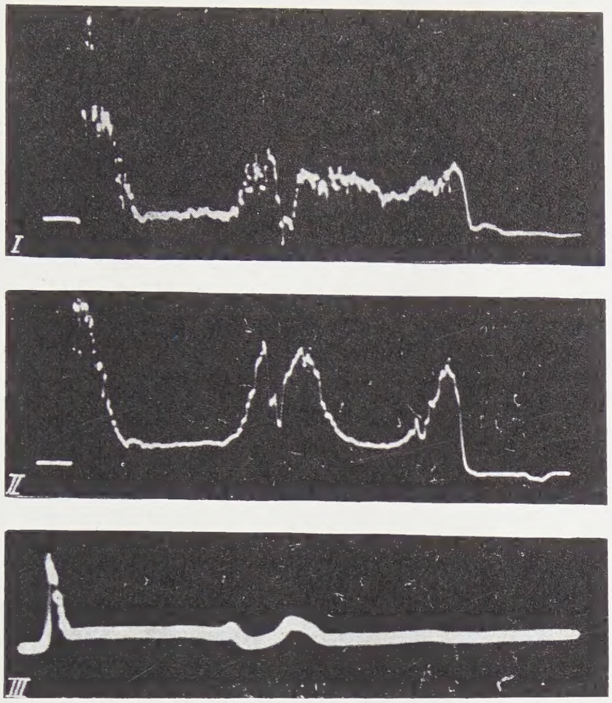

FIG. 7. Dependence of the probe current on the generator voltage at the same values of H_0, p, U_p and t_s as in Fig. 5. Oscillogram I – E = 9 kv, II – E = 6 kv, III – E = 3 kv.

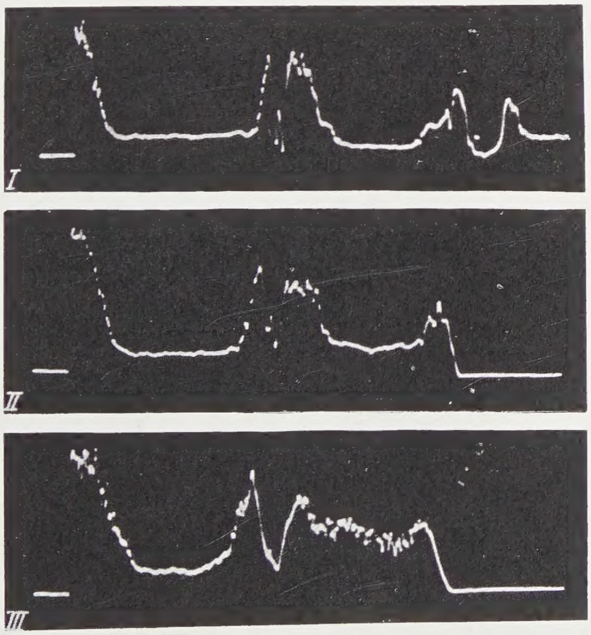

FIG. 8. Dependence of the probe current on the intensity of the magnetic field: I – H_0 = 8 koe, II – H_0 = 5.8 koe, III – H_0 = 4.2 koe; experimental conditions are the same as for Fig. 5.

Figure 9 shows an oscillogram of the quasi-static magnetic fields H_0 and the form of the sounding microwave signal pulse in the absence of plasma.

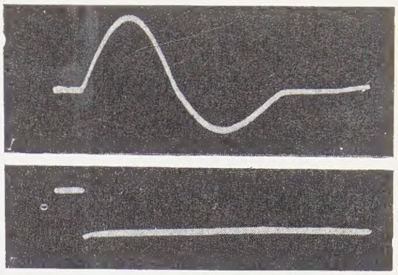

FIG. 9. Form of the quasi-static magnetic field (oscillogram I) and of the envelope of the microwave sounding signal (oscillogram II) at E = 0, $p = 10^{-6}$ mm Hg, t_s = 10 milliseconds.

We also plotted the characteristic of the probes, as shown in Fig. 10. The saturation of the probe current is evident.

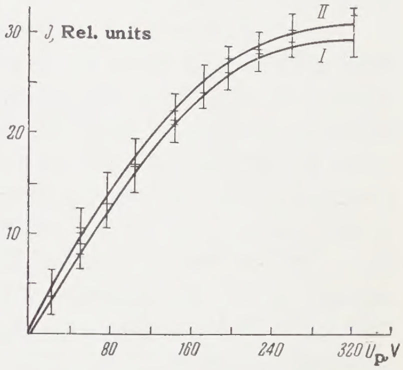

FIG. 10. Characteristics of the probes: Curve I – probe at the wall, II – probe on the chamber axis.

The probe was calibrated by comparing the oscillograms of the probe current with the oscillogram of the microwave sounding signal (see Fig. 5). It was assumed here that at the instant when the microwave signal is triggered the electron concentration passes through the value $n = 10^{12}$ cm^{-3}.

The oscillogram of Fig. 6 shows that the probe current has two maxima, corresponding to the following values of quasi-static magnetic field and electron concentration: $n = 6 \times 10^{12}$ cm^{-3} at H_0 = 650 oe and $n = 5 \times 10^{12}$ cm^{-3} at H_0 = 1580 oe.

The radial distribution of the plasma concentration, estimated with the aid of Fig. 5, is $n = 8.6 \times 10^{12}$ for probes located at the wall, and $n = 6.2 \times 10^{12}$ for probes located on the chamber axis.

3. DISCUSSION OF RESULTS

It has been shown in an earlier investigation[2] that a quasi-static magnetic field is varied, the amplitude of the alternating field goes through two or three resonant maxima. These were interpreted as magnetoacoustic resonances. In the present paper analogous resonant maxima were observed upon variation of the concentration of the plasma with time.

The resonant frequencies are close to the geometric mean of the electron and ion cyclotron frequencies ω_e and ω_i, as should be the case

	First maximum	Second maximum
$\omega^* = H_0\mu_i/\sqrt{4\pi\rho}\,R$	$6{,}0\cdot 10^7$	$3.1\cdot 10^8$
$\omega=\omega_i\,\omega_e\left[1+\frac{1}{\Pi^*}\frac{\omega_e}{\omega_i}\frac{k_z^2}{k_r^2}\right]\left[\Pi^*+1+\frac{\omega_e^2}{\omega_0^2}\right]$	$7.3\cdot 10^7$	$4\cdot 10^8$
$\sqrt{\omega_i\,\omega_e}$	$2.5\cdot 10$	$6.5\cdot 10^8$

when the number of electrons per unit plasma-cylinder length is small.[5] In this frequency region different types of oscillations are possible, to which the auxiliary resonances may indeed correspond. An accurate identification of the type of the resonant oscillations calls for a detailed measurement of the field configuration, and needs further investigation.

We can, however, draw the following preliminary conclusions from the data obtained on the radial distribution of the amplitude of the high-frequency magnetic field $\widetilde{H}_z$ and on the amplitudes $\widetilde{H}$ and $\widetilde{H}_z$ as given in reference 2. The resonance $H_0 = 650$ oe corresponds to the first radial number $k_r = 3.83$, while the resonance at $H_0 = 1580$ oe corresponds to the second radial number $k_r = 7.0$. Because of the symmetrical character of the excitation, we assume that the azimuthal number is $m = 0$ in either case. The resonant frequencies calculated under these assumptions are listed below; the generator frequency used is $\omega_g = 3.2 \times 10^8$.

Here ω^* is the circular frequency of the radial magnetoacoustic oscillations, ω is the circular frequency of the longitudinal-radial magnetoacoustic oscillations, and the remaining notation is that of reference 5. For ω^* we assume $k_z = 0$, and for ω we assume $k_z = 0.08$, corresponding to total reflection of the wave from the ends of the plasma cylinder. The calculation formulas were taken from references 1 and 5. The resonance at $H_0 = 1580$ oe corresponds to approximately one-half the "hybrid" frequency. The velocity of propagation of the magnetic sound differs little here from the Alfven velocity. The resonance at $H_0 = 650$ oe corresponds to a frequency close to "hybrid" but is somewhat higher. Purely radial oscillations are impossible in this case. The presence of a considerable component of the high frequency field H_φ confirms that actually the direction of the wave vector was in this case quite different from radial.

We thank E. K. Zavoiskiĭ for interest in this work.

---

[1] D. A. Frank-Kamenetskiĭ, J. Tech. Phys. (U.S.S.R.) **30**, 899, 1960, Soviet Phys.-Tech. Phys. **5**, 847 (1960).

[2] Akhmatov, Blinov, et al., JETP **39**, 536 (1960), Soviet Phys. JETP **12**, 376 (1961).

[3] L. A. Biberman and B. V. Panin, JETP **21**, 12 (1951) [sic!].

[4] The Characteristics of Electrical Discharge in Magnetic Fields. Edited by Guthrie, Wakerling, N. Y., (1949).

[5] D. A. Frank-Kamenetskiĭ, JETP **39**, 669 (1960), Soviet Phys. JETP **12**, 469 (1961).

Translated by J. G. Adashko
276

SOVIET PHYSICS JETP VOLUME 12, NUMBER 6 JUNE, 1961

GYROTROPIC PROPERTIES OF A PLASMA IN PROPAGATION OF THE EXTRAORDINARY WAVE

B. I. PATRUSHEV, V. D. RUSANOV, I. A. KOVAN, V. V. SAVICHEV, and D. A. FRANK-KAMENETSKIĬ

Submitted to JETP editor April 23, 1960

J. Exptl. Theoret. Phys. (U.S.S.R.) 39, 1503-1507 (December, 1960)

Rotation of the propagation and polarization vectors has been observed experimentally in a plasma for propagation of an electromagnetic wave at a frequency between the ion and electron cyclotron frequencies.

EXPERIMENTAL SECTION

IN the work reported here the propagation of electromagnetic waves along a cylindrical plasma column in a uniform quasistatic magnetic field H_0 has been studied. The plasma was produced in a cylindrical glass chamber by an ionizing oscillator which provided a nominal power of 150 kw at 50 Mc. The radio-frequency magnetic field was in the same direction as the static field. The experiments were carried out in hydrogen at a pressure $p = 8 \times 10^{-4}$ mm Hg. The plasma density was estimated by the blocking of pulses from a klystron which operated at a wavelength $\lambda = 3$ cm.

The basic parameters and a diagram of the apparatus are given in Fig. 1 of the preceding paper.[1]

Linearly polarized waves are excited in the plasma by a probing oscillator (pulsed) which delivers a power of 500 w at a frequency $f = 29$ Mc. The tank coil of the oscillator, which is located in a region of uniform quasistatic magnetic field (shown schematically in Fig. 1), is directly coupled to the plasma. It has been found that presence of the discharge in the chamber does not affect the operation of the oscillator except to cause a small frequency shift (of the order of 1%).

The detector system consists of magnetic radio-frequency probes; these are small coils consisting of Plexiglas forms on which 5 to 10 turns of type PEL wire (0.06 mm in diameter) are wound. The probes are used to measure the field components H_r, H_φ, and H_z; the orientations of the planes of these coils are different, but the product SW (where W is the number of turns and S is the area of a loop) is the same for all probes. A double magnetic probe has also been used. This probe differs from the one-coil probes in that two windings are wound on the frame and the planes of the windings are mutually perpendicular (a so-called double $H_r - H_\varphi$ probe).

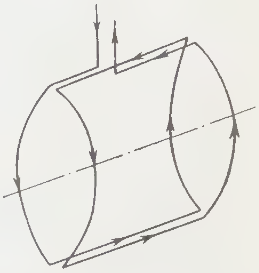

FIG. 1. Tank coil of the probing oscillator.

A block diagram of an experiment used to study the signal from a magnetic probe placed in the tank coil of the probing oscillator is shown in Fig. 2. Figure 3 shows oscillograms of the different wave components; here, the direction of H_r coincides with the direction of the field H in the tank coil of the oscillator.

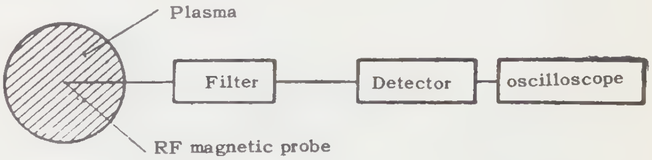

FIG. 2. Block diagram of the method used to measure the fields in the tank coil of the probing oscillator.

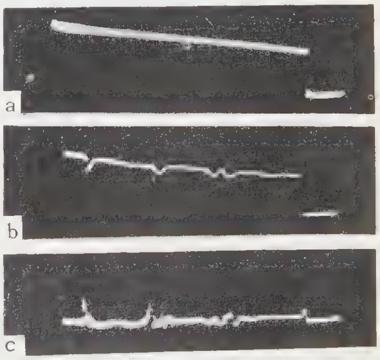

FIG. 3. Oscillogram showing the magnetic field in the tank coil of the probing oscillator (sweep length $t_s = 12$ msec.) a) the H_r component with vacuum in the chamber; b) and c) are the H_r and H_φ components with plasma present.

The oscillogram in Fig. 3a shows the time variation of the H_r component of the probing oscillator when the chamber contains nothing but vacuum; the oscillogram in Fig. 3b shows this same component with plasma in the chamber. The shallow dips in the second oscillogram correspond to times of maximum plasma concentration in the chamber. In Fig. 3c we show the time variation of the H_φ component. It is apparent from this figure that the peaks in the H_φ signal coincide with the dips in the H_r signal.

The absolute magnitudes of these signals have also been measured; a calibrated signal generator was used for this purpose. The measurements show that at an oscillator plate voltage of 750 v, the field at the center of the tank coil (in vacuum) $H_r = 0.33$ oe. When plasma is present this field is reduced to $H_r = 0.14$ oe. The other two components of the field are considerably smaller, being approximately 20% of H_r. The distributions of the field components H_r, H_φ, and H_z over the diameter of the vacuum chamber were also measured. These curves are shown in Fig. 4.

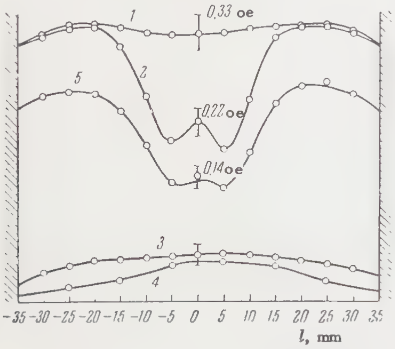

FIG. 4. Curves showing the distribution of the magnetic field components over the diameter of the vacuum chamber. Curve 1 shows the H_r component with vacuum in the chamber while curves 2, 3 and 4 show the components H_r, H_z and H_φ with plasma present but off resonance; curve 5 shows the H_r component at resonance (l is the distance from the center of the chamber).

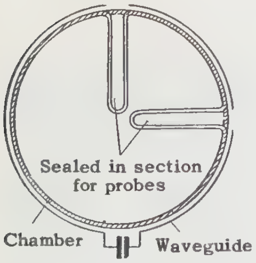

FIG. 5. Cross section of the chamber in the region of the waveguide.

The transmission of electromagnetic waves is studied in a plasma waveguide which is a glass plasma-filled chamber; the waveguide has an external copper shield which is 20 cm in length. The distance from the tank coil of the oscillator to the detector is approximately 25 cm. The radial distributions of the electromagnetic field components were measured by sealing two tubes into the vacuum chamber at an angle of 90° with respect to each other. A cross section of the vacuum chamber is shown in Fig. 5.

The vacuum wavelength of the probing oscillator is approximately 10 m; with the waveguide diameter which was used (7.5 cm) this wave is beyond cut off in the waveguide. With plasma in the chamber, but no static magnetic field, no transmitted signal can be observed. However, with plasma in the chamber in the presence of a quasistatic magnetic field, a transmission signal is observed at the rf magnetic probe in the plasma waveguide. The time variation of the transmission signal is shown in Figs. 6a, b and c. These photographs show four narrow transmission signals per period of the quasistatic magnetic field. These signals appear at times which correspond closely to the time of peak plasma concentration in the chamber. This result is corroborated by Fig. 7; in Fig. 7 one oscillogram (b) shows the transmission signal while the other (a) shows the time variation of plasma concentration in the chamber as measured by double electric probes.[1]

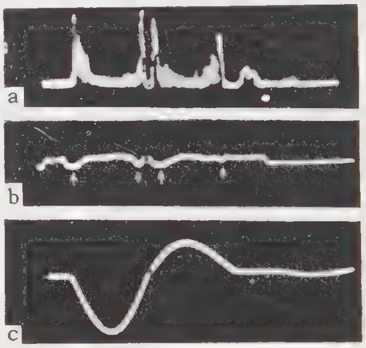

FIG. 6. a) Oscillogram of the transmission signal, b) oscillogram showing blocking of the signal at λ = 3 cm (the blocking time is shown by the arrows), c) oscillogram of the quasistatic magnetic field (the cross denotes the zero of the magnetic field).

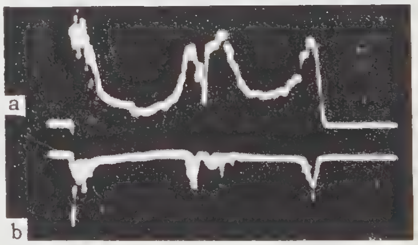

FIG. 7. a) Oscillogram showing the concentration, b) transmission signal ($t_s = 12$ msec).

The radial distribution of the various components of the electromagnetic field transmitted which by the plasma waveguide are shown in Fig. 8; these curves were obtained with radio-frequency magnetic probes. The amplitudes of the different components are within 20% of each other. The field at maximum transmission is 0.07 oe.

Even with asymmetric excitation the distribution of the field components in the waveguide is axially symmetric. From this we conclude that the linearly polarized wave is split into two circularly polarized waves; in the frequency region

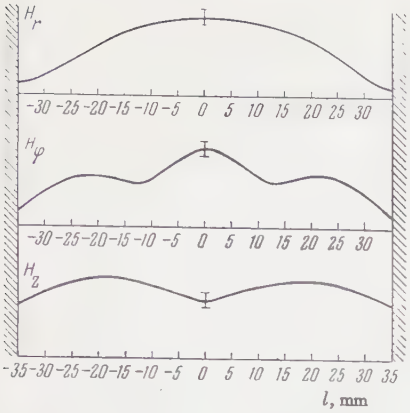

FIG. 8. Curves showing the distribution of the components of magnetic field of the wave in the plasma waveguide.

which has been investigated only one of these is transmitted through the waveguide. In a gyrotropic medium the wave can be rotated. If the wave is rotated at an angular frequency equal to the oscillator frequency, there should be a phase shift of 90° between signals from identical probes at a given cross section of the chamber which are oriented at an angle of 90° with respect to each other. The following experimental method was used to detect this phase shift. The signals from the probes were fed to amplifiers through equal lengths of cable (and low-frequency filters) and then compared in phase.

After calibration, the probes were placed in the plasma waveguide and checked to see that amplitude of the transmission signal was the same in both. Following this check the transmission signals were combined in a phase detector, but no appreciable change in the shape of the oscillogram was noted. However, when a section of cable $\lambda/4$ in length is inserted in one arm (before the filter) the transmission signal increases in the first half cycle of the magnetic field and decreases in the second half cycle. When the section of cable is placed in the other arm, the shape of the oscillograms is again changed. Now the transmission pulses increase in the second half cycle and decrease in the first half cycle. With the same arrangement, but with sections of cable which are $\lambda/2$ and $\lambda/8$ in length, no change is noted in the oscillograms. Thus, it has been shown that there is a phase shift of approximately 90° between the probe signals. This result corroborates our statement that the wave in the waveguide rotates at frequency ω.

By knowing the position of the probes in the plasma waveguide and introducing a fixed phase shift of 90° in the circuit of one or the other of the probes, we can determine the relative delay of the signals from the probes; thus, the direction of rotation of the wave can be determined. The direction of rotation of the wave is the same as the direction of rotation for an electron.

A similar experiment was carried out with the double probe. The oscillograms obtained in this case were similar to those obtained with two probes. It follows that there is a phase shift of approximately 90° between the H_r and H_φ components of the radio-frequency field which is transmitted in the plasma waveguide. The appropriate oscillograms are shown in Fig. 9.

From the oscillogram in Fig. 10, which shows the time behavior of the first transmission peak, it is apparent that the transmission signal exhibits a fine structure in the form of three satellites which coincide in time with the maximum concentrations. The results of these measurements are given in the table, where i is the number assigned to the peak of the transmission signal, n is the plasma concentration, $\epsilon_{||}$ and λ_{pl} are respectively the longitudinal component of the dielectric constant and the plasma wavelength computed for an infinite medium, ω_e and ω_i are respectively the

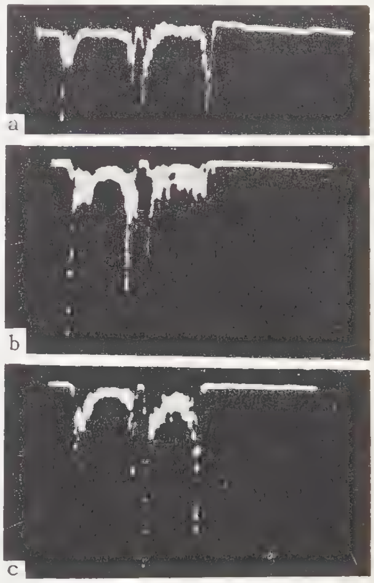

FIG. 9. a) Oscillogram of transmission signal, $t_s = 12$ msec; b) oscillogram showing the signal in the phase detector when a $\lambda/4$ cable is introduced into the arm containing one probe and then the other.

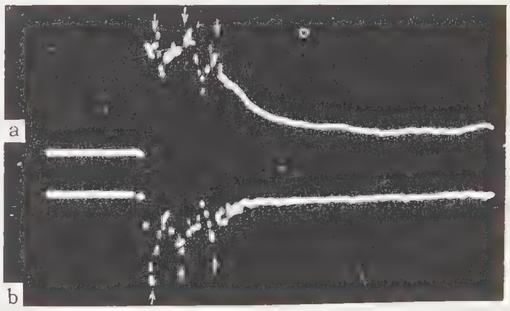

FIG. 10. a) Oscillogram showing the behavior of the concentration and b) transmission signal ($t_s = 3$ msec).

i	H_0, oe	n	$\varepsilon_{\parallel}$	λ_{pl} cm	ω_e	ω_i
1	450	$6 \cdot 10^{12}$	13300	8,6	$7,8 \cdot 10^9$	$4,3 \cdot 10^6$
2	1370	$6 \cdot 10^{12}$	4400	13	$24 \cdot 10^9$	$13,3 \cdot 10^6$
3	2280	$5 \cdot 10^{12}$	2200	19	$39 \cdot 10^9$	$22 \cdot 10^6$

electron and ion cyclotron frequencies. The frequency of the probing oscillator is $\omega = 18 \times 10^7$.

The shape of the transmission oscillogram may be interpreted as follows. The wave cannot be transmitted at very weak magnetic fields,[2-4] since $\omega > \omega_e$ and $\omega < \omega_0$. As the quasistatic magnetic field increases, ω_e becomes larger than ω and transmission becomes possible. However, the wave can propagate in the waveguide only for sufficient high concentrations (when the wavelength in the plasma is smaller than the cutoff wavelength) (cf. Fig. 6). The sharp rise in the transmission signal corresponds to the increase in plasma concentration in the waveguide. The subsequent behavior of the transmission then, in general, follows the variation in concentration. The termination of transmission at a sufficiently strong field H_0 is due to the reduction in concentration, which causes a marked increase in wavelength in the plasma, so that the waveguide is beyond cutoff.[5,6]

CONCLUSION

The results of these experiments indicate that if the frequency relations $\omega_i < \omega < \omega_e$ and $\omega < \omega_0$ are satisfied, it is possible to propagate a rotating circularly polarized electromagnetic wave in a plasma waveguide in a longitudinal magnetic field; this result is of interest from the point of view of plasma containment and radio-frequency heating.

The authors wish to thank E. K. Zavoĭskiĭ for his continued interest in this work and L. I. Rudakov for a number of valuable discussions.

---

[1] Rusanov, Patrushev, Kovan, Garkusha, and Frank-Kamenetskiĭ, JETP 1497.

[2] L. Spitzer, Physics of Fully Ionized Gases, Interscience, New York 1956.

[3] V. L. Ginzburg, JETP **21**, 788 (1951).

[4] Al'pert, Ginsburg, and Feĭnberg, Распространение радиоволн (Propagation of Radio Waves), Gostekhizdat, Moscow, 1953.

[5] G. Suhl and L. Walker, Problems of Waveguide Transmission and Gyrotropic Media. Russ. Transl. IIL, Moscow, 1955.

[6] Ya. B. Faĭnberg and M. F. Gorbatenko, J. Tech. Phys. (U.S.S.R.) **29**, 549 (1959, Soviet Phys.-Tech. Phys. **4**, 487 (1959).

Translated by H. Lashinsky
277

SOVIET PHYSICS JETP VOLUME 12, NUMBER 6 JUNE, 1961

STRIPPING REACTIONS ON Cu^{12}, O^{16}, *AND* Si^{28}

N. V. ALEKSEEV, K. I. ZHEREBTSOVA, V. F. LITVIN and Yu. A. NEMILOV

Radium Institute, Academy of Sciences, U.S.S.R.

Submitted to JETP editor June 15, 1960

J. Exptl. Theoret. Phys. (U.S.S.R.) **39**, 1508-1510 (December, 1960)

The energy spectra and angular distributions of protons from the reactions $C^{12}(d, p)C^{13}$, $O^{16}(d, p)O^{17}$ and $Si^{28}(d, p)Si^{29}$ were studied for proton energies from 3 to 15 Mev, using 6.3-Mev bombarding deuterons. A new magnetic analyzer, the multispectrograph, yields simultaneously the energy spectra of reaction products emitted at different angles. By comparing the observed angular distributions with stripping theory it was possible to derive the parities, spins, and reduced widths for a number of levels of the final nuclei.

EXCITED levels of light nuclei ($10 < Z < 15$) have been interpreted with encouraging success on the basis of a collective nuclear model.[1-4] It is therefore interesting to continue the study of stripping reactions for the same values of Z in order to determine the spins, parities, and reduced widths of higher excited levels.

The present work is a study of (d, p) reactions on Si^{28}, O^{16}, and C^{12}. A cyclotron furnished 6.25-Mev deuterons that were monoenergetic to within ~1%. The energy spectra of reaction products were obtained with a multispectrograph (multi-angle magnetic analyzer), which was described in earlier work.[5,6] This instrument obtains angular and energy distributions simultaneously; this is especially important for the study of weak spectral groups and for the identification of impurities.

The following targets (~1.5 mg/cm² thick) were used: a) polyethylene film (carbon target), b) quartz film (oxygen and silicon targets), and c) silicon (natural isotope mixture) deposited on a ~0.2μ silver backing (silicon target). Figure 1 is a typical energy spectrum from the silicon target, obtained in the seventh channel of the multispectrograph. Figure 2 shows the angular distributions of different proton energy groups from Si^{29} and the corresponding Born-approximation curves.[7] The table gives the theoretical orbital angular momentum l_n transferred to the final nucleus by the neutron, together with the parities, spins, and relative neutron capture probabilities Λ_n. Analogous results for O^{17} and C^{13} are also given.

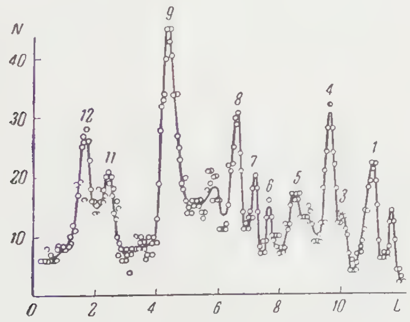

FIG. 1. Energy spectrum of protons at $\theta = 69°$. 4, 6, 7, 8 – proton groups from the reaction $Si^{28}(d, p)Si^{29}$; 1, 9, 11, 12 – from $C^{12}(d, p)C^{13}$; 3, 5 – from $O^{16}(d, p)O^{17}$. Group 2 is not shown, because at 69° it is masked by the strong group 1 resulting from carbon contamination of the target. N is the number of proton tracks in the microscope field of view; L is the coordinate along the photographic film.

Our results for the orbital angular momentum l_n transferred to Si^{29}, O^{17}, and C^{13} by a captured neutron agree with values given by other investigators.[8,9] We also obtained the angular distributions of three proton groups from Si^{29} which had previously not been resolved.[8] From a comparison of these angular distributions with stripping theory[7] it follows that the 5.946-Mev level of Si^{29} has odd parity and spin $3/2$ or $1/2$. Our data do not indicate

No. of group in Fig. 1	Energy level, Mev	l_n	Spin and parity	Λ_n (rel. units)
		$Si^{28}(d, p)Si^{29}$		
2	4.078	isotropic	—	—
4	4,934	1	$3/2^-$, $1/2^-$	10
6	5.946	1	$3/2^-$, $1/2^-$	0,93
7	6.105	1(2)	—	1,1 (for $l_n = 1$)
8	6.380	1	$3/2^-$, $1/2^-$	7,2
		$C^{12}(d, p)C^{13}$		
1	0	1	$1/2^-$	1
9	3.090	0	$1/2^+$	1.38
11	3,684	1	$3/2^-$	0,75
12	3.855	2	$5/2^+$	4,34
		$O^{16}(d, p)O^{17}$		
3	0	2	$5/2^+$	3.29
5	0.875	0	$1/2^+$	1

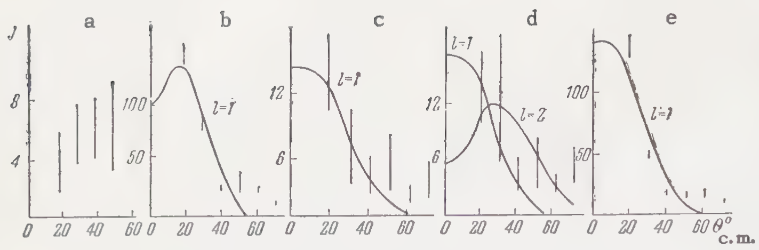

FIG. 2. Angular distributions of proton groups from silicon. J is the effective differential reaction cross section in relative units. Experimental results are represented by vertical lines, whose lengths correspond to the statistical errors. The solid curves were calculated from the formula of Bhatia et al. for $R = 6.4 \times 10^{-13}$ cm: a – group 2, E = 4.078 Mev; b – group 4, E = 4.934 Mev; c – group 6, E = 5.946 Mev; d – group 7, E = 6.105 Mev; e – group 8, E = 6.380 Mev. E is the excited level of the final nucleus.

uniquely either $l_n = 1$ or $l_n = 2$ for the 6.105-Mev level. However, for both levels $l_n = 1$ agrees qualitatively with Nilsson's scheme[2] when the deformation parameter $\delta = -0.15$ given in reference 3 is used. The almost isotropic angular distribution of the proton group corresponding to the 4.078-Mev level of Si^{29} in the measured angular range indicates that a direct-interaction mechanism makes only a small contribution to the production of this level.

---

[1] Alder, Bohr, Huus, Mottelson, and Winther, Revs. Modern Phys. **28**, 432 (1956),

[2] S. Nilsson, Kgl. Danske Videnskab, Selskab, Mat.-fys. Medd. **29**, 1 (1955).

[3] Bromley, Gove and Litherland, Can. J. Phys. **35**, 1057 (1957).

[4] V. G. Sukharevskiĭ, JETP **36**, 52 (1959), Soviet Phys. JETP **9**, 37 (1959).

[5] Yu. A. Nemilov and V. F. Litvin, Приборы и техника эксперимента (Instruments and Exptl. Techniques) No 3, (1960).

[6] V. F. Litvin, Труды РИАН (Trans. Radium Inst. Acad. Sci. U.S.S.R.) **9**, 141 (1959).

[7] Bhatia, Huang, Huby, and Newns, Phil. Mag. **43**, 485 (1952).

[8] J. R. Holt and T. N. Marsham, Proc. Phys. Soc. (London) **A66**, 467 (1953).

[9] F. A. Ajzenberg-Selove and T. Lauritsen, Nuclear Phys. **11**, 1 (1959).

Translated by I. Emin
278

SOVIET PHYSICS JETP VOLUME 12, NUMBER 6 JUNE, 1961

PRODUCTION OF NUCLEAR FRAGMENTS IN PHOTOGRAPHIC EMULSION BY 80-MEV POSITIVE PIONS

A. S. ASSOVSKAYA and N. S. IVANOVA

Radium Institute, Academy of Sciences, U.S.S.R.

Submitted to JETP editor June 18, 1960

J. Exptl. Theoret. Phys. (U.S.S.R.) **39**, 1511-1516 (December, 1960)

The production of multiply-charged particles by comparatively low-energy (80-Mev) π^+ mesons was investigated with nuclear emulsions. An analysis of the charge, energy, and angular distributions of the fragments and a comparison of the experimental data with calculations indicate that at the given incident meson energy the fragments are produced only by fast protons generated within the nucleus as a result of π^+ absorption by a nucleon pair (n, p). The experimental results permit the possibility that fragments are knocked out by these protons.

INTRODUCTION

THE production of multiply-charged particles in interactions between pions and complex nuclei is of considerable interest. It has been suggested[1] that when nuclei are struck by nucleons of sufficiently high energy, mesons are created which play an important part in the fragmentation process induced by the high-energy nucleons. The investigation of fragment production by pions could provide essential information for the understanding of this process.

In earlier work[2,3] we investigated the fragmentation of photoemulsion nuclei struck by 280-Mev π^+ mesons. It was concluded that in this case fragments were produced by fast nucleons resulting from interactions (absorption and scattering) of π^+ mesons with nucleons of the nucleus. The direct production of fragments by interactions between π^+ mesons and nuclear substructures was considered improbable, but was not entirely excluded.[3]

In the present work we investigated the production of multiply-charged particles in emulsion nuclei struck by 80-Mev π^+ mesons. This lower π^+ energy excluded the possibility that multiply-charged particles were produced by the ejection of nuclear substructures; the maximum possible energy of a fragment with $Z \geq 4$ was insufficient to surmount the Coulomb barrier. If the stated process were important for the production of fragments by π^+ mesons, we could expect a great reduction of the fragmentation cross section.

We investigated the fundamental features of the production of multiply-charged particles – the cross section for the process, and the angular, charge, and energy distributions of ejected fragments. We also compared the results with data on fragmentation produced by 280-Mev π^+ mesons and by high-energy nucleons.

EXPERIMENTAL PROCEDURE

We used the fine-grain P-R emulsion prepared in the laboratory of N. A. Perfilov at the Radium Institute. This emulsion possesses good discriminating power and permits sufficiently reliable visual detection of tracks produced by multiply-charged particles with $Z \geq 4$.

The plates were irradiated by a (80 ± 5)-Mev π^+ beam from the synchrocyclotron of the Joint Institute for Nuclear Research. For each interaction accompanied by the emission of a multiply-charged particle we investigated the nature of all particles in the star, and used Hodgson's technique,[4] taking the total charge of emitted particles into account, to distinguish disintegrations of heavy and light nuclei in the emulsion. The emission angle of each fragment relative to the incident pion was measured, together with its charge and energy whenever possible.

The charges of fragments were evaluated by measuring integrated track thicknesses.[5] Tracks having dip angles not greater than 30° in the undeveloped emulsion were selected. The calibration histograms show that fully reliable charge discrimination is possible for fragments with ranges greater than 24μ; less reliable discrimination is possible in the case of shorter ranges. The calibration was based on the observation in the same emulsion layers of alpha particles and Li_3^8 and B_5^8 ions having characteristic hammer tracks. The energy of a particle with a given charge was determined from its range in conjunction with range-energy curves.[6]

Fast singly-charged particles accompanying fragments were specially studied for the purpose of detecting fast emitted pions, and for determining angular correlations between fast emitted protons and fragments.

EXPERIMENTAL RESULTS

Scanning of the emulsions yielded 108 disintegrations in which a multiply-charged particle was produced by an 80-Mev π^+ meson. In accordance with the aforementioned criterion, 64% of these were attributed to interactions between π^+ mesons and heavy nuclei, and 36% to interactions with light nuclei.

Cross section. We obtained the following cross sections (in units of 10^{-27} cm^2) for the production of fragments with $Z \geq 4$:

Pion energy, Mev	80	280
Cross section for fragment production		
from heavy nuclei	1.2 ± 0.5	1.4 ± 0.5
from light nuclei	0.4 ± 0.2	0.56 ± 0.3

The cross sections for fragment production by 280-Mev π^+ mesons were taken from earlier work.[3] Only a slight reduction of the cross section is observed in the case of 80-Mev pions, if we neglect the considerable magnitude of the statistical errors.

Charge distribution. Figure 1 shows the charge distribution of fragments* in the case of heavy nuclei. Fragments with $Z \geq 6$ were not observed. A comparison with the charge distribution in the case of 280-Mev pions shows that the curve for 80-Mev pions falls off more rapidly toward larger values of Z. The charge distribution in the case of light nuclei is not given because of insufficient data.

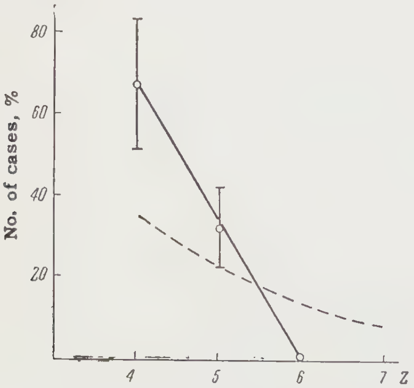

FIG. 1. Charge distribution of fragments from heavy emulsion nuclei: solid curve – for 80-Mev π^+ mesons; dashed curve – for 280-Mev π^+ mesons.[3]

Energy distribution. The solid line in Fig. 2 represents the energy distribution of fragments with $Z \geq 4$ emitted by heavy emulsion nuclei. Arrows indicate the potential-barrier heights for the emission of particles with $Z = 4$ and 5 from Br nuclei. The energy distribution of fragments with charges 4 and 5 produced by 280-Mev pions is given for comparison.[3] Both histograms are normalized in area. The maxima are found in the region of the potential barrier, and approximate correspondence of the two distributions is observed.

Angular distribution. Figure 3 shows the almost isotropic angular distribution of fragments with respect to the direction of incident 80-Mev pions. The forward-to-backward ratio is 1.3 ± 0.3, whereas for 280-Mev pions sharp forward peaking was observed, with the ratio[3] 2.8 ± 0.6.

Fast protons accompanying fragments. The fast singly-charged particles accompanying frag-

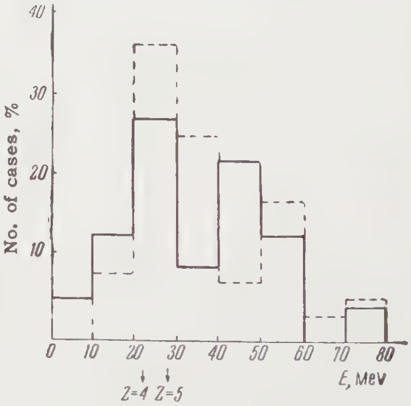

FIG. 2. Energy distribution of fragments with Z = 4 and 5, from heavy nuclei. Solid histogram – for 80-Mev pions; dashed histogram – for 280-Mev pions.

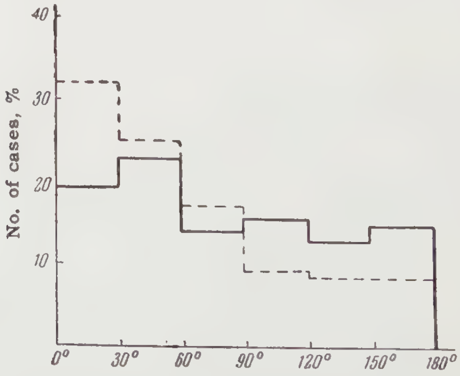

FIG. 3. Angular distribution of fragments with respect to the π^+ beam (projected on the plane of the emulsion). Solid histogram – for 80-Mev π^+ mesons; dashed histogram – for 280-Mev π^+ mesons[3] (both histograms for all emulsion nuclei).

---

*Some fragments with Z = 3 could have been overlooked visually. Therefore all data and comparisons are given for $Z \geqslant 4$.

ment emission were all identified as fast protons with energies > 50 Mev. No pion emission was observed in the case of $E_\pi = 80$ Mev.

Figure 4 gives the distribution of angles between multiply-charged particles and the accompanying fast protons. The angles of divergence lie predominantly in the interval 120-180°, especially in the case of light nuclei.

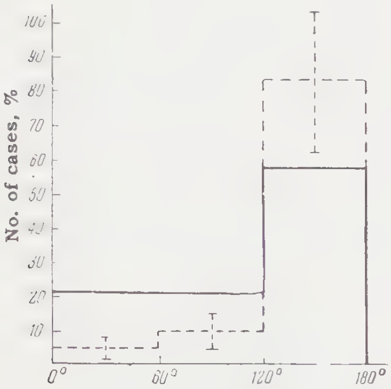

FIG. 4. Distribution of angles between fragments and fast protons (projected on the plane of the emulsion). Solid histogram – for heavy emulsion nuclei; dashed histogram – for light nuclei.

DISCUSSION

We can arrive at certain conclusions regarding the part played by a direct process of "substructure" ejection by pions, through a comparison of fragmentation cross sections in the cases of 80-Mev and 280-Mev π^+ mesons. The small difference between these cross sections suggests that this direct process does not occur, and that the fragmentation is produced only by fast nucleons generated within the nucleus. Some tendency toward a reduction of the cross section is probably associated with the change of energy of fragment-producing nucleons, from 200 — 150 Mev for $E_\pi = 280$ Mev to ~110 Mev for $E_\pi = 80$ Mev.

The angular distribution of fragments will now be discussed in greater detail. The strong forward directivity observed for $E_\pi = 280$ Mev is accounted for sufficiently well[3] by assuming that in this case fragments are produced not only by protons associated with π^+ absorption, but also to a considerable extent by fast recoil nucleons resulting from π^+ scattering on individual nucleons within the nucleus. For $E_\pi = 80$ Mev the angular distribution of fragments is almost isotropic. In order to determine the mechanism we computed the angular distribution of fragments in the case of 80-Mev π^+ mesons, assuming that fragments are produced only by fast protons resulting from π^+ absorption by a quasi-deuteron in the nucleus in the reaction

$$\pi^+ + d \rightarrow p + p \qquad (1)$$

and compared the calculation with experimental results. The calculation had to take into account a) the angular distribution of protons resulting from the absorption of 80-Mev π^+ mesons by deuterons, and b) the differential cross section for fragmentation of emulsion nuclei by protons of corresponding energies (~100-120 Mev). The angular distribution of protons associated with process (1) was taken to be $dN/d\Omega = A + \cos^2\theta$[7] in the center-of-mass system, where $A = 0.216$ and remains constant for π^+ energies from 70 to 150 Mev. We corrected this distribution for the motion of a quasi-deuteron in the nucleus, assuming 9 Mev as the average energy of the former. The angular distribution of fragments of emulsion nuclei produced by 100-Mev protons was taken from reference 8.

Figure 5 shows the spatial angular distribution of fragments that we obtained, together with the calculated curve, which is seen to furnish a good fit. The experimental $N_{\text{forward}}/N_{\text{backward}}$ ratio was 1.3, compared with the calculated value 1.33.

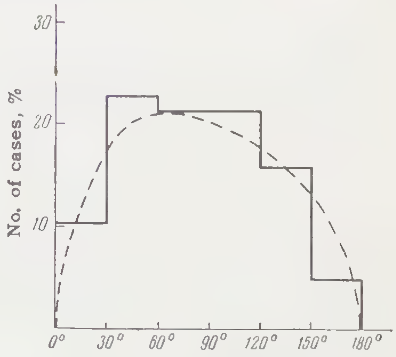

FIG. 5. Angular distribution of fragments produced by 80-Mev π^+ mesons. Experimental results are represented by the histogram; the dashed curve represents a calculation which takes into account only protons resulting from pion absorption.

It can therefore be stated that in the case of 80-Mev π^+ mesons the angular distribution is attributable entirely to protons resulting from π^+ absorption, and that the low-energy recoil nucleons associated with scattering play practically no part. The unimportance of recoil nucleons is also confirmed by the fact that pions are not emitted simultaneously with fragments.

The above-mentioned difference in the charge distributions of fragments for 80- and 280-Mev pions, respectively, (Fig. 1) can also be accounted for satisfactorily by assuming that fragments are knocked out by fast nucleons. In the case of 80-Mev π^+ mesons the highest energy of a fast nucleon is estimated at ~110 Mev in the nucleus when the π^+ mesons are absorbed by quasi-deuterons.* The maximum transfer of energy by this nucleon to a "substructure" of the form C_6^{12} is approximately equal to the height of the potential barrier for the ejection of this fragment from the residual nucleus, i.e., fragments with charge 6 are unlikely to be found in this case. For 280-Mev π^+ mesons, protons ejected in a similar process have ~210 Mev, and fragments with $Z \sim 6$ or more are energetically possible.

The angular correlation (Fig. 4) between fragments and fast protons also confirms the important role of protons associated with π^+ absorption. The predominance of angles in the range 120 – 180° agrees with the hypothesis that the fragments are produced by the protons, since the latter are emitted at 180° in the c.m. system, while the fragments mainly retain the dominant direction of the fragment-producing protons. Figure 4 shows that, as was to be expected, the correlation is more pronounced for light nuclei, in which case 85% of all fragments accompanied by fast protons fall in the range 120 – 180°. In the case of heavy nuclei the corresponding fraction is 58%.

Earlier work[3] indicated that fragments are generally produced most effectively by cascade nucleons of relatively small energy, since the energy spectrum of the fragments is approximately independent of incident-particle energy.† Figure 2 shows that the energy distribution of fragments produced by 80-Mev pions does not differ essentially from the previous results. This means that the energy of a fragment-producing nucleon can be as much as ~110 Mev inside the nucleus.

The foregoing experimental results and discussion do not appear to conflict with the hypothesis that under the given conditions fragments are knocked out by nucleons.

In conclusion the authors wish to thank A. I. Mukhin for assistance in irradiating the emulsions, V. I. Ostroumov for a discussion of the results, and Prof. N. A. Perfilov for his continued interest.

---

*Taking into account the depth of the potential well for interactions between π^+ mesons and emulsion nuclei, the energy of protons associated with the absorption of 80-Mev pions is estimated to be 120 Mev.

†By comparing the spectra of fragments produced by 660-Mev and 6.2-Bev protons and by 280-Mev π^+ mesons it was found that the latter are equivalent to 150–200 Mev protons.

---

[1] Wolfgang, Baker, Caretto, Cumming, Friedlander, and Hudis, Phys. Rev. **103**, 394 (1956); R. Wolfgang and G. Friedlander, Phys. Rev. **96**, 190 (1954).

[2] N. S. Ivanova, JETP **34**, 1381 (1958), Soviet Phys. JETP **7**, 955 (1958).

[3] Ivanova, Ostroumov and Pavlov, JETP **37**, 1604 (1959), Soviet Phys. JETP **10**, 1137 (1960).

[4] P. E. Hodgson, Phil. Mag. **45**, 190 (1954).

[5] V. I. Ostroumov and Yu. P. Yakovlev, JETP **35**, 1358 (1958), Soviet Phys. JETP **8**, 949 (1959).

[6] A. Papineau, Compt. rend. **242**, 2933 (1957).

[7] C. E. Cohn, Phys. Rev. **105**, 1582 (1957).

[8] Arifanov, Makarov, Perfilov, and Shamov, JETP **38**, 1115 (1960), Soviet Phys. JETP **11**, 806 (1960).

Translated by I. Emin
279

SOVIET PHYSICS JETP VOLUME 12, NUMBER 6 JUNE, 1961

INVESTIGATION OF ULTRASONIC ABSORPTION BY A METAL IN A MAGNETIC FIELD

A. A. GALKIN, É. A. KANER, and A. P. KOROLYUK

Institute of Radiophysics and Electronics, Academy of Sciences, Ukrainian S.S.R.

Submitted to JETP editor June 22, 1960

J. Exptl. Theoret. Phys. (U.S.S.R.) **39**, 1517-1528 (December, 1960)

Results are presented of a theoretical and experimental study of the magnetoacoustic resonance and of the absorption coefficient α of ultrasonic waves in a magnetic field H. The investigation refers to tin and indium single crystals and short-wave sound ($\lambda \ll l$) for $\mathbf{k} \perp \mathbf{H}$ ($\mathbf{k}$ is the wave vector, λ the wavelength of the sound, and l is the length of the electron path). It is shown that two types of oscillations occur in tin: resonance nonharmonic oscillations and sinusoidal oscillations. Those of the first type are ascribed to the existence of an open Fermi surface in tin. The period of the open surface, computed on the basis of the oscillation periods, is in agreement with crystallographic data. The anisotropy of the oscillation periods along various crystallographic directions is studied. The anisotropy and frequency dependence of saturation of α in a strong field is investigated. An analysis of the periods, amplitudes, oscillation phases, and absorption curve shapes in tin agree with the model of a Fermi surface in the form of a plane network of "corrugated" cylinders directed along the $[1\bar{1}0]$ and $[110]$ crystallographic axes. The reasons for some quantitative discrepancies between the theory and experiment are discussed.

1. INTRODUCTION

A large number of researches[1-19] have been devoted to the theoretical and experimental study of ultrasonic absorption in metals at low temperatures under conditions for which the mean free path of the electrons l is much greater than the sound wavelength λ. The effect of the irregular change of the absorption coefficient α in a magnetic field, first observed by Bömmel,[1] was explained qualitatively by Pippard[6] on the basis of the presence of a spatial periodicity of the field in the metal. Periodic changes in α as a function of H^{-1} are connected with an unusual spatial resonance, in which the diameter of the electron orbit in the magnetic field is an integral multiple of the wavelength λ.

The first theoretical calculations for closed Fermi surfaces were carried out in the work of Gurevich,[7] and were later developed in reference 8. Experimental verification of the theoretical deductions was made by a number of authors.[4,5,9,10] The behavior of α in a strong field, where $r \ll \lambda$ was also studied (r is the characteristic dimension of the electron orbit).[11-13]

Results are given in the present paper of a theoretical and experimental study of the peculiarities of ultrasonic absorption in a magnetic field. A comparison is given of the theory with experimental data for tin and indium.

1. OSCILLATORY EFFECTS

The nonmonotonic dependence of the absorption coefficient α on H is associated with the fact that the electrons periodically get into a plane of constant phase of the variable field under the action of a constant magnetic field, whereupon the periodic change of α as a function of H^{-1} can be of two types:[8] nonresonant oscillations of a harmonic type and resonant changes of nonsinusoidal form. In addition to these peculiarities, resonant oscillations, corresponding to sharp jumps in the absorption coefficient α, should be observed in the curve of the dependence of the derivative of the absorption coefficient $d\alpha/dH$ on the field. All the periodic field dependences occur under the condition $\lambda\!\!\!^{-} \ll 2\pi r \ll l$.

We shall cite the chief results of the theoretical investigations for the case in which the wave vector of the sound $\mathbf{k}$ is perpendicular to $\mathbf{H}$, inasmuch as the experimental data given below apply to this case.

The character of the oscillatory dependence of α on H depends in a fundamental way on the topology of the Fermi surface. For closed surfaces,[7] the oscillations are harmonic and are associated with electrons, the diameters of whose orbit D has an extremum in the direction of sound propagation ($D = D_{ext}$). In this case,

$$\alpha(H) \sim \alpha_0 \gamma^{-1} \{1 + A(kD_{ext})^{-1/2} \sin(kD_{ext} \pm \pi/4)\},$$
$$D_{ext} = c(eH)^{-1}(p_{y\,max} - p_{y\,min}), \tag{1}$$

where $\alpha_0 = \alpha(0) \sim N\mu\omega/\rho v s^2$ is the absorption for $H = 0$ (α has the dimensions cm^{-1}); N is the density, μ the chemical potential, v the electron velocity, ρ the density of the metal, $\omega/2\pi$ the frequency, s the sound velocity, c the light velocity, e the electron charge, and **p** the electron momentum; the wave vector **k** is directed along the x axis, the field **H**, along the z axis; $\gamma = r/l \ll 1$, $p_{y\,max} - p_{y\,min}$ is the extremal diameter of the Fermi surface in the $\mathbf{k} \times \mathbf{H}$ direction in momentum space; $A \sim 1$.

The oscillations of the given type take place on open periodic trajectories also if the vector **k** is parallel to the average direction of the open trajectory $\boldsymbol{\xi}$. The extremal diameter D_{ext} is determined by the difference $p_{y\,max} - p_{y\,min}$ on the cross section axis $p_z = 0$.* The oscillations associated with self-intersecting trajectories passing through a saddle point have an amplitude approximately $(kD)^{3/2} \gg 1$ times smaller, and the phase of the oscillations changes with the field with logarithmic slowness.

If the vector **k** deviates from the direction $\boldsymbol{\xi}$ by an angle $\vartheta[\vartheta \gtrsim (kl)^{-1}]$ in the plane $\mathbf{k} \perp \mathbf{H}$, then the nonoscillating part of the absorption, connected with the open trajectories, sharply decreases (by a factor of $kl\vartheta$) in comparison with (1). The amplitude of the oscillations changes appreciably for $\vartheta \sim (\bar{\lambda} r)^{1/2}/l$ and in the range of angles $(\bar{\lambda} r)^{1/2}/l \ll \vartheta \ll \bar{\lambda}/l$ it is comparable with the value of the monotonic part of the absorption $\alpha/\alpha_0 \sim (kr\vartheta)^{-1}$. Upon further increase in the angle, $\vartheta \ll (kr)^{-1}$, the nonresonant harmonic oscillations are replaced by oscillations of a new, resonant type.[8] The maxima in the curve of the absorption as a function of H are much narrower, and the minima are broad and less pronounced.

The presence of sharp resonant maxima is connected with the fact that the projections of the average (over the period of motion in the magnetic field) displacement of the electrons in the direction of the vector **k** differ from zero: $\mathbf{k} \cdot \overline{\mathbf{v}} T = k_y \bar{v}_y T = k_y c b_\xi / eH \neq 0$ (the y axis is perpendicular to **H** and $\boldsymbol{\xi}$; b_ξ is the period of the open trajectory in momentum space in the ξ direction). Resonance takes place for $|\mathbf{k} \cdot \overline{\mathbf{v}} T| = 2\pi n$ ($n = 1, 2, 3, \ldots$). Close to resonance,

$$\alpha \sim \frac{\alpha_0 \gamma}{\gamma^2 + (k_y b_\xi c/2\pi e H^{-n})^2} = \frac{\alpha_0 \gamma}{\gamma^2 + n^2(1 - H/H_n)^2}; \tag{2}$$

the line has a Lorentz shape and its relative width, $\Delta H/H_n = \gamma/n \sim (k_y l)^{-1}$, does not depend on the number n.

The maximum is obtained for $H_n = k_y c b_\xi / 2\pi n e$, and the period of the resonant oscillations is

$$\Delta H^{-1} = 2\pi e / k_y b_\xi c. \tag{3}$$

At the maximum,

$$\alpha_n \sim \alpha_0/\gamma \sim \omega H_n, \tag{4}$$

the absorption increases in proportion with the field and frequency and is comparable with the nonoscillating part of the absorption on closed trajectories. Far from resonance, $\alpha_{open} \sim \alpha_0$ and is much smaller than α_n.

Nonresonant oscillations of relatively small amplitude ($\alpha_{osc}/\alpha_n \lesssim (kr)^{-1/2}$) are superimposed on the resonant oscillations. The amplitude of the resonant oscillations falls off with approach of the vector **k** to the direction of the y axis. At $\vartheta = \vartheta_k$ (ϑ_k is the angle between **k** and $\boldsymbol{\xi}$ for which the line $\mathbf{k} \cdot \mathbf{v} = 0$ on the Fermi surface runs only along closed trajectories), the resonant oscillations associated with the open trajectories under consideration disappear. The amplitude of the resonance, along with the non-oscillating part of α, is strongly anisotropic relative to small departures of the vector **k** from the plane $\mathbf{k} \perp \mathbf{H}$ and of the magnetic field from the plane perpendicular to the axis of the cylinder.[8]

The conclusions of the theoretical analysis were the object of experimental study. The oscillatory effects for $\mathbf{k} \perp \mathbf{H}$ were investigated by means of the methods described previously[5,20] in the frequency region $\nu = \omega/2\pi = 180 - 220$ Mc on single crystals of tin and indium in the various crystallographic directions.

Typical dependences of the absorption coefficient on the magnetic field are shown in Fig. 1 for single crystals of tin and indium.* Figures 1a and 1c illustrate the harmonic nonresonant oscillations, the phase of which is equal to ($\pi/4$) sign ($d^2 D_{ext}/dp_z^2$). The resonance oscillations are shown in Fig. 1b; the phase of these oscillations is equal to zero. Figure 2 shows the dependence of the number of maxima of resonance and nonres-

---

*In what follows, in speaking of an open surface, we shall, for definiteness, have in mind an open surface of the "corrugated cylinder" type. The principal peculiarities of the absorption are the same for other types of open surfaces.[8]

*An error in notation exists in reference 5: the [110] and [100] axes should be interchanged.

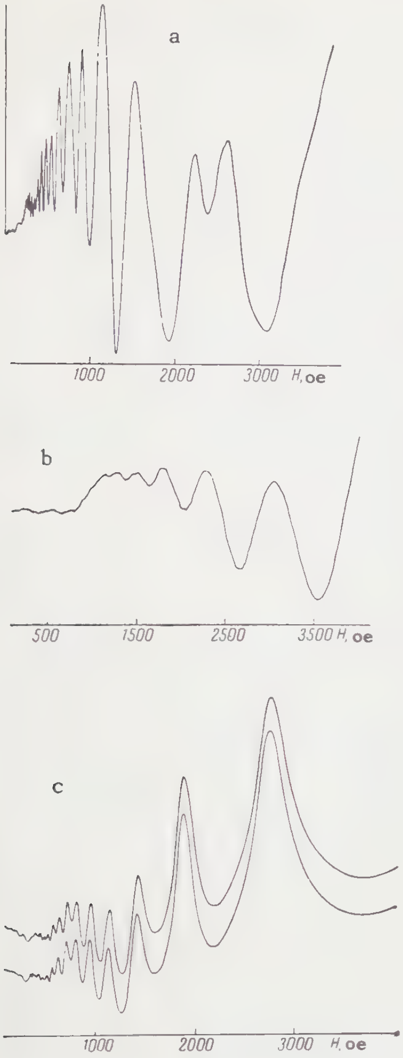

FIG. 1. Oscillations of the absorption coefficient of longitudinal sound in tin and indium at $\nu = 220$ Mc, $\mathbf{k} \perp \mathbf{H}$: a – sinusoidal oscillations in tin, the vector **k** in the (010) plane at an angle of 60° with respect to the [001] axis; b – resonance oscillations in tin, $\mathbf{k} \parallel [101]$ (the two curves illustrate the reproducibility of the record); c – indium, the **k** vector close to [110].

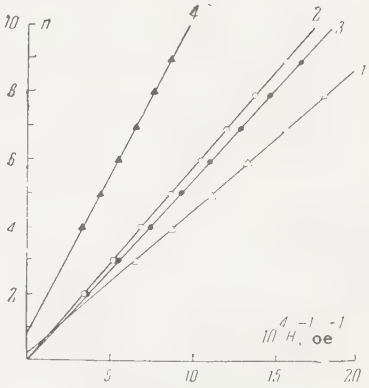

FIG. 2. Dependence of the number of maxima of oscillations on the inverse field. For tin: curve 1 – sinusoidal oscillations, 2 – resonance oscillations, the **k** vector ∥ [101], 3 – resonance oscillations, the **k** vector at an angle of 40° to the [001] direction; for indium: the curve 4 – sinusoidal oscillations.

onance oscillations on the reciprocal of the field H^{-1}.

It must be noted that it is impossible to separate the harmonic and resonance oscillations for all directions. In a number of cases, the oscillogram is the superposition of several oscillatory components with different periods and amplitudes, the treatment of which is extremely difficult.

Figure 3 shows the results of measurement of the anisotropy of the oscillation periods in the reciprocal field $\nu\Delta H^{-1}$ for tin in the rotation of the vector **H** in different planes $\mathbf{H} \perp \mathbf{k}$. These data form the starting point for the calculation of the extremal (in p_z) displacement of the electron in the magnetic field in the direction of sound propagation **k**.

A stereographic projection of the planes in which the magnetic field vector **H** was rotated for

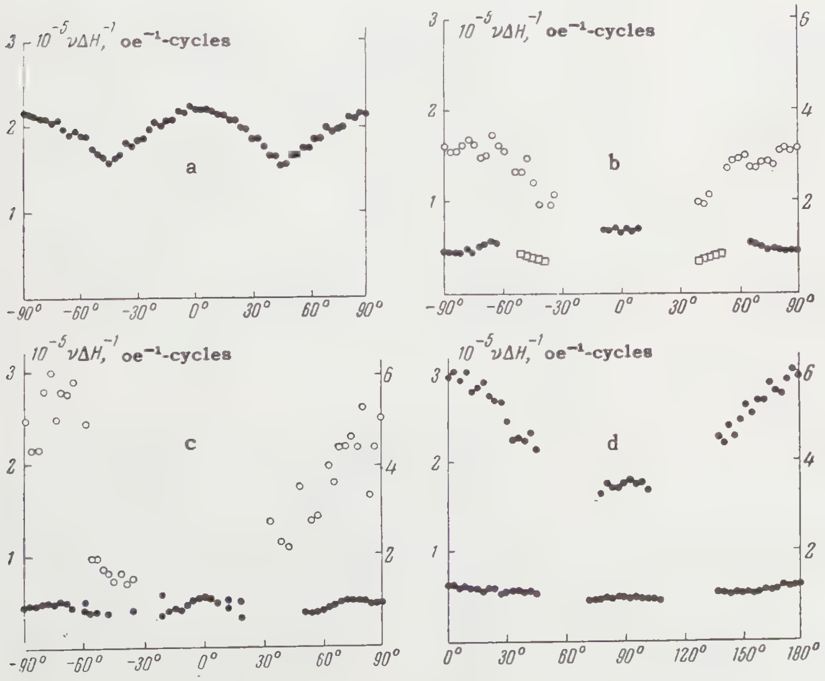

FIG. 3. Dependence of the periods: □ – resonance and ○, ● – non-resonance oscillations on the direction of the magnetic field in tin (□, ● – refer to the left hand scale, ○ to the right); a – the **k** vector along [001], b – **k** in the plane (010) at an angle of 40° to the [001] axis, c – **k** at an angle of 60° with respect to the [001] axis in the (010) plane, d – **k** along [110]; measurement of the field direction of a, b, c is from the [100] axis, for d, from [001].

all the specimens of tin studied is shown in Fig. 4. These directions of **H** in which the oscillations were observed most strongly are marked by the heavy lines.

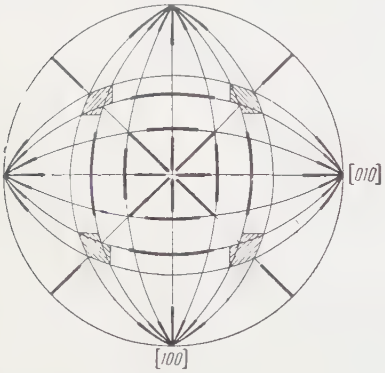

FIG. 4. Stereographic projection of the investigated directions of $\mathbf{H} \perp \mathbf{k}$ in tin. The shaded regions are those directions of **H** for which resonance oscillations are observed.

Figure 5 shows the results of measurement of the periods of oscillation in single crystals of indium for two directions of the vector **k**.

Considerable interest attaches to the resonance oscillations observed in tin with $\mathbf{k} \perp \mathbf{H}$ for two directions of the wave vector **k** and in a narrow range of directions of the magnetic field (see Fig. 4, shaded region). In the change of orientation of the vector **k**, the period of resonance oscillations changes (Fig. 2, curves 2, 3). For the first direction ($\mathbf{k} \parallel [101]$), $\Delta H^{-1} = 1.71 \times 10^{-4}$ oe^{-1}, for the second, $\Delta H^{-1} = 1.82 \times 10^{-4}$ oe^{-1} ($\nu = \omega/2\pi = 220$ Mc).

2. ANISOTROPY OF ULTRASONIC ABSORPTION IN A STRONG MAGNETIC FIELD

It is convenient to investigate absorption anisotropy in strong fields on the same specimens on which the oscillatory effects were measured. The latter take place only under the condition $\lambda\!\!\!^{-} \ll l$. Therefore, the region of strong fields corresponds to the inequality $r \ll \lambda\!\!\!^{-} \ll l$. The results given below of theoretical analysis and the measurements of the absorption coefficient refer to the case in which "deformation absorption" plays the principal role,[12,13] i.e., one can neglect the induction fields $\mathbf{G} = c^{-1}\dot{\mathbf{u}} \times \mathbf{H}$ and disregard the inhomogeneity of the variable electromagnetic field at distances of the order of the dimensions of the electron orbit r in the magnetic field.

The peculiarities of deformation ultrasonic absorption in a strong magnetic field are in many respects analogous to absorption at $H = 0$. The fact is that the rapid rotation of the electrons about the **H** direction leads to the averaging of all the characteristics over the period of precession, so that the formula for absorption has the same form as for $H = 0$,[15] in which, however, all the quantities are replaced by their average values on the trajectory $\epsilon(\mathbf{p}) = \mu$, $\mathbf{p} \cdot \mathbf{H}/H = \text{const}$ (denoted by the bar over the symbol):

$$\alpha(H) = h^{-3}W^{-1}\int d\tau\delta(\varepsilon - \mu)\,|\bar{g}|^2\bar{\nu}_0[\bar{\nu}_0^2 + (\mathbf{k}\bar{\mathbf{v}})^2]^{-1}, \quad (5)$$

where W is the energy density in the sound wave, $\nu_0 = t_0^{-1}$ is the frequency of collisions, and $d\tau$ is the element of momentum volume; $g = (\lambda_{ik}(\mathbf{p}) - \langle\lambda_{ik}\rangle)\dot{u}_{ik}$ is connected with the deformation change of the energy of the electron $\epsilon(\mathbf{p})$.

We write out the results for the case $\mathbf{k} \perp \mathbf{H}$. On the closed trajectories, $\mathbf{k} \cdot \bar{\mathbf{v}} \equiv 0$, the coefficient of absorption flattens out and its value is $kl \gg 1$ times larger than α_0:

$$\alpha(H) = h^{-3}W^{-1}\int d\tau\delta(\varepsilon - \mu)\,|\bar{g}|^2\,\bar{\nu}_0^{-1} \sim N\mu\omega^2 t_0/\rho s^3. \quad (6)$$

The sharp increase in the absorption in a strong field in comparison with α_0 is connected with the fact that all the electrons in the magnetic field on average (over one period) move along the field, i.e., for $\mathbf{k} \perp \mathbf{H}$ — in planes of equal phase, where they interact most effectively with the variable fields. For $H = 0$, the relative fraction of electrons moving in the plane of constant phase is of order $(kl)^{-1}$. Correspondingly, $\alpha(H)/\alpha_0 \sim kl$.

In the presence of open trajectories, the estimate given by (6) remains valid; however, upon rotation of **k** relative to **H** (or **H** relative to **k**) a sharp anisotropy of the absorption must take place in the plane $\mathbf{k} \perp \mathbf{H}$: $\alpha(H)$ can change by a

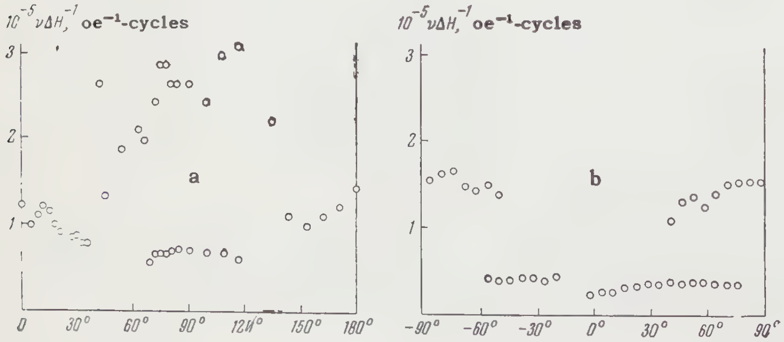

FIG. 5. Periods of the oscillations $\nu\Delta H^{-1}$ of the absorption coefficient in indium as a function of the direction of the vector **H**; a — **k** close to $[\bar{1}10]$, b — **k** near [100]. Two series of points correspond to two different periods of oscillation for the given direction of the magnetic field **H**, calculated from the [001] axis.

value of the order of α. This anisotropy is connected with the fact that $\bar{v}_y \neq 0$ on the open trajectories. (The y axis is parallel to the normal to the plane in which the magnetic field and the direction of the open trajectory lie.) If $k_y\bar{v}_y/\nu_0 \sim kl\vartheta \gg 1$, then the contribution of the open trajectories to the deformation absorption (5) is smaller by a factor of $(kl\vartheta)^2 \gg 1$ than the contribution from the closed trajectories.

The absorption in a strong magnetic field also possesses a strong anisotropy relative to the departure of the vector **k** (or **H**) from the plane **k** ⊥ **H**. If the angular departure $\varphi \gtrsim (kl)^{-1}$, the absorption falls off strongly:

$$\alpha(H) = \pi h^{-3} W^{-1} \int d\tau\, \delta(\varepsilon - \mu)\, \delta(k\bar{v})\, |\bar{g}|^2 \sim \alpha_0/\varphi. \qquad (7)$$

Violation of the inequality $\alpha(H) \gg \alpha_0$ for **k** ⊥ **H** in strong fields can be due both to insufficiently rigorous fulfillment of the condition **k** ⊥ **H** $(\varphi \gtrsim (kl)^{-1})$ and to the fact that for certain types of open Fermi surfaces, at definite directions of the wave vector **k** (for example, a weakly "corrugated cylinder" or a plane, the vector **k** parallel to the axis of the cylinder or plane) the quantity $\mathbf{k}\cdot\mathbf{v} \equiv 0$ and the order-of-magnitude estimate for α_0 is identical with (6).

Experimental investigation of the absorption in a strong field was carried out on a number of single crystals of tin and indium. In all cases, the difference $\alpha(H) - \alpha_0$ was determined experimentally. However, along with the given quantity, it is also desirable to know the absolute value of $\alpha(H)$. For this purpose the value of α_0 was determined by investigation of the temperature dependence of the absorption $\alpha_0(T)$ in the transition to the superconducting state. Extrapolating the curve $\alpha_0(T)$ as $T \to 0$, we can separate out the electronic part of the absorption, eliminating the losses connected with the transition layers, the lattice, and other factors. In those cases in which values of α_0 were not obtained, the anisotropy of the difference $\alpha(H) - \alpha_0$ was studied. Diagrams are given in Fig. 6 for the variation of $\alpha - \alpha_0$ as a function of the angle between the vector **H** and the [100] axis in tin for different directions of **k** in the (010) plane (here **k** ⊥ **H**). Figure 6d illustrates such a diagram for **k** ∥ [110] with measurement of the magnetic field from the [001] axis.

As is seen from Figs. 6a, b, c, the absorption coefficient decreases in comparison with its value for H = 0, and also increases as a function of the field orientation. With approach of the **H** vector to the [100] direction, the value of α always increases. The peculiar feature of Fig. 6d is that $\alpha(H) > \alpha_0$ for all directions.

The frequency dependence of the ultrasonic absorption coefficient in a strong field and without the field was studied for indium single crystals. In the absence of a magnetic field, the absorption coefficient α_0 increases linearly with frequency in the frequency range 50-150 Mc. The frequency dependence of α_0 is shown in Fig. 7 (curve 2). The single crystal was so rotated that the vector **k** was directed close to the [110] axis.

Application of a magnetic field of 8000 oe perpendicular to the **k** vector led to a sharp decrease in the absorption coefficient. At a frequency of 60 Mc, with a field orientation close to [001], the coefficient α fell off by a factor of more than 6.5. With increase in frequency, the relative decrease in the absorption coefficient in the strong field decreased. Figure 8 shows the anisotropy of the quantity α/α_0 in a field of 8000 oe for the three

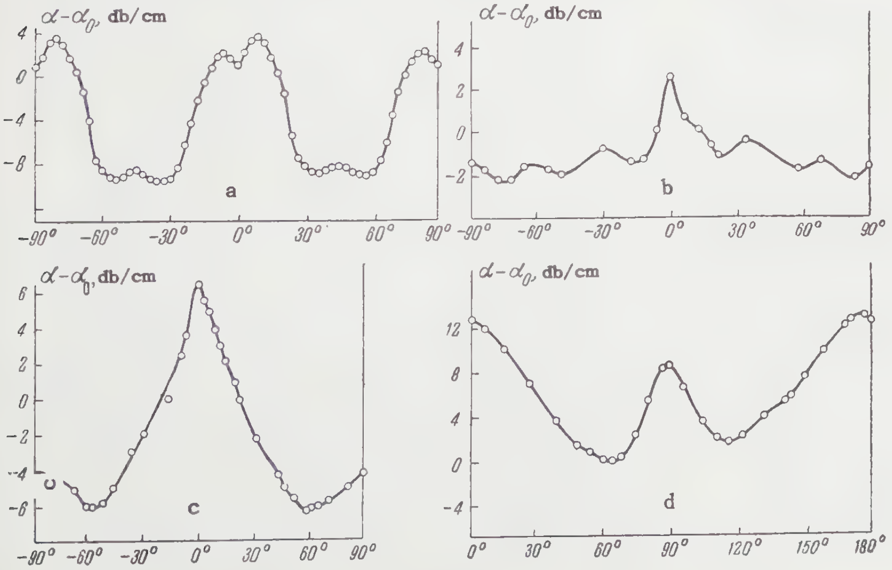

FIG. 6. The angular dependence of $\alpha - \alpha_0$ in a strong field for tin: a – **k** along [001], ν = 70 Mc, H ~ 10,000 oe; b – **k** at an angle of 40° to the [001] axis, ν = 60 Mc, H ~ 6500 oe; c – **k** at an angle at 60° to the [001] axis, ν = 60 Mc, H ~ 6500 oe; d – **k** along the [110] axis, ν = 60 Mc, H = 6500 oe. Measurement of the field direction was from the [100] axis for a, b, c, and from the [001] axis for d.

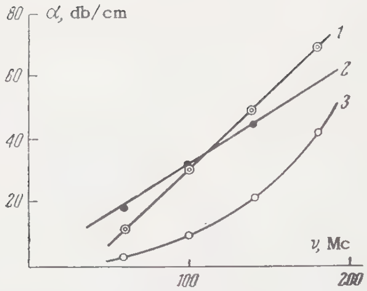

FIG. 7. The dependence of the ultrasonic absorption coefficient on the frequency in indium single crystals: 1 – H = 8000 oe, the direction of the **H** vector corresponds to the maximum absorption on the curves of Fig. 8; 2 – H = 0; 3 – H = 8000 oe, the direction of **H** corresponds to a minimum in the curves of Fig. 8.

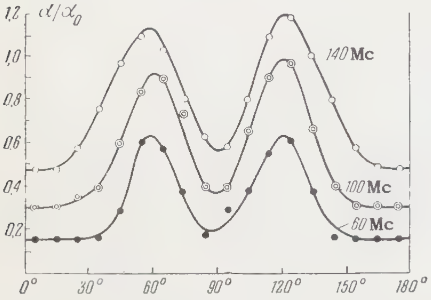

FIG. 8. Angular and frequency dependence of α/α_0 for H = 8000 oe on the direction of the vector **H** in indium. The vector **k** is close to [110], measurement of the direction of **H** is from the [001] axis.

frequencies of 60, 100 and 140 Mc, all for the same sample of indium. The study of the frequency dependence of α at the maximum (Fig. 7, curve 1) and at the minimum (Fig. 7, curve 3) of the absorption shows that in the first case $\alpha(H, \nu)$ increases linearly with frequency, but more rapidly than α_0; in the second case, the increase in $\alpha(H, \nu)$ is close to quadratic in the frequency.

3. DISCUSSION OF THE RESULTS

The experimental investigation of oscillation effects — the anisotropy of the periods, the phase of the oscillations, and also the form of the absorption curves — all make it possible to explain a number of characteristic peculiarities of the topology and form of the Fermi surface in metals. In the simplest case of a single closed convex surface possessing a center of symmetry, the study of only single oscillations of the absorption coefficient in the magnetic field makes it possible to establish its form and dimensions completely.

For more complicated surfaces (for example, non-convex, and all the more, open), the problem of defining them is very difficult, in the first place, because of the high sensitivity of the phenomenon to the various singularities on the Fermi surface, and in the second place, because of the periodicity of the absorption curves in the inverse field. Both these factors make the curve of the dependence of the absorption on the magnetic field the sum of many oscillating components with different periods, phases and amplitudes. Therefore the analysis of the experimental data is very complicated in many cases; frequently, it does not give unique solutions. The difficulties that were pointed out are typical for the majority of oscillatory effects, both at high frequencies (cyclotron resonance, ultrasonic absorption in a magnetic field), and in the case of diamagnetic quantum oscillations (the de Haas-van Alphen effect, the Shubnikov-de Haas effect, etc.).

Experimental investigations of the oscillations of the absorption coefficient in single crystals of tin and indium confirm, first, the validity of most of the conclusions of the theory.[6-9] Actually, in those cases in which one can easily determine the fundamental period of the oscillations, the curves are periodic in the inverse field, the initial phase of the vibrations is equal to zero for curves of the resonance type, and is different from zero for harmonic oscillations. Long-period oscillations and oscillations with relatively small amplitude do not have a definite phase; the latter depends on H. It is possible that these oscillations are connected with self-intersecting trajectories passing through saddle points.

In complete correspondence with the theory, the position of the maxima in the magnetic field is proportional to the ultrasonic frequency.[4,5] With increase in the frequency, the oscillations are increased, and the amplitude of most oscillations with small period increases upon increase of the field. Decrease in the temperature and purification of the samples, leading to an increase in the mean free path of the electrons, also increase the amplitude and number of observed peaks.

In single crystals of tin, nonharmonic resonance oscillations with narrow maxima are observed in a narrow range of directions of the magnetic field (Fig. 4). At the same time the oscillatory dependence of α on H^{-1} for most other directions is harmonic in first approximation.

Observation of resonance oscillations under conditions in which the vectors **k** and **H** are perpendicular makes it possible to draw the immediate conclusion that the Fermi surface of the given metal is open.[9] Measurement of the periods of these oscillations allows us to determine the direction and period of the open trajectory. In the first case, in which the wave vector **k** makes an angle of 28° with the four-fold axis [001] in the (010) plane, the period $\Delta H^{-1} = 1.71 \times 10^{-4}$ oe^{-1} (the magnetic field **H** lies in the (110) plane). From this start we can compute the value of the period of the open trajectory b_ξ by assuming that the Fermi surface is open along the [110] direction. (The ξ axis is parallel to [110], **H** is directed along the z axis.). With the aid of Eq. (3), we get

$$b_\xi = e\lambdabar/cn_y\Delta H^{-1} = 15\cdot10^{-20}\ \text{g-cm/sec}$$

$$(n_y = \cos(\widehat{ky}) = 0.942, \qquad \lambda = 1.5\cdot10^{-3}\,\text{cm}).$$

If the direction of the wave vector **k** is changed, then the product $k_y\Delta H^{-1}$ should remain unchanged if the oscillations are connected with this same open trajectory. Calculation of the period of the oscillations in the second case, in which the wave vector **k** is directed at an angle of 40° to the [001] axis in the same (010) plane, yields $\Delta H_2^{-1} = k_{y1}\Delta H^{-1}/k_{y2} = 1.81 \times 10^{-4}\ \text{oe}^{-1}$ (the anisotropy of the sound velocity can be neglected). This value agrees with the measured value of $\Delta H_2^{-1} = 1.82 \times 10^{-4}\ \text{oe}^{-1}$ with an accuracy to within better than one percent.

The direction of the open trajectory along [110] does not contradict the data of the galvanomagnetic measurements of Alekseevskiĭ and Gaĭdukov[20] for tin, and the value of the period in the open trajectory is in good agreement with the size of the Brillouin zone in this direction as obtained by Chambers.[22]

The fact that for other directions of the wave vector **k** (**k** parallel to the axes [001], [110]) resonance oscillations from open periodic trajectories are not observed has the explanation that the angle ϑ between the vector **k** and the direction of the open trajectory is bounded by the inequalities

$$\vartheta \gg (kr)^{-1}, \qquad |\vartheta - \vartheta_k| \gg (kr)^{-1}, \qquad \vartheta < \vartheta_k.$$

For **k** || [001], $\vartheta = \pi/2$ – the latter inequality is not satisfied, while for k || [110], the angle $\vartheta = 0$ and the first inequality is violated. In complete agreement with theory, the phase of these oscillations is equal to zero, and the breadth and height of the resonance maxima increase with the field.

For all the orientations studied, the extremal diameters $p_{y\,\max} - p_{y\,\min}$ for electrons in tin, computed from the period of the harmonic oscillations [Eq. (1)], are less than the dimensions of the first Brillouin zone.

It was shown above that the experimental curves are very complicated and are the superposition of several oscillating components. As a rule, it is relatively easy to separate the oscillations with widely differing periods. The small periods of ΔH^{-1} correspond to the fundamental dimensions of the Fermi surface, while the large periods can arise as a result of a small departure (in the limits of angle of the order of $k^{-1}l^{-1}$) of the wave vector **k** from the given crystallographic direction, or of the magnetic field from the crystallographic plane.

In the latter case, in the presence of open surfaces, the open periodic electron trajectories transform into extremely prolate or aperiodic open trajectories, which in turn lead to a large number of oscillations with relatively small amplitudes and large periods. Therefore, data are given on all the drawings for ΔH^{-1} on the anisotropy of the two principal periods of oscillation, measured in different directions for single crystals of tin and indium, and the results of the treatment of the long period oscillations (which are distinguished from the others by low accuracy) will not be discussed.

Making use of data on the anisotropy of the periods of oscillation, we can attempt to estimate certain dimensions of the Fermi surface in tin. All the results on the absorption anisotropy agree better with one another if we assume that the Fermi surface of tin is a "plane grid" of "corrugated cylinders"* with the open direction along [110]. The maximum diameter (height) of the cylinders in the [001] direction is about 11×10^{-20} g-cm/sec, the diameters in the [110] and [100] directions are respectively equal to 3×10^{-20} and 2×10^{-20} g-cm/sec. The first value is obtained from the periods of oscillation given in Fig. 3d, the latter two from Fig. 3a.

Generally speaking, caution is necessary in the treatment of periods of oscillation in the determination of the extremal diameters of the Fermi surface, inasmuch as the value of $p_{y\,\max} - p_{y\,\min}$ for a noncentral extremal cross section is not its diameter, but its projection on the direction **k** × **H**.

Study of the oscillatory effects in indium shows that the Fermi surface of this metal is rather complicated, just as in tin. Resonance oscillations were not observed in the directions we investigated. Attention is turned to the very large value of the maximum diameters of the Fermi surface (up to 20×10^{-20} g-cm/sec), which is appreciably larger than the maximum dimensions of the Brillouin zone in indium constructed on the planes (111) and (200); these dimensions are 3.75×10^{-20} g-cm/sec and 4.35×10^{-20} g-cm/sec, respectively.

The study of the oscillation dependence of the absorption coefficient makes it possible to estimate the mean free path lengths of the electrons from the number of oscillations ($l \sim n\bar{\lambda}$, where n is the number of clearly observed oscillations). In tin, the number of oscillations, and, consequently the path length, depends on the orientation; at T = 4.2° K, it has the order of 0.5 − 1 mm. In indium, the path length is somewhat less (about 0.3 mm). The purity of the metals studied is characterized by the ratio of resistances at helium and room temperatures: $R_{4.2}/R_{300} = 1.6 \times 10^{-5}$ for tin and $R_{4.2}/R_{300} = 8 \times 10^{-5}$ for indium. Our estimates agree well with the data of static measurements of Aleksandrov and Verkin,[24] who obtained a value of $l \approx 0.65$ mm for the mean path length in tin of such purity.

---

*This model corresponds to the galvanomagnetic data of Alekseevskiĭ and Gaĭdukov.[21,23]

The study of ultrasonic absorption in a strong magnetic field is of significant interest for the investigation of electron gas kinetics in a metal. The experimental data confirm qualitatively the predictions of the theory: the absorption coefficient levels off in a strong field, while the leveling off value is anisotropic. In single crystals of tin, as is seen from Fig. 6, the absorption coefficient always increases upon approach of the magnetic field to the (001) plane. The very fact of appreciable anisotropy of the absorption agrees with the open character of the Fermi surface in tin.

In single crystals of indium, at frequencies of the order of $\nu \approx 60 - 100$ Mc, the absorption levels off in a strong field; however, the value of the leveling off is much less than the absorption coefficient α_0 in the absence of the magnetic field. The saturation effect is very clear at fields of 6 — 8 koe, and the anisotropy of the absorption in the strong field is comparatively small.

It follows from the galvanomagnetic data that the Fermi surface in indium is closed.[21] Starting out from theory, one must expect a sharp increase in the absorption in a strong field for $\mathbf{H} \perp \mathbf{k}$. Such a sharp increase has been observed neither in indium nor in tin. This essential divergence between theory and experiment can be connected with the fact that the time of free flight decreases in a strong magnetic field.* It is known that the scattering amplitude, and consequently the collision probability of the charged particles, depend on the magnetic field. Moreover, in a strong magnetic field, the collision integral depends on the intensity of the resultant electric field.[25] The latter dependence can also have a significant effect on the effective relaxation time. Obviously, in the consideration of collisions, it is not possible to ignore quantum effects. Further experimental and theoretical investigation of this question can give interesting data on the mechanism of the interaction of the electrons with the lattice and with each other. In any case, if this assumption is valid, then we can satisfactorily account for the absorption coefficient curve in strong fields. In particular, it is seen from curve 3 of Fig. 7 that the frequency dependence of the absorption is evidently quadratic — in correspondence with the conclusions of the theory, although the rate of growth (which is proportional to the relaxation time t_0) is much less than expected.

It is seen from a comparison of theory with experiment that the observed oscillation effects are in much better agreement with the theory than the peculiarities of the absorption in strong fields. This is understood, since the oscillations are chiefly determined by the kinematic properties of the electrons in the metal and are not connected with the interaction, while the absorption in strong fields is very sensitive to the collision mechanism.

Thus, the results given above show that the study of magnetoacoustic resonance makes it possible to obtain a number of valuable data on the structure of the energy spectrum, and the study of the peculiarities of the absorption in strong fields gives information on the relaxation properties of the electrons in the metal. Further study of the peculiarities and anisotropies of resonance and absorption in strong fields, in other metals, and for nonperpendicular vectors **k** and **H** will be of interest.

---

*The authors are indebted to A. I. Akhiezer for this remark.

[1] H. E. Bömmel, Phys. Rev. **100**, 758 (1955).

[2] Morse, Bohm and Gavenda, Phys. Rev. **109**, 1394 (1958).

[3] D. H. Reneker, Phys. Rev. **115**, 303 (1959).

[4] A. A. Galkin and A. P. Korolyuk, JETP **36**, 1307 (1959), Soviet Phys. JETP **9**, 925 (1959).

[5] A. A. Galkin and A. P. Korolyuk, JETP **37**, 310 (1959), Soviet Phys. JETP **10**, 219 (1960).

[6] A. B. Pippard, Phil. Mag. **2**, 1147 (1957).

[7] V. L. Gurevich, JETP **37**, 71 (1959), Soviet Phys. JETP **10**, 51 (1960).

[8] Kaner, Peschanskiĭ, and Privorotskiĭ, JETP 1960 (in press).

[9] Galkin, Kaner, and Korolyuk, Dokl. Akad. Nauk SSSR **134**, 74 (1960); Soviet Phys.-Doklady, in press.

[10] A. A. Galkin and A. P. Korolyuk, JETP **38**, 1688 (1960), Soviet Phys. JETP **11**, 1218 (1960).

[11] E. A. Kaner, JETP **38**, 212 (1960), Soviet Phys. JETP **11**, 154 (1960).

[12] E. A. Kaner, JETP **39**, 1071 (1960), Soviet Phys. JETP **12**, 000 (1961).

[13] V. L. Gurevich, JETP **37**, 1680 (1959), Soviet Phys. JETP **10**, 1190 (1960).

[14] A. I. Akhiezer, JETP **8**, 1330 (1938).

[15] Akhiezer, Kaganov, and Lyubarskiĭ, JETP **32**, 837 (1957); Soviet Phys. JETP **5**, 685 (1957).

[16] T. Olsen, Phys. Rev. Lett. **4**, 324 (1960).

[17] T. Kjeldaas, Phys. Rev. **113**, 1473 (1959).

[18] E. I. Blount, Phys. Rev. **114**, 418 (1959).

[19] T. Mykosyra, J. Phys. Soc. Japan **13**, 759 (1958).

[20] A. A. Galkin and A. P. Korolyuk, Приборы и техника эксперимента (Instrum. and Exptl. Techniques) 1960 (in press).

[21] N. E. Alekseevskiĭ and Yu. P. Gaĭdukov, JETP **37**, 672 (1959), Soviet Phys. JETP **10**, 481 (1960).

[22] R. G. Chambers, Can. J. Phys. **34**, 1395 (1956).

[23] Alekseevskiĭ, Gaĭdukov, Lifshitz, and Peschanskiĭ, JETP **39**, (1960) (in press).

[24] B. N. Aleksandrov and B. I. Verkin, JETP **34**, 1655 (1958); Soviet Phys. JETP **7**, 1137 (1958).

[25] A. M. Kosevich and V. V. Andreev, JETP **38**, 882 (1960); Soviet Phys. JETP **11**, 637 (1960).

Translated by R. T. Beyer
280

SOVIET PHYSICS JETP VOLUME 12, NUMBER 6 JUNE, 1961

THE DECAY SCHEME OF Dy^{166}

L. I. RUSINOV,* A. V. BOROVIKOV, V. S. GVOZDEV, G. D. PORSEV, S. L. SAKHAROV, and Yu. L. KHAZOV

Leningrad Physico-Technical Institute Academy of Sciences, U.S.S.R.

Submitted to JETP editor June 29, 1960

J. Exptl. Theoret. Phys. (U.S.S.R.) 39, 1529-1533 (December, 1960)

Dy^{166} ($T_{1/2}$ = 80.2 hrs.) was obtained by double neutron capture from Dy^{164} and its decay scheme studied. The multipolarity of the following γ-ray transitions in Ho^{166} were determined: 28 kev (M1), 54.2 kev (E2) and 82.5 kev (M1). Branching ratios for the β decay of Dy^{166} to various levels in Ho^{166} were obtained and a level scheme for low lying states in Ho^{166} is proposed.

INTRODUCTION

HELMER and Burson[1] have studied the decay of Dy^{166} ($T_{1/2}$ = 80.2 hrs.), the Dy^{166} being made by double neutron capture from Dy^{164}. In the decay of Dy^{166} they found transitions with energies 28, 54.2, 82.5, 286, 346, 368, and 427 kev. On the basis of the observed $\gamma\gamma$ coincidences, they proposed the level scheme for Ho^{166} which is shown in Fig. 1. They did not determine the multipolarity of the γ transitions, nor the spins and parities of the levels in Ho^{166}.

Ho^{166} decays with a half life of 27 hr into Er^{166} (Fig. 2). The decay can go with approximately equal probabilities to either the ground state of Er^{166} or the first excited state (2^+). There are practically no transitions to the 4^+ level (the second excited state in the rotational band).[2] It follows that the spin of the ground state of Ho^{166} can not be greater than one.

Graham et al.[2] have studied the form of the β spectrum with a 1771-kev end point. The β spectrum was studied in coincidence with 81 kev γ rays. It was shown that the spectrum had a unique form, due to a spin change of two with change of parity. The $\beta\gamma$ correlation was also investigated. The authors concluded that the ground state of Ho^{166} had spin zero and negative parity.

According to the unified model of the nucleus, for the low lying intrinsic states, the quantum number K is equal to Ω, the projection of the angular momentum on the nuclear symmetry axis. For odd-odd nuclei Ω, and hence K, is equal to the sum or difference of the values of Ω for the last odd proton and the last odd neutron, $\Omega = |\Omega_p \pm \Omega_n|$.

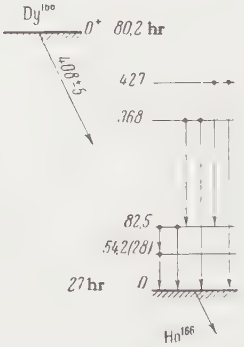

FIG. 1

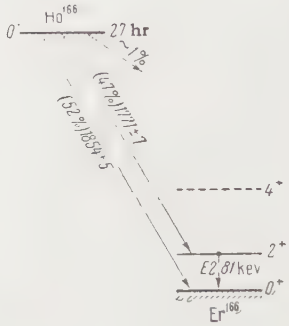

FIG. 2

FIG. 1. The decay scheme of Dy^{166} (the level which is the final state for the spectrum with end point 408 kev has not been established).

FIG. 2. The decay scheme of Ho^{166} (ref. 3).

The nuclear state has even parity if the last odd proton and neutron have the same parity, and is odd if the two parities are different.

From the above considerations it follows that information about the spins of excited states in an odd-odd nucleus can be obtained from the excited states of neighboring odd-even and even-odd nuclei. For $_{67}Ho^{166}$, the appropriate neighboring nuclei are $_{67}Ho^{165}$ and $_{68}Er^{167}$. The ground and first excited states of these nuclei are shown in Fig. 3.[3] The expected intrinsic states of Ho^{166} are shown schematically in Fig. 4. A rotational band can be associated with each of the levels shown in this figure.

From Fig. 4 it is clear that the ground state of the nucleus Ho^{166} should have the quantum number $K = 0^-$. However, since the shape of the nucleus is invariant under reflection in a plane perpendicular to the axis of symmetry, it follows that an odd parity intrinsic state implies odd

---

*Deceased.

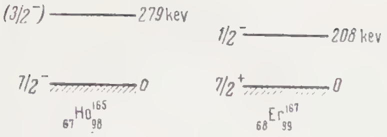

FIG. 3. The low lying levels in Ho^{165} and Er^{167}.

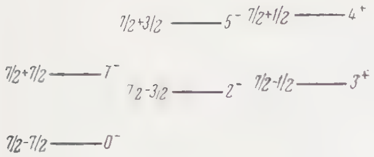

FIG. 4. Proposed intrinsic states for Ho^{166}.

values for the spins (i.e., the rotational band 1⁻, 3⁻, 5⁻, . . .).[4] Hence the ground state of Ho^{166} should be assigned a spin of one. This conclusion is in disagreement with the experimental result obtained by Graham et al.[2]

The contradiction between theory and experiment for Ho^{166} is important as a matter of principle. The purpose of the work reported here was to find the spins of the levels in Ho^{166} by studying the spectra of γ rays and conversion electrons from the β decay of Dy^{166}.

EXPERIMENTAL RESULTS

The spectra of the internal conversion electrons were measured on a Siegbahn type β spectrometer with focusing at an angle $\pi\sqrt{2}$, resolution $\Delta H\rho/H\rho = 0.25\%$, and aperture 0.25% of 4π. The source was dysprosium oxide enriched to 86.5% Dy^{164} and deposited on an aluminum foil 4 μ thick. The thickness of the dysprosium oxide layer was about 0.06 mg/cm^2. The source was irradiated by thermal neutrons from a reactor for 6 to 7 days. The measurements were made 36 hours after the irradiation in order to avoid effects due to Dy^{165} ($T_{1/2}$ = 2.4 hrs.).

Figure 5 shows the spectrum of internal conversion electrons from Ho^{166}. The spectrum contains conversion lines corresponding to transitions in Ho^{166} with energies 28; 54.2 and 82.5 kev. The spectrum also shows a line due to internal conversion electrons from the 81 kev transition in Er^{166}, arising from the β decay of Ho^{166}.

A search was made for conversion electrons due to transitions with energies > 82.5 kev in Ho^{166}. No such electrons were found. If there are any, their intensity is less than 0.5% of the intensity of the K line in the 82.5 kev transition.

The conversion electron spectrum shown in Fig. 5 was analyzed for the relative conversion coefficients associated with the three transitions. The results are shown in Table I. The table also shows values for the same internal conversion coefficients according to Sliv and Band.[5]

γ spectra and $\gamma\gamma$ coincidences were also measured. These measurements showed that the 28- and 54.2-kev γ rays were in coincidence while there was no coincidence between these γ rays and the one with energy 82.5 kev. This result agrees with the data of Helmer and Burson.[1]

The measurements of γ ray spectra showed that the combined intensity of all γ rays having energy greater than 82.5 kev must be less than 1 or 2% of the intensity of the 82.5 kev γ ray.

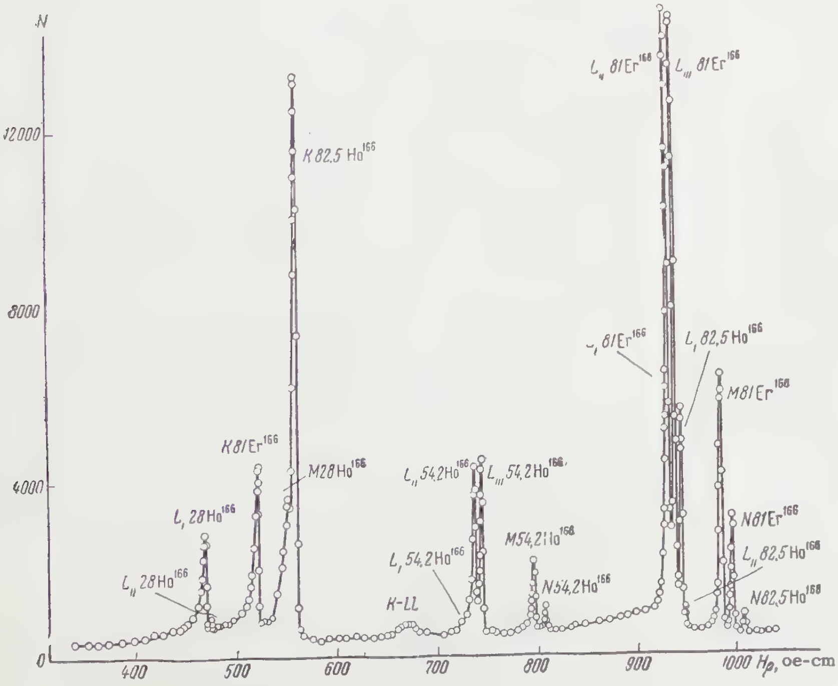

FIG. 5. Spectrum of internal conversion electrons from Ho^{166}.

TABLE I

E_γ, kev	Relative conversion coefficients							Intensity of the transition
	Experiment	Calculated						
		$E1$	$E2$	$E3$	$M1$	$M2$	$M3$	
	$\alpha_{L_{\mathrm{I}}} / \alpha_{L_{\mathrm{II}}}$							
28	10.5 ± 0,3	1,45	0,01	0,014	10,7	14,4	13.0	0,23 ± 0,01
	$\alpha_{L_{\mathrm{I}}}+\alpha_{L_{\mathrm{II}}} / \alpha_{L_{\mathrm{III}}}$							
54.2	0.85 ± 0,03	2.7	0.89	0.94	76	3.22	0,53	0.23 ± 0.01
	$\alpha_{L_{\mathrm{I}}} / \alpha_{L_{\mathrm{II}}}$							
82.5	11,0 ± 0,4	3.55	0,1	0.017	11,4	8,8	6,3	1
	α_K/α_L							
	7.6 ± 0.2	6,1	0,5	0,04	6,61	3,16	0,7	
81Er								1,05 ± 0,01

DISCUSSION OF THE RESULTS

Comparison of the experimental and theoretical ratios of internal conversion coefficients leads to the conclusion that the 28- and 82.5-kev γ rays are pure M1 transitions. The 54-kev γ ray is a pure E2 transition.

The intensities of the 28- and 54.2-kev γ rays were equal within 2 or 3% (see Fig. 1). The equality of these two intensities implies that the first excited state in Ho^{166} is essentially populated only by transitions from the second excited state at 82.5 kev (or at least that this occurs in the vast majority of cases). There is only a small probability that the first excited state in Ho^{166} be formed by decay from higher excited states or directly by β decay of Dy^{166}.

The probability that Dy^{166} decays to the ground state of Ho^{166} relative to the probability that it decays to the excited state at 82.5 kev can be inferred from a comparison of the sum of the intensities of the 28- (or 54-) and 82.5-kev transitions with the intensity of the 81-kev E2 transition in Er^{166}. Calculations with account of the fact that there is only a small probability that Dy^{166} decays to high excited states and using the results of Graham et al.[2] show that when Dy^{166} decays, the 82.5-kev state in Ho^{166} is formed (55 ± 2)% of the time. That only one or two per cent of the β decays of Dy^{166} are to high excited states follows from an estimate of the intensities of γ rays and conversion electrons connected with transitions having energies greater than 82.5 kev. The remaining ~ 43% of the decays of Dy^{166} lead to formation of Ho^{166} in the ground state.

It is not possible to determine uniquely the spins of the first two excited states in Ho^{166} from a knowledge of the multipolarity of the 28, 54.2, and 82.5-kev decays only, especially in view of the fact that the spin of the ground state is not known with certainty. However, the following considerations serve to narrow the range of possibilities.

1. Since there is no β decay to the first excited state in Ho^{166}, the spin of this level must be greater than the spins of the ground state and the excited state at 82.5 kev. [The spin and parity of the ground state of Dy^{166} is 0^+ (even-even nucleus].

2. In establishing the spins of the levels in the Ho^{166} nucleus, it should be borne in mind that the 54.2 and 82.5 kev transitions are pure — there is no admixture of other multipolarities. The same comment, though rather weakened, applies to the 28 kev transition.

3. It is not possible to measure directly the order of the 28- and 54.2-kev transitions, i.e., the energy of the first excited state in Ho^{166}. However, the intensity of the 82.5-kev γ transition relative to the intensities of the 28- and 54.2-kev γ transitions have been measured, and this can be compared with theoretical estimates[6] (Table II). One is led to the conclusion that the most likely process for de-excitation of the 82.5-kev level is

TABLE II

Possible transitions from the level at 82.5 kev	Ratio of transition probabilities	
	Theory	Experiment
	W_γ (82kev)/W_γ (28kev)	
$82.5 \xrightarrow[M1]{28} 54.2 \xrightarrow[E2]{54.2} 0$	25,6	13,5
	W_γ (82kev)/W_γ (54kev)	
$82.5 \xrightarrow[E2]{54.2} 28 \xrightarrow[M1]{28} 0$	10^6	25

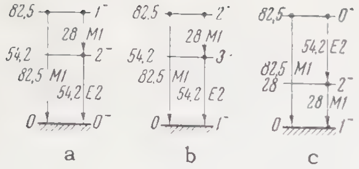

FIG. 6. Proposed level scheme for low-lying levels in Ho^{166}.

$$82{,}5 \xrightarrow[M1]{28} 54.2 \xrightarrow[E2]{54{,}2} 0.$$

In this case, the energy of the first excited state in Ho^{166} is 54.2 kev. It should be noted, however, that the process

$$82.5 \xrightarrow[E2]{54{,}2} 28 \xrightarrow[M1]{28} 0,$$

is not ruled out, since E2 transitions are often faster than estimated theoretically, while the M1 transition can be forbidden to a significant degree.

4. It should be borne in mind that Fig. 4 serves to eliminate a large number of spin assignments for the levels of Ho^{166}.

In view of the foregoing, Fig. 6 shows three possible level schemes for the low lying states of Ho^{166}. The most likely one of these is a, since it agrees best with the experimental data of reference 2 and the data being presented in this paper.

In conclusion, the authors consider it a pleasant duty to thank D. A. Varshalovich for discussion of results.

---

[1] R. G. Helmer and S. B. Burson, Bull. Am. Phys. Soc., Ser. II, **4**, 427 (1959).

[2] Graham, Wolfson, and Clark, Phys. Rev. **98**, 1173 (1955).

[3] V. S. Dzhelepov and L. K. Peker, Схемы распада радиоактивных ядер (Decay Schemes of Radioactive Nuclei) Acad. Sci. U.S.S.R. (1958).

[4] A. Bohr and B. Mottelson, Kgl. Danske Videnskab. Selskab, Mat.-fys. Medd. **27**, No. 16 (1953).

[5] L. A. Sliv and I. M. Band, Таблицы коэффициентов внутренней конверсии γ-излучения (Tables of γ Ray Internal Conversion Coefficients), Parts I, II, Acad. Sci. U.S.S.R. (1956-58).

[6] Nijgh, Wapstra, and Van Lieshout, Nuclear Spectroscopy Tables, Amsterdam, 1959.

Translated by R. Krotkov
281

SOVIET PHYSICS JETP VOLUME 12, NUMBER 6 JUNE, 1961

ANGULAR DISTRIBUTION OF SHOWER PARTICLES IN NUCLEAR INTERACTIONS OF FAST NUCLEONS WITH HEAVY EMULSION NUCLEI

S. A. AZIMOV, K. T. TESHABAEV, L. P. CHERNOVA, G. M. CHERNOV, and V. M. CHUDAKOV

Physico-Technical Institute, Academy of Sciences, Uzbek S.S.R.; Central Asia State University

Submitted to JETP editor June 27, 1960

J. Exptl. Theoret. Phys. (U.S.S.R.) 39, 1534-1539 (December, 1960)

The angular distribution of shower particles is studied for 70 showers (jets) produced by singly-charged or neutral cosmic-ray particles of $10^{10} - 10^{12}$ ev, and possessing more than eight strongly-ionizing particles.

IN the present experiment, the angular distribution of secondary particles in 70 interaction events of singly-charged and neutral cosmic-ray particles with heavy emulsion nuclei was studied. The showers were found in scanning Ilford G-5 emulsions exposed in the stratosphere during the 1955 Italian expedition, and possess five or more relativistic tracks, $n_s \geq 5$, and more than eight heavily ionizing particles, $n_h + n_g > 8$. Of these showers, 55 were produced by singly-charged particles and 15 by neutral ones. The maximum value of the Lorentz factor for the coordinate system with a symmetrical angular distribution is $\gamma_c = [1 - \beta_c^2]^{-1/2} = 11$. The measurements were carried out by the method already described by one of the authors.[1] For nuclear interactions of the charged particles, the angles with the direction of the primary particle were determined. In the range $\gamma_c < 3$ (31 showers out of 55), our measurements are rather good, since, for the majority of the particles, the distance from the point of intersection of the track with the sphere surrounding the vertex of the shower to the point of intersection of the primary-particle track with the same sphere is much greater than the errors in the determination of the coordinates of these points. For larger values of γ_c, this condition is not always satisfied.

The symmetry of the angular distribution of shower particles with respect to the $\pi/2$ angle in the center-of-mass system in collisions with complex nuclei has been studied by a number of investigators.[2,3] These investigations showed that such a symmetry exists in the frame of reference in which half of the particles have the angle $\theta^* > \pi/2$ (c system). The transformation from the angle θ in the laboratory system (l system) to the angle θ^* in the c system is given by the formula

$$\gamma_c \tan\theta = \tan(\theta^*/2), \qquad (1)$$

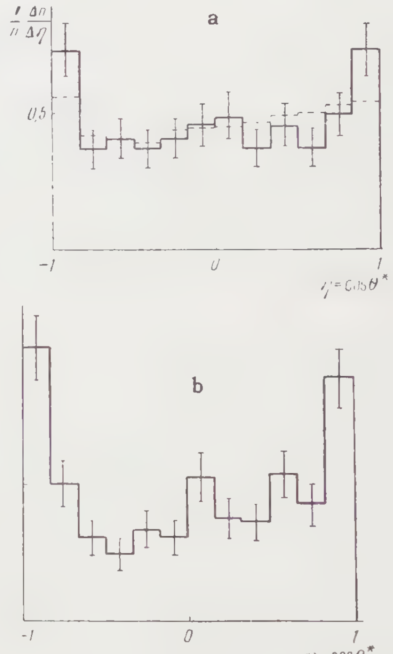

FIG. 1. Angular distribution in the c system of secondary particles in showers produced by charged particles; a – showers with $\gamma_c < 3$, b – showers with $\gamma_c > 3$. n – total number of secondary shower particles. $\Sigma\Delta n$ does not contain particles with $\theta > \pi/2$, so that $\Sigma\Delta n < n$. The dashed line represents the theoretical histogram to show the distortion of the isotropic distribution in the c system for m = 0.9 and for a transformation from the angle θ to the angle θ^* according to Eq. (1) for $\gamma_c = \bar{\gamma}_c$.

which has been obtained under the assumption that the velocity of the particle in the c system β^* is equal to the velocity β_c of the c system itself. The Lorentz factor γ_c of the c system was determined from the relations

$$(\gamma_c)_1 = \cot\theta_{1/2}, \qquad (2)$$

$$\log(\gamma_c)_2 = \overline{-\log\tan\theta}, \qquad (3)$$

The latter relation is correct for a symmetrical angular distribution of particles in the c system. The above-mentioned assumption that the secondary particles are monoenergetic in the c system, which has often been used in the analysis of experimental data, leads to an overestimate of γ_c.[4] However, such an overestimate does not considerably distort the angular and energy distribution of particles in the c system obtained by means of relativistic transformations.[5] Therefore, the earlier conclusions[2,3] about the symmetry and anisotropy of the angular distribution of particles in the c system and the increase of anisotropy with the energy of the primary particles are evidently correct. Henceforth, we shall also make use of the assumption that the secondary particles are monoenergetic in the c system, in order to investigate their angular distribution.

For a small γ_c, the analysis of the angular distribution is rendered difficult by the fact that the values $m = \beta_c/\beta^*$ can be different from 1. Figure 1a shows our data on the angular distribution in the c system for particles of 31 showers produced by charged particles for $\gamma_c < 3$. The angle transformation was carried out according to Eq. (1) for $\gamma_c = \overline{\gamma}_c = \frac{1}{2}[(\gamma_c)_1 + (\gamma_c)_2]$, i.e., assuming symmetry in the c system and $m = 1$. In determining γ_c from the angle $\theta_{1/2}$, the secondary relativistic particles emitted in the l system in the backward hemisphere were taken into account.*

The same figure shows the possible distortion of the isotropic distribution in the c system, due to the deviation of m from unity, calculated using Eq. (1). Our experimental data do not contradict the assumption of symmetry in the c system for small γ_c; the mean value of m can be less than one, but not by more than a few percent.

For the same group of showers, two values of the dispersion were also calculated:

$$\sigma_1 = \left[\sum_{i=1}^{N} \sum_{j=1}^{n_{1i}} [\log \tan \theta_{ij} - (\overline{\log \tan \theta})_i]^2 \Big/ \sum_{i=1}^{N} n_{1i} \right]^{1/2}, \tag{4}$$

$$\sigma_2 = \left[\sum_{i=1}^{N} \sum_{j=n_{1i}+1}^{n_{1i}+n_{2i}} [\log \tan \theta_{ij} - (\overline{\log \tan \theta})_i]^2 \Big/ \sum_{i=1}^{N} n_{2i} \right]^{1/2}, \tag{5}$$

where N is the number of showers, and n_{1i} and n_{2i} are the number of particles in the i-th shower with $\log \tan \theta < (\overline{\log \tan \theta})_i$ and $\log \tan \theta > (\overline{\log \tan \theta})_i$ respectively. The theoretical variation of σ_1 and σ_2 with m for an isotropic distribution in the c system is shown in Fig. 2. For an anisotropic angular distribution, the theoretical curves fall above those shown in Fig. 2. However, the character of the variation σ_1 and σ_2 with m remains the same. For a symmetrical distribution in the c system and for $m = 1$, we have $\sigma_1 = \sigma_2$. The experimental values $\sigma_1 = 0.50$ and $\sigma_2 = 0.52$ are close to each other, and confirm the conclusion concerning the symmetry of the angular distribution of particles in the c system, and concerning the mean value of m.

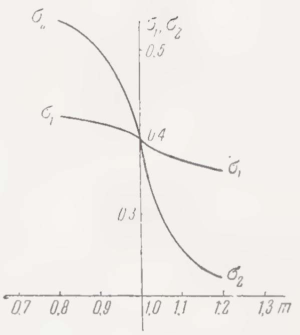

FIG. 2. Variation of the dispersion of the angular distribution σ_1 and σ_2 with $m = \beta_c/\beta^*$ for an isotropical distribution in the c system.

The study of the variation in the anisotropy of the angular particle distribution in the c system with the energy of the primary particle and with the impact parameter makes it possible to obtain some data on the character of the nuclear interaction. To this end, experimental values of n_s and γ_c are shown in the graph (see Fig. 3). In the paper of Takibaev et al.,[6] it is concluded that a certain fraction of shower particles is produced in secondary collisions of the nucleons inside the nucleus at energies below 10^{12} ev. This conclusion is based on the fact that, in many showers, the number of particles is greater than the maximum possible number predicted by the hydrodynamical theory.[7] However, this theory determines the number of particles N_0 (charged and neutral) to a constant factor $k \sim 1$ as follows:

$$N_0 = k(l+1)E_0^{1/4}, \qquad l < 3.7, \tag{6}$$

$$N_0 = 1.85k(l-0.25)^{3/4}E_0^{1/4}, \qquad l > 3.7. \tag{7}$$

Here l is the length of the tunnel in units of the nucleon diameter, and E_0 is the energy of the primary nucleon in the l system in units of the nucleon rest energy. Figure 3 shows theoretical curves, calculated assuming a symmetrical distribution in the center-of-mass system, and also that π mesons are produced only for $k = 1.7$. As can be seen, the agreement with the experimental data at high energy is not bad. In order to confirm the conclusions of reference 6 for secondary collisions, it might therefore be useful to study the variation of the anisotropy of the angular distribution in the c system with the impact parameter.

---

*A total of 24 such particles out of 480 were observed in the composite shower.

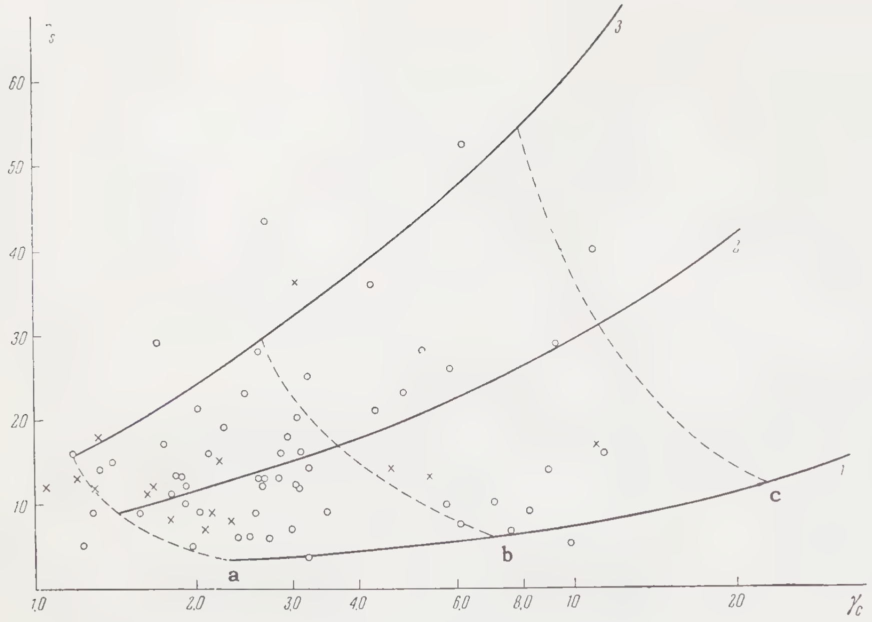

FIG. 3. Experimental values of n_s' and γ_c for 70 showers; o – showers produced by charged particles ($n_s' = n_s - 1$), x – showers produced by neutral particles ($n_s' = n_s$). Curves 1, 2, and 3 were calculated using Eqs. (6) and (7) for $k = 1.7$ and values of l equal to 1, 4, and 8 respectively. The dashed curves correspond to constant shower energy; a – for $E_0 = 10$, b – for $E_0 = 10^2$, and c – for $E_0 = 10^3$.

The curve 2 of Fig. 3 divides the showers according to their values of l and n_s for different γ_c. The showers corresponding to points lying below this curve (group I) are on the average produced in more central collisions with heavy emulsion nuclei than the showers with a smaller number of particles (group II), at least if considered from the point of view of the hydrodynamical theory. Hence, it follows that the angular distribution in group I should be closer to isotropic in the c system[8] if the multiple particle production occurs in one act of collision of the primary nucleon with a tunnel of nuclear matter.* Our experimental data presented in Fig. 4 contradict the theory qualitatively, and indicate clearly the important role played by consecutive collisions of the primary nucleon and of secondary particles with nucleons of the target nucleus in the energy range under consideration. As a quantitative characteristic of the average anisotropy of the angular particle distribution in the c system, we can use the quantity

$$\sigma = \left[\sum_{i=1}^{N}\sum_{j=1}^{n_i}[\log\tan\theta_{ij} - (\overline{\log\tan\theta})_i]^2 \Big/ \sum_{i=1}^{N}(n_i - 1)\right]^{1/2}, \quad (8)$$

where n_i is the number of charged particles with $\theta < \pi/2$ in the i-th shower. If we assume a normal distribution of the quantities $\log\tan\theta$ and the same anisotropy in different showers, then the value of σ corresponds to the standard deviation $\Delta\sigma = \sigma[2\sum_{i=1}^{N}(n_i - 1)]^{-1/2}$. For groups I and II of the showers produced by charged particles, the experimental values of σ equal 0.555 ± 0.016 and 0.479 ± 0.022 respectively. In the range $\gamma_c < 3$, where our measurements are certainly good, the corresponding values are equal to 0.549 ± 0.022 and 0.459 ± 0.031 respectively. We note that for showers which, according to their multiplicity, fall within the framework of the hydrodynamical

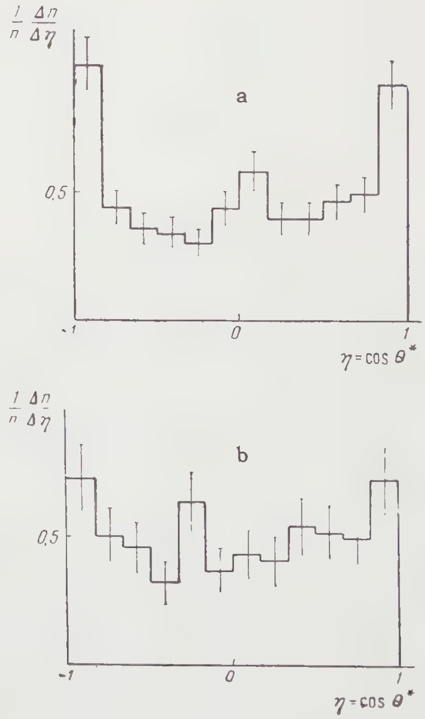

FIG. 4. Angular distribution in the c system of secondary particles in showers produced by charged particles; a – showers of group I (28 showers), b – showers of group II (27 showers).

---

*A quantitative comparison with theory is impossible since the shower energy is not sufficiently high.

Group	σ	σ_1	σ_2	$\overline{n_h + n_g}$
Showers produced by neutral particles (angles with the shower axis were measured)	0.44±0,02	0,36	0,50	17,6±1.1
Showers produced by charged particles (angles with the shower axis were measured)	0.44±0.02	0.37	0.47	19.2±1.1
Showers produced by charged particles (angles with the direction of the primary particle were measured)	0,51±0.03	0,47	0,50	19,2±1,1

theory for $k = 1$ in Eqs. (6) and (7), an increased anisotropy is observed with an increasing number of nucleons of the target nucleus taking part in the collision. Thus, those showers also cannot be considered to be the result of tunnel-effect collisions.

As far as the variation of the anisotropy of the angular particle distribution with energy γ_c is concerned, our data shown in Fig. 1 qualitatively agree with the results of Miesowicz et al.[3] Also, at large γ_c, the value of σ may be somewhat underestimated because of experimental errors. An increased σ with increasing γ_c is observed experimentally both for group I and group II.

We have also compared the characteristics of the showers produced by singly-charged and neutral particles. To this end, each of the 15 showers whose primary particles are neutral were compared with a shower produced by a charged primary particle and having similar values of n_s and $\theta_{1/2}$. The characteristics of these showers are given in the table, and they show that the singly-charged and neutral particles interact with the nuclei in a similar way. Hence, it apparently follows either that π mesons interact with nucleons in the same way as heavier particles, or that the admixture of π mesons among charged primary particles is negligible.

The authors thank G. B. Zhdanov for his comments on the results of the experiment.

---

[1] V. M. Chudakov, Приборы и техника эксперимента (Instruments and Exptl. Techniques) **6**, 37 (1959).

[2] A. P. Mishakova and B. A. Nikol'skiĭ, JETP **37**, 1594 (1959), Soviet Phys. JETP **10**, 1130 (1960).

[3] Bartke, Ciok, Gierula, Holyński, Miesowicz, and Saniewska, Nuovo cimento **15**, 18 (1960).

[4] Jain, Lohrmann, and Teucher, Phys. Rev. **115**, 643 (1959).

[5] Schein, Haskin, Lohrmann, and Teucher, Phys. Rev. **116**, 1238 (1959).

[6] San'ko, Takibaev, and Shakhova, JETP **35**, 574 (1958), Soviet Phys. JETP **8**, 396 (1959).

[7] S. E. Belen'kiĭ and G. A. Milekhin, JETP **29**, 20 (1955), Soviet Phys. JETP **2**, 14 (1956).

[8] G. A. Milekhin, JETP **35**, 1185 (1958), Soviet Phys. JETP **8**, 829 (1959).

Translated by H. Kasha
282

SOVIET PHYSICS JETP VOLUME 12, NUMBER 6 JUNE, 1961

EXCITED LEVELS OF Si^{30}

A. M. ROMANOV

Leningrad Physico-Technical Institute, Academy of Sciences, U.S.S.R.

Submitted to JETP editor June 30, 1960

J. Exptl. Theoret. Phys. (U.S.S.R.) 39, 1540-1541 (December, 1960)

The Si^{30} level scheme excited in the $Al^{27}(\alpha, p)Si^{30}$ reaction is determined.

EXPERIMENTAL data obtained until 1951 regarding the levels of Si^{30} were systematized by Alburger and Hafner,[1] and later data have been reviewed by Endt and Braams[2] and by Dzhelepov and Peker.[3] A large portion of this information was obtained from the energy spectra of protons in the reactions $Al^{27}(\alpha, p)Si^{30}$ and $Si^{29}(d, p)Si^{30}$. The four lowest excited levels of Si^{30} were determined exactly by magnetic analysis of the protons from these reactions.[4,5] Data on higher excited levels can be found in references 6 and 7. For the purpose of checking these data we have studied the energy spectra of protons from $Al^{27}(\alpha, p)Si^{30}$ using 10.4-, 13.65-, and 14.7-Mev α particles.

An α-particle beam from the cyclotron of the Physico-Technical Institute was focused by quadrupole lenses and collimated, before striking a thin (0.13 mg/cm^2) aluminum target which was positioned at 45° to the beam direction, in the center of a brass chamber. Ya-2 nuclear plates for registering protons from the $Al^{27}(\alpha, p)Si^{30}$ reaction were placed in holders on a circle of 206-mm radius inside the chamber. Windows in the holders were covered with thin aluminum foil. Following exposure the plates were processed in the usual manner. A MBI-2 microscope was used in measuring proton tracks.

The mean energies of proton groups were determined for two emission angles ($\theta = 60°$ and 90°) and three α-particle energies (E_α = 10.4, 13.65, 14.7 Mev). A more reliable identification of proton groups was thus possible, since separation could not be achieved with certainty in some individual cases. A certain amount of error is involved in the determination of mean proton-group energies by means of range-energy curves. This error could not exceed 1%, because the reference energies were those of the proton groups corresponding to the four lowest levels of Si^{30}, which had been determined reliably from magnetic analysis.[4,5] In addition, the proton-group energies were determined from three to six independent measurements (at different angles and α-particle energies). The energy levels were determined from the relationship

$$Q_i = E_{pi}(1 + m_p/m_r) - E_\alpha(1 - m_\alpha/m_r) - 2\cos\theta\sqrt{E_{pi}E_\alpha m_p m_\alpha}/m_r,$$

where Q_i is the reaction energy in the excitation

Energy levels of Si^{30}

No. of level	Energy level, Mev			
	Reference 5	Reference 6	Reference 7	Present work
1	2.258±0.006	2.23±0.02	—	2.26±0.05
2	3.518±0.007	3.52±0.02	3.65	3.50±0.06
3	3.798±0.009	3.80±0.04	—	3.82±0.06
4	4.85±0.01	4.83±0.02	—	4.80±0.06
5	—	5.28±0.02	—	5.30±0.08
6	—	5,52±0.03	5.60	5,48±0.08
7	—	5,94±0.04	—	5.70±0,08
8	—	—	—	6,08±0.07
9	—	6,52±0.03	—	6.68±0.07
10	—	7,10±0.03	—	7.06±0.07
11	—	7.38±0.05	7.34	7,40±0.08
12	—	—	—	7.76±0,09
13	—	—	8.36	8.44±0,09
14	—	—	—	8.80±0.10
15	—	—	9.42	9,38±0.10
16	—	—	—	9.70±0.10(?)
17	—	—	10.03	9,96±0.10
18	—	—	—	10,60±0.10
19	—	—	11.02	11.06±0.10

of the i-th level of the final nucleus; m_p, m_α, and m_r are the masses of the proton, α-particle, and final nucleus; E_α is the α-particle energy in the laboratory system; E_{pi} is the mean energy of a proton group from reactions leaving the final nucleus in the i-th state; θ is the laboratory angle of proton emission. The value $Q_0 = 2.38$ Mev was taken in accordance with the particle masses involved in the reaction.

Results obtained from our experimental data and from those of other investigators[5-7] are given in the table. The existence of a 5.08-Mev level is not confirmed, in agreement with reference 6.

Since the experimental technique could not be used to distinguish proton tracks from deuteron tracks, it was not fully demonstrated that a 9.70-Mev level is excited in the reaction $Al^{27}(\alpha, p)Si^{30}$.

I wish to thank L. N. Goryachaya for assistance in the treatment of the data.

[1] D. Alburger and E. Hafner, Revs. Modern Phys. **22**, 373 (1950), Russ. transl. 1952.

[2] P. M. Endt and C. M. Braams, Revs. Modern Phys. **29**, 683 (1957).

[3] B. P. Dzhelepov and L. K. Peker, Схемы распада радиоактивных ядер (Decay Schemes of Radioactive Nuclei), Acad. Sci. Press, 1958.

[4] D. M. Van Patter and W. W. Buechner, Phys. Rev. **87**, 51 (1952).

[5] Barros, Forsyth, Jaffe, and Taylor, Proc. Phys. Soc. (London) **73**, 793 (1959).

[6] Hassler, Steigert, and Pieper, Bull. Am. Phys. Soc. **1**, 280 (1956).

[7] Brolley, Sampson, and Mitchell, Phys. Rev. **76**, 624 (1949).

Translated by I. Emin
283

SOVIET PHYSICS JETP VOLUME 12, NUMBER 6 JUNE, 1961

RESONANCE AND MAGNETIC PROPERTIES OF YTTRIUM IRON GARNET AT LOW TEMPERATURES

K. P. BELOV, L. A. MALEVSKAYA, and V. I. SOKOLOV

Moscow State University

Submitted to JETP editor June 29, 1960

J. Exptl. Theoret. Phys. (U.S.S.R.) 39, 1542-1547 (December, 1960)

The variation in the anisotropy of a 8,500 Mc/sec resonance field in a single crystal of yttrium iron garnet on cooling from room temperature to 2°K was studied. At helium temperatures the magnetic anisotropy constant K_1 is 8 – 9 times greater than its room temperature value. The existence of such a sharp variation in K_1 is confirmed by the small slope of the magnetization curves at helium temperatures, measured on polycrystalline specimens. There are sharp maxima in the curves of the temperature dependence of the ferromagnetic resonance absorption line width for single crystals in the region 20 – 40°K. These maxima are smaller for polycrystalline specimens and are greatly spread out between 4 and 60°K. It was found that in this temperature range the magnetic viscosity is high (from the static magnetization curves measured).

A detailed study of the temperature dependence of the ferromagnetic resonance parameters in yttrium iron garnets (YIG) is of considerable interest. From the theoretical point of view, the low-temperature regions is of the most importance in this respect. Interesting anomalies in the temperature dependence of the ferromagnetic resonance line width and of the anisotropy of the resonance field were found at low temperatures by Dillon[1] and by Spencer et al.[2] Kittel et al.[3] have attempted a theoretical explanation of them.

We have studied the temperature dependence of the anisotropy in the resonance field and of the resonance line width in several single crystal specimens of yttrium ferrite with the garnet structure ($3Y_2O_3 \cdot 5Fe_2O_3$) in the temperature range from 2 to 300°K. We have also measure the line widths and static field magnetization curves on polycrystalline specimens of yttrium ferrite having the same composition. The ferromagnetic resonance studies were carried out at a frequency of 8500 Mc/sec by using a short-circuited waveguide section. The part of the waveguide contained in the helium Dewar was made of stainless steel to reduce the heat leakage. The upper end of the waveguide, firmly soldered to the cap, was sealed with mica to maintain a vacuum and its lower end was shorted by a brass wall. The positioning tube was soldered to the outer wall of the short-circuited section and the specimen holder was placed in it; a spur gear was attached to the end of the holder. The holder with the specimen could be turned through 360° by means of a second gear attached to a rod passing through the cap. A nonmagnetic nichrome heating coil was wound on the tube in order to obtain temperatures between nitrogen and room temperatures. The temperature was measured by a copper-constantan thermocouple. Unwanted field distortion was prevented by bifilar winding. The range from 4.2°K to 80°K was covered by boiling off liquid helium. In this region the temperature was measured by a carbon resistance thermometer and was maintained to an accuracy of 1 – 2°. The resonance line width

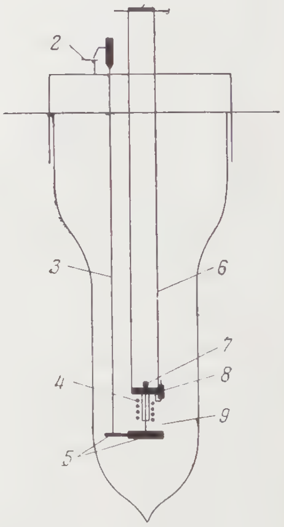

FIG. 1. Arrangement of the short-cuited waveguide section: 1 – mica window, 2 – dividing head, 3 – phosphor bronze rod, 4 – heater, 5 – gears, 6 – waveguide, 7 – specimen, 8 – thermometer, 9 – specimen holder.

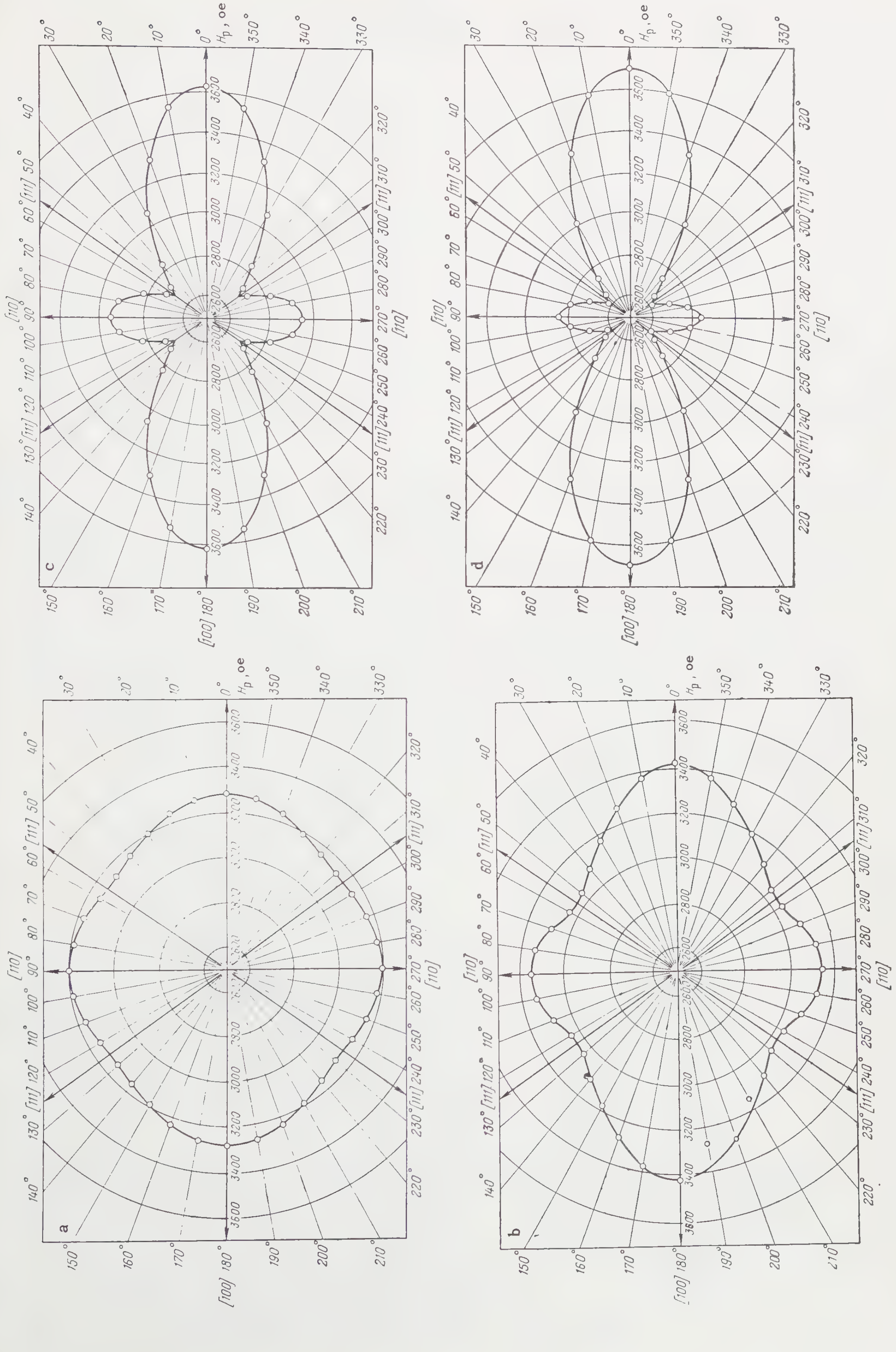

FIG. 2. The variation of resonance field with its direction relative to the crystallographic axes in the (110) plane in a YIG single crystal: a – at T = 300° K, b – at T = 77°K, c – at T = 20°K, d – at T = 2.0°K.

ΔH to the half-amplitude level was determined from the resonance curve (the resonance curve was measured point by point).

The YIG specimens were grown in the Crystallographic Institute of the Academy of Sciences by Timofeeva,[4] who crystallized them from molten mixtures with a cooling rate of 2 — 3° per hour. Polycrystalline YIG was prepared by a ceramic process and had a density of 4.97 g/cm^3. The specimens were given a spherical shape with diameter from 0.8 to 2 cm. The spheres were purposely not carefully polished as the large line width of the ferromagnetic resonance was advantageous in our cases — it made it easier to observe its variation on lowering the temperature. The magnetization curves (in weak fields) at low temperatures were measured ballistically on a small toroid of polycrystalline YIG having a density of 4.85 g/cm^3.

1. THE ANISOTROPY OF THE RESONANCE FIELD

We studied the variation in the magnitude of the resonance field with its direction relative to the crystallographic axes in the (110) plane (in which all the main crystallographic axes lie) for one of the single crystal specimens. The crystal orientation was determined magnetically with an accuracy of 30′. The accuracy of reading the angle on rotating the crystal was 2°.

The polar diagrams of the resonance field H_r at temperatures of 300, 77, 20.4 and 2.0°K are shown in Fig. 2. It can be seen that the anisotropy in H_r is very small at room temperature; the rotation diagram departs only insignificantly from a circle (the maximum change in H_r is of the order of 100 oe). The rotation diagram changes sharply as the temperature is lowered and maxima and minima are clearly seen in the values of H_r. At liquid helium temperatures the variation in H_r is of the order of 1000 oe. This can also be seen clearly in Fig. 3, where the dependence of H_r on temperature is shown for a single crystal for the two directions [111] and [100], and also for polycrystalline YIG. The change in H_r on rotating the crystal in the (110) plane reflects the crystal symmetry of the specimen sufficiently well.

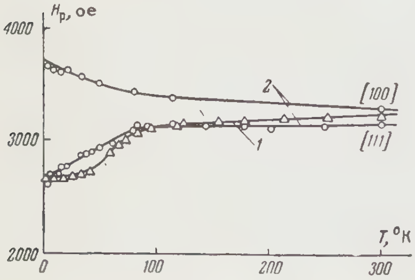

FIG. 3. The variation of resonance field with temperature: 1 — in polycrystalline YIG, 2 — in a YIG single crystal.

Dillon[1] measured the anisotropy in H_r on single crystals at low temperatures for a frequency of 23 700 Mc/sec. He found a very complicated variation of H_r with respect to the crystal axes at 4.2°K. In the (110) and (100) planes he obtained an eight-leaf rosette. The additional maxima in the diagram were ascribed to rare earth element impurities in the YIG.

Although there was an appreciable amount of rare earth impurities in our YIG, no complicated behavior of the resonance field relative to the crystallographic axes (at a frequency of 8,500 Mc/sec) appeared in our experiments.

As is well known, the dependence of H_r on the angle of rotation θ (measured from [100]) for the (110) plane can be expressed in the following form:

$$H_p = H_{\text{eff}} - \frac{K_1}{M_s}\left(2 - \frac{5}{2}\sin^2\theta - \frac{15}{8}\sin^2 2\theta\right).$$

The relative anisotropy constant K_1/M_s was calculated with the aid of this equation. The spontaneous magnetization M_s varies relatively little (10%) between room temperature and liquid-helium temperature, so that the temperature variation of the ratio K_1/M_s represents, qualitatively, the variation of the crystallographic anisotropy constant K_1 with temperature. The table shows values of K_1/M_s and also of M_s and g for a single crystal at different temperatures.

T, °K	K_1/M_s	M_s, G	g
300	40	136	1.89±0.02
77	110	160	1.90±0.02
20,4	263	160	1.97±0.02
4.2	286	160	1.98±0.02
2,0	328	—	1,99±0.02

It can be seen that in the region of hydrogen and helium temperatures there is a rapid increase in the anisotropy constant, compared with its value at room temperature (8 — 9 times). The existence of such a rapid change in K_1 is confirmed by the small slope of the magnetization curves in this temperature region, which we measured on polycrystalline specimens (toroidal) of YIG (see Fig. 4).

2. THE TEMPERATURE DEPENDENCE OF THE FERROMAGNETIC RESONANCE ABSORPTION LINE WIDTH

Our measurements showed that there is practically no anisotropy in the ferromagnetic resonance absorption line width not only at room tem-

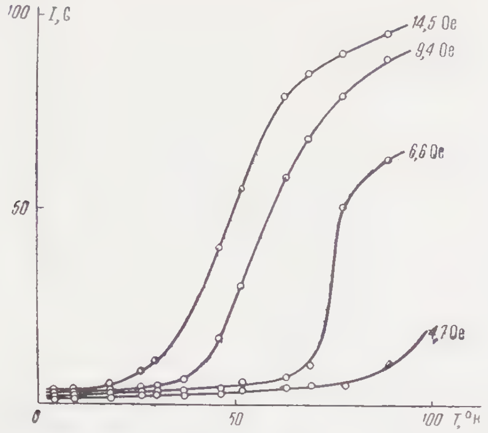

FIG. 4. Magnetization curves, I(T), measured in weak fields on polycrystalline YIG in the low temperature region.

perature but also at helium temperatures. The measured temperature dependence of the line width for a single crystal (at different orientations) and also for a polycrystalline specimen is shown in Fig. 5 in relative units $\Delta H/\Delta H_R$ (H_R is the line width at room temperature) for the range 2 — 300°K.

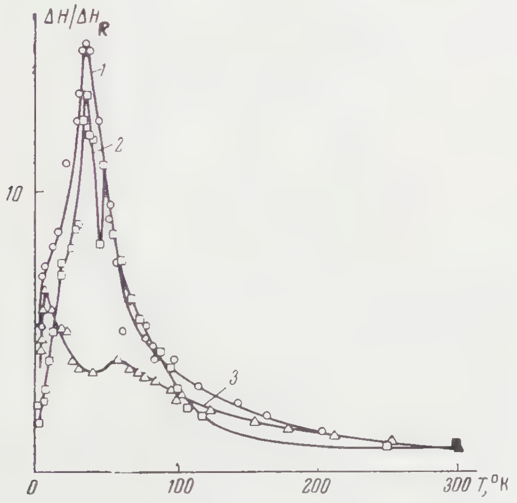

FIG. 5. The temperature dependence of the ferromagnetic resonance absorption line width in YIG, in relative units. Curves 1 and 2 are for single crystals of different orientations, curve 3 is for a polycrystalline specimen.

ΔH can be seen to increase on lowering the temperature. The line width for a single crystal has sharp maxima between 20 and 40°K, similar to those measured by Dillon[1] and by Spencer et al.[2] The line width at 40°K has increased to more than 15 times its room temperature value. These maxima are smaller for a polycrystalline specimen and they are spread out over a fairly wide temperature interval (40 — 60°K). Since the magnetic anisotropy constant changes smoothly at low temperatures (there are neither minima nor maxima on the curve) it follows that the mechanism of the anomalous broadening of the absorption line at low temperatures found in polycrystalline YIG is not connected with the magnetic anisotropy. According to Dillon[1] and to Spencer et al.[2] the appearance of the anomalous maxima on the ΔH(T) curves is due to the presence of rare earth impurities in the YIG. It appears that a terbium impurity in even insignificant amounts has an exceptionally strong influence.

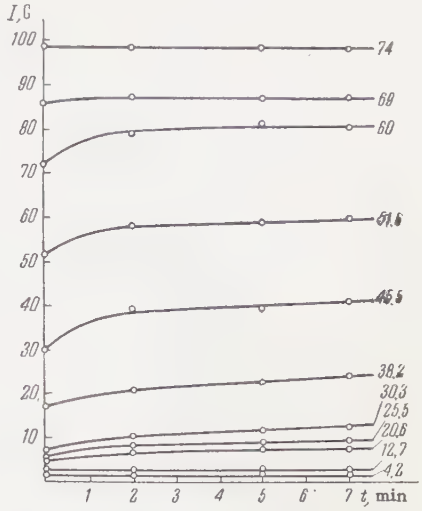

FIG. 6. Curves showing the establishment of magnetization with time for polycrystalline YIG specimens in the low temperature region (in a field of H = 9.4 oe). The numbers against the curves show the temperature in °K.

According to Kittel,[3] ions of rare earth impurities in the YIG sublattices have a short relaxation time, which produces a mechanism of line broadening which dominates other broadening mechanisms at low temperatures. There may also appear relaxation phenomena at low temperatures connected with rare earth impurity ions which influence the course of the magnetization at low temperatures. We found that in the range 20 — 60°K magnetization was not achieved immediately on applying the field, but after 5 — 6 minutes, i.e., there is a large magnetic viscosity in this temperature range in YIG (see Fig. 6).

In conclusion, we express our thanks to Professor A. I. Shal'nikov for his interest in our work and for his valued advice, and to V. A. Timofeeva for providing the YIG single crystals for our experiments.

---

[1] J. F. Dillon, Phys. Rev. **111**, 1476 (1958).

[2] Spencer, Le Craw, and Clogston, Phys. Rev. Letters **3**, 32 (1959).

[3] de Gennes, Kittel, and Portis, Phys. Rev. **116**, 323 (1959).

[4] V. A. Timofeeva, Кристаллография **5**, 476 (1960), Soviet Phys.-Crystallography **5**, 453 (1960).

Translated by R. Berman
284

SOVIET PHYSICS JETP VOLUME 12, NUMBER 6 JUNE, 1961

ELECTRON PARAMAGNETIC RESONANCE IN ANDALUSITE

A. L. BIL'DYUKEVICH, V. M. VINOKUROV, M. M. ZARIPOV, Yu. E. POL'SKIĬ, V. G. STEPANOV, G. K. CHIRKIN, and L. Ya. SHEKUN

Kazan' State University

Submitted to JETP editor July 2, 1960

J. Exptl. Theoret. Phys. (U.S.S.R.) **39**, 1548-1551 (December, 1960)

Electron paramagnetic resonance of Fe^{3+} ions which isomorphously replace the Al^{3+} ions in natural crystals of andalusite Al_2SiO_5 has been observed at frequencies from 9000 to 37000 Mc/sec. The spectrum is interpreted with the aid of a spin Hamiltonian of the form (2). Two magnetically nonequivalent ions exist, whose z axes lie in the plane of the ab axes and form and angle of 57.9° with each other.

THE CRYSTAL STRUCTURE

ANDALUSITE is one of the polymorphous modifications of Al_2SiO_5. In natural single crystals of andalusite a small portion of the aluminum ions is replaced by Fe^{3+} ions.[1] Andalusite crystalizes in a rhombic syngony, with a space group Pnnm. The unit-cell parameters are: $a_0 = 7.77$ A, $b_0 = 7.91$ A, and $c_0 = 5.57$ A. The unit cell contains four (Al_2SiO_5) molecules (reference 2).

The data of x-ray structure analysis (cf. Fig. 1) indicate that four of the Al^{3+} ions are surrounded by 5 oxygen ions, and the other four are surrounded by six oxygen ions (octahedron).

We have assumed that the Fe^{3+} ions replace in the main Al^{3+} ions that are surrounded by 6 oxygen ions. The experiment confirms this assumption, and therefore in the following we shall discuss Al^{3+} ions surrounded by 6 oxygen ions. These aluminum ions, in turn, are divided into two types which we shall designate I and II. If, for example, the Al1 ion will be classified as type I, then the ions Al2, Al3, Al4, and Al5 will be classified as type II, and vice versa.

From the data of the x-ray structure analysis it follows that the surrounding of the I ion coincides with the surrounding of the II ion if it is translated and then rotated by 59.37° about the crystallographic c axis. Thus, we are dealing here with two identical but differently oriented coordination polyhedra, so that it is sufficient to consider in more detail the vicinity of any one ion, for instance Al1.

The oxygen ions O6, O7, and O8 are located at distances of 1.884 A, 1.961 A, and 2.236 A from the Al1 ion. The distances O7 — O10, O6 — O7, and O6 — O11 are not equal. The quadrilateral formed by the O6, O7, O10, and O11 ions is not plane. Here there exists only one twofold symmetry axis which coincides with the c axis of the crystal. The electric field of such an ion system should have rhombic symmetry. The large stretching of the polyhedron allows us to assume that the component of the electric field along the O8 — O9 direction will be large.

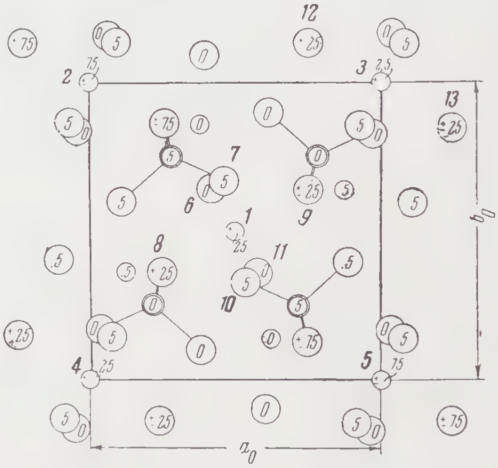

FIG. 1. The crystal structure of andalusite. The large circles represent oxygen, the small circles aluminum, and the double circles silicon.

THE ELECTRON PARAMAGNETIC RESONANCE SPECTRUM

The electron paramagnetic resonance spectra were observed at room temperature at 9000, 15,000, and 37,000 Mc/sec. The results of experiments at 9000 Mc/sec for the case when the constant magnetic field **H** lies in the ab plane are given in Fig. 2. It is seen that the experimental points straddle the curves given by

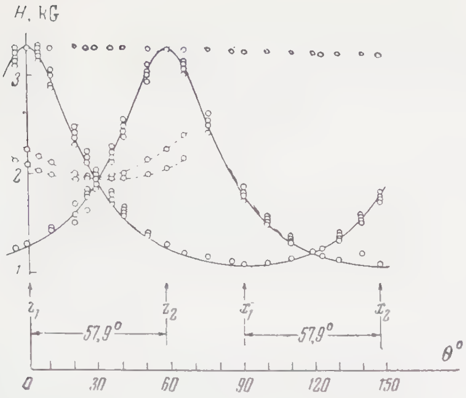

FIG. 2. Paramagnetic resonance in andalusite at 9000 Mc/sec. The solid lines are curves given by formula (1). The line of points in the upper part of the diagram represents the resonance field of the free radical.

$$H \sim (9\sin^2\vartheta + \cos^2\vartheta)^{1/2}, \tag{1}$$

displaced relative to each other by an angle of 57.9°.

Such an angular dependence is obtained in a case when we have an Fe^{3+} ion in an axial electric field, and the Zeeman energy is small compared with the energy of the ion in the electric field. We therefore described the spectrum with the aid of the spin Hamiltonian of the form[3]

$$\mathcal{H} = DS_z^2 + \beta[g_\perp(H_xS_x + H_yS_y) + g_\parallel H_zS_z] \tag{2}$$

with an effective spin $5/2$. The z axes of ions of type I (z_1) and II (z_2) lie, within the limits of experimental error, in the ab plane and form an angle of 57.9°. We can thus conclude that the z_1 and z_2 axes are very near to the O8 — O9 and O12 — O13 directions, which form an angle of 59.37°.

The spectrum at 15000 Mc/sec does not differ from the spectrum at 9000 Mc/sec. At 37000 Mc/sec a small deviation, which shall be discussed below, is observed.

DETERMINATION OF THE CONSTANTS OF THE SPIN HAMILTONIAN

The ground level of the Fe^{3+} ion in an axially symmetric electric field splits into three doublets with $M = \pm 5/2, \pm 3/2$, and $\pm 1/2$. When a constant magnetic field is applied along the z axis the doublets split linearly, so that there appear $\pm \frac{5}{2} g_\parallel \beta H$, $\pm \frac{3}{2} g_\parallel \beta H$, and $\pm \frac{1}{2} g_\parallel \beta H$ levels. One notices readily that the transitions within the $\pm 3/2$ and $\pm 5/2$ doublets are forbidden. If the magnetic field is perpendicular to the z axis, then the $\pm 5/2$ and $\pm 3/2$ doublets begin to split quadratically, and a very large field is required to observe resonance on these doublets. Thus, the peak observed in weak fields is due to the $\pm 1/2$ doublet.

To determine the constants of the Hamiltonian, we calculated the splitting $\Delta\epsilon$ of the $\pm 1/2$ doublet with the aid of perturbation theory, assuming that $g\beta H \ll D$. Taking into account the second and third approximations, we obtain the result

$$\Delta\varepsilon = \sqrt{9h_x^2 + h_z^2}\left(1 - \frac{h_x^2}{2D^2}\,\frac{9h_x^2 - 2h_z^2}{9h_x^2 + h_z^2}\right). \tag{3}$$

Here, $h_x = g_\perp \beta H_x$, $h_z = g_\parallel \beta H_z$; H_y was set equal to 0.

Measurements at 9000 and 15000 Mc/sec have shown that the correction containing D is rather small, and cannot be determined, so that one can only find the g factors:

$$g_\parallel = g_\perp = 2.004 \pm 0.001.$$

In this case $\Delta\epsilon \sim (9\sin^2\vartheta + \cos^2\vartheta)^{1/2}$ (the angle ϑ is measured from the z axis) which yields the result shown in Fig. 2.

At 37000 Mc/sec the correction containing D begins to have an effect, and we have found that $D \approx 1.8\ \mathrm{cm}^{-1}$. Thus, the distance between the $\pm 1/2$ and $\pm 3/2$ doublets should amount to about $3.6\ \mathrm{cm}^{-1}$, To obtain a more precise value of D and to estimate the errors measurements of frequencies exceeding 37000 Mc/sec are required.

As can be seen from Fig. 2, at angles ϑ other than 0 and 90°, the absorption line of each ion splits up into four closely located peaks. This splitting, which is not described by the Hamiltonian (2) is apparently connected with a small nonequivalency of ions belonging to the same type. The determination of the corrections to the Hamiltonian (2) to account for this nonequivalency requires additional investigation.

TRANSITION PROBABILITIES

The wave functions of the states between which the observed transitions take place can be written in the form

$$\Psi_1 = \cos\alpha\,|1/2\rangle + \sin\alpha\,|-1/2\rangle,$$

$$\Psi_2 = \sin\alpha\,|1/2\rangle - \cos\alpha\,|-1/2\rangle.$$

Here α is an auxiliary angle determined by the relation

$$\tan\alpha = \{(9\sin^2\vartheta + \cos^2\vartheta)^{1/2} - \cos\vartheta\}/3\sin\vartheta.$$

The probability of the transition is proportional to

$$w = |\gamma_1\langle 1|S_x|2\rangle + \gamma_2\langle 1|S_y|2\rangle + \gamma_3\langle 1|S_z|2\rangle|^2, \tag{4}$$

where γ_1, γ_2, and γ_3 are the direction cosines of the alternating magnetic field H_1. The matrix elements in (4) are:

$$\langle 1|S_x|2\rangle = -{}^3/_2 \cos 2\alpha, \qquad \langle 1|S_y|2\rangle = {}^3/_2 i;$$
$$\langle 1|S_z|2\rangle = {}^1/_2 \sin 2\alpha. \qquad (5)$$

The experimentally observed line intensities are in agreement with formulas (4) and (5). Thus, for instance, if $H \parallel z$ and $H_1 \parallel x$, then $w = 2.25$. If, however, $H \parallel x$ and $H_1 \parallel z$, then $w = 0.25$ (for the free Fe^{3+} ion $w = 8.75$).

CONCLUSION

Andalusite is the only investigated ionic crystal in which the Fe^{3+} ion has a Stark splitting exceeding 3 cm^{-1}. Such a large splitting has thus far been observed only in hemoglobin[4] (molecular crystal) and in glasses.[5] A possible reason for the large splitting is the strong stretching of the nearest vicinity of the Fe^{3+} ion. For the same reason the non-axial terms in the Hamiltonian are probably only small corrections.

In addition to the above absorption lines, the spectrum contains other weak peaks whose angular dependence (shown in Fig. 2 by a dotted curve) does not make it possible to refer them to ions of types I and II. These peaks are possibly due to ions surrounded by five oxygen atoms.

In conclusion, the authors express their deep gratitude to S. A. Al'tshuler for interest and attention to their work.

---

[1] A. G. Betekhtin, Минералогия (Mineralogy), 1950, p. 701.

[2] R. W. G. Wyckoff, The Structure of Crystals, 1957.

[3] A. Abragam and M. H. L. Pryce, Proc. Roy. Soc. **A205**, 135 (1951).

[4] J. E. Bennett and D. J. E. Ingram, Nature **177**, 275 (1956).

[5] Castner, Newell, Holton, and Slichter, J. Chem. Phys. **32**, 668 (1960).

Translated by Z. Barnea
285

SOVIET PHYSICS JETP VOLUME 12, NUMBER 6 JUNE, 1961

PARAMAGNETIC RESONANCE OF Mn^{2+} *IN DOLOMITE AND MAGNESITE*

V. M. VINOKUROV, M. M. ZARIPOV, and V. G. STEPANOV

Kazan State University

Submitted to JETP editor July 2, 1960

J. Exptl. Theoret. Phys. (U.S.S.R.) **39**, 1552-1553 (December, 1960)

The hyperfine structure spectrum of the electron paramagnetic resonance of Mn^{2+} in dolomite and magnesite has been studied both experimentally and theoretically. The values of the parameters of the spin Hamiltonian describing the position of the lines in the spectrum have been determined.

THE hyperfine structure of paramagnetic resonance of Mn^{2+} in dolomite $CaMg(CO_3)_2$ and magnesite $MgCO_3$ has been observed at room temperature at frequencies of $\sim 9 \times 10^9$ cps. Natural single crystals of dolomite and magnesite with a manganese contents of ~0.1 and 0.1% respectively were used in the investigation. The crystal structure of these minerals has a trigonal symmetry. The immediate surrounding of the Mn^{2+} ions which replace Mg and Ca isomorphously in these substances is an octahedron formed by six $(CO_3)^{2-}$ groups. This octahedron is deformed along the three-fold axis which coincides with the L_3 axis of the crystal.

We studied the spectra for $\mathbf{H} \parallel L_3$ and $\mathbf{H} \perp L_3$. Corresponding to the fact that the ground state of Mn^{2+} is $^6S_{5/2}$ and the spin of the Mn^{55} nucleus is $I = 5/2$, we observed 30 fundamental absorption lines with the expected intensity relations in each of the indicated orientations. In addition, lines of considerably lower intensity were observed in dolomite for $\mathbf{H} \parallel L_3$. In dolomite Mn^{2+} ions can isomorphously replace both the Ca^{2+} and the Mg^{2+}. It is known[1] that in this particular case the magnesium atoms are more readily displaced by manganese than the calcium atoms. On the basis of this we assume that the main absorption lines are due to the Mn^{2+} ions replacing the Mg^{2+}, and the additional lines are due to the Mn^{2+} ions replacing the calcium.

The spectra are described by the following spin Hamiltonian

$$\mathcal{H} = g\beta \mathbf{HS} + D\left[S_z^2 - \frac{1}{3}S(S+1)\right] + \frac{a}{6}[S_\xi^4 + S_\eta^4 + S_\zeta^4]$$
$$+ \frac{F}{180}[35\,S_z - 30\,S(S+1)\,S_z^2 + 25S_z^2 - 6S(S+1)$$
$$+ 3S^2(S+1)^2] + AS_zI_z + B(S_xI_x + S_yI_y).$$

Here $\mathbf{z} \parallel L_3$ is also the [111] direction in the ξ, η, ζ system.

For Mn^{2+} ions replacing Mg^{2+} in dolomite:

$$g = 2.003, \quad D = \pm 153.2 \text{ gauss}, \quad a - F = \mp 10.4 \text{ gauss},$$
$$A = \pm 93.4 \text{ gauss}, \qquad B = \pm 94.3 \text{ gauss};$$

for Mn^{2+} ions replacing Ca^{2+} in dolomite:

$$g = 2.003, \qquad 2D - \tfrac{2}{3}(a - F) = \pm 11 \text{ gauss},$$
$$A = \pm 93.4 \text{ gauss};$$

for magnesite:

$$g = 2.001, \quad D = \pm 85.5 \text{ gauss}, \quad a - F = \mp 12.1 \text{ gauss},$$
$$A = \pm 92 \text{ gauss}, \qquad B = \pm 93 \text{ gauss}.$$

The calculated values H_{res} in dolomite agree with the experimental values within the limits of ±3 gauss, and in magnesite within the limits of ±1 gauss. It turned out impossible to determine D and a − F separately for the Mn^{2+} ions replacing Ca^{2+} in dolomite, because the lines of the $\pm 3/2$, m $\leftrightarrow \pm 1/2$, m transitions coincide with the $+1/2$, m $\leftrightarrow -1/2$, m lines (m is the magnetic quantum number of the nuclear spin moment).

---

[1] Dana, Dana, Palache, Berman, and Frondel, System of Mineraolgy, v. II, Russ. Transl. IIL 1953, p. 252.

Translated by Z. Barnea
286

SOVIET PHYSICS JETP VOLUME 12, NUMBER 6 JUNE, 1961

SUPERCONDUCTIVITY OF CRYSTALLINE MODIFICATIONS OF BISMUTH

N. B. BRANDT and N. I. GINZBURG

Moscow State University

Submitted to JETP editor July 8, 1960

J. Exptl. Theoret. Phys. (U.S.S.R.) **39**, 1554-1556 (December, 1960)

The critical temperature T_c for the superconducting modification Bi III has been determined, it is found to equal 7.25° K for pressures $25{,}000 < p < 29{,}000$ atm. Superconductivity of the modification Bi II has been discovered with $T_c = 3.93°$ K ($p = 25{,}000$ atm). The derivative $\partial T_c/\partial p$ for Bi III is negligibly small; for Bi II $\partial T_c/\partial p \approx -3.5 \times 10^{-5}$ °K/atm. The stability of the Bi II and Bi III modifications has been investigated at liquid helium temperatures.

THE pT phase diagram (p = pressure, T = temperature) for bismuth[1] is shown in Fig. 1. As is well known,[2] Bi III is a superconductor with a critical temperature $T_c \sim 7°$ K. Since, however, the method employed by Chester and Jones[2] did not permit the attainment of adequately uniform pressures, the critical temperature for the superconducting modification Bi III was determined only approximately, while the Bi II modification was not investigated at all. It appeared, therefore, of interest to investigate superconductivity in the Bi II and Bi III modifications in greater detail, and also to investigate the stability of these modifications at helium temperatures.

A method previously described in detail[3] was employed for production of pressure. The monocrystalline bismuth sample 1 (Fig. 2) and a monocrystalline sample of tin 2, both covered with a layer of graphite lubricant, were placed within a sturdy yoke 3. The samples were compressed by a piston which transmitted pressure from the upper chamber of the multiplier or press, located in the liquid helium bath.* The transition of the samples into the superconducting state was indicated by a change in the mutual inductance of the coils 5 and 6.[4] The magnitude of the pressure p was determined from the displacement of the critical temperature of the tin specimen 2. The value of $\partial T_c/\partial p$ for tin was taken to be[5] 4.5×10^{-5} deg/atm. Above 4.2° K the temperature was determined with the aid of a carbon resistor 7, which was calibrated against the superconducting transition temperature of a sample of lead 8, taken equal to 7.22° K.

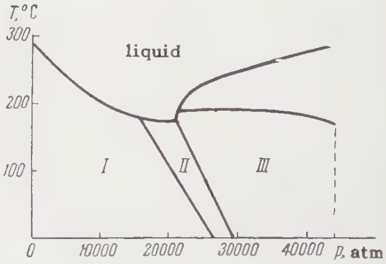

FIG. 1. Pressure-temperature phase diagram for bismuth.

The maximum inhomogeneity in the pressure, estimated from the width of the superconducting transition curves for the lead, did not exceed 1 - 2%. It was found that the Bi II and Bi III modifications are superconductors with critical temperatures, respectively, of 3.93° K (at $p = 25{,}000$ atm) and 7.25° K ($25{,}000 < p < 29{,}000$ atm) (Fig. 3). For Bi II, $\partial T_c/\partial p$ was approximately -3.5×10^{-5} deg/atm, while for Bi III it was negligibly small.

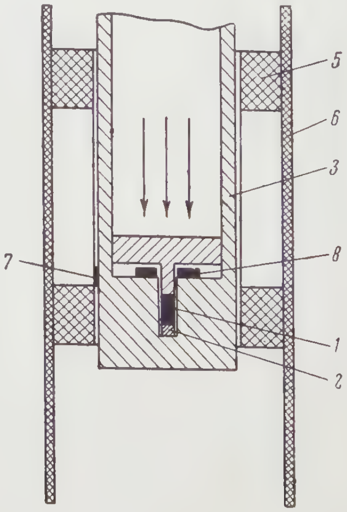

FIG. 2. Diagram of apparatus for production of high pressure.

---

*We take this opportunity to thank N. E. Alekseevskiĭ for his generous loan of the press.

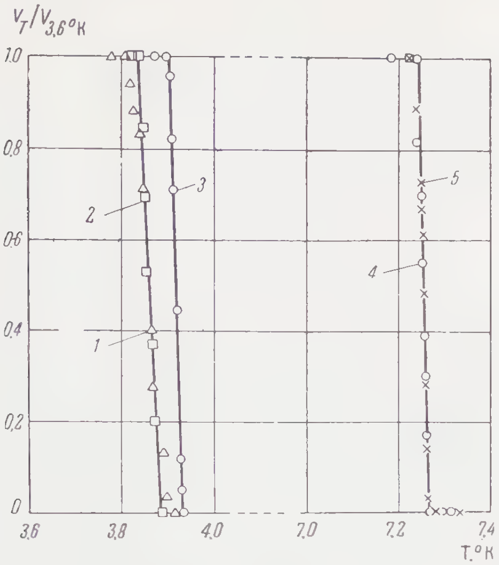

FIG. 3. Superconducting transition curves for the crystalline modifications Bi II (curves 1, 2, 3) and Bi III (4, 5): 1 – p = 26,800 atm; 2 – p = 26,600 atm; 3 – p = 25,000 atm; 4 – p = 27,000 atm.

In order to determine the stability of the superconducting modifications of bismuth in the helium temperature region, experiments were carried out in which pressure applied at room temperature was removed and reapplied at liquid helium temperatures.

Upon removal of pressure at helium temperatures the Bi II modification always transformed into the Bi I modification. The Bi III modification produced by compression of the monocrystalline bismuth sample transformed, upon removal of the pressure (T ~ 2.2° K), into the non-superconducting Bi I modification in the pressure region about 20,000 atm, which indicates the presence of strong hysteresis in the transition in the helium temperature region. Upon repeated compression of one and the same sample, a polycrystalline structure of small dispersion appeared. In these cases the superconducting modification persisted upon removal of the pressure, and transformed into the non-superconducting Bi I modification at a temperature of 6.5 – 7.5° K.

It may be suggested that the superconductivity of bismuth films sputtered at liquid-helium temperature[6,7] is associated with the formation of a crystalline modification analogous to Bi III. Nor is the possibility excluded that carbon sputtered on a diamond substrate cooled to liquid helium temperature, will crystallize in a diamond structure.

In conclusion, we take this opportunity to express our thanks to A. I. Shal'nikov and N. E. Alekseevskiĭ for their interest in this work, and to S. G. Obruchnikov for the high quality of his machine work.

---

[1] F. P. Bundy, Phys. Rev. **110**, 314 (1958).

[2] P. F. Chester and G. O. Jones, Phil. Mag. **44**, 1281 (1953).

[3] N. B. Brandt, P. T. É. **2**, 131 (1960).

[4] Alekseevskiĭ, Brandt, and Kostina, Izv. Akad. Nauk. U.S.S.R., Ser. Fiz. **16**, 233 (1952).

[5] D. H. Bowen and G. O. Jones, Proc. Roy. Soc. **A254**, 522 (1960).

[6] R. Hilsch, Rec. Intern. Conf. on Low Temperature Phys., Oxford, 1951, p. 119.

[7] N. V. Zavaritskiĭ, Doklady Akad. Nauk U.S.S.R. **91**, 787 (1953).

Translated by S. D. Elliott
287

SOVIET PHYSICS JETP VOLUME 12, NUMBER 6 JUNE, 1961

EFFECT OF NUCLEON BINDING ON THE SHAPES OF PION ENERGY SPECTRA

V. G. VOVCHENKO, G. GEL'FER, A. S. KUZNETSOV, M. G. MESHCHERYAKOV, and V. SVYATKOVSKIĬ

Joint Institute for Nuclear Research

Submitted to JETP editor July 9, 1960

J. Exptl. Theoret. Phys. (U.S.S.R.) 39, 1557-1570 (December, 1960)

A comparative investigation of the π^+ and π^- spectra produced by 654-Mev protons in free p-p collisions, and in p-p and p-n collisions in deuterons and carbon nuclei, has been carried out with a magnetic spectrometer. The observed difference between the shapes of pion spectra from deuterium and carbon is due to a) a higher degree of nucleon-pair correlation in carbon than in deuterons, b) differences in the nucleon momentum distribution, and c) secondary pion-nucleon interactions in carbon. The ratios 1 : 0.79 : 0.40 have been obtained for the differential cross sections for π^+ production on free protons and on protons in D and C at ~ 90° in the c.m. system of the two colliding nucleons. The π^- yields from D and C per neutron of the target nucleus are approximately equal. At the given angle the ratio of π^+ to π^- yield from D and C is 10.3 ± 1.3 and 6.0 ± 0.8, respectively. The difference is attributed to an appreciable contribution from the secondary exchange interaction $\pi^0 + n \rightarrow \pi^- + p$ to the π^- yield from carbon.

1. INTRODUCTION

THE differences between the elementary pion-production processes involved in the collisions of nucleons with free and with bound nucleons are not well understood. These differences, which undoubtedly exist, can be attributed to such obvious factors as internal motion and mutual shielding of nucleons, the Pauli exclusion principle for recoil nucleons, and meson reabsorption in initial nuclei, and also to specific effects associated with nuclear deformation and the overlapping of meson shells in groups of tightly correlated nucleons.

The present paper describes experiments undertaken for the purpose of obtaining quantitative information regarding the effect of nucleon binding in deuterons and carbon nuclei upon processes of charged-pion production. We approached the problem by comparing the shapes of energy spectra for pions produced in proton collisions with free protons and with nucleons bound in deuterons and carbon nuclei. Our experimental procedure insured the obtaining of pion spectra under strictly identical conditions and the discrimination of effects due to p-p and p-n collisions, respectively.

Experiments performed at 460, 660,[1,2] and 970 Mev[3] showed that p-d collisions without pion production represent mainly the quasi-elastic scattering of protons by individual nucleons in deuterons; this bears a general resemblance to proton scattering by free nucleons. An incident proton seldom reacts simultaneously with both nucleons of a deuteron. These triple collisions represent p-d scattering, with the differential cross section $\sim 10^{-29}$ cm^2/sr at large angles for 460 and 660 Mev.

In virtue of the proton-nucleon character of high-energy p-d collisions, possible reactions involving single-pion production in these collisions are

$$p + p + (n) \rightarrow \pi^+ + p + n + (n), \tag{1}$$

$$p + p + (n) \rightarrow \pi^0 + p + p + (n), \tag{2}$$

$$p + n + (p) \rightarrow \pi^+ + n + n + (p), \tag{3}$$

$$p + n + (p) \rightarrow \pi^0 + p + n + (p), \tag{4}$$

$$p + n + (p) \rightarrow \pi^- + p + p + (p). \tag{5}$$

Here (n) and (p) denote nucleons that are not struck directly by incident protons and that are therefore liberated with low energies. According to reference 3, "unstruck" protons in p-d collisions at 970 Mev are emitted with the probable energy of ~ 5 Mev, their angular distribution being weakly correlated with the primary-beam direction. Pions can also be produced in p-d collisions where either two or all three nucleons are bound in the final state, as follows:

$$p + p + (n) \rightarrow \pi^+ + d + (n), \tag{6}$$

$$p + n + (p) \rightarrow \pi^0 + d + (p), \tag{7}$$

$$p + d \rightarrow \pi^+ + H^3, \tag{8}$$

$$p + d \rightarrow \pi^0 + He^3. \qquad (9)$$

The same pion-production processes will evidently occur in collisions between protons and individual nucleons of carbon nuclei, the sole difference lying in the stronger effect of nuclear binding than in the p-d collisions.

2. EXPERIMENTAL PROCEDURE

The experiments were performed with the six-meter synchrocyclotron of the Joint Institute for Nuclear Research, using an internal unpolarized proton beam focused by quadrupole lenses and passed through a magnetic clearing field. In the measurements of charged-pion spectra from p-p and p-d collisions we used equipment for the prolonged storage of liquid hydrogen and for deuterium liquefaction. The target was a thin-walled cylinder 4 cm in diameter and 12 cm long, filled with liquid deuterium or liquid hydrogen. This vessel was placed inside a vacuum chamber cooled by liquid hydrogen, with an outer jacket cooled by liquid nitrogen. The densities of liquid deuterium and liquid hydrogen at the boiling point of liquid hydrogen were taken to be 0.169 and 0.0708 g/cm^2, respectively.[4] The empty cylinder produced less than 3% of the particle yield from hydrogen or deuterium. In the experiments with carbon the target was a 5×5 cm^2 graphite plate 3 mm thick. In order to minimize the deceleration losses of pions in graphite, the angle between the target and proton beam was such that the secondary particles to be analyzed emerged perpendicularly to the target.

The proton energy was 654 ± 5 Mev at the center of each target. The average deceleration losses of primary protons in hydrogen and deuterium were 1.4 and 1.7 Mev, respectively; the loss was 1.9 Mev in the carbon target. The losses of 150-Mev pions in hydrogen, deuterium, and carbon, averaged over the irradiated target volume, were 0.7, 0.8, and 0.5 Mev, respectively. At the target the proton flux in a beam of 2×3 cm^2 cross section was 2×10^8 protons/cm^2-sec.

The energy spectra of charged pions were measured with the magnetic spectrometer described in reference 5. As in the case of reference 5, two thin scintillation counters at the entrance of the spectrometer defined a beam of particles emitted at 56° from the primary-proton direction. In the case of the $p + p \rightarrow \pi^+ + d$ reaction this corresponds to a 90° emission angle in the center-of-mass system of the two colliding protons. Horizontal angular divergence of the analyzed beam was ± 2°. After traversing the spectrometer, particles were registered by a telescope consisting of four scintillation counters. The relative width $\Delta p/p$ of the momentum interval defined by the spectrometer scintillators in the solid angle 5×10^{-5} sr was about ± 3% for all measured momenta. The pion-registration threshold was 35 Mev. The way in which the mean momentum of particles traversing the spectrometer depended on the magnet current was determined from calibration measurements with simulation of trajectories by means of flexible conducting wires. The small admixture of secondary protons was separated from the pions by an absorber placed between the scintillators at the spectrometer exit. The muon and electron constituents of the beam passing through the spectrometer were determined from measurements of ranges in copper. The background of accidental coincidences was determined by means of delay lines for the different sets of counters; the selection of delay times took into account the temporal fine structure of the proton beam from the synchrocyclotron.

The measurements furnished corrections accounting for the decay of pions in flight as well as their deceleration and absorption in the target, scintillators, and absorber for removing secondary protons. Absolute values of the differential cross sections $d^2\sigma/d\omega dE$ were calculated to within 7% by comparing the pion yield with the yield of recoil protons from p-p scattering, which was also observed with the spectrometer. The differential cross section for elastic p-p scattering at 654 Mev at the laboratory angle 56° was taken to be $(6.7 \pm 0.35) \times 10^{-27}$ cm^2/sr, which corresponds to $(3.41 \pm 0.13) \times 10^{-27}$ cm^2/sr at the center-of-mass angle 120°.[6] Special control measurements detected no difference between the registration efficiency for 150-Mev pions and that for protons with the same energy.

Assuming that pions are produced in collisions of protons with individual nucleons in a nucleus, and neglecting the internal motion of nucleons in deuterons and carbon nuclei, the observed spectra were transformed to the c.m. system of two colliding nucleons. In this system the majority of pions from p-d collisions were emitted between 90° and 97°. In the case of p-C collisions the angular range was 88° to 110°.

3. RESULTS

A. Energy spectra of charged pions from p-p and p-d collisions. The observed energy spectra of positive and negative pions from p-p and p-d collisions, along with the statistical errors, are shown in Figs. 1 and 2. All additional errors associated with the determination of the absolute values of $d^2\sigma/d\omega dE$ and with the estimation of corrections to be introduced were taken into account in determining the differential cross sections $d\sigma/d\omega$ of the investigated pion-producing reactions. Below 70 Mev experimental data on spectrum shapes are not very reliable, because it is very difficult to determine the admixture of muons and electrons in this energy range.

If pion pair production in a single nucleon-nucleon interaction is extremely improbable, it can be assumed that π^- mesons result only from p-n collisions, whereas π^+ mesons are created in both p-p and p-n collisions. From charge symmetry the differential cross sections for the reactions $p + n \to \pi^+ + n + n$ and $p + n \to \pi^- + p + p$ are related by

$$\frac{d\sigma}{d\omega}[p+n\to\pi^+ + n + n]_\vartheta = \frac{d\sigma}{d\omega}[p+n\to\pi^- + p + p]_{180^\circ-\vartheta}, \tag{1}$$

where ϑ is the c.m. angle of pion emission. At $\vartheta = 90°$ the differential cross sections for the given reactions should be equal and the π^+ and π^- spectra should have similar shapes. We can therefore expect that when the π^- spectrum from the reaction (5) is subtracted from the observed combined π^+ spectrum from reactions (1), (3), and (6), the remainder represents the π^+ spectrum from only p-p collisions in deuterons.

The π^+ spectrum in Fig. 1 (dashed curve) extends to higher energies than the π^+ spectrum from free p-p collisions. The obvious cause, which is the motion of struck protons in deuterons, can account for the fact that the π^+ spectrum from p-p collisions in deuterons does not exhibit a peak from the reaction $p + p \to \pi^+ + d$, although a peak is observed clearly at 196 Mev in the case of free

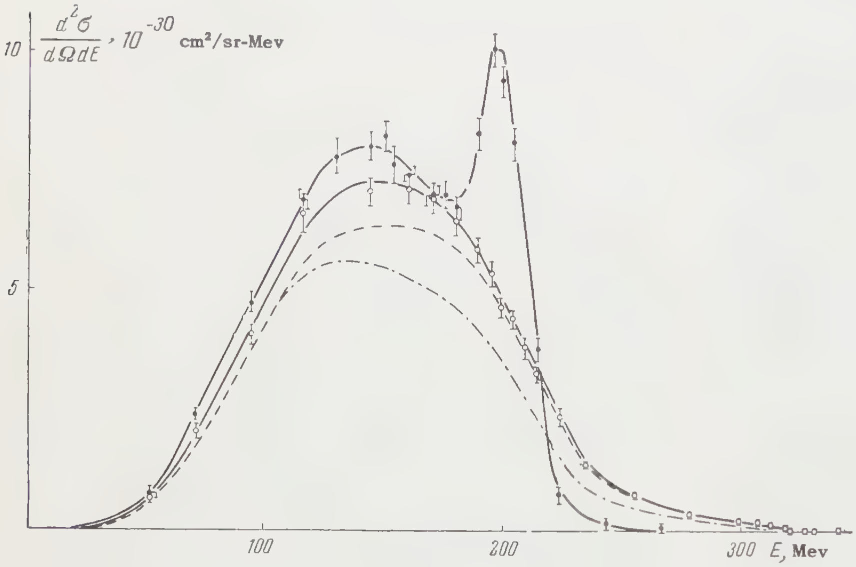

FIG. 1. Energy spectra of π^+ mesons measured at 56° from the 654-Mev proton beam: ● – from free p-p collisions, ○ – from p-d collisions. The dashed curve represents the π^+ spectrum from $[p\text{-}p]_D$ collisions alone, while the dash-dot curve isolates the contribution of the reaction $[p\text{-}p]_D \to \pi^+ + p + n$ in this spectrum.

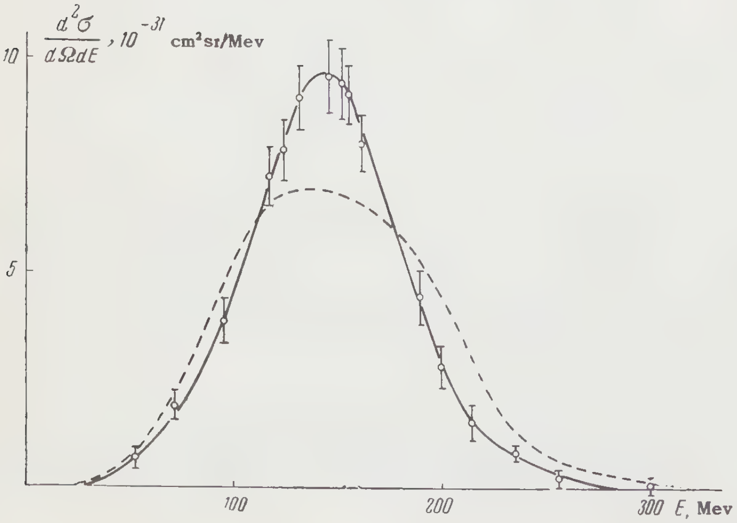

FIG. 2. Energy spectrum of π^- mesons from $[p\text{-}n]_D$ collisions at 56° from the 654-Mev proton beam. The dashed curve represents the π^+ spectrum from the reaction $[p\text{-}p]_D \to \pi^+ + p + n$, normalized to the same area as the π^- spectrum.

Table I. Differential cross sections for charged-pion production in p-p, p-d, and p-C collisions at 654 Mev, observed at 56° from the proton-beam direction (~ 90° in the c.m. system)

Process	Differential cross sections, 10^{-28}cm²/sr			
	$\frac{\partial\sigma+}{\partial\omega}$, 56° (l. s.)	$\frac{\partial\sigma-}{\partial\omega}$, 56° (l. s.)	$\frac{\partial\sigma+}{\partial\omega}$, ~90° (c. m. s.)	$\frac{\partial\sigma-}{\partial\omega}$, ~90° (c. m. s.)
$p+p\rightarrow\pi+$nucleons	10,2±1,0	—	6.7±0.7	—
$p+d\rightarrow\pi+$nucleons	9.1±0.9	0,88±0,12	5.9±0.6	0.57±0,08
$p+C\rightarrow\pi^{+}+$ nucleons	30.2±3,0	5.0±0.8	19,5±1,9	3.2 ±0.5

p-p collisions. Nevertheless, if the spectra of π^+ mesons formed on protons in deuterons and on free protons are normalized to the same area, and the contribution of the reaction p + p → π^+ + d is then subtracted from the π^+ spectrum associated with free p-p collisions, it is found that at the peak representing p + p → π^+ + d, the values of $\frac{d^2\sigma}{d\omega dE}[p + p + \pi^+ + \text{nucleons}]_D$ exceed those of $\frac{d^2\sigma}{d\omega dE}[p + p \rightarrow \pi^+ + p + n]_N$. This indicates that reaction (6) actually occurs in proton-proton collisions in deuterons.

The spread of the π^+ peak from the reaction p + p → π^+ + d on protons in deuterons as a result of intranuclear motion has been estimated by Prokoshkin,[7] who assumed that the nucleon momentum distribution in deuterons can be approximated by the Salpeter-Goldstein distribution[8] for an exponential potential.* His calculated π^+ spectrum from reaction (6) was normalized to the differential cross section $\frac{d\sigma}{d\omega}[p + p \rightarrow \pi^+ + d]_H$ for $\vartheta = 90°$, which is $(1.00 \pm 0.19) \times 10^{-28}$ cm²/sterad at 660 Mev,[9] and was subtracted from the π^+ spectrum for p-p collisions in deuterons. Figure 1 thus distinguishes the contributions of reactions (1) and (6) to the observed π^+ spectrum.

A comparison of the π^+ and π^- spectra from reactions (1) and (5), as in Fig. 2, shows that with increasing energy beyond the peak the π^- spectrum falls off more rapidly than the π^+ spectrum. This difference, which exceeds the limits of experimental error, can be accounted for if the reactions p + p → π^+ + p + n and p + n → π^- + p + p are not affected to the same degree by nucleon interactions in the final state. Indeed,† in the first of these reactions the dominant role is played by the isotopic-spin transition T = 1 → T = 0 from the initial to the final state of the two-nucleon system, leaving the neutron and proton in the ^{3}S state. Because of the strong interaction between nucleons in this state, they are emitted for the most part with small energies of relative motion; π^+ mesons consequently carry away an increased fraction of the energy. In contrast thereto, in the second reaction the transition T = 1 → T = 1 makes a considerable contribution, leaving the protons in ^{3}P states, where their interaction produces a less pronounced effect.

For π^+ mesons from p-d collisions the absence of a peak representing reaction (8) is not unexpected, since at 340 Mev[11] the total cross section for this reaction is only ~ 10^{-29} cm². From the π^+ yield near the upper boundary $E_\pi = 310$ Mev, where a π^+ peak from reaction (8) could have been expected, we can conclude that if reaction (8) does occur at 660 Mev, its differential cross section for π^+ emission at 56° from the proton beam does not exceed 5×10^{-30} cm²/sr.

Table I gives the differential cross sections for the production of charged pions in p-p and p-d collisions, integrated with respect to energy.

The cross section for π^+ production in free p-p collisions at 654 Mev for the c.m. angle ~ 90° is close to the value $(6.8 \pm 1.5) \times 10^{-28}$ cm²/sr in reference 12, but is considerably smaller than the result $(9.3 \pm 0.7) \times 10^{-28}$ cm²/sr reported in reference 13.

It follows from the data that for the c.m. angle 90° the π^+/π^- yield ratio from deuterium is 10.3 ± 1.3. If in nucleon-nucleon collisions pions were produced only by resonance interaction through the $J = T = 3/2$ state, the ratio of the total cross sections for π^+ and π^- production in p-d collisions would be $\sigma^+/\sigma^- = 11$.[14]

The total π^+ yield from p-p collisions in deuterium corresponds to the cross section

$$\frac{d\sigma}{d\omega}[p+p\rightarrow\pi^{+}+\text{nucleons}]_{D} = \frac{d\sigma}{d\omega}[p+d\rightarrow\pi^{+} + \text{nucleons}] - \frac{d\sigma}{d\omega}[p+d\rightarrow\pi^{-}+\text{nucleons}] = (5{,}30\pm 0{,}7)\cdot 10^{-28}\ \text{cm}^2/\text{sr}$$

The ratio of the differential cross sections for π^+

---

*Prohoshkin[7] also showed that the Salpeter-Goldstein momentum distribution for an exponential potential leads to an accurate prediction for the shape of the π^+ spectrum from the reaction $[p + p \rightarrow \pi^+ + p + n]_D$, using data regarding the π^+ spectrum from the same reaction on free protons.

†At 660 Mev the isotopic cross sections σ_{10}, σ_{11}, and σ_{01} are (10.9 ± 0.5), (3.22 ± 0.17), and $(1.7 \pm 1.1) \times 10^{-27}$ cm², respectively.[10]

production in collisions of protons with bound and free protons is therefore

$$\frac{d\sigma}{d\omega}[p+p\to\pi^+ + \text{nucleons}]_{\mathrm{D}} \Big/ \frac{d\sigma}{d\omega}[p+p\to\pi^+ + \text{nucleons}]_{\mathrm{H}} = 0.79\pm0.08.$$

Since the pion spectra from p-p and p-d collisions were measured with strictly identical geometry, the accuracy of this ratio depends only on the statistical errors in measurements of the pion yields and of muon and electron impurities.

B. Energy spectra of charged pions from p-C collisions. In the course of the present experiments it was found that the π^+ and π^- spectra from p-C collisions at energies below 250 Mev were measured with insufficient accuracy in reference 5. Figure 3 shows the new measurements of π^+ and π^- spectra and the statistical errors. It must be emphasized that for pion energies above 250 Mev our values for $d^2\sigma/d\omega dE$ agree, within error limits, with those given in reference 5, thus confirming the long tail extending beyond 350 Mev in the charged-pion spectrum from p-C collisions. On this basis the high-energy portions of the spectra in Fig. 3 were plotted from the combined results of the present experiments and those reported in reference 5, disregarding the small difference in incident-proton energy (654 Mev and 670 Mev, respectively).

Integration over energies furnished the differential cross sections for π^+ and π^- production on carbon nuclei, which are also given in Table I. In this case at ~ 90° (c.m.) the ratio of integrated π^+ and π^- yields is 6.0 ± 0.8. For p-C collisions we should also have had $\sigma^+/\sigma^- = 11$, if pion production took place only through the $J = T = 3/2$ state. We again followed the procedure of subtracting the π^- spectrum from the combined π^+ spectrum in order to isolate the effect of p-p collisions in carbon nuclei. The differential cross sections for π^+ (π^-) production in p-C collisions, per proton (neutron), are, respectively,

$$\frac{1}{Z}\left\{\frac{d\sigma}{d\omega}[p+\mathrm{C}\to\pi^+ + \text{nucleons}] - \frac{d\sigma}{d\omega}[p+\mathrm{C}\to\pi^- + \text{nucleons}]\right\} = (2.7\pm0.3)\cdot10^{-28}\ \mathrm{cm}^2/\mathrm{sr}$$

$$\frac{1}{N}\frac{d\sigma}{d\omega}[p+\mathrm{C}\to\pi^- + \text{nucleons}] = (0.53\pm0.08)\cdot10^{-28}\ \mathrm{cm}^2/\mathrm{sr}\ .$$

It will be clear from the sequel that the difference

$$\frac{1}{Z}\left\{\frac{d\sigma}{d\omega}[p+\mathrm{C}\to\pi^+ + \text{nucleons}] - \frac{d\sigma}{d\omega}[p+\mathrm{C}\to\pi^- + \text{nucleons}]\right\}$$

obtained in this manner can be equated approximately to $\frac{d\sigma}{d\omega}[\mathrm{p}+\mathrm{p}\to\pi^+ + \text{nucleons}]_{\mathrm{C}}$. $(1/\mathrm{N})\frac{d\sigma}{d\omega}[\mathrm{p}+\mathrm{C}\to\pi^- + \text{nucleons}]$ cannot be associated with the π^- yield from a single p-n collision in a carbon nucleus.

4. COMPARISON OF OBSERVED PION SPECTRA

In Fig. 4 the smooth experimental curves, which were represented in preceding figures, provide a comparison of the charged-pion spectra from the investigated collisions. All curves were normalized to the same area. Table II gives the mean pion energies and the energies at the spectral maxima. The maxima of all π^+ spectra and the maximum of the π^- spectrum from p-d collisions are found in approximately the same energy region. As could be expected, we observed pion spectra different in shape from the spectrum corresponding to only a single statistical weight of the final states. The maxima of spectra trans-

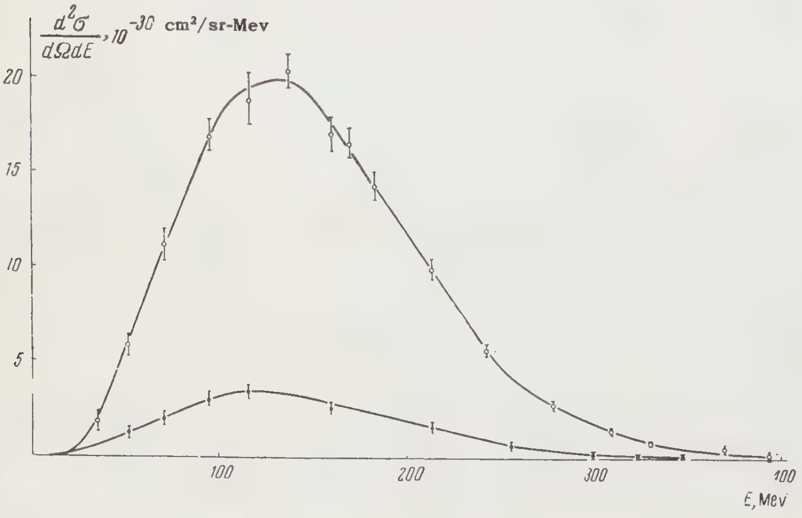

FIG. 3. Energy spectra of charged pions from p-C collisions at 56° from the 654-Mev proton beam: ○ – π^+ mesons, ● – π^- mesons.

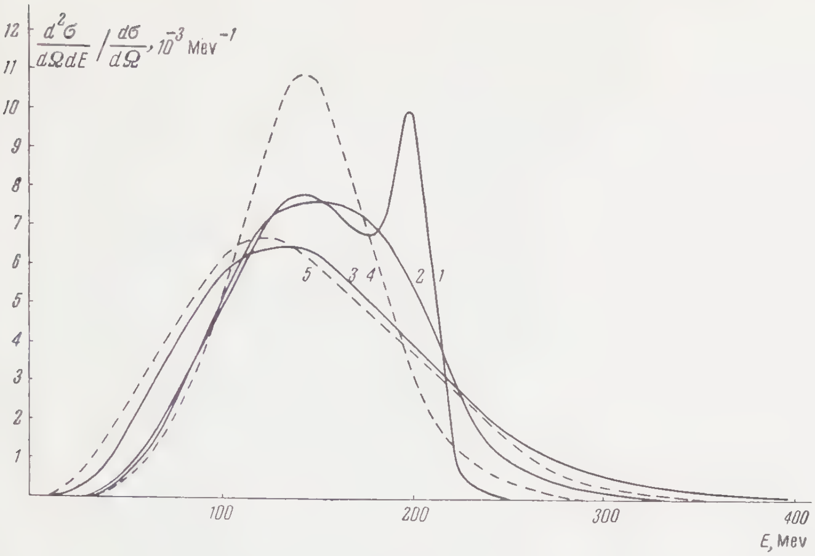

FIG. 4. Comparison of the energy spectra of charged pions: 1 – π^+ mesons from free p-p collisions, 2 – π^+ mesons from $[\text{p-p}]_D$ collisions, 3 – π^+ mesons from $[\text{p-p}]_C$ collisions, 4 – π^- mesons from $[\text{p-n}]_D$ collisions, 5 – π^- mesons from $[\text{p-n}]_C$ collisions. All spectra were normalized to the same area.

Table II. Data regarding energy spectra of charged pions from p-p, p-d, and p-C collisions*

Reaction	Energy at maximum of spectrum, Mev (l.s.)	Energy at maximum of spectrum, Mev (c.m.s.)	Mean pion energy, Mev (l.s.)	Mean pion energy, Mev (c.m.s.)
$[p+p]_H \rightarrow \begin{cases} \pi^+ + p + n \\ \pi^+ + d \end{cases}$	143 ± **	106 ± 6 **	—	—
$[p+p]_D \rightarrow \begin{cases} \pi^+ + p + n \\ \pi^+ + d \end{cases}$	145 ± 8	109 ± 8	151	116
$[p+n]_D \rightarrow \pi^- + p + p$	143 ± 5	107 ± 5	144	108
$[p+p]_C \rightarrow \pi^+ +$nucleons	132 ± 8	100 ± 5	148	114
$p+_C \rightarrow \pi^- +$nucleons	120 ± 12	87 ± 5	141	107

*The errors indicated in the second and third columns took spectrometer resolution and the experimental spread at the maximum into account.

**These values pertain only to the π^+ spectrum from the reaction $p + p \rightarrow \pi^+ + p + n$.

formed to the center-of-mass system of the two colliding nucleons correspond closely to the maximum of the curve representing the energy dependence of the total cross section for π^+-p scattering. This characteristic of pion spectra in nucleon-nucleon collisions is also exhibited for the given energy at a different angle of pion registration,[15] as well as at 1000 and 2300 Mev,[16] and indicates that a resonance interaction between a pion and nucleon in the J = T = 3/2 state plays an important part in pion production.*

The most obvious differences between the spectra under discussion are as follows:

1. The π^+ spectrum from p-p collisions in carbon extends considerably farther on the high-energy side than the π^+ spectrum from p-p collisions in deuterium. An analogous difference is observed between π^- spectra; a 300-Mev π^- yield from deuterium could not be detected, whereas the π^- yield from carbon extends to ~ 350 Mev. The different yields of high-energy pions in the given spectra result primarily from the fact that carbon is more strongly affected by the correlation of nuclear matter and therefore contains more high-momentum nucleons than deuterium.

2. The π^+ and π^- spectra from carbon are considerably broader than the corresponding spectra from deuterium, in accordance with the fact that the mean nucleon momentum in carbon nuclei is greater than that in deuterons. Since above 650 Mev the excitation curves for pion production in p-p and p-n collisions rise slowly, while below 650 Mev they drop rapidly, the efficiency of pion production on nucleons inside carbon nuclei must be somewhat less than in the case of free nucleons

---

*The shape of the observed pion spectrum from the reaction $p + p \rightarrow \pi^+ + p + n$ will be compared elsewhere with that predicted from the resonance model for pion production in nucleon-nucleon collisions.

or of nucleons bound in deuterons.* Table II shows that the internal motion of protons in deuterons and in carbon nuclei has no appreciable effect on the mean energy of pions in the spectra.

3. The real shift (~ 20 Mev) of the π^- maximum from carbon toward lower energy than the π^- maximum from deuterium considerably exceeds the difference between the shifts of these spectra resulting from Coulomb attraction between the pions and initial nuclei. This dissimilarity between the π^- spectra, which is much more pronounced than that between the corresponding π^+ spectra, cannot be explained easily if it is assumed that only p-n collisions produce π^- mesons in carbon nuclei.

A similar difficulty arises in connection with the differential cross sections for π^+ (π^-) emission in p-d and p-C collisions per proton (neutron) of the target nucleus, and also in connection with the difference between the π^+/π^- yield ratios of deuterium and carbon. The pertinent data are collected in Table III. For hydrogen, deuterium, and carbon the ratios of the differential cross sections for π^+ emission per proton are represented by

$$\frac{d\sigma}{d\omega}\,[p+p\rightarrow\pi^+]_{\mathrm{H}}:\frac{d\sigma}{d\omega}[p+p\rightarrow\pi^+]_{\mathrm{D}}:\frac{d\sigma}{d\omega}[p+p\rightarrow\pi^+]_{\mathrm{C}}$$

$$=1:0{,}79:0{,}40,$$

while for deuterium and carbon the differential cross sections for π^- emission per neutron agree within experimental error.

Table III. Differential cross sections for π^+ production in $[\text{p-p}]_{\text{H}}$, $[\text{p-p}]_{\text{D}}$, and $[\text{p-p}]_{\text{C}}$ collisions. Differential cross sections for π^- emission in p-d and p-C collisions per neutron. π^+/π^- yield ratios at ~ 90° (c.m. system)

	Collisions		
	$p+p$	$p+d$	$p+\mathrm{C}$
$\frac{1}{Z}\left[\frac{d\sigma^+}{d\omega}-\frac{d\sigma^-}{d\omega}\right]$, 10^{-28} cm²/sr	6,7 ± 0.7	5.3±0,7	2.7±0.3
$\frac{1}{N}\frac{d\sigma^-}{d\omega}$, 10^{-28} cm²/sr	—	0,57±0,08	0.53±0,08
$\left(\frac{d\sigma^+}{d\omega}\right)/\left(\frac{d\sigma^-}{d\omega}\right)$	—	10.3±1,3	6,0±0,8

The causes, in addition to the internal motion of nucleons, of reduced efficiency of pion production on bound nucleons are: 1) the exclusion principle for recoiling nucleons, 2) the mutual shielding of nucleons in deuterons or the absorption of incident protons in nuclear matter in the case of more complex nuclei, and 3) meson reabsorption in the initial nuclei. The efficiency of pion production in collisions between protons and free or bound nucleons, respectively, can differ in general if nuclear binding changes essentially the character of interference between the amplitudes of possible pion-nucleon states. Calculations show[7] that at 660 Mev a) the exclusion principle has very little effect on pion production in p-d and p-C collisions, and b) mutual nucleon shielding in deuterons reduces pion-production cross sections by only a few percent.

The reduced efficiency of pion-production on nucleons inside nuclei resulting from incident-proton absorption and pion reabsorption is given by[17,18]

$$F=\frac{1}{V}\int\exp\{-(k's'+k''s'')\}\,dV, \tag{I}$$

which is the probability, averaged over the nuclear volume V, that a pion will emerge from the nucleus in which it is created. Here s' is the distance traversed by the proton within the nucleus before pion creation, s'' is the distance traversed by the pion within the nucleus before its emergence, k' and k'' are the proton and meson absorption coefficients in nuclear matter. From the measured cross sections for nucleon-nucleus interactions over a broad energy range[19–23] we have the nuclear radius $R = 1.26\,A^{1/3}\times10^{-13}$ cm and $k' = 0.5\times10^{13}$ cm^{-1}. Values of k'' were estimated in the approximation of the quasi-deuteron model of pion capture in nuclei, using the expression

$$k''=\left(\Gamma\sigma\,[\pi^+ + d\rightarrow 2p]\,\frac{A}{2}\right)/V.$$

Below 150 Mev the cross section for the reaction $\pi^+ + d \rightarrow 2p$ was obtained by detailed balancing from the resonance curve for excitation of the inverse reaction $p + p \rightarrow \pi^+ + d$;[9] for higher energies the data of Neganov and Parfenov[24] were used. The normalization factor Γ, which is the factor by which the probability for the creation of correlated nucleon pairs in carbon nuclei exceeds that in deuterons, was derived by comparing the total cross sections for pion absorption in carbon at 62 and 125 Mev given in references 25 and 26, with the total cross sections for the reaction $\pi^+ + d \rightarrow 2p$ at these energies; the calculation yielded $\Gamma \approx 3.8$.

If only proton absorption, or only pion reabsorption, occurs, we know that[17]

---

*Prohoshkin[7] has estimated that at 660 Mev proton-nucleon collisions in deuterons are, because of nuclear motion, about 4% less efficient in pion production than collisions of protons with free nucleons.

$$F(x) = 3\,[1/2x - 1/x^3 + e^{-x}(1+x)/x^3], \tag{II}$$

where $x = 2Rk$. For proton absorption alone $F \approx 0.42$ in the case of carbon nuclei. This value of F is undoubtedly too low, because no account was taken of the fact that after a first collision some of the colliding nucleons have energies sufficient for pion production.

The combined effect of proton absorption and pion reabsorption can be estimated simply only for backward emission of pions, in which case F is expressed by (II) but with $x = 2R(k' + k'')$, and for forward pion emission,[27] in which case

$$F = \frac{3}{x' - x''}\left[\frac{1-(1+x'')\exp\{-x''\}}{x''^2} - \frac{1-(1+x')\exp\{-x'\}}{x'^2}\right], \tag{III}$$

where $x' = 2Rk'$ and $x'' = 2Rk''$, with $x' > x''$ even at the maximum energy on the excitation curve for the reaction $\pi^+ + d \rightarrow 2p$. F can also be calculated approximately for 56° emission with different pion energies; in this case F averaged over the pion energy spectrum has the value ~ 0.30.* This is in qualitative agreement with the fact that the observed π^+-production efficiency in p-p collisions is smaller for carbon than for hydrogen. The 20% lower efficiency of π^+ production in p-p collisions in deuterium compared with free p-p collisions evidently results mainly from the more considerable reabsorption of pions in the final three-nucleon system.†

Proton absorption and pion reabsorption in carbon must lead to identical relative reductions in the yields of positive and negative pions, if the proton and neutron distributions in the nucleus are identical. In this case the invariance of $(1/N) \times (d\sigma^-/d\omega)$ must be accounted for by assuming again that π^- production in carbon results not only from p-n collisions, but also from additional processes whose contribution compensates the reduced efficiency of p-n collisions that is brought about by proton absorption and pion reabsorption. Both pion production by pions and exchange scattering of pions on nucleons can serve as additional sources of π^- mesons. In the present experiments the first of these processes resulted in the disappearance of an extremely small number of pions with highest energies; secondary pions from this process were altogether unobservable because of the high registration threshold. It is easily seen that the exchange reactions $\pi^+ + n \rightleftarrows \pi^0 + p$ and $\pi^0 + n \rightleftarrows \pi^- + p$ led to a relative increase of the π^- yield.

We have attempted to evaluate exchange scattering of pions in carbon, using the customary charge-independent relationships a) between cross sections for different pion-nucleon scattering processes $(\sigma[\pi^+ + n \rightarrow \pi^0 + p] = \sigma[\pi^- + p \rightarrow \pi^0 + n] = {}^2\!/_9\,\sigma[\pi^+ + p \rightarrow \pi^+ + p])$, and b) between cross sections for π^+, π^0, and π^- production by protons on a nucleus with isotopic spin $T = 0$ $(\sigma^+ + \sigma^- = 2\sigma^0)$. We also assumed that pion production in nucleon-nucleon collisions inside a nucleus takes place only through the resonance $J = T = {}^3\!/_2$ state and that, consequently, in the case of carbon the cross sections for the production of positive, neutral, and negative pions must be in the ratios 11 : 6 : 1. The charge-exchange coefficient of pions with different energies in nuclear matter was found from the equation

$$k = \left(\gamma \cdot \frac{2}{9}\,\sigma\,[\pi^+ + p \rightarrow \pi^+ + p]\,\frac{A}{2}\right)/V,$$

where γ takes into account the changes of cross sections for pion-nucleon interactions that result from nuclear binding. We assumed $\gamma = 0.5$.* The probability that a pion with given energy undergoes charge exchange in a nucleus before leaving the nucleus can be represented by

$$W = 1 - \frac{\int \exp\{-[k's' + (k'' + k)s'']\}\,dV}{\int \exp\{-[k's' + k''s'']\}\,dV}.$$

A doubly approximate estimate indicates that in 56° emission the energy-averaged probability of charge exchange for a pion with the proper sign in carbon is about 0.12 to 0.16. When the energy-averaged probability of pion charge exchange is taken to be 0.14, and we take into account the fact that the π^- yield from the reaction $\pi^0 + n \rightarrow \pi^- + p$ is six times greater than the loss from the inverse reaction $\pi^- + p \rightarrow \pi^0 + n$, it is found that secondary exchange reactions in the initial nuclei increase the overall π^- yield by ~ 70% and reduce the π^+ yield by ~ 7%. This must cause some shift of the π^- spectrum from p-C collisions toward lower energies, and should fully compensate the reduced efficiency of π^- production in p-n collisions due to proton absorption and pion reabsorption, as a result of which the ratio σ^+/σ^- is reduced from 11 to 6. Confirmation of the fact that this situation is generally realized comes from the present experiments and from other experiments where $(d\sigma^+/d\omega)/(d\sigma^-/d\omega)$ was measured under similar conditions for different emission angles.[15,31]

---

*The very approximate character of such estimates results from difficulties in taking account of the diffuse nuclear surface, elastic pion scattering on bound nucleons, Coulomb interaction, etc.

†This conclusion is supported by the fact that in pion photoproduction on deuterons the probability of pion reabsorption in the final two-nucleon system is 10-20%.[28,29]

*According to reference 30, $\gamma \approx 0.5$ in the scattering of 300-Mev $\pi^\pm$ mesons on nucleons in helium. One cause of this large reduction in the cross sections for pion scattering by bound nucleons compared with free nucleons is the forbiddenness of collisions in which the struck nucleon is transferred to a momentum state already occupied by a similar nucleon.

5. CONCLUDING REMARKS

The present experiments have shown that as the nuclear binding of nucleons is strengthened when we pass from deuterium to carbon, there is a change of shape in the spectra of pions produced in these nuclei in p-p and p-n collisions at 654 Mev. There can be no doubt about the nucleon-nucleon character of all the considered primary pion-production processes, with the possible exception of the rare events when ingoing protons interact within a carbon nucleus with nucleons which at the instant of collision are bound to other nucleons in tightly correlated groups.

Our results furnish evidence that even in the case of light nuclei the π^+/π^- yield ratio is sensitive to secondary exchange reactions of pions in nuclear matter. Therefore measurements of this ratio do not provide a basis for conclusions regarding the properties of nucleon-nucleon systems in which pions were produced, such as the relative contributions of states in a p-n system with $T = 1$ or $T = 0$. The difference between the value of this ratio for the deuteron and for another nucleus containing equal numbers of protons and neutrons can be regarded as a measure of the extent to which, with increasing nuclear size and as a result of exchange reactions in nuclear matter, the pion current that is created with strong isotopic "polarization" in the primary p-p and p-n collisions becomes isotopically "depolarized."

---

[1] Meshcheryakov, Bogachev, Leksin, Neganov, and Piskarev, Proc. CERN Symposium **2**, 124 (1956).

[2] G. A. Leksin, JETP **32**, 440 (1957), Soviet Phys. JETP **5**, 371 (1957).

[3] Batson, Culwick, Klepp, and Riddiford, Proc. Roy. Soc. (London) **A251**, 233 (1959).

[4] D. B. Chelton and D. B. Mann, Cryogenic Data Book, UCRL-3421, 1956.

[5] Azhgireĭ, Vzorov, Zrelov, Meshcheryakov, and Petrukhin, JETP **34**, 1357 (1958), Soviet Phys. JETP **7**, 939 (1958).

[6] N. P. Bogachev and I. K. Vzorov, Dokl. Akad. Nauk SSSR **99**, 931 (1954).

[7] Yu. D. Prokoshkin, JETP **38**, 455 (1960), Soviet Phys. JETP **11**, 334 (1960).

[8] E. Salpeter and J. Goldstein, Phys. Rev. **90**, 983 (1953).

[9] M. G. Meshcheryakov and B. S. Neganov, Dokl. Akad. Nauk SSSR **100**, 677 (1955).

[10] A. F. Dunaĭtsev and Yu. D. Prokoshkin, JETP **38**, 747 (1960), Soviet Phys. JETP **11**, 540 (1960).

[11] Frank, Bandtel, Madey, and Moyer, Phys. Rev. **94**, 1716 (1954).

[12] B. S. Neganov and O. V. Savchenko, JETP **32**, 1265 (1957), Soviet Phys. JETP **5**, 1033 (1957).

[13] Meshkovskiĭ, Shalamov, and Shebanov, JETP **35**, 64 (1958), Soviet Phys. JETP **8**, 46 (1959).

[14] D. C. Peaslee, Phys. Rev. **94**, 1085 (1954); **95**, 1580 (1954).

[15] Meshcheryakov, Vzorov, Zrelov, Neganov, and Shabudin, JETP **31**, 55 (1956), Soviet Phys. JETP **4**, 79 (1957).

[16] L. C. Yuan and S. J. Lindenbaum, Phys. Rev. **103**, 404 (1956).

[17] Brueckner, Serber, and Watson, Phys. Rev. **84**, 258 (1951).

[18] A. A. Ansel'm and V. M. Shekhter, JETP **33**, 481 (1957), Soviet Phys. JETP **6**, 376 (1958).

[19] V. A. Nedzel, Phys. Rev. **94**, 174 (1954).

[20] H. G. de Carvalho, Phys. Rev. **96**, 398 (1954).

[21] Coor, Hill, Hornyak, Smith, and Snow, Phys. Rev. **98**, 1369 (1955).

[22] Chen, Leavitt, and Shapiro, Phys. Rev. **99**, 857 (1955).

[23] Booth, Ledley, Walker, and White, Proc. Phys. Soc. (London) **A70**, 209 (1957).

[24] B. S. Neganov and L. B. Parfenov, JETP **34**, 767 (1958), Soviet Phys. JETP **7**, 528 (1958).

[25] Byfield, Kessler, and Lederman, Phys. Rev. **86**, 17 (1952).

[26] J. O. Kessler and L. M. Lederman, Phys. Rev. **94**, 689 (1954).

[27] A. A. Tyapkin, Dissertation, Joint Institute for Nuclear Research, 1959.

[28] N. Austern, Phys. Rev. **100**, 1522 (1955).

[29] R. R. Wilson, Phys. Rev. **104**, 218 (1956).

[30] Kozodaev, Kulyukin, Sulyaev, Filippov, and Shcherbakov, JETP **38**, 409 (1960), Soviet Phys. JETP **11**, 300 (1960).

[31] V. M. Sidorov, JETP **28**, 727 (1955), Soviet Phys. JETP **1**, 600 (1955).

Translated by I. Emin
288

SOVIET PHYSICS JETP VOLUME 12, NUMBER 6 JUNE, 1961

THE THERMAL CONDUCTIVITY OF HIGH PURITY THALLIUM AND TIN

N. V. ZAVARITSKIĬ

Institute for Physics Problems, Academy of Sciences U.S.S.R.

Submitted to JETP editor July 11, 1960

J. Exptl. Theoret. Phys. (U.S.S.R.) 39, 1571-1577 (December, 1960)

The thermal conductivity of several thallium and tin single crystals of various purity has been studied in the normal (K_n) and superconducting (K_s) states. A deviation from additivity was found in the electron scattering processes in the normal state. The variation in K_s/K_n when the scattering of electrons changes from being due to lattice defects to being due to thermal vibrations is investigated. The results obtained are compared with the theoretical predictions.

As is well known, the magnitude of the thermal conductivity of metals is limited by the scattering of electrons by lattice defects, by the boundaries of the specimen and by thermal vibrations. For most superconductors which have been studied the scattering of electrons is mainly determined by the first process at temperatures below the transition temperature. The characteristics of the thermal conductivity change at the transition from the normal to the superconducting state have been studied sufficiently fully for this case, both experimentally[1-4] and theoretically.[5,6]

The results of these investigations are in satisfactory agreement with one another.

The characteristics of the heat transfer associated with the scattering of electrons by thermal vibrations have not been studied in such detail, since for most metals this scattering process only predominates in the superconducting state for specimens of the greatest purity. The only results for this case are for lead and mercury,[1,7] which are metals with an anomalously large ratio T_c/Θ (T_c is the superconducting transition temperature and Θ is the Debye temperature). These results[1] show that the change in thermal conductivity on passing from the normal to the superconducting state is of a very different nature from the case of scattering of electrons by lattice defects. The theoretical treatment of this problem by Bardeen et al.[6] led to results contradictory to the experimental facts.

It seemed of interest to examine how the thermal conductivity varies on changing from scattering of electrons by lattice defects to scattering by thermal vibrations for a superconductor with a smaller ratio T_c/Θ.

Thallium and tin were chosen for this study. The investigation of the latter metal was started in collaboration with L. G. Koreneva.

The purification of the tin, essential for performing this work, was carried out in the technological section of the Institute under the direction of N. N. Mikhaĭlov. The method of preparing the specimens and of measuring the thermal conductivity was similar to that used previously.[3]

Table I shows the main characteristics of the specimens studied.

THERMAL CONDUCTIVITY IN THE NORMAL STATE

The thermal and electrical conductivities of the specimens in the normal state were measured in order to compare the contributions of the different processes to the electron scattering. For temperatures below T_c the measurements were made in a magnetic field directed along the axis of the specimen, and Kohler's rule was used to extrapolate them to zero field.

At sufficiently low temperatures the electronic thermal conductivity* in the normal state, K_n, can be represented by

$$T/K_n = \rho_0/L + TW_i(T), \qquad (1)$$

where the first term is determined by scattering of electrons by lattice defects and by the specimen boundaries (ρ_0 is the residual resistivity and L is the Lorenz number) and the second is determined by scattering by lattice vibrations, and according to Makinson,[9] $TW_i(T) = \alpha T^3$. The results obtained for thallium (Fig. 1) show that (1) holds

---

*The lattice conductivity, the magnitude of which can be calculated on the basis of the measurements of Sladek and of Garfinkel and Lindenfeld[8] is, for all the specimens studied, negligibly small in the normal state.

Characteristics of Investigation Specimens

Specimen	Orientation	Diameter, mm	$10^{10}\rho_0$, Ω·cm	d/l*	T/K_n ($T\to 0°$K)	$10^4\alpha_0$	$\rho_0/L\alpha T_c^3$	K_s/K_n, $T/T_c=$ 0,9	0,8	0,6
Sn-1	[001]	2,6	1±0,5	2.6	—	2.8	0.25÷0.35	0,83	0,7	0,48
Sn-2	[001]	1,1	1.65±0,2	1,7	—					
Sn-3	[001]	1,5	6,1	8,6	—	5	1	0,89	0,77	—
Sn-4	[110]	2,1	1.2 ±0.5	2,5	—	2.0	0,3÷0,5	0,75	0,6	—
Tl-7	30°**	1,6	2.4 ±0,3	1	0,7	30(±10%)	0,14÷0,2	0.86	0.67	0.35
Tl-8***	30°	0,9	4,5	1	1.8	35	0,28	0,84	0,74	0.46
Tl-1	80°	1	8,1	2,2	3	35	0.6	0.9	0,82	0,47
Tl-2	40°	1.3	6,5	4,7						
Tl-3	20°	1	26	6,7	11	48	1,6	0.9	0.80	0,62
Tl-4	80°	1,1	50	13,5	20	56	2,6	0,95	0,86	0,64

*Rough values. For Sn we took $\rho_0 l = 1.05 \times 10^{-11}$; anisotropy is neglected. Tl we took $\rho_0 l = 4 \times 10^{-11}$ as a result of an analysis of the results of measuring ρ for specimens Tl-7 and Tl-8.

**Angles made with the hexagonal axis.

***Obtained by etching specimen Tl-7.

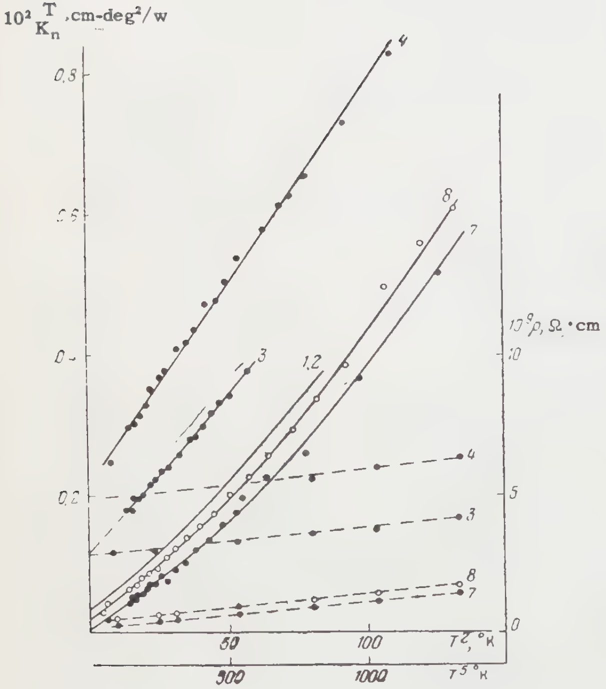

FIG. 1. The thermal conductivity (full curves) and the electrical resistivity (dashed curves) of thallium specimens in the normal state. The ordinate scales have been chosen so that $(T/K_n)_{T=0°} = \rho_0/L$. The specimen numbers are marked on the curves.

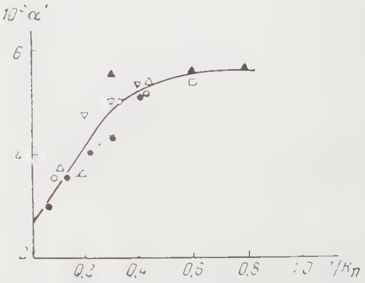

FIG. 2. The variation of α' with T/K_n for thallium specimens: △ – Tl-1, Tl-2, ▽ – Tl-3, ▼ – Tl-4, ● – Tl-7, ○ – Tl-8, □ – according to reference 10.

only to a first approximation. While the magnitude of $(T/K_n)_{T\to 0°K}$ coincides within the experimental accuracy with ρ_0/L, $TW_i(T)$ is only nearly the same for all specimens at the highest temperatures covered by the measurements (4 – 5°K) where the maximum differences between $TW_i(T)$ is not more than ~20%. At lower temperatures there is a systematic reduction in $TW_i(T)$ with increasing purity of the specimens.* There is also a change in the quantity $\alpha' = d[TW_i(T)]/dT^3$, which on the simplest theory[9] should be a constant. The change in $TW_i(T)$ (or in α' — see Fig. 2) lies outside all possible experimental errors and can, evidently, only be explained by a lack of additivity in the scattering of electrons. The possibility of such an effect follows from a general consideration of transport phenomena.†[11]

Figure 3a shows the results of measurements of the thermal conductivity of tin in the normal state. They are similar to those obtained for thallium. However, while the anisotropy of $\alpha_0 = \alpha_{T\to 0°K}$ does not exceed ~10% for thallium, for tin α along the [001] axis is 1.4 times greater than α along the [110] axis (see Table I). The

---

*The temperature dependent part of the electrical resistivity of the thallium specimens depends on purity to a small extent. Between 2.4 and 4.2° K the electrical resistivity of all the specimens obeys the relation $\rho = \rho_0 + bT^5$. b is 10^{-12} ohm-cm/deg⁵ and for increasing impurity content does not increase by more than 20-30%.

†It appears that Hulm[1] first observed a non-additivity in the scattering of electrons, similar to that found in our experiments, in his study of mercury. In his experiments, however, a possible appearance of lattice conductivity could not be excluded and the results remained unexplained.

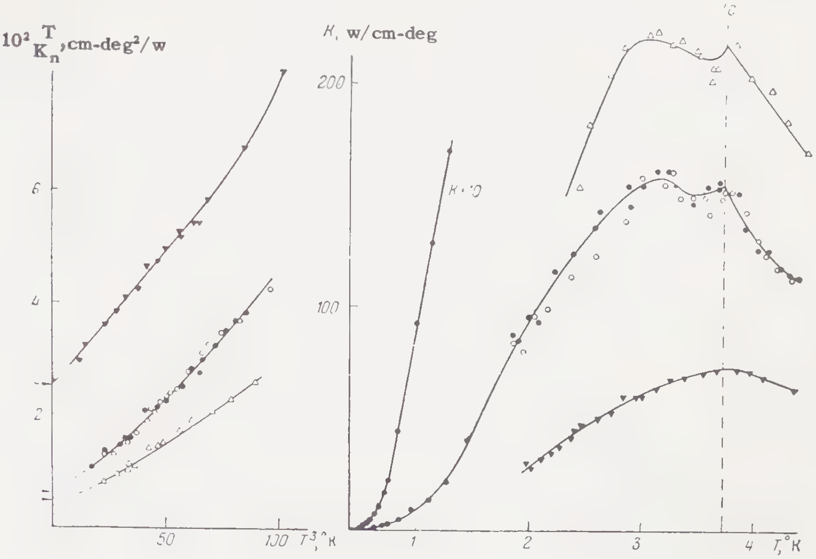

a

b

FIG. 3. The thermal conductivity of tin specimens: a – in the normal and b – in the superconducting states: ○ – Sn-1, ● – Sn-2, ▼ – Sn-3, Δ – Sn-4. The arrows show the values of ρ_0/L.

magnitude and nature of the anisotropy of α in tin agrees with the data on the anisotropy of the temperature dependent part of the electrical resistance, determined by Zernov and Sharvin.[12]

By using the data of Figs. 1 — 3 the contributions of different electron scattering processes can be determined. Table I shows the ratio at $T = T_c$ of the scattering by lattice imperfections to the scattering by thermal vibrations, which is determined by the value of $\rho_0/L\alpha T^3$. It can be seen from the table that for the purest specimens measured, the conductivity at temperatures near T_c is limited by scattering of electrons by thermal vibrations.

THERMAL CONDUCTIVITY IN THE SUPERCONDUCTING STATE

The thermal conductivity of a superconductor, K_s, is determined not only by the thermal conductivity of its electrons, but also by the thermal conductivity of the lattice. The transition from the temperature region where the electronic conductivity is dominant to the region where the lattice conductivity predominates is usually accompanied by a change in the $K_s(T)$ dependence. The thermal conductivity of the thallium specimens is shown in Fig. 4. Figure 3b shows the thermal conductivity of the tin specimens. For thallium the change in the $K_s(T)$ dependence occurs at 0.3 — 0.4°K. Below this temperature the conductivity of all specimens has nearly the same value and varies, to a first approximation as T^n, where $n = 3 — 3.5$. Apparently, below 0.3 — 0.4°K the lattice conductivity* is dominant in heat transport, the electronic conductivity showing up at higher temperatures. In what follows we shall use the results obtained for temperatures where the electronic thermal conductivity predominates ($T \geq 0.8$°K) and the correction for the contribution of the lattice conduction is less than 10 — 15%.

We shall first consider the change in conductivity on going from the normal to the superconducting state in thallium specimens of different purity. The values of K_s/K_n obtained are shown as functions of T/T_c in Fig. 5, together with the results of various theoretical calculations. The dashed curve, marked G, shows the form of the variation of this quantity for the case of scattering of electrons by lattice defects, according to the theory of Geĭlikman[5] and of Bardeen et al.,[6] on the assumption that the energy gap $\Delta = 1.7T_c$. The values of K_s/K_n for the specimen with the greatest impurity concentration (Tl-4) agree with this dependence over the whole range: from Table I it can be seen that the scattering of electrons by lattice defects predominates in this specimen. For specimens with smaller impurity concentration there is a different form of the dependence of K_s/K_n on T/T_c near the transition temperature, but on lowering the temperature the ratio K_s/K_n approaches the value given by curve G. For specimens Tl-3 and Tl-4, for example, below temperatures of respectively ~0.55°K and ~0.4°K, the difference

---

*Calculating the phonon mean free path l_g according to Casimir's relation (see, e.g., references 2 and 3) shows that for the thallium specimens $l_g \sim 0.2$ mm and for the tin specimen Sn-2 (measured down to 0.2° K) $l_g \sim 2$ mm.

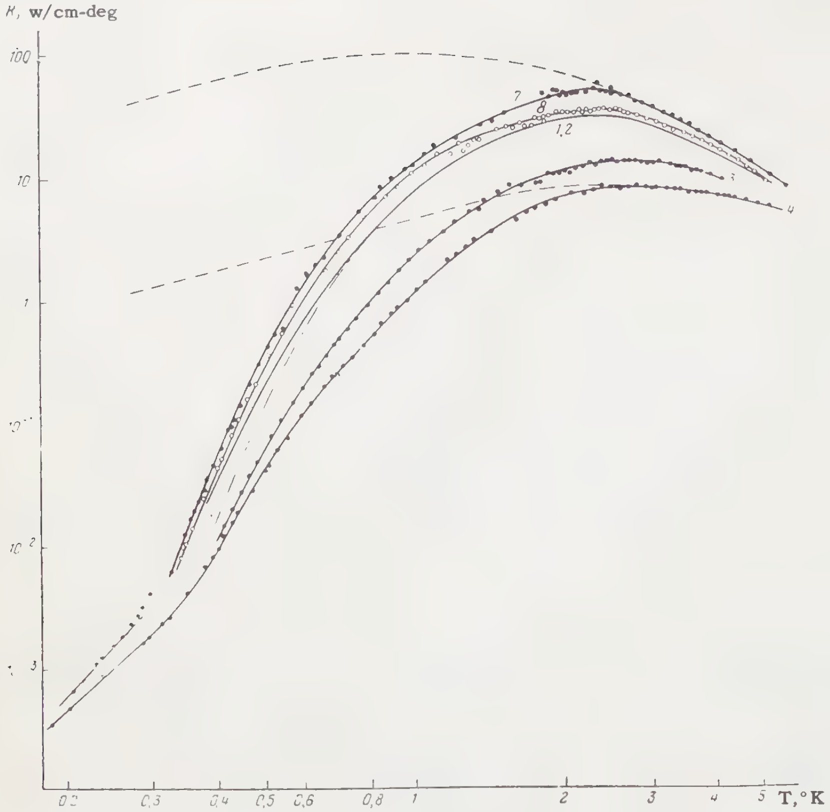

FIG. 4. The thermal conductivity of thallium specimens. The numbers of the corresponding specimens are shown on the curves. The dashed curves show the thermal conductivity in the normal state.

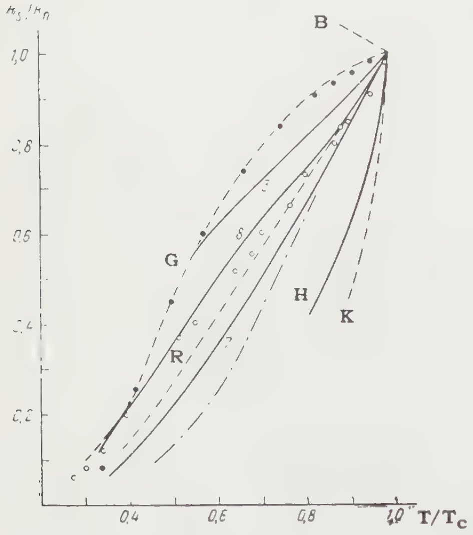

FIG. 5. The dependence of K_s/K_n on T/T_c. The points and full curves represent experimental data; the numbers on the curves refer to the corresponding specimens: the points are for: ● – for Tl-4, ○ – for Sn-1, Sn-2. Curve H is for mercury and lead according to reference 1. The dashed and dotted curve is for scattering of electrons only by lattice vibrations, derived by extrapolating the values of $1/K_s$ for specimens Tl-7, Tl-8, Tl-1 and Tl-2. The dashed curves are theoretical relations: curve G is for the case of scattering of electrons by lattice defects according to Geĭlikman,[5] curves B, K and R are for the case of scattering by thermal vibrations according to Bardeen et al.[6] Kresin[16] and Eq. (2).

between the experimental and theoretical values of K_S/K_n is already no greater than the accuracy in determining these quantities (5 – 10%).*

Graham[13] has recently suggested that the dependence of K_S/K_n on T/T_c is different for scattering of electrons by lattice defects and by the specimen boundaries. Our results do not support this hypothesis. For example, for $T/T_c \leq 0.4$ the values of K_S/K_n for specimens Tl-1, Tl-2, Tl-3, Tl-4 and Tl-8 agree, although for the first four specimens the scattering of electrons is determined by the first process and for the last specimen by the second (see d/l in Table I). Similar results follow from an analysis of the thermal conductivity of the tin specimens. The value of K_S/K_n for specimen Sn-2 is close to the value obtained by Loredo,[2] although the scattering is mainly at the specimen boundaries for Sn-2 (see the table), while for Laredo's specimen it is by lattice defects. The values of K_S/K_n obtained for specimens Sn-2 are 5 – 10 times greater, at 1 – 0.7°K, than the values of K_S/K_n which would follow from Graham's hypothesis.

The data of Fig. 5 and of Table I show that for a relative increase in thermal vibration scattering

*There is only agreement between K_s/K_n and the theoretical curve G for temperatures where $\rho_0/LTW_i(T)$ reaches 5–9.

(a reduction in $\rho_0/L\alpha T_c^3$) K_s/K_n decreases near T_c. K_s/K_n is then close for specimens of thallium and tin* with the same ratios $\rho_0/L\alpha T_c^3$ (specimens Tl-8, Sn-1 and Sn-2). For thallium and tin, therefore, as was found earlier[1] in the experiments on mercury and lead, the reduction in the electronic thermal conductivity at the transition from the normal to the superconducting state is sharper when the scattering by electrons is by thermal vibrations than when it is by lattice defects.

We can explain qualitatively the different form of the dependence of K_s/K_n on T/T_c for scattering by imperfections and by thermal vibrations in the following way. The electron mean free path in the former case is the same in the normal and superconducting states of the metal. For the latter case it is rather the mean collision time, τ, between electrons and phonons which should stay constant, assuming an unchanged interaction between them. As a result of the change in the electron energy spectrum in the superconducting state, this leads to a reduction in the electron mean free path and therefore in the value of K_s/K_n. A calculation of the heat conductivity for the case τ = const. can be made easily, using Geĭlikman's formulation,[5] and leads to the following result:†

$$K_s \sim \frac{\tau}{T}\int_0^\infty \varepsilon^2 \frac{\partial n}{\partial \varepsilon}\left(\frac{\partial \varepsilon}{\partial \xi}\right)^2 d\xi \sim \frac{\tau}{T}\int_0^\infty \frac{\Delta^2 \cosh 2\varphi}{\exp\{\Delta T^{-1}\cosh\varphi\}+1}\, d\varphi,$$

$$\frac{K_s}{K_n} = \frac{3}{2\pi^2}\int_0^\infty x^2 \operatorname{sech}^2\left(\frac{1}{2}\sqrt{x^2+(\Delta/T)^2}\right)dx, \qquad (2)$$

where $\epsilon = \sqrt{\xi^2 + \Delta^2}$ is the excitation energy in the superconductor and $n = (e^{\epsilon/T} + 1)^{-1}$.

The dependence of K_s/K_n on T/T_c calculated according to (2) is shown in Fig. 5 (curve R). It can be seen that (2) only describes the variation of K_s/K_n with T/T_c qualitatively.‡ It is possible that this is due to the phonon electron interaction being different in the normal and superconducting states (we are, of course, concerned with the so-called "normal" electrons of the superconductor). It may be that different dependences of K_s/K_n on T/T_c for thallium, tin, mercury and lead (Fig. 5) are produced by the differences in Δ/T_c for these metals.[17] The extent to which these suggestions are correct can only be decided after a detailed theoretical analysis of the problem.

In conclusion, I take this pleasant opportunity of expressing my deep indebtedness to P. L. Kapitza and A. I. Shal'nikov for their interest in the work and also to L. G. Koreneva who carried out the measurements of the thermal conductivity of the series of tin specimens.

---

*There appears to be some anisotropy in the $K_s/K_n - T/T_c$ relation in tin. The change of K_s/K_n with T/T_c for specimens along the [110] axis follows a steeper law than for specimens along the [001] axis. This anisotropy is similar in form to the anisotropy in the ultrasonic absorption near T_c.[15]

†We have recently seen a preprint of the work of Kadanov and Marti in which a similar formula is obtained.

‡The results of two further theoretical calculations[6,16] dealing with this problem are shown in Fig. 5, and these also do not agree with the experimental K_s/K_n dependence.

[1] J. K. Hulm, Proc. Roy. Soc. **A204**, 98 (1950).

[2] S. J. Laredo, Proc. Roy. Soc. **A229**, 473 (1955).

[3] N. V. Zavaritskiĭ, JETP **33**, 1085 (1957), Soviet Phys. JETP **6**, 837 (1958); JETP **34**, 1116 (1958), Soviet Phys. JETP **7**, 773 (1958); JETP **37**, 1506 (1959), Soviet Phys. JETP **10**, 1069 (1960).

[4] C. B. Satterthwaite, Superconductivity Conference, Cambridge (1959).

[5] B. T. Geĭlikman, JETP **34**, 1042 (1958), Soviet Phys. JETP **7**, 721 (1958).

[6] Bardeen, Rickayzen, and Tewordt, Phys. Rev. **113**, 982 (1959).

[7] W. J. de Haas and A. Rademakers, Physica **7**, 992 (1940).

[8] R. J. Sladek, Phys. Rev. **97**, 902 (1955); M. Garfinkel and P. Lindenfeld, Phys. Rev. **110**, 883 (1958).

[9] R. E. B. Makinson, Proc. Camb. Phil. Soc. **34**, 474 (1938).

[10] H. M. Rosenberg, Phil. Trans. Roy. Soc. **A247**, 441 (1955).

[11] E. H. Sondheimer, Proc. Roy. Soc. **A203**, 75 (1949).

[12] V. B. Zernov and Yu. V. Sharvin, JETP **36**, 1038 (1959), Soviet Phys. JETP **9**, 737 (1959).

[13] G. M. Graham, Proc. Roy. Soc. **A248**, 522 (1958).

[14] A. M. Guenault, Superconductivity Conference, Cambridge (1959).

[15] Bezuglyĭ, Galkin, and Korolyuk, JETP **36**, 1951 (1959), Soviet Phys. JETP **9**, 1388 (1959); Morse, Olsen, and Gavenda, Phys. Rev. Letters **3**, 15 (1959).

[16] V. Z. Kresin, JETP **36**, 1947 (1959), Soviet Phys. JETP **9**, 1385 (1959).

[17] M. Tinkham, Superconductivity Conference, Cambridge (1959).

Translated by R. Berman
289

SOVIET PHYSICS JETP VOLUME 12, NUMBER 6 JUNE, 1961

AN INVESTIGATION OF THE $Sn^{120}(\gamma, p)$ *REACTION*

KUO CH'I-DI and B. S. RATNER

P. N. Lebedev Physics Institute, Academy of Sciences, U.S.S.R.

Submitted to JETP editor July 12, 1960

J. Exptl. Theoret. Phys. (U.S.S.R.) **39**, 1578-1584 (December, 1960)

The cross sections for the reactions $Sn^{120}(\gamma, p)In^{119}$ and $Sn^{120}(\gamma, pn)In^{118}$ were measured by recording the induced radioactivity. The maximum of the (γ, p) cross section, at $E_{\gamma\,\max} = 20.8 \pm 0.5$ Mev, is 6.5 ± 0.6 mb. The integral cross sections are 28 ± 3 and 5.0 ± 1 mb-Mev for the (γ, p) and (γ, pn) reactions, respectively. A new half-life $T = 2.1 \pm 0.2$ min has been detected which corresponds to the ground state in the presented decay scheme of In^{119}. The results are discussed on the basis of the Wilkinson model.

THE investigation of photonuclear reactions involving the direct emission of particles that acquire most of the γ-ray energy (the so-called "resonance direct" process) is of interest for the understanding of reactions between γ rays and nuclei, and for the determination of nuclear structure. Dipole models cannot account for the excessive emission of protons and fast neutrons by certain nuclei, or for the character of their angular and energy distributions. The fundamental features of photonuclear reactions appear to be described correctly by the direct-interaction model proposed by Courant[1] and developed by Wilkinson using nuclear shell structure.[2] However, some important aspects of the process remain unclear, partly because of insufficient information regarding the cross section for the direct photoeffect.

The present work is a study of the (γ, p) reaction on a tin isotope having a closed proton shell. In the Sn^{120} nucleus there is a positive difference between the binding energies of the proton (E_{p0}) and neutron (E_{n0}): $E_{p0} - E_{n0} = 11.3 - 9.14 = 2.16$ Mev.[3] The probability for proton emission by a compound nucleus is therefore very small, and the observed yield of the (γ, p) reaction can therefore be attributed confidently to a direct interaction.

EXPERIMENTAL PROCEDURE

Our γ-ray source $(E_{\gamma\,\max} = 30$ Mev$)$ was the synchrotron of the Physics Institute of the U.S.S.R. Academy of Sciences. The 2000-mg tin sample,* which was enriched in Sn^{120}, contained the following isotopes:

Isotope	Sn^{124}	Sn^{122}	Sn^{120}	Sn^{119}	Sn^{118}	$Sn^{112-117}$
Content, %	<0.1	0.1	99.1	0.6	0.1	<0.07

The 40 × 30 × 0.2-mm tin sample and a copper sample of the same shape were irradiated with γ rays at a distance of 20 cm from the synchrotron target. The reaction $Cu^{63}(\gamma, n)Cu^{62}$ served as the principal monitor, supplemented by an integrating ionization chamber under 2 mm of lead, which registered deviations of beam intensity. The decay of β activity induced in tin was measured by two SI-2B end-window counters. In measurements of the reaction $Sn^{120}(\gamma, p)In^{119}$ $(T = 17.5$ min$)$ a 380-mg/cm^2 aluminum absorber was used to eliminate the small amount of activity induced by the reaction $Sn^{124}(\gamma, n)Sn^{123}$ $(T = 39.5$ min, $E_\beta = 1.3$ Mev$)$.

The energies of γ rays accompanying the β decay of In^{119} were measured by means of two parallel scintillation counters, consisting of 40 × 40-mm NaI(Tl) crystals and FÉU-29 photomultipliers. Pulses from the counters were fed to a single-channel analyzer, scaler and time discriminator. A 2.5-mm aluminum absorber of electrons was placed between the sample and the crystals.

RESULTS AND DISCUSSION

1. Our measurements detected an activity with $T = 2.1 \pm 0.2$ min,* in addition to the known activities of In^{119} $(T = 17.5 \pm 0.2$ min according to our data$)$ and In^{118} $(T = 4.5$ min$)$ from the reaction $Sn^{120}(\gamma, np)$, beginning at $E_{\gamma\,\max} = 24$ Mev. The maximum energy of β-decay electrons was deter-

---

*The authors are greatly indebted to the workers in the laboratory of V. S. Zolotarev who prepared the sample.

*The results given in Sec. 1 were reported at the Tenth All-Union Conference on Nuclear Spectroscopy, held during January, 1960.

mined from absorption in aluminum. Because of the poor geometry for induced-activity registration, the energy of electrons was determined from a comparison with the absorption in aluminum of β rays with known energies from C^{11} (E_β = 0.99 Mev) and Cu^{62} (E_β = 2.87 Mev). It follows from these experiments that for the activity with T = 2.1 min we have E_β = 1.8 Mev, and for T = 17.5 min, E_β = 2.6 Mev. A control experiment employing a 90-mg/cm² lead absorber yielded agreement within experimental error with the results for the aluminum absorber in the case of the 2.1-min emission; this indicates that electrons, rather than soft γ rays, were registered. The induced β-ray yield from a Sn^{120}-enriched sample was measured without absorbers for different values of $E_{\gamma\,max}$. Figure 1 shows that the value of α, denoting the ratio of 2.1-min activity to 17.5-min activity from $Sn^{120}(\gamma, p)In^{119}$, is almost constant over a broad range of $E_{\gamma\,max}$ from 20 to 28 Mev, but increases rapidly for $E_{\gamma\,max}$ < 20 Mev.

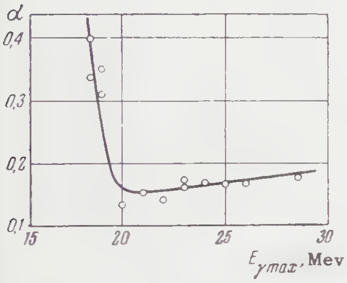

FIG. 1. Yield ratio of activities with T = 2.1 min and 17.5 min as a function of $E_{\gamma max}$.

If the discovered half-life corresponds to a (γ, n) reaction on a tin isotope, α should diminish appreciably as $E_{\gamma\,max}$ increases, because the yields of (γ, n) and (γ, p) reactions depend differently on $E_{\gamma\,max}$; this evidently applies also to the (γ, γ′) reaction. The (γ, 2n) threshold for most tin isotopes lies above the energy $E_{\gamma\,max}$ at which the 2.1-min activity is observed. Finally, the sample contained very small amounts of all isotopes except Sn^{120}, and if the former were responsible for the 2.1-min activity, this activity would be observed with much greater probability in a natural tin-isotope mixture.[4] We believe that the 2.1-min activity can be attributed with the highest probability to In^{119} produced in the reaction $Sn^{120}(\gamma, p)In^{119}$.*

The increase of α as $E_{\gamma\,max}$ diminishes indicates that the 2.1-min half-life belongs to the ground state of In^{119}. The previously known 17.5-min half-life evidently belongs to an isomeric state of In^{119}. A change in the ratio of activities corresponding to the formation of the ground and isomeric states near the photonuclear threshold was previously observed in the case of (γ, n) reactions.[6] The fact that in the present case α begins to increase at about 8 Mev from the threshold is attributable to the emission of protons having considerable energy.

A preliminary measurement of the γ rays associated with the In^{119} activities of present interest detected a 0.70 ± 0.02-Mev line with T = 2.1 min. The data suggest the In^{119} decay scheme given in Fig. 2.

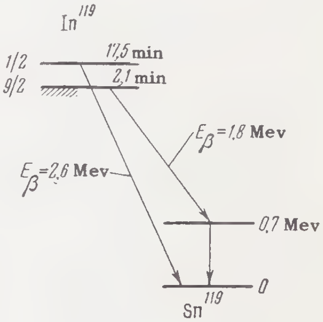

FIG. 2. Decay scheme of In^{119}

2. Figure 3 shows the curve for the relative yields of $Sn^{120}(\gamma, p)In^{119}$* and $Cu^{63}(\gamma, n)Cu^{62}$. The root-mean-square errors of several measurements for the same $E_{\gamma\,max}$ are indicated. The curve for the relative yields of $Sn^{120}(\gamma, pn)In^{118}$* and $Cu^{63}(\gamma, n)Cu^{62}$ is also shown.

The energy dependence of the cross sections was determined as follows. The yield a of the investigated reaction, relative to that of the reaction $Cu^{63}(\gamma, n)Cu^{62}$, together with the well-known energy dependence of the cross section for the latter, was used to calculate $\sigma(E_\gamma)$. Let us consider the case in which the threshold of our reaction lies above that of the reference reaction. We divide our curves for $\sigma^{Cu}(E_\gamma)$ and $a(E_{\gamma\,max})$ into intervals, and denote values beginning at the threshold for $Cu^{63}(\gamma, n)Cu^{62}$ as σ^{Cu}_{-i}, σ^{Cu}_{-i+1}, . . . , σ^{Cu}_1, σ^{Cu}_2, . . . σ^{Cu}_n (mean values) and a_1, a_2, . . . a_n. The subscript 1 denotes the first interval in the relative yield curve of our reaction. We then have

$$\sigma_1 = \frac{a_1}{N_1(E_1)} \sum_{k=-i}^{1} \sigma_k^{Cu} N_k(E_1),$$

$$\sigma_2 = \frac{a_2}{N_2(E_2)} \left[\sum_{k=-i}^{2} \sigma_k^{Cu} N_k(E_2) - \sigma_1 N_1(E_2) \right], \ldots,$$

$$\sigma_n = \frac{a_n}{N_n(E_n)} \left[\sum_{k=-i}^{n} \sigma_k^{Cu} N_k(E_n) - \sum_{l=1}^{n-1} \sigma_l N_l(E_n) \right],$$

---

*The isotope tables in reference 5 contain a reference to a private communication regarding the existence of a ~2-min activity of In^{119}.

*Data for the (γ, pn)-reaction yield are much less accurate, since it is difficult to discriminate 2.1-min and 4.5-min activities.

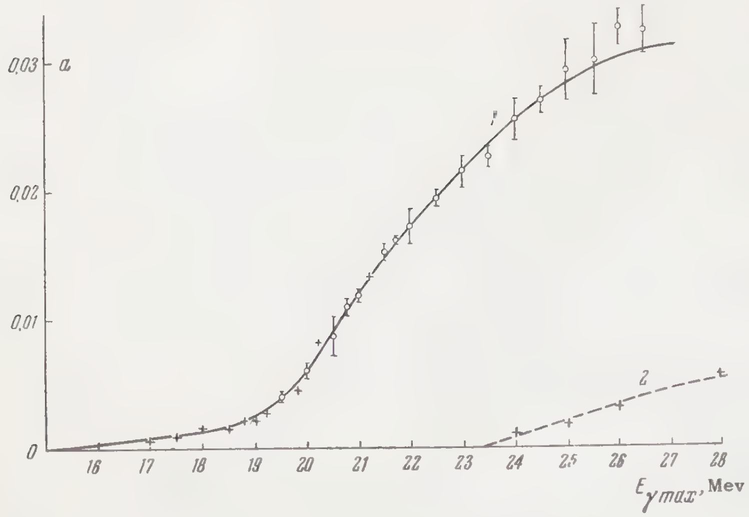

FIG. 3. Yields of the reactions $Sn^{120}(\gamma, p)In^{119*}$ (curve 1) and $Sn^{140}(\gamma, pn)In^{118}$ (curve 2) relative to the yield of $Cu^{63}(\gamma, n)Cu^{62}$ as a function of $E_{\gamma max}$.

where $N_k(E_n)$ is the number of photons in the k-th interval for maximum bremsstrahlung energy E_1. This procedure obviates measurement of the monitor-reaction yield with an absolute ionization chamber. The cross section for $Cu^{63}(\gamma, n)$ was taken from reference 7. The curves of the cross sections for $Sn^{120}(\gamma, p)$ and $Sn^{120}(\gamma, pn)$ are shown in Fig. 4. The maximum for (γ, p), at $E_\gamma = 20.8$ Mev, is 6.5 ± 0.6 mb, and the integrated cross section is 28.0 ± 2 mb-Mev. The integrated cross section for $Sn^{120}(\gamma, pn)$ is 5.0 ± 1 mb-Mev. The described procedure was used to calculate (γ, p) cross sections on cadmium isotopes from earlier data,[8] and from our measurements on a sample 90% enriched in Cd^{116}. These results differ from those given in reference 8 because of improved data on registration efficiency.

The data on (γ, p) reactions unassociated with compound-nucleus formation are collected in Table I, which gives the values of E_{max} and the corresponding maximum cross sections σ_{max}, the integrated cross sections, and the half-widths Γ of the resonance curves for a number of nuclei. (Data for Mo^{100} were taken from reference 9.) It follows from the experimental results that 1) the resonance widths for the direct (γ, p) reaction are only slightly (1.0 — 1.5 Mev) less than those for the (γ, n) reaction; 2) for the tin nucleus with filled proton shell ($Z = 50$) Γ is smaller than for neighboring nuclei; 3) the resonance peak for direct-interaction protons is shifted by 5 — 6 Mev from the giant resonance (for $Z = 40 — 50$).

For the purpose of interpreting the data we shall attempt a rough estimate of the contributions from different proton transitions, based on Wilkinson's single-particle model. Sn^{120}, for which there is a minimum number of possible proton transitions, will be used as an example.

a) Neutron and proton transitions make approximately equal contributions to the total γ-ray absorption cross section. The fact that the width of the absorption cross section curve for tin is only 5.0 Mev[10] permits us to assume that the energies of the principal proton transitions and neutron transitions are concentrated in the giant-resonance

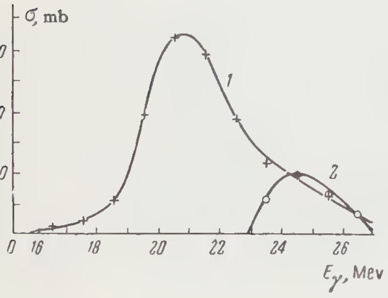

FIG. 4. Cross section for the reactions $Sn^{120}(\gamma, p)In^{119}$ (curve 1) and $Sn^{120}(\gamma, pn)In^{118}$ (curve 2).

TABLE I. (γ, p)-reaction cross sections for direct interaction

Nuclide	E_{max}, Mev	σ_{max}, mb	Γ, Mev	$\int \sigma dE$, mb-Mev
Sn_{50}^{120}	20.8 ± 0,5	6,5 ± 0,6	3.5 ± 0,5	28 ± 3
Cd_{48}^{112}	21.0 ± 0.5	12,0 ± 1	5.2 ± 0,5	67 ± 7
Cd_{48}^{113}	20,5 ± 0.5	8.3 ± 0,8	4,0 ± 0,5	36 ± 4
Cd_{48}^{114}	21,0 ± 0,5	6.65 ± 0.7	4,4 ± 0.5	31 ± 3
Cd_{48}^{116}	21,2 ± 0.5	3,3 ± 0.3	4.4 ± 0,5	16 ± 2
Mo_{42}^{100} [9]	22,0	15,0	5,0	100 ± 20

TABLE II. Proton dipole transitions in the tin nucleus

Transition	Transition energy, rel. units			Transition intensity	Transition energy, Mev*	Energy of emitted proton, Mev	Penetration factor	Probability of proton emission
	[12]	[13]	[14]					
1	2	3	4	5	6	7	8	9
$1g_{9/2} \rightarrow 1h_{11/2}$	1,0	1.0	1.0	1.45	15.3	4.0	$0,1 \cdot 10^{-4}$	$0,15 \cdot 10^{-4}$
$1f_{5/2} \rightarrow 1g_{7/2}$	1.05	1.3	1,1	0.84	16.0	0.7	0	0
$1f_{5/2} \rightarrow 2d_{3/2}$	1.6	1,5	1,4	0.06	24.2	8.9	0.85	0,051
$2p_{1/2} \rightarrow 2d_{3/2}$	1,4	1,1	1.3	0,19	20.8	9.0	0.85	0.16
$2p_{3/2} \rightarrow 2d_{5/2}$	0.85	1,0	1.2	0.33	13.0	—	—	0
$2p_{3/2} \rightarrow 3s_{1/2}$	1.6	1.3	1,5	0.08	24,6	10.1	1.0	0.08

*Assuming that the transitions $1g_{9/2} \rightarrow 1h_{11/2}$ and $1f_{5/2} \rightarrow 1g_{7/2}$ form the giant resonance at 15.5 Mev when using the scheme of reference 12.

region with a peak at 15.5 Mev.[11] Table II gives results for the principal proton dipole transitions; the respective energies compared with that of the $1g_{9/2} - 1h_{11/2}$ transition have been taken from the literature[12–14] (the latter for the case of no nuclear deformation). The estimated transition intensities show, according to Wilkinson,[2] that $1g_{9/2} \rightarrow 1h_{11/2}$ and $1f_{5/2} \rightarrow 1g_{7/2}$ play the principal roles in absorption. Taking additional energy-level data from reference 12, we equate the giant resonance energy 15.5 Mev to the "center of gravity" of the two indicated transitions, and thus derive the energies of the remaining transitions.

b) It is also necessary to determine which of the proton transitions are responsible for the appearance of "direct" photoprotons. We determine the binding energies of protons on different levels, equating the binding energy of the $g_{9/2}$ level to the known value $E_{p0} = 11.3$ Mev, and obtain the energy of emitted protons. In determining the potential-barrier penetration factor we used Evans' data for Sn^{118}.[15] By comparing the emission probabilities of separate proton groups it is easily found that the proton transitions $1g_{9/2} \rightarrow 1h_{11/2}$ and $1f_{5/2} \rightarrow 1g_{7/2}$, which play the principal parts in γ-ray absorption, make a negligibly small contribution to the yield of direct-transition protons. The principal contribution comes from p-shell protons, with transition energies above 20 Mev. The emission of "direct" photoprotons from other nuclides in the range $Z = 40 - 50$ is apparently analogous.

The foregoing discussion supplies a reasonable explanation of the experimental fact that resonance for "direct" photoprotons is shifted by 5 — 6 Mev from giant resonance. The appreciable anisotropy observed for high-energy photoprotons from Cd^{114} [16] and silver[17–18] corresponds qualitatively to a p → d transition.*

We shall note one additional circumstance. It has been indicated above that the reaction $Sn^{120}(\gamma, p)In^{119}$ involves two half-lives: $T_1 = 2.1$ min and $T_2 = 17.5$ min. The ratio of the corresponding activities is $\alpha \approx 0.16$. We assume that $T = 17.5$ min is associated with an isomeric state of In^{119}. We shall make use of the reasonable hypothesis that cascade transitions take place predominantly between levels with close spin values.[6] Then a dominant transition to the isomeric level In^{119*}, which apparently has spin ½, will occur only if the protons emitted by $Sn^{120}(I = 0)$ have small angular momentum. This is confirmed by the evaluation of proton transitions.

Finally, we shall discuss the observed difference in the (γ, p) cross sections for cadmium isotopes. At resonance $E_\gamma = 21$ Mev, the ratio of these cross sections is ~4 for Cd^{112} and Cd^{116}. From qualitative considerations this effect would be expected from increased proton binding energy as the number of neutrons increases, with correspondingly reduced penetrability. Unfortunately, a quantitative evaluation is difficult, because the p-proton binding energy is not known with sufficient accuracy. In earlier work[8] we assumed that the given effect is specifically associated with the photoeffect. However, Levkovskiĭ has shown,[20] that cross sections for the emission of charged particles depend on the number of neutrons in the nucleus even in the case of neutron-induced reactions.

In conclusion the authors wish to thank O. V. Bogdankevich, L. E. Lazareva and B. A. Tulupov for valuable discussions of the results.

---

*Anisotropy close to ~ $\sin^2 \theta$ is obtained, according to reference 19, from the interference of p → d and p → s transitions.

[1] E. D. Courant, Phys. Rev. **82**, 703 (1951).
[2] D. H. Wilkinson, Physica **22**, 1039 (1956).
[3] V. A. Kravtsov, Usp. Fiz. Nauk **54**, 3 (1954).
[4] Mock, Waddel, Fagg, and Tobin, Phys. Rev. **74**, 1536 (1948).
[5] Strominger, Hollander and Seaborg, Revs. Modern Phys. **30**, 585 (1958).

[6] Katz, Baker, and Montalbetti, Can. J. Phys. **31**, 250 (1953).

[7] A. I. Berman and K. L. Brown, Phys. Rev. **96**, 83 (1954).

[8] Kuo Ch'i-di and B. S. Ratner, Doklady Akad. Nauk SSSR **125**, 761 (1959), Soviet Phys.-Doklady **4**, 369 (1959).

[9] Ferrero, Hanson, Malvano, and Tribuno, Nuovo cimento **6**, 585 (1957).

[10] Fuller, Petree, and Weiss, Phys. Rev. **112**, 554 (1958).

[11] Kuo Ch'i-di, Ratner, and Sergeev, JETP (in press).

[12] Ross, Mark, and Lawson, Phys. Rev. **102**, 1613 (1956).

[13] A. Schröder, Nuovo cimento **7**, 461 (1958).

[14] S. G. Nilsson, Kgl. Danske Videnskab. Selskab, Mat.-fys. Medd. **29**, 1 (1955).

[15] J. A. Evans, Proc. Phys. Soc. (London) **73**, 33 (1959).

[16] Akindinov, Amirov, Osokina, and Ratner, Ядерные реакции при малых и средних энергиях (Nuclear Reactions at Low and Intermediate Energies) IIL, 1958, p. 403

[17] K. H. Lokan, Proc. Phys. Soc. (London) **73**, 697 (1959).

[18] H. Wäffler, Helv, Phys. Acta **26**, 785 (1953).

[19] J. Eichler and H. A. Weidenmüller, Z. Physik **152**, 261 (1958).

[20] V. H. Levkovskiĭ, JETP **33**, 1520 (1957), Soviet Phys. JETP **6**, 1174 (1958).

Translated by I. Emin
290

SOVIET PHYSICS JETP VOLUME 12, NUMBER 6 JUNE, 1961

RATIO OF CROSS SECTIONS FOR PRODUCTION OF NEGATIVE AND POSITIVE PHOTO-MESONS IN BERYLLIUM

M. I. ADAMOVICH, N. M. PANOVA, V. M. POPOVA, and F. R. YAGUDINA

P. N. Lebedev Physics Institute, Academy of Sciences of the U.S.S.R.

Submitted to JETP editor July 12, 1960

J. Exptl. Theoret. Phys. (U.S.S.R.) **39**, 1585-1588 (December, 1960)

We have measured the ratio of the yields of the charged mesons emitted at 90° to a photon beam irradiating a beryllium target. The spectrum of the photons was a bremsstrahlung one with maximum energy 250 Mev. The energy spectra of the mesons were obtained in the energy range 12 to 40 Mev. The ratio of the cross sections for photo production of π^- and π^+ mesons is $\sigma^-/\sigma^+ = 1.8 \pm 0.15$. These results are discussed.

IT is well known that the yield of charged photomesons from various nuclei is proportional to $A^{2/3}$, where A is the mass number. However, the ratio N^-/N^+ of the yields of π^- and π^+ mesons in some nuclei is considerably greater than would be expected from such a rule.

The largest discrepancy is for beryllium. For mesons having energy 56 Mev and made by photons having maximum energy $E_{max} = 256$ Mev, the ratio $N^-/N^+ = 3.3 \pm 0.3$.[1] According to the "$A^{2/3}$ law" this ratio should be 1.51. For slow mesons made in beryllium ($E_\pi < 3$ Mev, $E_{max} = 250$ Mev), the ratio $N^-/N^+ = 1.9 \pm 0.38$,[2] which does not contradict the value 2.1 calculated assuming the same law but including correction for the Coulomb interaction between the emitted mesons and the residual nucleus.

The work reported here was undertaken in order to understand this difference and to measure the value of the ratio of cross sections for photoproduction of π^- and π^+ mesons with intermediate energies. The experiments were carried out on beryllium.

The photons were obtained from the synchrotron of the Physics Institute of the Academy of Sciences and had maximum energy 250 Mev. They were incident on a beryllium plate 3 mm thick. The mesons emitted at 90° to the photon beam were detected in a stack of 400μ type NIKFI – R emulsions. The detection efficiency was the same for π^- and π^+ mesons, and no more than 2% were not counted. Of all tracks ending in the emulsion, we selected those π^- and π^+ mesons which had energies in the range 12 to 40 Mev. This interval was chosen because for such mesons the corrections for Coulomb interactions between the mesons and the residual nucleus are small and may be neglected. Furthermore, the ratio σ^-/σ^+ for free nucleons is known in this energy range. We counted 981 π^- and 370 π^+ mesons.

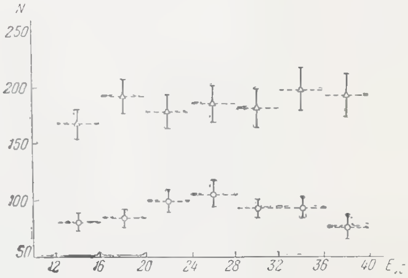

FIG. 1. Energy distribution of mesons from beryllium: ○ – π^+ mesons, △ – π^- mesons ($E_{max} = 250$ Mev, $\theta = 90°$).

Figure 1 shows the energy distribution of these mesons. The ratio of the yields of negative and positive mesons is $N^-/N^+ = 2.65 \pm 0.22$. As is evident from the figure, the yields are practically independent of the energy of the mesons. The general nature of these spectra can be explained by assuming that photoproduction takes place on the nucleus as a whole, and not on free nucleons. Mesons emitted in a definite direction and with a definite energy can be made by photons having energies in the range from $E_n^\pm$ to E_{max}, where E_n^- and E_n^+ are thresholds for production of mesons with the given energy E_π and the given direction of emission θ.

The yields of π^- and π^+ mesons on beryllium can then be written as follows:

$$N^-(E_\pi, \theta) = \int_{E_n^-}^{E_{max}} C\sigma^-(E_\pi, \theta) f(E_\gamma)\, dE_\gamma,$$

$$N^+(E_\pi, \theta) = \int_{E_n^+}^{E_{max}} C\sigma^+(E_\pi, \theta) f(E_\gamma)\, dE_\gamma, \qquad (1)$$

where C is the number of nuclei per cm^2 in the target, $\sigma^\mp(E_\pi, \theta)$ is the cross section for the production of mesons of the appropriate sign with energy E_π and at an angle θ, while $f(E_\gamma)$ is the photon spectrum. Upon averaging over the energy spread of the photons, we obtain the following expression for the ratio of the mean cross sections for photoproduction of charged π mesons on the nucleus:

$$\frac{\sigma^-}{\sigma^+} = \frac{N^-}{N^+} \int\limits_{E_n^- + \Delta}^{E_{max}} Cf(E_\gamma)\, dE_\gamma \left[\int\limits_{E_n^-}^{E_{max}} Cf(E_\gamma)\, dE_\gamma \right]^{-1} = k\, \frac{N^-}{N^+}. \qquad (2)$$

Here $\Delta = E_n^- - E_n^+$ is the difference between the thresholds for production of π^- and π^+ mesons with energy E_π and at an angle θ. Because of this difference, the quantity k can be different from 1.[3] Indeed, from Eq. (2) it follows that for Δ sufficiently large and for fixed meson energy E_π, a decrease in E_{max} implies an increase in the ratio N^-/N^+. This is experimentally verified by the data shown in the table.

E_{max}, Mev	E_π, Mev	N^-/N^+
500	40	1.65±0.14 [4]
310	54	1.65±0.06 [5]
270	54	2.0 ±0.1 [5]
250	54	2.4 ±0.3 [5]
225	54	3.3 ±0.5 [5]
250	<3	1.88±0.35 [2]

The quantity Δ is determined by the final products of the reaction and depends on the mechanism for photo-production of mesons in the nucleus. It is reasonable to accept the single nucleon model for photo-production of mesons. This model is supported by the results of Gorzhevskaya and Panova.[6] The model is further supported by Fig. 2, which shows the correlation between observed values of N^-/N^+ and values for Δ, the latter being calculated using the single nucleon model for fixed E_{max} and E_π. The values for N^-/N^+ were taken from the work of Littauer and Walker.[1]

According to the single nucleon model, Δ for beryllium is determined by the energy relations in the reactions

$$\gamma + \mathrm{Be}_4^9 \rightarrow \pi^- + p + \mathrm{Be}_4^8,$$
$$\gamma + \mathrm{Be}_4^9 \rightarrow \pi^+ + n + \mathrm{Li}_3^8. \qquad (3)$$

In general, the residual nuclei could be either in their ground states or in excited states, but the thresholds for the reactions are determined by formation of the residual nuclei in their ground states. The difference between the thresholds of these reactions is 18.7 Mev. This large value of Δ implies that the number of photons which have energy enough to make positive mesons is small compared to the number of photons which can make negative mesons. As a consequence, the ratio N^-/N^+ is quite different from σ^-/σ^+ and depends on E_{max}. This explains the results in the table.

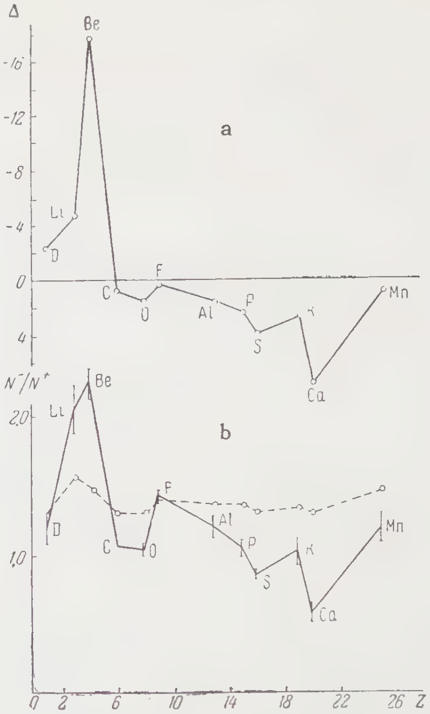

FIG. 2. a – Difference between thresholds for photoproduction of π^- and π^+ mesons on the nucleus, plotted as a function of Z; b – ratio of yields of positive and negative photomesons on the nucleus, plotted as a function of Z; the dotted line shows the predictions of the $A^{2/3}$ law.

From the bremsstrahlung spectrum with $E_{max} = 250$ Mev, and taking $\bar{E}_\pi = 26$ Mev, $\theta = 90°$, we obtain $k = 0.68$.

Substituting this value of k into formula (2), together with $N^-/N^+ = 2.65 \pm 0.22$, we find that the ratio of cross sections for photoproduction of negative and positive mesons on beryllium is $\sigma^-/\sigma^+ = 1.8 \pm 0.15$. This is a ratio of cross sections that are averaged over photons in the energy range $E_n^\pm$ to E_{max} and over mesons in the energy range 12 to 40 Mev. The correction for the dependence of cross sections on photon energy has only a negligible effect on the ratio σ^-/σ^+. The value 1.8 ± 0.15 agrees well with the yield ratios 1.9 ± 0.38 obtained[2] for $E_\pi < 3$ Mev, $E_{max} = 250$ Mev and 1.6 ± 0.14 obtained[4] for $E_\pi = 40$ Mev, $E_{max} = 500$ Mev. In comparing our result with that obtained by Waters,[4] his value $N^-/N^+ = 1.6 \pm 0.14$ must be increased by about 10% to correct for pair production by photons with $E_{max} = 500$ Mev. This comparison can be justified by noting that in the experiments quoted the threshold energy of γ rays is much less than E_{max} and the ratio of the numbers of photons making π^- and π^+ mesons is practically one.

Thus it appears that the anomalous values obtained for the yield ratios N^-/N^+ on beryllium are due to a difference in the thresholds for π^- and π^+ meson production.

The ratio of cross sections for photoproduction of charged π mesons on beryllium is $\sigma^-/\sigma^+ = 1.8 \pm 0.15$, which is somewhat larger than the number $1.3\,(N/Z)^{2/3} = 1.51$ to be expected when $\sigma^- + \sigma^+ \sim A^{2/3}$ (1.3 is the ratio σ^-/σ^+ for free nucleons). Let us compare the data for beryllium with the data for helium and carbon, all at approximately the same meson energy. It should be recalled that for helium and carbon the ratio of yields of π^- and π^+ mesons is close to 1.3 for both slow[2] and fast[7,5] mesons. Perhaps the peculiarities observed in photoproduction of mesons on neighboring nuclei are due to peculiarities in the structure of these nuclei; both He_2^4 and C_6^{12} have filled shells, while in Be_4^9 one of the shells is not filled.

It is reasonable to suppose that meson production on nucleons in closed shells is inhibited, while production on nucleons in unfilled shells is enhanced. As a rough measure of how much production on nucleons in closed shells is inhibited we can take the following data for He_2^4:

$$\varepsilon = N^+(E_\pi)/ZN_p^+(E_\pi) = 0.51 \pm 0.05\ [^7], \qquad (4)$$

In Eq. (4), $N^+(E_\pi)$ is the meson yield from helium, and $N_p^+(E_\pi)$ is the meson yield from free protons. For nucleons in open shells we take $\epsilon = 1$. Then the ratio of cross sections for formation of π^- and π^+ mesons on beryllium should be 1.73 ± 0.1, which agrees better with the experimental data. At the same time, for carbon the ratio σ^-/σ^+ should be 1.3. We have thus used the experimental data for He to obtain a value of σ^-/σ^+ for beryllium which takes into account shell structure in the nucleus.

There have been a number of attempts[8-10] to explain the anomalous photo-production of mesons on beryllium in terms of a "weakly bound" neutron. From the point of view of the shell model, such a singling out of one nucleon can be justified in terms of pair interactions between nucleons in unfilled shells. If all nucleons in Be_4^9 were equally inhibited in making mesons, except for the single odd one, then σ^-/σ^+ would turn out to be 1.95 ± 0.1, which does not contradict our experimental results. This model could be checked by measuring σ^-/σ^+ for Ne_{10}^{22}, since the unfilled shell in this nucleus has two neutrons.

In conclusion, we should like to thank Prof. P. A. Cerenkov, Prof. V. I. Gol'danskiĭ, É. G. Gorzhevskaya and S. P. Kharlamov for discussion of our results.

---

[1] R. M. Littauer and D. Walker, Phys. Rev. **86**, 838 (1952).

[2] Popova, Semashko, and Yagudina, JETP **36**, 1357 (1959), Soviet Phys. JETP **9**, 965 (1959).

[3] Kharlamov, Adamovich, and Larionova, JETP **36**, 945 (1959), Soviet Phys. JETP **9**, 668 (1959).

[4] J. R. Waters, Phys. Rev. **113**, 1133 (1959).

[5] D. Luckey, Phys. Rev. **97**, 469 (1955).

[6] E'G. Gorzhevskaya and N. M. Panova, Doklady Akad. Nauk SSSR, **111**, 1205 (1956), Soviet Phys.-Doklady **1**, 757 (1957).

[7] Jakobson, Schulz, and White, Phys. Rev. **91**, 695 (1953).

[8] S. T. Butler, Phys. Rev. **87**, 1117 (1952).

[9] H. A. Medicus, Phys. Rev. **83**, 662 (1951).

[10] R. M. Littauer and D. Walker, Phys. Rev. **82**, 746 (1951).

Translated by R. Krotkov
291

ACCELERATION OF POSITIVE IONS IN EXPANSION OF THE PLASMA IN A VACUUM SPARK

A. A. PLYUTTO

Submitted to JETP editor July 14, 1960

J. Exptl. Theoret. Phys. (U.S.S.R.) **39**, 1589-1592 (December, 1960)

Acceleration of positive ions to energies of $10^3 - 10^4$ ev has been detected in the rapid expansion of the plasma in a vacuum spark. A brief description is given of a mechanism capable of explaining the experimental facts; this mechanism involves the acceleration of ions by electrons.

A number of ionic spectra of "hot" vacuum-sparks have been obtained by means of a Thomson mass spectrometer (parabola method) in the development of a spark ion source.[1] Analysis of these spectra has made it possible to study the ionic composition of the plasma and ion formation; in this analysis, positive ions with energies of $10^3 - 10^4$ ev, which originate in the spark-plasma in a number of cases, have been observed. In later experiments it was found that the ions are not accelerated in the spark region; rather, acceleration occurs as the plasma expands into the vacuum region. For this reason it has been proposed that the ions are accelerated by electrons. Subsequently a theory was developed for a simple mechanism by which the ions are accelerated by electrons; this theory allows us to explain the general features of the experimental results.

The ionic spectra of the sparks were obtained with an extraction-acceleration voltage $V_0 = 0 - 70$ kv which is applied in a narrow region (approximately 4 cm) between the source and extraction electrode;[1] the beam then enters the mass spectrometer. No special provision is made for focusing. An ionic spectrum with a clearly defined fast component is shown in the figure. This spectrum has been obtained under the following conditions: $V_0 = 9$ kv; spark voltage $V_S = 7$ kv, spark-circuit inductance $L = 6\,\mu h$, spark capacity $C = 0.005\,\mu f$. The line $V_0 - V_0$ corresponds to the normal energy ZeV_0 (Ze is the charge of the ion). In the ionic spectrum the fast component is found in parabolic segments below the line $V_0 - V_0$ and is characterized by a so-called "plus-spread" in energy. A "minus-spread" (ions with energies less than ZeV_0) is also observed, but is due to other physical causes.

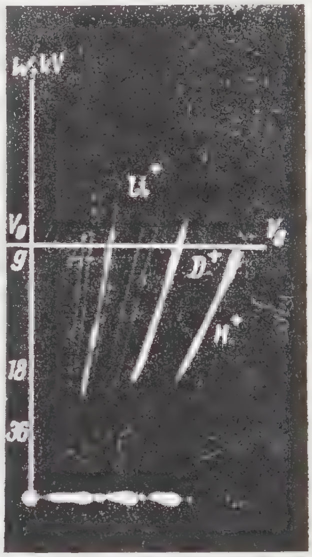

Ionic spectrum of a vacuum spark with a clearly defined fast positive-ion component.

As is apparent from the figure, the maximum energies are as follows: for H^+ and D^+ 18 kv; for Li^+ 24 kv; for C^+ 35 kv. These values are to be compared with the mean energy, which is 2.5 kv. It should be noted that in the majority of cases the fast component is not as well defined, the maximum energies reach several kev for a mean energy of 200 — 500 ev, and the ion energy is independent of mass. In a number of cases the fast component is not observed.

An important characteristic of the fast component is the fact that the maximum energy and the mean energy depend on the extraction voltage V_0. In the majority of cases the fast component vanishes when $V_0 = 30 - 50$ kv; if it does not disappear the maximum and mean ion energies are reduced by large factors. When V_0 is reduced to $5 - 10$ kv the "plus-spread" increases, reaching a maximum value at $V_0 = 0$. Since a change in V_0 does not affect the spark, the fact that the "plus-spread" depends on V_0 would seem to indicate that the ions are accelerated outside the spark, in the region of expanding plasma. The region occupied by the plasma and the degree of expansion are both rapidly reduced as V_0 is increased, causing a reduction of the "plus-spread." If the plasma expands strongly before entering the draw-out region and the ions are accelerated, the "plus spread" becomes independent of V_0. At appreciable fast-component energies the ionic spectra can be photographed without the application of the extraction-acceleration voltage ($V_0 = 0$). In this case the spark ion source becomes a "plasma gun" with energies of $10^3 - 10^4$ ev for some ions. Direct time-of-flight measurements of the velocity of the forward edge of a plasma propagating over a known distance (through the use of a sensitive method) have verified that some ions have velocities up to 10^8 cm/sec (mean velocity of 2×10^7 cm/sec), in good agreement with the mass-spectrometer results. It should be noted that the energy of the fast component does not vary to any great extent when the current is varied by a large factor; the time derivative and the spark-circuit frequency are proportional to Ze.

The results given above and certain other experimental findings indicate that a possible mechanism for this effect is the acceleration of ions by electrons in the expanding, highly ionized plasma. The acceleration mechanism can be analyzed conveniently in terms of a spherical drop model. The light fast electron component of the plasma tends to escape from the drop but is constrained by the Coulomb forces, which are produced by the separation of charges; thus the electrons remain within the volume of the drop. The drop expands from inside because of the electron gas, and the ions are accelerated radially toward the surface. This collective process of energy transfer from electrons to ions is reminiscent of the acceleration of a heavy piston (ions) by a gas (electrons). In carrying out the appropriate calculations we shall use thermodynamic expressions. In particular, assuming an isothermal expansion (electron gas heated externally) we obtain the following expression for the mean ion energy $\overline{W}_i$

$$\overline{W}_i = 4.6\overline{Z}\,\overline{W}_e \log (r/r_0), \qquad (1)$$

where $\overline{W}_e$ is the mean electron energy (in ev), $\overline{Z}$ is the mean charge multiplicity of the ions, r_0 and r, are the initial and final radii of the drop. For a plasma in a vacuum spark $\overline{W}_e = 25$ ev and $\overline{Z} = 1-2$; assuming that $\log(r/r_0) = 2$, we have $\overline{W}_i = 230 - 460$ ev, in good agreement with most of the experimental data. The plasma which escapes from the extraction aperture of the spark source will be approximately spherical at high degrees of expansion and the inflow of new particles is unimportant, so that Eq. (1) applies. In direct proximity to the spark, in spite of the strong expansion of the plasma the ions are not accelerated because of the magnetic field which is transverse to the motion of the plasma. The energy generated in the spark provides isothermal expansion if the thermal conductivity of the plasma is high. Equation (1) also applies for small condensations which expand in a rarified plasma. In order to explain the value $\overline{W}_i = 2.5$ kev, we must assume that under certain conditions, for example, in induction heating, $\overline{W}_e$ can be $100 - 150$ ev.

In order to explain the acceleration of some ions to energies of $(1-3) \times 10^4$ ev, we must study the expansion in detail. We may divide the drop into two regions, in which expansion proceeds differently, viz., a narrow double layer at the surface and the remaining volume. The acceleration of ions in the volume may be described on the basis of ambipolar acceleration of ions by electrons with ambipolar diffusion in the highly ionized plasma. The electric field in the drop is such as to provide expansion of the plasma as a whole, and the expression for ion energy is approximately the same as Eq. (1).

If we assume that the double layer stretches the surface of the drop elastically, acceleration of the ions in the double layer must be realized in such a way that the ions are in a region of high field $10^4 - 10^5$ v/cm at all times; then the ions acquire an energy of $10^4 - 10^5$ ev in a distance of approximately 1 cm. A calculation indicates the following ion energy

$$\overline{W}_i = 3.8 \cdot 10^{-3}\,\overline{Z}\,\overline{W}_e^{1/2} n_{0e}^{1/2} r_0^{3/2} (r_0^{-1/2} - r^{-1/2}), \qquad (2)$$

where n_{0e} is the initial electron concentration in the plasma. For a vacuum spark with $\overline{W}_e = 25$ ev, $n_{0e} = 10^{14}$ cm^{-3}, $r_0 = 0.1 - 1$ cm and $r \gg r_0$, we have $\overline{W}_i/\overline{Z} = 2 \times 10^3 - 2 \times 10^4$ ev for a relative fast component content of $10 - 1\%$, which is of the same order of magnitude as that indicated by the experimental data.

The mechanism considered here for acceleration of ions by electrons does not explain the sporadic appearance of the "plus-spread." This feature may require that some conditions must be satisfied in the plasma in order for acceleration to take place. There are also experiments which indicate that the direction of ionic acceleration in the plasma does not always coincide with the axial direction of the device; in these cases the ions are not recorded in the ionic spectrum.

This mechanism for ion acceleration by electrons can be applied in the analysis of physical processes in an inhomogeneous plasma. If there is a high degree of inhomogeneity in a plasma at a high electron temperature (10^5 degrees and higher) the collective processes for the transfer of energy from electrons to ions may predominate over the elementary processes. In thermal plasmas at temperatures of $10^7 - 10^8$ degrees, these processes can predominate even for a very slight inhomogeneity. In this connection, we may note that the electrical conductivity of an inhomogeneous plasma may be much lower than that of a plasma of uniform density. In particular, the anomalously low electrical conductivity in the Zeta system may be due to the inhomogeneity in plasma density, which, because of instabilities, lasts for the entire pulse.

On the other hand, in an inhomogeneous plasma, the expansion of a condensation can result in the production of fast ions (0.1 — 1%) with energies of $10^4 - 10^5$ ev directed along the electric field. This fast component may be responsible for neutron radiation in highly ionized inhomogeneous plasmas, for example, in linear pinches and induction pinches In inhomogeneous plasmas in a magnetic field, ions can be accelerated along the lines of force by electrons if the Larmor radius is smaller than the electron mean free path.

It is interesting to note that high-velocity gas flows with particle energies of $10^2 - 10^3$ ev have been observed in stationary vacuum arcs.[2] This effect, which is not understood at the present time, may be due to the acceleration of ions by electrons in plasmas which expand from cathode sparks. Using Eq. (1), and taking $\overline{W}_e = 10$ ev, $\overline{Z} = 1 - 2$, $r_0 = 10^{-2} - 10^{-3}$ cm (the dimensions of a cathode spot) and $r = 10$ cm, we have $\overline{W}_i = 140 - 380$ ev, which is in approximate agreement with the experimental data. In moving from the cathode spots the ions undergo charge exchange and form a flux of neutral gas. A detailed analysis of the results of these investigations is contained in papers which are being prepared for publication.

In conclusion the author wishes to express his gratitude to I. F. Kvartskhava and K. N. Kervalidze, who helped with this work, and Academician K. D. Sinel'nikov, Professor E. S. Borovik, and B. S. Akshavov for valuable discussions concerning the acceleration of ions by electrons.

---

[1] Plyutto, Kervalidze, and Kvartskhava, Атомная энергия (Atomic Energy) **3**, 153 (1957).

[2] R. Tanberg, Phys. Rev. **35**, 1080 (1930); R. M. Robertson, Phys. Rev. **53**, 578 (1938).

Translated by H. Lashinsky
292

SOVIET PHYSICS JETP VOLUME 12, NUMBER 6 JUNE, 1961

THE GAMMA SPECTRUM OF Na^{24} *IN THE 2.5 – 5.5 MEV ENERGY RANGE*

K. P. ARTAMONOVA, L. V. GUSTOVA, Yu. N. PODKOPAEV, and O. V. CHUBINSKIĬ

Leningrad State University

Submitted to JETP editor July 15, 1960

J. Exptl. Theoret. Phys. (U.S.S.R.) **39**, 1593-1595 (December, 1960)

The hard γ radiation from Na^{24} was investigated. The previously known γ lines corresponding to the transitions $h\nu = 2.75$ and 3.85 Mev have been observed, and a more precise determination yielded for the intensity of the latter transition a value $(9 \pm 2) \times 10^{-4}$ quantum per decay. Gamma rays from the transition $h\nu = 4.24$ Mev (4230 ± 50 kev), the intensity of which is $(1.5 \pm 0.5) \times 10^{-5}$ quantum per decay, have been detected. The upper limit of the intensity of the 5.22-Mev γ transition, which is possible according to the Na^{24} decay scheme, is estimated at $I_{5.22} \leq 2 \times 10^{-7}$ quantum per decay. The reduced half-lives for β transitions with $E_p = 0.29$ and 1.27 Mev are estimated at log ft = 6.6 and log ft = 10.7, respectively.

In references 1 and 2, devoted to the investigation of the hard γ radiation of Na^{24}, values were found for the intensity of the transition with $h\nu = 3.85$ Mev and for the estimated upper limits of the intensities of the γ transitions of energy higher than 4 Mev, which are possible according to the decay scheme of Na^{24}. The present paper reports on further investigation of the hard radiation of Na^{24}.

Using the γ hodoscope of the Physics Research Institute of the Leningrad State University,[3,4] we investigated the γ spectrum of Na^{24} in the region above 2.5 Mev. The γ-ray source was an Na_2CO_3 compound in which the Na^{24} isotope was produced by the (n, γ) reaction. The activity of the compound was 3.4 C at the start of the reaction. Five series of measurements were at different magnetic field intensities. The table lists the values of the magnetic field intensity of each series of measurements and the values of H/H_0, which characterize the conditions under which the spectral γ lines were registered at a given H (H_0 is the value of the magnetic field at which optimum conditions are produced for the registration of γ rays of given energy).

No. of series	H, oe	*H/H₀*				
		2.75 Mev	3,85 Mev	4.12 Mev	4.24 Mev	5,22 Mev
I	1675	(1,83)	1.34	1,26	1,22	1.00
II	1377	(1.51)	1.10	1.03	1.00	0.82
III	1252	1.37	1.00	0,94	0.91	0.75
IV	1226	1.34	0.98	0.92	0.89	0.73
V	913	1.00	0.73	(0.68)	(0.67)	(0.55)

The values of H/H_0 in the parenthesis indicate that the corresponding line is not registered by the instrument at the given H.

The figure shows the form of the γ spectrum of Na^{24}, with the background eliminated, for H = 1675 oe. Resolution of the spectrum (dotted lines) with allowance for the dependence of the instrument line shape on h and on H, makes it possible to separate the γ line of energy 4230 ± 0.050 Mev. The continuous curve on the left of the figure corresponds to the "hard fall-off" of the known 3850-Mev line.

The intensity ratio of the 3.85- and 4.24-Mev γ transitions, determined from the ratio of the areas under the corresponding lines in the measurement series I, II, and III, is 1: 0.018 (averaged over the three series). The error in the determination of the intensity ratio reaches 35 or 45%.

We have determined the relative intensities of the γ transitions with $h\nu = 2.75$, 3.85, and 4.24 Mev by comparing the areas under the 3.85-Mev line in measurement series II, III, and IV, and under the 4.24-Mev line in series I with the area under the 2.75-Mev line in series V. The comparison was made with allowance for the probability of registration of the line at the given field H, the decay of the Na^{24} compound, and the efficiency of the apparatus in each measurement series. The average value (over three series) of $I_{3.85}/I_{2.75}$ is $(9 \pm 2) \times 10^{-4}$, while $I_{4.24}/I_{2.75} = (1.5 \pm 0.5) \times 10^{-5}$. If it is assumed that the intensity of the 2.75-Mev transition is one quantum per decay, then the intensities of the 3.85- and 4.24-Mev transitions are 9×10^{-4} and 1.5×10^{-5} quantum per decay, respectively. This method of determining the relative transition intensities can be regarded as the more accurate, since the compared lines are obtained under the most favorable

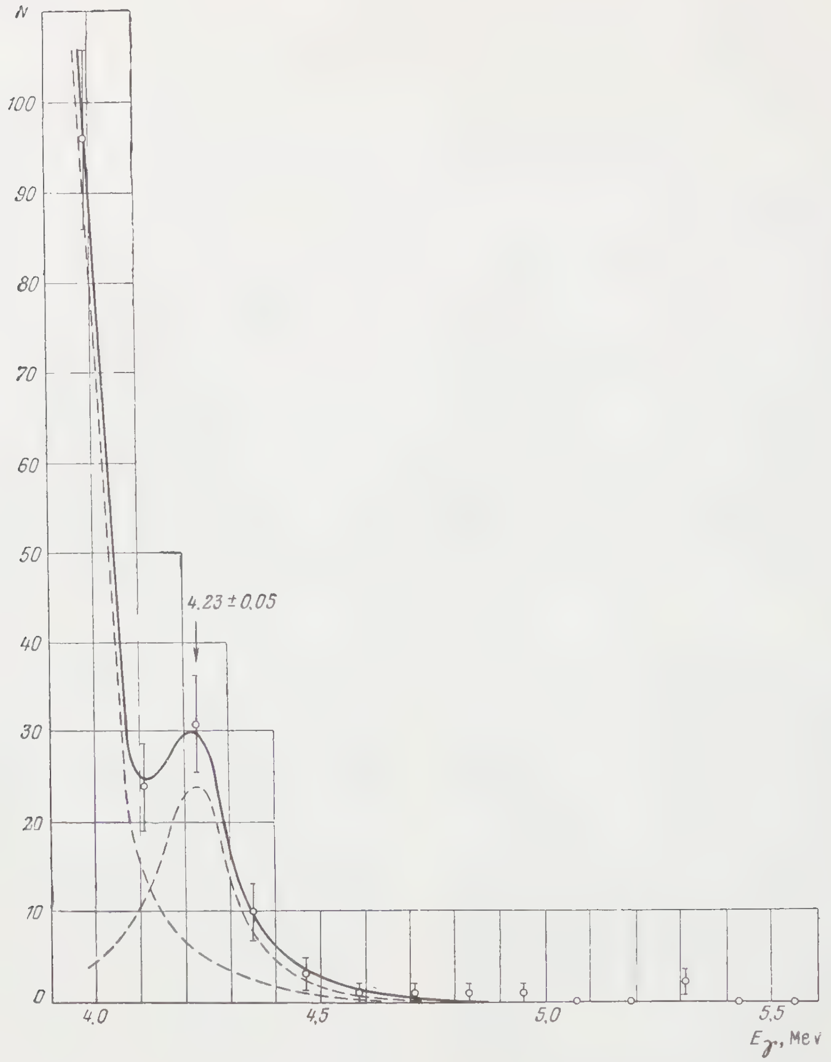

registration conditions. The errors in the determination of the intensities are due to the inaccuracy in the resolution of the spectrum, to statistical measurement errors, and to errors in the values of the registration probability.

In the energy region ~ 5.3 Mev (see the figure), the experimental points are observed to exceed the background slightly. This enables us to estimate the upper limit of the intensity of the γ transition with $h\nu \approx 5.22$ Mev, which is possible in accordance with the decay scheme of Na^{24}. We find that $I_{5.22} \leq 2 \times 10^{-7}$ quantum per decay.

Within the limits of the spectral resolution (see the figure), we observed no 4.12-Mev transition.

The observed γ rays with $h\nu = 4.24$ Mev and intensity 1.5×10^{-5} quantum per decay allow us to assume that the Na^{24} decay is accompanied by a β transition with $E_{\lim} = 1.27$ Mev (see reference 5) with intensity not lower than $1.5 \times 10^{-3}\%$ decays and log ft = 10.7. The intensity of the β transition with $E_{\lim} = 0.29$ Mev (reference 5) is apparently of the same order as the intensity of the 3.85-Mev γ transition, i.e., $9 \times 10^{-2}\%$ decays, so that no other γ transitions are observed from the 5.22-Mev level. For this transition we have log ft = 6.6.

The authors are grateful to B. A. Emel'yanov for aid in preparing the source and in the measurement, and to N. D. Novosil'tseva for providing the project with a good source.

---

[1] Gustova, Dzhelepov, Ermolov, and Chubinskiĭ, Izv. Akad. Nauk SSSR, Ser. Fiz. **22**, 211 (1958), Columbia Tech. Transl. p. 208.

[2] O. V. Chubinskiĭ, Dissertation, Phys. Res. Inst. Leningrad State Univ. 1959.

[3] B. S. Dzhelepov, Izv. Akad. Nauk SSSR, Ser. Fiz. **21**, 1580 (1957), Columbia Tech. Transl. p. 1569.

[4] O. V. Chubinskiĭ, ibid. p. 1583, transl. p. 1572.

[5] B. S. Dzhelepov and L. K. Peker, Схемы распада радиоактивных ядер (Decay Schemes of Radioactive Nuclei), Acad. Sci. Press, 1958.

Translated by J. G. Adashko
293

SOVIET PHYSICS JETP VOLUME 12, NUMBER 6 JUNE, 1961

FERROMAGNETIC RESONANCE IN SILICON-IRON CRYSTALS AND ITS RELATION TO DOMAIN STRUCTURE

A. S. SHUR and O. I. SHIRYAEVA

Institute of Metal Physics, Academy of Sciences, U.S.S.R.

Submitted to JETP editor July 19, 1960

J. Exptl. Theoret. Phys. (U.S.S.R.) **39**, 1596-1601 (December, 1960)

Measurements of the resonance absorption curves at 9370 Mc/sec were made on monocrystalline disks of silicon iron, with surface orientations (001) and (011), at different magnitudes and directions of the constant magnetic field in the plane of the specimen. The domain structure was observed by the powder-pattern method. It was established that besides the resonance peak observed in fields sufficient to saturate the crystal, an additional resonance peak may appear in very weak fields in the presence of a multidomain structure, if the orientation of the alternating magnetic field is parallel to the domain walls. This makes possible the use of the phenomenon of ferromagnetic resonance for exhibiting the domain structure and for determining its form qualitatively.

1. INTRODUCTION

ALTHOUGH ferromagnetic resonance was discovered comparatively recently, this phenomenon has already been studied in detail on many materials. Ferromagnetic resonance is usually observed in large enough constant magnetic fields to saturate the ferromagnet. The existing theories of ferromagnetic resonance[1] satisfactorily explain the resonance that occurs with parallel orientation of the spins and of the constant external magnetic field. In some cases, however, two resonance peaks are detected in measurement of the absorption curves; one of the peaks is observed in comparatively weak magnetic fields, insufficient to saturate the specimen.[2-4]

It has been shown theoretically[4,5] that in the presence of a certain form of domain structure, a high-frequency field oriented parallel to the domain walls can produce a resonance phenomenon in weak fields. Thus there has been predicted theoretically a direct relation between the form of the domain structure of a ferromagnetic crystal and the additional peaks on the absorption curve. If there actually is such a relation, then new possibilities are thereby opened up for experimental study of domain structure. The fact is that in many cases there is no possibility of observing this structure by the existing methods of direct observation (the powder-pattern method and the magneto-optical methods). Perhaps in such cases it may be possible, through measurement of the absorption curves of a ferromagnetic crystal, to show the presence of a domain structure and even to establish some of its details.

The present research was undertaken with the aim of establishing experimentally, in crystals of silicon iron, the relation between the course of the absorption curve and the form of the domain structure.

2. SPECIMENS AND METHOD OF OBSERVATION

As the ferromagnetic material to be investigated, silicon iron (3.5% Si) was chosen because its magnetic structure has been studied in considerable detail. In addition, production of resonance absorption does not require very high frequencies, since the anisotropy constant of this ferromagnetic material is comparatively small.

The investigations were carried out on 15 monocrystalline specimens in the form of disks with various diameters (from 4 to 15 mm) and various thicknesses (0.07 to 0.2 mm). The surfaces of these crystals were close to the crystallographic planes (001) and (011). The specimens were etched from sheets containing large crystals, then were subjected to annealing in a vacuum at 1100° C. Then the specimens underwent an electrolytic polishing. To insure the possibility of comparing the results obtained by observation of the magnetic structure and by measurement of the resonance absorption, both investigations were made on the same specimens.

The investigation of the ferromagnetic resonance phenomenon was made at frequency 9370 Mc/sec. The generator of high-frequency oscillations was composed of a wave-guide track with a resonant cavity in the form of a cylinder, in which oscillations of the H_{112} mode were excited. In the cylinder there were two coupling apertures, which were used to measure the high-frequency power transmitted through the cavity. For measurement of the transmitted power, the cavity was connected to a detector cell. The specimen was fastened to the head of the cylinder, which could be rotated. The cylinder was placed between the poles of an electromagnet in such a way that the orientations of the constant magnetic field (H) and of the alternating field (h_{∞}) were mutually perpendicular and lay in the plane of the disk. By rotating the cavity head, it was possible to measure the absorption curve for various orientations of the specimen with respect to the constant magnetic field.

The magnetic structure of the specimens was studied by the powder-pattern method.[6] For observation of these patterns, the head, together with the specimen attached to it, was removed from the cavity and placed between the poles of the electromagnet, in the same position as in the observation of the resonance absorption. Then the surface of the specimen was covered with a magnetic suspension, and observation of the powder patterns was carried out with gradual increase of the magnetic field, which was parallel to the surface of the specimen. Just as in the measurement of resonance absorption, it was possible to rotate the specimen about an axis perpendicular to its surface; that is, it was possible to observe the magnetic structure for various orientations of the constant magnetic field in the plane of the specimen. In silicon-iron crystals, at the frequency of alternating field used in this work, the depth of penetration is about 10^{-5} cm. Therefore the absorption curves will be determined by the properties of a thin surface layer and by its domain structure. The powder-pattern method reveals the domain structure only of a surface layer. Thus in our case there is a possibility of comparing the absorption curves with the form of the domain structure.

3. COMPARISON OF THE COURSE OF THE ABSORPTION CURVE WITH THE FORM OF DOMAIN STRUCTURE

The investigations of ferromagnetic resonance and of domain structure were carried out on two groups of specimens, whose surfaces coincided with a (001) plane [(001) specimens] or with a (011) plane [(011) specimens]. Qualitatively similar results were obtained on all specimens with the same orientation of the surface. Therefore we shall restrict ourselves to the detailed consideration of data obtained on two crystals whose surfaces were nearly parallel to (001) and to (011) planes. The dimensions of these monocrystals were respectively as follows: diameter, 7.0 and 9.0 mm; thickness, 0.22 and 0.10 mm.

(011) Specimen. The plane of this specimen contains all three principal crystallographic directions of a cubic crystal: [100], [110], and [111].

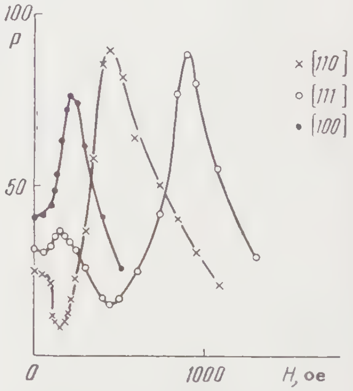

FIG. 1. Absorption curves. Crystal surface close to plane (011). Constant field **H** parallel to axis [110], [111], or [100].

Figure 1 shows resonance absorption curves obtained with the constant field oriented along these crystallographic axes (P is the energy absorbed). For magnetization in direction [100] we have a resonance curve with a single maximum, at a field of order 220 oe. A curve with a single maximum is also observed for direction [110]. On the resonance absorption curve in direction [111] there are two clear maxima: the first at field 160 oe, the second at field 900 oe.

(001) Specimen. The plane of this specimen contains two directions of easy magnetization, [100] and [010]; the difficult direction of magnetization is the axis [110]. Figure 2 shows absorption curves for two directions of magnetization: the easy, [100], and the difficult, [110]. The resonance absorption curve for axis [100] has a single

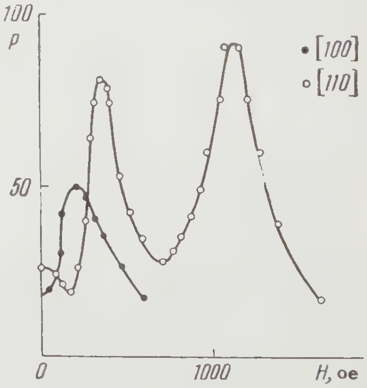

FIG. 2. Absorption curves. Crystal surface close to plane (001). Constant field parallel to axis [100] or [110].

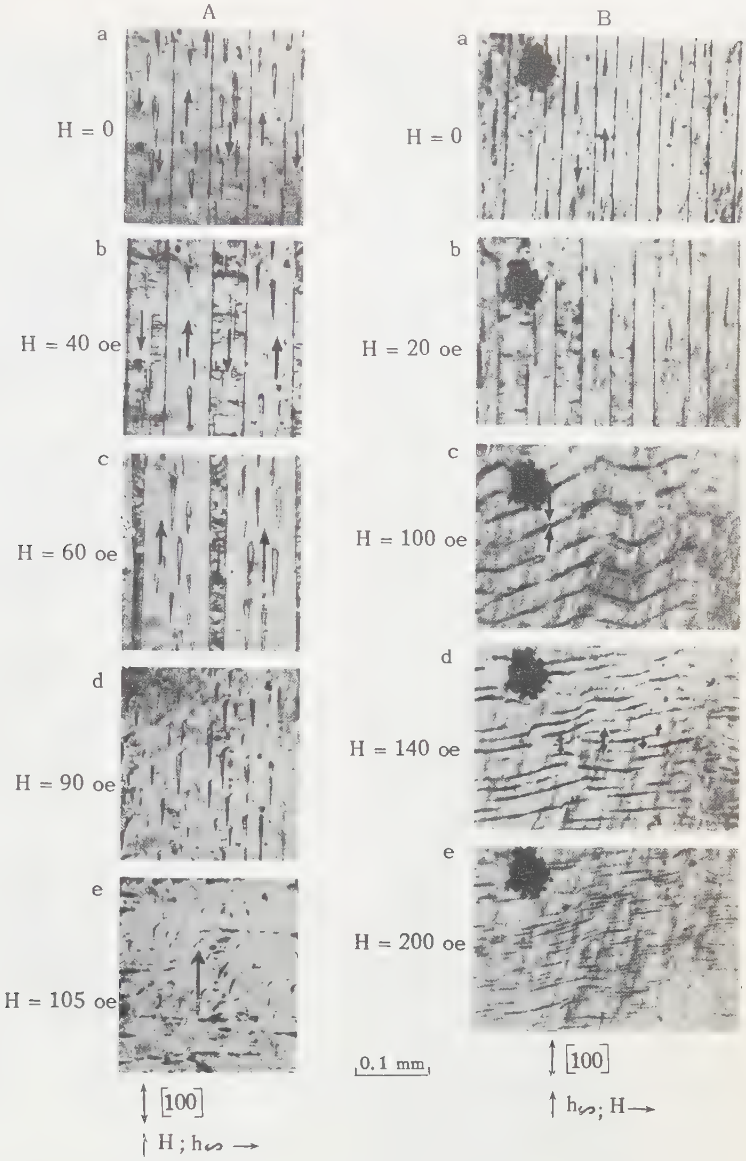

FIG. 3. Powder-pattern photographs on surface of (011) specimen.

maximum at a field of about 200 oe. On the absorption curve for direction [110] there are two maxima, of which the first is obtained at a value of the external field of about 370 oe and the second in a field of about 1150 oe. Similar results for a (001) specimen were obtained earlier by Kip and Arnold.[2]

From the curves of Figs. 1 and 2 it is clear that for magnetization in a difficult direction — [110] for a (001) specimen and [111] for a (011) specimen — two clearly separated resonance peaks are observed on the resonance absorption curve. As has already been indicated, according to existing theoretical ideas,[4,5] the peak in weak fields is connected with the presence of a domain structure. This peak is retained also when the orientation of the field deviates by a small angle from the [111] axis in the plane of the (011) specimen and from the [110] axis in that of the (001) specimen. It is observed at the same value of the constant field as when the field is oriented parallel to the difficult direction in the plane of the specimen. However, the height of the peak decreases with increase of the angle of deviation, and for angles of 10 to 15 degrees the additional peak disappears.

We pass on to the results of the direct observations of domain structure. Figures 3 and 4 show photographs of the powder patterns for the (011) specimen. In the initial state (Fig. 3 A and B, and Fig. 4 A, case a), this specimen has a simple magnetic structure, the so-called type-A structure:[6] it breaks up into basic domains with 180° walls. The orientation of the magnetization in these domains coincides with the axis of easy magnetization closest to the specimen surface

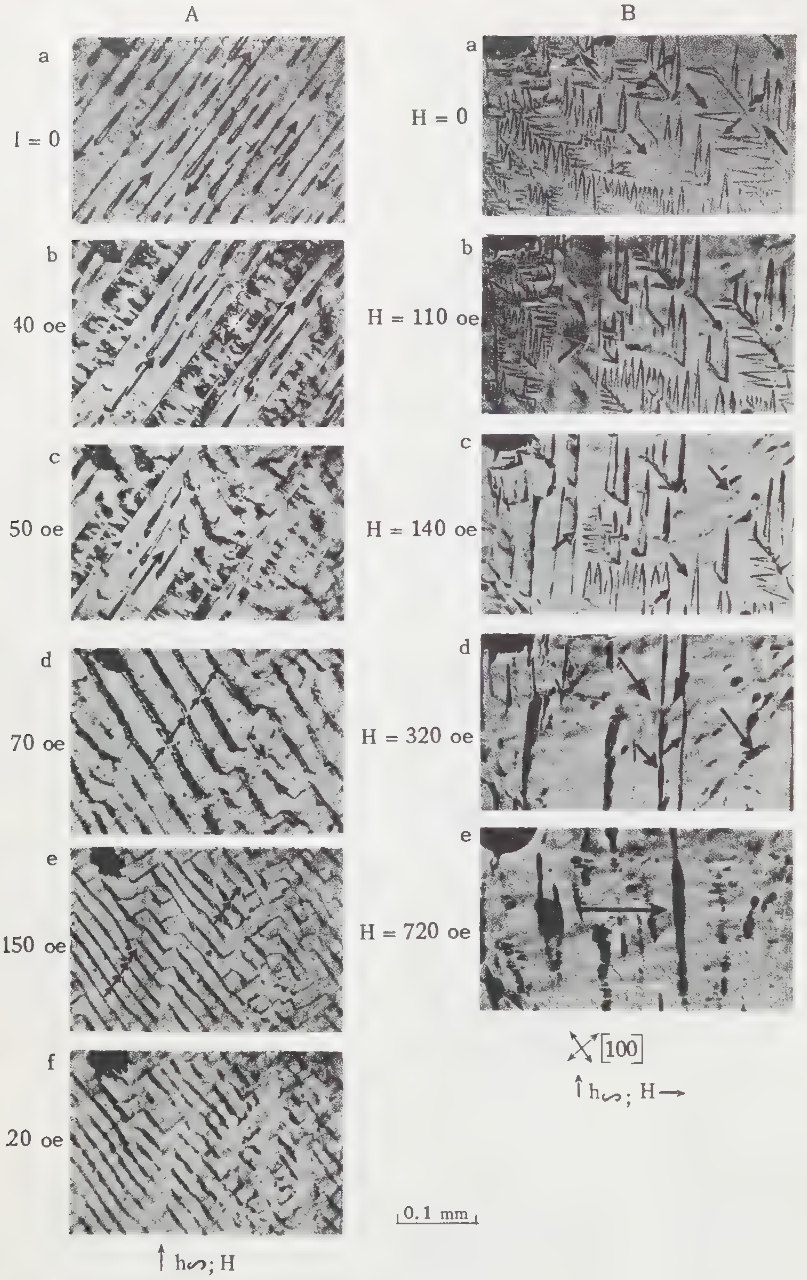

FIG. 4. Powder-pattern photographs: A, surface of specimen (011); B, surface of specimen (001).

(the [100] axis). In consequence of the fact that the [100] axis makes a small angle with the surface, there appear on this surface closure domains of droplet shape, whose magnetization is antiparallel to the magnetization in the basic domains.[6]

Figure 3 A shows photographs of the powder patterns for the case of magnetization in direction [100].* The arrows on the photographs show the orientation of the magnetization in the domains. On application of the magnetic field and gradual increase of it, there occurs a displacement of 180° walls between adjacent domains (Fig. 3 A, cases b and c). In a field of 90 oe, the displacement process is completed, but the closure domains remain (Fig. 3 A, case d). In fields of order 200 oe the specimen reaches magnetic saturation (Fig. 3 A, case e).

Figure 3 B shows photographs of powder patterns for magnetization of the specimen in direction [110]. On increase of the magnetic field the walls between the basic domains disappear, and after them the closure domains in the "droplet" form (Fig. 3 B, case c). At the same time a new

series of strips are formed; they mark the appearance of a new type of domain structure, the so-called type-B structure.[6,7] The peculiarity of this structure is that the basic domains are located within the crystal, with their magnetization oriented along the axes of easy magnetization [010] and [001]. Visible on the surface are closure domains, having the form of prisms, whose bases come out of the surface of the specimen. The orientation of the magnetization in these closure domains is not favorable in relation to the external magnetic field; therefore with increase of the field, a breaking up of them occurs (Fig. 3 B, cases d and e), leading to a diminution of volume of these domains.[7]

---

*More precisely, along the projection of the [100] direction on the plane of the specimen. However, in view of the smallness of the angle of deviation of the axis from the surface, we will assume that the field is parallel to the axis. The same holds with respect to axes [110] and [111].

Figure 4 A shows the transformation of magnetic structure under the influence of a magnetic field in the direction [111] — a difficult direction of magnetization. As is evident from Fig. 4 A (case a), in the initial state there is the usual type-A structure; on application of the magnetic field (Fig. 4 A, case b), there begins a process of displacement of 180° walls. On gradual increase of the field, there occurs a transformation of the type-A structure. The beginning of the transformation is evident in Fig. 4 A, case c. In a field of order 70 oe (Fig. 4 A, case d), a new type of magnetic structure is seen, the so-called B structure.[7] Located on the surface are prismatic closure domains; the magnetization vectors in adjacent domains are directed in opposite senses, parallel to the [100] axis. The basic domains are located inside the specimen, and their magnetization is oriented along the two other axes of easy magnetization, [010] and [001]. With further increase of the magnetizing field, the type-A structure completely disappears; and on the surface the closure domains, with an unfavorable orientation of the magnetization with respect to the external field, contract (Fig. 4 A, case d). On subsequent increase of the field, there remain on the surface of the specimen only closure domains with a single direction of magnetization (case e); but the walls between these domains remain, thanks to the antiparallel orientation of the basic domains. Further increase of the field causes disappearance of the walls, which indicates approach to a state of saturation (case f).

We shall compare the powder-pattern photographs of the (011) specimen with the resonance absorption curve (Fig. 1). In the measurement of the absorption curves in the direction of the [100] axis, the resonance maximum is observed in a field of order 220 oe. From the form of the powder patterns (Fig. 3 A) it can be noted that at this field the specimen is magnetized to saturation. A similar picture is obtained also for magnetization along the [110] axis (Fig. 3 B). Furthermore, in this case the walls between domains are, throughout the process of magnetization, always oriented approximately perpendicular to the direction of the alternating magnetic field. It is otherwise for magnetization of the specimen along the difficult direction [111] (Fig. 4 A). In this case two resonances are observed on the absorption curve — the first in a field or order 150 oe, at which there is visible on the surface a clear magnetic domain structure with parallel walls (Fig. 4 A, case e). It should be noted that the high-frequency magnetic field h_∞ in this case has a component parallel to the walls. The second resonance peak was observed in a field of order 900 oe, at which the specimen is already magnetized to saturation.

Figure 4 B gives powder-pattern pictures of the (001) specimen for magnetization along direction [110]. In the initial state (Fig. 4 B, case a), one sees on the surface of the crystal a type-A magnetic structure, with closure domains of "tree" and "trunk" type.[6] On application of the magnetic field, the branches of the "trees" and "trunks" with one direction begin to grow, and on gradual increase of the field they are transformed to "wedges." Some of these "wedges" are converted to basic domains (Fig. 4 B, cases b and c). Further increase of the field leads to disappearance of the closure domains, and the whole crystal consists of basic domains, whose magnetization is oriented along the two axes of easy magnetization. In fields of 700 to 800 oe the process of magnetization is completed, and the crystal becomes magnetized to saturation.

We shall compare these results with the resonance absorption curve for direction [110]. It is clear from Fig. 2 that the first maximum is observed at a field of order 370 oe. The magnetic structure in this field consists of domains whose walls (Fig. 4 B, case d) are parallel to the direction of the alternating field.

Upon magnetization of the (001) specimen along the [100] axis, only displacement of 180° walls is observed; the high-frequency field is perpendicular to the domain walls, as in the case shown in Fig. 3 A.

When the orientation of the constant field in the plane of the crystal is inclined to the [111] axis in the (110) specimen, or to the [110] axis in the (100) specimen, by an angle less than 10 to 15 degrees, the observed transformation of the magnetic structure is of the same nature as that illustrated in Fig. 4 A and B. At large angles of inclination, domain structures of another form are produced: in them, the walls between domains are perpendicular to the direction of the alternating field. As was mentioned above, at these angles the additional peaks in the absorption curves likewise disappear.

Thus comparison of the powder-pattern photographs and of the resonance absorption curves for a (011) specimen magnetized in a [111] direction has shown that the additional resonance peak in weak fields occurs in the presence of a multidomain structure. Under these conditions the high-frequency field has a component parallel to the walls between domains. For specimen magnetization in directions [100] and [110] either saturation occurs in comparatively small fields, or there is a multidomain structure of such nature that the alternating magnetic field has no component parallel to the walls between domains.

Comparison of the powder-pattern pictures and of the resonance absorption curves for a (001) specimen magnetized in a [110] direction has shown that to the resonance peak in weak fields there corresponds a multidomain structure such that the high-frequency field is parallel to the walls between domains.

CONCLUSION

Measurements of the resonance absorption curves at frequency 9370 Mc/sec and observations of the domain structure on the same crystals of silicon iron have shown that the additional resonances exhibited in weak fields for certain orientations of the specimen surface are observed only in case the crystal has a multidomain structure and the high-frequency magnetic field is parallel, or has a component parallel, to the domain walls. These results provide experimental confirmation of the correctness of theoretical ideas,[4,5] which relate the appearance of additional resonance peaks to a definite form of domain structure in the crystals. Thanks to the existence of such a relation, it is possible to use the phenomenon of ferromagnetic resonance for detection of the domain structure of ferromagnets and for establishment of some details of the structure. Such a method of studying the domain structure is of great interest, especially in those cases in which it is not possible to use the known methods of direct observation of this structure.

---

[1] C. Kittel, Phys. Rev. **73**, 155 (1948); D. Polder, Phil. Mag. **40**, 99 (1949); J. H. Van Vleck, Phys. Rev. **78**, 266 (1950).

[2] A. F. Kip and R. D. Arnold, Phys. Rev. **75**, 1556 (1949).

[3] L. R. Bickford, Phys. Rev. **78**, 449 (1950); K. H. Reich, Phys. Rev. **101**, 1647 (1956).

[4] J. Smit and H. G. Beljers, Philips Res. Rep. **10**, 113 (1955).

[5] J. O. Artman, Phys. Rev. **105**, 62 and 74 (1957); T. Nagamiya, Progr. Theoret. Phys. (Kyoto) **10**, 72 (1953).

[6] Ya. S. Shur and V. R. Abel's, Физика металлов и металловедение (Phys. of Metals and Metallography) **1**, 11 (1955).

[7] Ya. S. Shur and V. R. Abel's, ibid. **6**, 556 (1958).

Translated by W. F. Brown, Jr.
294

SOVIET PHYSICS JETP VOLUME 12, NUMBER 6 JUNE, 1961

MAGNETIC-MIRROR CONFINEMENT OF A PLASMA

M. S. IOFFE, R. I. SOBOLEV, V. G. TEL'KOVSKIĬ and E. E. YUSHMANOV

Submitted to JETP editor July 20, 1960

J. Exptl. Theoret. Phys. (U.S.S.R.) **39**, 1602-1611 (December, 1960)

The containment of a hydrogen plasma (density 10^9 cm^{-3}) in a cylindrical magnetic-mirror system has been studied. The mean ion energy in the plasma is $1-2$ kev, the mean electron energy is approximately 10 ev, and the minimum neutral-gas pressure under operating conditions is $3-4\times10^{-7}$ mm Hg. Plasma confinement is investigated by measuring the fast-ion lifetime. It has been found that ions escape from the confinement system much more rapidly than would be expected on the basis of charge exchange and scattering. Anomalous ion losses are observed only with plasma in the trap. These losses are not observed when the density of charged particles is reduced to values such that the Debye distance becomes comparable to the dimensions of the confinement system.

FORMULATION OF THE PROBLEM

THEORETICALLY, a plasma cannot be contained for long periods of time in a magnetic-mirror system; the containment time is not limited by Coulomb scattering of charged particles or escape through the mirrors,[1] but by the instabilities that arise in the plasma. Field instabilities may arise in a magnetic-mirror because the field falls off radially (interchange instability)[2,3] and because of the anisotropy in the longitudinal and transverse temperatures of the charged particles.[4] At small values of β $[\beta = 8\pi n(T_e + T_i)/H^2]$ the greatest danger lies apparently in the interchange instability; this effect is frequently called the flute instability.

However, magnetic compression experiments are not in accord with theoretical predictions.[5,6] In these experiments ($n \sim 10^{14}$ cm^{-3}, $T_e = 10-20$ kev, $T_i = 1$ kev, $H = 40{,}000$ oe) plasma containment was observed for several milliseconds; this time is considerably in excess of the time required for the development of instabilities under these conditions. The authors have explained this discrepancy as due to a number of experimental conditions which are not taken into account by the theory. In particular, they point out the stabilizing effect of the cold plasma in the regions beyond the mirrors which is in contact with conducting walls.[6]

Because of the complexity of the problem, a final evaluation of the possibility of stable plasma confinement cannot be made on the basis of the experiments which have been reported. For this reason it is of interest to carry out investigations under other conditions.

In the work reported here we have investigated a magnetic-mirror system with dimensions of the order of tens of centimeters, filled with a hydrogen plasma with a mean density of approximately 10^9 cm^{-3} at a minimum neutral-gas pressure of approximately 3×10^{-7} mm Hg. The mean ion energy is $1-2$ kev. The mean electron energy is small, of the order of 10 ev. The magnetic field is $(5-8)\times10^3$ oe. Under these conditions both the adiabaticity requirement (the ion Larmor radius must be small compared with the dimensions of the mirror system) and the neutrality requirement (the Debye radius must be small compared with the dimensions of the region occupied by plasma) are well satisfied.

Plasma containment was investigated by observing the rate of reduction of the density of fast ions after the plasma production process was terminated. Because of the appreciable ion energy and the low plasma density, processes such as the scattering of fast ions on the plasma components (which result in entry into the escape cone and loss from the confinement system) and slowing down of ions on electrons are relatively weak. The scattering time is of the order of tens of seconds while the slowing-down time is of the order of a tenth of a second (cf. for example reference 7).

The fast-ion loss caused by charge exchange on the neutral gas is a much greater effect. Thus, at a hydrogen pressure of $3-5\times10^{-7}$ mm Hg the mean charge-exchange time for ions with energies of $1-2$ kev is several milliseconds at most. Other processes involving the interaction of ions with the neutral gas, such as excitation, ionization, and scattering are much weaker than charge exchange for the ion energies indicated here.

Thus, if a plasma with the parameters indicated above is produced in the mirror system, its subsequent decay (i.e., the reduction in the density of fast ions) should take place primarily as a result of charge exchange. If, however, there is some additional mechanism which removes fast ions from the confinement system, the lifetime is reduced still further.

EXPERIMENTAL APPARATUS AND METHOD OF MEASUREMENT

The apparatus used in these experiments is shown schematically in Fig. 1. A fixed magnetic field is produced by means of four coils 1. The maximum field intensity $H_0 = 8000$ oe at the center and $H_{max} = 12{,}400$ oe at the mirrors; the corresponding mirror ratio is $\alpha = H_{max}/H_0 = 1.55$.

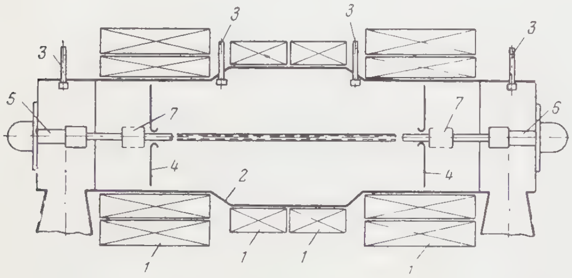

FIG. 1. Diagram of the apparatus; 1) coils for magnetic field, 2) vacuum chamber, 3) titanium evaporators, 4) apertured walls, 5) plasma source, 6) detection electrode, 7) caps.

The vacuum chamber 2 is made of stainless steel; the chamber is 2 m in length, the diameter of the central portion is 50 cm and the diameter at the mirrors 37 cm. The chamber is evacuated by two N-5T oil-diffusion pumps to a pressure of 10^{-6} mm Hg; the pumps are provided with nitrogen traps. Lower pressures are achieved by absorption of titanium which is evaporated directly at the inner surface of the chamber. The system is provided with four titanium evaporators 3 each of which provides a hydrogen pumping rate up to 20,000 liters/sec at 4×10^{-7} mm Hg. The minimum residual gas pressure after the titanium is flashed on the chamber walls is 5×10^{-8} mm Hg.

The cold plasma is produced in a source which uses a hot-cathode hydrogen arc discharge in a longitudinal magnetic field.[8] The source 5 is located near one of the mirrors. The plasma, with electron and ion temperatures characteristic of this kind of discharge, is emitted through an aperture in the discharge chamber and moves along the axis of the magnetic field in a beam approximately 10 mm in diameter. Near the opposite mirror the beam is collected by a detection electrode 6 which is at the anode potential of the source. With a hydrogen consumption of 300 cm^3 per hour in the source, the plasma density in the beam is approximately 10^{12} cm^{-3}.

To produce fast ions in the plasma, we set up a radial electric field between the beam and the chamber walls by applying a positive potential to the source (up to 45 kv with respect to the walls). The ions in the beam and the low-density plasma which surround it are accelerated by this field and execute cycloidal motion in the crossed electric and magnetic fields. The accelerating voltage U_0 is applied in single rectangular pulses 25 — 30 μsec long; the length of the leading edge is 2 μsec while the length of the trailing edge is 0.2 μsec.

After the accelerating voltage pulse is terminated the ions in the plasma retain part of the kinetic energy acquired in the electric field. In order to prevent the entry of cold plasma from the source into the system after the electric field is switched off, the discharge in the source is turned off at the trailing edge of the accelerating voltage pulse.

To minimize the neutral-gas pressure in the system, we use a differential pumping system; the vacuum chamber is divided into three sections by two metal walls 4. These walls are located in the region of maximum magnetic field and have center apertures 5 cm in diameter to permit passage of the plasma beam. For this reason there is a rather high impedance to the flow of neutral gas into the central part of the mirror system from both the source and the detection electrode on which ions of the plasma beam are neutralized. To ensure that the beam is not affected by the strong electric fields close to the edges of the aperture in the walls while the accelerating voltage pulse is on, special caps 7 are used to block off the source and the detection electrode. With the source in operation the pressures are as follows: in the central section $(3-4) \times 10^{-7}$ mm Hg, in the source chamber 4×10^{-6} mm Hg, in the detection chamber 1.5×10^{-6} mm Hg.

Under the conditions described here, at the end of the accelerating voltage pulse the system is filled by plasma with a mean density of approximately 10^9 cm^{-3} and a mean ion energy of 1 — 2 kev. The determination of plasma density and particle energy will be discussed below in connection with the experimental results.

Plasma containment in the mirror system is studied by observing the fast-ion lifetime. If the only loss mechanism is charge exchange, the mean fast-ion lifetime in the system τ should equal the charge-exchange time τ_{ce}, which is $\tau_{ce} = 1/n_0\sigma_{ce}v_i$, where n_0 is the neutral-gas concentration, σ_{ce} is the charge-exchange cross section and v_i is the ion velocity. Hence, for the charge-exchange case the dependence of reciprocal lifetime $1/\tau$ on pressure p should be given by a line which starts from the origin and has a slope $\sigma_{ce}v_i$.

The lifetime τ is determined experimentally by observing the rate of decay of the fast-ion density at the end of acceleration by the radial electric field (i.e., after the end of the accelerating voltage pulse). For this purpose we record the flux of fast neutral particles reaching the side walls of the chamber as a function of time. Since these particles are formed by charge exchange of fast ions on the neutral gas, for a given neutral-gas pressure and ion energy the flux at the walls should be proportional to the mean density of fast ions in the volume of the system.

The neutral particles are detected by the device which is shown schematically in Fig. 2. The detector consists of two insulated metal plates, A and B, which are enclosed in a grounded guard chamber C; there is a rectangular slit $0.5 \times 2\ cm^2$ in the front wall of the box. A fixed potential difference of 20 — 40 v is applied between the plates. Neutral particles which enter through the slit and strike plate A cause the emission of secondary electrons from this plate. The electrons are collected by the collector B and flow through the resistance R. The signal across the resistance is applied to a cathode follower and then, after suitable amplification, to the plates of an OK-17M oscilloscope. The detector is located in a special housing in the central portion of the system and can be moved radially.*

A typical oscillogram obtained in the detection of neutral particles is shown in Fig. 3 (the neutral particle flux is shown above and the accelerating voltage pulse is shown below). The quantity τ is found by plotting the oscillogram on a semilogarithmic scale. The error in the determination of τ is not greater than 20%.

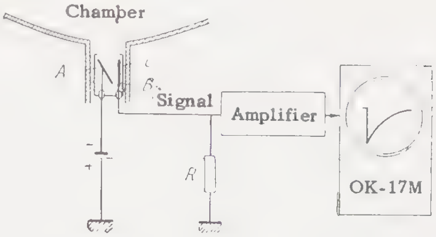

FIG. 2. Diagram of the neutral-particle detector.

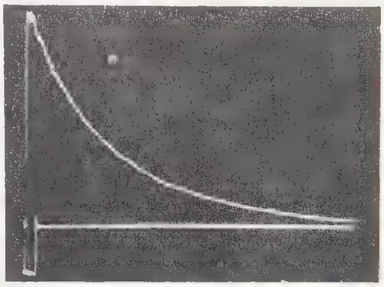

FIG. 3. Oscillogram of the neutral particle flux. $H_0 = 8000$ oe; $U_0 = 30$ kv; $\alpha = 1.55$; $p = 6 \times 10^{-7}$ mm Hg. The sweep length is 2.5 millisec.

RESULTS

The pressure dependence of τ has been measured at various accelerating voltages, magnetic fields, and mirror ratios in the hydrogen pressure range $3 \times 10^{-7} - 2 \times 10^{-5}$ mm Hg. The results of these measurements for several values of U_0 and H_0 are shown in Figs. 4 and 5. It is apparent from these figures that the experimental points lie on straight lines, as is to be expected for charge exchange.

The slope of the lines must equal the product $\sigma_{ce}v_i$ so that this slope can be used to determine the ion energy E. The experimental values of $\sigma_{ce}v_i$ and data on the proton charge exchange cross sections[9,10] yield the following ion energies:*

U_0, kev	11	20	45
$10^8\,\sigma_{ce}v_i$, cm^3/sec	1.3	3.1	4.2
E, kev	0.7	1.3	1.7

It should be noted that these quantities represent some mean energy since there is no reason to believe that the ions in the system are monoenergetic.

Knowing $\sigma_{ce}v_i$ we can estimate the mean density of the fast ions $\bar{n}_+$ from the neutral-particle flux at the walls of the system. The relation between $\bar{n}_+$ and the neutral-particle flux j_0 is given by $2\pi R j_0 = n_0\sigma_{ce}v_i\bar{n}_+\pi R^2$ (R is the radius of the system). If the current measured in the neutral

---

*In general, the current in the collector circuit need not be caused exclusively by the secondary emission produced by fast neutral particles, but can also be caused by photoemission due to ultraviolet radiation excited by the plasma electrons. It is easy to show, however, that for the electron and ion energies considered here (and the fact that their densities are equal, in accordance with the neutrality condition) the photocurrent cannot amount to more than several percent of the secondary electron current.

*The relative percentages of protons and molecular ions in the system have not been measured. On the basis of investigations of the mass spectrum of hydrogen ions in a source similar to that used in the present work, it can be assumed that for the modes of operation of the discharge in which the life times were measured the proton content is at least 75%.

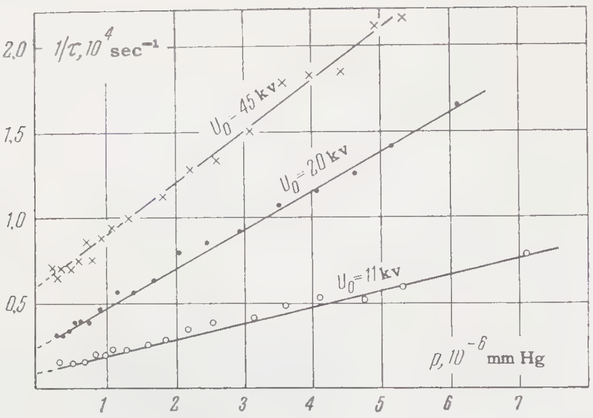

FIG. 4. The reciprocal lifetime for fast ions as a function of pressure for various values of the accelerating voltage. $H_0 = 5000$ oe, $\alpha = 1.55$

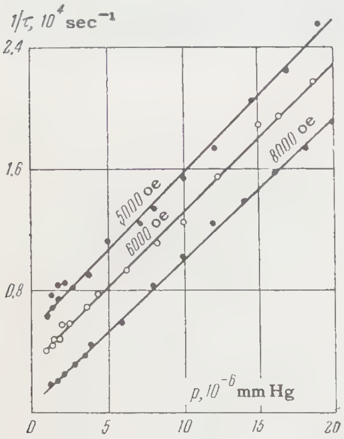

FIG. 5. The reciprocal lifetime for fast ions as a function of pressure for various magnetic fields. $U_0 = 30$ kv, $\alpha = 1.55$.

particle detector circuit (the secondary electron current) is i_e, then $j_0 = i_e/kS$, where k is the secondary-emission coefficient for neutral particles and S is the area of the detector slit. In making the density estimates the coefficient k is set equal to unity.[11]

The secondary electron current from the neutral-particle detector i_e varies from fractions of a microampere to hundreds of microamperes, depending on the chamber pressure. The magnetic field strength, the mirror ratio, and the acceleration voltage also have an effect on i_e, although this effect has not been studied in detail in the present work. The values of $\overline{n}_+$ found from the values of i_e, σ_{ce}, v_i, n_0, R and S lie within the limits $0.5 \times 10^9 - 5 \times 10^9$ cm^{-3}, depending on the mode of operation of the source and the quantities H_0 and U_0. The values indicated correspond to the end of the accelerating voltage pulse.

The most important feature found in an analysis of the pressure dependence of τ is the fact that the $1/\tau = f(p)$ lines do not pass through the origin when extrapolated to zero pressure. These lines intersect the ordinate axis at values greater than zero and the intersection point $1/\tau_p$ differs for different values of U_0 and H_0. This displacement of the lines would seem to indicate that in addition to charge exchange, there is another mechanism which causes additional loss of fast ions from the system; this mechanism is pressure independent. Before reaching this conclusion, however, we must investigate the effects of possible errors in the method of measurement on the validity of the results which have been obtained.

The fact that the $1/\tau = f(p)$ lines intersect the ordinate axis above the origin could result from errors in the measurement of the neutral-gas pressure. If there is a residual pressure in the working volume which is not recorded by the vacuum gauges, charge exchange on this "residual" gas might show up as additional loss. In order to explain the observed values of τ_p on this basis, however, we would have to increase the hydrogen pressure to $(3-5) \times 10^{-6}$ mm Hg over the entire pressure range for which measurements have been carried out. Analysis of possible causes for this increase (for example, occlusion of gas from the walls because of bombardment by fast particles during the accelerating voltage pulse and in the subsequent plasma decay period) shows that an error of this kind cannot exist. This result also follows directly from an analysis of the pressure dependence of the fast neutral-particle flux. In Fig. 6 this dependence is shown for the pressure range $2 \times 10^{-7} - 3 \times 10^{-6}$ mm Hg; the measured pressure is plotted along the abscissa axis while the secondary electron current I caused by neutral particles at the detector plate (at the instant of termination of the accelerating-voltage pulse) is plotted along the ordinate axis. It is

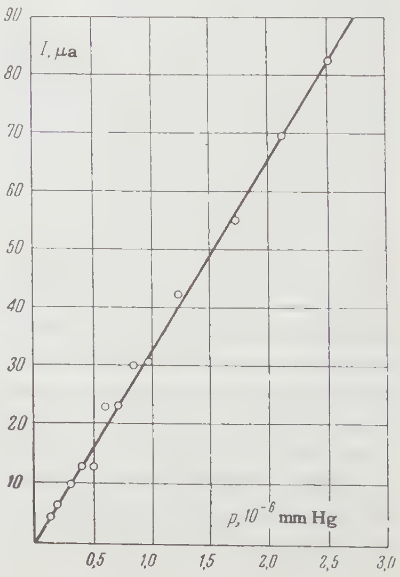

FIG. 6. The fast neutral particle flux as a function of pressure. $H_0 = 5000$ oe, $U_0 = 45$ kv.

apparent from the figure, that as the pressure read by the vacuum gauge is reduced, the neutral-particle flux approaches zero, not some finite value, which would correspond to a "residual" pressure.

Other possible causes for these measured results are charge exchange of fast protons on molecular ions, according to the scheme

$$H^+ + H_2^+ \rightarrow H + 2H^+.$$

The possibility that this process may occur has been pointed out by G. I. Budker. Data on the cross sections of this charge exchange process are not available. However, if this process were important in the present experiments, the flux of charge-exchange particles would remain finite upon reduction of the pressure instead of becoming vanishingly small.

Finally, the anomalously rapid decay in the neutral particle flux might result from a change in the direction of the fast ion velocities. We assume that initially the velocities of all ions are perpendicular to the magnetic field and that the neutral-particle flux lies in a plane. If for some reason the directions of these velocities should change (i.e., if a longitudinal component should arise), there would be an additional decay in the neutral-particle flux over and above the decay due to the reduction in the density of fast ions in the system. If such a mechanism actually operates, it should be possible to observe this redistribution in velocities by varying the position of the detector in the chamber, that is to say, the decay time τ should change. However, no such effect has been observed; the time constant for the decay of the neutral-particle flux is the same in any position.

Thus, none of the mechanisms cited above can explain the displacement of the $1/\tau = f(p)$ lines. This leads us to the conclusion that for the experimental conditions reported here there are additional ion losses which are caused by a mechanism which is not related to charge exchange. These losses may be considerably greater than the losses due to charge exchange; at minimum system pressures they may exceed the charge exchange losses by a factor of eight or ten.

The additional loss rate is characterized by a decay time τ_p so that the mean lifetime of ions in the system can be written in the form $\tau = \tau_{ce}\tau_p/(\tau_{ce} + \tau_p)$. When the accelerating voltage is increased or the magnetic field is decreased the points at which the $1/\tau = f(p)$ lines intersect the ordinate move upwards, that is to say, the decay time for the additional loss τ_p is reduced. The values of τ_p for a number of values for U_0 and H_0 are given in Table I for $\alpha = 1.55$.

TABLE I

U_0, kv	τ_p, μsec		
	H_0=8000 oe	H_0=6000 oe	H_0=5000 oe
45	700	170	130
35	900		
30	1500	400	200
20			400
11			1000

It is apparent from the table that these additional losses are very sensitive to the magnetic field. When H_0 is changed from 8000 to 5000 oe, the losses increase by a factor of six or eight. The mirror ratio has an effect on the additional loss rate only when $\alpha < 1.6$; the losses increase sharply when α is reduced. For values of α greater than 1.6 no appreciable variation in loss rate is observed.

In Table II we show values of τ_p corresponding to different mirror ratios for $U_0 = 30$ kv and $H_0 = 5000$ and 8000 oe.

TIME DEPENDENCE OF ADDITIONAL FAST-ION LOSSES

On the basis of the experimental data which have been presented we cannot draw any conclusion as to the nature of the additional loss mechanism, nor can we determine whether this mechanism is to be associated with the collective interaction of charged plasma* or whether it is also effective for single particles which move independently. In the latter case the energy losses might be attributed to the fact that the adiabaticity condition is not strictly observed in the magnetic field of the system described here.

In order to investigate this problem, we measured the time dependence of the rate of additional loss. If the escape of particles from the system is due to a collective plasma interaction, this interaction should be weakened as the plasma density is reduced in the course of time, and the particle motion should become more and more independent. For this reason the additional loss mechanism should weaken after some time. On the other hand, if the additional loss is due to a single-particle interaction between a single fast ion and the magnetic field in the present configuration, the ion losses should be independent of density and should not fall off with time.

---

*"Collective interactions" in a plasma generally refer to those slowing-down and scattering processes which take place by virtue of remote Coulomb interactions. However, as we have shown in the introduction, these processes can be neglected under the present conditions. Here we may be dealing with more complicated collective interaction, say the development of plasma instabilities.

TABLE II

α	τ_p, μsec		α	τ_p, μsec	
	H_0=8000 oe	H_0=5000 oe		H_0=8000 oe	H_0=5000 oe
1.25	200	100	1.55	1500	200
1.33	740		2.0		230
1.45	830	160	2.35		230

To find the effect of the fast ion density on the additional loss, we must plot the pressure dependence of $1/\tau$ for different concentrations. However, in finding this dependence we must plot the line $1/\tau = f(p)$ at later values of the time, which is measured from the trailing edge of the accelerating voltage pulse. A change in lifetime need not be due solely to the change in additional loss, but may be caused by the change in the probability for charge exchange. The point is that the fastest ions experience charge exchange first, causing a change in the shape of the ion energy spectrum. The maximum in the ion energy distribution is shifted toward lower energies and the mean charge exchange probability is reduced while the mean charge exchange time is increased.

In order to take this change into account at different pressures, we must consider times at which the ionic spectra are identical. If this condition is satisfied and we plot $1/\tau = f(p)$, the curve should be a line corresponding to charge exchange, with a slope $\sigma_{ce}v_i$, to which the quantity τ_p is added at each point. If all the ions in the spectrum for a given ion energy distribution have the same probability of escape from the system via the additional loss mechanism, the change in the spectrum is due to charge exchange only. The rate of change of the spectrum will be proportional to the pressure p. Hence, at different pressures the spectra will vary identically in a time t, which is inversely proportional to p, that is to say, the condition that the spectrum remains unchanged is pt = const.

The decay time for the charge-exchange flux at different times is measured by means of the detector described earlier; now, however, an appropriate delay (with respect to the trailing edge of the accelerating voltage pulse) is inserted in the amplifier. In Fig. 7 we show the experimental dependence of τ on delay time for $p = 2 \times 10^{-6}$ mm Hg with $H_0 = 5000$ oe and $U_0 = 30$ kv. Similar curves are obtained at other pressures.

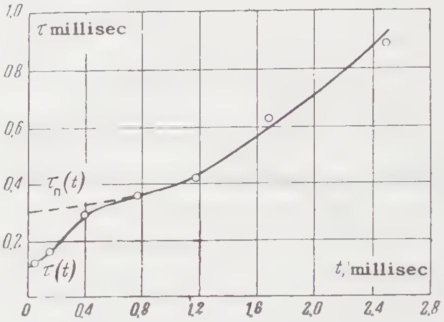

FIG. 7. Change in the fast ion lifetime τ with time t. $H_0 = 5000$ oe, $U_0 = 30$ kv, $p = 2 \times 10^{-6}$ mm Hg.

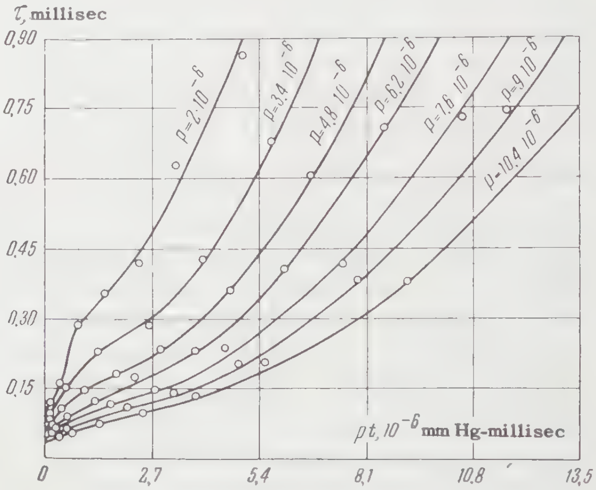

FIG. 8. The dependence of lifetime on the quantity pt for various pressures. $H_0 = 5000$ oe, $U_0 = 30$ kv.

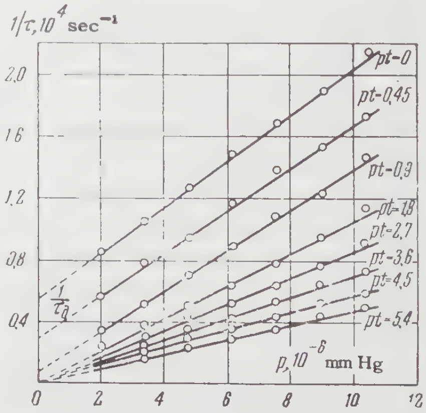

FIG. 9. The dependence of reciprocal lifetime on pressure for various values of pt (in units of 10^{-6} mm Hg × millisec). $H_0 = 5000$ oe, $U_0 = 30$ kv.

In Fig. 8 we show a family of curves for the dependence of τ on pt; the parameter is the pressure p. In Fig. 9 we have plotted $1/\tau = f(p)$ for several given values of pt. Increasing values of the parameter pt (for fixed pressure) correspond to later and later times. It is apparent from the last figure that as pt is increased the $1/\tau = f(p)$ lines are displaced downward (the quantity $1/\tau_p$ is reduced) and, that at some value of pt, the lines can be extrapolated through the origin. Thus, in the course of time these losses, which are independent of charge exchange, grow smaller and finally vanish completely; at this point only the charge-exchange mechanism remains.

The decrease of the additional losses with time shows that these losses are not due to individual interaction between the ions and the magnetic field in the system, but are typical plasma processes, which appear only at sufficiently high densities, when the motion of the charged particles is no longer independent. The fact that the particle motion is not independent means that there are intrinsic potential differences in the plasma, which are comparable with the ion energy. This condition can be expressed quantitatively by saying that the Debye radius for the fast ions [$r_D = \sqrt{kT_i/4\pi ne^2}$] must be small compared with the characteristic dimensions of the region occupied by the plasma. Hence, the transition from collective motion to single-particle motion occurs at that density for which the Debye radius for the fast ions becomes comparable to the system dimensions. Under the present conditions this density is of the order of 10^7 cm^{-3}.

The experimental results indicate that the additional loss mechanism is suppressed in a time equal to several lifetimes. At this point the density estimated from the fast neutral particle flux is reduced to several percent of its initial value, i.e., it is of the order of 10^7 cm^{-3}, in accordance with the considerations given above.

The characteristic downward bend at the beginning of the $\tau(t)$ curve in Fig. 7 is due to the additional losses in this region. This can be shown if, using the family shown in Fig. 9, we determine the dependence of the additional loss constant $1/\tau_p$ on time t (for $p = 2 \times 10^{-6}$ mm Hg); then, from the relation $1/\tau = 1/\tau_p + 1/\tau_{ce}$ we find the dependence of the charge exchange time τ_{ce} on t. The approximate behavior of this curve is shown in Fig. 7 by the dashed line. The convergence of the $\tau(t)$ and $\tau_{ce}(t)$ curves then shows the approximate suppression time for the additional loss mechanism.

In conclusion the authors wish to express their gratitude to Academician L. A. Artsimovich and B. B. Kadomtsev for their interest in this work and for valuable discussions.

The authors also wish to thank V. M. Petrov for the construction of the apparatus, É. N. Braverman, for the design of the titanium evaporators, and Yu. T. Baĭborodov, for the development and installation of the electrical system.

---

[1] G. I. Budker, Физика плазмы и проблема управляемых термоядерных реакций (Plasma Physics and the Problem of Controlled Thermonuclear reactions), Academy of Sciences USSR Press, 1958, Vol. 3, p. 3.

[2] M. N. Rosenbluth and C. Longmire, Ann. Phys. 1, 120 (1957).

[3] B. B. Kadomtsev, op. cit. ref. 1, Vol. 4, p. 380.

[4] A. A. Vedenov and R. Z. Sagdeev, ibid., p. 278.

[5] F. Coensgen and F. Ford, 2nd Int. Conference on the Peaceful Uses of Atomic Energy, Geneva, 1958, p. 378.

[6] Post, Ellis, Ford and Rosenbluth, Phys. Rev. Letters, 4, 166 (1960).

[7] R. Post, Revs. Modern Physics **28**, 328 (1956).

[8] E. E. Yushmanov, op. cit. ref. 1, Vol 4, p. 235.

[9] Afrosimov, Il'in, and Fedorenko, JETP **36**, 1398 (1959), Soviet Phys. JETP **9**, 995 (1959).

[10] Fite, Brackmann, and Snow, Phys. Rev. **112**, 1161 (1958).

[11] V. G. Tel'kovskiĭ, Secondary Electron Emission by Ions and Neutral Particles, Dissertation Nuclear Phys. Res. Inst., Moscow State University, 1959.

Translated by H. Lashinsky
295

SOVIET PHYSICS JETP VOLUME 12, NUMBER 6 JUNE, 1961

CHARGED PRODUCTS OF THE REACTIONS $He^4 + d$ *(20 Mev)*

K. P. ARTEMOV and N. A. VLASOV

Submitted to JETP editor July 23, 1960

J. Exptl. Theoret. Phys. (U.S.S.R.) **39**, 1612-1614 (December, 1960)

The spectra and angular distributions of the charged products of the reactions between 20.2-Mev deuterons and He^4 were measured using photographic emulsions. The angular distributions of elastically-scattered deuterons and of the protons from the $He^4(d, p)He^5$ and $He^4(d, pn)He^4$ reactions are presented. The proton group from the $He^4(d, p)He^5$ (ground state) reaction is intense at small angles. A broad continuous proton spectrum is observed at large angles. The angular distribution of the continuous proton spectrum is similar to that of the elastically-scattered deuterons. The elastic scattering and the (d, pn) cross sections are approximately equal.

In the study of neutron spectra produced by bombarding light nuclei with 15 — 20 Mev deuterons, it was found that there is a large probability of deuteron stripping (d, pn) accompanied by the production of neutrons with a continuous spectrum.[1] It is evident that, as a result of the stripping, protons having a continuous spectrum should also be observed. The study of the nucleons produced in stripping is of interest in attempting to explain the mechanism of the reaction and the states of the produced nuclei. The He^4 nucleus is very convenient as a target for the study of the stripping mechanism. The reactions (d, 2n) and (d, 2p) have high thresholds and, for 20-Mev deuterons, stripping (d, pn) is the only reaction yielding nucleons with a continuous spectrum.

In the present experiment, the spectra and the angular distribution of charged products of the $He^4 + d$ (20 Mev) reaction were studied by means of emulsions. The deuteron energy of 20.2 Mev was determined from the range in emulsion after scattering. The plates were placed at angles ranging from 15 to 165° in steps of 15°, and at a distance of 12.5 cm from the gaseous target. The target was at an angle of 8° to the reaction-product beams, which were selected by collimating slits in different directions. In the scanning of the plates, these tracks were selected that began on the surface of the emulsion and had a given direction. The background measured with the target without He^4 was not greater than 10% in the region of the continuous spectrum.

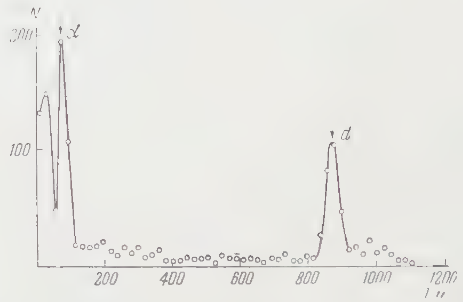

FIG. 1. Range spectrum of charged products of the reaction $He^4 + d$ (20 Mev) at an angle of 30°. The number N of tracks in the range 20.6μ is shown as a function of the track length l.

The range spectrum of the particles in the plate placed at an angle of 30° is shown in Fig. 1. We can easily distinguish in the spectrum the monoenergetic group of elastically-scattered deuterons and the recoil α particles. The continuous spectrum is composed of the stripping protons and of the recoil α particles from the $He^4(d, pn)$ reaction, which can be seen only at small angles in the short-range portion of the spectrum. The group of protons from the $He^4(d, p)He^5$ (ground state) reaction is visible less clearly, but still well enough, against the background of the continuous spectrum, near its upper limit.

After separating the monoenergetic groups of deuterons and α particles, the continuous spectra of the protons were constructed. One of these spectra, corresponding to a laboratory angle of 90°, is shown in Fig. 2.

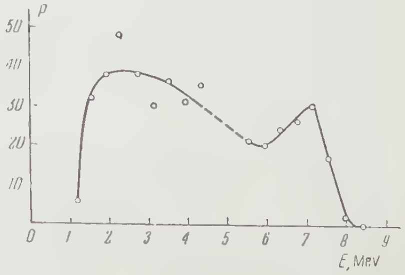

FIG. 2. Spectrum of protons of the reaction $He^4 + d$ (20 Mev) at an angle of 90°. The number of protons P in the interval 0.4 Mev is shown as a function of the energy E.

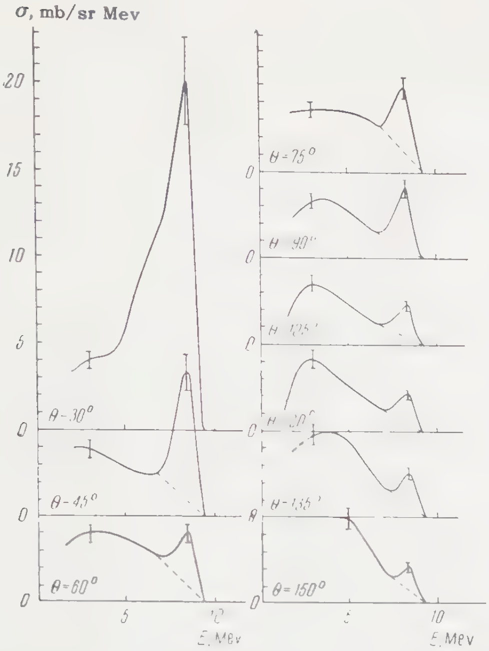

FIG. 3: Spectrum of protons of the reaction He^4 + d (20 Mev) at various angles in the c.m.s.

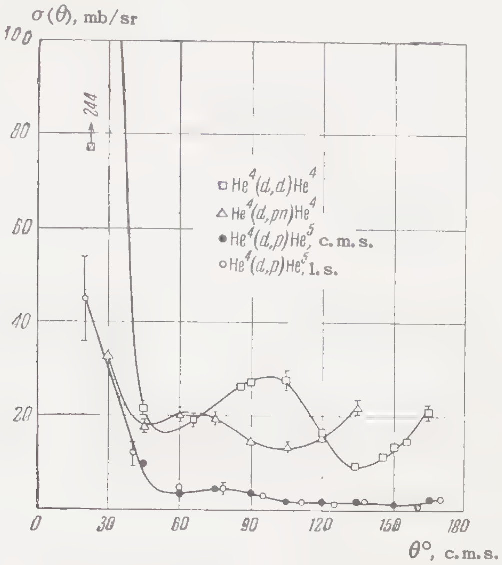

FIG. 4. Angular distributions of deuterons and protons in the processes indicated in the figure.

The spectra of protons at different angles in the center-of-mass system are shown in Fig. 3. The vertical lengths marked in the different parts of the spectrum indicate the errors in the solid curves, which are mainly due to the statistical spread of the points. In the region of small ranges, small (< 30%) corrections were applied for the scattering of the particles in the gas of the target. Those portions of the spectrum which needed corrections > 30% were considered unreliable and were not used.

In all spectra, and especially at small angles, a group of protons from the $He^4(d, p)He^5$ reaction can be observed. Its intensity decreases strongly with the angle, and, for angles > 50°, amounts to less than 15% of the continuous-spectrum intensity. In studying the neutron spectrum,[2] the analogous large group of neutrons of the mirror reaction $He^4(d, n)Li^5$ was observed at an angle of 0°.

The continuous spectrum of protons having its maximum shifted from the medium towards the low energies is not related to the production of the He^5 and Li^5 nuclei. The upper limit of the proton spectrum produced in the reaction cascade $He^4(d, n)Li^5 \rightarrow He^4 + p$ lies at an energy of 3.3 Mev. This range of the proton spectrum has practically not been investigated. The shape of the continuous spectrum does not change greatly with the angle.

Figure 4 shows the angular distributions of the elastically scattered deuterons, of protons of the $He^4(d, p)He^5$ (ground state) reaction, and of protons of the continuous spectrum in the 2 – 9.3 Mev energy range in the c.m.s. The elastic dHe^4 scattering at $E_d = 19$ Mev has already been observed by Freemantle et al.[3] Taking into account the general tendency of the cross section to decrease with energy, both results can be regarded as being in good agreement. The cross section for the production of a proton of the continuous spectrum at angles > 45° varies little with the angle, and is approximately equal to the elastic-scattering cross section. The cross sections integrated over the angles from 45 to 135° are:

$$\sigma(d, d) = 189 \pm 25 \text{ mb}, \qquad \sigma(d, pn) = 152 \pm 25 \text{ mb}.$$

This means that a 20 Mev deuteron undergoes stripping in about half of the collisions with an α particle.

The continuous spectra of protons obtained in deuteron stripping at 10.3 Mev on He^4 have already been observed by Allred et al.[4] In experiments on the elastic scattering of deuterons on medium and heavy nuclei (see, e.g., reference 5), a strong deviation of the cross section from the Rutherford value is observed, which increases with the angle of scattering. The direct observation of the large deuteron-stripping probability is in full agreement with this experiment, and can serve as an explanation of the strong deviations. It should be mentioned that, in our case, the stripping is almost solely due to the nuclear interaction, since the Coulomb interaction is very small.

[1] Bogdanov, Vlasov, Kalinin, Rybakov, and Sidorov, JETP **30**, 185 and 981 (1956), Soviet Phys. JETP **3**, 113 and 793 (1956).

[2] Vlasov, Rybakov, and Sidorov, Nucl. Phys. (in print).

[3] Freemantle, Grotdal, Gibson, McKeague, Prowse, and Rotblat, Phil. Mag. **45**, 1090 (1954).

[4] Allred, Froman, Hudson, and Rosen, Phys. Rev. **82**, 786 (1951).

[5] J. L. Yntema, Phys. Rev. **113**, 261 (1959).

Translated by H. Kasha
296

SOVIET PHYSICS JETP VOLUME 12, NUMBER 6 JUNE, 1961

THE REACTION (d, t) ON ZIRCONIUM ISOTOPES

N. A. VLASOV, S. P. KALININ, A. A. OGLOBLIN, and V. I. CHUEV

Submitted to JETP editor July 23, 1960

J. Exptl. Theoret. Phys. (U.S.S.R.) **39**, 1615-1617 (December, 1960)

The spectra of tritons of the reaction (d, t) on $Zr^{91,92,94}$ have been investigated at E_d = 20 Mev. Two groups of tritons of different energy and angular distribution are produced on zirconium isotopes. One corresponds to the ejection of a neutron from the N = 50 filled shell, and the other to the ejection of an external neutron. The intensity of the latter group is approximation proportional to the number of super-magic neutrons. The intensity of the first group slowly decreases from Zr^{90} to Zr^{94}.

In a study of the (d, t) reaction on medium and heavy elements, it was observed that a level band 1.5 — 2.0 Mev wide was excited near the ground state, and there were practically no excitations of higher states.[1] The reason was either the absence of sufficiently pure single-particle neutron states with high binding energy in the closed subshells, or that screening prevented their ejection. We report here the results of an investigation of the (d, t) reaction on the isotopes $Zr^{91,92,94}$, which are of interest in that they have one, two, and four neutrons on top of the closed shell N = 50.

The triton spectra were obtained, as before,[1-3] from the tritium activity. The tritons emitted from a thin target, 3 — 5 mg/cm², were caught in stacks of aluminum foils placed at different angles 15 cm from the target. The deuterons were accelerated in a cyclotron to 20 Mev. The targets used were the oxide of zirconium enriched with Zr^{91} (79.5%), Zr^{92} (88.6%), and Zr_{94} (90.0%).

The triton spectra, measured at 13° are shown in Fig. 1. For all the three zirconium isotopes, excitation of two groups of states is observed. The first narrow group of tritons corresponds to excitation of the ground state. Its angular distribution, shown in Fig. 2, agrees with the value of orbital momentum $l = 2$ corresponding to the state $d_{5/2}$, as expected from the order of filling of the nuclear nucleon shells. An orbital momentum $l = 2$ was obtained also in the radiation of the reaction (d, p) on isotopes Zr^{90} and Zr^{91} (reference 4). The intensity of this group of tritons or, in other words, the probability of ejection of a neutron from the $d_{5/2}$ shell, is proportional to the number of neutrons in this shell, as can be seen from Fig. 3a.

The second broad group of tritons is a series of unresolved lines. Figure 2 shows the angular distributions of the group as a whole. The presence

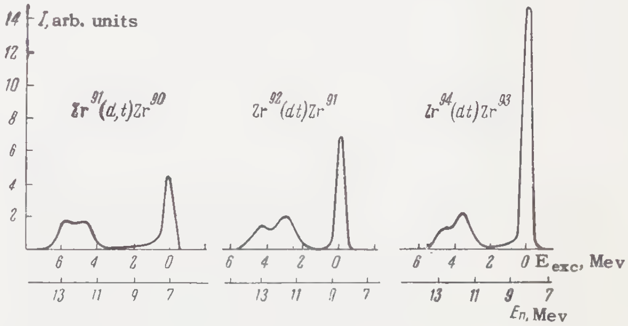

FIG. 1. Spectra of tritons in the reaction (d, t) on zirconium isotopes at an angle of 13°. Upper abscissas — excitation energy of the residual nucleus, lower abscissas — binding energy of the neutron of the target nucleus (I — intensity).

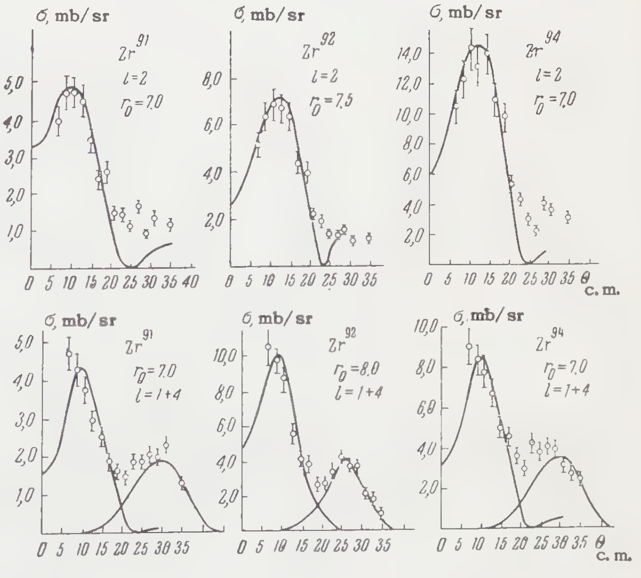

FIG. 2. Angular distributions of tritons in the reaction (d, t) on zirconium isotopes. The solid curves were calculated on the basis of the Butler theory. Upper figures — for the ground states, lower figures — for the group of excited states.

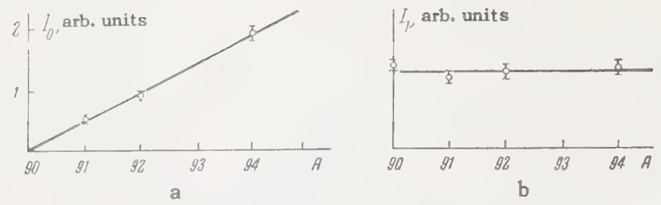

FIG. 3. Dependence of the probability of ejection of a neutron in the (d, t) reaction on zirconium isotopes on the mass number: a – ejection of neutrons from external shell $d_{5/2}$, b – ejection of neutrons from the closed shell (N = 50).

of two components with different momenta is evident by the deformation of the group with a variation of the angle. Corresponding to the smaller value of l is a higher binding energy of the ejected neutron. In accordance with the shell model, we can assign to it orbital momentum values $l = 1$ and 4.

Thus, this group (approximately 2 Mev wide) corresponds to the ejection of neutrons from the closed shell with a neutron binding energy approximately equal to 11 — 13 Mev for all isotopes of zirconium. In the (d, t), reaction on the isotope Zr^{90} (reference 1), this group alone was observed. The intensity and form of this group differ little for the different isotopes from Zr^{90} to Zr^{94}. This is evidence that the screening of the internal shell by the external nucleons is weak (Fig. 3b).

Owing to pairing effects, the state of the two external neutrons in Zr^{92} should be mixed. The greatest impurity to the state $2d_{5/2}$ should be introduced by the state $1g_{7/2}$, since they are located close to each other in the Nilsson scheme. In this case we should observe, upon ejection of an external neutron in the (d, t) reaction, tritons emitted with two values of l, 2 or 4. However, only the excitation of the ground state was observed upon ejection of the d-neutron. The impurity of the g-state would have been noted were it higher than 20%.

---

[1] N. A. Vlasov, S. P. Kalinin, A. A. Ogloblin, and V. I. Chuev, JETP **38**, 280 (1960), Soviet Phys. JETP **11**, 203 (1960).

[2] N. A. Vlasov, A. A. Ogloblin, JETP **37**, 54 (1959), Soviet Phys. JETP **10**, 39 (1960).

[3] N. A. Vlasov, S. P. Kalinin, A. A. Ogloblin, and V. I. Chuev, JETP **37**, 1187 (1959), Soviet Phys. JETP **10**, 844 (1960).

[4] Preston, Martin, and Sampson, Bull. Am. Phys. Soc. Ser. II, **5**, 267 (1960).

Translated by J. G. Adashko
297

SOVIET PHYSICS JETP VOLUME 12, NUMBER 6 JUNE, 1961

THE REACTION $B^{11}(d, t)B^{10}$

N. A. VLASOV, S. P. KALININ, A. A. OGLOBLIN, and V. I. CHUEV

Submitted to JETP editor July 23, 1959

J. Exptl. Theoret. Phys. (U.S.S.R.) 39, 1618-1620 (December, 1960)

The $B^{11}(d, t)B^{10}$ reaction has been studied for 20-Mev deuterons. In accordance with the level scheme of the B^{10} nucleus, excitation of the lower levels of B^{10} occurs as a result of ejection of a neutron with $l = 1$. The probability of the ground state is several times higher than that of the excited states. The reduced widths from the reactions $B^{11}(d, t)B^{10}$ and $Be^9(d, n)B^{10}$ are compared.

In the present investigation we studied the reaction $B^{11}(d, t)B^{10}$ at a deuteron energy of 20 Mev.

The measurement of the triton spectra was based, as before,[1-4] on the activity of tritium accumulated in stacks of foils placed around the target. The target of thickness 3 mg/cm^2 was made of natural boron (81% B^{11}), deposited in the form of the suspension on a magnesium substrate 0.4 mg/cm^2 thick.

Figure 1 shows one of the measured spectra (at an angle 11°). The groups of tritons corresponding to the formation of B^{10} in the ground and known excited states with energies 0.72, 1.74, 2.15, 3.58, 5.1 and 6.2 Mev, are clearly pronounced. We see that the two last groups of tritons correspond to more than one level each. The low-intensity continuous spectrum of tritons with energy less than 10 Mev is apparently connected with the excitation of unresolved high-lying states of B^{10}. The weak group of tritons ($E_t = 16.0$ Mev) pertains apparently to the reaction $B^{10}(d, t)$ with formation of B^9 in the first excited state.

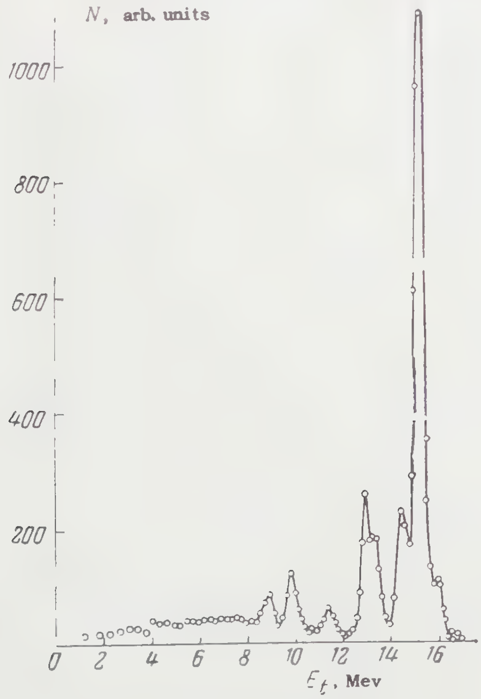

FIG. 1. Spectrum of tritons in the reaction $B^{11}(d, t)^{10}$ at an angle of 11°.

The results of the measurements are listed in the table. The ground state and the first three excited states of B^{10} are formed upon ejection of a neutron with orbital momentum $l = 1$. This value of the momentum is in agreement with the known values of the spin and parity of these states. The group of tritons corresponding to the 3.58-Mev level contains components of approximately equal intensity with $l = 1$ and an isotropic component. The group of tritons corresponding to the excitation energy 5.1 Mev does not fit any definite value of the momentum l. It corresponds to two unresolved levels 5.11 and 5.16 Mev, and possibly contains an admixture of the 4.77-Mev level ($\lesssim 20\%$). The states 5.11 and 5.16 Mev have apparently opposite parity,[5] and consequently the angular distribution of the unresolved group can contain components with $l = 0$, 1, and 2. From the form of the angular distribution it follows that the main contribution to the angular distribution is made by tritons from the level 5.16 Mev ($l = 1$). The group connected with the 6.2-Mev level (or levels) has an almost isotropic angular distribution.

The table lists also data on the reaction $Be^9(d, n)B^{10}$ (reference 6). The distribution of the reduced widths Θ^2 over the different levels in the (d, t) and (d, n) reactions, is shown in Fig. 2. We see that the probability of excitation of the same states is quite different. Thus, the levels 0.72 and 1.74 Mev in the (d, n) reaction are formed with a greater probability than the ground state, while in the (d, t) reaction they are formed

Level of B^{10}, Mev	$B^{11}(d, t)B^{10}$				$Be^9(d, n)B^{10}$	
	l	r_0, ϕ	σ_{max} in c.m.s., mb/sr	Θ^2, %	l	Θ^2
Ground state	1	6.0	6.4 (15°)	2.47	1	1,7
0.72	1	6.0	1.75(15°)	0.71	1	3.5
1.74	1	7.0	0.95(15°)	0.39	1	2.5
2.15	1	6.0	1,55(15°)	0.72		
3.58	(1)		0.45(15°)	~0.1	1	0.7
4.77			<0.2 (15°)	<0.1 (l=1)	(1)	0,3
5.11	} (1)		0.9 (10—15°)	~0.3		
5.16					(0)	1,3
5.93					(1)	(0,5)
6.2	isotropic		0.6		(1)	0,5

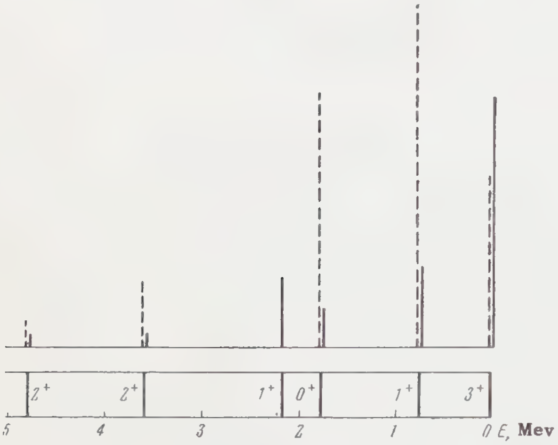

FIG. 2. Reduced widths in reactions $B^{11}(d, t)B^{10}$ (solid lines) and $Be^9(d, n)B^{10}$ (dashed).

with a probability which is several times smaller. At the same time, the 2.15 Mev level, not observed in the (d, n) reaction, appears with noticeable probability in the (d, t) reaction.

---

[1] N. A. Vlasov and A. A. Ogloblin, JETP **37**, 54 (1959), Soviet Phys. JETP **10**, 39 (1960).

[2] Vlasov, Kalinin, Ogloblin, and Chuev, JETP **37**, 1187 (1959), Soviet Phys. JETP **10**, 844 (1960).

[3] Vlasov, Kalinin, Ogloblin, and Chuev, JETP **38**, 280 (1960), Soviet Phys. JETP **11**, 203 (1960).

[4] Vlasov, Kalinin, Ogloblin, and Chuev, Izv. Akad. Nauk SSSR, Ser. Fiz., in press.

[5] F. Ajzenberg-Selove, and T. Lauritsen, Nucl. Phys. **10**, 1 (1959).

[6] W. E. Meyerhof and L. F. Chase, Phys. Rev. **111**, 1348 (1958).

Translated by J. G. Adashko
298

SOVIET PHYSICS JETP VOLUME 12, NUMBER 6 JUNE, 1961

REACTIONS LEADING TO THE FORMATION OF THE Pb^{205m} *ISOMER*

V. L. GLAGOLEV, A. M. MOROZOV, and P. A. YAMPOLSKIĬ

Institute of Chemical Physics, Academy of Sciences, U.S.S.R.

Submitted to JETP editor July 29, 1960

J. Exptl. Theoret. Phys. (U.S.S.R.) 39, 1621-1624 (December, 1960)

More accurate data on the short-lived γ-radiation emitted from thallium irradiated by 19.2-Mev protons and 14.7-Mev neutrons are presented. It is demonstrated that the observed radiation is from the Pb^{205m} isomer. The cross sections for the production of Pb^{205m} nuclei in proton and neutron reactions are measured. Calculations show that about half of the Pb^{205} nuclei produced in the Pb^{206} (n, 2n) reaction are produced in the metastable state.

UPON bombardment of thallium with 20-Mev protons[1] γ radiation was observed having an energy $E_\gamma \sim 0.9$ Mev and a half-life $T_{1/2} = (6.5 \pm 0.05)$ milliseconds. Irradiation of lead by 14-Mev neutrons[2] resulted in a short-lived radiation with similar characteristics: $T_{1/2} = (5.0 \pm 0.5)$ milliseconds, $E_{\gamma_1} = (0.94 \pm 0.02)$ Mev, and $E_{\gamma_2} = (0.48 \pm 0.01)$ Mev. In comparing these data, it was assumed in reference 2 that the radiation observed in the proton and neutron reactions belongs to the same lead isomer, Pb^{205m}. This identification was seemingly confirmed by Pryce,[3] who used the shell model and certain data on the levels of Pb^{205} to predict the existence of a level with a lifetime in the millisecond region. The transition from this level to the ground state of Pb^{205} should be accompanied by the emission of a γ quantum of energy 0.4 ± 0.2 Mev via an intermediate 0.7033-Mev level. Vegors and Health,[4] in an investigation of the decay of Bi^{205}, observed delayed γ radiation with a half-life $T_{1/2} = (4.7 \pm 1.5)$ milliseconds and an energy $E_\gamma = 0.987$ Mev, which was attributed to the Pb^{205m} isomer.

The aim of the present investigation was to obtain more accurate characteristics of the radiation in the reactions between protons and thallium and between neutrons and lead. The results confirm that this radiation is due to the lead isomer Pb^{205m}.

The procedure for the investigation of the proton-induced short-lived radiation ($E_p = 19.2$ Mev) was described in detail earlier.[5] Many measurements have shown that the energy of the short-lived radiation is 0.97 ± 0.01 Mev. It was also found that the spectrum of the short-lived radiation has lines with energies 0.73 ± 0.01 and 0.27 ± 0.02 Mev. Both lines appear against a considerable background of other γ radiation, and are therefore difficult to investigate. The intensity of the 0.73-Mev radiation is roughly estimated at ~ 0.1 of the intensity of the 0.97-Mev radiation. The half-life of the 0.97-Mev activity is $T_{1/2} = 5.2 \pm 0.3$ milliseconds. Experiments with natural thallium (70.5% Tl^{205} and 29.5% Tl^{203}) and enriched thallium (96.2% Tl^{205} and 3.8% Tl^{203}) have shown that the observed short-lived isomer radiation ($T_{1/2} = 5.2$ milliseconds) is the result of a reaction between protons and Tl^{205} nuclei (the single-channel analyzer was set in the experiments at the 0.97-Mev line).

The minimum energy E_p of the protons participating in the reaction that gave rise to the 0.97-Mev short-lived radiation was found to be about 7.7 ± 0.4 Mev. A calculation of the thermal effect of the most probable reactions between the protons and the Tl^{205} nuclei, with allowance for the excitation energy of the final nucleus ($E_\gamma = 0.97$ Mev) leads to the following values: $-Q_{(p,\, n)} = 1.8$ Mev, $-Q_{(p,\, 2n)} = 8.6$ Mev, and $-Q_{(p,\, pn)} = 8.6$ Mev. The value of E_p which we obtained can be explained under the assumption that the isomer is produced in the reaction $Tl^{205}(p, n)Pb^{205m}$. Using a thin thallium target (32.3 mg/cm^2) we found the cross section of this reaction at 19.2 Mev to be $\sigma_m = 20 \pm 4$ mb.

We used a procedure described elsewhere[2] to investigate the short-lived radiation produced in neutron reactions ($E_n = 14.7$ Mev) with lead. Certain improvements in this procedure made it possible to obtain more reliable data on the spectrum of the short-lived radiation and to measure the cross section of the isomer-producing reaction. The use of additional instruments made it possible to calculate the background more reliably. To measure the registration efficiency we used radioactive sources of γ radiation of energy close to 0.94 Mev. This made it possible to determine more reliably the efficiency of the scintillations spectrometer. The neutrons were obtained from a separate beam of deterium ions. We could therefore determine the spectrum of the neutrons and the average cross section of the reaction Cu^{63} (n, 2n) Cu^{62}, with which the measured cross section was compared. The monitor circuitry was modified to effect more accurate control of the monitor operation, thus increasing the accuracy of measurement of the neutron yields.

The revised value obtained in the present experiments for the isomer half-life is $T_{1/2} = 5.0 \pm 0.2$ milliseconds. The radiation spectrum was measured as before,[2] with a single-channel amplitude analyzer. An investigation of the spectrum has shown that the greatest intensity of short-lived radiation corresponds to an energy 0.94 ± 0.02 Mev; this result coincides with the value obtained earlier.[2] To identify the 0.48-Mev line it is necessary to take into account the Compton effect for 0.94-Mev photons. For this purpose we measured the radiation spectrum of Nb^{92} compounds ($E\gamma = 0.94$ Mev) placed between lead plates; this spectrum simulated the source of the isomer radiation. After normalizing the spectrum obtained in this manner and subtracting it from the spectrum of the short-lived radiation of the neutron-bombarded lead, we established that the 0.48-Mev line was due to the background and could not be ascribed to the lead Pb^{205m} isomer, as was assumed earlier.[2] A certain increase in the amplitude distribution of the momenta is observed in the vicinity of 0.7 Mev. If it is assumed that this increase is due to the 0.7-Mev γ radiation, then the yield of this radiation is less than 0.1 of the yield of the 0.94-Mev radiation. The cross section of the reaction, measured for 0.94 Mev radiation energy, is 0.28 b (calculated for lead of natural isotopic composition). As follows from the work of Ashby et al.,[6] the cross section can assume this value at the neutron energy used only through a reaction of the type (n, 2n). Since the radiation produced in the reaction of lead with neutrons is quite similar to the radiation accompanying the bombardment of thallium by protons, it follows that the radiation belongs to the same isomer. The only possible (n, 2n) reaction that leads to the formation of such an isomer is the reaction Pb^{206} (n, 2n) Pb^{205m}. The cross section of this reaction is $\sigma_m = 1.1 \pm 0.2$ b.

The results of the present experiments are listed in the table, which includes also all the previously published data on the lead isomer Pb^{205m}.

It is thus established that the short-lived γ radiations from thallium bombarded by 19.2-Mev protons and from lead bombarded by 14.7-Mev neutrons belong to the lead isomer Pb^{205m} obtained from the reactions Tl^{205} (p, n) and Pb^{206} (n, 2n), respectively.

From a comparison of all the known data on the radiation of Pb^{205m} (see table) it is seen that the half-lives determined in different investigations agree with each other within the limits of experimental error. Further experiments are necessary, since the 0.73-Mev radiation observed in experiments with protons has a low intensity and is also quite weak in experiments with neutrons, while the 0.27-Mev radiation was not investigated in the neutron experiments. We note here that no information on the short-lived 0.7- and 0.27-Mev lines is contained in the paper by Vegors and Health.[4] The data obtained in the experiments on the radiation energies of the Pb^{205m} isomer did not confirm the computations by Pryce.[3]

The high probability of production of the lead isomer Pb^{205m} in experiments with neutrons is very difficult to explain on the basis of the existing level scheme of Pb^{205}. Actually, the calculated cross section of the inelastic processes is approximately 2.5 b. Thus, from this result and from our measurements it follows that approximately half the nuclei produced in the (n, 2n) reaction is de-excited through the metastable level with a half life of 5 milliseconds.

Calculations show that the most probable value

Radiation energy, Mev	Half-life of isomer, msec	Method of obtaining the isomer	Reaction cross sections, b	Reference
~0.9	6.5±0.5	$Tl + p$	—	[1]
0.94±0.2 0.48±0.01	5.0±0.5	$Pb^{206}(n, 2n)Pb^{205m}$	—	[2]
0.4±0.2 0.7033	**several units**	**calculation**	—	[3]
0.987	4.7±1.5	$Bi^{205} \xrightarrow{\varepsilon} Pb^{205m}$	—	[4]
0.97±0.01	5.2±0.3	$Tl^{205}(p, n)Pb^{205m}$	$(20\pm4)\cdot10^{-3}$	**present work**
0.73±0.01	—	—	—	
0.27±0.02	—	—	—	**present work**
0.94±0.02	5.0±0.2	$Pb^{206}(n, 2n)Pb^{205m}$	(1.1±0.2) b	
0.7(?)	—	—	—	

of the spin of the residual nucleus produced in the $Pb^{206}(n, 2n)Pb^{205}$ reaction is $^{11}/_2$. From the data on the levels of Pb^{205} (reference 7) it follows that there are many levels with spins $^9/_2$ and $^{11}/_2$. It is clear that the residual nucleus with spin $^{11}/_2$ should decay principally to these levels. Yet, as follows from the accepted scheme,[7] the high-spin levels include no states with lifetimes $\sim 10^{-3}$ sec. Taking this result into consideration, as well as the fact that the calculation[3] based on the characteristics of known levels of Pb^{205} has not been verified, it would be desirable to review the level scheme of Pb^{205}.

In conclusion, we consider it our pleasant duty to express sincere gratitude to A. P. Klyucharev for continuous interest in the present investigation, to the accelerator crew of the Physico-Technical Institute of the Academy of Sciences of the Ukrainian S.S.R. and the Institute of Chemical Physics of the Academy of Sciences U.S.S.R., and also to V. M. Nikishova who participated in the experiments with the neutrons.

[1] Leĭpunskiĭ, Miller, Morozov, and Yampol'skiĭ, Dokl. Akad. Nauk SSSR **109**, 935 (1956), Soviet Phys.-Doklady **1**, 505 (1957).

[2] Glagolev, Kovrizhnykh, Makarov, and Yampol'skiĭ, JETP **36**, 1046 (1959), Soviet Phys. JETP **9**, 742 (1959).

[3] M. H. Pryce, Nucl. Phys. 2, 226 (1956).

[4] S. H. Vegors and R. L. Health, Bull. Amer. Phys. Soc. **3**, 209 (1958).

[5] Morozov, Remaev, and Yampol'skiĭ, JETP **39**, 973 (1960), Soviet Phys. JETP **12**, 674 (1961).

[6] Ashby, Catron, Newkirk, and Taylor, Phys. Rev. **111**, 616 (1958).

[7] B. S. Dzhelepov and L. K. Peker, Схемы распада радиоактивных ядер (Decay Schemes of Radioactive Nuclei), U.S.S.R. Acad. Sci. Press, 1958.

Translated by J. G. Adashko
299

SOVIET PHYSICS JETP VOLUME 12, NUMBER 6 JUNE, 1961

SECONDARY PROCESSES IN THE PRODUCTION OF PIONS ON NUCLEI

V. M. MAL'TSEV and Yu. D. PROKOSHKIN

Joint Institute for Nuclear Research

Submitted to JETP editor July 30, 1960

J. Exptl. Theoret. Phys. (U.S.S.R.) 39, 1625-1629 (December, 1960)

The production of π mesons in p-C collisions at an energy of 660 Mev is calculated by the Monte Carlo method. It is shown that the scattering of π mesons changes appreciably the π-meson angular distributions and the ratio of the positive and negative π-meson yields. The angular dependence obtained for this ratio agrees with the experimental data.

1. INTRODUCTION

THE study of the processes of π-meson production in collisions of high-energy nucleons with nuclei permits one, in principle, to obtain information on both the nucleon-nucleon and meson-nucleon interactions. Within the framework of the existing theory of the nucleus, this problem, however, cannot be accurately solved, and therefore attempts are being made, for the present, to find at least an approximate solution. Interest in solutions of this type springs from the fact that they permit one to obtain some knowledge of the characteristics of nucleon-nucleon processes not by carrying out complicated experiments, but on the basis of the results of comparatively simpler investigations of interactions between nucleons and nuclei (see, for example, references 1 — 3). All similar studies make use of the circumstance that the fast particles interact with nuclear matter primarily via two-particle collisions. This makes it possible to apply the simple optical model of the nucleus, where the parameters of this model are directly related to the nucleon-nucleon and meson-nucleon reaction cross sections. The calculation then reduces to the determination of the corrections for the scattering of the nucleons of the nucleus and for the change in the π-meson yield due to the secondary processes, namely absorption and scattering inside the nucleus.

In the case of light nuclei, where secondary effects are small, these corrections prove to be small for intense reactions (such as $p + p \rightarrow \pi^+$ and $p + n \rightarrow \pi^0$), so that it is possible to describe the experimental data with sufficient accuracy by means of a model that takes the emission of nucleons and π mesons from the meson production process into account.[1] However, in the analysis of low-intensity reactions (for example, $p + n \rightarrow \pi^-$), such a simplified model, in which π-meson scattering is neglected, cannot be used, for even in light nuclei the relative yield of negative π mesons should increase significantly, owing to scattering (with charge exchange) of π^0 mesons,* the loss of which is compensated, in turn, by the charge exchange of π^+ mesons. For this reason, the ratio Y^+/Y^- of the integrated yields of the π^+ and π^- mesons in collisions of protons with a complex nucleus should be smaller than in the case of free nucleons, firstly, owing to the increase in the π^--meson yield, and, secondly, owing to the comparatively small decrease in the π^+-meson yield. It also follows from the above that Y^+/Y^- should be a decreasing function of the weight of the bombarded nucleus. This mechanism for the variation of the ratio Y^+/Y^- is apparently a basic one and accounts for the difference[5-7] in the values of Y^+/Y^- for deuterium and carbon.† The purpose of the present article is a quantitative verification of this hypothesis by comparison of the results of the calculations with the existing experimental data.

2. METHOD OF CALCULATION

The π-meson production process was simulated by the Monte Carlo method (see, for example, reference 8). The light nucleus C_6^{12} was chosen as the target to be bombarded by 660 Mev protons. This proved to be convenient, since, on the one hand, the probability of secondary interactions in such a nucleus is already sufficiently large, and, on the other hand, the role of multiple collisions is not yet important, which considerably facilitates the calculations.

---

*If this process is overlooked, then one may arrive at an an incorrect conclusion as regards the value of the cross section for the $p + n \rightarrow \pi^-$ reaction and overestimate the π-meson production probability in the state with a total isotopic spin T = 0, as was the case in the paper of Azhgireĭ et al.[4]

†As shown by B. Pontecorvo (private communication), the relative yield of negative π mesons can also be increased as a result of their production by recoil neutrons due to the scattering of primary protons inside the nucleus. We have estimated that the ratio Y^+/Y^- then decreases by approximately 10%. In the region of higher energies, the above-mentioned process should be important.

Since the aim of the calculation was to explain the role of secondary processes and scattering in particular, and not to obtain a complete picture of the production of π mesons in a nucleus, we used a simplified model of the nucleus in which, with no detrimental effect on the accuracy, the motion inside the nucleus was not taken into account (its role is small at the energy considered[3]) and the density of the nuclear matter was taken to be constant over the volume of the nucleus. The problem was solved in two steps: the process for the production of π mesons was "drawn" with and without allowance for scattering. The results were then compared. Thus the calculations were made by a relative method. We studied, for example, not the π-meson angular distribution, but its change due to scattering within the framework of the same model, owing to which the aforementioned simplifications could not appreciably distort the final results.

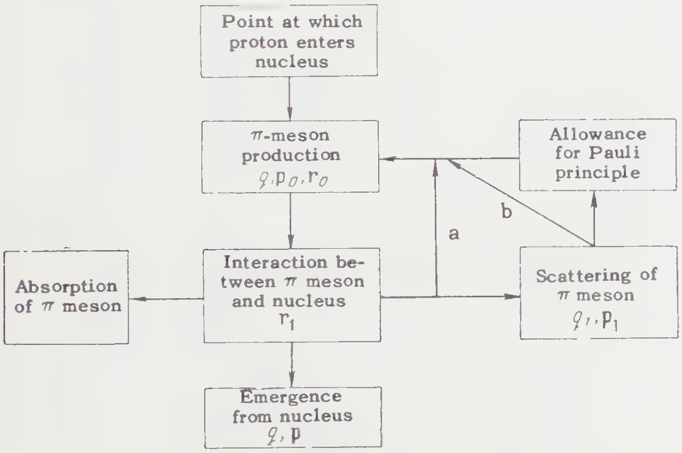
Point at which proton enters nucleus
π-meson production
q, p_0, r_0
Allowance for Pauli principle
b
a
Absorption of π meson
Interaction between π meson and nucleus
r_1
Scattering of π meson
q_1, p_1
Emergence from nucleus
q, p

FIG. 1. Scheme of calculations. The processes and the quantities determined are shown in the rectangles of the block diagram.

The calculations were carried out according to the scheme shown in Fig. 1. We determined the following quantities: the π-meson charge q, its momentum p, and the point r at which the event took place. The arrow a on the diagram refers to the first stage of the calculations, in which the π-meson scattering was not taken into account. At the same time, the role of the Pauli principle was also estimated (calculated along arrow b and along the basic scheme). In the latter case, events in which the recoil nucleon, after the scattering, has an energy lying below the limiting Fermi energy are excluded. The calculations were performed on the Ural electronic computer. To determine the probability of the various processes, we used the existing experimental data on the sizes of the cross sections (see the literature cited in references 3 and 8). A total of 500 cases of production of a π meson inside the nucleus were simulated. Of these, 314 mesons left the nucleus without experiencing secondary interactions, and 15 mesons interacted twice with nucleons of the nucleus.

3. RESULTS OF THE CALCULATIONS AND DISCUSSION

A. Variation of the total cross sections. In collisions of 660-Mev protons with free protons and neutrons, π mesons of different charge are produced in the following proportions:* $Y^+/Y^0 = 1.70 \pm 0.12$[9] and $Y^+/Y^- = 9.0 \pm 0.8$.[5,6,9] The simulation showed that as a result of charge-exchange scattering the value of the first ratio, as should have been expected, changes slightly: for carbon $Y^+/Y^0 = 1.6$. At the same time, the ratio of the yields of positive and negative π mesons is $1/(1.5 \pm 0.1)$ of the value for free nucleons.

$$Y^+/Y^- = 6{,}1 \pm 0{,}6.$$

This value is in good agreement with the experimentally found value $Y^+/Y^- = 6.2 \pm 0.5$[5–7] (see last footnote).

The effect of the Pauli principle for π-meson energies as large as in our case turns out to be slight. Only 15% of all acts of scattering are forbidden because of this principle.

B. Change in the angular distributions. The scattering of the produced π mesons on the nucleons of the nucleus leads to a decrease in the asymmetry of the π-meson angular distribution with respect to 90°, in the laboratory system. Correspondingly, there is a decrease in the asymmetry of the π-meson angular distribution in the center-of-mass system (c.m.s.) of the colliding nucleons $f(\theta)$, which, even without allowance for the scattering of the π mesons, should be essentially asymmetric, owing to the scattering of protons and the absorption of the π mesons.[10] If we describe the asymmetry of the angular distribution by means of the quantity $\eta = [f(180°) - f(0°)]/f(90°)$, then, as is seen from Fig. 2, the increase in the asym-

---

*We also used the data shown in Fig. 3 privately communicated by V. G. Vovchenko, G. Gel'fer, A. S. Kuznetsov, M. G. Meshcheryakov, and V. Svyatkovskiĭ.

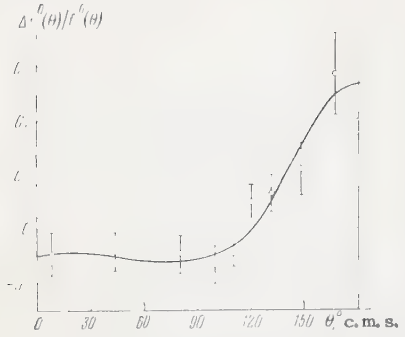

FIG. 2. Relative change of the π^0-meson angular distribution $f^0(\theta)$ as a result of scattering. The points were obtained by the Monte Carlo method. The curve, fitted by the method of least squares, represents a polynomial of the third degree in cos θ.

metry due to the scattering of the π mesons reaches approximately 30% for the case of the production of neutral π mesons, and constitutes an appreciable part of the experimentally observed value for carbon: $\eta = 80 - 100\%$.[10] It follows therefore that even in the case of intensive reactions taking place in light nuclei, the scattering process should not be neglected in the calculation of the π-meson angular distributions.* If we consider the angular distributions of the reactions of low intensity ($p + n \rightarrow \pi^-$ in our case), then the scattering processes already play a decisive role here. In particular, they lead to a sharp drop in the value of the differential π^+- and π^--meson yield ratios y^+/y^- at large angles, as is seen in Fig. 3. From this figure it also follows that the calculated and measured values of the ratios y^+/y^- at various angles are in good agreement with one another. It would be desirable to detect experimentally the fast decrease in the value of y^+/y^- in the region of angles 120 — 180°, as predicted by the calculations. It is also of interest to compare the experimental asymmetries of the angular distributions of π^- and π^+ (or π^0) mesons. The simulation showed that, owing to the scattering, the asymmetry of the angular distributions of π^- mesons produced on carbon is 20 — 30% greater than in the case of π^+ mesons.

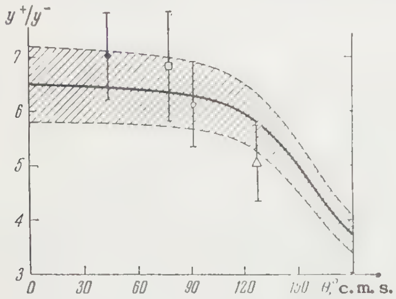

FIG. 3. Ratio of π^+- and π^--meson yields y^+/y^- at various angles for carbon. The solid curve is the result of the Monte Carlo calculation, the dotted curve indicates the error zone, the points are the experimental data: ● – from ref. 7, □ – from ref. 6, △ – from ref. 5, ○ – data of Vovchenko at al. (see footnote, page 1135).

4. CONCLUSION

The above comparison of the results of the Monte Carlo calculations with the experimental data showed that the simple model of the nucleus in which the scattering of the mesons produced in the nucleus is taken into account can be used with success to explain the observed picture of π-meson production on light nuclei. In the case of heavy nuclei, it should be noted that the scattering processes should play a still greater role here. As a result, with increasing weight of the nucleus, one should observe a decrease in the value of the ratio Y^+/Y^-, the occurrence of a still sharper dependence of the value of y^+/y^- on the angle, and also a fast increase in the asymmetry η of the π-meson angular distribution. The last conclusion is in qualitative agreement with the experimental data of reference 10. It should be noted that in the work of Metropolis et al.[8] the contrary result was obtained: their value of η calculated for aluminum (at an energy of 460 Mev) proved to be even greater than that for lead. It is possible that this is due to the small statistical accuracy of the calculations.

In conclusion, it is our duty to thank B. Pontecorvo for helpful discussions.

---

*Comparison of Fig. 2 of the present article with Fig. 5 of reference 1 indicates that the change in the π-meson angular distribution caused by scattering and absorption bears approximately the same character. This makes it possible to take into account the effect of meson scattering on their angular distribution in the model used in reference 1 by means of a small increase in the absorption coefficient for mesons in the nucleus.

[1] Yu. D. Prokoshkin, Proc. CERN Symposium **2**, 385 (1956).

[2] A. M. Segar and R. Rubinstein, Nuclear Phys. 14, 222 (1959).

[3] Yu. D. Prokoshkin, JETP **38**, 455 (1960), Soviet Phys. JETP **11**, 334 (1960).

[4] Azhgireĭ, Vzorov, Zrelov, Meshcheryakov, and Petrukhin, JETP **34**, 1357 (1958), Soviet Phys. JETP **7**, 939 (1958).

[5] V. M. Sidorov, JETP **28**, 727 (1955), Soviet Phys. JETP **1**, 600 (1955); V. M. Sidorov, Proc. CERN Symposium **2**, 366 (1956).

[6] Meshkovskiĭ, Pligin, Shalamov, and Shebanov, JETP **32**, 1328 (1957), Soviet Phys. JETP **5**, 1085 (1957).

[7] Meshcheryakov, Vzorov, Zrelov, Neganov, and Shabudin, JETP **31**, 55 (1956), Soviet Phys. JETP **4**, 79 (1957).

[8] Metropolis, Bivins, Storm, Miller, Friedlander, and Turkevich, Phys. Rev. **110**, 204 (1958).

[9] A. F. Dunaĭtsev and Yu. D. Prokoshkin, JETP **38**, 747 (1960); Soviet Phys. JETP **11**, 540 (1960).

[10] Tyapkin, Kozodaev, and Prokoshkin, Dokl. Akad. Nauk SSSR **100**, 689 (1955).

Translated by E. Marquit
300

SOVIET PHYSICS JETP VOLUME 12, NUMBER 6 JUNE, 1961

PHENOMENOLOGICAL QUANTUM ELECTRODYNAMICS IN THE CASE OF TWO MEDIA

G. M. GARIBYAN

Physics Institute, Academy of Sciences, Armenian S. S. R.

Submitted to JETP editor April 7, 1960

J. Exptl. Theoret. Phys. (U.S.S.R.) **39**, 1630-1636 (December, 1960)

A macroscopic quantum electrodynamics of transition phenomena is constructed. The probabilities for the following first order processes are computed: transition and Cerenkov radiation, electron-positron pair conversion of photon incident on boundary of the medium.

THE theory of transition radiation,[1] based on the classical Maxwell equations, has been considered in a number of papers (see reference 2). It appears interesting to give a quantum theory of this phenomenon, with account of the recoil of the charge. As is well known, the correction from the quantum theory of Cerenkov radiation (see the review of Bolotovskiĭ[3] and the article of Ryazanov[4]) to the usual classical formula is not large; this is connected with the fact that Cerenkov frequencies are optical, and therefore the recoil of the charge caused by radiation of such quanta is entirely negligible. But a condition of the Cerenkov type $[\beta^2\epsilon(\omega) > 1]$ does not apply to the quantum frequencies of the transition radiation, which may contain quanta with frequencies greater than optical. Therefore the quantum theory of transition radiation is expected to change the results of classical theory at higher frequencies. Besides, the apparatus of quantum theory also makes it possible to calculate other effects which take place during transition of charges or photons from one medium to another and which have no classical analog. By way of an example, we calculate below the probability of conversion of a photon into an electron-positron pair when the photon is incident on the boundary of a medium, or emerges from it.

1. GENERAL SCHEME OF THE THEORY

To construct the quantum theory of electromagnetic phenomena one must first discuss the free electromagnetic and electron-positron fields.* Since the formalism of second quantization of the electron-positron field does not depend on the properties of the medium, we shall use all the results of such a quantization (see, for example, reference 5). A fresh analysis must be given, however, for the electromagnetic field.

We shall use a gauge for the potentials in which the scalar potential $\varphi = 0$. Let the medium have a dielectric constant ϵ_1 in the region $z < 0$ and ϵ_2 in the region $z > 0$. Then the components of the vector potential, $A_j(x)$ $(j = 1, 2, 3)$, satisfy the equation $(\hbar = c = 1)$

$$\{\nabla^2 - [\theta(-z)\hat{\varepsilon}_1(\omega) + \theta(z)\hat{\varepsilon}_2(\omega)]\,\partial^2/\partial t^2\}\, A_j(x) = 0, \quad (1)$$

where $\theta(z)$ is a function which equals zero for negative values and unity for positive values of the argument, and the operator $\hat{\epsilon}(\omega) = \epsilon(i\partial/\partial t)$.

The general solution of the wave equation in a homogeneous medium is a superposition of plane waves with arbitrary amplitudes. If two media are present it is natural to subdivide all waves into waves moving away from the interface of the media and waves moving toward the interface. Here the motion may be directed either along or opposite to the positive z direction. In order that these waves be solutions of Eq. (1), two additional waves must be added to each of them. Thus we obtain several types of solution of Eq. (1), as shown in Figs. 1 and 2. The heavy arrow indicates the fundamental wave, and the two other arrows correspond to the waves accompanying it. As independent solutions, in terms of which the general solution of (1) can be expanded, it is enough to take either waves of type (1) (Fig. 1), or waves of type

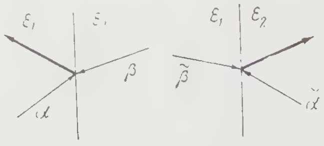

a b

FIG. 1

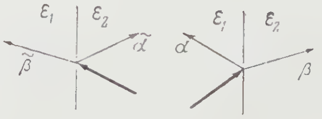

a b

FIG. 2

---

*It is clear that the results obtained will be correct for spin-½ particles of arbitrary mass.

2 (Fig. 2). It is not difficult to verify that either type can be expressed as a linear combination of the other.

The expansion of the general solution of Eq. (1) in terms of waves of type (1) can be put in the form

$$A_j(x) = A_j^{(1a)}(x) + A_j^{(1b)}(x), \tag{2}$$

where

$$A_j^{(1a)}(x) = V^{-1/2} \sum_{\substack{\varkappa,\ \omega \geqslant 0 \\ l=1,2}} \frac{1}{\sqrt{2\omega g^{(l)}}} \Big\{ \theta(-z) \frac{e_j^{(l)}}{\sqrt{\varepsilon_1}} (a_- e^{ik_{1-}x} + \overset{+}{a}_- e^{-ik_{1-}x})$$

$$+ \theta(-z) \frac{e_{j1}^{(l)}}{\sqrt{\varepsilon_1}} \alpha^{(l)} (a_- e^{ik_{1+}x} + \overset{+}{a}_- e^{-ik_{1+}x})$$

$$+ \theta(z) \frac{e_{j2}^{(l)}}{\sqrt{\varepsilon_2}} \beta^{(l)} (a_- e^{ik_{2-}x} + \overset{+}{a}_- e^{-ik_{2-}x}) \Big\}, \tag{3}$$

$$A_j^{(1b)}(x) = V^{-1/2} \sum_{\substack{\varkappa,\ \omega \geqslant 0 \\ l=1,2}} \frac{1}{\sqrt{2\omega \tilde{g}^{(l)}}} \Big\{ \theta(z) \frac{e_j^{\prime(l)}}{\sqrt{\varepsilon_2}} (a_+ e^{ik_{2+}x} + \overset{+}{a}_+ e^{-ik_{2+}x})$$

$$+ \theta(z) \frac{e_{j1}^{\prime(l)}}{\sqrt{\varepsilon_2}} \tilde{\alpha}^{(l)} (a_+ e^{ik_{2-}x} + \overset{+}{a}_+ e^{-ik_{2-}x})$$

$$+ \theta(-z) \frac{e_{j2}^{\prime(l)}}{\sqrt{\varepsilon_1}} \tilde{\beta}^{(l)} (a_+ e^{ik_{1+}x} + \overset{+}{a}_+ e^{-ik_{1+}x}) \Big\};$$

$$xk_{1,2\pm} = \varkappa\rho \pm \lambda_{1,2} z - \omega t, \qquad \lambda_{1,2} = + \sqrt{\omega^2 \varepsilon_{1,2} - \varkappa^2},$$

$$g^{(l)} = 1 + \alpha^{(l)2} + \beta^{(l)2}, \qquad \tilde{g}^{(l)} = 1 + \tilde{\alpha}^{(l)2} + \tilde{\beta}^{(l)2}. \tag{4}$$

In order to simplify the notation, we denote the wave amplitudes $a_{\kappa,\omega,l,\pm}$ simply by $a_\pm$. The remaining notation is as follows: V is the normalization volume, located either in the first or the second medium; κ and ρ are the wave vector of the radiation field and the radius vector of a field point in the xy plane; e (with various indices) are unit polarization vectors of the corresponding waves. Summation over polarization directions is carried out over the values $l = 1, 2$; the polarization direction is perpendicular to the propagation direction of the wave (the potentials satisfy the Lorentz condition div A = 0). It is clear that the propagation directions of each of the three waves shown in the figure are coplanar. We shall choose polarization vectors with $l = 1$ to lie in the plane of the three waves, and those with $l = 2$ to be perpendicular to this plane. The coefficients $\alpha^{(l)}, \ldots, \tilde{\beta}^{(l)}$ must be determined by equating the radiation fields at the interface between the media. We obtain the following expressions for them by the standard method used to derive the Fresnel formulas (see reference 6):

$$\alpha^{(1)} = (\lambda_1 \varepsilon_2 - \lambda_2 \varepsilon_1) / (\lambda_1 \varepsilon_2 + \lambda_2 \varepsilon_1),$$

$$\alpha^{(2)} = (\lambda_1 - \lambda_2) / (\lambda_1 + \lambda_2), \qquad \beta^{(1)} = 2\lambda_1 \varepsilon_2 / (\lambda_1 \varepsilon_2 + \lambda_2 \varepsilon_1),$$

$$\beta^{(2)} = 2\lambda_1 \sqrt{\varepsilon_2 / \varepsilon_1} / (\lambda_1 + \lambda_2). \tag{5}$$

The coefficients with a tilde are obtained from formula (5) by exchanging the indices 1 and 2.

As already mentioned, the general solution of Eq. (1) can also be expanded in terms of solutions of type 2:

$$A_j(x) = A_j^{(2a)}(x) + A_j^{(2b)}(x), \tag{6}$$

where the solutions $A_j^{(2a)}(x)$ and $A_j^{(2b)}(x)$ can be obtained respectively from $A_j^{(1b)}(x)$ and $A_j^{(1a)}(x)$ by the simple substitution

$$k_{1,2\pm} \rightleftarrows k_{1,2\mp}, \qquad a_+ \rightleftarrows a_-, \qquad \overset{+}{a}_+ \rightleftarrows \overset{+}{a}_-.$$

To quantize the radiation field we demand that

$$[a_\pm, \overset{+}{a}_\pm] = [a_{\varkappa,\omega,l,\pm}, \overset{+}{a}_{\varkappa',\omega',l',\pm}] = \delta_{\varkappa\varkappa'} \delta_{ll'} \delta_{\omega\omega'}, \tag{7}$$

and that all remaining commutators be equal to zero. From Eq. (7) it follows that the amplitudes with a cross correspond to the creation of any one of the three waves shown in Figs. 1 and 2, and those without a cross to their annihilation. For the energy of the field we then obtain an expression appropriate to the corpuscle picture.

Using formulas (2) — (4) and (7) one can calculate the commutators of the field operators, but we shall not do this, since these expressions are not needed for the purposes of the present work.

After introducing the scattering matrix in the form of a series in powers of the charge, we can calculate the probability of any process that takes place when a charge or a photon crosses from one medium into another. For example, the Feynman diagram for transition radiation is shown in Fig. 3 (the vertical line through the vertex of the diagram indicates that an interaction of a special type takes place there). The form of a matrix element corresponding to Fig. 3 differs basically from the usual case in that in the general case a conservation law will not apply to the z components of the momenta of the particles that participate in the process. This is so because a fraction of the momentum is transferred to the medium whose density changes discontinuously along the z axis.

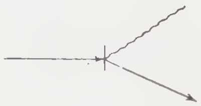

FIG. 3

Since the theory we are developing is macroscopic, it can only be applied if the volume in which the process takes place contains a large number of atoms. This criterion must apply to each of the processes separately, and thus determines the limits of applicability of the formulas obtained.

2. TRANSITION RADIATION

Let a charge moving along the z axis hit the interface between the two media normally. We shall calculate the probability of radiating a quantum of frequency ω in the second medium. Let the momentum of the particle be $\mathbf{p}_1$ before the emission of the quantum and $\mathbf{p}_2$ afterwards. The process under investigation is an effect of first order (Fig. 3). Since the radiation emitted in the second medium corresponds to creation of a photon of type 1b, the matrix element for this process,

$$M_{12} = -e\int d^4xN(\bar{\psi}(x)\hat{A}(x)\psi(x)),$$

is equal to

$$M_{12} = \frac{(2\pi)^3}{\sqrt{V}}\frac{e}{\sqrt{2\omega\widetilde{g}^{(l)}}}f_{12}\delta(\mathbf{p}_{2t}+\varkappa)\delta(E_1-E_2-\omega), \quad (8)$$

where

$$f_{12} = \bar{u}(p_2)\Big[\Big(\pi\delta(p_1-p_{2z}-\lambda_2)+\mathrm{P}\frac{i}{p_1-p_{2z}-\lambda_2}\Big)\frac{\hat{e}'^{(l)}}{\sqrt{\varepsilon_2}}$$
$$-\Big(\pi\delta(p_1-p_{2z}-\lambda_1)-\mathrm{P}\frac{i}{p_1-p_{2z}-\lambda_1}\Big)\frac{\hat{e}_2'^{(l)}\widetilde{\beta}^{(l)}}{\sqrt{\varepsilon_1}}$$
$$+\Big(\pi\delta(p_1-p_{2z}+\lambda_2)+\mathrm{P}\frac{i}{p_1-p_{2z}+\lambda_2}\Big)\frac{\hat{e}_1'^{(l)}\widetilde{\alpha}^{(l)}}{\sqrt{\varepsilon_2}}\Big]u(p_1). \quad (9)$$

The letter P means that the integral of the expression following it is to be taken in the sense of a principal value.

We shall limit our investigation to the medium — vacuum case ($\epsilon_1 = \epsilon$, $\epsilon_2 = 1$) and shall study the radiation in the vacuum, i.e., we put $\kappa = \omega \sin \vartheta$, where ϑ is the angle between the propagation direction of the quantum and the z axis. Then

$$f_{12} = \bar{u}(p_2)\Big[\mathrm{P}\Big(\frac{i\hat{e}'^{(l)}}{p_1-p_{2z}-\lambda_2}-\frac{i\hat{e}_2'^{(l)}\widetilde{\beta}^{(l)}}{(p_1-p_{2z}-\lambda_1)\sqrt{\varepsilon}}$$
$$+\frac{i\hat{e}_1'^{(l)}\widetilde{\alpha}^{(l)}}{p_1-p_{2z}+\lambda_2}\Big)+\frac{\pi}{\sqrt{\varepsilon}}\hat{e}_2'^{(l)}\widetilde{\beta}^{(l)}\delta(p_1-p_{2z}-\lambda_1)\Big]u(p_1). \quad (10)$$

The first three terms in the last formula correspond to non-conservation of the z component of momentum of the participating particles (i.e., to the presence of the boundary). It is natural to associate these terms with transition radiation. Concerning the term with the δ function, we shall see below that it describes Cerenkov radiation which is generated in the medium and passes into the vacuum.

We first calculate the probability of generating transition radiation (Heaviside units):

$$dw = \frac{1}{V}\frac{e^2}{2\omega}|f'_{12}|^2\delta(\mathbf{p}_{2t}+\varkappa)\delta(E_1-E_2-\omega)\frac{ST}{(2\pi)^3}d\mathbf{p}_2 d\mathbf{k}_{2+}, \quad (11)$$

where f'_{12} is defined by the first three terms of (10), $dk_{2+} = \omega^2 d\omega d\Omega$, S is the cross section of the volume in which the process takes place, T is the time it takes for the process, i.e., $V = S\beta T$. By integrating over the electron momentum we find

$$dw = \frac{e^2}{4\pi}\frac{\omega\, d\omega\, d\Omega}{4\pi^2\beta}\frac{E_2}{p_{2z}}|f'_{12}|^2, \quad (12)$$

where we recall that

$$p_{2z} = \sqrt{p_1^2 - 2E_1\omega + \omega^2\cos^2\vartheta}, \qquad E_2 = E_1 - \omega.$$

Next we must average $|f'_{12}|^2$ over the polarizations of the initial electron state, and sum over the electron and photon polarizations in the final state. Let us look at two limiting cases. In the first case we shall not limit the electron speed, but shall suppose that the energy of the emitted quantum is much lower than the electron energy. In the second case we shall suppose that the electron is highly relativistic, and $\omega \gg \sigma$, where $\sigma = 4\pi ne^2/m$. For the first case, after appropriate approximations and calculations, we obtain a formula which agrees with the classical formula for transition radiation emitted in the foreward direction[7] (by an entirely analogous method one could obtain also the classical formula for transition radiation emitted backwards).

In the second case we may suppose $\widetilde{\alpha}^{(l)} = 0$, $\widetilde{\beta}^{(l)} = 1$.

As a result we have

$$dw = \frac{e^2}{16\pi^3}\frac{\omega\, d\omega\, d\Omega}{E_1p_{2z}}(E_1E_2 - p_1p_{2z}\cos^2\vartheta - m^2)$$
$$\times\Big(\frac{1}{p_1-p_{2z}-\lambda_2}-\frac{1}{p_1-p_{2z}-\lambda_1}\Big)^2. \quad (13)$$

We confine our attention to frequencies satisfying the condition

$$1-\omega/\beta_1p_1 \gg \sqrt{1-\beta_1^2},$$

i.e., not very close to $E_1 - m$, and integrate over the angles in (13). We obtain

$$w(\omega) = \frac{e^2}{2\pi^2\omega b^2}\Big\{\Big(\frac{1+a}{2}+\frac{\omega^2b(1-\beta_1^2)}{\sigma}\Big)\ln\Big(1+\frac{\sigma}{\omega^2b(1-\beta_1^2)}\Big)$$
$$-1-\frac{a}{2}+\frac{a}{2(1+\sigma/\omega^2b(1-\beta_1^2))}\Big\},$$
$$a = \frac{\omega^2/p_1^2}{2(1-\omega/\beta_1p_1)^2}, \qquad b = 1+\frac{\omega/p_1}{1-\omega/\beta_1p_1}. \quad (14)$$

For frequencies $\omega \ll E_1$, when we can put $a \sim 0$ and $b \sim 1$, we obtain the usual classical formula for highly relativistic particles.[8] Quantum corrections become substantial for $\omega \lesssim E_1$. In this case, however, the frequencies satisfy the relation $\omega \gg [\sigma/(1-\beta_1^2)]^{1/2}$, for normal electron densities. Therefore the intensity of transition radiation becomes insignificant,[2] and the quantum corrections do not appear particularly interesting. Quantum corrections will become interesting if the electron is incident from the vacuum on very dense matter, for example, on the atomic nucleus. In this case $\sqrt{\sigma} \sim 5$ Mev and $\omega < [\sigma/(1-\beta_1^2)]^{1/2}$ always. It is clear from (14) that the quantum calculation makes the probability of emitting frequencies $\omega \approx p_1$ vanish.

We finally consider the question of the limits of applicability of the formulas obtained. For frequencies $\omega \lesssim p_1$ the linear extent of the zone of formation of transition radiation is (in standard units)

$$R \sim \frac{\hbar}{mc} \frac{1}{\sqrt{1-\beta_1^2}} \left(1 - \frac{\omega}{\beta_1 p_1}\right).$$

If we recall that the radiation is emitted into an angle $\sim \sqrt{1-\beta_1^2}$, we find as the condition of applicability of the theory

$$E_1 / mc^2 \gg (\hbar / mc)^{-3} n^{-1} (1 - \omega / \beta_1 p_1)^{-3},$$

where n is the number of dispersing particles per unit volume.

From the term with the δ function in the brackets of Eq. (10) we can calculate the Cerenkov radiation which is emitted in the medium and passes into the vacuum. In the classical case we put $p_1 = p_2 = p$ and obtain a relationship which agrees with formula (29) of reference 7.

3. PAIR PRODUCTION

As another effect of first order we consider electron-positron pair production by a γ quantum (which moves along the z axis) crossing from one medium into the other (the boundary surface is the $z = 0$ plane). This process corresponds to annihilation of a photon of type 2b, and its graph is shown in Fig. 4. It is clear that this boundary effect can occur because the conservation law of the z component of momentum of particles participating in the process is not fulfilled.* On the other hand, the law of conservation of energy demands that the quantum be hard, and therefore we shall put $\alpha^{(l)} = 0$, $\tilde{\beta}^{(l)} = 1$. Using expansion (6) for the vector potential we find for the matrix element the expression

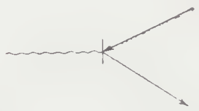

FIG. 4.

$$M_{12} = \frac{i\,(2\pi)^3 e}{2\sqrt{V\omega}} f_{12} \delta(\mathbf{p}_{1t} + \mathbf{p}_{2t})\, \delta(\omega - E_1 - E_2), \qquad (15)$$

where

$$f_{12} = (\bar{u}(p_1)\, \hat{e}'^{(l)} v(p_2)) \left(\frac{1}{p_{1z} + p_{2z} - \omega\sqrt{\varepsilon_1}} - \frac{1}{p_{1z} + p_{2z} - \omega\sqrt{\varepsilon_2}}\right). \qquad (16)$$

In these formulas p_1 and p_2 are the momenta of the electron and the positron.

The probability of the process equals

$$dw = \frac{e^2}{16\pi^3} |f_{12}|^2 \frac{E_1}{p_{1z}\omega} dp_2,$$

$$E_1 = \omega - E_2, \qquad p_{1z} = \sqrt{\omega^2 + p_{2z}^2 - 2E_2\omega}. \qquad (17)$$

Next we carry out the averaging and summation over the polarizations of the photon, electron, and positron, and obtain

$$dw = \frac{e^2}{8\pi^2} \frac{(E_1E_2 - p_{1z}p_{2z} + m^2)\, p_2^2\, dp_2 \sin\vartheta\, d\vartheta}{E_2 p_{1z} \omega} \times \left(\frac{1}{p_{1z} + p_{2z} - \omega\sqrt{\varepsilon_1}} - \frac{1}{p_{1z} + p_{2z} - \omega\sqrt{\varepsilon_2}}\right)^2, \qquad (18)$$

where ϑ is the angle between the direction of motion of the positron and the z axis. If we limit the momentum of the positrons by the condition $m \ll p_2 \ll \omega - m$, then after some transformations and integration over all directions of positron emission we find the following expression:

$$dw = \frac{e^2}{16\pi^2} \frac{p_2^3}{\omega^3} \left(\frac{\varepsilon_1 - \varepsilon_2}{m^2}\right)^2 \frac{dp_2}{E_2}. \qquad (19)$$

The length of the zone of pair production is, to the same approximation, $R \sim (\hbar/mc)(p_2/mc^2)$ (ordinary units). Hence the condition of applicability of the theory has the form

$$p_2 / mc^2 \gg (\hbar / mc)^{-3} n^{-1}.$$

Let us compare the probability of pair production due to the boundary effect with the probability of the usual mechanism for pair production in the field of atomic nuclei in the range $R_{\min} \sim (\hbar/mc)^{-2} n^{-1}$. Estimates show that in the case when a photon enters from the vacuum into a medium of typical electron density, the probability of the boundary effect is insignificant compared with the probability of pair production in the field of atomic nuclei. Therefore it is interesting to consider the incidence of a γ quantum on dense matter, for example on an atomic nucleus, and compare the probability of pair production from the boundary effect with the usual probability of pair production inside the nucleus on the separate protons,[5] regarded as infinitely heavy. Here, as in the previous section, we shall approximate the nucleus by an infinite half-space, supposing that such an approximation gives good estimates if the size of the nucleus is larger than the region in which the process takes place.

---

*Saakyan[9] has discussed the production of pairs of charged particles by a γ quantum in a homogeneous medium, with all conservation laws satisfied; this corresponds in our method to terms with δ functions in formulas of type (9).

Estimates show that the probability of electron-positron pair production from the boundary effect is by one order larger than the probability of the usual mechanism of pair production; however, the process of interest to us will not occur in nuclei, because the length of the zone of pair production is at least two orders larger than the nuclear size. In this connection we note that the region of μ-meson pair production is less than the dimensions of heavy nuclei; however, the probability of the process itself is roughly two orders less than the usual probability of production of a muon pair. Here we have taken the particles that constitute the dispersing medium to be protons. On the other hand, it is well known[10] that anomalous nuclear magnetic moments can be qualitatively explained by the assumption that for some fraction (approximately one third) of the eigentime the nuclei are in a dissociated state, having decayed into another nucleon and a charged π meson. If we consider the π mesons as the particles that make up the dispersive medium, then estimates show that the boundary effect will constitute roughly one third of the usual effect of μ-meson pair production in the field of the separate protons in the nucleus.

In conclusion the author expresses his thanks to I. I. Gol'dman, A. Ts. Amatuni, and G. S. Saakyan for helpful discussions while this work was in progress.

---

[1] V. L. Ginzburg and I. M. Frank, JETP **16**, 15 (1946).

[2] G. M. Garibyan, JETP **37**, 527 (1959), Soviet Phys. JETP **10**, 372 (1960).

[3] B. M. Bolotovskiĭ, Usp. Fix. Nauk **62**, 201 (1957).

[4] M. I. Ryazanov, JETP **32**, 1244 (1957), Soviet Phys. JETP **5**, 1013 (1957).

[5] A. I. Akhiezer and V. B. Berestetskiĭ, Квантовая электродинамика (Quantum Electrodynamics), Fizmatgiz, M. 1959. [2d ed.].

[6] L. D. Landau and E. M. Lifshitz, Электродинамика сплошных сред (Electrodynamics of Continuous Media), Gostekhizdat, M. 1957.

[7] G. M. Garibyan, JETP **33**, 1403 (1957), Soviet Phys. JETP **6**, 1079 (1958).

[8] G. M. Garibyan, JETP **39**, 332 (1960), Soviet Phys. JETP **12**, 237 (1961).

[9] G. S. Saakyan, JETP **38**, 843 (1960), Soviet Phys. JETP **11**, 610 (1960).

[10] E. Fermi, Nuclear Physics, The University of Chicago Press, 1950.

Translated by D. Brill
301

SOVIET PHYSICS JETP VOLUME 12, NUMBER 6 JUNE, 1961

ON SLOW AND RAPID NEUTRON-CAPTURE PROCESSES IN THE THEORY OF ORIGIN OF THE ELEMENTS

G. S. MALKIÉL'

Submitted to JETP editor May 13, 1960

J. Exptl. Theoret. Phys. (U.S.S.R.) **39**, 1637-1640 (December, 1960)

A hypothesis concerning the synthesis of the elements with $Z > 30$ by means of neutron capture is discussed. It is shown that the time required for the synthesis of stable nuclei is of the order of 100 days. Arguments are presented which indicate that neutron numbers 98, 108, and 116 may be favored.

THE peculiarities of the isotopic composition of elements with an atomic number $Z > 30$, and the connection between the isotope abundance and the neutron-capture cross section, definitely indicate that the greater part of matter with $Z > 30$ has been produced by means of neutron capture.

Burbidge et al.[1] assume that the main processes of the production of medium and heavy elements are slow and rapid neutron capture. In the slow-capture process, the neutron flux remains constant for $\sim 10^6$ years, while, for the rapid-capture process, it remains constant for only $10 - 100$ sec.

In the present paper it is shown that it is not necessary to assume the existence of two processes to explain the observed regularities in the abundance of the nuclei. It is sufficient instead to assume one process by which the neutron flux attains its maximum value within 0.1 to 1 hour, and then, for the following 10 to 100 days, remains at $0.01 - 0.1\%$ of the maximum value.

All stable nuclei, from the point of view of neutron-capture production, can be divided into three groups:

1. Unshielded nuclei, i.e., nuclei obtained as a result of the β^- decay of nuclei with a neutron excess.
2. Shielded nuclei, i.e., nuclei which could not have been produced by the consecutive decay of nuclei with a neutron excess, but were obtained by the capture of a neutron by stable nuclei.
3. "By-passed" nuclei, i.e., nuclei whose production requires processes other than neutron capture.

For the production of many unshielded nuclei, the process of neutron capture need not be very slow, since the decay periods of the β^--active isotopes involved in the consecutive neutron-capture processes are ≥ 1 hour. Shielded isotopes, on the other hand, cannot be produced in considerable quantities if the time-scale of the processes are much less than the time of production (by β^- decay) of the corresponding stable nucleus to which a neutron must be added to obtain the required isotope or its β^--active isobar. The fraction of the various isotopes for each group of nuclei is listed in the table. For unshielded nuclei, the fraction of all unshielded nuclei of each element is given, while for shielded and "by-passed" nuclei the percentage of each isotope is shown separately. Only data for even-Z nuclei in the table are presented since nuclei with odd Z cannot be shielded and "by-passed" at the same time.

From the data presented, it can be seen that all shielded isotopes present in quantities greater than 2% do not need more than several days for their production. An exception is the isotope ${}_{42}\mathrm{Mo}^{52}$, which constitutes 9% of the element, and for whose production $\sim 10^6$ years are necessary, but it can be produced within a short time from ${}_{42}\mathrm{Mo}^{50}$, which is a magic "by-passed" nucleus whose content is 15%. Among the shielded isotopes, we also have three isotopes with a content $\leq 2\%$, and for whose production times longer than for the remaining nuclei are needed. These are ${}_{36}\mathrm{Kr}^{44}$, ${}_{48}\mathrm{Cd}^{60}$, and ${}_{64}\mathrm{Gd}^{88}$, and their times of production are 6×10^4, 7×10^6, and 93 years respectively. However, their fractions, equal to 2, 1, and 0.2% respectively, are not greater than those of by-passed nuclei, which indicates the absence of a slow ($10^4 - 10^6$ years) neutron-capture process in the element synthesis.

Thus, for nuclei produced by neutron capture, there is not a single isotope for whose production a time greater than $10 - 100$ days is necessary.

The proposed lifetime of the neutron flux should not only satisfy the observed abundance of the separate isotopes, but should also be in agreement with the abundance maxima of the elements. The abundance H of the elements as a function of the

Z	Isotope fraction, %		
	Unshielded nuclei	Shielded nuclei (with corresponding decay periods)	By-passed nuclei
32	80	20 (1 hour)	
34	90	10 (8 min)	1
36	87	11 (30 min); 2 (6·10^4 years)	0.3
38	82	9 (4 hours)	0.5
40	100		
42	60	16 (65 days); 9 (10^6 years)	15
44	81	12 (60 hours)	2;5
46	89	10 (39 days)	1
48	87	12 (13 hours); 1 (7.10^6 years)	1
50	85	14 (53 hours)	1
52	92	4.6 (39 min); 2.4 (27 hours)	0.1
54	94	4 (72 min); 2 (9 hours)	0.1
56	90	7.8 (9 hours); 2.4 (5 days)	0.1

Z	Isotope fraction, %		
	Unshielded nuclei	Shielded nuclei (with corresponding decay periods)	By-passed nuclei
48	100		0.2
60	73	27 (33 days)	
62	79	7 (2 hours); 11 (11 days)	3
64	98	2 (47 hours); 0.2 (93 years)	
66	98	2 (18 hours)	
68	98		1.5
70	97	3 (9 days)	
72	95		5
74	100		
76	98	1.5 (75 days)	0.02
78	99	0.8 (16 days)	0.01
80	90	10 (18 hours)	0.15
82	99	1.4 (46 days)	

atomic weight is shown in Fig. 1, taken from Suess and Urey.[2] To explain the maxima in the range of magic nuclei, it is necessary to assume that the corresponding isotopes (whether shielded or unshielded) were produced within a time shorter than the lifetime of the neutron flux. In that case, the small value of the neutron-capture cross section for magic isotopes would lead to their great abundance. The time of production corresponds, in such a case, to the time of production of the magic isotope itself, and not to that of the β^--active isobar as in the case of shielded nuclei.

In addition to the maxima corresponding to magic numbers, maxima are also observed for $A = 128$ and 194. Burbidge et al.[1] relate these maxima with $N = 82$ and $N = 126$, assuming that the synthesis of the element was accompanied by a very short ($\sim 10 - 100$ sec) neutron pulse that produced nuclei with a neutron excess up to $18 - 24$. If we do not accept the hypothesis of such a rapid neutron-capture process, then the maximum for $A = 128$ can be attributed to the small cross section for neutron capture and to the long half-lives of the β^- decays of the isotopes $\mathrm{Sn}^{124-132}$ which produce this maximum. The maximum for $A = 194$ can be partially ascribed to the neutron number 116.

The connection between the maximum for $A = 194$, and also the less marked maxima at $A = 180$ and 164, and the neutron numbers 98, 108, and 116 is clear from the comparison of Figs. 1 and 2.

In Fig. 2, stable isotopes with an odd Z are shown. The kinks correspond to the neutron numbers for which the corresponding nuclei have an increased stability. At these points, the stable nucleus is not the next one, formed by addition of two protons and four neutrons, but the nucleus with two protons and only two neutrons more than

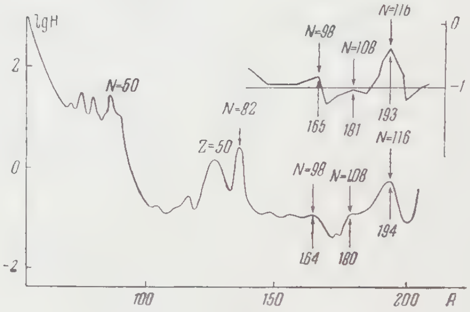

FIG. 1

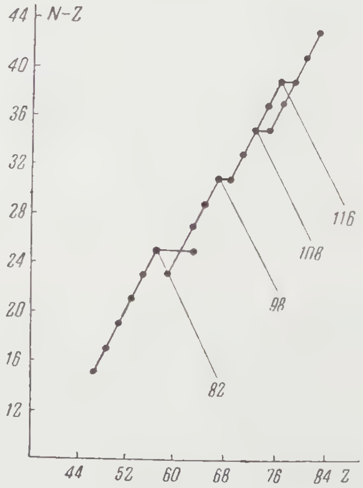

FIG. 2

the preceding one, owing to the decreased binding energy of the neutrons beyond the especially-stable numbers. The mass-spectroscopic data of Demirkhanov et al.[3] also point to the special character of the number 116. The time necessary for the production of maxima can be estimated sufficiently accurately for the maxima corresponding to $N = 50$ and $N = 82$, and also for $A = 128$.

The period of isotope production for $N = 50$ is less than 50 days, and that for $N = 82$ is less than 33 days. For the maximum for $A = 128$, the lifetime of the neutron flux should be of the order of the period of the Sn^{131} β^- decay, so that this time should be sufficient to produce the isotope Sn^{132}. Since the β^--decay period of Sn^{131} equals 3.4 min, the period of existence of the neutron flux necessary for the production of this maximum is of the order of 5 min.

Thus, for the production of shielded nuclei and maxima in the region of magic nuclei, nucleon capture with a duration on the order of 100 days is necessary. This time should be less than 1 hour to explain the production of unshielded nuclei, and about 5 min for the production of the $A = 128$ maximum. For a qualitative explanation of the observed regularities in the isotope abundance at $Z > 30$, one can assume that the neutron flux was in the form of a pulse with a duration of 0.1 — 1 hours, followed by a tail having a characteristic time of ~100 days. Since the abundance of shielded and unshielded isotopes is of the same order of magnitude, the ratio of the neutron fluxes at the maximum and in the tail should be inversely proportional to the ratio of their duration, i.e., the flux in the tail amounts to 0.01 — 0.1% of thė pulse height.

Evidently, if the shape of the neutron-pulse is such that first the unshielded isotopes and then the shielded ones are synthesized, the synthesis process of shielded isotopes has only little influence on the fraction of the unshielded ones by increasing the abundance of isotopes with a smaller neutron excess, since these can also be produced in a slow-capture process. However, in processes proposed by Burbidge et al.,[1] where the shielded nuclei are produced first, followed by the short neutron pulse necessary for the production of unshielded nuclei, the shielded nuclei can be almost completely destroyed by the neutron flux during the pulse.

In conclusion, the author expresses his gratitude to Prof. D. A. Frank-Kamenetskiĭ for his useful comments.

---

[1] Burbidge, Burbidge, Fowler, and Hoyle, Revs. Modern Phys. **29**, 548 (1957).

[2] H. E. Suess and H. C. Urey, Revs. Modern Phys. **28**, 53 (1956).

[3] Demirkhanov, Gutkin, and Dorokhov, JETP **37**, 1217 (1959), Soviet Phys. JETP **10**, 866 (1960).

Translated by H. Kasha
302

SOVIET PHYSICS JETP VOLUME 12, NUMBER 6 JUNE, 1961

PROPERTIES OF THE SCATTERING AMPLITUDE RESULTING FROM THE UNITARITY CONDITION

M. A. BRAUN and L. V. PROKHOROV

Leningrad State University

Submitted to JETP editor May 25, 1960

J. Exptl. Theoret. Phys. (U.S.S.R.) **39**, 1641-1646 (December, 1960)

The restrictions imposed on the two-particle scattering amplitude by the unitarity condition are investigated. It is shown that 1) the imaginary part of the scattering amplitude is a bounded function of the energy and possesses no discontinuities of the first kind in the physical region of the variables; 2) as the energy tends to infinity the amplitude cannot grow without bound, except possibly for some particular values of the scattering angle; 3) under certain reasonable assumptions the total scattering cross section cannot grow indefinitely with increasing energy.

1. As a result of the unsatisfactory state of the theory of strong interactions based on a specific Hamiltonian, attempts have been made to clarify the general properties of quantum field theory without invoking specific interactions, but making use only of principles that would be normally required of any theory: relativistic invariance, causality, the existence of a complete set of positive energy states, and unitarity. Use of the first three conditions has led to the establishing of important analyticity properties for transition amplitudes for the simplest processes. The application of the unitarity condition has turned out to be so restrictive as to even permit the formulation of approximate equations for the two-particle scattering amplitude (although only after assuming the validity of the double representation of Mandelstam and postulating a definite behavior at infinity). In this paper certain general conclusions are obtained regarding the two-particle scattering amplitude, starting from only the unitarity condition and the established analyticity properties. It turns out that only some very general estimates can be made, but these estimates are independent of any approximations.

The fact that the unitarity condition severely restricts the growth of the amplitude is well known in the case of partial wave amplitudes; in this case the unitarity condition takes the form [accurate to within irrelevant factors — see Eq. (7) below]

$$\operatorname{Im} A_l = |A_l|^2 + \text{inelastic-scattering terms}$$

It therefore follows immediately that $|A_l| \leq 1$. However when this result is generalized to the entire scattering amplitude treated as a function of two variables certain definite mathematical complications arise, which it is the aim of the present paper to overcome.

For simplicity we limit ourselves to the scattering of two spinless neutral particles of mass μ. The amplitude for the process will be denoted by $A(s, t) \equiv \overline{A}(s, x)$, where s and t are the invariants introduced by Mandelstam, x being the cosine of the scattering angle in the barycentric frame. If q^2 denotes the square of the particle momentum in that frame then, as is well known,

$$s = 4(q^2 + \mu^2), \qquad t = -2q^2(1 - x).$$

2. Let us show that Im A(s, t) is bounded as a function of s for $s > 4\mu^2$ and possesses no discontinuities of the first kind. We write the unitarity condition for forward scattering as

$$\operatorname{Im} A(s, 0) = \frac{q}{\sqrt{s}} \int_0^2 dy\, |A(s, -2q^2 y)|^2 + \Sigma, \qquad (1)$$

where Σ denotes terms involving amplitudes for inelastic processes, $\Sigma \geq 0$.

We show first that Im A(s, t) is bounded. Let us assume that as $s \rightarrow s_0$ the Im A(s, t) increases without bound for some interval of the variable t. It then follows from the inequality proved below that

$$\operatorname{Im} A(s, 0) \geqslant |\operatorname{Im} A(s, t)| \quad \text{for} \quad -s + 4\mu^2 \leqslant t \leqslant 0; \qquad (2)$$

in any case, Im A(s, 0) will increase no slower. If it is assumed that Im A(s, 0) and Im A(s, t), where t lies in the indicated interval, increase in approximately the same fashion, then this assumption will be sufficient to prove the impossibility of Im A(s, t) growing without bound.

More precisely we shall prove that if the function $\rho(s)$ is monotonic and $\rho(s) \to \infty$ as $s \to s_0$, then there exists no sequence

$$s_1, s_2, \ldots, s_k \quad (s_k \to s_0 \text{ as } k \to \infty), \tag{3}$$

such that the following conditions are satisfied

$$\frac{1}{\rho(s_k)} |\operatorname{Im} A(s_k, -2q_k^2 y)| \geqslant \chi(y) \not\equiv 0,$$
$$\frac{1}{\rho^2(s_k)} |\operatorname{Im} A(s_k, 0)| \to 0 \text{ as } k \to \infty, \tag{4}$$

where $\chi(y)$ is some non-negative function. Indeed, let us suppose that such a sequence exists. Then, by leaving out from Eq. (1) non-negative terms, we find

$$\operatorname{Im} A(s, 0) \geqslant \frac{q}{\sqrt{s}} \int_0^2 dy \, |\operatorname{Im} A(s, -2q^2 y)|^2. \tag{5}$$

Dividing both sides of Eq. (5) by $\rho^2(s)$ and studying the resultant inequality with the sequence (3) we find, upon passing to the limit and taking into account Eq. (4), that

$$0 \geqslant \frac{q_0}{\sqrt{s_0}} \int_0^2 dy \, \chi^2(y),$$

which is obviously impossible.

The sequence (3) (and analogous sequences later) is considered here to enable us to take into account the case of nonmonotonic behavior of the function near the limiting point. We note that with the help of the method utilized below to study the amplitude as $s \to \infty$, it is also possible to show that $\operatorname{Im} A(s, t)$ cannot increase as $s \to s_0$ in an arbitrary interval of positive measure of the variable t under more general assumptions.

Let us consider the inequality (2). It is an elementary consequence of the unitarity relation. It was shown by Lehmann[1] that for those values of s for which $\bar{A}(s, x)$ exists, both it and its imaginary part are analytic functions of x within an ellipse, which contains the physical region $|x| \leq 1$, and, consequently, may be expanded in partial waves, e.g.,

$$\operatorname{Im} A(s, t) = \sum_{l=0}^{\infty} (2l+1) \operatorname{Im} A_l(s) P_l(x). \tag{6}$$

From the unitarity relation for partial waves:

$$\operatorname{Im} A_l(s) = (2q/\sqrt{s}) |A_l(s)|^2 + \text{inelastic-scattering terms} \tag{7}$$

it follows that $\operatorname{Im} A_l(s) \geq 0$. This fact, together with the inequality $|P_l(x)| \leq P_l(1)$ for $|x| \leq 1$, immediately leads to Eq. (2).

Thus we have proved that $\operatorname{Im} A(s, t)$ is bounded. It is easy to see that $\operatorname{Im} A(s, t)$ cannot have discontinuities of the first kind in s for an interval of positive measure in t, since then $\operatorname{Re} A(s, t)$ would have a logarithmic singularity at the discontinuity point leading to the violation of the inequality [which results from (1)]

$$\operatorname{Im} A(s, 0) \geqslant \frac{q}{\sqrt{s}} \int_0^2 dy \, |\operatorname{Re} A(s, -2q^2 y)|^2,$$

as a consequence of the boundedness of $\operatorname{Im} A(s, 0)$.

3. Let us turn now to a study of the behavior of $\bar{A}(s, x)$ as $s \to \infty$. The unitarity condition (7) permits us to conclude that for sufficiently large s

$$|A_l(s)| \leqslant 2. \tag{8}$$

Using this inequality we shall show that there exists no sequence

$$s_1, s_2, \ldots, s_k \quad (s_k \to \infty \quad \text{as } k \to \infty), \tag{9}$$

such that $|\bar{A}(s_k, x)|$ increases without bound at all points of an interval of positive measure in the variable x, so that

$$\min_{x \in [\alpha, \beta]} |\bar{A}(s_k, x)| \to \infty \text{ as } k \to \infty.$$

Let us suppose this to be false and that in some interval $[\alpha, \beta] \subset [-1, 1]$ with the sequence (9) the quantity $|\operatorname{Re} \bar{A}(s_k, x)|$ or $|\operatorname{Im} \bar{A}(s_k, x)|$ (or both together) increases without bound as $k \to \infty$ uniformly in $x \in [\alpha, \beta]$. For the sake of definiteness let it be $|\operatorname{Re} \bar{A}(s_k, x)|$. Let us define

$$a_k = \min_{x \in [\alpha, \beta]} |\operatorname{Re} \bar{A}(s_k, x)|.$$

According to our assumption the a_k form an increasing sequence. Let us choose from the sequence (9) a subsequence

$$s_{i_1}, s_{i_2}, \ldots, s_{i_k} \quad (s_{i_k} \to \infty \quad \text{as } k \to \infty), \tag{10}$$

for which a_k increases monotonically. It is obvious then that, for sufficiently large k, the quantity $\operatorname{Re} \bar{A}(s_k, x)$ does not change sign in the interval $x \in [\alpha, \beta]$ and we will take it to be, for example, positive. Let us introduce a continuous nonnegative function $v(x)$ with the following properties:

1) $v(x) = 0$ for $x \,\bar{\in}\, [\alpha, \beta]$;
2) $v(x) > 0$ for $x \in (\alpha, \beta)$;
3) if $v(x) = \sum_{n=0}^{\infty} (2n+1) v_n P_n(x)$.

$$\text{then } \sum_{n=0}^{\infty} |v_n| (2n+1) < \infty. \tag{11}$$

Such properties are possessed, for example, by the following function

$$v(x) = \begin{cases} 0, & x \in [\alpha, \beta] \\ \exp\{-(\alpha - x)^{-2} - (\beta - x)^{-2}\}, & x \in [\alpha, \beta] \end{cases}.$$

It can now be asserted that on the sequence (10)

$$(v(x)/a_k)\,\mathrm{Re}\,\bar{A}(s_k,x)\geqslant v(x). \tag{12}$$

The inequality (12) together with the premise about the growth of a_k contradict the unitarity relation. In fact, if the left side of Eq. (12) is expanded in Legendre polynomials, one obtains

$$B(s_k,x)\equiv\frac{v(x)}{a_k}\mathrm{Re}\,\bar{A}(s_k,x)=\sum_{l=0}^{\infty}(2l+1)B_l(s_k)P_l(x),$$

$$B_l(s_k)=\frac{1}{a_k}\sum_{n=0}^{\infty}\sum_{m=0}^{\infty}(2n+1)(2m+1)v_n\,\mathrm{Re}\,\bar{A}_m(s_k)\,C_l^{nm},$$

$$C_l^{nm}=\frac{1}{2}\int_{-1}^{+1}P_l(x)P_n(x)P_m(x)\,dx.$$

The coefficients C_l^{nm} are different from zero only if

$$n+l\geqslant m\geqslant|n-l|,$$

and from their definition follows the estimate

$$|C_l^{nm}|\leqslant(2n+1)^{-1/2}(2m+1)^{-1/2}.$$

Making use of Eq. (8) we find

$$|B_l(s_k)|\leqslant\frac{2}{a_k}\sum_{n=0}^{\infty}\sum_{m=0}^{\infty}(2n+1)(2m+1)|v_n||C_l^{nm}|$$

$$\leqslant\frac{2}{a_k}\sum_{n=0}^{\infty}(2n+1)^{1/2}|v_n|\sum_{m=|l-n|}^{l+n}(2m+1)^{1/2}.$$

From here we obtain for $l=0$ and with Eq. (11) taken into account

$$|B_0(s_k)|\leqslant\frac{2}{a_k}\sum_{n=0}^{\infty}(2n+1)|v_n|\leqslant\frac{c}{a_k}, \tag{13}$$

where c is some constant, independent of k. On the other hand it follows from Eq. (12) that

$$B_0(s_k)\geqslant\frac{1}{2}\int_{\alpha}^{\beta}v(x)\,dx, \tag{14}$$

which is in contradiction with Eq. (13) since $B_0(s_k)\to 0$ as $k\to\infty$.

The above proof does not apply to functions, for which for an arbitrary x in a given interval it is possible to find a sequence $s_1(x)\ldots s_k(x)$ such that the functions increase, but nevertheless the conditions of the above formulated theorem are not fullfilled. Such are, for example, functions of the type $s\cos xs$ (this particular function can be excluded by a slight modification of the method used in Sec. 2, namely by replacing $\chi(y)$ by a quantity $\chi(s,y)$ such that its square integrated over y is bounded from below by a positive number independent of s). It is possible that there exist functions of a kind that do not contradict unitarity at all.

4. Within the indicated limitations, we have thus proved that the amplitude $\bar{A}(s,x)$ does not increase as $s\to\infty$, with the possible exception of particular values of the variable x. Apparently it is not possible to deduce limitations on the behavior of the amplitude for particular values of the angle from the unitarity condition alone, because of the integral character of unitarity. However, it seems most unlikely from physical considerations, that as $s\to\infty$ the amplitude $\bar{A}(s,x)$ should increase without bound for some particular values of the angle other than 0 or π. This statement can also be given some mathematical foundation based on the Mandelstam assumption,[2] that $\bar{A}(s,x)$ is for finite s an analytic function of x except for cuts on the real axis in the intervals $(-\infty,-1-8\mu^2/(s-4\mu^2)]$ and $[1+8\mu^2/(s-4\mu^2),\infty)$. As $s\to\infty$ these cuts go over into the rays $(-\infty,-1]$ and $[1,+\infty)$.

The points $|x|<1$ are located, for arbitrarily large values of s, inside the region of analyticity in x and it is natural to believe that also in the limit, as $s\to\infty$, no singularities in the variable x will develop at these points. On the other hand, in the limit $s\to\infty$, the points $|x|=1$ fall on the beginnings of the cuts and are therefore exceptional. We can therefore suppose that $\bar{A}(s,1)$ and $\bar{A}(s,-1)$ behave in a singular fashion as $s\to\infty$, for example increase. Let us note here that the usual assumption of constancy for the total cross section in the high energy limit corresponds to $\mathrm{Im}\,\bar{A}(s,1)$ increasing as s for $s\to\infty$.

To study the behavior of $\bar{A}(s,x)$ in the vicinity of the points $|x|=1$ (to be definite we have in what follows in mind the point $x=1$) it is convenient to pass to the variables s and t. It follows from the Mandelstam representation that for finite s the quantity $A(s,t)$ is an analytic function of t except for the cuts $(-\infty,-s]$ and $[4\mu^2,\infty)$ along the real axis. The entire physical region of t, including the point $t=0$, finds itself inside the region of analyticity in t for arbitrarily large values of s (at a distance $\geq 4\mu^2$ from the nearest singularity). Based on this we assume that also in the limit $s\to\infty$ the point $t=0$, or any point $t=t_1$ in the physical region, is no more singular than other points in the physical region, i.e., that if $A(s,0)$ or $A(s,t_1)$ increases as $s\to\infty$ then there must exist a finite interval $[\alpha_1,\beta_1]$ in the physical region of t, such that for fixed $t\in[\alpha_1,\beta_1]$ the amplitude $A(s,t)$ increases with s uniformly in t and not slower than $A(s,0)$ or $A(s,t_1)$. Let us note that we exclude here from consideration functions of the form $s^{1/(4\mu^2-t)}$.

If the above assumption is taken to be satisfied then it turns out to be possible to prove that as s increases the amplitude $A(s, t)$ grows no faster than s, for t fixed in the physical region. Whence, in particular, it follows that the total scattering cross section cannot increase without bound with increasing s.

Let us assume the contrary, i.e. that for $t = t_1$ (in particular $t = 0$) the quantity $A(s, t_1)$ grows faster than s, or, more precisely, that there exists a sequence

$$s_1,\ s_2, \ldots, s_k \qquad (s_k \to \infty \text{ as } k \to \infty), \tag{15}$$

such that $(1/s_k)|A(s_k, t_1)|$ increases monotonically. There are two possibilities: 1) there exists a subsequence

$$s_{i_1},\ s_{i_2}, \ldots, s_{i_k} \qquad (s_{i_k} \to \infty \text{ as } k \to \infty), \tag{16}$$

such that $(1/s_{i_k})|A(s_{i_k}, 0)|$ grows monotonically and faster than $(1/s_{i_k})|A(s_{i_k}, t_1)|$; in this case we set $b_k = (1/s_{i_k})|A(s_{i_k}, 0)|$ and in the following use this subsequence instead of the sequence (15); 2) no such subsequence exists, in which case we consider the sequence (15) having set $b_k = (1/s_k)|A(s_k, t_1)|$. In both cases

$$\frac{1}{s_k b_k}|A(s_k, 0)| \leqslant \text{const},$$

$$\frac{1}{s_k b_k^2}|A(s_k, 0)| \to 0 \quad \text{as} \quad k \to \infty. \tag{17}$$

It follows from our assumption that for the sequence so determined, for values of k larger than some number n, the condition

$$(1/s_k b_k)|A(s_k, t)| \geqslant \psi(t) \not\equiv 0, \tag{18}$$

will be satisfied, where t lies in some finite interval $[\alpha_1, \beta_1]$, and $\psi(t)$ is an integrable nonnegative function. Let us call attention to the fact that conditions (17) and (18) are analogous to condition (4) in Sec. 2.

Let us show that the increase of b_k as $k \to \infty$ contradicts unitarity. Passing in Eq. (1) to the integration variable t and throwing away nonnegative terms we obtain the inequality (for large s_k)

$$\operatorname{Im} A(s_k,\ 0) \geqslant \frac{1}{s_k}\int_{\alpha_1}^{\beta_1} dt\,|A(s_k,\ t)|^2. \tag{19}$$

We divide this inequality by $s_k b_k^2$ and let $k \to \infty$. It then turns out, as a consequence of Eqs. (17) and (18), that

$$0 \geqslant \int_{\alpha_1}^{\beta_1} dt\,\psi^2(t),$$

which is impossible.

We have thus found that there exists no sequence $s_1, s_2, \ldots s_k$, $s_k \to \infty$, for which $|A(s_k, t_1)|$ increases faster than s for any fixed physical t_1. On the basis of qualitative considerations the same conclusion was reached by Pomeranchuk.[3]

In conclusion the authors express their gratitude to Yu. V. Novozhilov for interest in this work and useful discussions, and to K. K. Golovkin for consultations on mathematical problems.

---

[1] H. Lehmann, Nuovo cimento **10**, 579 (1958).

[2] S. Mandelstam, Phys. Rev. **112**, 1344 (1958).

[3] I. Ya. Pomeranchuk, JETP **34**, 725 (1958), Soviet Phys. JETP **7**, 499 (1958).

Translated by A. M. Bincer
303

SOVIET PHYSICS JETP VOLUME 12, NUMBER 6 JUNE, 1961

FLUCTUATION THERMODYNAMICS OF NON-EQUILIBRIUM PROCESSES

R. L. STRATONOVICH

Moscow State University

Submitted to JETP editor May 25, 1960

J. Exptl. Theoret. Phys. (U.S.S.R.) 39, 1647-1659 (December, 1960)

A connection is established between the two-dimensional distribution of equilibrium fluctuations and the one-dimensional distribution of a non-equilibrium process. As a consequence of this relation the equations of the theory of equilibrium fluctuations and of non-equilibrium thermodynamics are derived. It is shown that the residual correlations and the ergodicity of the system are determined by the behavior of its thermodynamic functions. In correspondence with this the Onsager relations are generalized for the case of nonlinear non-equilibrium processes.

1. INTRODUCTION

THE recent developments in theoretical thermodynamics have mainly been in the direction of establishing relations between the statistical characteristics of the fluctuations of thermodynamic parameters for equilibrium and non-equilibrium processes. In accordance with the thermodynamic method, the relations studied bear a universal character, i.e., they do not depend on the choice of the particular dynamic model for the process. The main results of the quantum thermodynamics of non-equilibrium processes[1-4] were obtained by applying perturbation-theory methods. In contradistinction to those papers, the fundamental relation (9) in the present paper, which gives the connection between the two-dimensional characteristic function of equilibrium fluctuations and the one-dimensional characteristic function of a non-equilibrium process, is derived as an exact equation without use of perturbation theory. This is made possible by an application of the very exact quantum method (which uses the "ordering" index") worked out by Feynman.[5]

The universal connection which we find between the two-dimensional equilibrium distribution of the fluctuations, on the one hand, and the non-equilibrium fluctuation process, on the other, enables us to obtain both the main previous results and a number of new results. When we change over to the one-dimensional distribution, we obtain an important formula which gives us a quantum generalization of the theory of equilibrium fluctuations by Terletskiĭ and Magalinskiĭ.[6] On the other hand, the equations of the theory of non-equilibrium fluctuations, which can be found in the papers by Callen and others,[1,3] are obtained by differentiation, from the basic Eq. (9) which serves thus as a generating equation for these relations. It is clear from what has been said that we establish a connection between these two theories.

The basic Eq. (9) [or (25)] enables us to study also what we call the residual correlations, a phenomenon which is of great interest (from the point of view of the principles involved). This phenomenon consists of the fact that when there are equilibrium fluctuations the correlations between the values of thermodynamic parameters do not vanish when the time interval is increased, i.e., non-ergodicity exists. The residual correlations and the non-ergodicity coefficient which we introduce can be expressed in terms of the thermodynamic functions of the system. When the volume of the system and its number of particles are given proportional increases, the residual correlations and the non-ergodicity coefficient remain equal to well defined finite values. Contact with an external thermostatic bath, which is a surface phenomenon, plays a relatively smaller and smaller role when this increase takes place so that references to such a contact can not diminish the essential importance of this phenomenon. The non-ergodicity of a maximally increased system which by itself is a thermostatic bath, is in our opinion an essential one. It is not possible for us to dwell here on the conclusions that follow from this in relation to the dynamic foundation of statistical thermodynamics, and we restrict ourselves only to a reminder that in the opinion of several authors the ergodicity of a system is neither necessary nor sufficient for such a foundation.

Applying the principle of time reversal to the basic formula, we can derive the reciprocity relations. In view of the fact that this formula does not presuppose that the perturbation is small, the deviation of the non-equilibrium process from the equilibrium one need not be small and the equations describing the relaxation process (Onsager relations) need not be linear. The linearity of Onsager's theory[7,8] has been considered by several people to be a flaw of the theory and the problem was raised in this connection whether the coefficients should satisfy some reciprocity relations which would supplement the Onsager relations when there are non-linear terms. This question is answered in the present paper in the affirmative. It turns out that the complete set of reciprocity relations affects not only the coefficients for non-linear terms in the equations for average values, but also the coefficients in the equations for the fluctuation characteristics of the process (dispersion, asymmetry coefficient, and so on). The quantum-theoretical generalization introduces into the reciprocity relations additional complications. Callen et al.[4] have considered quantum reciprocity relations by using the usual linear approximation, but applied to non-Markovian processes.

2. DERIVATION OF THE BASIC EQUATION

Let the system under consideration be described by a Hamiltonian H which depends not only on the dynamic variables but also on external thermodynamic parameters $a^0 = a_1^0, a_2^0, \ldots$ We shall assume that this latter dependence is linear

$$H = H_0 - \sum a_j^0 F_j \equiv H_0 - a^0 F. \tag{1}$$

Here $F = F_1, F_2, \ldots$ are internal parameters, the statistical characteristics of which are studied.

The equilibrium state corresponding to a temperature $T = 1/k\beta$ is described by a density matrix

$$\rho = e^{\beta\Psi - \beta H}, \tag{2}$$

where $\Psi \equiv \Psi(T, a) = -\beta^{-1} \ln \operatorname{Sp} e^{-\beta H}$ is the free energy which is a thermodynamic c-function.

It is well known that in the Heisenberg representation any dynamical operator L satisfies as a function of time the law

$$L_\tau = e^{i\tau H/h} L e^{-i\tau H/h} \qquad (L_\tau = L(t+\tau),\ L = L(t)).$$

Introducing the operator of differentiation with respect to time, $p = \partial/\partial t$, we can write the last equation as

$$e^{\tau p} L = e^{i\tau H/h} L e^{-i\tau H/h}. \tag{3}$$

We use the ordering parameter s introduced by Feynman;[5] this describes the order in which operators act (an operator acts earlier if it has a lower value of this index). In accordance with the Feynman rules we have

$$e^{-\beta H + uF} = \exp\left\{\int_0^1 [-\beta(H)_s + u(F)_s]\, ds\right\}. \tag{4}$$

We shall "extricate" the operator H from this last equation (the meaning of this operation and the means to carry it out are explained in the cited paper by Feynman). This gives us immediately

$$\exp\left\{\int_0^1 [-\beta(H)_s + u(F)_s]\, ds\right\}$$
$$= e^{-\beta H} \exp\left\{u \int_0^1 (e^{\beta s H} F e^{-\beta s H})_s ds\right\}.$$

Using (3) we have hence

$$e^{-\beta H + uF} = e^{-\beta H} \exp\left\{u \int_0^1 e^{-ih\beta s p_s} (F)_s\, ds\right\}, \tag{5}$$

where the operator p_s refers to the corresponding $(F)_s$ $[p_s(F)_s = (\partial F/\partial t)_s]$.

Besides ρ and Ψ, we introduce the density matrix and the free energy of an auxiliary state

$$\rho_u = \exp\{\beta\Psi_u - \beta H + uF\},$$

$$\Psi_u = -\beta^{-1} \ln \operatorname{Sp} e^{-\beta H + uF} = \Psi(T,\ a^0 + kTu). \tag{6}$$

This auxiliary state is an equilibrium state in the case of a system with changed external parameters

$$a = a^0 + \Delta a = a^0 + kTu. \tag{7}$$

For the original system this state is a non-equilibrium one. We shall call the increments in the parameters $\Delta a = kTu = u/\beta$ additional external forces.

Multiplying (5) by $e^{\beta\Psi}$ and using (2) and (6) we get

$$\rho \cdot \exp\left\{u \int_0^1 e^{-ih\beta s p_s} (F)_s\, ds\right\} = \exp\{\beta\Psi - \beta\Psi_u\}\, \rho_u. \tag{8}$$

If we multiply this last equation by $\exp\{u_\tau F_\tau\}$, say, and take the trace we get

$$\left\langle \exp\left\{u \int_0^1 e^{-ih\beta s p_s} (F)_s\, ds\right\} \exp\{u_\tau F_\tau\} \right\rangle$$

$$= \exp\{\beta\Psi - \beta\Psi_u\} \langle \exp\{u_\tau F_\tau\} \rangle_{kTu}. \tag{9}$$

The formula which we have obtained connects the statistical characteristics of the equilibrium fluctuations with a non-equilibrium process. The latter is defined by stating that we know at $t = t_0$ its non-equilibrium state ρ_u, which is the same as the equilibrium state when the additional forces (7) are applied. For $t > t_0$ or $t < t_0$ there are transient non-equilibrium processes in the system. The resultant process consists of two non-equilibrium processes in opposite directions. The average values over such a process will be denoted by the symbol $<\ldots>_{\Delta a}$. One of these opposing processes (the direct one) can be represented as the result of the action of an external force $f(t)$ which is equal to Δa for $t < t_0$ and equal to zero for $t > t_0$. The other is produced by a force $\tilde{f}(t) = \Delta a - f(t)$ when the time is reversed.

In the classical limit $h = 0$ Eq. (9) changes to

$$\langle \exp\{uF + u_\tau F_\tau\}\rangle = \exp\{\beta\Psi - \beta\Psi_u\}\langle \exp\{u_\tau F_\tau\}\rangle_{kTu}, \quad (10)$$

which can be easily derived directly from Gibbs' classical formula both for the equilibrium and for the non-equilibrium state.

3. THE THEORY OF EQUILIBRIUM FLUCTUATIONS

If we put $u_\tau = 0$ in (9), the average over the non-equilibrium distribution disappears and there remains the thermodynamic equation

$$\langle \exp\left\{u\int_0^1 e^{-ih\beta s p_s}(F)_s\, ds\right\}\rangle = \exp\{\beta\Psi - \beta\Psi_u\}, \quad (11)$$

which refers to equilibrium fluctuations. This equation is a quantum generalization of the formula $<\exp\{uF\}> = \exp\{\beta\Psi - \beta\Psi_u\}$ which is the basis of Magalinskiĭ and Terletskiĭ's theory.[6] In the classical case the derivatives

$$\mu_{j_1\ldots j_r} = \left[\frac{\partial^r}{\partial u_{j_1}\ldots\partial u_{j_r}}\exp\{\beta\Psi - \beta\Psi_u\}\right]_{u=0}$$
$$= \frac{1}{\beta^r}e^{\beta\Psi}\frac{\partial^r}{\partial a_{j_1}\ldots\partial a_{j_r}}e^{-\beta\Psi} \quad (12)$$

determine the moments $<F_{j_1}\ldots F_{j_r}>$ of the fluctuation process. In the quantum case differentiation of (10) leads to the relations

$$\int_0^1\ldots\int_0^1 \exp\{-ih\beta s_1 p_1 - \ldots$$
$$- ih\beta s_r p_r\}\langle (F_{j_1})_{s_1}\ldots(F_{j_r})_{s_r}\rangle\, ds_1\ldots ds_r = \mu_{j_1\ldots j_r} \quad (13)$$

The domain over which the integration over $s_1, \ldots, s_r$ takes place, which is a cube in r-dimensional space, is divided into r! subdomains corresponding to different ways of ordering the indices $s_\alpha > \ldots > s_\omega$ by magnitude. If we take into account that the order in which the indices increase corresponds to the order in which the operators act, we get from (12)

$$\sum P_r \int_{s_\alpha > \ldots > s_\omega}\ldots\int \exp\{-ih\beta s_\alpha p_\alpha - \ldots$$
$$- ih\beta s_\omega p_\omega\}\, ds_\alpha\ldots ds_\omega\, \langle F_{j_\alpha}\ldots F_{j_\omega}\rangle = \mu_{j_1\ldots j_r}. \quad (14)$$

The sum which contains r! terms is extended here over all possible permutations P_r of the indices $s_1, \ldots, s_r$. Each operator p_γ refers only to its own F_{j_γ}.

Introducing the function

$$\Phi_r(x_r, \ldots, x_1) = \int_0^1 dy_r \int_0^{y_r} dy_{r-1}\ldots\int_0^{y_2} dy_1 \exp\{-x_r y_r - \ldots - x_1 y_1\} \quad (15)$$

and removing Φ_r from under the summation sign, we can write Eq. (14) in the form

$$\Phi_r(ih\beta p^r, \ldots, ih\beta p^1)\langle \sum P_r F_{j_\alpha}\ldots F_{j_\omega}\rangle = \mu_{j_1\ldots j_r}, \quad (16)$$

if we stipulate that p^1 refers to the operator F_{j_ω} which stands on the right (in the first place) in the product $F_{j_\alpha}\ldots F_{j_\omega}$, p^2 to the operator standing in the second place, and so on; finally, the operator p^r refers to F_{j_α} which stands in the r-th place, i.e., on the left.

In particular, when $r = 1$ (first-order effect) we have

$$\Phi_1(x_1) = (1 - e^{-x_1})/x_1. \quad (17)$$

Because the fluctuation process is a stationary one, we have $p_1<F_{j_1}> = 0$, so that $\Phi_1<F_{j_1}> = F_{j_1}$, and (16) leads to the usual classical formula (equation of state)

$$\langle F_j\rangle = \mu_j = -\frac{\partial\Psi}{\partial a_j}(T, a^0). \quad (18)$$

When $r = 2$ (second order effect) we get from (16)

$$\Phi_2(ih\beta p^2, ih\beta p^1)\langle F_{j_1}F_{j_2} + F_{j_2}F_{j_1}\rangle$$
$$= \mu_{j_1 j_2} = \langle F_{j_1}\rangle\langle F_{j_2}\rangle - kT\partial^2\Psi/\partial a_{j_1}\partial a_{j_2}. \quad (19)$$

Since the process is stationary, the value of $<F_{j_1}(t_1)F_{j_2}(t_2)>$ depends only on the difference in the time coordinates $t_2 - t_1 = \tau$ so that $p^2 = -p^1$. Taking into account the relation

$$\Phi_2(-x_1, x_1) = (e^{x_1} - 1 - x_1)/x_1^2,$$

that follows from (15) we find from (19)

$$[e^{ih\beta p_\tau} - 1 - ih\beta p_\tau](ih\beta p_\tau)^{-2}\langle F_{j_1}F_{j_2\tau} + F_{j_2}F_{j_1\tau}\rangle$$
$$- \langle F_{j_1}\rangle\langle F_{j_2}\rangle = -kT\partial^2\Psi/\partial a_{j_1}\partial a_{j_2}, \quad (20)$$

when $\tau = 0$ ($p_\tau = \partial/\partial\tau$).

4. EQUATIONS FOR THE MOMENTS

By differentiating Eq. (9) we get formulae connecting the moments of equilibrium and of non-equilibrium processes. Thus, differentiating both sides of the equation with respect to u_j and $u_{l\tau}$ and then putting $u = u_\tau = 0$, we find

$$\frac{1 - e^{-ih\beta p}}{ih\beta p} \langle F_j F_{l\tau} \rangle - \langle F_j \rangle \langle F_l \rangle = \frac{\partial}{\partial u_j} \langle F_{l\tau} \rangle_{kTu}. \tag{21}$$

Because the process is stationary we can replace p here by $-p_\tau = -\partial/\partial\tau$. In front of the term $\langle F_j \rangle \langle F_l \rangle$ we can also write the operator $\Phi_1(-ih\beta p_\tau)$ which becomes equal to unity because that term is constant. Dividing after that both sides of the equation by the above mentioned operator and taking the real and the imaginary part of the expressions thus obtained, we get

$$\operatorname{Re} \langle F_j F_{l\tau} \rangle - \langle F_j \rangle \langle F_l \rangle = \frac{h\beta p_\tau}{2} \cot \frac{h\beta p_\tau}{2} \frac{\partial}{\beta \partial a_j} \langle F_{l\tau} \rangle_{\Delta a}, \tag{22}$$

$$\operatorname{Im} \langle F_j F_{l\tau} \rangle = -\frac{h\beta p_\tau}{2} \frac{\partial}{\beta \partial a_j} \langle F_{l\tau} \rangle_{\Delta a}. \tag{22'}$$

If we set the spectral components in the left and the right hand sides of Eq. (22) equal to each other we obtain the fluctuation-dissipation theorem.[1,2] The corresponding equation for the classical case

$$\langle F F_\tau \rangle - \langle F \rangle^2 = kT (\partial / \partial a) \langle F_\tau \rangle_{\Delta a}$$

was first obtained by Vladimirskiĭ.[9]

Multiple differentiation of (9) leads to the relations

$$\Phi_r (ih\beta p^r, \ldots, ih\beta p^1) \langle (\sum P_r F_{j_\alpha} \ldots F_{j_\omega}) F_{l_1\tau} \ldots F_{l_n\tau} \rangle$$
$$= (kT)^r e^{-\beta\Psi} \frac{\partial^r}{\partial a_{j_1} \ldots \partial a_{j_r}} [e^{-\beta\Psi} \langle F_{l_1\tau} \ldots F_{l_n\tau} \rangle_{\Delta a}]. \tag{23}$$

In the classical case there are closed formulae for the cumulants

$$K[F_{j_1}, \ldots, F_{j_r}, F_{l_1\tau}, \ldots, F_{l_n\tau}] = \frac{\partial^{r+n} \ln \langle \exp(uF + u_\tau F_\tau) \rangle}{\partial u_{j_1} \ldots \partial u_{j_r} \partial u_{l_1\tau} \ldots \partial u_{l_n\tau}}.$$

These formulae which are obtained by taking the logarithm of Eq. (10) and differentiating are of the form

$$K[F_{j_1}, \ldots, F_{j_r}, F_{l_1\tau}, \ldots, F_{l_n\tau}]$$
$$= \frac{(kT)^r \partial^r}{\partial a_{j_1} \ldots \partial a_{j_r}} K[F_{l_1\tau}, \ldots, F_{l_n\tau}]. \tag{24}$$

5. THE RESIDUAL CORRELATIONS AND ERGODICITY

It is convenient for what follows to use instead of (9) an equation which is symmetric in the times $t_1 = t$ and $t_2 = t + \tau$. Multiplying (8) by the operator

$$\exp\left\{u_\tau \int_0^1 e^{-ih\beta sp} (F(t_2))_s ds\right\}^* = \exp\left\{u_\tau \int_0^1 e^{ih\beta sp} (F(t_2))_{-s} ds\right\},$$

we get

$$\left\langle \exp\left\{u \int_0^1 e^{-ih\beta sp} (F(t_1))_s ds\right\} \exp\left\{u_\tau \int_0^1 e^{ih\beta sp} (F(t_2))_{-s} ds\right\}\right\rangle$$
$$= \exp\{\beta\Psi - \beta\Psi_u\} \left\langle \exp\left\{u_\tau \int_0^1 e^{ih\beta sp} (F(t_2))_{-s} ds\right\}\right\rangle_{kTu}$$
$$= \exp\{\beta\Psi - \beta\Psi_{u_\tau}\} \left\langle \exp\left\{u \int_0^1 e^{-ih\beta sp} (F(t_1))_s ds\right\}\right\rangle_{kTu_\tau}, \tag{25}$$

The average $\langle \ldots \rangle_{kTu}$ is here taken over a non-equilibrium process which has a density matrix ρ_u at time $t_0 = t_1$, and the average $\langle \ldots \rangle_{kTu_\tau}$ corresponds to a process with the matrix ρ_{u_τ} at time $t_0 = t_2$.

We consider the residual correlations, i.e., the correlations between F and F_τ, which occur as $\tau \to \infty$. After a time interval τ the non-equilibrium process in the system dies out and the system changes into some equilibrium state described by a density matrix ρ'. If contact between the system and a thermostatic bath is maintained, the final limiting density matrix ρ' will be the same as ρ from (2). However, contact with a thermostatic bath cannot occur; on the contrary, fixing the Hamiltonian H presupposes that it is absent. A thermostatic bath which exists in reality can, moreover, always be included as part of the system under consideration. Finally, if the thermostatic bath is not included in the system but the contact with it is weak, the state ρ', which is not the same as ρ, will correspond to a quasi-equilibrium state.

Be that as it may, the state ρ' and the new temperature $T' = (k\beta)^{-1}$ and the free energy $\Psi' = \Psi(T', a)$ corresponding to it can be found from the condition that the non-equilibrium process be an adiabatic one. If we apply Eq. (11) to the equilibrium state ρ' we get as $\tau \to \infty$

$$\left\langle \exp\left\{u \int_0^1 e^{ih\beta sp} (F(t_2))_{-s} ds\right\}\right\rangle \to \exp\{\beta'\Psi' - \beta'\Psi'_u\}.$$

We get thus from (25)

$$\left\langle \exp\left\{u \int_0^1 e^{-ih\beta sp_1} (F(t_1))_s ds\right\} \exp\left\{u_\tau \int_0^1 e^{ih\beta sp_2} (F(t_2))_{-s} ds\right\}\right\rangle$$
$$\to \exp\{\beta\Psi - \beta\Psi_u + \beta'\Psi' - \beta'\Psi'_{u_\tau}\}. \tag{26}$$

To evaluate the required correlations we need only find T' as a function of $kTu = \Delta a$. To do this we need perform a simple thermodynamic calculation, which takes the energy balance into consideration. The energy of the equilibrium state with the additional forces Δa, which is described by a density matrix ρ_u, is equal to $U(T, a^0 + \Delta a)$

where U(T, a) is a given thermodynamic function of the system. The energy of the non-equilibrium state ρ_u (without the external additional forces) is equal to

$$U = U(T,\ a^0 + \Delta a) + \langle F\rangle_{\Delta a}\Delta a.$$

As the transient process develops further, the energy does not change because the process is adiabatic. We get thus the following equation for T′:

$$U(T',\ a^0) = U(T,\ a^0 + \Delta a) + \langle F\rangle_{\Delta a}\Delta a.$$

If we express the internal energy in terms of the free energy $U = \Psi - T\partial\Psi/\partial T$ and use (18) we can write this equation in terms of one function $\Psi(T, a)$

$$\Psi(T', a^0) - T'\frac{\partial\Psi}{\partial T}(T', a^0) = \Psi(T, a^0 + \Delta a) - T\frac{\partial\Psi}{\partial T}(T,\ a^0 + \Delta a) - \frac{\partial\Psi}{\partial a}(T, a^0 + \Delta a)\,\Delta a. \qquad (27)$$

The equation obtained is best solved by using a power series expansion. We get for the first term of the expansion of T′ − T in powers of Δa

$$T' - T = \left(\frac{\partial^2\Psi}{\partial T\partial a}\Big/\frac{\partial^2\Psi}{\partial T^2}\right)\Delta a = \left(\frac{\partial S}{\partial a}\Big/\frac{\partial S}{\partial T}\right)\Delta a. \qquad (28)$$

Let us consider pair correlations. Returning to Eq. (26) we differentiate it with respect to u_j and $u_{l\tau}$ and put $u = u_\tau = 0$. In view of the fact that the function $\langle F_j F_{l\tau}\rangle$ tends to a constant as $\tau \to \infty$, we can put $p_1 = -p_2 = 0$, so that the quantum corrections to the pair correlations vanish. As a result we get

$$\langle F_j F_{l\tau}\rangle = \frac{\partial^2}{\partial u_j \partial u_{l\tau}} \exp\{\beta\Psi - \beta\Psi_u + \beta'\Psi' - \beta'\Psi'_{u_\tau}\}$$

$$= \langle F_j\rangle\langle F_{l\tau}\rangle - \frac{\partial^2\Psi}{\partial T\partial a_l}\frac{\partial T'}{\partial u_j}$$

or, if we take (28) into account,

$$\langle F_j F_{l\tau}\rangle - \langle F_j\rangle\langle F_l\rangle = -kT\frac{\partial^2\Psi}{\partial T\partial a_j}\frac{\partial^2\Psi}{\partial T\partial a_l}\Big/\frac{\partial^2\Psi}{\partial T^2}. \qquad (29)$$

It is well known that in order that a random function F(t) be ergodic it is necessary that the correlation functions $\langle FF_\tau\rangle - \langle F\rangle\langle F\rangle$ vanish as $\tau \to \infty$. The residual correlations (29) are evidence that the process is non-ergodic. The magnitude of the correlation coefficients

$$R_{jl} = (D_j D_l)^{-1/2}[\langle F_j F_{l\tau}\rangle - \langle F_j\rangle\langle F_l\rangle]$$

$$(D_j = \langle F_j^2\rangle - \langle F_j\rangle^2)$$

as compared to unity tells us how strongly non-ergodic the chosen system is. Substituting here (29) and evaluating the dispersion $D_j = -kT\partial^2\Psi/\partial a_j^2$ we obtain for the non-ergodicity indices which we have just introduced the equation

$$R_{jl} = \frac{\partial^2\Psi}{\partial T\partial a_j}\frac{\partial^2\Psi}{\partial T\partial a_l}\Big/\left(-\frac{\partial^2\Psi}{\partial T^2}\right)\left(\frac{\partial^2\Psi}{\partial a_j^2}\frac{\partial^2\Psi}{\partial a_l^2}\right)^{1/2}, \qquad (31)$$

from which it is clear that the degree of non-ergodicity of a system can be estimated from the form of its thermodynamic functions.

Let us consider as an example a perfect gas of N molecules, each of which possesses i degrees of freedom, and let us choose as thermodynamic parameters the pressure and the volume: $a = -p$; $A = \langle V\rangle = V_0$. When we choose the parameters in that way we must take instead of $\Psi(T, a)$ the thermodynamic potential

$$\Phi(T, -p) = U_0 + pV_0 - ST$$

$$= \frac{i+2}{2}NkT(1 - \ln T) + NkT\ln p.$$

In that case Eq. (27) gives

$$\frac{i+2}{2}Nk(T' - T) = -V_0\Delta p(u) = V_0 kTu,$$

$$k(T' - T) = \frac{2}{i+2}\frac{(kT)^2}{p}u.$$

Substituting these equations into (26) and neglecting quantum corrections, we get as $\tau \to \infty$

$$\langle\exp\{uV + u_\tau V_\tau\}\rangle$$

$$= \left(1 - \frac{kT}{p}u\right)^{-N}\left(1 - \frac{kT}{p}u_\tau - \frac{2}{i+2}\left(\frac{kT}{p}\right)^2 uu_\tau\right)^{-N}. \qquad (32)$$

In particular, the residual pair correlation is equal to

$$\langle VV_\tau\rangle - \langle V\rangle^2 = \frac{2}{i+2}N\left(\frac{kT}{p}\right)^2, \qquad (33)$$

and the index of non-ergodicity has the value $R = 2/(i + 2)$.

It is clear from this expression that the denominator of the index of non-ergodicity contains the number of "passive" degrees of freedom, i.e., the degrees of freedom on which the external force a does not act directly. If a thermostatic bath is included in the system, the number of "passive" degrees of freedom increases steeply and the non-ergodicity coefficient decreases. When the thermostatic bath has far more degrees of freedom than the "active" system, the non-ergodicity coefficient is practically equal to zero. This occurs in the case of a Brownian particle or in the case of thermal electrical noise. It can be seen, however, from the formula $R = 2/(i + 2)$ that the non-ergodicity coefficient does not change when one simply increases the number N of particles in the system. Thermodynamic phenomena that depend on the volume are thus essentially non-ergodic, as noted in the introduction.

To study the residual correlations of higher order we must perform a multiple differentiation of the logarithms of both sides of Eq. (26). In the classical approximation $(h = 0)$ the following formulae hold $(n > 1)$

$$K[F_{j_1}, \ldots, F_{j_r}, F_{l_1\tau}, \ldots, F_{l_n\tau}]$$

$$= -\left[\frac{\partial^{r+n}}{\partial u_{j_1} \ldots \partial u_{j_r} \partial u_{l_1\tau} \ldots \partial u_{l_n\tau}} \frac{\Psi(T', a^0 + kT'u_\tau)}{kT'}\right]_{u=u_\tau=0}. \quad (34)$$

The quantum generalization of this formula is obtained by the following rule. The cumulant on the left hand side of (34) is expressed in terms of moments. Each term of the corresponding sum is a product of moments of the type $\langle F_{j_1} \ldots F_{j_\alpha} F_{l_1\tau} \ldots F_{l_\gamma\tau} \rangle$. To obtain the quantum formula one must replace each of those moments by

$$\langle \Phi_\alpha(ih\beta p^\alpha, \ldots, ih\beta p^1)\left(\sum P_\alpha F_{l_1} \ldots F_{l_\alpha}\right)\Phi_\beta(ih\beta p^\gamma, \ldots, ih\beta p^1)$$

$$\times \left(\sum P_\gamma F_{l_1\tau} \ldots F_{l_\gamma\tau}\right)\rangle$$

(the symbol P_α indicates a permutation of the α factors that follow it).

6. THE RECIPROCITY RELATIONS

The reciprocity relations which characterize the non-equilibrium process are a generalization of the well-known Onsager relations.[7,8] Just as the latter, they follow from the symmetry of the dynamic equations governing the motion of the system as regards the direction of the time. When the time is reversed, t → − t, these equations do not change (provided, however, that the sign of the magnetic field and the order in which operators act are reversed; see below) and therefore the statistical characteristics of the fluctuation process also remain unchanged.

Before we write down the analytical condition for reversibility, we shall change the form of Eq. (25) somewhat. In the expression $\langle \ldots \rangle_{kTu}$ which occurs in (25) the density matrix ρ_u is fixed at the time $t_0 = t_1$. At another time $t_2 = t_1 + \tau$ a transient process is taking place and it is convenient to denote the operators $F(t_2)$ pertaining to this time by F_τ. In the second expression $\langle \ldots \rangle_{kTu_\tau}$ the averaging takes place with respect to another process, which corresponds to a density matrix ρ_{u_τ} at time $t_0 = t_2$. The operators $F(t_1)$ taken at the time $t_1 = t_2 - \tau$ can be written relative to the time t_2 as $F_{-\tau}$. If τ is positive and increases, $F_{-\tau}$ generates a transient process that evolves in reverse time. Using these notations Eq. (25) will be of the form

$$\exp\{-\beta\Psi_u\}\left\langle \exp\left\{u_\tau \int_0^1 e^{ih\beta s p_\tau} (F_\tau)_{-s} ds\right\}\right\rangle_{kTu}$$

$$= \exp\{-\beta\Psi_{u_\tau}\}\left\langle \exp\left\{u \int_0^1 e^{ih\beta s p_\tau} (F_{-\tau})_s \, ds\right\}\right\rangle_{kTu_\tau}. \quad (35)$$

We now go over to use the condition of symmetry in the time. When applied to the expressions in (35), this condition clearly gives

$$\mathrm{Sp}\left[\exp\left\{u \int_0^1 e^{ih\beta s p_\tau} (F_\tau')_{-s} \, ds\right\} \rho'_{u_\tau}\right]$$

$$= \mathrm{Sp}\left[\exp\left\{u \int_0^1 e^{ih\beta s p_\tau} (F_\tau)_{-s} \, ds\right\} \rho_{u_\tau}\right], \quad (36)$$

where the prime indicates the operators into which the original operators are changed when the time is reversed, t → − t (L → L′, . . .). In the quantum case the position is somewhat complicated by the fact that one must take into account the change in the order in which the operators follow one another under time reversal. The fact is that when we perform the simple transformation $H' = H$, $q' = q$, $p' = -p$, $L' = \pm L$, the equations of motion and the commutation relations,

$$ih\partial L/\partial t = LH - HL, \quad qp - pq = ih$$

do not remain invariant. To attain invariance we must also perform a transposition. Operators of one kind (the Hamiltonian, the density matrix, coordinates) change then into their transposed ones ($H' = H^T$, $\rho' = \rho^T$, $q' = q^T$), while at the same time operators of the second group (momenta, spin, magnetic field) change their sign ($p' = -p^T$, . . .). If F belongs to the first group of operators, $F'_\tau = F^T_{-\tau}$, $\rho'_{u_\tau} = \rho^T_{u_\tau}$ and we have from (36)

$$\mathrm{Sp}\left[\exp\left\{u \int_0^1 e^{ih\beta s p_\tau} (F^T_{-\tau})_{-s} \, ds\right\} \rho^T_{u_\tau}\right]$$

$$= \mathrm{Sp}\left[\exp\left\{u \int_0^1 e^{ih\beta s p_\tau} (F_\tau)_{-s} \, ds\right\} \rho_{u_\tau}\right].$$

Performing the transposition in the left hand side, we have

$$\left\langle \exp\left\{u \int_0^1 e^{ih\beta s p_\tau} (F_{-\tau})_s \, ds\right\}\right\rangle_{kTu_\tau}$$

$$= \left\langle \exp\left\{u \int_0^1 e^{ih\beta s p_\tau} (F_\tau)_{-s} \, ds\right\}\right\rangle_{kTu_\tau}. \quad (37)$$

Substituting (37) into (35) and taking the complex conjugates of both sides of the equation, we get the formula

$$\exp\{-\beta\Psi_u\}\Big\langle \exp\Big\{u_\tau\int_0^1 e^{-ih\beta sp_\tau}(F_\tau)_s\,ds\Big\}\Big\rangle_{kTu}$$

$$=\exp\{-\beta\Psi_{u_\tau}\}\Big\langle \exp\Big\{u\int_0^1 e^{-ih\beta sp_\tau}(F_\tau)_s\,ds\Big\}\Big\rangle_{kTu_\tau}, \quad (38)$$

which can be used as a generating equation for the reciprocity relations. These are derived by taking the logarithm of (38), differentiating the result with resepct to $u_{j_1}, \ldots, u_{j_r}, u_{l_1\tau}, \ldots, u_{l_n\tau}$, and setting u and u_τ equal to zero. It is then useful also to take into account the connection between u, u_τ, and the additional forces $\Delta a = kTu$, $\Delta a = kTu_\tau$. The result is

$$\frac{(kT)^r\,\partial^r}{\partial a_{j_1}\ldots\partial a_{j_r}}\frac{\partial^n}{\partial u_{l_1\tau}\ldots\partial u_{l_n\tau}}\ln\Big\langle\exp\Big\{u_\tau\int_0^1 e^{-ih\beta sp}(F)_s\,ds\Big\}\Big\rangle_{\Delta a}$$

$$=\frac{(kT)^n\,\partial^n}{\partial a_{l_1}\ldots\partial a_{l_n}}\frac{\partial^r}{\partial u_{j_1}\ldots\partial u_{j_r}}$$

$$\times\ln\Big\langle\exp\Big\{u\int_0^1 e^{-ih\beta sp}(F)_s\,ds\Big\}\Big\rangle_{\Delta a}. \quad (39)$$

The magnitude of the additional forces $\Delta a = a - a^0 = kTu$ characterizes the degree in which the non-equilibrium state ρ_u (or ρ_{u_T}) deviates from an equilibrium one. Because of this deviation, the averages $A = \langle F\rangle_{\Delta a}$ differ from the corresponding equilibrium values $A^0 = \langle F\rangle$. The deviations $A - A^0$ can in their turn be used as a measure of the deviation of the non-equilibrium state from an equilibrium one. During the transient process, the averages $\langle F\rangle$ go over into the equilibrium values A^0. Both the values $F = \langle F\rangle_{\Delta a}$ at the initial time and the equilibrium values A^0 are connected with a and a^0 by the equations of state (18)

$$A_j=-\frac{\partial\Psi}{\partial a_j}(T,\ a),\qquad A_j^0=-\frac{\partial\Psi}{\partial a_j}(T,\ a^0).$$

Similar formulae for all the times during which the transient process takes place

$$A_j(\tau)=-\frac{\partial\Psi}{\partial a_j}(T,\ a(\tau)) \quad (40)$$

must simply be regarded as equations for a change of variables. Although the variables a, which are conjugate to the A, have a less obvious physical meaning, they have the advantage that they result in equations of very simple form.

1. Let us first of all consider the simpler formulae of the classical case. Differentiation of the logarithm of the characteristic function in (39) gives immediately the cumulants of the non-equilibrium process

$$k_{\alpha\ldots\omega}(a,\ \tau)=\frac{\partial\ldots\partial}{\partial u_\alpha\ldots\partial u_\omega}\ln\langle\exp\{uF_\tau\}\rangle_{\Delta a}. \quad (41)$$

We get thus from (39) (when $a = a^0$)

$$\frac{(kT)^r\,\partial^r}{\partial a_{j_1}\ldots\partial a_{j_r}}k_{l_1\ldots l_n}(a,\ \tau)=\frac{(kT)^n\,\partial^n}{\partial a_{l_1}\ldots\partial a_{l_n}}k_{j_1\ldots j_r}(a,\ \tau). \quad (42)$$

The reciprocity relations which we have established refer to the dependence of the characteristics of the non-equilibrium process on the non-equilibrium initial data, which are described by the variables A, or (which comes to the same) by the conjugate variables a. One can also derive similar relations for $\langle F_{\alpha\tau}\ldots F_{\omega\tau}\rangle_{\Delta a}$ [if one does not take the logarithm of Eq. (38)].

The relations which refer to the dependence of the rate of change of the non-equilibrium characteristics on the values of the non-equilibrium parameters at the same instant of time are also of interest. To find these relations we differentiate (42) with respect to τ and let $\tau \to 0$. If we differentiate once only, this gives

$$\frac{(kT)^r\,\partial^r}{\partial a_{j_1}\ldots\partial a_{j_r}}\dot k_{l_1\ldots l_n}(a^0,\ 0)=\frac{(kT)^n\,\partial^n}{\partial a_{l_1}\ldots\partial a_{l_n}}\dot k_{j_1\ldots j_r}(a^0,\ 0). \quad (43)$$

The equations obtained impose a number of restrictions on the phenomenological equations that describe the dependence of the rate of change of the characteristics of the non-equilibrium process on the evolving non-equilibrium values of the parameters. Let us assume that these are of the form

$$\dot A_j\equiv\dot k_j=\tilde f_j(A,\ A^0)=f_j(a,\ a^0),$$

$$\dot k_{jk}=\tilde f_{jk}(A,\ A^0)=f_{jk}(a,\ a^0),\ \ldots,$$

$$\dot k_{j_1\ldots j_r}=\tilde f_{j_1\ldots j_r}(A,\ A^0)=f_{j_1\ldots j_r}(a,\ a^0),\ \ldots \quad (44)$$

or, if we use Taylor expansions for the functions on the right hand side,

$$\dot A_j=L_j^l(a^0)\Delta a_l+\tfrac{1}{2}L_j^{lm}(a^0)\,\Delta a_l\Delta a_m+\ldots;$$

$$\dot k_{jk}=L_{jk}^l(a^0)\,\Delta a_l+\tfrac{1}{2}L_{jk}^{lm}(a^0)\,\Delta a_l\Delta a_m+\ldots;\ \ldots$$

$$\dot k_{j_1\ldots j_r}=L_{j_1\ldots j_r}^l(a^0)\,\Delta a_l+\tfrac{1}{2}L_{j_1\ldots j_r}^{lm}(a^0)\,\Delta a_l\Delta a_m+\ldots \quad (45)$$

and so on. Here $\Delta a_l = a_l - a_l^0$,

$$L_{j_1\ldots j_r}^l=\frac{\partial f_{j_1\ldots j_r}}{\partial a_l}=\frac{\partial\tilde f_{j_1\ldots j_r}}{\partial A_p}\frac{\partial A_p}{\partial a_l},$$

$$L_{j_1\ldots j_r}^{lm}=\frac{\partial^r f_{j_1\ldots j_r}}{\partial a_l\,\partial a_m}=\frac{\partial^2\tilde f_{j_1\ldots j_r}}{\partial A_p\,\partial A_q}\frac{\partial A_p}{\partial a_l}\frac{\partial A_q}{\partial a_m}$$

$$+\frac{\partial\tilde f_{j_1\ldots j_r}}{\partial A_p}\frac{\partial^2 A_p}{\partial a_l\partial a_m},\ \ldots$$

Substitution of (45) into (44) leads to the reciprocity relations

$$(kT)^r L_{j_1\ldots j_r}^{l_1\ldots l_n}=(kT)^n L_{l_1\ldots l_n}^{j_1\ldots j_r}. \quad (46)$$

If we put r = n = 1, we get the usual Onsager relations

$$L_j^l = L_l^j. \tag{47}$$

Putting then r = 2 and n = 1 we obtain the relations

$$L_{jk}^l = kTL_l^{jk}, \tag{48}$$

which establish another connection between the equation for the average value and the equation for the dispersion. Finally putting r = n = 2 in (46) we get relations between the coefficients of the quadratic terms in the equation for the dispersion

$$L_{jk}^{lm} = L_{lm}^{jk}. \tag{49}$$

Let us note the following regarding the case where F_1 refers to operators that change sign when the time is reversed ($F'_\tau = -F^T_{-\tau}$). In that case

$$\exp\{-\beta\Psi_u\}\rho'_u = \exp\{-\beta\Psi_{-u}\}\rho^T_{-u}$$

and from (35) and (36) follows the equation

$$\exp\{-\beta\Psi_u\}\left\langle\exp\left\{u_\tau\int_0^1 e^{-ih\beta sp_\tau}(F_\tau)_s ds\right\}\right\rangle_{kTu}$$
$$= \exp\{-\beta\Psi_{-u_\tau}\}\left\langle\exp\left\{-u\int_0^1 e^{-ih\beta sp_\tau}(F_\tau)_s\, ds\right\}\right\rangle_{-kTu_\tau}, \tag{50}$$

which replaces (38). The further discussion in this case is completely analogous to the preceding one. The only difference is that now Eqs. (39), (42), (43), and (46) contain an additional factor $(-1)^{r+n}$. In general, if F_j transforms as $F_j \rightarrow (-1)^{k_j} F_j^T$, there will occur in the above mentioned reciprocity relations a factor $(-1)^k$, where $k = j_1 + \ldots + j_r + l_1 + \ldots + l_n$.

2. Going over to the quantum case, we put r = n = 1 in (39). We then get

$$\frac{\partial}{\partial a_j}\Phi_1(ih\beta p)\langle F_l\rangle_{\Delta a} = \frac{\partial}{\partial a_l}\Phi_1(ih\beta p)\langle F_j\rangle_{\Delta a}.$$

Since the same operator $\Phi_1(ih\beta p)$ occurs on both sides of this equation, we can drop it. The resulting relation

$$\frac{\partial}{\partial a_j}\langle F_l\rangle_{\Delta a} = \frac{\partial}{\partial a_l}\langle F_j\rangle_{\Delta a} \tag{51}$$

is the same as the classical one when $\Delta a = 0$. If we assume that the first equation in (44), $\dot{A} = \tilde{f}(A, A^0)$, remains valid also in the quantum case, the usual relation (47) will follow from (51). If, however, the transient process is not a Markov process and is not described by this equation, we must take Eq. (51) directly into account and it follows from this equation that in this case we can derive a reciprocity relation for the admittance matrix.[4]

If we put r = 2 and n = 1 and 2, we get from (39)

$$\frac{kT\partial^2}{\partial a_j \partial a_k}\Phi_1(ih\beta p)\langle F_l\rangle_{\Delta a}$$
$$= \frac{\partial}{\partial a_l}[\Phi_2(ih\beta p^2,\ ih\beta p^1)\langle F_jF_k + F_kF_j\rangle_{\Delta a}$$
$$- \Phi_1(ih\beta p^2)\Phi_1(ih\beta p^1)\langle F_j\rangle_{\Delta a}\langle F_k\rangle_{\Delta a}],$$
$$\frac{\partial^2}{\partial a_j \partial a_k}[\Phi_2(ih\beta p^2, ih\beta p^1)\langle F_lF_m + F_mF_l\rangle_{\Delta a}$$
$$- \Phi_1(ih\beta p^2)\Phi_1(ih\beta p^1)\langle F_l\rangle_{\Delta a}\langle F_m\rangle_{\Delta a}]$$
$$= \frac{\partial^2}{\partial a_l \partial a_m}[\Phi_2(ih\beta p^2, ih\beta p^1)\langle F_jF_k + F_kF_j\rangle_{\Delta a}$$
$$- \Phi_1(ih\beta p^2)\Phi_1(ih\beta p^1)\langle F_j\rangle_{\Delta a}\langle F_k\rangle_{\Delta a}]. \tag{52}$$

These equations are the quantum generalizations of relations (48) and (49).

Performing the differentiation of the left hand side of Eq. (39) with respect to $u_{l_1\tau}, \ldots, u_{l_n\tau}$ and of the right hand side with respect to $u_{j_1}, \ldots, u_{j_r}$, we verify easily that the following rules for writing down the quantum reciprocity relations in the general case are correct.

To obtain the quantum relation corresponding to the classical Eq. (42), we must express the correlation function (41) $k_{j_1}\cdots_{j_r}$ in terms of the moments $\langle F_\alpha \ldots F_\omega\rangle_{\Delta a}$ and then replace each of these moments by their quantum analogue

$$\Phi_m(ih\beta p^m, \ldots, ih\beta p^1)\langle\sum P_m F_\alpha \ldots F_\omega\rangle_{\Delta a}.$$

The correspondence between the classical moment and the quantum analogue just mentioned is apparently an essential one and it goes beyond the framework of the thermodynamics.

In conclusion we note once more that the discussion given here refers to the case where the Hamiltonian of the thermodynamic system depends linearly on the external parameters. The problem whether the relations of the thermodynamics of fluctuations allows a generalization to the case of a non-linear dependence is of great interest.

---

[1] H. B. Callen and T. A. Welton, Phys. Rev. **83**, 34 (1951).

[2] L. D. Landau and E. M. Lifshitz, Статистическая физика (Statistical Physics), Engl. Transl.

Pergamon Press, 1958; Электродинамика сплошных сред (Electrodynamics of Continuous Media), Gostekhizdat, 1957.

[3] W. Bernard and H. B. Callen, Revs. Modern Phys. **31**, 1017 (1959).

[4] Callen, Barasch, and Jackson, Phys. Rev. **88**, 1382 (1952).

[5] R. P. Feynman, Phys. Rev. **84**, 108 (1951).

[6] V. B. Magalinskiĭ and Ya. P. Terletskiĭ, JETP **34**, 729 (1958), Soviet Phys. JETP **7**, 501 (1958).

[7] L. Onsager, Phys. Rev. **37**, 405 (1931); **38**, 2265 (1931).

[8] S. R. de Groot, Thermodynamics of Irreversible Processes, North-Holland Publishing Company, Amsterdam, 1951.

[9] V. V. Vladimirskiĭ, JETP **12**, 199 (1942).

Translated by D. ter Haar
304

SOVIET PHYSICS JETP VOLUME 12, NUMBER 6 JUNE, 1961

DETERMINATION OF THE DEFORMATION AND QUADRUPOLARIZATION OF ALPHA-ACTIVE NUCLEI FROM THE ENERGY AND ANGULAR DISTRIBUTIONS OF THE ALPHA PARTICLES

V. G. NOSOV

Submitted to JETP editor May 31, 1960

J. Exptl. Theoret. Phys. (U.S.S.R.) **39**, 1660-1667 (December, 1960)

The theory of the α decay of nonspherical nuclei developed previously by the author is employed to treat the experimental data on the relative intensities of the fine structure lines in the α radiation, the half-lives, and the angular distributions of the α particles emitted by oriented nuclei. The dependence of the nuclear deformation on the atomic weight in the region $A > 220$ is deduced from fine structure data. It is shown that, by taking into account the effect of these deformations on the half-lives, it is possible to remove the anomalies in the variation of the radii of α-active nuclei which result from the comparison of the old theories of α decay with experiment. The quadrupolarization of the parent U^{233} nuclei was determined in the corresponding experiments from the angular distribution of the α particles.

1. INTRODUCTION

In a number of papers,[1] the author has developed a theory of the α decay of nonspherical nuclei; a more systematic exposition has been given in reference 2 (below referred to as I). In the case of the so-called favored α transitions, which conform to the selection rules (I, 1.8), formulas were obtained for the relative probability w_J of exciting each of the rotational levels of the daughter nucleus (J is the angular momentum of the daughter nucleus) and for the total decay rate. Now the natural question arises as to how these formulas can be used in the most rational way to account for the experimental data.

The w_J are usually known from experiment. The formula (I, 2.22) is therefore used to determine the deformation α_n (we use everywhere the notation of reference I). The solution of this problem is facilitated by the circumstance that the quadrupole term $\alpha_2 P_2(\mu)$ predominates almost always in the sum over n on the right-hand side of the equation for the shape of the surface of the daughter nucleus (I, 2.1). The subsequent terms of the expansion α_4, α_6, α_8, etc., are significantly smaller.* In many cases it suffices, therefore, to take account only of the quadrupole deformation α_2, i.e., to make the replacement $\tilde{X}_l \rightarrow X_l(\beta)$, where the integrals $\tilde{X}_l$ and X_l are defined by (I, 2.20), (I, 2.14), and (I, 2.23). As a result, the quadrupole deformation of the daughter nucleus, α_2, can be determined in practically all cases in which there are any trustworthy data on the relative intensities of the fine structure lines in favored α decay. In isolated cases the 2^4-pole deformation α_4 can also be determined.

The values of the quadrupole deformations of the various nuclei, which are of considerable interest in themselves, are also very important for the calculation of the α decay constant W. Indeed, it is well known that in the old theories of α decay, in which the effect of the nuclear deformations α_n was neglected, one had to depart from the natural assumption

$$R_0 = r_0 A^{1/3}. \tag{1}$$

in order to achieve agreement with the experimental data on the half-lives. If we set $\alpha_n = 0$ and compute R_0 from the experimental data on W for different nuclei,* setting the internal probability w_α equal to some constant value, we obtain the well-known so-called "reverse trend of the radii":[4] the quantity r_0 becomes a function of A which mainly decreases with increasing A, so that

---

*The "monopole" deformation α_0 is not an independent parameter characterizing the shape of the nucleus. It is expressed in terms of the other deformations $\alpha_2, \alpha_4, \alpha_6, \ldots$ by the condition that the total volume of the nonspherical nucleus be equal to $(4/3)\pi R_0^3$. Here it appears that for $\alpha_n \ll 1$ the quantity α_0 is quadratic in α_n and should therefore not be taken into account at all in the approximation considered in references 1 to 3.

*In our view the interval $222 \leqslant A \leqslant 250$, to which the considered daughter nuclei belong, is too narrow for the w_α to exhibit any dependence on A. We therefore regard the assumption that the internal probability w_α is constant as eminently reasonable.

R_0 does not become larger. It is therefore reasonable to inquire whether the account of the deformations will lead to a rectification of this unnatural "reverse trend" of the radii.

If we solve the formula for the α decay probability (I, 2.18) with respect to the internal probability w_α, we find that the latter is inversely proportional to the penetration factor of the Coulomb barrier Γ, which is extremely sensitive to the choice of the radius R_0. To improve the accuracy of our calculations, it is therefore expedient to reverse the problem: assuming the validity of the relation (1) (where r_0 is a constant), we attempt to show that w_α is constant in the whole region $A > 222$ of nonspherical daughter nuclei.*

Above we have not touched the problem of the angular distribution of the α particles emitted by oriented nonspherical nuclei; the corresponding formulas have been given in reference I. It is seen from these formulas that the degree of orientation (quadrupolarization) of the parent nucleus can be determined from the angular distribution of the α particles. We shall do this for a special case in Sec. 4.

2. THE FINE STRUCTURE OF THE α DECAY AND THE DEFORMATIONS OF THE DAUGHTER NUCLEI

Sign of the deformation. The shape of the nucleus can be either prolate ($\alpha_2 > 0$) or oblate ($\alpha_2 < 0$) with respect to the nuclear symmetry axis. In the region $150 < A < 190$ the sign of α_2 has been determined by optical measurements of the quadrupole moments.[5] However, for $A > 222$ the attempts to establish the sign of the quadrupole deformation have for a long time led to contradictory results.[6] The theory of the α decay of nonspherical nuclei allows us to solve this problem in a completely unambiguous way. In order to keep the discussion simple, we consider the simplest case of even-even nuclei.

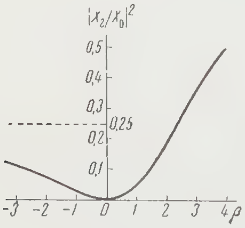

FIG. 1

The relative probability of excitation of the level 2^+ of the daughter nucleus, w_2, is mainly determined by the quadrupole deformation α_2 and is therefore proportional to the expression $|X_2(\beta)/X_0(\beta)|^2$. As is seen from Fig. 1, the function $|X_2/X_0|^2$ is strongly asymmetric with respect to the ordinate.* This was to be expected, because according to (I, 2.23) the asymptotic value of $|X_2/X_0|^2$ for $\beta \rightarrow \infty$ is equal to unity, while the corresponding limit for $\beta \rightarrow -\infty$ is only $\frac{1}{4}$ (Fig. 1, dotted line).† As a result, we find that for $\beta < 0$ the theoretical value of w_2 remains smaller than the experimental value in the case of many nuclei, even if $|\beta|$ is arbitrarily large. The corresponding daughter nuclei are: $Ra^{222,224,226,228}$, $Th^{226,228,230,232,234}$, and U^{232} (here and in the following we borrow most of the experimental data from the review article of Perlman and Rasmussen[8]). We are thus led to the conclusion that in the region $A \geq 222$ the nuclei are prolate, i.e., have positive values of β, α_2, and Q_0, where

$$Q_0 = \tfrac{6}{5} Z R_0^2 \alpha_2 \tag{2}$$

is the so-called internal quadrupole moment of a nonspherical nucleus.

Behavior of the quadrupole deformations. The values of α_2 were determined with the help of formula (I, 2.22) [with the replacement $\widetilde{X}_l \rightarrow X_l(\beta)$] from the experimentally observed first excited rotational level above the level with $J = \Omega$, where J is the angular momentum of the daughter nucleus, and Ω is the angular momentum of the parent nucleus in the initial (ground) state. The values of the ratio X_l/X_0 needed for the calculations are listed in Table I. The results corresponding to the assumption $r_0 = 1.4 \times 10^{-13}$ cm are shown in Fig. 2 (if the radius is lowered to r_0

---

*If the internal probability w_α is computed under the assumption (1) without account of the surface deformations of the daughter nucleus, it decreases by about one order of magnitude over the region $222 \leqslant A \leqslant 250$.

*This fact demonstrates that perturbation theory cannot be applied to the α decay of nonspherical nuclei. Such methods for measuring the deformations as Coulomb excitation or the determination of the lifetime of the excited rotational state[5] do not allow us to fix the sign of α_2. Indeed, both Coulomb excitation and the emission of γ quanta by the nucleus are described by perturbation theory. Hence the probability of the process is quadratic in the perturbation, which in this case is the deformation α_2. On the other hand, the curve shown in Fig. 1 has the form of a parabola only in the region $\beta \ll 1$; this corresponds to such a small value of α_2 that it apparently does not occur in nature. In the region of actually occurring values of α_2 the dependence of this effect on the deformation is more complicated, which is just the reason why the sign ot the deformation can be determined from the fine structure of the α decay.

†This teature ot the α decay of nonspherical nuclei was already noted earlier by the author.[7]

TABLE I

β	X_2/X_0	X_4/X_0	X_6/X_0	X_8/X_0	β	X_2/X_0	X_4/X_0	X_6/X_0	X_8/X_0
0	0	0	0	0	2,2	0.478	0,149	0.0341	0,0061
0,2	0,041				2.4	0,513	0.173	0.0430	0,0084
0.4	0,084	0.0049			2,6	0,546	0,198	0.0529	0.0112
0.6	0.129	0.011			2.8	0,577	0,223	0.0637	0,0143
0,8	0.174	0,020	0.0019		3,0	0,605	0.247	0,0752	0,0182
1.0	0.220	0,032	0.0035		3.2	0,631	0.271	0.0873	0,0224
1.2	0,267	0,047	0.0058		3.4	0,654	0.295	0.1000	0,0271
1.4	0,312	0,063	0.0094		3.6	0.675	0,318	0.1131	0.0322
1.6	0.356	0,083	0.0138	0.0023	3.8	0,694	0.340	0.127	0,0377
1,8	0.398	0.103	0,0195	0.0029	4,0	0,712	0,361	0,140	0.0437
2.0	0,439	0,126	0.0263	0.0043					

TABLE II

Daughter nucleus	w_4 theor	w_4 exp	Daughter nucleus	w_4 theor	w_4 exp	α_2	α_4
Ra^{222}	0,0010	0,0076	U^{232}	0,0072	0,0026	0.22	—0.04
Ra^{224}	0,0030	0,0028	U^{234}	0,0054	0,0013	0.20	—0.04
Ra^{226}	0,0023	0,0027	U^{236}	0.0034	0,0013	0.17	—0,03
Ra^{228}	0,0016	0.0026	Pu^{238}	0,0050	0.00047	0,19	—0.04
Th^{226}	0,0062	0.0045	Pu^{240}	0.0036	0,00021	0,17	—0.04
Th^{228}	0,0063	0,0047	Cm^{242}	0,0036	0.0021		
Th^{230}	0,0039	0.0041	Cm^{248}	0,0013	0,0024		
Th^{232}	0,0034	0.0035	Cf^{250}	0.0020	0.0048		
Th^{234}	0,0020	0.0030					

$R_0 = 1.4\ A^{1/3} \cdot 10^{-13}$ cm.

$= 1.0 \times 10^{-13}$ cm the deformation increases by 20 to 25%).* We see that practically all points lie on a rather clearly defined curve, there being no noticeable difference in the behavior of the deformations of even-even and odd nuclei.

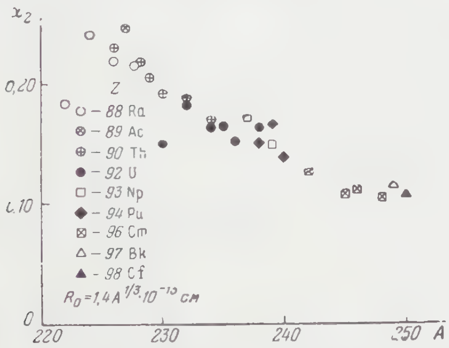

FIG. 2

Excitation of the 4^+ level and the 2^4-pole deformation α_4. In the case of even-even nuclei, the values of β obtained from the excitation of the 2^+ level were used to compute the probability of excitation of the 4^+ level of the daughter nucleus. The results of the calculation with the help of the formula (I, 2.22) [with the replacement $\widetilde{X}_l \rightarrow X_l(\beta)$] are compared with experiment in Table II (in the case of the daughter nuclei Ra^{228} and $Th^{232,234}$ the experimental data were taken from the work of Kocharov et al.[9]). For most of the nuclei we observe good agreement within the limits of accuracy of the experimental data.* However, for the isotopes of uranium and plutonium there is a considerable discrepancy, since the experimental value of w_4 drops rapidly in this region, leading to a deep minimum for the daughter nucleus Pu^{240}, while the theoretical value of w_4 continues to vary rather smoothly. In our opinion the most natural explanation of this anomaly is the following. In the calculation of $w_{4\,\text{theor}}$ we took only the quadrupole deformation α_2 into account. But the probability of excitation of the 4^+ level may turn out to be very sensitive to relatively small contributions to the 2^4 pole deformation α_4. If both deformations α_2 and α_4 are included we have the expression

$$\widetilde{X}_l = \int_0^1 \{\exp[\beta P_2(\mu) + \beta_4 P_4(\mu)]\} P_l(\mu)\, d\mu, \qquad (3)$$

where

$$\beta_4 = \frac{20}{21} \varkappa R_0 \left(1 - \frac{3}{50}\frac{k^2}{\varkappa_b^2} - \frac{2}{25}\frac{k^4}{\varkappa_b^4} - \frac{4}{25}\frac{k^6}{\varkappa_b^6}\right) \alpha_4. \qquad (4)$$

---

*The values of the deformations of the nuclei quoted in reference 1 correspond to the experimental data of Perlman and Asaro,[4] which are now partially obsolete.

*The discrepancy in the case of Ra^{222} should not be taken seriously. The spectrum of the weakly excited states of this nucleus follows the J(J + 1) law very poorly, which seems to indicate a strong interaction between the rotation of the nucleus and the oscillations of its shape.

For $l = 4$ there may be destructive interference between α_2 and α_4 even for very small negative α_4, which leads to a sharp decrease in X_4 and, hence, w_4. It is natural to assume that this is what happens in the region under consideration. Owing to the destructive interference, the value of w_4 is very sensitive to the values of the two deformations α_2 and α_4, which allows us to determine the latter from the observed excitation of the levels 2^+ and 4^+ with the help of the formulas (3), (4), and (I. 2.22).* The results of this calculation for the isotopes of uranium and plutonium are listed in the last two columns of Table II. We direct attention to the near-constancy of the value of α_4 for all isotopes of these elements.

Certain ratios that do not depend on the magnitude of the deformations. In references 1 and 2 we obtained the formula (I, 2.21) for the ratio

$$\Lambda_{J'J}^{(l)} = w_{J'l} / w_{Jl}, \tag{5}$$

where w_{Jl} is the probability of excitation of a rotational level with angular momentum J accompanied by the emission of an α particle with angular momentum l. It appeared that the quantity $\Lambda_{J'J}^{(l)}$ is independent of the deformations; thus the comparison with experiment serves only to test the validity of the theory developed in references 1 and 2. Unfortunately, the experiments do not give us w_{Jl}, but the total probabilities

$$w_J = \sum_l w_{Jl}. \tag{6}$$

We must therefore select those cases where some value of the orbital angular momentum predominates:

$$w_J \approx w_{Jl}. \tag{7}$$

In particular, $l = 2$ usually predominates in the decay to the two rotational levels of the above-mentioned band lying immediately above the level $J = \Omega$. Thus the theoretical value of the ratio (5) can be compared with the observed ratio

$$\Lambda_{J'J} = w_{J'}/w_J \tag{8}$$

for these two levels.

TABLE III

Daughter nucleus	K	$\Lambda_{J'J}^{(2)}$ theor	$\Lambda_{J'J}$ exp
Ac^{227}	1/2	1.6	1.5
Th^{229}	5/2	0.14	0,11
U^{235*}	1/2	0.86	0.65
Np^{237}	5/2	0.17	0.12
Np^{239}	5/2	0.16	0.10
Pu^{239}	5/2	0.17	0.16
Cm^{245}	9/2	0.09	0,09
Bk^{249}	7/2	0.16	0.23

$\Lambda^{(4)}_{9/2\,7/2\,\text{theor}} = 0.48$; $\Lambda_{9/2\,7/2\,\text{exp}} = 0,35$.

The theoretical and experimental values of Λ are compared in Table III. The decay $Pu^{239} \xrightarrow{\alpha} U^{235}$, where $\Omega = K = 1/2$, is especially pronounced (K is the projection of the angular momentum of the daughter nucleus on the axis of symmetry). With the help of the conservation laws for angular momentum and parity, we can thus easily verify that to each J there corresponds a single definite l, so that the relation (7) is rigorous. Hence the expressions (5) and (8) can be identified and for $l = 4$, $J' = K + 4$ and $J = K + 3$; the theoretical and experimental values of $\Lambda^{(4)}$ are listed above in Table III (the experimental values of $w_{9/2}$ and $w_{7/2}$ were taken from the work of Novikova et al.[10]).

It is seen from Table III that the agreement between theory and experiment is good, although Λ_{theor} is usually somewhat larger than the experimental value. Apparently, this can be explained by the interaction of the rotation of the nucleus with the motion of the odd nucleon. In the final count such an interaction does not conserve the quantum number K, and the admixture of states with $K \neq K_0$ becomes gradually larger as J increases. On the other hand, favored α decay proceeds without change of the quantum number K, i.e., it goes to a state with $K = K_0$, where K_0 is the projection of the angular momentum of the parent nucleus on its axis of symmetry. Therefore the theoretical value of $\Lambda_{J'J}^{(l)}$ [see (I, 2.21)], calculated in references 1 and 2 under the assumption that K is a strict integral of the motion of the daughter nucleus, must be somewhat larger than Λ_{exp}.*

3. LIFETIMES, INTERNAL PROBABILITIES, AND RADII OF DAUGHTER NUCLEI

The data on the half-lives $t_{1/2} = (\log 2)/W$ were used to compute the internal probabilities w_α. In our case only the quadrupole deformation α_2 plays a role, i.e., we can make the replacement $\widetilde{X}_l \rightarrow X_l(\beta)$; the values of β were determined from the fine structure (see above). The results of the calculation for $R_0 = 1.4 A^{1/3} \times 10^{-13}$ cm were given in Tables I and II of reference 3. It follows from these tables that the quantity w_α does not undergo any significant systematic changes with increasing

---

*Here the value of the quadrupole deformation α_2 differs slightly from the values shown in Fig. 2 (see above).

*We choose everywhere $J' > J$.

A, but only fluctuates about some average value. Thus the account of the deformations permits us to remove the anomalies in the behavior of the radii (or of the internal probabilities) which are so characteristic of the old theories of α decay (see the introduction). It must be emphasized that the removal of these anomalies has not been achieved by adjusting the deformation α_2 to the observed half-lives $t_{1/2}$: the deformations were determined from the fine structure, i.e., from data which have nothing to do with the experimental data on the half-lives.

As was already noted in the introduction, the quantity w_α is extremely sensitive to the choice of R_0. If the radius is decreased, w_α grows very rapidly (for example, if R_0 is lowered to the value $1.0\,A^{1/3} \times 10^{-13}$ cm, the internal probability is increased by 4 to 5 orders of magnitude). Thus we have for α decay

$$R_0 \geqslant 1.4 A^{1/3} \cdot 10^{-13}\,\mathrm{cm} \tag{9}$$

otherwise we have a contradiction to the condition (I. 1.3).[3] We note that the inequality (9) is in good agreement with the data on the interaction of α particles with energies above the barrier and heavy nuclei.[11] At the same time, for phenomena caused only by the electromagnetic interaction of the incoming particle with the nucleus (scattering of electrons, Coulomb excitation), a somewhat smaller radius is required.[5,12] This situation is very natural, for in electromagnetic processes the volume $(4/3)\pi R_0^3$ over which the nuclear charge is distributed comes into play. However, in α decay (and also in the interaction of α particles with energies above the barrier and nuclei) the region of the strong interaction of the α particles with the nucleus is important; the volume of this region is related to the extension of the α particle and also to the existence of a finite range of interaction of the nuclear forces.

4. ANGULAR DISTRIBUTION OF THE α PARTICLES AND THE QUADRUPOLARIZATION OF THE PARENT NUCLEI

For weakly oriented parent nuclei the angular distribution of the α particles is given by the formulas (I, 3.3). The values of the ratio A_2/f_2 calculated by the second of formulas (I, 3.3) (A_2 is the anisotropy parameter of the angular distribution, f_2 is the quadrupolarization) for various nuclei are given in Table IV.

TABLE IV

Parent nucleus	K	A_2/f_2
U^{233}	5/2	1.25
Am^{241}	5/2	1.14
Am^{243}	5/2	1.09

So far only the angular distributions of the α particles emitted by $U^{233,235}$ and Np^{237} (reference 13) have been measured. However, in the last two cases the level schemes of the corresponding daughter nuclei Th^{231} and Pa^{233} indicate a significant interaction between the rotational bands, so that K is not an integral of the motion, and the theory developed in references 1 and 2 cannot be applied directly.

On the other hand, the favored transition $U^{233} \xrightarrow{\alpha} Th^{229}$ goes to a rotational band of Th^{229} which corresponds to the definite value $K = \Omega = 5/2$. According to reference 13, $A_2 = -0.0625/T$, where T is the Kelvin temperature. It follows from Table IV that $f_2 = -0.050/T$. The spin energy of the nucleus U^{233} in the crystal field is given by the formula

$$H = P\left[\Omega_z^2 - \tfrac{1}{3}\Omega(\Omega+1)\right]. \tag{10}$$

f_2 and P can be related to each other by the Boltzmann distribution; as a result we find $P = 0.027°$. It is desirable to verify this value with the help of the magnetic resonance in the salt $U^{233}O_2Rb(NO_3)_3$, with which the experiments of Dabbs et al. were carried out.[13]

5. CONCLUSIONS

The comparison with experiment completely confirms the validity of the theory developed in references 1 to 3. This comparison also leads us to suggest some very definite experiments. Let us list a few of these.

1. The basic difficulty in the investigation of the decay $Pa^{231} \xrightarrow{\alpha} Ac^{227}$ $(K = 1/2)$ is the fact that the distance between the levels $J = \Omega = 3/2$ and $J = 1/2$ of the daughter nucleus is only 27 kev. For not too high resolution, the experimental energy distribution of the α particles in the region of favored decay has the following form: there is a basic maximum corresponding to the transition to the state $J = \Omega$ and a small "growth" on top of it corresponding to the decay to the level with $\Delta E_J = 27$ kev (ΔE_J is the excitation energy of the daughter nucleus reckoned from the level $J = \Omega$; $\Delta E_\Omega = 0$). The quadrupole deformation of the daughter nucleus Ac^{227} depends very strongly on the ratio of the intensities of these two maxima.

It is seen from Fig. 2 that the value of α_2 obtained from the available experimental data[8] is apparently somewhat too high. It is therefore necessary to make new measurements with a better resolution. Besides this, it is desirable to investigate also the transitions to the levels $J = 7/2$ and $5/2$ in order to substantiate the assumption $K = 1/2$. Experimentally we have $\Delta E_{7/2} = 58$ kev; the ratio of intensities $w_{7/2}/w_{1/2}$ is in good agreement with the formula (I, 2.21) (see Table III). For $J = 5/2$ the theoretical formula describing the rotational energy levels of a nonspherical nucleus with $K = 1/2$ (reference 5) gives $\Delta E_{5/2} = 121$ kev. However, the corresponding α decay has not been observed yet, since, according to (I, 2.21), its intensity amounts to only 0.13% of the total probability for the decay $Pa^{231} \xrightarrow{\alpha} Ac^{227}$.

2. It is seen from Fig. 2 that the deformation of the nucleus U^{230} deviates markedly from the general behavior of the deformations. This is not surprising, since, according to reference 8, the data on the fine structure of the decay $Pu^{234} \xrightarrow{\alpha} U^{230}$ are based on some unpublished work in which the excitation probability of the 2^+ level was determined with insufficient accuracy. More careful measurements of the relative probability of excitation of the 2^+ level in this process are needed to determine whether the deformation of U^{230} conforms to the general pattern of Fig. 2.

I express my gratitude to E. L. Feĭnberg for a discussion of the results of this work, and also to A. G. Zelenkov and G. E. Kocharov for the discussion of a number of questions concerning the experimental data. The author is grateful to L. A. Martynov and T. V. Novikova for helping with the tables and figures.

---

[1] V. G. Nosov, Doklady Akad. Nauk SSSR **112**, 414 (1957) Soviet Phys.-Doklady **2**, 48 (1957); JETP **33**, 226 (1957), Soviet Phys. JETP **6**, 176 (1958); Izv. Akad. Nauk SSSR, Ser. Fiz. **21**, 1551 (1957) Columbia Tech. Transl. p. 1541; Ядерные реакции при малых и средних энергиях (Nuclear Reactions at Small and Intermediate Energies), Report of the All-Union Conference, November 1957, U.S.S.R. Acad. Sci. Press 1958, p. 589.

[2] V. G. Nosov, JETP **39**, 141 (1960), Soviet Phys. JETP **12**, 102 (1961).

[3] V. G. Nosov, JETP **36**, 1580 (1959), Soviet Phys. JETP **9**, 1122 (1959).

[4] I. Perlman and F. Asaro, Ann. Rev. Nucl. Sci. **4**, 157 (1954). Gol'din, Peker, and Novikova, Usp. Fiz. Nauk **59**, 459 (1956).

[5] Alder, Bohr, Huus, Mottelson, and Winther, Revs. Modern Phys. **28**, 432 (1956).

[6] Fred, Tomkins, and Meggers, Phys. Rev. **98**, 1514 (1955) and **111**, 1747 (1958). K. L. van der Sluis and J. R. McNally, J. Opt. Soc. Am. **44**, 87 (1954). Bleany, Hutchison, Llewellyn, and Pope, Proc, Phys. Soc. **B69**, 1167 (1956). M. H. L. Pryce, Phys. Rev. Lett. **3**, 375 (1959).

[7] V. G. Nosov, Doklady Akad. Nauk SSSR **103**, 65 (1955).

[8] I. Perlman and J. Rasmussen, Alpha-Radioactivity (Russ. Transl.) IIL (1959).

[9] Kocharov, Komar, and Korolev, JETP **36**, 68 (1959), Soviet Phys. JETP **9**, 48 (1959). G. E. Kocharov, Dissertation, Radiophysics Institute, Academy of Sciences, Leningrad (1960).

[10] Novikova, Kondrat'ev, Sobolev, and Gol'din, JETP **32**, 1018 (1957), Soviet Phys. **5**, 832 (1957).

[11] J. Jungerman, Phys. Rev. **79**, 632 (1950). Wing, Ramler, Harkness, and Hizenga, Phys. Rev. **114**, 163 (1959).

[12] R. Hofstadter, Revs. Modern Phys. **28**, 214 (1956).

[13] Dabbs, Roberts, and Parker, Physica Suppl. **24**, 69 (1958).

Translated by R. Lipperheide
305

SOVIET PHYSICS JETP VOLUME 12, NUMBER 6 JUNE, 1961

LOW ENERGY INTEGRAL EQUATIONS FOR $\pi\pi$ SCATTERING

HSIEN DING-CHANG, HO TSO-HSIU, and W. ZÖLLNER

Joint Institute for Nuclear Research

Submitted to JETP editor June 31, 1960

J. Exptl. Theoret. Phys. (U.S.S.R.) **39**, 1668-1676 (December, 1960)

A critical analysis of the Chew-Mandelstam equations for $\pi\pi$ scattering is presented. With the help of fixed momentum transfer dispersion relations and the unitarity condition new equations are derived, which are entirely different from the Chew-Mandelstam equations as far as the contribution from the unphysical region is concerned.

1. INTRODUCTION

RECENTLY Chew and Mandelstam[1] derived a set of integral equations for $\pi\pi$ scattering. These authors determine the singularities of the partial wave scattering amplitudes by making use of the double dispersion relations proposed by Mandelstam.[2-4] The unitarity condition in the unphysical region is obtained by analytic continuation from the physical region with the help of an expansion in terms of Legendre polynomials. This method was also used by other authors[5,6] in discussing πN scattering and NN annihilation.

Efremov, Meshcheryakov, Chu, and Shirkov[7] have shown that the analytic continuation by means of the Legendre polynomial expansion leads to serious difficulties. Large errors result from the neglect of higher partial waves in the unphysical region, and the legitimacy of the Legendre expansion is limited by the borders of the region in which the spectral functions are nonvanishing. However, if the contributions from the unphysical region are not neglected for high energies $\nu > L$ (ν is the square of the pion momentum in the barycentric frame; the pion mass is set equal to unity, L is the cut-off parameter) then divergences are obtained in the resultant integral equations. The larger l, the higher is the degree of divergence of the coefficients of the Legendre polynomials $P_l(\cos\theta)$, and this divergence cannot be overcome by a finite number of subtractions. As a consequence, the neglect of the contributions from the unphysical region beyond some limit is unavoidable.

Even if contributions for $\nu' \geq L = 10$ are neglected there still remains a sizable region for which the distance from the physical region is comparable to the distance to the borders of the region where the spectral functions are nonzero. In this region the scattering amplitude cannot be approximated by only the first two terms of the Legendre expansion.

In this paper the $\pi\pi$ scattering problem is reexamined. With the help of only one unitarity condition together with fixed momentum transfer dispersion relations we obtain a set of integral equations for $\pi\pi$ scattering. In order to avoid a loss in accuracy when higher partial waves are neglected subtractions are performed at points different from those proposed by Chew and Mandelstam.

In Sec. 2 the limitations on the analytic continuation of the Legendre expansion are discussed. In Sec. 3 the integral equations are obtained and the subtraction problem is discussed. In the last section the error arising from the neglect of higher partial waves is determined. It is shown that in the region where the unitarity condition is rigorously fulfilled this error amounts to less than 10%.

2. LIMITATIONS ON THE ANALYTIC CONTINUATION OF THE LEGENDRE EXPANSION

The following three reactions:

$$\begin{aligned}
&(\mathrm{I}) && (p_1, \alpha) + (p_2, \beta) \to (-p_3, \gamma) + (-p_4, \delta),\\
&(\mathrm{II}) && (p_1, \alpha) + (p_4, \delta) \to (-p_2, \beta) + (-p_3, \gamma),\\
&(\mathrm{III}) && (p_1, \alpha) + (p_3, \gamma) \to (-p_2, \beta) + (-p_4, \delta)
\end{aligned} \tag{1}$$

are described by the single Green's function

$$T = A(s, t, \bar{t})\,\delta_{\alpha\beta}\delta_{\gamma\delta} + B(s, t, \bar{t})\,\delta_{\alpha\gamma}\delta_{\beta\delta} + C(s, t, \bar{t})\,\delta_{\alpha\delta}\,\delta_{\beta\gamma}. \tag{2}$$

Here p are the momenta, chosen for convenience as incident, and α, β, γ, δ are isotopic spin indices. The invariants s, t, and $\bar{t}$ are defined as follows:

$$s = -(p_1 + p_2)^2 = -(p_3 + p_4)^2,$$
$$t = -(p_1 + p_4)^2 = -(p_2 + p_3)^2,$$
$$\bar{t} = -(p_1 + p_3)^2 = -(p_2 + p_4)^2. \tag{3}$$

In particular, if ν and θ are respectively the square of the pion momentum and the scattering angle in the barycentric frame of reaction (I), then

$$s = 4(\nu + 1), \qquad t = -2\nu(1 - \cos\theta),$$
$$\bar{t} = -2\nu(1 + \cos\theta). \tag{4}$$

Let us denote by A^I the scattering amplitude in the isotopic spin state I for reaction (I). The A^I and the functions A, B, C are related by

$$A^0 = 3A + B + C, \qquad A^1 = B - C, \qquad A^2 = B + C. \tag{5}$$

The scattering amplitude may be expanded in partial waves:

$$A^I(\nu, \cos\theta) = \sum_l (2l + 1)\, A_l^I(\nu)\, P_l(\cos\theta),$$
$$A_l^I(\nu) = \sqrt{(1+\nu)/\nu}\, \exp(i\delta_l^I) \sin\delta_l^I. \tag{6}$$

Here l denotes the orbital angular momentum, δ_l^I is the scattering phase shift, and the summation is over even l for I = 0, 2 and over odd l for I = 1.

In the two-meson approximation the unitarity condition may be expressed in the form

$$\operatorname{Im} A_l^I(\nu) = \sqrt{\nu/(1+\nu)}\, |A_l^I(\nu)|^2. \tag{7}$$

Chew and Mandelstam use the following representation for the function A:

$$A(s, t, \bar{t}) = \frac{1}{\pi^2} \int ds' \int dt' \frac{a_{13}(s', t')}{(s - s')(t - t')}$$
$$+ \frac{1}{\pi^2} \int ds' \int d\bar{t}' \frac{a_{12}(\bar{t}', s')}{(s - s')(\bar{t} - \bar{t}')}$$
$$+ \frac{1}{\pi^2} \int dt' \int d\bar{t}' \frac{a_{23}(t'; \bar{t}')}{(t - t')(\bar{t} - \bar{t}')}, \tag{8}$$

where a_{12}, a_{13}, a_{23} are spectral functions. The functions B and C may be represented in an analogous manner.

The limits of validity of the Legendre expansion in the unphysical region can be immediately deduced as follows. Chew and Mandelstam obtained their integral equations from the dispersion relation for partial wave amplitudes (Eq. (V.1) of Chew and Mandelstam[1])

$$A_l^I(\nu) = \frac{1}{\pi} \int_0^\infty \frac{d\nu'}{\nu' - \nu} \operatorname{Im} A_l^I(\nu') + \frac{1}{\pi} \int_{-\infty}^{-1} \frac{d\nu'}{\nu' - \nu} \operatorname{Im} A_l^I(\nu'). \tag{9}$$

According to Eq. (IV.5) of Chew and Mandelstam[1]

$$\operatorname{Im} A_l^I(\nu')$$
$$= \sum_{I'} \alpha_{II'} \int_0^{-\nu'-1} \frac{d\nu''}{\nu'} P_l\left(1 + 2\frac{\nu'' + 1}{\nu'}\right) \operatorname{Im} A^{I'}(\nu'', \cos\theta'') \tag{10}$$

in the unphysical region $\nu' \leq -1$, where

$$\cos\theta'' = 1 + 2(\nu' + 1)/\nu''. \tag{11}$$

By substitution of Eq. (6) into Eq. (10), and then of Eq. (10) into Eq. (9), we obtain

$$A_l^I(\nu) = \frac{1}{\pi} \int_0^\infty \frac{d\nu'}{\nu' - \nu} \operatorname{Im} A_l^I(\nu')$$
$$+ \frac{1}{\pi} \int_0^\infty d\nu' \sum_{l', I'} \alpha_{II'} (2l' + 1) \beta_{ll'}(\nu', \nu) \operatorname{Im} A_{l'}^{I'}(\nu'), \tag{12}$$

$$\beta_{ll'}(\nu', \nu) = \int_{-\infty}^{-\nu'-1} \frac{d\nu''}{\nu''(\nu'' - \nu)} P_l\left(1 + 2\frac{\nu' + 1}{\nu''}\right)$$
$$\times P_{l'}\left(1 + 2\frac{\nu'' + 1}{\nu'}\right). \tag{13}$$

Expression (13) diverges for $l' \geq 1$. By means of one subtraction the divergence of the coefficient of the p wave can be eliminated and the $\pi\pi$ interaction constant λ introduced into the theory. However the remaining divergences cannot be eliminated by a finite number of subtractions. This circumstance results from an unjustified use of analytic continuation by means of the Legendre expansion whose validity fails at the borders of the region where the spectral functions become nonzero.

Chew and Mandelstam cut off the dispersion integral at $|\nu'| = L \approx 10$, i.e. at approximately the limit of validity of the Legendre expansion, and then neglected the contributions from d and higher partial waves. However even for $|\nu'|$

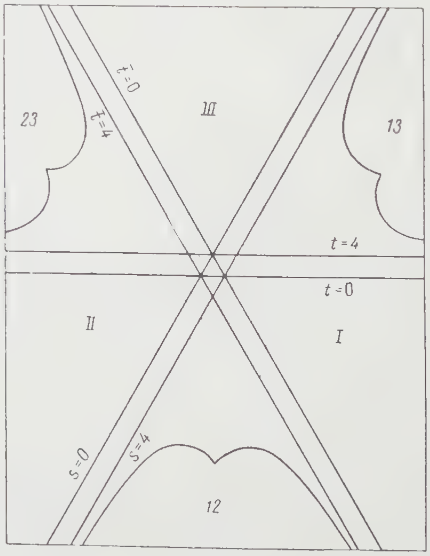

FIG. 1

≤ 10 there exists a sizable region, whose distance from the borders of the spectral functions is comparable with the distance from the physical region, as can be seen from Fig. (1). It is therefore doubtful whether the first two terms of the Legendre expansion are sufficient to represent the scattering function in the indicated region.

The error resulting from this circumstance may be roughly determined as follows. It follows from the double dispersion relation and crossing symmetry that

$$\operatorname{Im} A^0(\nu'', \cos\theta'') = \frac{1}{\pi}\int\limits_{t_0(\nu'')}^{\infty} \frac{dt'}{2\nu''}(2a_{13}+b_{13}+c_{13})\left\{\frac{1}{\tau-\cos\theta''}+\frac{1}{\tau+\cos\theta''}\right\},$$

$$\operatorname{Im} A^1(\nu'', \cos\theta'') = \frac{1}{\pi}\int\limits_{t_0(\nu'')}^{\infty} \frac{dt'}{2\nu''}(b_{13}-c_{13})\left\{\frac{1}{\tau-\cos\theta''}-\frac{1}{\tau+\cos\theta''}\right\}, \tag{14}$$

$$\operatorname{Im} A^2(\nu'', \cos\theta'') = \frac{1}{\pi}\int\limits_{t_0(\nu'')}^{\infty} \frac{dt'}{2\nu''}(b_{13}+c_{13})\left\{\frac{1}{\tau-\cos\theta''}+\frac{1}{\tau+\cos\theta''}\right\}, \tag{15}$$

where

$$\tau = 1 + t'/2\nu''.$$

$t_0(\nu'')$ is the border of the spectral functions a_{13}, b_{13} and c_{13}, which are functions of the quantities $s'' = 4(1+\nu'')$ and t'. They do not depend on $\cos\theta''$. The dependence of $\operatorname{Im} A^I(\nu'', \cos\theta'')$ on $\cos\theta''$ is therefore exhibited explicitly in the denominators in the curly braces.

According to Heine's theorem (see Whittaker and Watson[8]) we have

$$\frac{1}{\tau-\cos\theta''} = \sum_{l'}(2l'+1)\,Q_{l'}(\tau)\,P_{l'}(\cos\theta''); \tag{16}$$

where $Q_{l'}(\tau)$ is the Legendre function of the second kind. Keeping only the first two terms in the Legendre expansion is equivalent to the approximation:

$$R_+ \equiv \frac{1}{\tau-\cos\theta''}+\frac{1}{\tau+\cos\theta''} \approx 2Q_0(\tau),$$
$$R_- \equiv \frac{1}{\tau-\cos\theta''}-\frac{1}{\tau+\cos\theta''} \approx 6\cos\theta'' Q_1(\tau). \tag{17}$$

Now the error we are interested in can be easily estimated. Let us discuss the case $\nu'' = 3$, for which the unitarity condition begins to be violated. The nearest singular point, giving the largest contribution to Eq. (14), lies in the neighborhood of the border of the spectral functions $t_0(\nu'' = 3) = 64/3$. The corresponding value of τ equals 41/9. For this value, and for scattering angles $\theta = 0, \pi/2$, it is easy to obtain the data shown in the Table.

	$\theta = 0$	$\theta = \pi/2$
$\cos\theta''$	1	$^{11}/_3$
R_+	0.46	1.25
$2Q_0(\tau)$	0.44	0.45
R_-	0.101	1.00
$6\cos\theta'' Q_1(\tau)$	0.099	0.36

For $\theta = 0$ the error introduced by the approximation (17) amounts to only $2-4\%$. However for $\theta = \pi/2$ the error amounts to a factor of 3. It is clear from Fig. 1 that, even if the expansion is cut off at $|\nu'| = 10$ as was done by Chew and Mandelstam,[1] a large region of integration exists in which the imaginary part of the scattering function cannot be approximated by just two terms of the Legendre expansion.

These results also indicate that the approximation (17) is fully adequate for $\theta = 0$.

In accordance with the considerations developed by Efremov et al.[7] we derive in the following section integral equations for ππ scattering from the dispersion relation for fixed momentum transfer, which was proved rigorously by Bogolyubov, Medvedev, and Polivanov.[9] Our method is analogous to the method used by Chew, Goldberger, Low, and Nambu[10] in their work on πN scattering.

3. DERIVATION OF INTEGRAL EQUATIONS

In what follows we shall neglect g and higher partial waves in comparison with s waves, and h and higher partial waves in comparison with p waves. In this case we obtain with the help of Eq. (6) the following expressions:

$$A_0^0(\nu) \approx A^0(\nu, t=0) - \frac{2\nu}{3}\frac{\partial A^0(\nu, t)}{\partial t}\bigg|_{t=0},$$
$$A_1^1(\nu) \approx \frac{2}{5}A^1(\nu, t=0) - \frac{2\nu}{15}\frac{\partial A^1(\nu, t)}{\partial t}\bigg|_{t=0},$$
$$A_0^2(\nu) \approx A^2(\nu, t=0) - \frac{2\nu}{3}\frac{\partial A^2(\nu, t)}{\partial t}\bigg|_{t=0}. \tag{18}$$

When crossing symmetry is taken into account the dispersion relations for ππ scattering at fixed momentum transfer may be written in the form

$$\begin{pmatrix} A(\nu, t) \\ B(\nu, t) \\ C(\nu, t) \end{pmatrix} = \frac{1}{\pi}\int\limits_0^{\infty}\frac{d\nu'}{\nu'-\nu}\operatorname{Im}\begin{pmatrix} A(\nu', t) \\ B(\nu', t) \\ C(\nu', t) \end{pmatrix}$$
$$+\frac{1}{\pi}\int\limits_0^{\infty}\frac{d\nu'}{1+\nu+\nu'+t/4}\operatorname{Im}\begin{pmatrix} C(\nu', t) \\ B(\nu', t) \\ A(\nu', t) \end{pmatrix} \tag{19}$$

The following expressions are then obtained for the derivatives of the scattering amplitudes:

$$\begin{pmatrix}\partial A(\nu, t)/\partial t\\ \partial B(\nu, t)/\partial t\\ \partial C(\nu, t)/\partial t\end{pmatrix} = \frac{1}{\pi}\int_0^\infty \frac{d\nu'}{\nu'-\nu}\operatorname{Im}\begin{pmatrix}\partial A(\nu', t)/\partial t\\ \partial B(\nu', t)/\partial t\\ \partial C(\nu', t)/\partial t\end{pmatrix}$$

$$+\frac{1}{\pi}\int_0^\infty \frac{d\nu'}{1+\nu+\nu'+t/4}\operatorname{Im}\begin{pmatrix}\partial C(\nu', t)/\partial t\\ \partial B(\nu', t)/\partial t\\ \partial A(\nu', t)/\partial t\end{pmatrix}$$

$$-\frac{1}{4\pi}\int_0^\infty \frac{d\nu'}{(1+\nu'+\nu+t/4)^2}\operatorname{Im}\begin{pmatrix}C(\nu', t)\\ B(\nu', t)\\ A(\nu', t)\end{pmatrix} \tag{20}$$

It is well known that the expansion of the imaginary part of the scattering amplitudes in Legendre polynomials converges better, than the expansion of the real part, and therefore in the following we neglect the imaginary parts of d (f) and higher waves in comparison with s (p) waves. The validity of this approximation follows from the estimates made in the preceding section.

With the help of Eqs. (5), (6), and (18) – (20) we obtain the following equations for the s and p waves, in which no subtractions were performed:

$$A_0^0(\nu) = \frac{1}{\pi}\int_0^\infty \frac{d\nu'}{\nu'-\nu}\operatorname{Im} A_0^0(\nu') + \frac{1}{3\pi}\int_0^\infty \frac{d\nu'}{1+\nu+\nu'}[\operatorname{Im} A_0^0(\nu')$$

$$+\left(3\frac{\nu}{\nu'}-9\right)\operatorname{Im} A_1^1(\nu') + 5\operatorname{Im} A_0^2(\nu')]$$

$$+\frac{1}{18\pi}\int_0^\infty \frac{d\nu'}{(1+\nu+\nu')^2}[\operatorname{Im} A_0^0(\nu')$$

$$-9\operatorname{Im} A_1^1(\nu') + 5\operatorname{Im} A_0^2(\nu')], \tag{21}$$

$$A_1^1(\nu) = \frac{1}{\pi}\int_0^\infty \frac{d\nu'}{\nu'-\nu}\operatorname{Im} A_1^1(\nu') + \frac{1}{5\pi}\int_0^\infty \frac{d\nu'}{\nu'}\operatorname{Im} A_1^1(\nu')$$

$$+\frac{1}{15\pi}\int_0^\infty \frac{d\nu'}{1+\nu+\nu'}[-2\operatorname{Im} A_0^0(\nu') + \left(9-\frac{3}{2}\frac{\nu}{\nu'}\right)\operatorname{Im} A_1^1(\nu')$$

$$+5\operatorname{Im} A_0^2(\nu')] + \frac{\nu}{180\pi}\int_0^\infty \frac{d\nu'}{(1+\nu+\nu')^2}[-2\operatorname{Im} A_0^0(\nu')$$

$$+9\operatorname{Im} A_1^1(\nu') + 5\operatorname{Im} A_0^2(\nu')], \tag{22}$$

$$A_0^2(\nu) = \frac{1}{\pi}\int_0^\infty \frac{d\nu'}{\nu'-\nu}\operatorname{Im} A_0^2(\nu') + \frac{1}{6\pi}\int_0^\infty \frac{d\nu'}{1+\nu+\nu'}[2\operatorname{Im} A_0^0(\nu')$$

$$+\left(9-3\frac{\nu}{\nu'}\right)\operatorname{Im} A_1^1(\nu') + \operatorname{Im} A_0^2(\nu')]$$

$$+\frac{\nu}{36\pi}\int_0^\infty \frac{d\nu'}{(1+\nu+\nu')^2}[2\operatorname{Im} A_0^0(\nu')$$

$$+9\operatorname{Im} A_1^1(\nu') + \operatorname{Im} A_0^1(\nu')]. \tag{23}$$

The following expressions may be used to estimate the order of magnitude of d and f waves:

$$\frac{A_2^0(\nu)}{\nu} = \frac{1}{5\pi}\int_0^\infty \frac{d\nu'}{\nu'(1+\nu+\nu')}\operatorname{Im} A_1^1(\nu')$$

$$-\frac{1}{30\pi}\int_0^\infty \frac{d\nu'}{(1+\nu+\nu')^2}\left\{\frac{1}{3}\operatorname{Im} A_0^0(\nu')\right.$$

$$\left.-3\operatorname{Im} A_1^1(\nu') + \frac{5}{3}\operatorname{Im} A_0^2(\nu')\right\},$$

$$\frac{A_3^1(\nu)}{\nu} = \frac{3}{70\pi}\int_0^\infty \frac{d\nu'}{\nu'(1+\nu+\nu')}\operatorname{Im} A_1^1(\nu')$$

$$+\frac{1}{70\pi}\int_0^\infty \frac{d\nu'(1+2\nu+\nu')}{(1+\nu')(1+\nu+\nu')^2}$$

$$\times\left\{-\frac{1}{3}\operatorname{Im} A_0^0(\nu') + \frac{3}{2}\operatorname{Im} A_1^1(\nu) + \frac{5}{6}\operatorname{Im} A_0^2(\nu')\right\},$$

$$\frac{A_2^2(\nu)}{\nu} = \frac{1}{10\pi}\int_0^\infty \frac{d\nu'}{\nu'(1+\nu+\nu')}\operatorname{Im} A_1'(\nu') - \frac{1}{30\pi}\int_0^\infty \frac{d\nu'}{(1+\nu+\nu')^2}$$

$$\times\left\{\frac{1}{3}\operatorname{Im} A_0^0(\nu') + \frac{3}{2}\operatorname{Im} A_1^g(\nu') + \frac{1}{6}\operatorname{Im} A_0^2(\nu')\right\}. \tag{24}$$

It is necessary to keep in mind that these formulas are less accurate than Eqs. (21) – (23) since g waves are neglected in comparison with d waves, and h waves in comparison with f waves.

Chew and Mandelstam carry out a subtraction at the point $\nu = -2/3$ $(s = 4/3)$ at a stage in the calculation when it is still necessary to integrate along the straight line $s = 4/3$ between the points $\cos\theta = \pm 1$. They relate the given value λ of the scattering amplitude at the symmetric point $s = t = \bar{t} = 4/3$ to other points of this straight line by means of the Legendre polynomial expansion. In that expansion they keep only the leading terms and this may lead to further loss in accuracy due to the neglect of unphysical terms.

We avoid this loss in accuracy by carrying out the subtraction for A and C at the point 0″ $(s = \bar{t} = 2,\ t = 0)$ (see Fig. 2), where

$$A\left(\nu = -\tfrac{1}{2},\ t = 0\right) = C\left(-\tfrac{1}{2}, 0\right) = \Lambda,$$

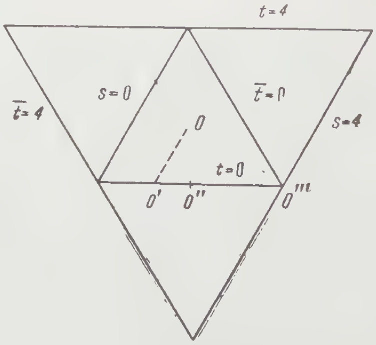

FIG. 2

and for A^1 at the point $0'''$ ($s = 4$, $t = \bar{t} = 0$), where

$$A^1(0,0) = B(0,0) - C(0,0) = 0.$$

It is therefore necessary to introduce but one new parameter. It should be noted that Λ differs from the constant λ utilized by Chew and Mandestam.[1] The connection between them is given in the Appendix.

After subtraction the Eqs. (21) – (23) for the s and p waves take on the form

$$\begin{aligned}A_0^0(\nu) = 5\Lambda &+ \frac{1}{\pi}\int_0^\infty d\nu' \,\mathrm{Im}\, A_0^0(\nu')\left\{\frac{\nu + {}^1\!/_2}{(\nu' - \nu)(\nu' + {}^1\!/_2)} - \frac{{}^2\!/_3(\nu + {}^1\!/_2)}{(\nu' + {}^1\!/_2)(1 + \nu + \nu')}\right.\\ &\left.+ \frac{{}^1\!/_3\nu}{(1 + \nu')(1 + \nu + \nu')} + \frac{{}^1\!/_{18}\nu}{(1 + \nu + \nu')^2}\right\}\\ &+ \frac{1}{\pi}\int_0^\infty d\nu' \,\mathrm{Im}\, A_1^1(\nu')\left\{\frac{{}^9\!/_2(\nu + {}^1\!/_2)}{(\nu' + {}^1\!/_2)(1 + \nu + \nu')} - \frac{{}^3\!/_2}{\nu'(\nu' + {}^1\!/_2)}\right.\\ &\left.- \frac{{}^3\!/_2\nu}{(1 + \nu')(1 + \nu + \nu')} + \frac{\nu}{\nu'(1 + \nu + \nu')} - \frac{{}^1\!/_2\,\nu}{(1 + \nu + \nu')^2}\right\}\\ &- \frac{5}{6\pi}\int_0^\infty \frac{d\nu'}{1 + \nu + \nu'}\\ &\times \mathrm{Im}\, A_0^2(\nu')\left\{\frac{\nu + {}^1\!/_2}{\nu' + {}^1\!/_2} + \frac{\nu}{1 + \nu'} - \frac{{}^1\!/_3\nu}{1 + \nu + \nu'}\right\},\end{aligned} \tag{25}$$

$$\begin{aligned}A_1^1(\nu) = \frac{\nu}{90\pi}\int_0^\infty &\frac{d\nu'}{(1+\nu')(1 + \nu + \nu')}\,\mathrm{Im}\, A_0^0(\nu')\left\{11 + \frac{\nu}{1 + \nu + \nu'}\right\}\\ &+ \frac{\nu}{\pi}\int_0^\infty d\nu' \,\mathrm{Im}\, A_1^1(\nu')\left\{\frac{1}{\nu'(\nu' - \nu)} - \frac{{}^1\!/_{10}}{\nu'(1 + \nu + \nu')}\right.\\ &\left.- \frac{1}{20}\,\frac{11 + \nu\,[1 + \nu + \nu']^{-1}}{(1 + \nu')(1 + \nu + \nu')}\right\}\\ &- \frac{\nu}{36\pi}\int_0^\infty d\nu' \,\mathrm{Im}\, A_0^2(\nu')\,\frac{11 + \nu\,[1 + \nu + \nu']^{-1}}{(1 + \nu')(1 + \nu + \nu')},\end{aligned} \tag{26}$$

$$\begin{aligned}A_0^2(\nu) = 2\Lambda &+ \frac{1}{\pi}\int_0^\infty d\nu' \mathrm{Im} A_0^0(\nu')\left\{- \frac{{}^2\!/_3(\nu + {}^1\!/_2)}{(1 + \nu + \nu')(\nu' + {}^1\!/_2)}\right.\\ &\left.+ \frac{{}^1\!/_3\nu}{(1 + \nu')(1 + \nu + \nu')} + \frac{{}^1\!/_{18}\nu}{(1 + \nu + \nu')^2}\right\}\\ &+ \frac{1}{\pi}\int_0^\infty d\nu' \mathrm{Im} A_1^1(\nu')\left\{- \frac{{}^3\!/_2}{\nu'(\nu' + {}^1\!/_2)} - \frac{{}^3\!/_2\nu}{(1 + \nu')(1 + \nu + \nu')}\right.\\ &\left.- \frac{{}^1\!/_2\nu}{\nu'(1 + \nu + \nu')} + \frac{{}^1\!/_4\nu}{(1 + \nu + \nu')^2}\right\}\\ &+ \frac{1}{\pi}\int_0^\infty d\nu' \mathrm{Im} A_0^2(\nu')\left\{\frac{\nu + {}^1\!/_2}{(\nu' + {}^1\!/_2)(\nu' - \nu)}\right.\\ &+ \frac{{}^2\!/_3(\nu + {}^1\!/_2)}{(\nu' + {}^1\!/_2)(1 + \nu + \nu')}\\ &\left.- \frac{{}^5\!/_6\nu}{(1 + \nu + \nu')(1 + \nu')} + \frac{{}^1\!/_{36}\nu}{(1 + \nu + \nu')^2}\right\}\end{aligned} \tag{27}$$

Here the coefficients of the p wave on the right-hand sides of the equations differ from the corresponding expressions in the Chew-Mandelstam equations.

The above-mentioned difficulties with analytic continuation in the unphysical region, the divergence of the coefficients and the need for a cut-off, can be avoided in our equations.

4. ESTIMATE OF THE ERROR DUE TO THE NEGLECT OF HIGHER WAVES IN THE PHYSICAL REGION

The error arising from the neglect of d and higher waves in the imaginary part, and g and higher waves in the real part of the scattering amplitude, can be determined by a method similar to the one used in Sec. 2.

We start by estimating the error arising in the imaginary part. We have

$$\left(1 - \gamma\frac{\nu}{\nu''}\frac{d}{d\cos\theta''}\right)\left(\frac{1}{\tau - \cos\theta''} + \frac{1}{\tau + \cos\theta''}\right)\Big|_{\cos\theta'' = 1} \approx 2Q_0(\tau), \tag{28a}$$

$$\left(1 - \gamma\frac{\nu}{\nu''}\frac{d}{d\cos\theta''}\right)\left(\frac{1}{\tau - \cos\theta''} - \frac{1}{\tau + \cos\theta''}\right)\Big|_{\cos\theta'' = 1} \approx 6\left(1 - \gamma\frac{\nu}{\nu''}\right)Q_1(\tau). \tag{28b}$$

Here $\gamma = {}^1\!/_3$ in the s-wave and $\gamma = {}^1\!/_6$ in the p-wave equations. As before, the quantity τ will be taken equal to ${}^{41}\!/_9$. For lower energies τ is larger and the error is smaller. At higher energies τ decreases, however the unitarity condition (7) gets violated. After simple calculations we find that in the region in which the unitarity condition (7) is satisfied the error of the approximate formula (28a) is less than 3%, and the error of formula (28b) is less than 8%.

An estimate of the error in the real part of the scattering amplitude is more difficult. The most serious limitation to the validity of the Legendre expansion is due to distant singularities in a thin layer of the region of integration, and they contribute insignificantly to the scattering amplitude. However a rough estimate shows that in the region in which the unitarity condition holds, the error in the real part of the scattering amplitude should be less than 10%.

The authors express their gratitude to professor Chu Hung-Yuan and D. V. Shirkov for suggesting this problem and for valuable remarks, and also to Chou Kuang-Chao and Wang Jung for useful discussions.

APPENDIX

The relation between the subtraction constant λ introduced by Chew and Mandelstam, and our constant Λ is given by the formula

$$\begin{aligned}\lambda = \Lambda &- \frac{1}{30\pi}\int_0^\infty \frac{d\nu'}{(\nu' + {}^2/_3)(\nu' + {}^1/_2)}\operatorname{Im}A_0^0(\nu') \\ &- \frac{3}{10\pi}\int_0^\infty \frac{d\nu'}{\nu'(\nu' + {}^1/_2)}\operatorname{Im}A_1^1(\nu') \\ &- \frac{1}{15\pi}\int_0^\infty \frac{d\nu'}{\nu'(\nu' + {}^1/_3)}\operatorname{Im}A_1^1(\nu') + \frac{2}{15\pi}\int_0^\infty \frac{d\nu'}{(\nu' + {}^1/_3)(\nu' + 1)} \\ &\times \operatorname{Im}\left\{-\frac{1}{3}A_0^0(\nu') + \left(\frac{1}{2} - \frac{1}{\nu'}\right)A_1^1(\nu') + \frac{5}{6}A_0^2(\nu')\right\} \\ &+ \frac{1}{30\pi}\int_0^\infty \frac{d\nu'}{(\nu' + {}^1/_3)(\nu' + {}^1/_2)}\operatorname{Im}\left\{\frac{2}{3}A_0^0(\nu')\right. \\ &\left.- \frac{9}{2}A_1^1(\nu') + \frac{5}{6}A_0^2(\nu')\right\} + \frac{1}{30\pi}\int_0^\infty \frac{d\nu'}{(\nu' + {}^1/_3)^2} \\ &\times \operatorname{Im}\left\{-\frac{1}{3}A_0^0(\nu') + 3A_1^1(\nu') - \frac{5}{3}A_0^2(\nu')\right\}.\end{aligned}$$

Due to the neglect of partial waves of higher order this formula is not exact. We find that the corresponding error is less than 6%.

Note added in proof (November 2, 1960). After the present article was sent to press we received a preprint from Chew and Mandelstam (UCRL 9126), in which they remark that if the p wave is large at low energies, a cut-off must be introduced. In their theory there arise at least two new parameters. The solutions to their equations are unstable, which confirms our conclusions regarding these equations.

---

[1] G. Chew and S. Mandelstam, Phys. Rev. **119**, 467 (1960).

[2] S. Mandelstam, Phys. Rev. **112**, 1344 (1958).

[3] S. Mandelstam, Phys. Rev. **115**, 1741 (1959).

[4] S. Mandelstam, Phys. Rev. **115**, 1752 (1959).

[5] S. McDowell, Phys. Rev. **116**, 774 (1959).

[6] W. Frazer and J. Fulco, Phys. Rev. **117**, 1603 (1960).

[7] Efremov, Meshcheryakov, Shirkov, and Tzu, Joint Inst. Nucl. Res. Preprint E 539.

[8] E. Whittaker and G. Watson, Modern Analysis, Cambridge, Univ. Press. 1946, p. 321.

[9] Bogolyubov, Medvedev, and Polivanov, Вопросы теории дисперсионных соотношений (Problems in Dispersion Relations Theory), Gostekhizdat, M., 1958.

[10] Chew, Goldberger, Low, and Nambu, Phys. Rev. **106**, 1337 (1957).

Translated by A. M. Bincer
306

SOVIET PHYSICS JETP VOLUME 12, NUMBER 6 JUNE, 1961

ANGULAR DISTRIBUTIONS OF HIGH-ENERGY MUONS IN THE ATMOSPHERE AND THEIR PRODUCTION MECHANISM

G. T. ZATSEPIN and V. A. KUZ'MIN

P. N. Lebedev Physics Institute, Academy of Sciences, U.S.S.R.

Submitted to JETP editor July 10, 1960

J. Exptl. Theoret. Phys. (U.S.S.R.) **39**, 1677-1685 (December, 1960)

The kinetic equation for μ mesons in the atmosphere in which the decay and energy losses are taken into account is solved. The angular distributions of $10^{11}-10^{14}$ ev μ mesons in the atmosphere are computed for two possible production mechanisms: $\pi \rightarrow \mu + \nu$ and $K \rightarrow \mu + \nu$ decays. The results indicate that in the energy range of $10^{11}-5\times10^{12}$ ev the μ-meson angular distributions depend significantly on the mechanism of their production.

1. INTRODUCTION

ON the basis of their experiments, a number of authors[1-3] have recently discussed the suggestion that heavy particles constitute the overwhelming share of all secondary particles produced in ultrahigh energy nuclear interactions. In particular, it may be that the largest part consists of K mesons. In this case, the role of K mesons in the production of high-energy μ mesons can prove to be important. Therefore experiments that would make it possible to determine which of the two possible mechanisms for the production of μ mesons, $\pi \rightarrow \mu + \nu$ or $K \rightarrow \mu + \nu$, plays the basic role would be of considerable interest. In the $1\times10^{11}-5\times10^{12}$ ev μ-meson energy region, the study of the angular distribution of μ mesons in the atmosphere[4] is, as is shown below, an experiment of this type.

The production of μ mesons in the atmosphere as a result of π-meson decay was first considered for the simpler case by Greisen; subsequently various forms of production of this type were studied by many authors. Detailed references to the literature on this question can be found in the work of Smith and Duller,[5] where calculations are given for the angular distributions of 40 — 160 ev μ mesons associated with π-μ decays for the case of a plane atmosphere and several other simplifying assumptions. In the present article we give a more accurate solution of the problem. The solution of the problem for μ mesons, roughly speaking, is divided into two parts: 1) solution of the kinetic equation for the parent particles (π, K) whose decay results in the production of μ mesons, and 2) the solution of the kinetic equation for the μ mesons.

2. SOLUTION OF THE KINETIC EQUATIONS FOR π AND K MESONS IN THE ATMOSPHERE

We shall consider the one-dimensional problem in which it is assumed that the trajectories of the primary nucleon, the π or K meson produced by it, and also the μ meson form one straight line. The path of the particles x is measured in units of the nucleon mean free path λ_0 (we take $\lambda_0 = 75$ g/cm²). The beginning of the path is taken at the point of entry of the nucleon into the atmosphere.

We assume that the intensity of production of η mesons (understood to be π or K mesons) can be written in the form $I_0^{(\eta)} E^{-(\gamma+1)} e^{-\mu x}$, i.e., the production spectrum follows a power law and the dependence on the depth, which is exponential with an absorption coefficient μ, does not depend on the energy, depth, or angle of inclination of the particle trajectory to the vertical. The graphical results shown at the end of the article were obtained for values of $1/\mu$ corresponding to an absorption mean free path of 120 g/cm².

We assume that the mean free path of the η particles is equal to the mean free path of the nucleons and that the regeneration of the η particles can be neglected. If the η-meson flux of energy E, E + dE at the depth x is equal to $P^{(\eta)}(x, E)\,dE$, then it decreases over a path dx by the quantity $P^{(\eta)}(x, E)\,dE\,dx$, owing to nuclear collisions.

We shall consider the probability of the decay of η particles $dW_d(x, E, \theta)$ on a path between x and x + dx for motion along a line directed towards the point of observation at an angle θ to the vertical. Let $\rho(x, \theta)$ be the air density at the point

x, θ. Then

$$dW_d(x, E, \theta) = [M_\eta c\lambda_0/\tau_{0\eta}\rho(x,\theta)E]dx, \qquad (1)$$

where M_η and $\tau_{0\eta}$ are the mass and lifetime (at rest) of the η particle, and c is the velocity of light.

The equation for the diffusion of nuclear-active particles with allowance for decay is readily solved by the method of successive generations if $\rho = \alpha x$, where $\alpha = \text{const}$, which is valid for a plane isothermal atmosphere. The isothermal approximation can obviously be used, since the effective production of high-energy mesons takes place over a small segment of the path, where the temperature of the atmosphere varies slowly along the path. It is also shown in the Appendix that although the relation between ρ and x for θ close to $\pi/2$ is more complicated than simple proportionality, in the region of the effective values of x, even for $\theta = \pi/2$, an approximation of the type $\rho(x, \theta) = \alpha(\theta)x$ is quite satisfactory, except for the narrow region of very small x. Replacing ρ in (1) by $\alpha(\theta)x$, we obtain

$$dW_d = [M_\eta c\lambda_0/\tau_{0\eta}\alpha(\theta)xE]dx = [E_\eta(\theta)/xE]dx, \qquad (2)$$

where $E_\eta(\theta)$ is the critical energy at which, for a path $x = 1$, the probability of decay of an η meson is equal to probability of a nuclear collision.

As a result, we obtain the kinetic equation for η particles in the form

$$\partial P^{(\eta)}(x, E)/\partial x = -[1 + E_\eta(\theta)/xE]P^{(\eta)}(x, E) + I_0^{(\eta)}E^{-(\gamma+1)}e^{-\mu x}. \qquad (3)$$

The solution of this equation has the form

$$P^{(\eta)}(x, E) = e^{-x}\sum_{i=1}^{\infty}\frac{x^i}{i!}F_i^{(\eta)}(E),$$

$$F_i^{(\eta)}(E) = I_0^{(\eta)}a^{i-1}E^{-(\gamma+1)}[1 + E_\eta(\theta)/iE]^{-1}, \qquad (4)$$

where $a = 1 - \mu$. The deviation from the obtained solution resulting from the inaccuracy of the adopted assumptions will be discussed below.

3. SOLUTION OF THE KINETIC EQUATION FOR μ MESONS IN THE ATMOSPHERE

The kinetic equation for μ mesons is written in the form

$$\frac{\partial P^{(\mu)}(x, E, \theta)}{\partial x} = -\frac{mc\lambda_0}{\tau_{0\mu}\rho(x, \theta)E}P^{(\mu)}(x, E, \theta) + \frac{\partial}{\partial E}[\beta(E)P^{(\mu)}(x, E, \theta)] + G(x, E, \theta), \qquad (5)$$

where m and $\tau_{0\mu}$ are the mass and the lifetime (at rest) of the μ meson, and $\beta(E)$ is the energy loss of a μ meson (of energy E) over a unit path. The first term in (5) takes into account the μ-meson decay, the second the energy losses and the third the production of μ mesons. We shall assume that the losses occur continuously, i.e., fluctuations can be neglected. Then

$$-dE/dx = \beta(E) = (\beta_0 + cE)\lambda_0,$$

where β_0 is the ionization loss, which we shall take to be constant along the μ-meson path and equal to

$$\beta_0 = 2.8 \text{Mev cm}^2/\text{g}.$$

The losses that are proportional to the energy are the radiation loss and the pair-production loss. For the energy region in which there is no complete screening, c is a slowly varying function of the energy. We shall assume that c is constant along the μ-meson path. The values of c (in 10^{-6} cm^2/g) for energies of $10^{11} - 10^{14}$ ev are as follows:*

E, ev	10^{11}	10^{12}	10^{13}	10^{14}
c_{rad}	0.77	1.02	1.11	1.16
c_{pair}	1,15	1.195	1.20	1,205
c_{tot}	1.92	2.22	2,31	2.36

A solution of Eq. (5) satisfying the condition $P^{(\mu)}(0, E, \theta) = 0$ is

$$P^{(\mu)}(x, E, \theta) = \exp\{-v(x, E, \theta) + c\lambda_0 x\}\int_0^x G(t, \varepsilon(E, x-t)) \times \exp\{v(t, E, \theta) - c\lambda_0 t\}\,dt, \qquad (6)$$

where

$$v(x, E, \theta) = (mc\lambda_0/\tau_{0\mu})\int_{x_0}^{x} dt/\rho(t, \theta)\,\varepsilon(E, x-t);$$

$$\varepsilon(E, x-t) = Ee^{c\lambda_0(x-t)} + (\beta_0/c)(e^{c\lambda_0(x-t)} - 1)$$

is the energy at the point t for a μ meson passing through the point x with an energy E, and x_0 is an arbitrary constant; it is convenient to take $x_0 = 1$.

We shall find the source function for μ mesons $G(x, \epsilon)$. We shall consider the μ-meson production process to be the decay $\pi \to \mu + \nu$, or, alternatively, the decay $K \to \mu + \nu$. In the rest system of the π and K mesons, the decay takes place isotropically. Therefore in the laboratory system (1.s.) the probability for the production of a μ meson of energy ϵ, $\epsilon + d\epsilon$ in the decay of an η meson of energy E is

$$W_{\eta\mu}(E, \varepsilon)d\varepsilon = [E(1 - m^2/M_\eta^2)]^{-1}d\varepsilon \quad \text{for } \varepsilon < E < M_\eta^2\varepsilon/m^2$$

---

*In the calculations, we made use of the results in the thesis of I. S. Alekseev, Phys. Faculty, Moscow State University, 1958.

and $W_{\eta\mu} \equiv 0$ for a value of E lying outside the indicated energy interval. The total number of μ mesons of the given energy ϵ produced in a layer of thickness dx can be determined if the value obtained above for $P^{(\eta)}(x, E)\,dE$ is multiplied by the probability of η-meson decay on the path dx: $dW_d = E_\eta(\theta)\,dx/xE$ and by the probability $W_{\eta\mu}(E, \epsilon)$ for the production of a μ meson of energy E in such a decay, and if we then integrate over all energies E in the interval $\epsilon < E < M_\eta^2\epsilon/m^2$. We obtain

$$G(x, \varepsilon) = e^{-x} \sum_{i=1}^{\infty} \frac{x^{i-1}}{(i-1)!} F_i^{(\mu)}(\varepsilon, \theta),$$

$$F_i^{(\mu)}(\varepsilon, \theta) = \frac{I_0^\eta a^{i-1}}{1 - m^2/M_\eta^2} \int\limits_{\varepsilon}^{M_\eta^2 \varepsilon/m^2} \frac{E^{-(\gamma+2)}}{1+iE/E_\eta(\theta)}\,dE. \qquad (7)$$

Expression (6) for the μ-meson flux now takes the form

$$P^{(\mu)}(x, E, \theta) = \exp\{-v(x, E, \theta) + c\lambda_0 x\} \int\limits_0^x \sum_{i=1}^{\infty} F_i^{(\mu)}(\varepsilon, \theta) \frac{t^{i-1}}{(i-1)!} \times \exp\{v(t, E, \theta) - c\lambda_0 t\}\,dt. \qquad (8)$$

We shall calculate the integral in the last expression.

Since the function $G(t, \epsilon)$ is appreciably different from zero only in a narrow interval of small t (~ 1), then, owing to the smallness of the quantity $c\lambda_0$, we can neglect the dependence of ϵ on t in $F_i^{\mu}(\epsilon, \theta)$ and in $\exp\{v(t, E, \theta)\}$ and take $\epsilon(E, x-t)$ equal to $\epsilon(E, x)$. Then $\exp\{v(t, E, \theta)\}$ is approximated well by the function t^δ. In fact, as was shown above, for $t \sim 1$ the dependence of $\rho(t, \theta)$ in the region of effective μ-meson production is satisfactorily approximated by the function $\rho(t, \theta) \approx \alpha(\theta)t$. Then

$$\exp\{[mc\lambda_0/\alpha(\theta)\tau_{0\mu}\varepsilon] \int\limits_1^t dz/z\} = t^\delta,$$

where $\delta = mc\lambda_0/\tau_{0\mu}\,\alpha(\theta)\,\epsilon(E, x)$ is a small quantity at the energies under consideration $E \gtrsim 1 \times 10^{11}$ ev. It can be seen that at large t, the integrand is a rapidly decreasing function, and the level of observation x lies deep in the atmosphere. Therefore the upper limit of integration over t can be replaced by ∞. We obtain

$$\sum_{i=1}^{\infty} \int\limits_0^x F_i^{(\mu)}(\varepsilon, \theta) \frac{t^{i-1+\delta}}{(i-1)!} e^{-(1+c\lambda_0)t}\,dt$$

$$\approx \sum_{i=1}^{\infty} \frac{F_i^{(\mu)}(\varepsilon, \theta)}{(i-1)!} \int\limits_0^{\infty} e^{-(1+c\lambda_0)t} t^{i-1+\delta}\,dt$$

$$= \sum_{i=1}^{\infty} F_i^{(\mu)}(\varepsilon, \theta) \frac{\Gamma(i+\delta)}{(i-1)!\,(1+c\lambda_0)^{i-1+\delta}},$$

where $\Gamma(i+\delta)$ is a Γ function. For the energy we are considering $E \gtrsim 1 \times 10^{11}$ ev, the factor

$$\Gamma(i+\delta)\,[(i-1)!\,(1+c\lambda_0)^{i-1+\delta}]^{-1} = 1$$

for all i makes an appreciable contribution, owing to the smallness of the quantities δ and $c\lambda_0$.

We introduce the notation $\sum\limits_{i=1}^{\infty} F_i^{(\mu)}(\epsilon, \theta) \equiv P_0^{(\mu)}(\epsilon, \theta)$.

We shall calculate the integral in the expression for $F_i^{(\mu)}(\epsilon, \theta)$. Since only values of E close to ϵ give a contribution to the last integral, the integral can be replaced by its approximate value

$$\int\limits_{\varepsilon}^{M_n^2 \varepsilon/m^2} \frac{E^{-(\gamma+2)}\,dE}{1+iE/E_\eta(\theta)} \approx \frac{1-(m/M_\eta)^{2(\gamma+1)}}{\gamma+1} \frac{\varepsilon^{-(\gamma+1)}}{1+ib_\eta\varepsilon/E_\eta(\theta)},$$

$$b_\eta = \frac{\gamma+2}{\gamma+1} \frac{1-(m/M_\eta)^{2(\gamma+1)}}{1-(m/M_\eta)^{2(\gamma+2)}}.$$

This substitution leads to an accurate approximation for $\epsilon \ll E_\eta/i$ and $\epsilon \gg E_\eta/i$; in the region $\epsilon \sim E_\eta/i$, for $\gamma = 1.5$, it gives an error of less than 4% for the case of the $\pi \to \mu + \nu$ decay and an error of less than 7% for the $K \to \mu + \nu$ decay. The accuracy increases with γ.

Inserting the values of the constants, we obtain for $\gamma = 1.5$:

1) when the generating component are π mesons

$$P_{0\pi}^{(\mu)}(\varepsilon, \theta) = A_\pi I_0^{(\pi)}(\varepsilon)^{-(\gamma+1)} S_\pi(\varepsilon, \theta); \qquad (9a)$$

2) in the case of K mesons

$$P_{0k}^{(\mu)}(\varepsilon, \theta) = A_k I_0^{(k)} \mathscr{K}_{\mu 2} \varepsilon^{-(\gamma+1)} S_k(\varepsilon, \theta), \qquad (9b)$$

where

$$S_\eta(\varepsilon, \theta) = \sum_{i=1}^{\infty} \frac{a^{i-1}}{1+ib_\eta\varepsilon/E_\eta(\theta)}, \quad A_\eta = \frac{1-(m/M_\eta)^{2(\gamma+1)}}{(\gamma+1)(1-m^2/M_\eta^2)},$$

$\mathscr{K}_{\mu 2}$ is the relative frequency of $K_{\mu 2}$ decay.

The values of the coefficients A_η and b_η are given in Table I, for several values of γ.

Table II lists the values of $S_\eta(E, 0)$ for various values of E; the decrease of S_η with an increase in E reflects the fact that the probability of η-meson decay decreases with increasing energy.

The complexity of the integrand makes it diffi-

TABLE I

	γ		
	1.5	2.0	2.5
b_π	1.22	1.21	1.20
b_K	1.40	1.33	1.28
A_π	0.706	0.635	0.575
A_K	0.419	0.350	0.300

TABLE II

E, ev	S_π (0)	$S_K(0)$
10^{11}	0,64	1.27
10^{12}	0,11	0,50
10^{13}	0.012	0,074
10^{14}	0.0012	0.0076

cult to calculate the quadrature $\int_1^x dt/\rho(t,\theta)\times$ $\epsilon(E, x-t)$ in the factor that accounts for the decay in expression (8) for the μ-meson flux at a depth x. However, the decay can be taken into account with good accuracy by means of an approximation. We set $\epsilon(E, x-t) \approx \epsilon(E,x)$. This corresponds to the assumption that the μ mesons traverse a large portion of their goemetric path in an atmosphere of low density, where they experience a slight energy loss, and are subject to an intensive energy loss only during the last segment of their path, this segment being short and therefore not important as regards the decay. As shown by the estimates, such an approximation is permissible even if it is assumed that the mesons traverse the entire path with an energy $\epsilon(E,x)$.

Then $\int_1^x \lambda_0 dt/\rho(t,\theta)$ is the geometric path $L(x,\theta)$ traversed by the μ mesons from their point of production to the point of observation.

Finally, for the μ-meson flux of energy E, E+dE at the point of observation x, we now obtain an expression convenient for the approximate calculations:

$$P_\eta^{(\mu)}(x, E, \theta) = \exp\{-mcL(x,\theta)/\tau_{0\mu}\varepsilon(E,x)$$

$$+ c\lambda_0 x\} P_{0\eta}^{(\mu)}(\varepsilon(E,x),\theta). \tag{10}$$

The results of the calculations of $P_\eta^{(\mu)}(x, E, \theta)$ for the two μ-meson production mechanisms are shown in Fig. 1. The values of $\cos\theta$ are laid off on the abscissa axis and $P^{(\mu)}(x, E, \theta)/P^{(\mu)}(x, E, 0)$, on the ordinate axis on a logarithmic scale. The calculations were carried out for the value $\gamma = 1.5$.

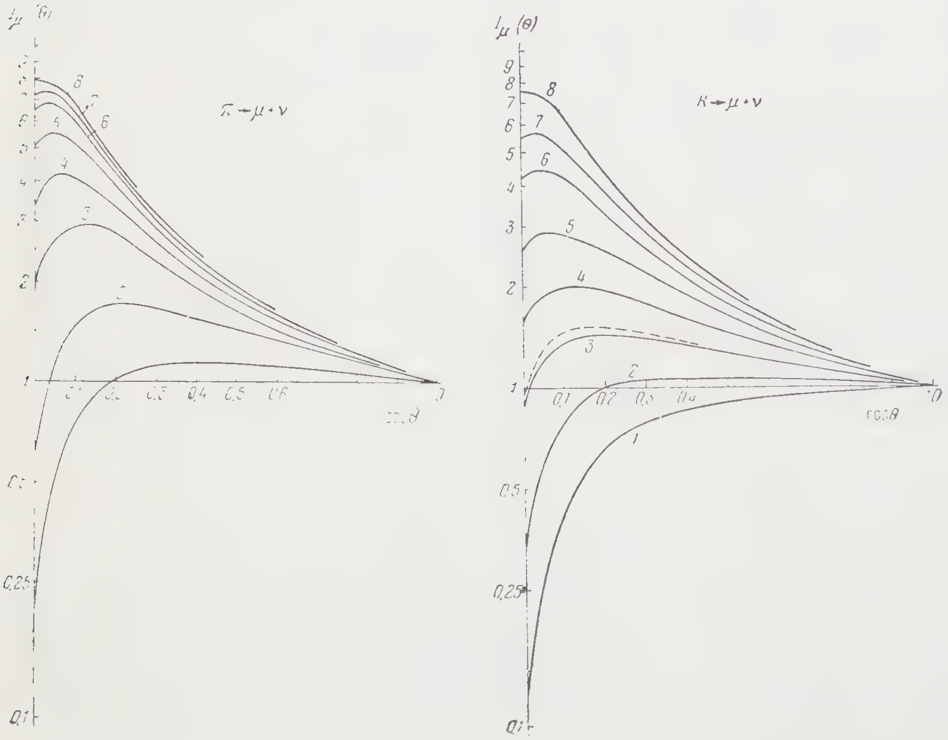

FIG. 1. Angular distribution of μ mesons of different energy E in the atmosphere for the two mechanisms of production. 1 – E = 1 × 10^{11} ev; 2 – E = 2 × 10^{11} ev; 3 – E = 5 × 10^{11} ev; 4 – E = 1 × 10^{12} ev; 5 – E = 2 × 10^{12} ev; 6 – E = 5 × 10^{12} ev; 7 – E = 1 × 10^{13} ev; 8 – E = 1 × 10^{14} ev. All curves are normalized to the corresponding intensity in the vertical direction.

TABLE III

$\cos\theta$	$\cos\theta_{\text{eff}}$	h_{eff}, km	L_{eff}, km	x, atm	E_π, ev	E_K, ev
0.00	0.111	34.0	660	35.4	$1.14\cdot10^{12}$	$8.41\cdot10^{12}$
0.05	0.123	33.3	406	15.2	$1.025\cdot10^{12}$	7,58
0.1	0.148	32.0	265	9.18	$8.46\cdot10^{11}$	6.25
0.2	0.226	29.1	140	4.88	5.40	3.99
0,3	0.315	26.8	90	3.30	3,81	2.82
0.4	0.410	25.0	60	2.48	2.87	2.12
0.6	0.603	22.4	38	1,67	1,93	1.43
1.0	1.0	19.0	19	1,00	1.16	$8.58\cdot10^{11}$

In Table III are listed the values of the effective heights of μ-meson production, the geometric path lengths from the effective points of generation to sea level, the ranges (in g/cm^2) for various zenith angles, and the values of the critical energies $E_\pi(\theta)$ and $E_K(\theta)$. The computational procedure is described in the Appendix.

4. DISCUSSION OF RESULTS

The kinetic energies $E_\pi(\theta)$ and $E_K(\theta)$ differ approximately by a factor of seven (owing to the difference in lifetimes and rest masses of the π and K mesons). This results from the different μ-meson angular distributions for the two production mechanisms over a considerable energy interval. Indeed, Fig. 1 shows that the μ-meson angular distribution curves for the energies $1 \times 10^{11} - 5 \times 10^{12}$ in the case of the π-meson mechanism of production lie on a level 1.5 to 2 times that for the K-meson mechanism in the zenith angle interval $0 < \cos\theta < 0.2$. At ultra-high μ-meson energies $E \gg E_\eta(\pi/2)$, the angular distributions are determined only by the properties of the atmosphere.[6] From Table II it is seen that $E_\eta(\pi/2) \approx 10\, E_\eta(0)$. Since for ultra-high energy μ mesons, by (9a) and (9b),

$$P_{0\eta}^{(\mu)}(\varepsilon, \theta) / P_{0\eta}^{(\mu)}(\varepsilon, 0) \sim E_\eta(\theta) / E_\eta(0),$$

then the μ-meson production increases about tenfold for both mechanisms as θ varies from 0 to $\pi/2$. Inclusion of the μ-meson energy loss limits the increase in intensity to a factor of eight at $\gamma = 1.5$ for $E = 1 \times 10^{14}$ ev.

As we have already mentioned, the calculations of the angular distributions were carried out under an assumed mean free path of 75 g/cm^2 for the nuclear interaction of π and K mesons. The obtained distributions, however, are extremely insensitive to a change in the mean free path λ_0 in the direction of higher values. Thus, when we set λ_0 for K mesons equal to the mean free path for absorption of the generating component $1/\mu = 120$ g/cm^2 (which is equivalent to the assumption that a substantial number of K mesons is produced in nuclear collisions), we obtained a decrease in the maxima of the angular distributions at large angles by 6 — 10% for energies of $10^{11} - 10^{12}$ ev. Also, the difference in the distributions for the two mechanisms of production increased. The distribution curves are more sensitive to a decrease in λ_0, but in order to bring the distributions for the two mechanisms quite close together λ_0 must be made 1/2.5 — 1/3 as large, i.e., it must be reduced to 30 — 25 g/cm^2, which is improbable. Thus, no reasonable change in the mean free path of the mesons can eliminate the difference in the distributions for the two production mechanisms.

In solving the diffusion equations for π and K mesons, we have assumed that they are produced only by stable particles, chiefly nucleons. Such a simplification is permissible, owing to the fact that the π- and K-meson flux is small ($\lesssim 5\%$) at the heights of effective production of μ mesons in comparison with the nucleon flux over the entire energy range.[7-10] The production of π mesons in the decay of K mesons does not have to be taken into account. According to an estimate made under the assumption of a power-law spectrum for the production of K mesons with an exponent $\gamma = 1.5$, in which the large probability of $K_{\mu 2}$ decay in comparison with $K_{\pi 2}$ decay was taken into account, the contribution of K mesons to the μ-meson flux via decay with direct production of μ mesons is 3.5 times the contribution of the two-stage decay $K \to \pi \to \mu$, even at small energies ($E \lesssim 10^{11}$ ev). This effect is apparently the most important of all those not taken into account. It appears most strongly at energies $E_\pi(0) < E < E_\pi(\pi/2)$. The dotted curve of Fig. 1b represents the angular distribution of 5×10^{11} ev μ mesons with allowance for the $K \to \pi \to \mu$ process.

Nor does the presence of complex nuclei in primary cosmic radiation have a great effect on the obtained results. We have estimated that the μ-meson angular distribution curves are lowered by several percent at large zenith angles when the contribution of nuclei in the π- (or K-) meson flux is taken into account.

The scattering of μ mesons in the atmosphere can be neglected, since even for μ mesons with an energy of $E \sim 1 \times 10^{11}$ ev and a horizontal direction of flight the scattering at the point of observation is $\sim 0.4°$. The deviation of the direction of flight of the meson from the direction of motion of the primary particle is of the same order for a transverse momentum of ~ 0.3 Bev/c.

The method used to account for the decay separately from the energy loss reduces the μ-meson decay for energies of $E = (1-2) \times 10^{11}$ ev and horizontal directions approximately by 5%, i.e., the distribution curves for these energies are enhanced by about 10% for angles $0 < \cos\theta < 0.2$.

The calculated distributions depend on the value of the γ-spectrum exponent for the production of π or K mesons almost entirely because of the μ-meson energy losses. Thus, for a change of γ from 1.5 to 1.75, the points of the distributions corresponding to the angle $\theta = \pi/2$ decrease by 18 — 11% for energies of $(1-2) \times 10^{11}$ ev.

The dependence of the angular distributions on the level of observation for the lower half of the atmosphere is reflected in the results also only because of the μ-meson energy losses, since the effective layer of matter through which the μ mesons pass is changed. However, for a considerable angular interval $0.1 < \cos\theta$, in which the difference in the distributions of the two μ-meson production mechanisms is important and the losses small, it is not necessary to know the exact value of γ, since the distributions are then almost independent of the value of γ.

Thus the contribution of μ mesons from K mesons to the flux can be determined on the basis of the appropriate experimental data if the contribution attains the value of $\gtrsim 20\%$.

Comparison of our curve for μ mesons from π-μ decays with a similar curve obtained by Smith and Duller[5] for $E = 10^{11}$ ev indicates that the curves differ by no more than 6% at the maximum.

APPENDIX

The path traversed in a spherical isothermal atmosphere by a particle traveling at sea level at an angle θ is expressed in g/cm^2 in the following way:

$$x = \rho_0 \int_h^\infty e^{-u/h_0} du/\cos\psi = \rho_0 e^{-h/h_0} \int_0^\infty \left(1 + \frac{u+h}{R}\right)$$
$$\times \left[\cos^2\theta + 2\frac{u+h}{R} + \left(\frac{u+h}{R}\right)^2\right]^{-1/2} e^{-u/h_0} du,$$

where R is the radius of the earth, ψ is the flux angle with the vertical. After simple calculations, we obtain

$$x = \rho_0 e^{-h/h_0} z^{-1/4} e^{z/2} \sqrt{Rh_0/2}\, W_{-1/4,\,1/4}(z), \tag{11}$$

where $z = h/h_0 + R\cos^2\theta/2h_0$, $W_{-1/4,1/4}(z)$ is the Whittaker function. Depending on the problem being considered — the calculation of the layer of matter in g/cm^2 traversed by μ mesons in the atmosphere to sea level or the determination of the relation between ρ and x at great heights — we choose different values of the quantities ρ_0 and h_0 which best approximate the dependence of ρ on the height h over the range of variation of h of interest to us.

Using for great heights the asymptotic form of the function $W_{-1/4,1/4}(z)$, we obtain

$$x = \rho_0 e^{-h/h_0} z^{-1/2} \sqrt{Rh_0/2}\left[1 + \sum_{k=1}^{\infty} (-1)^k \frac{(2k-1)!!}{2^k z^k}\right]$$
$$= \alpha(h, \theta)\, \rho(h). \tag{12}$$

Figure 2 shows the values of α/h_0 as a function of the traversed path for the angle $\theta = \pi/2$. It is seen that α varies little over the range of effective production. A natural simplification is to replace relation (12) by the approximate expression

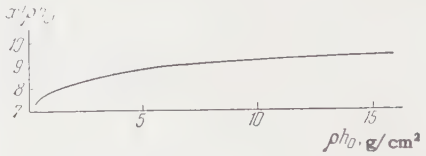

FIG. 2. Variation of the path x referred to the pressure ρh_0 along the trajectory of a particle in the atmosphere for the angle $\theta = \pi/2$ (values of ρh_0 equal to 5, 10, 15, g/cm^2 correspond to values of x equal to 44, 99 140, g/cm^2).

$$x \approx \alpha_{\text{eff}}(\theta)\, \rho(h), \tag{13}$$

where $\alpha_{\text{eff}}(\theta)$ is calculated at the point of "half-production" (i.e., at a depth above which half of the total μ-meson flux is produced. For $\lambda_0 = 75$ g/cm^2 and $1/\mu = 120$ g/cm^2, the half-production depth is $x_{\text{eff}} = 65$ g/cm^2. The meaning of the simplification is that the part of the path on which the nuclear-active shower effectively generates μ mesons is replaced by a straight line making some effective angle to the vertical. The effective angles calculated by us are also shown in Table III.

Generally speaking, the atmosphere is not isothermal. However, at heights in which we are interested and over small segments of path the temperature changes slowly. Therefore the calculations were made under the assumption of an isothermal atmosphere, but for each zenith angle we took the experimentally known temperature at the corresponding effective height. The experimental values of the pressure, density, and temperature at various heights were taken from the data of Alekseev et al.[11]

---

[1] Duthie, Fisher, Fowler, Kaddoura, Perkins, and Pinkau, Proceedings of the International Conf. on Cosmic Rays, Moscow, 1960.

[2] Fujimoto, Hasegawa, Kazuno, Nishimura, Niu, and Ogita, ibid.

[3] A. I. Alikhanyan, Proceedings ibid.

[4] I. S. Alekseev and G. T. Zatsepin, ibid.

[5] J. A. Smith and N. M. Duller, J. Geophys. Research **64**, 2297 (1959).

[6] Oda, Oshio, Watanabe, Watanase, Preprint.

[7] A. Subramanian and S. D. Werma, Nuovo cimento **13**, 572 (1959).

[8] G. T. Zatsepin, Dissertation, Physics Institute, Academy of Sciences, 1954.

[9] N. L. Grigorov, Usp. Fiz. Nauk **58**, 599 (1956).

[10] Pine, Davisson, and Greisen, Proceedings of the International Conf. on Cosmic Rays, Moscow, 1960.

[11] Alekseev, Besyadovskiĭ, Golyshev, Izakov, Kasatkin, Kokin, Livshitz, Masanova, and Shvidkovskiĭ, Метеорология и гидрология (Meteorology and Hydrology) **8**, 3 (1957).

Translated by E. Marquit
307

SOVIET PHYSICS JETP VOLUME 12, NUMBER 6 JUNE, 1961

CALCULATION OF THE TRANSITION EFFECT AT VARIOUS DISTANCES FROM THE ELECTRON-PHOTON SHOWER AXIS

O. I. DOVZHENKO

P. N. Lebedev Physics Institute, Academy of Sciences, U.S.S.R.

Submitted to JETP editor June 11, 1960

J. Exptl. Theoret. Phys. (U.S.S.R.) **39**, 1686-1692 (December, 1960)

A method for calculating the transition effect in thin layers of matter ($t < 1$ radiation length) is developed for radiation consisting of electrons and photons with an arbitrary spectrum. The results obtained are used for calculating the transition effect between the air and the ionization-chamber wall at various distances r from the electron-photon shower axis for $s = 1$ and for an infinite primary energy. Electron- and photon-energy spectra at various distances r from the shower axis are derived by the moment method.

1. In a number of experiments (see the article by Greisen[1]) on the lateral distribution of charged particles in extensive air showers (EAS), thin-walled ionization chambers and cloud chambers with covers made of heavy matter (brass, steel, etc.) were used as detectors. Since, in the passage of the electron-photon shower through a thin layer of matter, the absolute number of electrons depends substantially on the magnitude of the air-to-counter-wall transition effect, the question arises as to whether it is possible to compare the lateral distributions of charged particles obtained by means of different detectors.

For the case of an equilibrium energy spectrum of the electrons and photons, the transition effect in a thin layer of matter has been treated in detail in the monograph of Belen'kiĭ.[2] However, the formulae given there cannot be used in those cases where it is necessary to determine the transition effect at various distances r from the shower axis, since, for a given r, the energy spectra of electrons and photons are not in equilibrium, even though the electrons and photons may be in equilibrium over the whole shower. For small distances from the electron-photon shower axis, Bethe[3] obtained the following approximate formula, which is customarily used for calculating the air-to-counter-wall transition effect:

$$\Delta N/N = 2(1-7.2/Z)\,t, \qquad (1)$$

where Z is the atomic number of the counter-wall matter, 7.2 is the atomic number of air, and t is expressed in radiation lengths. However, Eq. (1) does not take the variation of the transition effect with the distance from the shower axis into account, and its usefulness is therefore greatly limited.

The variation of the transition effect with varying distance from the shower axis was discussed by Heinemann.[4] However, an insufficiently substantiated choice of the lateral distribution functions of electrons and photons for energies $E < 2\beta$ (where β is the critical energy) prevents us from accepting the results of Heinemann as being certain.

2. Let us consider the transition effect of radiation consisting of electrons and photons passing from medium 1 into medium 2 without assuming the equilibrium between electrons and photons in medium 1.

Let $P_1^{\pi}(E, r)$ be the number of electrons in medium 1 with energy in the range E, $E+dE$ at a distance range of r, $r+dr$ from the axis of the electron-photon showers at the observation level, and let $P_1^{\gamma}(E, r)$ be the analogous function for photons. If we neglect the deflection of particles in medium 2, then the variation of the number of electrons $P_2^{\pi}(E, r, t)$ and photons $P_2^{\gamma}(E, r, t)$ with the depth t in this medium is described by the following equations:[2]

$$\frac{\partial P_2^{\pi}(E,r,t)}{\partial t} = L_1[P_2^{\pi}(E,r,t)] + 2\int_E^{\infty}\frac{\sigma_{p2}(E')}{\sigma_0 E'}P_2^{\gamma}(E',r,t)\,u\left(\frac{E}{E'}\right)dE' + g_2\int_E^{\infty}P_2^{\gamma}(E',r,t)\,v_{\text{Compton}}(E',E'-E)\,dE' + \beta_2\frac{\partial P_2^{\pi}(E,r,t)}{\partial E}, \qquad (2)$$

$$\frac{\partial P_2^{\gamma}(E,r,t)}{\partial t} = L_2[P_2^{\pi}(E,r,t)] - P_2^{\gamma}(E,r,t)\,\sigma_2(E) + g_2\int_E^{\infty}P_2^{\gamma}(E',r,t)\,v_{\text{Compton}}(E',E)\,dE' \qquad (3)$$

with the boundary conditions $P_2^{\pi}(E, r, 0) = P_1^{\pi}(E, r)$ and $P_2^{\gamma}(E, r, 0) = P_1^{\gamma}(E, r)$.

$L_1[P_2^{\pi}]$ and $L_2[P_2^{\pi}]$ are integral operators acting on the function P_2^{π} and corresponding to bremsstrahlung, $\sigma_{p2}(E')$ is the photon-absorption coefficient in medium 2 due to pair production, $\sigma_0 = 0.773$ is the limiting value of the photon-absorption coefficient, and $\sigma_2(E')$ is the total photon-absorption coefficient in medium 2,

$$u\left(\frac{E}{E'}\right) = \left(\frac{E}{E'}\right)^2 + \left(1 - \frac{E}{E'}\right)^2 + \left(\frac{E}{E'}\right)\left(1 - \frac{E}{E'}\right)\left(\frac{2}{3} - 2b\right), \quad b \approx 0{,}0135, \tag{3'}$$

$$v_{\mathrm{Compton}}(E', E)\, dE \approx \frac{dE'}{EE'}\left[1 + \left(\frac{E}{E'}\right)^2\right]. \tag{3''}$$

The values of g_2 for various media are given in reference 2, and β_2 is the critical energy in medium 2.

Following the procedure of Belen'kiĭ,[2] we shall solve Eq. (2) by the successive-approximation method.* In calculating the first approximation, we shall assume that:

1. The photon spectrum does not change greatly in the layer under consideration of the second medium, i.e., $t < 1/\sigma_2$. This gives $P_2^{\gamma}(E, r, t) \approx P_1^{\gamma}(E, r)$.

2. The variation of the electron spectrum $P_2^{\pi}(E, r, t)$ due to the radiation losses, which are considerable in the high-energy range, does not greatly affect the number of electrons detected by the counter. This enables us to assume that $L_1[P_2^{\pi}] = 0$.

In fact, as has been shown by Eyges[5] for $t < 1$, the integral variation of the number of electrons due to bremsstrahlung, and the ensuing absorption due to ionization losses, is a higher-order effect than the change in the number of electrons due to single-ionization absorption. This enables us to set $L_1[P_2^{\pi}] = 0$ for a first approximation, which greatly simplifies the solution of the problem since it makes it possible to pass from the integro-differential Eq. (2) to the partial differential equation

$$\frac{\partial P_2^{\pi}(E, r, t)}{\partial t} - \beta_2 \frac{\partial P_2^{\pi}(E, r, t)}{\partial E} = 2\int_E^{\infty} \frac{\sigma_{p2}(E')}{\sigma_0 E'} P_1^{\gamma}(E', r)\, u\left(\frac{E}{E'}\right) dE' + g_2 \int_E^{\infty} P_1^{\gamma}(E', r)\, v_{\mathrm{Compton}}(E', E' - E)\, dE', \tag{4}$$

with the boundary condition $P_2^{\pi}(E, r, 0) = P_1^{\pi}(E, r)$.

The integration of this equation leads to the following result:

$$P_2^{\pi}(E, r, t) = \frac{2}{\beta_2}\int_E^{E+\beta_2 t} dE'' \int_{E''}^{\infty} \frac{\sigma_{p2}(E')}{\sigma_0 E'} P_1^{\gamma}(E', r) u\left(\frac{E''}{E'}\right) dE' + \frac{g_2}{\beta_2}\int_E^{E+\beta_2 t} dE'' \int_{E''}^{\infty} P_1^{\gamma}(E', r)\, v_{\mathrm{Compton}}(E', E' - E'')\, dE' + P_1^{\pi}(E + \beta_2 t, r). \tag{5}$$

The total number of particles $N_2^{\pi}(R, t)$ under the transition layer $t < 1$ of the second medium can be written in the following form:

$$N_2^{\pi}(r, t) = \int_0^{\infty} P_2^{\pi}(E, r, t)\, dE = [N_2^{\pi}(r, t)]_{\mathrm{pair}} + [N_2^{\pi}(r, t)]_{\mathrm{Compton}} + N_1^{\pi}(\beta_2 t, r), \tag{6}$$

$$[N_2^{\pi}(r, t)]_{\mathrm{pair}} = \frac{2}{\beta_2}\int_0^{\infty} dE \int_E^{E+\beta_2 t} dE'' \int_{E''}^{\infty} \frac{\sigma_{p2}(E')}{\sigma_0 E'} P_1^{\gamma}(E', r) u\left(\frac{E''}{E'}\right) dE', \tag{6'}$$

$$[N_2^{\pi}(r, t)]_{\mathrm{Compton}} = \frac{g_2}{\beta_2}\int_0^{\infty} dE \int_E^{E+\beta_2 t} dE'' \int_{E''}^{\infty} P_1^{\gamma}(E', r)\, v_{\mathrm{Compton}}(E', E' - E'')\, dE', \tag{6''}$$

$$N_1^{\pi}(\beta_2 t, r) = \int_{\beta_2 t}^{\infty} P_1^{\pi}(E, r)\, dE. \tag{6'''}$$

In the integral (6′), the range of relatively low energies is most important, and we therefore set $u(E''/E') = 1$. For the term v_{Compton} appearing in the integral (6″), we substitute the expression (3″). Changing the order of integration twice and integrating expressions (6′) and (6″), we have

$$[N_2^{\pi}(r, t)]_{\mathrm{pair}} = \frac{1}{\beta_2 \sigma_0}\int_0^{\beta_2 t} P_1^{\gamma}(E', r)\, E' \sigma_{p2}(E')\, dE' + \frac{1}{\sigma_0}\int_{\beta_2 t}^{\infty} \frac{P_1^{\gamma}(E', r)}{E'} \sigma_{p2}(E')[2tE' - \beta_2 t^2]\, dE', \tag{7}$$

$$[N_2^{\pi}(r, t)]_{\mathrm{Compton}} = \frac{g_2}{\beta_2}\left\{\int_{\beta_2 t + mc^2/2}^{\infty} P_1^{\gamma}(E', r) V_1(E')\, dE' + \int_{mc^2/2}^{\beta_2 t + mc^2/2} P_1^{\gamma}(E', r) V_2(E')\, dE'\right\}, \tag{8}$$

where

$$V_1(E') = \ln\frac{E'}{E' - \beta_2 t} + \frac{\beta_2 t}{E'}\left[\ln\frac{2(E' - \beta_2 t)}{mc^2} - \frac{1}{2}\right] + \frac{1}{6}\left(\frac{\beta_2 t}{E'}\right)^3\left[1 - 3\left(\frac{mc^2}{2\beta_2 t}\right)^2\right] - \frac{1}{2}\left(\frac{\beta_2 t}{E'}\right)^2, \tag{8'}$$

$$V_2(E') = \ln\frac{2E'}{mc^2} - \frac{5}{6} + \frac{mc^2}{2E'} - \frac{1}{2}\left(\frac{mc^2}{2E'}\right)^2 + \frac{1}{3}\left(\frac{mc^2}{2E'}\right)^3. \tag{8''}$$

---

*Since the commonly-used detectors (cloud chambers, ionization and diffusion chambers) are sensitive only to charged particles, the solution is sought for electrons only.

The expression (6) for $N_2^{\pi}(r,t)$ has a clear physical meaning: the lateral distribution of electrons below the layer $t < 1$ of the second medium is determined, on the one hand, by the lateral distribution of electrons with energy $\geq \beta_2 t$ in the first medium, and on the other by the lateral distributions $[N_2^{\pi}(r,t)]_{\text{pair}}$ and $[N_2^{\pi}(r,t)]_{\text{Compton}}$ of electrons produced in the layer t by photons as the result of pair production and Compton effect, respectively.

3. Thus, the lateral distribution of electrons $N_2(r,t)$ under the transition layer $t < 1$ can be calculated by means of simple quadratures if the differential energy spectra of electrons and photons in the first medium are known, i.e., $P_1^{\pi}(E,r)$ and $P_1^{\gamma}(E,r)$. For the high-energy range, where we can neglect the ionization losses, $P_1^{\pi}(E,r)$ and $P_1^{\gamma}(E,r)$ are calculated for different values of r by the moment method for the various stages of shower development and infinite primary energy.[6] We shall attempt to find approximate expressions for $P_1^{\pi}(E,r)$ and $P_1^{\gamma}(E,r)$, which describe the differential energy spectra of electrons and photons in the low-energy range $E < \beta_1$, since the low-energy particles are the ones mainly responsible for the magnitude of the transition effect.

In order to find $P_1^{\pi}(E,r)$ and $P_1^{\gamma}(E,r)$ by the moment method, it is necessary to know the behavior of these functions for $r \to 0$. Since the behavior of P_1^{π} and P_1^{γ} in the low-energy range near zero is unknown, we shall assume that the lateral distribution of electrons having a given energy near zero at the shower maximum is the same for all energies, and is represented by the Molière distribution for high energies,[7] i.e., $P_1^{\pi}(E,r) \sim r^{-1/3}$ for $r \to 0$. An analogous assumption is made for photons: $P_1^{\gamma}(E,r) \sim r^{-1}$ for $r \to 0$.

We expect $P_1^{\pi}(E,r)$ to be of the following form:

$$P_1^{\pi}(E, r) \sim r^{-1/3} P_1^{\pi}(E) e^{-\alpha r^{\nu}}, \tag{9}$$

where $P_1^{\pi}(E)$ is the differential energy spectrum of electrons over the whole shower, and the parameters α and ν are determined from the known values of $\overline{r^2}^{\pi}$ and $\overline{r^4}^{\pi}$.[6,8] If we assume that the ratio $[\overline{r^2}^{\pi}(E)]^2/\overline{r^4}^{\pi}(E) = \text{const}$ is independent of energy, which is correct in the high-energy range, then we can determine the parameters α and ν and obtain the following analytical expression for $P_1^{\pi}(E,r)$:

$$P_1^{\pi}(E, r) = \frac{\alpha^{10/3}}{4\pi\Gamma(10/3)} r^{-1/3} P_1^{\pi}(E) e^{-\alpha\sqrt{r}},$$

$$\alpha = \left[\frac{\Gamma(22/3)}{\Gamma(10/3)} \frac{1}{\overline{r^{2\pi}}}\right]^{1/4}, \tag{10}$$

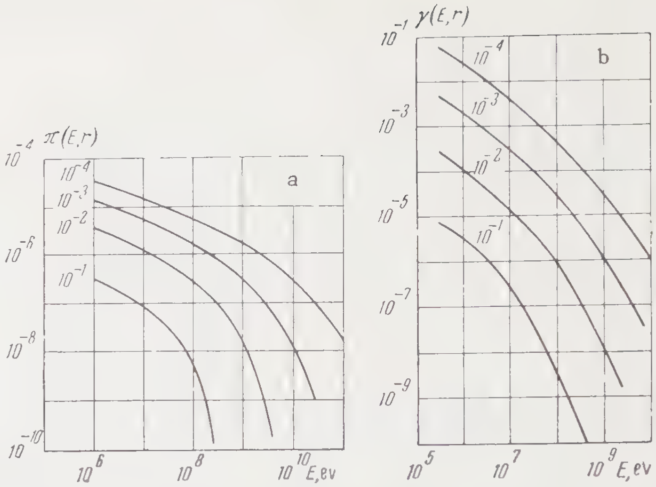

FIG. 1. Differential energy spectra of a – electrons, b – photons, in air for s = 1, normalized to the total number of electrons. The numbers at the curves denote the distance (in radiation lengths) from the shower axis.

where $\Gamma(x)$ is the Γ function.

Analogously for photons

$$P_1^{\gamma}(E, r) = \frac{\zeta^3}{6\pi\Gamma(3)} \frac{P_1^{\gamma}(E)}{r} \exp(-\zeta r^{1/3}),$$

$$\zeta = \left[\frac{\Gamma(9)}{\Gamma(3)} \frac{1}{\overline{r^{2\gamma}}}\right]^{1/6}, \tag{11}$$

where $P_1^{\gamma}(E)$ is the differential energy spectrum of photons in air over the whole shower.

Figure 1a shows the normalized electron energy spectra $\pi(E,r) = P_1^{\pi}(E,r)\left[\int_0^{\infty} 2\pi r N_1^{\pi}\, dr\right]^{-1}$ in air at various distances from the axis, calculated according to formula (10), while Fig. 1b shows the analogous spectra of photons $\gamma(E,r) = P_1^{\gamma}(E,r) \times \left[\int_0^{\infty} 2\pi r N_1^{\pi}\, dr\right]^{-1}$, calculated from formula (11)

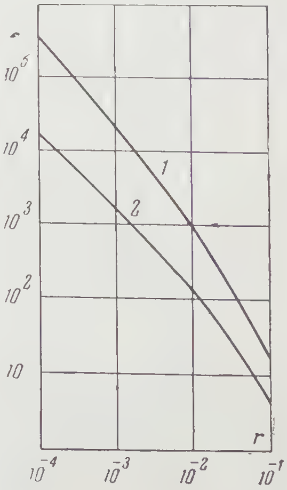

FIG. 2. Lateral distributions in air: $f_1^{\pi}(r)$ of electrons with energy >0 (curve 2) and $f_1^{\gamma}(r)$ of photons with energy $\gtrsim 5 \times 10^5$ ev (curve 1), normalized to the total number of electrons for $s = 1$ (r in radiation lengths).

using the following expressions for the equilibrium spectra:[2]

$$P_1^{\pi}(E) = \frac{E_0}{\beta_1}\frac{[1-(\varepsilon+1)\,G(\varepsilon,1)]}{E},$$

$$P_1^{\gamma}(E) = \frac{E_0}{\beta_1}\frac{G(\varepsilon,1)}{\sigma_1 E}, \qquad (12)$$

where σ_1 is the total absorption coefficient of photons in air, $\epsilon = 2.29\ E/\beta_1$, and $\beta_1 = 72$ Mev is the critical energy in air, and

$$G(\varepsilon,1) = 1 - \varepsilon e^{\varepsilon}\int_{\varepsilon}^{\infty} e^{-x}x^{-1}\,dx.$$

The values of $G(\epsilon, 1)$ for various ϵ are given in the review of Belen'kiĭ and Ivanenko.[9] The values of $\overline{r^2}^{\pi}$ and $\overline{r^2}^{\gamma}$ are taken from the papers of Kamata and Nishimura[8] and Roberg and Nordheim.[10]

The integral lateral distributions of electrons with energy greater than 0* and photons with energy $\gtrsim 5 \times 10^5$ ev† corresponding to differential spectra (10) and (11) are shown in Fig. 2.

It can be seen that the total number of photons is considerably greater than the total number of electrons. In addition, photons have a different lateral distribution than electrons, so that the ratio of the number of electrons to photons depends on the distance from the axis. In the end, this should also be felt in the variation of the transition effect with the distance from the shower axis.

4. The differential energy spectra of electrons and photons shown in Figs. 1a and 1b make it possible to use formulas (6) — (8) to determine the magnitude of the transition effect in the absorbing layer with thickness $t < 1$ for different distances from the axis of the electron-photon shower. In Fig. 3, the lateral distributions of electrons calculated from the above formulas for the case $t \approx 0.18$, $\beta_2 = 16.6$ Mev (copper) are shown. As can be seen from these distributions, the increase in the number of electrons because of the transition effect is mainly due to the pair production by photons, and the Compton effect plays only a small part even at relatively large distances (for $r \approx 0.1$ and $t \approx 0.18$, we have $N^{\pi}_{\mathrm{Compton}} \approx 0.3\ N^{\pi}_{\mathrm{p}}$).

Analogous distributions were obtained for other values of t. The results of the calculation are shown in Fig. 4, where the function $F = 1 + [f_2^{\pi}(r,t) - f_1^{\pi}(r)]/f_1^{\pi}(r)$ shows the variation of the number of electrons at a distance r from the shower axis with absorber thickness. (The values of t are indicated by the numbers near the curve.) It is clear that for small distances from the shower axis ($r \sim 3 \times 10^{-4}$, which corresponds to ~ 10 cm for mountain altitudes), this increase is very great for $t \approx 0.5$ (~ 10 times). Although the calculation has been carried out for copper, the magnitude of the transition effect is mainly due to the pair production by photons, so that the curve shown in Fig. 4 can be used to determine the transition effect in any substance whose atomic number is not very small, if we express the thickness of the transition layer in radiation-length units.

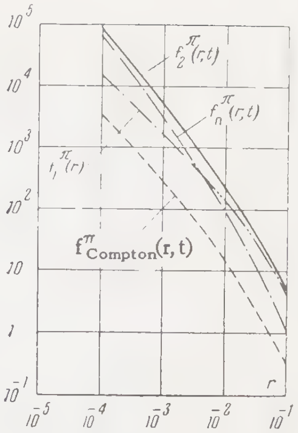

FIG. 3. Normalized lateral distributions of electrons for $t \approx 0.18$ and $\beta_2 = 16.6$ Mev.

It should be noted that, in the calculations, we have not taken the scattering of the particles in the transition layer and the angular distribution of the particles in air into account. The influence of the angular distribution of the electrons and photons in air should lead to a somewhat smaller change of the transition effect with distance. This follows from the curves of Fig. 4 since, with increasing distance from the shower axis, the angular distribution of the particles becomes ever wider, which effectively leads to an increase of the transition-layer thickness. However, at small distances from the axis, this correction may be neglected.

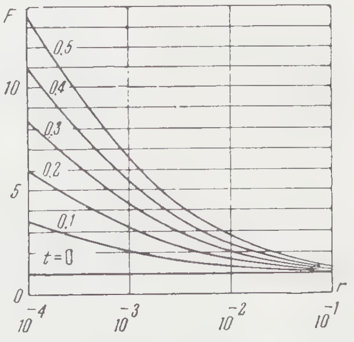

FIG. 4

---

*The lateral distribution of electrons with energy >0 corresponds fully with the distribution obtained by Kamata and Nishimura[8] by another method.

†The lateral distribution of photons with energy >0 is difficult to calculate, since it is necessary to take into account effects that play a considerable role in the range of very low energies ($E < 10^5$ ev).

5. As has been mentioned above, the differential energy spectra of electrons and photons [Eqs. (10) and (11)] have been obtained for the maximum development of the electron-photon cascade ($s = 1$). The lateral distribution of charged particles in EAS corresponds best to a value[8] $s = 1.2 - 1.4$, so that it would be desirable to determine how the magnitude of the transition effect varies with increasing shower age. Such estimates were carried out for $s = 1.4$ and for infinite primary energy. It was found that, if for $s = 1$, $t \approx 0.18$, and $\beta_2 = 16.6$ Mev the number of particles of the whole shower increases by $\sim 31\%$, then, for $s = 1.4$, the corresponding increase amounts to $\sim 29\%$. This indicates that the magnitude of the transition effect varies little with s near $s = 1$.*

In conclusion, the author wishes to thank A. A. Emel'yanov, G. T. Zatsepin, and S. I. Nikol'skiĭ for their discussion of the results.

---

*With increasing s, one should expect the greatest change in the transition effect to occur at small values of r. However, it is not possible to indicate the magnitude of such a change.

[1] K. Greisen, Progress in Cosmic Ray Physics (North Holland Publishing Co., Amsterdam 1956), Vol. III.

[2] S. Z. Belen'kiĭ, Лавинные процессы в космических лучах (Cascade Processes in Cosmic Rays) Gostekhizdat, 1948, p. 128.

[3] R. W. Williams, Phys. Rev. **74**, 1689 (1949).

[4] R. E. Heinemann, Phys. Rev. **96**, 174 (1954).

[5] L. Eyges, Phys. Rev. **76**, 264 (1949).

[6] V. V. Gužavin and I. P. Ivanenko, Suppl. Nuovo cimento **8**, 749 (1958).

[7] Cosmic Radiation, ed. by Heisenberg, N.Y. 1946.

[8] K. Kamata and J. Nishimura, Suppl. Progr. Theoret. Phys. **6**, 93 (1958).

[9] S. Z. Belen'kiĭ and I. P. Ivanenko, Usp. Fiz. Nauk **69**, 591 (1959), Soviet Phys.-Uspekhi **2**, 912 (1960).

[10] J. Roberg and L. W. Nordheim, Phys. Rev. **75**, 444 (1949).

Translated by H. Kasha
308

SOVIET PHYSICS JETP VOLUME 12, NUMBER 6 JUNE, 1961

RESONANCE EFFECTS OF RADIATION IN A LAMINAR MEDIUM

M. L. TER-MIKAELYAN and A. D. GAZAZYAN

Erevan State University and Physics Institute, Academy of Sciences, Armenian S. S. R.

Submitted to JETP editor June 10, 1960

J. Exptl. Theoret. Phys. (U.S.S.R.) **39**, 1693-1698 (December, 1960)

Resonance radiation is studied in a periodic medium which is most convenient for experimentation, that is, in a laminar medium. Laminar media consisting of sets of two arbitrary layers with different or equal thicknesses are considered. Formulas for the spectral distribution and for the total number of radiated quanta are derived. The frequency ranges (for each harmonic $r = 1, 2, 3 \ldots$) and the energy threshold of the radiation are determined.

In an earlier paper[1] we have studied the radiation which occurs when a charged particle moves in an arbitrary periodic medium. For the particular case of a laminar medium consisting of two plates of equal thickness, and when $\Delta = |(N_1 - N_2)/(N_1 + N_2)| \ll 1$, it was pointed out that the resonance radiation is given by a formula which differs from formula (19) of reference 1 by the factor $16/\pi^2$. Here N_1 and N_2 are the electron densities in the first and second medium.

It should be mentioned that the case of a layered medium has already been discussed in the literature. As I. M. Frank emphasized in his Nobel lecture, when the distances between layers become large compared to the formation zone, the total radiation from a layered medium equals the sum of the radiations from the different layers; this is the well known transition radiation of V. L. Ginzburg and I. M. Frank. In our interpretation this limit means radiation of high order, or, as we shall say, radiation of high harmonics, when the summation over r can be replaced by integration.

The exact solution of the problem of radiation in a layered medium is given in a paper by Khizhnyak and Faĭnberg,[2] who cite a condition the physical gist of which is equivalent to our resonance condition (8). Khizhnyak and Faĭnberg analyze the case when the wavelength of the radiated quantum exceeds the length of a period. As is shown in reference 1, the more interesting case occurs precisely when the opposite inequality holds. The exact solution is also given in a paper of Garibyan. Garibyan's results do not appear convincing to us, since he neglected resonance effects.

From the experimental point of view a laminar medium is the most convenient for detection of resonance radiation. We therefore derive and discuss in this paper the corresponding formulas for the general case of different thicknesses and arbitrary Δ. We shall use the formulas obtained in reference 1 in the semiclassical approximation. In order to apply the semiclassical theory to a layered medium, the boundaries between the layers must be smoothed over. This can always be done, because it is the larger distances traversed by the particle that are important for emission of radiation [see Eqs. (4) – (6)], and therefore the result of interest does not depend on the sharpness of the boundary.

Let us further note that the semiclassical approximation leads to incorrect results for the reflected waves. Therefore we must demand that effects connected with reflected waves be negligible. This will be the case if there is only a small change in the dielectric properties of the medium from a layer with dielectric constant ϵ_1 to a layer with ϵ_2, i.e.,

$$|(\varepsilon_2 - \varepsilon_1)/(\varepsilon_2 + \varepsilon_1)| \ll 1. \tag{1}$$

This condition is always satisfied in the high-frequency region, which will occupy our interest below.

In addition to (1) we must also suppose that the radiation is confined to small angles at $v \approx c$. This condition turns out to be fulfilled if

$$\lambda \ll l \tag{2}$$

($\lambda = \omega\sqrt{\epsilon}/c$, l is the period of the layers).

Let the particle move along the z axis through a plane which is perpendicular to its trajectory, and at a distance $z \rightarrow \infty$ from the origin of coordinates. The energy radiated by the particle is then given by Eq. (18) of reference 1:

$$S = \frac{8\pi^3}{c^3}\,\omega^4\varepsilon^{3/2}(z)\,d\omega\int\sin^3\theta\cos^2\theta\,|A(q, z, \omega)|^2\,d\theta, \tag{3}$$

where A (q, z, ω) is calculated from formula (14) of reference 1:

$$A(q, z, \omega) = \frac{iev}{4\pi^2 c}\left(\frac{\varepsilon(z)}{\varkappa(z)}\right)^{1/2} I, \tag{4}$$

$$I = \int\limits_{-\infty}^{+\infty}\exp\Big\{i\omega t + i\Big|\int\limits_{vt}^{z}\varkappa dz\Big|\Big\}\frac{dt}{[\varkappa(vt)\,\varepsilon(vt)]^{1/2}}. \tag{5}$$

The calculation of A (q, z, ω) amounts to calculating I for a layered medium. Consider first a finite number of arbitrary layers of two different materials with dielectric constants ϵ_1 and ϵ_2:

$$\varkappa_1 = (\omega\sqrt{\varepsilon_1}/c)\cos\theta, \qquad \varkappa_2 = (\omega\sqrt{\varepsilon_2}/c)\cos\theta.$$

Let the layers of the first material (ϵ_1, κ_1) have a thickness Δz_1 ($\Delta z_1 = v\Delta t_1$) and those of the second material (ϵ_2, κ_2) have a thickness Δz_2 ($\Delta z_2 = v\Delta t_2$). Let us number the layers with integers from 1 to n (odd numbers characterize the first medium, even ones the second medium). For convenience we take n even, so that we have n/2 layers of the first, and n/2 layers of the second medium. Later on we shall let n tend to infinity; actually this means that the factor $|\sin(n\alpha/2)/\sin\alpha|^2$ contained in $|I|^2$ [see Eq. (6)] can be replaced by

$$\tfrac{1}{2}n\pi\sum_{r=-\infty}^{\infty}\delta(\alpha - \pi r).$$

Let us denote by $t_1, t_2, \ldots t_n$ the times when the particle enters the first, second, etc. layer, and by t_{n+1} the time of leaving the last layer. Then the integral I can be broken up into a sum of integrals over t (from $-\infty$ to t_1; from t_1 to t_2 etc.; from t_{n+1} to ∞). We are not interested in the first integral from $-\infty$ to t_1, or in the last one from t_{n+1} to ∞, because they are connected with transient effects on the first and last layer (below we must let z tend toward infinity faster than the number of layers).

Once the integrals have been calculated, their summation amounts to the summing of a geometric series. For I we obtain a final expression

$$|I| = 2\sin\left\{\frac{(\omega - \varkappa_2 v)}{2}\,\Delta t_2\right\}\Bigg|\frac{1}{(\varepsilon_1\varkappa_2)^{1/2}(\omega - \varkappa_1 v)} - \frac{1}{(\varepsilon_2\varkappa_2)^{1/2}(\omega - \varkappa_2 v)}\Bigg|\frac{\sin(n\alpha\;2)}{\sin\alpha}, \tag{6}$$

$$2\alpha = (\omega - \varkappa_1 v)\,\Delta t_1 + (\omega - \varkappa_2 v)\,\Delta t_2. \tag{7}$$

For sufficiently large n, the integral I differs from zero only when the resonance condition

$$\alpha = \pi r \tag{8}$$

is fulfilled (here r is an arbitrary integer).

We introduce the notation

$$(\sqrt{\varepsilon_1}\,\Delta t_1 + \sqrt{\varepsilon_2}\,\Delta t_2)/\Delta t = \sqrt{\varepsilon}, \tag{9}$$

where $v\Delta t = v(\Delta t_1 + \Delta t_2) = l$ is the sum of the thicknesses of two adjacent layers. Condition (8) defines the cosine of the angle at which the quantum is emitted,

$$\cos\theta = c/v\sqrt{\varepsilon} - 2\pi rc/\omega l\sqrt{\varepsilon}. \tag{10}$$

By demanding $|\cos\theta| \le 1$ we have

$$\frac{\omega l}{2\pi v}\left(1 + \frac{v}{c}\sqrt{\varepsilon}\right) \geqslant r \geqslant \frac{\omega l}{2\pi v}\left(1 - \frac{v}{c}\sqrt{\varepsilon}\right). \tag{11}$$

If we confine our attention to the cases when Cerenkov radiation can occur, we see that $r \gg 1$. We also note that the polarization of the resonance radiation agrees with the polarization of the Cerenkov radiation.

From (6), (5), and (3) we find the total radiated energy when a particle crosses n layers

$$S = 2\,\frac{e^2v^2}{c^3\varepsilon}\;nd\omega\sum_{r=1}^{r_{max}}\int\sin^3\theta\,d\theta\,\sin^2\frac{\omega\Delta t_2}{2}\left(1 - \frac{v}{c}\sqrt{\varepsilon_2}\cos\theta\right)$$
$$\times\frac{|\varepsilon_2^{3/4} - \varepsilon_1^{3/4} + (v/c)\cos\theta\,(\varepsilon_1^{5/4} - \varepsilon_2^{5/4})|^2}{(1 - (v\sqrt{\varepsilon_1}/c)\cos\theta)^2(1 - (v\sqrt{\varepsilon_2}/c)\cos\theta)^2}\,\delta$$
$$\times\left(\omega\Delta t - \omega\Delta t\,\frac{v}{c}\cos\theta\sqrt{\varepsilon} - 2\pi r\right). \tag{12}$$

Let us integrate (12) over the emission angles θ, using the formula

$$\int\sin^3\theta d\theta\delta\left(\omega\Delta t - \omega\Delta t\,\frac{v}{c}\cos\theta\sqrt{\varepsilon} - 2\pi r\right)$$
$$= (c/l\omega\sqrt{\varepsilon})\,[1 - (c/v\sqrt{\varepsilon} - 2\pi rc/\omega l\sqrt{\varepsilon})^2]. \tag{13}$$

Since we suppose that the angles θ are small, formula (13) can be simplified by putting

$$1 + (c/v\sqrt{\varepsilon} - 2\pi rc/\omega l\sqrt{\varepsilon}) \approx 2.$$

The final formula for the radiation from relativistic particles of frequencies which appreciably exceed atomic frequencies has the form

$$S = \frac{d\omega}{\omega}\,\frac{e^2n}{l}(\varepsilon_2 - \varepsilon_1)^2\sum_{r=1}^{r_{max}}\sin^2\frac{\omega\Delta t_2}{2}\left(\frac{2\pi rv}{l\omega} - \frac{2\pi e^2}{m\omega^2}\,\frac{\Delta t_1}{\Delta t}\,(N_1 - N_2)\right)$$
$$\times\left[\frac{2\pi}{l}\,r\,\frac{v}{\omega} - \left(1 - \frac{v}{c}\right) - \frac{2\pi e^2}{m\omega^2}\left(N_1\frac{\Delta t_1}{\Delta t} + N_2\frac{\Delta t_2}{\Delta t}\right)\right]$$
$$\times\left[\frac{2\pi}{l}\,r\,\frac{v}{\omega} - \frac{2\pi e^2}{m\omega^2}\,\frac{\Delta t_1}{\Delta t}(N_1 - N_2)\right]^{-2}$$
$$\times\left[\frac{2\pi}{l}\,r\,\frac{v}{\omega} - \frac{2\pi e^2}{m\omega^2}\,\frac{\Delta t_2}{\Delta t}(N_2 - N_1)\right]^{-2}. \tag{14}$$

To find the total number of radiated quanta we must divide S by $\hbar\omega$ and integrate over all possible emitted frequencies. From the right part of inequality (11) we obtain a condition on the range of the emitted frequencies

$$\frac{2\pi vr}{\omega l}-\left(1-\frac{v}{c}\right)-\frac{2\pi e^2}{m\omega^2}\left(N_1\frac{\Delta t_1}{\Delta t}+N_2\frac{\Delta t_2}{\Delta t}\right)=0. \tag{15}$$

We note that an analogous expression occurs in the square brackets of the numerator in Eq. (14). The left part of inequality (11) leads to the condition

$$\pi vr/\omega l \leqslant 1. \tag{2'}$$

Whenever (2) is satisfied, (2′) is certainly satisfied for $r = 1$.

We must note that in cases of practical interest condition (2′) turns out to be weaker than the condition on $\omega_{\min}$ which follows from Eq. (15) [cf. (17) and (21)]. It is easy to see that in order that this be so, l must exceed $l_1 = [4\pi e^2(N_1 + N_2)/m]^{-1/2}\pi vr$.

To simplify the calculations we introduce the notation

$$\frac{2\pi rv}{l}=a,\qquad \frac{2\pi e^2}{m}\left(N_1\frac{\Delta t_1}{\Delta t}+N_2\frac{\Delta t_2}{\Delta t}\right)=b \tag{16}$$

and a new variable of integration ξ, which equals

$$a/\omega = 2\pi vr/\omega l = \xi. \tag{17}$$

With the new notation, Eq. (15) can be written in the form

$$\xi-(1-v/c)-b\xi^2/a^2=0, \tag{15'}$$

and the solution of Eq. (15′) gives us the limits of the interval of the emitted frequencies,

$$\xi_{1,2}=\frac{1\pm\sqrt{1-4(1-v/c)b/a^2}}{2b/a^2}. \tag{18}$$

In order that different real roots exist, it is clearly necessary that the expression under the square root in (18) be positive. This requirement determines the energy threshold at which the radiation begins:

$$E/mc^2 \geqslant \sqrt{2b}/a. \tag{19}$$

Let us proceed to the analysis of Eq. (14) for the case when $\Delta t_1 = \Delta t_2$. For layers of equal thickness formula (19) can be rewritten in the form

$$\frac{E}{mc^2}\geqslant\sqrt{\frac{2\pi e^2}{m}(N_1+N_2)}\,\frac{l}{2\pi rv}. \tag{20}$$

If the energy considerably exceeds the threshold value, a simple expression can be obtained for ξ_1 and ξ_2, since the expression under the root in Eq. (18) can be expanded. We then have the following condition on the radiated frequency interval

$$\xi_1=a^2/b-(1-v/c)\gtrsim\xi\gtrsim(1-v/c)=\xi_2, \tag{21}$$

i.e., the only frequencies radiated are in the interval from

$$\omega_{min}=a/\xi_1=l\pi e^2(N_1+N_2)/2\pi rvm \tag{22}$$

to

$$\omega_{max}=a/\xi_2=4\pi rv(E/mc^2)^2/l. \tag{23}$$

Let us pass to the calculation of the intensity and number of quanta per unit of particle path. For this we rewrite formula (14) for the case of equal thickness ($\Delta t_1 = \Delta t_2$) and for variable ξ. We also divide by $\hbar\omega$ and by the total distance covered, $nl/2$. Then the number of quanta radiated in 1 cm is given by the expression

$$\begin{aligned}dM &= \left(\frac{4\pi e^2}{m}\right)^2(N_2-N_1)^2\frac{e^2}{\hbar l^2}\,2\\ &\times\sum_{r=1}^{\infty}\frac{d\omega}{\omega^6}\left\{\frac{2\pi r}{l}\frac{v}{\omega}-\left(1-\frac{v}{c}\right)-\frac{\pi e^2}{m\omega^2}(N_1+N_2)\right\}\\ &\times\sin^2\left(\frac{\pi r}{2}-\frac{\pi e^2}{m}(N_1-N_2)\frac{l}{4\omega v}\right)\\ &\times\left\{\left(\frac{2\pi rv}{l\omega}\right)^2-\left(\frac{\pi e^2}{m\omega^2}(N_1-N_2)\right)^2\right\}^{-2}.\end{aligned} \tag{24}$$

Equation (24) becomes considerably simpler when

$$\Delta=|(N_1-N_2)/(N_1+N_2)|\ll 1. \tag{25}$$

In this case it can be rewritten as follows

$$\begin{aligned}dM &= \frac{4}{\pi}(N_1-N_2)^2\frac{r_0^2}{137}\frac{d\omega}{\omega^3}\\ &\times\sum_r\frac{lc^2}{r^3}\left[1-\frac{l\omega}{2\pi vr}\left(1-\frac{v}{c}+\frac{\pi e^2}{m\omega^2}(N_1+N_2)\right)\right].\end{aligned} \tag{26}$$

Here r_0 denotes the classical electron radius. A characteristic property of the frequency distributions (24) and (26) is their sharp concentration near $\omega_{\min}$.

As already pointed out above, formula (26) differs by a factor $16/\pi^2$ from the formula for radiation when the dielectric constant of the medium varies as $\epsilon = \epsilon_0 + \Delta\cos(2\pi z/l)$. A. Amatuni kindly informed us that he and O. Korkhmazyan have investigated this case, starting out with a Mathieu-type equation. Formula (19) of reference 1 was confirmed, however they managed to obtain the result without using the condition $\lambda \ll l$, but confined attention to radiation of the zeroth and first harmonic only.

The number of radiated quanta decreases as the inverse cube of the frequency (the intensity of the radiation consequently decreases as the inverse square of the frequency with increasing ω). At $\omega = \omega_{\min}$ and $\omega = \omega_{\max}$ the intensity and number of radiated quanta become zero, owing to the presence of the factor

$$1-\frac{v}{c}+\frac{\pi e^2}{m\omega^2}(N_1+N_2)-\frac{2\pi rv}{l\omega}$$

in Eqs. (24) and (26). We must also turn attention to the factor

$$\sin^2\left(\frac{\pi r}{2} - \frac{\pi e^2}{m}(N_1 - N_2)\frac{l}{4v\omega}\right), \qquad (27)$$

which occurs in Eq. (24). Since under the integral the effective value of ω is $\omega_{\min}$, (27) will be of the order

$$\cos^2\left(\frac{\pi e^2}{m}(N_1 - N_2)\frac{l}{4v\omega}\right) \approx \cos^2\left(\frac{\pi}{2} r \frac{N_1 - N_2}{N_1 + N_2}\right) \qquad (28)$$

for even r, and

$$\sin^2\left(\frac{\pi e^2}{m}(N_1 - N_2)\frac{l}{4v\omega}\right) \approx \sin^2\left(\frac{\pi}{2} r \frac{N_1 - N_2}{N_1 + N_2}\right) \qquad (29)$$

for odd r. Thus when (25) is fulfilled and r is not very large, only odd values of r contribute in the sum over r in Eq. (26).

In the range of frequencies which interest us, the term with r = 1 makes the principal contribution (if we consider the term r = 3, $\omega_{\min}$ decreases by a factor of three compared to the $\omega_{\min}$ with r = 1, and the number of radiated quanta for r = 3 will also be three times smaller than for the case r = 1). The total number of radiated quanta per unit of path for the case $\Delta \ll 1$ is found by integrating (26) over all frequencies. The result is

$$M = \sum_{r=1,\,3,\,5} \left(\frac{N_1 - N_2}{N_1 + N_2}\right)^2 \frac{1}{137\, lr} \frac{8}{3\pi}. \qquad (30)$$

We now consider formula (24) for the case when (25) is not satisfied. We write (24) using the notation of (16) and (17). Then the number of radiated quanta per unit path is

$$M = \sum \frac{16}{\pi l} \frac{\Delta^2}{137\, r} \int\limits_{b\xi_{min}/a^2}^{b\xi_{max}/a^2} \frac{[y - (1 - v/c)\, b/a^2 - y^2]\, dy}{\{1 - \Delta^2 y^2\}^2} \begin{matrix}\cos^2\\ \sin^2\end{matrix} \left(y\Delta \frac{\pi r}{2}\right), \qquad (31)$$

where y = bξ/a^2. The $\cos^2$ under the integral applies when r is even, and the $\sin^2$ when r is odd [cf. (27) – (29)].

If this formula is evaluated for energies appreciably in excess of the threshold value, we obtain the following number of quanta emitted in one centimeter: for Δ = 0.4; 0.6; 0.8; 1.0 the corresponding M is 0.095/100l, 0.21/100l, 0.36/100l, 0.54/100l (for r = 1); for Δ = 0.6 and 0.8 the respective values of M are 0.095/100l and 0.26/100l (for r = 2) or 0.03/100l and 0.13/100l (for r = 3).

As we have already noted, the majority of quanta are concentrated near $\omega_{\min}$, the value of which is given by expression (22). The radiation threshold is defined by formula (20). The intensity of higher harmonics is less, fewer quanta are radiated, and the threshold energy is lower, than for r = 1.

The case of layers of unequal thickness can be investigated by starting with formula (15). By introducing the variable y one can easily bring it into a form convenient for numerical calculation:

$$M = \frac{4}{137} \frac{1}{l\pi} (q + p)^2 \sum_r \frac{1}{r} \int \frac{dy\, [y - (b/a^2)(1 - v/c) - y^2]}{(1 - py)^2 (1 + qy)^2}$$

$$\times \sin^2\left[\frac{q}{p + q}\, \pi r - y\pi r\, \frac{pq}{p + q}\right],$$

$$p = \Delta t_1 (N_1 - N_2) / (N_1 \Delta t_1 + N_2 \Delta t_2), \quad q = p\Delta t_2 / \Delta t_1. \qquad (32)$$

---

[1] M. L. Ter-Mikaelyan, Doklady Akad. Nauk SSSR **134**, 318 (1960), Soviet Phys.-Doklady, in press.

[2] Ya. B. Faĭnberg and N. A. Khizhnyak, JETP **32**, 883 (1957), Soviet Phys. JETP **5**, 720 (1957).

[3] G. M. Garibyan, JETP **35**, 1435 (1958), Soviet Phys. JETP **8**, 1003 (1959).

Translated by D. Brill
309

SOVIET PHYSICS JETP VOLUME 12, NUMBER 6 JUNE, 1961

THEORY OF THE KAPITZA THERMAL DISCONTINUITY OF THE BOUNDARY BETWEEN LIQUID He^3 AND A SOLID BODY

I. L. BEKAREVICH and I. M. KHALATNIKOV

Institute for Physical Problems, Academy of Sciences U.S.S.R.

Submitted to JETP editor June 13, 1960

J. Exptl. Theoret. Phys. (U.S.S.R.) **39**, 1699-1712 (December, 1960)

The problem of motion in a Fermi liquid due to vibrations of the boundary is treated. The energy transferred to the liquid during thermal vibrations of the solid body and the related heat transfer at various temperatures of the liquid and the solid are computed by applying the resulting solutions. The thermal resistance derived is proportional to T^{-3}.

As is known,[1,2] in the transfer of heat between liquid He II and bodies surrounding it, a temperature discontinuity appears on the boundary, connected with the difficulty of the energy exchange between the phonons of the solid and He II. A similar temperature discontinuity also appears on the boundary of He^3 and a solid. The surface of the heated solid executes small vibrations. In such a case motion of the liquid takes place, and carries away part of the energy. However, this energy is shown to be small, thus, as in the case of He II, leads to the appearance of a temperature discontinuity.

We shall consider liquid He^3 in contact with the vibrating surface of a solid. At low temperatures, He^3 is a Fermi liquid, and its state is characterized by the distribution function of the excitations, which satisfies the kinetic equation

$$\frac{\partial n}{\partial t}+\frac{\partial n}{\partial r}\frac{\partial \varepsilon}{\partial p}-\frac{\partial n}{\partial p}\frac{\partial \varepsilon}{\partial r}=I(n). \qquad (1)$$

Here n is the distribution function, ϵ is the energy of the excitation, which is a functional of n, and I(n) is the collision integral.

Inasmuch as the velocity of sound in a solid is much greater than the velocity of the excitations on the Fermi surface, it can be assumed that all the points of the surface are vibrating with the same phase. Therefore, the distribution function will depend only on the z coordinate, which is perpendicular to the boundary of the body.

We seek a distribution function in the form $n = n_0 + n_1$, where n_0 is the equilibrium Fermi function for the temperature of absolute zero. The excitation energy in this case will be

$$\varepsilon=\varepsilon_0+\int f(p, p')\, n_1(p')\, dp', \quad f(p, p')=\delta\varepsilon(p)/\delta n(p'), \qquad (2)$$

where ϵ_0 is the excitation energy at T = 0.

By considering the linearized kinetic equation (1), it is easy to see that n_1 is proportional to $\partial n_0/\partial\epsilon \sim \delta(p - p_0)$, where p_0 is the limiting momentum. Therefore, n_1 can be represented in the form of the product of $\partial n_0/\partial\epsilon$ and some function ν, which depends on the direction of the momentum (and, naturally, on the coordinates and time); moreover, the momentum can everywhere be set equal to the limiting value.

Introducing a spherical set of coordinates, we can consider ν as a function of the angles θ and χ, where θ is the angle between the direction of p and the z axis, and χ is the azimuthal angle, measured from the direction of the tangential component of the velocity u_t of the wall.

Substituting n_1 in the expression for the energy of the excitation, and integrating over the absolute value of the momentum, we obtain the energy in the form of a series of spherical functions [by expanding $f(p, p')p_0$ in spherical harmonics]. For the case of He^3, we limit ourselves to the first two terms,[3] which are determined from experimental data:

$$\varepsilon=\varepsilon_0(p)-F_0\int \nu'\frac{d\Omega'}{4\pi}-3F_1\int \nu'\cos\vartheta\,\frac{d\Omega'}{4\pi}, \qquad (3)$$

where ϑ is the angle between the direction of the momentum p and the momentum of the integration p'; $\cos\vartheta = \cos\theta\cos\theta' + \sin\theta\sin\theta'\cos(\chi - \chi')$. The constants F_0 and $3F_1$ are respectively 4.65 and 1.3.

Substituting all these expressions in the kinetic equation and linearizing it, we obtain

$$-i\omega\nu+v_0\cos\theta\,\frac{\partial}{\partial z}\left[\nu+F_0\int \nu'\frac{d\Omega'}{4\pi}+3F_1\int \nu'\cos\vartheta\,\frac{d\Omega'}{4\pi}\right]=I(\nu), \qquad (4)$$

where ω is the vibration frequency and $v_0 = (\partial\epsilon_0/\partial p)_{p_0}$ is the velocity on the Fermi surface.

The characteristic frequency of the thermal vibrations of the surface of a solid has the value $\omega \sim kT/h$. Taking the value of the collision frequency of the excitations $1/\tau$ from the work of Abrikosov and Khalatnikov,[3] we obtain the result that for all temperatures, within the limits of applicability of the theory of a Fermi liquid (below 0.2° K), the condition $\omega\tau \gg 1$ is satisfied, which means a negligibly small role for the collisions. From considerations of mathematical convenience, one should not immediately drop the collision integral in the kinetic equation. However, it can be taken in the extremely simple form $I = -\nu/\tau$, which guarantees the convergence of the mathematical expressions. The quantity τ does not appear in the final result, because of the transition to the limit $\omega\tau \to \infty$.

As is seen from (4), it is convenient to introduce a new function

$$\varphi = \nu + F_0 \int \nu' \frac{d\Omega'}{4\pi} + 3F_1 \int \nu' \cos\vartheta \frac{d\Omega'}{4\pi}. \tag{5}$$

We denote

$$\varphi_0 = \int \varphi \frac{d\Omega}{4\pi}, \qquad \varphi_{1n} = \int \varphi \cos\theta \frac{d\Omega}{4\pi},$$
$$\varphi_{1t} = \int \varphi \sin\theta \cos\chi \frac{d\Omega}{4\pi}. \tag{6}$$

It is easy to see that

$$\int \nu \frac{d\Omega}{4\pi} = \frac{\varphi_0}{1+F_0}, \qquad \int \nu \cos\theta \frac{d\Omega}{4\pi} = \frac{\varphi_{1n}}{1+F_1},$$
$$\int \nu \sin\theta \cos\chi \frac{d\Omega}{4\pi} = \frac{\varphi_{1t}}{1+F_1}.$$

With the aid of these expressions the energy ϵ is written in the form

$$\varepsilon = \varepsilon_0 - \frac{F_0}{1+F_0}\varphi_0 - \frac{3F_1\cos\theta}{1+F_1}\varphi_{1n} - \frac{3F_1 \sin\theta\cos\chi}{1+F_1}\varphi_{1t}. \tag{7}$$

The values of φ_0 and $\varphi_{1n,t}$ depend on z. We shall omit the periodic dependence of all the quantities on the time. Finally, denoting $\cos\theta$ by μ and measuring the z coordinate in lengths of the mean free path $l = \nu_0\tau$, we get, going where possible to the limit $\omega\tau \to \infty$:

$$\mu \frac{\partial\varphi}{\partial z} + (1 - i\omega\tau)\varphi = -\frac{i\omega\tau F_0}{1+F_0}\varphi_0 - \frac{3i\omega\tau F_1}{1+F_1}\mu\varphi_{1n}$$
$$- \frac{3i\omega\tau F_1}{1+F_1}\sqrt{1-\mu^2}\cos\chi\varphi_{1t}. \tag{8}$$

It is necessary to add some boundary conditions to this equation. Inasmuch as the latter are shown to be non-trivial, we shall discuss these specially.

BOUNDARY CONDITIONS

The boundary conditions are determined by the character of the scattering of the excitations on the surface of the solid. Let us first consider the case of specular reflection of excitations from a moving surface. In the collision of an excitation with a smooth surface, the components of the momentum of the excitation parallel to the surface are conserved. The change in the normal component is determined by the law of energy conservation, which holds in the system of coordinates moving with the wall. As before, let p be the momentum in the stationary system of coordinates. Then the energy of the excitation in a set of coordinates moving with velocity u will be, in accord with the Galilean transformation,

$$\varepsilon' = \varepsilon(p) - \mathbf{pu}. \tag{9}$$

Writing out the expression for the energy of the excitation (7), and taking into account the conservation of the tangential component of the momentum, we get an equation which expresses the conservation of energy in the moving system of coordinates

$$\varepsilon_0(p_1) - \frac{3F_1}{1+F_1}\frac{p_{1z}}{p_0}\varphi_{1n}(z=0) - p_{1z}u_z = \varepsilon_0(p_2)$$
$$- \frac{3F_1}{1+F_1}\frac{p_{2z}}{p_0}\varphi_{1n}(z=0) - p_{2z}u_z,$$

where p_1 is the momentum before the collision with the wall and p_2 the momentum after the collision. Then we get, with accuracy up to the small quantity $u(\partial\epsilon_0/\partial p)^{-1}$

$$p_{2z} + p_{1z} = \frac{2p_0}{\partial\varepsilon_0/\partial p}\left[u_z + \frac{3F_1\varphi_{1n}(0)}{p_0(1+F_1)}\right]. \tag{10}$$

The requirement of equality of the number of incident excitations to the number of reflected excitations in the system in which the wall is at rest leads to the condition

$$n(p_1)(\partial\varepsilon/\partial p_{1z} - u_z)\,\partial p_{1z}\,dp_{1x}\,dp_{1y}$$
$$= n(p_2)(\partial\varepsilon/\partial p_{2z} - u_z)\,dp_{2z}\,dp_{2x}\,dp_{2y}. \tag{11}$$

Then, by making use of (9) and recalling than n is equal to $n_0 + n_1$, we get

$$n_0(\varepsilon_0(p_1)) + \frac{\partial n_0}{\partial\varepsilon}\nu\left(\frac{p_{1z}}{p_0}\right) = n_0(\varepsilon_0(p_2)) + \frac{\partial n_0}{\partial\varepsilon}\nu\left(\frac{p_{2z}}{p_0}\right). \tag{12}$$

Substituting p_{1z} from (10) and limiting ourselves to the first term in the expansion in powers of the difference $n_0(p_2) - n_0(p_1)$, we get [taking into account the definition (6) of the function φ],

$$\psi(\mu) = \psi(-\mu) - 2p_0u_z\mu. \tag{13}$$

Here and in what follows we shall denote by $\psi(\mu)$ the value of $\varphi(z, \mu)$ at $z = 0$.

In the case of diffuse reflection, in a system in which the surface is at rest, particles are emitted from it with an equilibrium distribution function. On the basis of (9), the quantity $\epsilon(\mathbf{p}) - \mathbf{p}\cdot\mathbf{u}$ will appear in the argument of the function. Moreover, one must take it into account that the mass flow through the moving surface must be equal to zero. This leads to the result that the particles emitted from the wall are distributed according to the Fermi distribution function, with a chemical potential differing from the limiting energy by a small constant value which we shall denote by $p_0u_z\xi$. We then have

$$n(p_z>0) = n_0\Big\{\varepsilon_0 - \frac{F_0\varphi_0}{1+F_0} - \frac{3\mu F_1\varphi_{1n}}{1+F_1} - \frac{3F_1\varphi_{1t}}{1+F_1}\sqrt{1-\mu^2}\cos\chi - p_0u_z(\mu+\xi) - p_0u_t\sqrt{1-\mu^2}\cos\chi\Big\}. \quad (14)$$

Expanding the right hand side in a series, and recalling the definition of φ, we obtain

$$\psi = -p_0u_z(\mu+\xi) - p_0u_t\sqrt{1-\mu^2}\cos\chi, \quad \mu>0. \quad (15)$$

The constant ξ is determined from the condition $j'_z = 0$, where

$$\mathbf{j}' = m\int n(\partial\varepsilon/\partial\mathbf{p} - \mathbf{u})\,d\tau \quad (16)$$

is the mass flow through the moving surface.

Substituting for n and ϵ and integrating over the absolute value of the momentum, we obtain the condition that determines ξ:

$$\varphi_{1n} = \frac{1}{2}\int_{-1}^{+1}\mu\psi(\mu)\,d\mu = -p_0u_z/3. \quad (17)$$

We note that this condition is automatically satisfied for specular reflection. Moreover, in order to determine the energy transferred to the liquid, we must know the force with which the liquid acts on the wall. It is expressed in terms of the momentum flux tensor Π_{ik}[3]

$$\Pi_{ik} = \int np_i\frac{\partial\varepsilon}{\partial p_k}\,d\tau + \delta_{ik}\Big[\int n\varepsilon\,d\tau - E\Big]. \quad (18)$$

In the approximation linear in φ we find

$$\Pi_{\alpha z} = -3\rho m^{-1}\psi_{2\alpha},$$

where

$$\psi_{2n} = \frac{1}{4\pi}\int\cos^2\theta\,\psi(\theta,\chi)\sin\theta\,d\theta\,d\chi,$$
$$\psi_{2t} = \frac{1}{4\pi}\int\sin\theta\cos\theta\cos\chi\,\psi(\theta,\chi)\sin\theta\,d\theta\,d\chi, \quad (19)$$

$\rho m^{-1} = N$ is the number of excitations per unit volume.

One can solve this problem exactly for the limiting cases of completely diffuse or completely specular reflection. In the first case, the Hopf-Wiener method is used for the solution of the problem. In the second case the problem is solved by expansion in a Fourier integral.

As a result of the solution (see below), the quantity ψ_2 can be written in the form

$$\psi_{2n} = -ap_0u_z, \qquad \psi_{2t} = -bp_0u_t, \quad (20)$$

Where the coefficients of proportionality a and b depend on the conditions of reflection of the particles at the wall and the characteristics of the liquid (F_0 and F_1). Inasmuch as the wavelength of the excitation $L/p_0 \sim 10^{-8}$ is of the order of interatomic distances, the reflection will rapidly become diffuse. However, as calculations show, the character of the reflection depends only weakly on the result.

We shall set down the solution of the problem in both cases.

1. DIFFUSE REFLECTION. LONGITUDINAL VIBRATIONS

The distribution function φ is a solution of Eq. (8) with the boundary conditions (1) and (17). A slightly modified Hopf-Wiener method can be used for its solution (the modification is connected with the fact that one must solve an inhomogeneous integral equation). A similar mathematical problem was solved previously by Fock.[4]

Because of the linearity of the problem, the solution can be broken up into two parts, corresponding to the two terms in the boundary condition (15) — proportional to u_z and u_t. The solution corresponding to the normal vibrations of the surface will be called longitudinal; that corresponding to tangential vibrations will be called transverse.

In this section we consider longitudinal vibrations. As follows from the boundary condition, φ does not depend on the angle χ and is a function of the coordinates z and $\mu = \cos\theta$. We change from the functions $\varphi(z,\mu)$, $\varphi_0(z)$, $\varphi_{1n}(z) \equiv \varphi_1(z)$ (inasmuch as $\varphi_{1t} = 0$) to their Laplace transforms.

$$\varphi(s,\mu) = \int_0^\infty\varphi(z,\mu)e^{-sz}\,dz, \quad \varphi_{01,}(s) = \int_0^\infty\varphi_{01,}(z)e^{-sz}\,dz. \quad (1.1)$$

Further, we operate everywhere only with functions of the argument s, so that the designation of the transform and the original by one and the same letter φ cannot lead to any misunderstanding. It follows from the boundedness of the initial functions that their Laplace transforms are analytic in the right half-plane.

Multiplying Eq. (8) by e^{-sz} and integrating over z, we get

$$(\mu s+1-i\omega\tau)\,\varphi(s,\mu)-\mu\psi(\mu)$$
$$=-\frac{i\omega\tau F_0}{1+F_0}\varphi_0(s)-\frac{3i\omega\tau F_1}{1+F_1}\mu\varphi_1(s) \tag{1.2}$$

Integrating the left and right hand sides of this expression over μ, we find the relation between φ_0 and φ_1:

$$\varphi_1(s)=\frac{\psi_1}{s}+\frac{i\omega\tau}{s}\,\frac{\varphi_0(s)}{1+F_0}. \tag{1.3}$$

In this case we neglect unity in comparison with $\omega\tau$. The transition to the limit $\omega\tau\to\infty$ is possible everywhere except for the factor $(\mu s+1-i\omega\tau)$ which stands in front of φ in the first term of (1.2), where the 1 is necessary to define the region of analyticity of the functions.

It follows from (17) that $\psi_1=-p_0u_t/3$; therefore, for the condition that $\varphi_1(s)$ be bounded at zero (which means the absence of undamped solutions) we have

$$[i\omega\tau/(1+F_0)]\varphi_0(0)=p_0u_z/3. \tag{1.4}$$

This solution replaces (17).

We substitute (1.3) in (1.2), and express φ in terms of φ_0. Then, integrating over μ, we obtain the equation relative to the function φ_0

$$\varphi_0\left\{1+\frac{1}{2}\int_{-1}^{+1}\frac{i\omega\tau F_0/(1+F_0)+3\mu(i\omega\tau)^2F_1/s(1+F_0)(1+F_1)}{\mu s+1-i\omega\tau}d\mu\right\}$$
$$=\frac{p_0u_z\,i\omega\tau F_1}{s(1+F_1)}\,\frac{1}{2}\int_{-1}^{+1}\frac{\mu d\mu}{\mu s+1-i\omega\tau}+\frac{1}{2}\int_{-1}^{+1}\frac{\mu\psi(\mu)\,d\mu}{\mu s+1-i\omega\tau}. \tag{1.5}$$

Substituting $\psi(\mu)$ for $\mu>0$, we have from the boundary condition (longitudinal part)

$$\varphi_0\left\{\frac{1}{1+F_0}+\left[\frac{F_0}{1+F_0}+\frac{3(i\omega\tau)^2F_1}{s^2(1+F_0)(1+F_1)}\right]w(s)\right\}$$
$$=-\frac{p_0u_z}{s^2}\left(\frac{i\omega\tau}{1+F_1}+\xi s\right)w(s)$$
$$+\frac{1}{2}\int_{-1}^{0}\frac{\mu[\psi(\mu)+p_0u_z(\mu+\xi)]}{\mu s+1-i\omega\tau}d\mu, \tag{1.6}$$

where

$$w(s)=1-\frac{i\omega\tau}{2s}\ln\frac{1-i\omega\tau-s}{1-i\omega\tau+s}. \tag{1.7}$$

When $\mu<0$, the function $\psi(\mu)$, which enters in the last term of the right-hand side of (1.6), can be expressed in terms of $\varphi_0(s)$. Thus the resultant equation (1.6) is an inhomogeneous integral equation in φ_0. To solve it, by the Hopf-Wiener method, it is necessary to construct from the expressions at hand a certain function of complex variable analytic in the entire plane.

Let us investigate the properties of the quantities entering into (1.6). We denote the quantity in the curly brackets on the left hand side of (1.6) by $\Delta(s)$:

$$\Delta(s)=\frac{1}{1+F_0}+\frac{F_0}{1+F_0}\,\frac{s^2-s_1^2}{s^2}\,w(s), \tag{1.8}$$

where

$$s_1^2=3(\omega\tau)^2F_1/F_0(1+F_1). \tag{1.9}$$

The function $\Delta(s)$ is analytic in the strip $|\mathrm{Re}\, s|<1$. Moreover, we are interested in the roots of $\Delta(s)$ located inside this strip. They correspond to sound vibrations in a Fermi liquid, more accurately to "zero sound,"[3] since they are found in the region $\omega\tau\gg1$.

As is seen from (1.7) and (1.8), the dispersion equation depends on the argument $s/i\omega\tau$. The width of the strip corresponding to this variable is equal to $2/\omega\tau$. Therefore, inside this strip and at a sufficiently large $\omega\tau$, no roots are expected excepting those corresponding to zero sound and lying on the real axis.

Using the results of reference 3, we shall establish the fact that the roots are found at the points $s=\pm s_0$ ($\mathrm{Re}\, s_0>0$).

Starting out from this point, we represent the quantity $\Delta(s)$ in the form

$$\Delta(s)=\frac{s^2-s_0^2}{s^2-(1-i\omega\tau)^2}G(s). \tag{1.10}$$

The function $G(s)$ is analytic in the strip $|\mathrm{Re}\, s|<1$, contains no zeros in it and, as is easy to establish, approaches unity for $s\to\infty$.

Therefore, $\ln G(s)$ can be written in the form

$$\ln G(s)=\ln g_+(s)-\ln g_-(s), \tag{1.11}$$

according to the Cauchy formula, where

$$g_\pm(s)=\exp\left\{\frac{1}{2\pi i}\int_{\pm\beta-i\infty}^{\pm\beta+i\infty}\frac{\ln G(u)}{u-s}du\right\}. \tag{1.12}$$

Here $0<\beta<1$; $g_+(s)$ is analytic for $\mathrm{Re}\, s<\beta$ and $g_-(s)$ for $\mathrm{Re}\, s>-\beta$.

The integral on the right hand side of (1.6) is denoted by $Q(s)$. It is analytic for $\mathrm{Re}\, s<1$.

We shall express $w(s)$ and $\Delta(s)$ in terms of the functions g_+ and g_-. Substituting the resultant expressions in (1.6) and multiplying the left and right hand sides by

$$(s-s_1)(s-1+i\omega\tau)/(s-s_0)g_+(s),$$

we obtain

$$\left[\varphi_0(s)(s-s_1)+\frac{F(s)}{s+s_1}\right]\frac{s+s_0}{s+1-i\omega\tau}\,\frac{1}{g_-(s)}$$
$$=Q(s)\frac{(s-s_1)(s-1+i\omega\tau)}{(s-s_0)g_+(s)}-\frac{F(s)}{s+s_1}\,\frac{\Delta(-s_1)(s-1+i\omega\tau)}{(s-s_0)g_+(s)}, \tag{1.13}$$

where

$$F(s) = p_0 u_z \frac{1+F_0}{F_0}\left(\frac{i\omega\tau}{1+F_1} + \xi s\right). \qquad (1.14)$$

The right hand side of (1.13) has a pole at $s = -s_1$, where s_1 is that root of (1.9) which has a positive real part. In order to get rid of the pole, we add the quantity

$$\frac{F(-s_1)(s_1+1-i\omega\tau)\,\Delta(s_1)}{2s_1(s_1+s_0)\,g_+(-s_1)}\,\frac{s-s_1}{s+s_1} \qquad (1.15)$$

to both sides of the equation. Then, on the right hand side of (1.13) we shall have a function which is analytic for $\operatorname{Re} s < \min(\beta, \operatorname{Re} s_0)$ and, as follows from the integral representation of $Q(s)$, is bounded as $s \to \infty$.

On the left hand side we shall have a function which is analytic and bounded (if we assume that $\varphi_0 \sim 1/s$ as $s \to \infty$) in the half-plane $\operatorname{Re} s > 0$.

Inasmuch as these two functions are identical at the pole $0 < \operatorname{Re} s < \min(\beta, \operatorname{Re} s_0)$, then one is the analytic continuation of the other and, consequently, according to Liouville's theorem, the total function is equal to a constant. It is easy to determine this constant by setting $s = s_1$ on the left hand side.

Finally, the solution will be (for $\operatorname{Re} s > 0$)

$$\varphi_0(s) = -\frac{F(s)}{s^2-s_1^2} + \frac{s+1-i\omega\tau}{s+s_0}\,g_-(s)$$
$$\times\left[\frac{F(s_1)(s_1+s_0)}{2s_1(s_1+1-i\omega\tau)\,g_-(s_1)}\,\frac{1}{s-s_1}\right.$$
$$\left. - \frac{F(-s_1)\,\Delta(s_1)(s_1+1-i\omega\tau)}{2s_1(s_1+s_0)\,g_+(-s_1)}\,\frac{1}{s+s_1}\right]. \qquad (1.16)$$

Thus, actually, $\varphi_0(s) = \mathrm{const}/s$ as $s \to \infty$, and is analytic in the right half-plane.

The function $F(s)$, which is determined by Eq. (1.14), contains ξ. Substituting the solution of $\varphi_0(s)$ in (1.4), we get, after several transformations,

$$\frac{g_-(0)}{2s_0}\left[\frac{i\omega\tau}{1+F_1}(A+B) + \xi s_1(A-B)\right] = -1,$$

where

$$A = \frac{s_1+s_0}{(s_1+1-i\omega\tau)\,g_-(s_1)}, \quad B = \frac{(s_1+1-i\omega\tau)\,\Delta(s_1)}{(s_1+s_0)\,g_+(-s_1)}, \qquad (1.17)$$

from which ξ is determined.

Finally, expanding the right and left sides of (1.5) in a series in s, and equating coefficients for the first powers of s, we obtain an expression for ψ_{2n}

$$\psi_{2n} = -\frac{(i\omega\tau)^2}{(1+F_0)(1+F_1)}\left(\frac{d\varphi_0}{ds}\right)_{s=0}$$
$$= \frac{p_0 u_z}{3F_1}\left\{\xi - i\omega\tau\left[\frac{g'_-(0)}{g_-(0)} - \frac{s_0+i\omega\tau}{i\omega\tau s_0}\right]\right.$$
$$\left. + \frac{i\omega\tau g_-(0)}{2s_0 s_1}\left[\frac{i\omega\tau}{1+F_1}(A-B) + \xi s_1(A+B)\right]\right\}. \qquad (1.18)$$

We introduce the notation $s_1 = x_1\omega\tau$ and $s_0 = x_0(1-i\omega\tau)$. The numerical value of x_0 is found in reference 3 and is equal to 0.58. The quantity x_1 is equal to $\sqrt{3F_1/F_0(1+F_1)}$ and its numerical value is equal to 0.44.

We shall compute the function $\ln g(\omega\tau y)$, where $y > 0$ is a real quantity. This function entered into the final formula. From the definition (1.12) we have

$$\ln g_-(\omega\tau y) = \frac{1}{2\pi i}\int_{-\beta-i\infty}^{-\beta+i\infty} \frac{\ln G(u)}{u-\omega\tau y}\,du. \qquad (1.19)$$

To compute the integral, we proceed in two ways. First we close the path of integration by another large circle $R \to \infty$ in the right half-plane, as is shown in the drawing. In this case, it is necessary to go around the cut along the line $u = x(1-i\omega\tau)$, $x \geq 1$ (x is real), which removes the ambiguity of the function $G(u)$ for $|\operatorname{Re} u| > 1$ [according to Eqs. (1.7) – (1.10) the function $G(u)$ contains a logarithmic term]; moreover, it is necessary to take into account the presence of a pole in the expression under the integral when $u = \omega\tau y$.

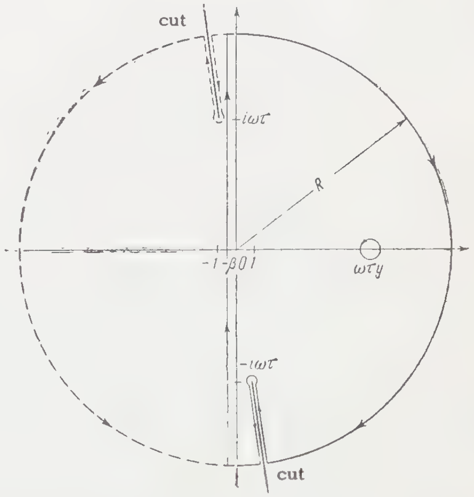

Integration contour for the integral in (1.19). The solid curve is the contour of integration in the first case and the dashed curve is the contour in the second.

We then close the contour of integration in the left hand plane where the cut is taken along the line $u = -x(1-i\omega\tau)$, $x \geq 1$. Carrying out the calculation at the pole and transforming to the variable x in the integration around the cut, we obtain in the two cases

$$\ln g_-(\omega\tau y) = -\ln G(\omega\tau y) - \frac{1}{\pi}\int_1^\infty \frac{\tan^{-1} S}{x-iy}\,dx,$$

$$\ln g_-(\omega\tau y) = \frac{1}{\pi}\int_1^\infty \frac{\tan^{-1} S}{x+iy}\,dx, \qquad (1.20)$$

respectively, where

$$S=\pi F_0\left(1+\frac{x_1^2}{x^2}\right)\Big/\,2x\left[1+F_0\left(1+\frac{x_1^2}{x^2}\right)\left(1+\frac{1}{2x}\ln\frac{x-1}{x+1}\right)\right].$$

The arctangent appearing in the formulas is the difference of the expression in the integrand on the two edges of the cut and is determined in the interval $(0, \pi)$.

Equating these two expressions, we find

$$g_-(\omega\tau y)=\frac{1}{\sqrt{G(\omega\tau y)}}\,e^{-iy\Phi(y)}, \tag{1.21}$$

where

$$\Phi(y)=\frac{1}{\pi}\int_1^\infty\frac{\tan^{-1}S}{x^2+y^2}\,dx. \tag{1.22}$$

Differentiating $g_-(\omega\tau y)$ with respect to y and then setting $y = 0$, we get

$$g_-'(0)/g_-(0)=-i\Phi(0)/\omega\tau. \tag{1.23}$$

Making use of Eq. (1.12) and the evenness of the function $G(u)$, it is not difficult to show that the quantity $g_+(-s_1)$ appearing in (1.17) is expressed in terms of $g_-(s_1)$:

$$g_+(-s_1)=1/g_-(s_1). \tag{1.24}$$

Substituting the resultant expressions in Eqs. (1.17) and (1.18), and going to the limit as $\omega\tau \to \infty$, we get

$$\psi_{2n}=\frac{p_0u_z}{3F_1}\left\{\frac{2\sqrt{1+F_1}-(2+F_1)\cos\delta}{x_1(1+F_1)\sin\delta}-\frac{1-x_0}{x_0}-\Phi(0)\right\}, \tag{1.25}$$

where

$$\delta=x_1\Phi(x_1)-\tan^{-1}\frac{x_0}{x_1}+\tan^{-1}\frac{1}{x_1}. \tag{1.26}$$

As a result of the numerical computations, we find $\psi_{2n} \approx -0.3\, p_0u_z$.

2. DIFFUSE REFLECTION. TRANSVERSE VIBRATIONS

We now consider the solution connected with the tangential vibrations of the surface. In this case, the equation will be proportional to $\cos\chi$, which corresponds to an angular dependence on χ of the second term in the boundary condition (15). The normalization condition (17) need not be considered since, for $\varphi \sim \cos\chi$, the flow of particles through the surface vanishes after integration of $\cos\chi$ over the angle χ.

Proceeding as before to the Laplace transform, and taking it into account that φ_0, and the current $j \sim \varphi_{1n}$, is equal to zero, we obtain from Eq. (8)

$$(s\cos\theta+1-i\omega\tau)\varphi-\cos\theta\psi(\theta,\chi)$$
$$=-3i\omega\tau F_1/(1+F_1)^{-1}\sin\theta\cos\chi\varphi_{1t}, \tag{2.1}$$

with the boundary condition

$$\psi(\theta,\chi)=-p_0u_t\sin\theta\cos\chi,\qquad 0<\theta<\pi/2. \tag{2.2}$$

In what follows, it will be convenient for us to use the angle θ in place of μ.

Multiplying (2.1) by $\sin\theta\cos\chi/(s\cos\theta+1-i\omega\tau)$ and integrating over the solid angle, we obtain

$$\varphi_{1t}(s)\left[1+\frac{3i\omega\tau F_1}{4\pi(1+F_1)}\int\frac{\sin^3\theta\cos^2\chi\,d\theta\,d\chi}{s\cos\theta+1-i\omega\tau}\right]$$
$$=\frac{1}{4\pi}\int\frac{\sin\theta\cos\theta\cos\chi\psi(\theta,\chi)}{s\cos\theta+1-i\omega\tau}\sin\theta\,d\theta\,d\chi. \tag{2.3}$$

Substituting $\psi(\theta, \chi)$ for $\theta < \pi/2$ from (2.2), and carrying out the integration, we find

$$\varphi_{1t}\Delta(s)=-\frac{p_0u_t}{2s}\left[\frac{1}{3}-\frac{s^2-(i\omega\tau)^2}{s^2}w(s)\right]$$
$$+\int_0^{2\pi}d\chi\int_{\pi/2}^{\pi}\frac{\sin^2\theta\cos\theta\cos\chi\cdot[\psi(\theta,\chi)+p_0u_t\sin\theta\cos\chi]}{s\cos\theta+1-i\omega\tau}\,d\theta\,d\chi, \tag{2.4}$$

where

$$w(s)=1-\frac{i\omega\tau}{2s}\ln\frac{1-i\omega\tau-s}{1-i\omega\tau+s}, \tag{2.5}$$

$$\Delta(s)=1+\frac{3F_1}{2(1+F_1)}\left\{\left[1-\frac{(i\omega\tau)^2}{s^2}\right]w(s)-1\right\}. \tag{2.6}$$

Equation (2.4) is similar to Eq. (1.6) and is solved in the same way. As was shown in reference 3, there does not exist a "transverse zero sound" (which propagates at frequencies $\omega\tau \gg 1$) which means the absence of roots of $\Delta(s)$; as $s \to \infty$, the quantity $\Delta(s) \to 1$. Therefore, by analogy to Eqs. (1.11) – (1.13), we can write

$$\Delta(s)=\Delta_+(s)/\Delta_-(s), \tag{2.7}$$

where $\Delta_+(s)$ is analytic in the region $\operatorname{Re} s < \beta < 1$ and $\Delta_-(s)$ is analytic for $\operatorname{Re} s > -\beta$ (β has the same meaning as before).

We write down an expression for $\Delta_-(s)$:

$$\Delta_-(s)=\exp\left\{\frac{1}{2\pi i}\int_{-\beta-i\infty}^{-\beta+i\infty}\frac{\ln\Delta(u)}{u-s}\,du\right\}. \tag{2.8}$$

With the help of these expressions, Eq. (2.4) can be rewritten in the form

$$\left(s\varphi_{1t}(s)-\frac{p_0u_t}{3}\frac{1+F_1}{F_1}\right)\frac{1}{\Delta_-(s)}=\frac{sQ(s)}{\Delta_+(s)}-\frac{p_0u_t\Delta(0)(1+F_1)}{3F_1\Delta_+(s)}, \tag{2.9}$$

where $Q(s)$ denotes the last term in the right hand side of (2.4), which is analytic for $\operatorname{Re} s < 1$.

Repeating all of the discussions of the previous section, we obtain the solution

$$\varphi_{1t}(s)=\frac{p_0u_t}{3}\frac{1+F_1}{F_1}\frac{1}{s}\left[1-\frac{\Delta_-(s)}{\Delta_-(0)}\right]. \tag{2.10}$$

Making use of this expression, it is easy to obtain the quantity ψ_{2t} which is of interest to us and which is defined in (19). Setting s = 0 in (2.3), we find

$$\psi_{2t} = -\frac{i\omega\tau}{1+F_1}\varphi_{1t}(0) = p_0u_t\frac{i\omega\tau}{3F_1}\frac{\Delta'_-(0)}{\Delta_-(0)}. \qquad (2.11)$$

By analogy to the previous section, we can obtain (only now $\Delta(s)$ is given by Eq. (2.6))

$$\frac{\Delta'_-(0)}{\Delta_-(0)} = -\frac{1}{i\omega\tau}\frac{1}{\pi}\int\limits_1^\infty \frac{\tan^{-1}S'}{x^2}\,dx,$$

$$S' = \frac{\dfrac{3\pi F_1}{4x(1+F_1)}\left(1-\dfrac{1}{x^2}\right)}{\left\{1-\dfrac{3F_1}{2(1+F_1)}\left[1-\dfrac{x^2-1}{x^2}\left(1+\dfrac{1}{2x}\ln\dfrac{x-1}{x+1}\right)\right]\right\}}. \qquad (2.12)$$

The arctangent in the expression under the integral sign is determined in the interval $(0, \pi)$.

Substituting (2.12) in (2.11), we find the final expression $\psi_{2t} = -bp_0u_t$, where

$$b = \frac{1}{3\pi F_1}\int\limits_1^\infty \frac{\tan^{-1}S'}{x^2}\,dx. \qquad (2.13)$$

The numerical value of $b \approx 0.05$.

3. SPECULAR REFLECTION

In this case the solution can be obtained by an expansion in a Fourier integral, for which one must determine the function $\varphi_0(z)$ and $\varphi_{1n} \equiv \varphi_1(z)$ for the value $z < 0$. We continue $\varphi_0(z)$ into negative values of the argument as an even function fashion, and $\varphi_1(z)$ as an odd one. The validity of this continuation will be confirmed by the solution.

We seek the function $\varphi(z, \mu)$ in the form

$$\varphi(z,\mu) = \chi(z,\mu) + \begin{cases} -2p_0u_z\mu\exp\{-z(1-i\omega\tau)/\mu\}, & \mu > 0, \\ 0, & \mu < 0. \end{cases} \qquad (3.1)$$

As follows from (13), the boundary condition for χ will be

$$\chi(z=0,\mu) = \chi(z=0,-\mu). \qquad (3.2)$$

The equation for χ is obtained by the substitution of (3.1) in (8):

$$\mu\frac{\partial\chi}{\partial z} + (1-i\omega\tau)\chi = -\frac{i\omega\tau F_0}{1+F_0}\chi_0$$
$$-3\mu\frac{i\omega\tau F_1}{1+F_1}\chi_1 + \Phi_0 + 3\mu\Phi_1, \qquad (3.3)$$

where

$$\Phi_0(z) = 2p_0u_z\frac{i\omega\tau F_0}{1+F_0}\frac{1}{2}\int\limits_0^1\mu\,\exp\left\{-\frac{z}{\mu}(1-i\omega\tau)\right\}d\mu,$$

$$\Phi_1(z) = 2p_0u_z\frac{i\omega\tau F_1}{1+F_1}\frac{1}{2}\int\limits_0^1\mu^2\exp\left\{-\frac{z}{\mu}(1-i\omega\tau)\right\}d\mu. \qquad (3.4)$$

We make the continuation of Φ_0 even for negative values and that of Φ_1 odd. Further, we transform to the Fourier components

$$\chi(z,\mu) = \frac{1}{2\pi}\int\chi(k,\mu)\,e^{ikz}\,dk,$$

$$\chi_{0,1}(z) = \frac{1}{2\pi}\int\chi_{0,1}(k)\,e^{ikz}dk. \qquad (3.5)$$

Equation (3.3) reduces to an algebraic equation relative to the Fourier components

$$(ik\mu + 1 - i\omega\tau)\chi(k,\mu)$$
$$= -\frac{i\omega\tau F_0}{1+F_0}\chi_0 - \frac{3\mu i\omega\tau F_1}{1+F_1}\chi_1 + \Phi_0(k) + 3\mu\Phi_1(k), \qquad (3.6)$$

where

$$\Phi_{0,1}(k) = \int\limits_{-\infty}^{+\infty}\Phi_{0,1}(z)\,e^{-ikz}\,dz. \qquad (3.7)$$

Integrating the left and right sides of (3.6) with respect to μ, we can express χ_0 in terms of χ_1.

$$\chi_0(k) = \frac{1+F_0}{i\omega\tau}[ik\chi_1(k) - \Phi_0(k)]. \qquad (3.8)$$

Substituting this expression in (3.6), dividing the left and right sides by $(ik\mu + 1 - i\omega\tau)/\mu$ and integrating over μ, we get

$$\chi_1(k) = \frac{w(k)}{ik}\frac{(1+F_0)\Phi_0(k) - 3\omega\tau k^{-1}\Phi_1(k)}{\Delta(k)}, \qquad (3.9)$$

where

$$w(k) = 1 - \frac{\omega\tau}{2k}\ln\frac{1-i\omega\tau-ik}{1-i\omega\tau+ik},$$

$$\Delta(k) = 1 + \left(F_0 + \frac{3(i\omega\tau)^2F_1}{(ik)^2(1+F_1)}\right)w(k). \qquad (3.10)$$

Let us prove that the boundary condition (3.2) is satisfied. It follows from (3.6) — (3.9) that

$$\chi(z=0,\mu) = \frac{1}{2\pi}\int\limits_{-\infty}^{+\infty}\frac{A_0(k)+\mu A_1(k)}{ik\mu+1-i\omega\tau}\,dk, \qquad (3.11)$$

where $A_0(k)$ is an even function and $A_1(k)$ is odd. If we replace k by $-k$ in the integral, it is easy to see that

$$[\chi(\mu) - \chi(-\mu)]_{z=0} = 0.$$

The solution (3.9) and Eq. (3.8) demonstrate the validity of the continuation of $\varphi_0(z)$ and $\varphi_1(z)$ for negative z.

Let us calculate the quantity

$$\psi_{2n} = \frac{1}{2}\int\limits_{-1}^{+1}\mu^2\psi(\mu)\,d\mu.$$

It follows from (3.1) that

$$\varphi_2(z) = \frac{1}{2\pi}\int\chi_2(k)\,e^{ikz}\,dk$$

$$+\frac{1}{2}\int\limits_0^1(-2p_0u_z)\,\mu^3\exp\left\{-\frac{z}{\mu}(1-i\omega\tau)\right\}d\mu. \qquad (3.12)$$

We find $\chi_2(k)$ by multiplying (3.6) on both sides by μ and integrating:

$$ik\chi_2(k) = i\omega\tau(1+F_1)^{-1}\chi_1(k) + \Phi_1(k). \qquad (3.13)$$

By determining the functions $\Phi_0(k)$ and $\Phi_1(k)$ from (3.4) and (3.7), and substituting $\chi_1(k)$ from (3.9), we get after lengthy transformations and transition to the limit as $\omega\tau \to \infty$

$$\psi_{2n} = -\frac{2}{3}\frac{p_0 u_z}{1+F_1}\frac{1}{2\pi i}$$

$$\times \int_{-\infty}^{+\infty} \frac{\omega\tau}{k^2} \frac{1+[F_0+3(\omega\tau/k^2)]\,w(k)}{1+[F_0+3(\omega\tau/k)^2 F_1/(1+F_1)]\,w(k)}\,dk. \qquad (3.14)$$

The integrand has a pole in the upper half plane at the point $k = \omega\tau x_0(1+i\epsilon)$ $(x_0 = 0.58;\ \epsilon = 1/\omega\tau)$ which corresponds to "zero sound," and also a cut along the line $k = x\omega\tau(1+i\epsilon)$, $x \geq 1$ (x is real).

Closing the integration contour from above and going around the cut and the pole, we find

$$\psi_{2n} = -2\frac{p_0 u_z}{(1+F_1)^2}\left\{\frac{1}{F_0 x_0^3}\left[F_0\frac{x_0^2}{1-x_0^2}\left(1+\frac{x_1^2}{x_0^2}\right)^2 - \left(1+3\frac{x_1^2}{x_0^2}\right)\right]^{-1}\right.$$

$$+\frac{1}{2}\int_1^{\infty}\left(\frac{\pi^2 F_0^2}{4x^2}\left(1+\frac{x_1^2}{x^2}\right)^2 + \left[1+F_0\left(1+\frac{x_1^2}{x^2}\right)\right.\right.$$

$$\left.\left.\left.\times\left(1+\frac{1}{2x}\ln\frac{x-1}{x+1}\right)\right]^2\right)^{-1} x^{-5}dx\right\}, \qquad (3.15)$$

where

$$x_1^2 = 3F_1/F_0(1+F_1).$$

The numerical value of ψ_{2n} is determined essentially by the first term in the curly brackets, which is equal to the residue at the pole. The second term, which corresponds to the circuit around the cut, is much less. Numerically, we have $\psi_{2n} \approx -0.3\, p_0 u_z$.

4. THERMORESISTANCE

Knowing the pressure exerted by the liquid, it is easy to compute the energy transferred per unit time. It is equal to the work of the pressure forces in moving the wall

$$\Delta E = -\frac{1}{2}\sum_\alpha \int \Pi_{\alpha z} u_\alpha dS, \qquad (4.1)$$

where the integration is carried out over the surface of the solid; the factor ½ appears as a result of averaging over the period of vibration of the wall ($\Pi_{\alpha z} \sim u_\alpha$).

Expressing $\Pi_{\alpha z}$ in terms of the velocity of the surface by Eqs. (19) and (20), we write

$$|\Delta E| = \frac{3}{2} p_0 \frac{\rho}{m}\int (a|u_z|^2 + b|u_t|^2)\,dS. \qquad (4.2)$$

Further, we can use the results of the work of one of the authors[2] on the determination of the thermal discontinuity between He II and the solid. The energy flow directed from the surface of a solid having a temperature T into the liquid is equal to[2]

$$W = \frac{3}{2} p_0 \frac{\rho}{m}\int n\left(\frac{h\omega}{kT}\right)\left\{(au_{z1}^2 + bu_{t1}^2)\frac{\omega^2 V d\Omega}{2(2\pi c_1)^3}\right.$$

$$\left. + (au_{z2}^2 + bu_{t2}^2)\frac{\omega^2 V\, d\Omega}{2(2\pi c_2)^3} + (au_{z3}^2 + bu_{t3}^2)\frac{2\pi\omega s}{(2\pi c_3)^2}\right\} d\omega, \qquad (4.3)$$

where c_i ($i = 1, 2, 3$) are the velocities of the longitudinal (1), transverse (2) and surface (3) waves; u_{zi} are the velocity components normal to the boundary, u_{ti} are the velocity amplitudes tangential to the boundary, associated with the different types of vibrations; n is the Planck distribution function for the phonons.

Using the results of quantization of the surface vibrations[2] we get

$$W(T) = \frac{3}{2} p_0 \frac{\rho}{m}\frac{4\pi^5}{15\rho_T}\frac{(kT)^4}{(2\pi h c_2)^3}\left[aF\left(\frac{c_1}{c_2}\right) + b\Phi\left(\frac{c_1}{c_2}\right)\right], \qquad (4.4)$$

where ρ_T is the density of the solid; F and Φ are functions of the elastic constants of the solid, arising as the result of integration over the angles of incidence of the phonons in Eq. (4.4) (u_z and u_t depend on the direction of the momentum of the incident phonon).

The function F was computed in reference 2 for certain bodies, and has the order of unity. The function Φ is equal to

$$\Phi = \frac{1}{4\pi h\omega}\left\{\int\left[\left(\frac{c_2}{c_1}\right)^3 u_{t1}^2 + u_{t2}^2\right]\frac{V d\Omega}{2} + \frac{(2\pi)^2}{\omega}\frac{c_2^3}{c_3^2}u_{t3}^2 s\right\} \qquad (4.5)$$

and is also of the order of unity.

When the temperatures of the liquid and solid are equal, the heat fluxes from one to the other are equal and are given by Eq. (4.4). For different temperatures, the resulting energy flux is equal to the flux difference

$$Q = W(T+\Delta T) - W(T) = \frac{1}{R(T)}\Delta T, \qquad (4.6)$$

where the thermoresistance of the boundary R(T) is equal to

$$R = \frac{1}{aF + b\Phi}\frac{5\rho_T}{8\pi^5}\left(\frac{2\pi h c_2}{kT}\right)^3\frac{1}{kp_0\rho/m}. \qquad (4.7)$$

As is seen, on the basis of the values obtained for a and b under different reflection conditions at the wall, R depends weakly on the character of the reflection. The thermoresistance is proportional to T^{-3} as in the case of He II.

The formula thus derived is valid in the low-temperature region, where a linear law applies for the temperature dependence of the specific heat of He^3 (below 0.2° K). For temperatures above 0.2°, the principal mechanism of heat transfer from the solid to the liquid He^3 will be radiation of sound by the heated surface of the solid. The corresponding formula was obtained in reference 2:

$$Q_{\mathbf{so}} = \frac{\rho}{\rho_T} c_l \frac{16\pi^5}{15}\left(\frac{kT}{2\pi hc_2}\right)^3 Fk\Delta T, \qquad (4.8)$$

where c_l is the sound velocity in the liquid.

It is interesting to compare the thermoresistance of the boundary at low and high temperatures, inasmuch as their temperature dependences are identical. We get the following expression for the thermoresistance ratio from Eqs. (4.7) and (4.8):

$$\frac{R_{He^3}}{R_{\mathbf{so}}} = \frac{2\pi^2 h^3 (\rho c)_{He^3}}{p_0^4} \frac{F}{aF + b\Phi}. \qquad (4.9)$$

This ratio is approximately 3. Thus, in the transition to low temperatures (less than 0.2° K), a relative increase in the thermoresistance should be observed (change in the coefficient of T^{-3}).

The experiments of Lee and Fairbank[5] were carried out at high temperatures. The temperature dependence R(T) obtained in their experiments agree with Eq. (4.8). The ratio Q_{He^4}/Q_{He^3} was also measured in their research. According to (4.8), it is equal to the ratio of the acoustic resistances of He^4 and He^3

$$Q_{He^4}/Q_{He^3} = (\rho c)_{He^4}/(\rho c)_{He^3} \approx 2,$$

which agrees with the results of reference 5.

So far as the absolute values of R in He^3 are concerned, calculation by Eq. (4.8) with known values of the elastic constants for copper give results which, as in the case of He II differ several fold from the measured values.

In conclusion, the authors express their deep gratitude to Academician L. D. Landau for participation in the discussion of this question.

---

[1] P. L. Kapitza, JETP **11**, 1 (1941).

[2] I. M. Khalatnikov, JETP **22**, 687 (1952).

[3] A. A. Abrikosov and I. M. Khalatnikov, Usp. Fiz. Nauk **66**, 177 (1958), Soviet Phys. Uspekhi **1**, 68 (1959).

[4] V. A. Fock, Математический сборник (Mathematical Collection) **14**, 3 (1944).

[5] D. M. Lee and H. A. Fairbank, Phys. Rev. **116**, 1359 (1959).

Translated by R. T. Beyer
310

SOVIET PHYSICS JETP VOLUME 12, NUMBER 6 JUNE, 1961

ON THE BOND IN THE $C^{12} - C^{12}$ *NUCLEAR MOLECULE*

A. S. KOMPANEETS

Institute of Chemical Physics, Academy of Sciences, U.S.S.R.

Submitted to JETP editor June 13, 1960; resubmitted August 31, 1960

J. Exptl. Theoret. Phys. (U.S.S.R.) **39**, 1713-1715 (December, 1960)

It is shown that "molecular" states of two nuclei may exist as the result of a common orbit of a strongly excited neutron.

RECENTLY data have appeared on the scattering of nuclei of carbon on carbon targets, which indicate the existence of resonance quasi-levels.[1] These levels are described by a "molecular" state with a lifetime of the order of 10^{-21} sec.

The present note does not aim at giving an explanation of the experiments of Almquist, which are not yet complete. It will only be shown that quasi-stable states of two nuclei can exist as distances exceeding the dimensions of the zone of diffuseness of the nuclear boundary. This state must be regarded as a certain limiting case, which demonstrates the possibility of a less than a complete separation, the mechanism of which is less clearly developed.

A bond can exist in such a quasi-molecule because of an orbit of a strongly excited neutron common to both nuclei. If the energy of such a neutron is close to the extraction threshold (for example, by 1 Mev less), then the wave function outside the nucleus falls off at distances greater than the radius of action of the nuclear forces. Calculation shows that the resulting force of interaction between the nuclei due to the energy of this neutron and the Coulomb repulsion becomes attractive at such distances from the nucleus for which one can already speak of a separate existence of both nuclei, i.e., outside the zone of diffuseness of the nuclear boundary.

In the series of experiments of Almquist, the energy of the colliding nuclei was evidently insufficient for excitation of the single-particle neutron level (this was pointed out to us by A. S. Davydov). One can therefore assume that the limiting case which we are considering here did not exist in those experiments, but rather some intermediate case in which the zones of diffuseness of the nuclear boundaries partially overlapped. In other words, the present note does not have any direct relation to these experiments.

Thus the situation here is similar to that which exists in the deuteron. Therefore, we can carry out quantum mechanical calculations of the binding energy with sufficient accuracy by considering both nuclei as potential wells. At an infinite distance from one another, they have identical neutron levels. As the nuclei come together, this level splits into two levels, symmetric and antisymmetric relative to the nuclei. The first of these is the lower. Its energy can be computed in the adiabatic approximation as a function of the distance between the nuclei. For this purpose, it is necessary to apply a method similar to that which was applied in reference 2 for one-dimensional potential wells.

It might appear that a bond of this kind could exist in the collision of C^{13} nuclei with C^{12}, where there is simply one excess neutron, but not in the collision of two C^{12} nuclei. In fact, however, in the collision of sufficiently energetic C^{12} nuclei, the neutron can be excited in one of the nuclei. A hole is formed in place of this neutron in the $P_{3/2}$ shell, while the neutron from the corresponding level of the other nucleus enters partially into the hole. Owing to this second neutron, which partially fills the hole, the excited neutron moves in two similar potential wells. The nucleus will have two "common" neutrons — excited and unexcited. Since different quantum numbers correspond to these, the Pauli principle does not prevent their being found in states of arbitrary symmetry. Even in states with different symmetry, their actions cannot compensate for one another because of the difference in the damping decrements of the wave functions. Naturally, the actions of the unexcited neutrons in closed shells are compensated, since pairs of neutrons with wave functions of opposite symmetry are necessarily obtained.

If the z axis is directed along the line connecting the nuclear centers, and the origin of the coordinates is placed at the midpoint, then the shift in the energy of the state which is symmetric relative to the nuclei is given by

$$\Delta E = -\frac{2\pi\hbar^2}{m}\int_0^\infty r\,dr\left(\psi_0\frac{\partial\psi_0}{\partial z}\right)_{z=0}. \qquad (1)$$

Here ψ_0 is the state in the individual nucleus, and the integration is carried out in the central plane perpendicular to the axis. For ψ_0 we use the functions of the p and s states of the neutron. If the density distribution of the excited neutron stretches along the axis connecting the nuclei (as is the case in the p state), then the binding between the nuclei is greater than for the s state of the neutron with the same energy.

The resulting curve of the potential energy is similar in form in the two cases. It has the form of a crater, inside of which a molecular quasilevel is possible. In the given example, the distance of the vertex of the crater from the center of the nucleus for the p state is 2.41 times greater than the nuclear radius.

Denoting the distance of the vertex from the "edge" of the nucleus by the radius of the nucleus by r_0, $\kappa = \sqrt{2m\,|E_{\text{bond}}|}$, we can compute from the equations

$$\frac{12\,\pi\hbar^2}{Z^2e^2mr_0}e^{-2\Delta\varkappa}\left(1+\frac{3}{\varkappa r_0}+\frac{3}{\varkappa^2 r_0^2}\right)^{-1}$$
$$\times\left(3+2\varkappa(r_0+\Delta)+\frac{3}{\varkappa(r_0+\Delta)}+\frac{3}{2\varkappa^2(r_0+\Delta)^2}\right)=1 \qquad (2)$$

(p neutron) and

$$\frac{4\pi\hbar^2}{Z^2e^2mr_0}\left(1+\frac{1}{\varkappa r_0}\right)^{-1}(1+2\varkappa(r_0+\Delta))\,e^{-2\varkappa\Delta}=1 \qquad (3)$$

(s neutron) with the aid of (1).

In the derivation of these formulae we have neglected the energies of the neutron outside the well in comparison with its kinetic energy in the well.

For the numerical factors in Eqs. (2) and (3), the radius of the nucleus was set equal to 3.2 f (assuming that $r_0 = 1.4\ A^{1/3}$ f). We set the binding energy of the neutron in the nucleus equal to 1 Mev. We note that, according to the data of reference 3, there is a level with such a binding energy in the C^{12} nucleus, to which is ascribed the state 0^+, as to the ground state of C^{12}. Therefore, the excited state can be attributed to the p neutron. The question of the possibility of the excitation of just this state in the experiments of reference 1 we leave to one side, since we are more interested in the problem of the existence of a quasimolecule. We then obtain from (2) $\Delta_p = 4.53$ f, and from (3), $\Delta_s = 3.91$ f. Both these values, and especially the first, are larger than the range of action of nuclear forces. When the binding energy of the neutron is equal to 4 Mev, $\Delta_p = 3.55$ f.

It would have been very interesting to explain from this point of view why Almquist did not observe resonance phenomena in collisions of O^{16} nuclei. Unfortunately, we must limit ourselves to suppositions here. For example, it can be assumed that in the interaction of the O^{16} nuclei the excitation of neutrons takes place with a smaller probability than in the case of C^{12}, as a consequence of the greater stability of the O^{16}. But this assumption must be verified by independent experiments.

In order that the nuclei in the "crater" be in a quasi-stable state, they must not adhere together in each contact (this was pointed out to us by K. A. Ter-Martirosyan). If the actual picture for the C^{12} nuclei corresponds to the model considered here, this will mean that the adhesion coefficient for these nuclei is much less than unity. Then another possibility arises for explaining the fact that there are no resonances in O^{16}: this may be connected with the large adhesion probability of these nuclei. In the scattering problem, the possibility of adhesion can be taken into account by the introduction of some complex boundary condition at the point of contact of the nuclei.

---

[1] Bromley, Kuehner, and Almquist, Phys. Rev. Lett. **4**, 365 (1960).

[2] L. D. Landau and E. M. Lifshitz, Квантовая механика (Quantum Mechanics), Moscow, Gostekhizdat 1948, p. 208. [Engl: Pergamon, 1958].

[3] F. Ajzenberg-Selove and T. Lauritsen, Nucl. Phys. **11**, 117 (1959).

Translated by R. T. Beyer
311

SOVIET PHYSICS JETP VOLUME 12, NUMBER 6 JUNE, 1961

CALCULATION OF *l*-FORBIDDEN TRANSITION PROBABILITIES

G. M. BUKAT

Leningrad Physico-Technical Institute, Academy of Sciences, U.S.S.R.

Submitted to JETP editor June 17, 1960

J. Exptl. Theoret. Phys. (U.S.S.R.) **39**, 1716-1717 (December, 1960)

The reduced matrix element for l-forbidden M1 transitions were calculated by employing a configuration mixture. The results of the calculation are compared with the experimental data.

THE probability of M1 transitions is given by the expression[1]

$$W_\gamma = 1/\tau_\gamma = 0.419\cdot 10^{13} E^3 m^2/(2j+1)\ \mathrm{sec}^{-1}, \qquad (1)$$

where E is the energy of transition in Mev, $m = (j \parallel \Sigma\mu_j \parallel j')$ is the reduced matrix element of the transition operator (in nuclear magnetons). An M1 transition is possible for $\Delta j \leq 1$, $\Delta\pi = 0$ (without change in parity). In calculations with functions of the shell model, the matrix element differs from 0 only for $\Delta l = 0$. However, there is a large number of transitions which, from the point of view of the shell model, take place with a change in the orbital angular momentum of the nucleon by two units. In the work of Arima et al.,[1] such transitions were considered by means of a configura-

Nucleus	j	j'	E, kev	τ_γ, sec	Configuration		Type	m^2 theoret	m^2 exp
					proton	neutron			
Fe^{57}	$f^5/_2$	$p^3/_2$	122	$1.23\cdot10^{-8}$	$(f^7/_2)^6$	$(f^5/_2)^2p^3/_2$	U	0.0339	0.0643
Co^{59}	$p^3/_2$	$f^5/_2$	191	$<1.6\cdot10^{-9}$	$(f^7/_2)^6f^5/_2$	$(f^7/_2)^8(p^3/_2)^4$	L	0,817	>0.0845
Zn^{67}	$f^5/_2$	$p^3/_2$	90	$2.02\cdot10^{-8}$	$(f^5/_2)^2$	$(f^5/_2)^6(p^3/_2)^3$	U	0.0513	0.0974
Rb^{85}	$p^3/_2$	$f^5/_2$	150	$1.14\cdot10^{-9}$	$(p^3/_2)^4(f^5/_2)^5$	$(g^9/_2)^{10}$	U	0.00846	0.236
Sn^{119}	$d^3/_2$	$s^1/_2$	24	$1.85\cdot10^{-8}$	$(g^9/_2)^{10}$	$(h^{11}/_2)^4s^1/_2$	L	0.804	0,512
Te^{121}	$d^3/_2$	$s^1/_2$	213	$<2\cdot10^{-9}$	$(g^7/_2)^2$	$(h^{11}/_2)^4s^1/_2$	L	0,708	$>0,0458$
						$(d^3/_2)^4s^1/_2$	U	0.155	
Xe^{129}	$d^3/_2$	$s^1/_2$	40	$0,7\cdot10^{-9}$	$(g^7/_2)^4$	$(h^{11}/_2)^{10}s^1/_2$	L	1,11	2,51
					$(g^7/_2)^2(d^5/_2)^2$	$(h^{11}/_2)^{10}s^1/_2$	L	1,20	
					$(d^5/_2)^4$	$(h^{11}/_2)^{10}s^1/_2$	L	1,22	
Cs^{131}	$g^7/_2$	$d^5/_2$	122	$4\cdot10^{-9}$	$(g^7/_2)^4d^5/_2$	$(h^{11}/_2)^{10}(s^1/_2)^2$	L	0,144	0,201
					$(g^7/_2)^4d^5/_2$	$(h^{11}/_2)^8(d^3/_2)^2$ $(s^1/_2)^2$	L	0,109	
					$(g^7/_2)^4d^5/_2$	$(h^{11}/_2)^{12}$	L	0,183	
					$(g^7/_2)^4d^5/_2$	$(h^{11}/_2)^{10}(d^3/_2)^2$	L	0.144	
Cs^{133}	$s^1/_2$	$d^3/_2$	53	$\leqslant 2.37\cdot10^{-8}$	$(g^7/_2)^4d^3/_2$	$(h^{11}/_2)^{10}(d^3/_2)^2$ $(s^1/_2)^2$	L	0.639	$\geqslant 0,134$
					$(g^7/_2)^2$ $(d^5/_2)^2d^3/_2$	$(h^{11}/_2)^{10}(d^3/_2)^2$ $(s^1/_2)^2$	L	0.837	
					$(d^5/_2)^4d^3/_2$	$(h^{11}/_2)^{10}(d^3/_2)^2$ $(s^1/_2)^2$	L	1,07	
La^{137}	$d^5/_2$	$g^7/_2$	10	$<10^{-7}$	$g^7/_2(d^5/_2)^6$	$(h^{11}/_2)^{10}(d^3/_2)^4$ $(s^1/_2)^2$	U	0,103	$>0,104$
					$(g^7/_2)^3(d^5/_2)^4$	$(h^{11}/_2)^{10}(d^3/_2)^4$ $(s^1/_2)^2$	L	0,114	
					$g^7/_2(d^5/_2)^6$	$(h^{11}/_2)^{12}(d^3/_2)^4$	U	0,118	
Pr^{143}	$g^7/_2$	$d^5/_2$	57,4	$<10^{-6}$	$(g^7/_2)^8d^5/_2$	$(h^9/_2)^2$	U	0,00784	>0.00146
					$(g^7/_2)^6(d^5/_2)^3$	$(h^9/_2)^2$	L	0.0185	
					$(g^7/_2)^6(d^5/_2)^3$	$(h^9/_2)^2$	U	0,676	
Ir^{193}	$s^1/_2$	$d^3/_2$	73	$6\cdot10^{-9}$	$(h^{11}/_2)^8(d^3/_2)^3$ $(s^1/_2)^2$	$(i^{13}/_2)^4$	U	0,00293	0,00968
					$(h^{11}/_2)^{10}(d^3/_2)^3$	$(i^{13}/_2)^4$	L	0.0963	
Au^{197}	$s^1/_2$	$d^3/_2$	77	$1.9\cdot10^{-9}$	$(h^{11}/_2)^{10}(d^3/_2)^3$ $(s^1/_2)^2$	$(i^{13}/_2)^6$	U	0,0606	0,0133
					$(h^{11}/_2)^{12}(d^3/_2)^3$	$(i^{13}/_2)^6$	L	0,139	
Tl^{207}	$d^3/_2$	$s^1/_2$	353	$\leqslant 1,2\cdot10^{-9}$	$(d^3/_2)^4s^1/_2$	$(i^{13}/_2)^{14}$	U	0,0618	$\geqslant 0,0142$

tion mixture produced by the residual interaction of the nucleons. For the majority of cases good agreement was obtained with experiment.

We have carried out a detailed calculation for 80 configurations of 14 nuclei. The values of m^2_{theoret} that were computed were compared with m^2_{exp}, obtained from (1) for the partial lifetimes τ_γ found from the experimental data. The results are given in the table. In it are given the configurations for which m^2_{theoret} is in best agreement with m^2_{exp}. Only configurations of final states are given. The initial states can be determined from the type of transition, L or U. L indicates the case in which the nucleon undergoes a transition from a shell with an odd number of nucleons to a shell with an even number of nucleons, while U transitions are of the opposite kind. There is no agreement with experiment for Rb^{85}, for which $m^2_{\text{exp}}/m^2_{\text{theoret}} \sim 30$. The large deviation of m^2_{theoret} from m^2_{exp} for Co^{59} can be explained if we assume that the lifetime of the level with energy 191 kev is smaller by one order of magnitude than the upper limit given in reference 2. Unfortunately, the absence of exact experimental data (on lifetimes, internal conversion coefficients, and the mixture of M1 and E2 transitions) does not permit us to decide how much deviation exists for Cs^{133}, Pr^{143}, Ir^{193}, Au^{197}, Tl^{207}. In these cases $m^2_{\text{theoret}}/m^2_{\text{exp}} \sim 3 - 5$. For the remaining nuclei with the corresponding choice of configurations, this ratio is about 0.5 — 2.

Analysis of the results confirms the fact that by consideration of the configuration mixture, it is possible to explain the M1 transition between the states with $\Delta l = 2$. Configurations for which the best agreement with experiment was obtained yield the correct sign of the quadrupole moment of the ground state. They display the same regularities as observed in the work of Arima et al.:[1] the neutron shell $2d^{3/2}$ begins to be filled earlier than the shell $1h^{11/2}$ is filled, and in the proton configurations the shells $1g^{7/2}$ and $2d^{5/2}$ are competing.

The author is grateful to Professor L. I. Rusinov for his direction of the work and also to D. A. Varshalovich for discussion of the results.

---

[1] Arima, Horie, and Sano, Progr. Theor. Phys. 17, 567 (1957).

[2] B. S. Dzhelepov and L. K. Peker, Схемы распада радиоактивных ядер (Nuclear Radioactive Decay Schemes) Moscow, 1958.

Translated by R. T. Beyer
312

SOVIET PHYSICS JETP VOLUME 12, NUMBER 6 JUNE, 1961

PERIPHERAL π-π INTERACTIONS BETWEEN HIGH-ENERGY NUCLEONS

P. A. USIK and V. I. RUS'KIN

Nuclear Physics Institute, Academy of Sciences, Kazakh S.S.R.

Submitted to JETP editor June 21, 1960

J. Exptl. Theoret. Phys. (U.S.S.R.) 39, 1718-1720 (December, 1960)

Peripheral collisions of two fast nucleons in a π-π interaction are considered. The results of the calculations are compared with the experimental data.

TAMM[1] and Chernavskiĭ et al.[2] developed a method of calculating the peripheral interactions of two nucleons, based on the use of perturbation theory. The purpose of the present note is to consider the special case of peripheral interactions described by the Feynman diagram in Fig. 1. An interaction of this type can lead to the creation of two centers of emission of shower particles (i.e., a "two-center" angular distribution).* It is possible that in the case of a large scattering cross section for the two π mesons ($\sigma_{\pi\pi}$) the given process considerably increases the contribution of peripheral collisions. An estimate of the total cross section for this process, however, is made difficult by the following circumstances: 1) neither experimental nor reliable theoretical values of $\sigma_{Q\pi}$ are known; 2) the nature of the propagation function Q is not known.

We made a preliminary investigation of the propagation function of the diagram of Fig. 2 under the assumption that the π-π interaction proceeds via the exchange of a boson of 4-momentum Q and mass M. ($\mathfrak{M}_1$ and $\mathfrak{M}_2$ are the masses of the excited states, which rapidly decay into secondary particles.) Since the nuclear-active particle with the smallest mass is a π meson, we have $M \geq \mu$, where μ is the mass of the π meson. We have considered three assumptions as regards the value of the mass M: M = 2μ, M = 2m, and M = 4m (m is the mass of the nucleon).

Following Romanov and Chernavskiĭ,[2] we write the probability for the process described by the diagram of Fig. 2 in the form

$$dw \sim w^2_{Q\pi}\frac{p_1}{2E_0}\frac{d(\cos\theta)\,\mathfrak{M}_1\,d\mathfrak{M}_1\mathfrak{M}_2\,d\mathfrak{M}_2}{(Q^2+M^2)^2}, \qquad (1)$$

where E_0 is the virtual π-meson energy, which, according to reference 2, can be taken equal to

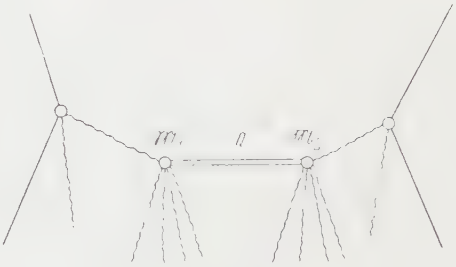

FIG. 1

$\mu\gamma_c$ (γ_c is the Lorentz factor of the colliding nucleons in their c.m.s.) Here we assume that for high energies of the nucleons ($\gamma_c \gg 1$) the quantity $w_{Q\pi}$ is constant.

For $E_0 > M, \mathfrak{M}_1, \mathfrak{M}_2$ we have

$$Q^2 + M^2 = M^2 + \varkappa^2 + 2E_0^2(1-\cos\theta), \qquad (2)$$

where

$$\varkappa^2 = \mathfrak{M}_1^2\mathfrak{M}_2^2/4E_0^2 + \mathfrak{M}_1^2\mathfrak{M}_2^2(\mathfrak{M}_1^2+\mathfrak{M}_2^2)/16E_0^4.$$

Integrating (1) over angles from 0 to $(1 - \cos\theta) = M^2/2E_0^2$, we have

$$dw \sim w^2_{Q\pi}\frac{P_1\mathfrak{M}_1\mathfrak{M}_2\,d\mathfrak{M}_1\,d\mathfrak{M}_2}{E_0^3(M^2+\varkappa^2)(2M^2+\varkappa^2)}. \qquad (3)$$

We shall confine ourselves to the case of a symmetric excitation ($\mathfrak{M}_1 \sim \mathfrak{M}_2$). The denominator of (3) increases rapidly starting with $\varkappa^2 \sim M^2$. Then $Q^2 + M^2 \sim 2M^2$, and the most probable values of the masses of the excited states are

$$\mathfrak{M}_1 \sim \mathfrak{M}_2 \sim \sqrt{2E_0M - M^2}. \qquad (4)$$

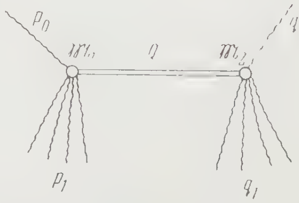

FIG. 2

---

*The possibility of such a process was first discussed by Zatsepin and Chernavskiĭ (private communication) and also by Bubelev.[3]

No.	Type of event	γ_c	n_s		
			$M = 2\mu$	$M = 2$	$M = 4$
1	0+ 4p	150(245)	11.4(14.5)	30.9(39.9)	42.7(55.6)
2	0+14p	450(218)	19.7(13.7)	54.4(37.5)	76.3(53.2)
3	1+15p	260(201)	15.0(13.2)	41.1(36.0)	57.3(50.0)
4	0+32p	71(81)	7.5(8.3)	20.7(22.3)	27.7(30.0)
5	0+20p	79(77)	8.2(8.1)	21.9(21.6)	29.6(29.4)
6	0+20p	34(69)	5.4(7.4)	13.5(20.4)	16.6(27.2)
7	0+22p	26(65)	4.7(7.4)	11.3(19.7)	12.8(29.2)
8	1+11p	55(53)	6.8(6.8)	17.9(17.7)	23.6(23.0)
9	0+21p	38(48)	5.7(6.4)	14.4(16.6)	18.1(21.5)
10	0+16p	50(45)	6.5(6.2)	17.0(16.0)	22.1(20.6)
11	0+13p	44(43)	6.1(6.1)	15.8(15.6)	20.3(19.9)
12	0+16p	20(43)	4.1(6.1)	9.4(15.6)	9.4(19.9)
13	0+16p	30(40)	5.0(6.0)	12.5(14.9)	14.9(18.9)

Using the experimental value $\bar{E}_\pi \approx 0.4$ for the mean energy of π mesons in the center-of-emission system (c.e.s.), we can find the mean multiplicity of the shower particles and compare it with that observed experimentally. Such a comparison is made in the table, which gives data on 12 showers reported by Cocconi[4] and one shower (No. 5) investigated in our laboratory.* The obtained results favor the exchange of a boson Q with a mass equal to the mass of a nucleon-antinucleon pair.

This is some confirmation of the assumption[5] that in the case of high-energy interactions the creation and subsequent annihilation of nucleon-antinucleon pairs play an important role. It is interesting to note in this connection that the mean value of the π-meson c.e.s. energy coincides with the corresponding value for nucleon-antinucleon annihilation.[6] Taking this fact into account, we can obtain, by a method similar to that suggested by Meier,[7] the more accurate value of γ_c:

$$\gamma_c = \left[\frac{0.84}{2\mu}(\gamma_1 + \gamma_2)\frac{3}{4}n_s\bar{E}_\pi\right]^{1/2}.$$

The values of γ_c thus obtained and the expected mean multiplicity of shower particles are given in parentheses in the table.

As can be seen from the table, the exchange of a boson Q with mass $M = 2\mu$ leads to very low values of the masses of the excited states. Cases of this type with large multiplicity ($n_s \gtrsim 10$) can therefore occur only at ultra-high energies ($\gamma_c \sim 150 - 200$).

In the case of the exchange of a boson Q of mass $M = 2$, the threshold of the process, as is readily seen, is at $\gamma_c \approx (M + \mu)/\mu = 7.7$, which, possibly, also explains the result of Kaneko and Okazaki.[8]

The authors thank D. S. Chernavskiĭ for suggesting the topic and for his constant interest in the work, and Professor Zh. S. Takibaev for helpful discussions.

---

*Strictly speaking, upon setting $E_0 = \mu\gamma_c$ we should compare the results of the calculations only with cases characterized by small values of the inelasticity coefficient. The inelasticity coefficients, however, were estimated only for a few of the showers listed in the table.

[1] I. E. Tamm, Report at the International Conference on High Energy Physics, Kiev, 1959.

[2] I. M. Dremin and D. S. Chernavskiĭ, JETP **38**, 229 (1960), Soviet Phys. JETP **11**, 167 (1960).

[3] É. G. Bubelev, Proceedings International Conf. on Cosmic Rays, 1959, vol. 1, Moscow, Press of the Acad. Sci. U.S.S.R., 1960 (Russian ed.) p. 284.

[4] G. Cocconi, Phys. Rev. **111**, 1699 (1958).

[5] P. A. Usik, Report, Institute of Nuclear Physics, Acad. Sci. Kazakh S.S.R., 1959.

[6] K. Niu, Nuovo cimento **10**, 994 (1958).

[7] H. W. Meier, Nuovo cimento **11**, 307 (1959).

[8] S. Kaneko and M. Okazaki, Nuovo cimento **8**, 521 (1958).

Translated by E. Marquit
313

SOVIET PHYSICS JETP VOLUME 12, NUMBER 6 JUNE, 1961

INTERNAL BREMSSTRAHLUNG AND ELECTROMAGNETIC CORRECTIONS TO $\mu - e$ *DECAY*

V. P. KUZNETSOV

Moscow Physico-Technical Institute

Submitted to JETP editor July 7, 1960

J. Exptl. Theoret. Phys. (U.S.S.R.) 39, 1722-1726 (December, 1960)

We derive electromagnetic corrections to the electron polarization and to the electron and μ - e decay and determine the polarization and angular distribution of γ quanta in internal bremsstrahlung. Electromagnetic corrections to the spectrum, to the angular distribution, and to the electron polarization in μ - e decay are computed in the low-energy region.

1. Kinoshita and Sirlin[1] and the author[2] investigated the electromagnetic corrections to the spectrum and to the angular distribution of $\mu - e$ decay in the theory of Gell-Mann and Feynman.[3]

Let us consider the polarization of the electrons in $\mu - e$ decay. It is known that the theory of Gell-Mann and Feynman predicts for the electron spin a polarization vector $\boldsymbol{\xi}_2$ equal to $-\mathbf{n}_2$ ($\mathbf{n}_2$ is a unit vector in the direction of emission of the electron). Using the vertex part (2) of reference 2, we find that in the approximation where $m_1/m_2 \gg 1$ (m_1 and m_2 are the muon and electron masses) the radiative corrections do not change the character of the polarization of the electron.

Since the radiative corrections to the spectrum of the $\mu - e$ decay and to the term proportional to $\boldsymbol{\xi}_2\mathbf{n}_2$ are the same, the infrared divergence does not enter in the expression for $\boldsymbol{\xi}_2$. Thus we have, as before, $\boldsymbol{\xi}_2 = -\mathbf{n}_2$.

Let us consider the corrections due to the internal bremsstrahlung. Its probability with emission of a polarized electron and a polarized γ quantum, integrated over the momenta and summed over all possible neutrino polarizations, has the following form (we use the Lagrangian (1) from reference 2 and write a_1 for the 4-vector of the muon polarization, a_2 for the electron polarization, ξ_γ for the photon Stokes parameter, and p_1, p_2, and k for the 4-momenta and ϵ_1, ϵ_2, and ϵ_γ for the respective energies of the muon, electron, and photon):

$$\left(\frac{dw}{dt}\right)_i = \frac{\alpha}{2\pi}\frac{G^2}{6\,(2\pi)^5\varepsilon_1} R\,\frac{1}{2}\,(1 + \xi_d\xi_\gamma)\,\frac{d^3p_2}{\varepsilon_2}\frac{d^3k}{\varepsilon_\gamma}, \tag{1}$$

$$\begin{aligned}
R = {} & \left[\tfrac{1}{2}(m_1^2 - m_2^2)^2 - Q^2\left(Q^2 + \tfrac{1}{2}(m_1^2 + m_2^2)\right)\right]\Phi \\
& + \frac{(kQ)^2}{(kp_1)\,(kp_2)}(m_1^2 + m_2^2 - 2Q^2) - 4Q^2 - m_1\Big\{(m_1^2 - m_2^2 \\
& + 2Q^2)\left[(a_1p_2)\,\Phi + (kQ)\,\Phi_1 - \frac{(ka_1)}{(kp_1)}\frac{(kQ)^2}{(kp_1)\,(kp_2)}\right] - 4\,\frac{(ka_1)}{(kp_1)}\,Q^2\Big\} \\
& - m_2\Big\{(m_2^2 - m_1^2 + 2Q^2)\Big[(a_2p_1)\,\Phi + (kQ)\,\Phi_2 \\
& - \frac{(ka_2)}{(kp_2)}\frac{(kQ)^2}{(kp_1)\,(kp_2)}\Big] - 4\,\frac{(ka_2)}{(kp_2)}\,Q^2\Big\} + m_1m_2\Big\{\Big[Q^2\,(a_1a_2) \\
& - 2\,(a_1p_2)\,(a_2p_1) - Q^2\,(kQ)\,\frac{(ka_1)}{(kp_1)}\frac{(ka_2)}{(kp_2)}\Big]\Phi \\
& + (kQ)\Big[\left(Q^2\frac{(ka_2)}{(kp_2)} - 2\,(a_2p_1)\right)\Phi_1 + \left(Q^2\frac{(ka_1)}{(kp_1)} - 2\,(a_1p_2)\right)\Phi_2 \\
& - 2\,(kQ)\,\Phi_{12}\Big] + \frac{(kQ)^2}{(kp_1)\,(kp_2)}\Big[2\,(a_2p_1)\frac{(ka_1)}{(kp_1)} + 2(a_1p_2)\frac{(ka_2)}{(kp_2)} \\
& - 2\,(a_1a_2) + (2\,(kQ) - Q^2)\,\frac{(ka_1)}{(kp_1)}\frac{(ka_2)}{(kp_2)}\Big] - 4Q^2\,\frac{(ka_1)}{(kp_1)}\frac{(ka_2)}{(kp_2)}\Big\};
\end{aligned}$$

$$(\xi_\gamma)_i = F_i\,/\,R \qquad (i = 1,\,2), \qquad (\xi_\gamma)_3 = F_3\,/\,R \quad 1,$$

$$\begin{aligned}
F_1 = {} & i\,\frac{(kQ)}{(kp_1)\,(kp_2)}\,e_{\alpha\beta\gamma\delta}\,p_{1\beta}\,p_{2\gamma}\,k_\delta\Big\{\frac{m_1a_{1\alpha}}{(p_1k)}\Big[m_1^2 - m_2^2 + 2Q^2 \\
& - m_2\left[Q^2\frac{(ka_2)}{(kp_2)} - 2\,(a_2p_1) - 2\,(kQ)\,\frac{\Phi_2}{\Phi}\right]\Big] - \frac{m_2a_{2\alpha}}{(p_2k)}\Big[m_2^2 - m_1^2 \\
& + 2Q^2 - m_1\left[Q^2\frac{(ka_1)}{(kp_1)} - 2(a_1p_2) - 2\,(kQ)\,\frac{\Phi_1}{\Phi}\right]\Big]\Big\},
\end{aligned} \tag{2}$$

$$\begin{aligned}
F_2 = {} & [(m_1^2 - m_2^2)\,(kQ) - 2Q^2\,(Pk)]\left[\Phi - \frac{(kQ)}{(kp_1)\,(kp_2)}\right] \\
& + m_1\Big[2m_2^2(kQ)\,\frac{(kp_1)}{(kp_2)}\left[\frac{(ka_1)}{(kp_1)}\Phi - \Phi_1\right] + [(m_1^2 + m_2^2)\,(kQ) \\
& + 2Q^2\,(Pk)]\left[\Phi_1 - \frac{(kQ)}{(kp_1)(kp_2)}\frac{(ka_1)}{(kp_1)}\right]\Big] \\
& + m_2\Big[2m_1^2\,(kQ)\,\frac{(kp_2)}{(kp_1)}\left[\Phi_2 - \frac{(ka_2)}{(kp_2)}\Phi\right] - [(m_1^2 + m_2^2)\,(kQ) \\
& - 2Q^2\,(Pk)]\left[\Phi_2 - \frac{(kQ)}{(kp_1)\,(kp_2)}\frac{(ka_2)}{(kp_2)}\right]\Big] + m_1m_2\,[(m_1^2 - m_2^2)\,(kQ) \\
& + 2Q^2\,(Pk)]\Big[\frac{(ka_1)}{(kp_1)}\frac{(a_2p_1)}{(kp_1)\,(kp_2)} + \frac{(ka_2)}{(kp_2)}\frac{(a_1p_2)}{(kp_1)\,(kp_2)} \\
& + \frac{(kQ)}{(kp_1)\,(kp_2)}\frac{(ka_1)}{(kp_1)}\frac{(ka_2)}{(kp_2)}\Big],
\end{aligned}$$

$$\begin{aligned} F_3 = {} & (m_1^2 + m_2^2 - 2Q^2)\frac{(kQ)^2}{(kp_1)\,(kp_2)} - 4Q^2 + m_1\frac{(ka_1)}{(kp_1)}\Big[\frac{(kQ)^2}{(kp_1)\,(kp_2)} \\ & \times (m_1^2 - m_2^2 + 2Q^2) + 4Q^2] + m_2\frac{(ka_2)}{(kp_2)}\Big(\frac{(kQ)^2}{(kp_1)\,(kp_2)}(m_1^2 \\ & - m_2^2 + 2Q^2) + 4Q^2\Big] + m_1 m_2\Big[\frac{(kQ)^2}{(kp_1)\,(kp_2)}\Big[2(a_1p_2)\frac{(ka_2)}{(kp_2)} \\ & + 2\,(a_2p_1)\frac{(ka_1)}{(kp_1)} + (2\,(kQ) - Q^2)\ \frac{(ka_1)}{(kp_1)}\frac{(ka_2)}{(kp_2)} - 2\,(a_1a_2)\Big] \\ & - 4Q^2\frac{(ka_1)}{(kp_1)}\frac{(ka_2)}{(kp_2)} - \frac{4\,(kQ)^2}{(kp_1)^3\,(kp_2)^3\Phi} \\ & \times e_{\alpha\beta\gamma\delta}a_{1\alpha}p_{1\beta}p_{2\gamma}k_\delta e_{\lambda\mu\rho\sigma}a_{2\lambda}p_{1\mu}p_{2\rho}k_\sigma\Big], \end{aligned}$$

where

$$\Phi = B_\mu^2, \qquad \Phi_1 = B_\mu B_{1\mu}, \qquad \Phi_2 = B_\mu B_{2\mu}, \qquad \Phi_{12} = B_{1\mu}B_{2\mu},$$

$$B_\mu = \frac{p_{2\mu}}{(p_2k)} - \frac{p_{1\mu}}{(p_1k)}, \qquad B_{1\mu} = \frac{(ka_1)}{(kp_1)}\frac{p_{2\mu}}{(p_2k)} - \frac{a_{1\mu}}{(p_1k)},$$

$$B_{2\mu} = \frac{a_{2\mu}}{(p_2k)} - \frac{(ka_2)}{(kp_2)}\frac{p_{1\mu}}{(p_1k)},$$

and $Q = p_1 - p_2 - k$, $P = p_1 + p_2$, ξ_d is the polarization vector, measured by the detector. For the unit vectors used in the determination of the Stokes parameter we choose

$$\mathbf{e}_1 = \frac{[\mathbf{p}_2\times\mathbf{k}]}{|[\mathbf{p}_2\times\mathbf{k}]|}, \qquad \mathbf{e}_2 = \frac{[\mathbf{k}\times\mathbf{e}_1]}{|\mathbf{k}|}, \qquad \mathbf{e}_3 = \frac{\mathbf{k}}{|\mathbf{k}|}$$

in the muon rest system. When $a_2 = 0$ and $\xi_\gamma = 0$ formula (1) becomes identical with (6) of reference 2.

Integrating (1) over d^3k and summing over the photon polarizations we obtain, in the muon rest system with $m_1/m_2 \gg 1$,

$$\begin{aligned} \tau_0\,(dw\,/\,dt)_i = {} & \alpha\,[8\pi^2]^{-1}\varepsilon^2 d\varepsilon\, d\Omega_2\Big\{f_i(\varepsilon) - \boldsymbol{\xi}_1\mathbf{n}_2 h_i(\varepsilon) \\ & - \boldsymbol{\xi}_2\mathbf{n}_2\Big[f_i(\varepsilon) - \tfrac{1}{3}\,\varepsilon^{-2}(1-\varepsilon)^2(5-2\varepsilon)\Big] + (\boldsymbol{\xi}_1\mathbf{n}_2)\,(\boldsymbol{\xi}_2\mathbf{n}_2) \\ & \times\Big[h_i(\varepsilon) - \tfrac{1}{3}\,\varepsilon^{-2}(1-\varepsilon)^2(1+2\varepsilon)\Big]\Big\}. \end{aligned} \tag{3}$$

Here

$$\begin{aligned} f_i(\varepsilon) = {} & 2\,(3-2\varepsilon)\,u_i(\varepsilon) + \tfrac{1}{3}\,\varepsilon^{-2}(1-\varepsilon)(5+17\varepsilon-34\varepsilon^2) \\ & \times(\ln\varepsilon + \omega - 1) + \tfrac{5}{3}\,\varepsilon^{-2}(1-\varepsilon)^2, \end{aligned}$$

$$\begin{aligned} h_i(\varepsilon) = {} & 2\,(2\varepsilon-1)\,u_i(\varepsilon) + \tfrac{1}{3}\,\varepsilon^{-2}(1-\varepsilon)(1+\varepsilon+34\varepsilon^2) \\ & \times(\ln\varepsilon + \omega - 1) + \tfrac{2}{3}\,\varepsilon^{-2}(1-\varepsilon)^2(2-\varepsilon), \end{aligned}$$

$$\begin{aligned} u_i(\varepsilon) = {} & -2\omega_<(\ln\varepsilon + \omega - 1) + 2\Big[\ln\varepsilon + \omega - 1 \\ & - \tfrac{1}{2}\,\varepsilon^{-1}(1-\varepsilon)\Big]\ln(1-\varepsilon) - (\ln\varepsilon - \omega)(\ln\varepsilon + \omega - 1) \\ & - \pi^2/6 + \sum_{n=1}^{\infty}\varepsilon^n/n^2, \end{aligned}$$

$$\omega = \ln(m_1/m_2), \qquad \omega_< = \ln(\lambda/m_2),$$

where λ is the fictitious photon mass, introduced to eliminate the infrared catastrophe, $\tau_0 = 192\,\pi^3/m_1^5G^2$, $d\Omega_2$ is the solid angle in the direction of the electron emission, and ξ_1 is the vector of muon polarization.

In the present paper ϵ does not stand for $\epsilon_2/\epsilon_{2\max}$, as in reference 2, but $\epsilon = 2\epsilon_2/m_1$.

We see from (3) that the longitudinal electron polarization is modified by the corrections due to the internal bremsstrahlung. The vector of electron polarization in $\mu - e$ decay, with allowance for electromagnetic second-order corrections in the approximation where $m_1/m_2 \gg 1$, has the form

$$\boldsymbol{\xi}_2 = -\,\mathbf{n}_2\frac{r_1(\varepsilon) - \boldsymbol{\xi}_1\mathbf{n}_2 s_1(\varepsilon)}{r_2(\varepsilon) - \boldsymbol{\xi}_1\mathbf{n}_2 s_2(\varepsilon)},$$

where

$$\begin{aligned} & r_1(\varepsilon) = 3 - 2\varepsilon + \frac{\alpha}{2\pi}\Big[f(\varepsilon) - \frac{1}{3}\,\varepsilon^{-2}(1-\varepsilon)^2(5-2\varepsilon)\Big], \\ & s_1(\varepsilon) = 2\varepsilon - 1 + \frac{\alpha}{2\pi}\Big[h(\varepsilon) - \frac{1}{3}\,\varepsilon^{-2}(1-\varepsilon)^2(1+2\varepsilon)\Big], \\ & r_2(\varepsilon) = 3 - 2\varepsilon + \frac{\alpha}{2\pi}f(\varepsilon), \qquad s_2(\varepsilon) = 2\varepsilon - 1 + \frac{\alpha}{2\pi}h(\varepsilon); \end{aligned} \tag{4}$$

the quantities $f(\epsilon)$ and $h(\epsilon)$ are given in reference 2 [see formula (9)].

In the decay of an unpolarized muon ($\xi_1 = 0$) we have

$$\boldsymbol{\xi}_2 = -\,\mathbf{n}_2[1-\Delta], \qquad \Delta = \frac{\alpha}{2\pi}\,\frac{1}{3}\,\frac{1}{\varepsilon^2}(1-\varepsilon)^2\frac{5-2\varepsilon}{r_2(\varepsilon)}, \tag{5}$$

i.e., the corrections are significant only in the region $\epsilon \lesssim 0.1$, in which the electron polarization is small.

2. The correction functions for the $\mu - e$ decay increase rapidly as $\epsilon \to \epsilon_{\min}$. It has been assumed heretofore (see references 1 and 2) that it is essential to take account of multi-photon internal bremsstrahlung and of pair production in the low-energy part of the spectrum. However, an estimate of the matrix elements of these processes (for additional quanta and pairs with energy $\sim m_1/4$) shows that the branching ratio of such processes, relative to the single-photon bremsstrahlung (photon energy $\sim m_1/2$), is of order α.

In the region $\epsilon_{\min} < \epsilon \lesssim 0.02$, where $\epsilon_{\min} = 2m_2/m_1 = 0.00966$, the correction function for the electron spectrum fits quite well the expression

$$f(\varepsilon) = {}^5/_6\,(m_1/m_2)\,\varepsilon^{-1},$$

and in the region $0.02 < \epsilon < 0.1$ it fits the formula

$$f(\varepsilon) = {}^5/_3\,\varepsilon^{-2}(\ln\varepsilon + \omega),$$

which is obtained from Eq. (9) of reference 2 if the terms $\sim\epsilon^{-2}$ are retained.

These two formulas can be obtained by using the internal bremsstrahlung matrix element and neglecting in it the Green's function of the muon compared with the electron Green's function, further neglecting in the latter the term $\hat{p}_2 + im_2$ in the numerator (compared with $\hat{k}$). Such an approximation presupposes that when $\epsilon \lesssim 0.1$ the main contribution is produced by the radiation of hard quanta of energy $\sim m_1/2$; this radiation is more isotropic than when $\epsilon > 0.1$. (In the integration over d^3k we can assume that $\epsilon_{\gamma\max}(\vartheta) = m_2/2$, where $\epsilon_{\gamma\max}(\vartheta)$ is the maximum energy of the γ quantum at a given angle ϑ relative to the electron momentum.)

When $\epsilon < 0.1$, calculation yields for the corrected decay probability of the polarized muon, in the muon rest system.

$$\begin{aligned}\tau_0\frac{dw}{dt} = 8\left(\frac{m_2}{m_1}\right)^3\frac{d\Omega_2}{4\pi}\sinh^2\theta\cosh\theta\, d\theta\Big\{3-2\varepsilon+\frac{\alpha}{2\pi}f(\theta)\\ -\xi_1\mathbf{n}_2\left[(2\varepsilon-1)\tanh\theta+\frac{\alpha}{2\pi}h(\theta)\right]\\ -\xi_2\mathbf{n}_2\left[(3-2\varepsilon)\tanh\theta+\frac{\alpha}{2\pi}g(\theta)\right]\\ +(\xi_1\mathbf{n}_2)(\xi_2\mathbf{n}_2)\left[(2\varepsilon-1)\frac{\cosh\theta-1}{\cosh\theta}+\frac{\alpha}{2\pi}l(\theta)\right]\\ -\xi_1\xi_2\left[2\frac{m_2}{m_1}\frac{1-\varepsilon}{\varepsilon}+\frac{\alpha}{2\pi}m(\theta)\right]\Big\},\end{aligned} \tag{6}$$

where

$$f(\theta)=\frac{5}{6}\left(\frac{m_1}{m_2}\right)^2\frac{\theta}{\sinh 2\theta}, \qquad h(\theta)=\frac{1}{6}\left(\frac{m_1}{m_2}\right)^2\frac{\theta\coth\theta-1}{\sinh 2\theta},$$

$$g(\theta)=5h(\theta), \qquad l(\theta)=\frac{1+2\cosh\theta}{\sinh\theta}h(\theta)-\frac{1}{5}f(\theta),$$

$$m(\theta)=\frac{1}{\sinh\theta}h(\theta), \qquad \cosh\theta=\frac{1}{2}\frac{m_1}{m_2}\varepsilon=\frac{\varepsilon_2}{m_2}. \tag{7}$$

These formulas are valid when $0 < \theta \lesssim 3$ ($\epsilon_{\min} < \epsilon \lesssim 0.1$). In the nonrelativistic case ($\theta \ll 1$ and $\epsilon \sim 0.01$) we get

$$f(\theta)=\frac{5}{12}\left(\frac{m_1}{m_2}\right)^2, \qquad h(\theta)=\frac{1}{36}\left(\frac{m_1}{m_2}\right)^2\theta,$$

$$g(\theta)=\frac{5}{36}\left(\frac{m_1}{m_2}\right)^2\theta, \qquad l(\theta)=\frac{1}{120}\left(\frac{m_1}{m_2}\right)^2\theta^2,$$

$$m(\theta)=\frac{1}{36}\left(\frac{m_1}{m_2}\right)^2. \tag{8}$$

In the region $1 \lesssim \theta \lesssim 3$ ($0.02 \lesssim \epsilon \lesssim 0.1$), neglecting the terms $\sim m_2/m_1$ in (7), we get

$$f(\varepsilon)=\tfrac{5}{3}(\ln\varepsilon+\omega)/\varepsilon^2, \qquad h(\varepsilon)=\tfrac{1}{3}\varepsilon^{-2}(\ln\varepsilon+\omega-1),$$

$$g(\varepsilon)=\tfrac{5}{3}\varepsilon^{-2}(\ln\varepsilon+\omega-1), \qquad l(\varepsilon)=\tfrac{1}{3}\varepsilon^{-2}(\ln\varepsilon+\omega-2),$$

$$m(\varepsilon)=0. \tag{9}$$

As indicated above, these expressions are also obtained in the usual way if the terms that increase as ϵ^{-2} in the initial part of the spectrum are retained. (In formula (9) of reference 2, in the expression for $h(\epsilon)$, the minus sign in front of the term $4\epsilon^{-1}(1-\epsilon)$ in the square brackets should be replaced by a plus sign.) The asymmetry coefficient introduced by Kinoshita and Sirlin,[4] with allowance for the electromagnetic corrections in the initial part of the spectrum, has the following form

$$\begin{aligned}a_r(\theta)=\Big[\frac{2}{3}+\frac{1}{3}\cosh^3\theta-\cosh\theta-\frac{m_2}{m_1}\sinh^4\theta\\ -\frac{\alpha}{2\pi}\frac{1}{12}\left(\frac{m_1}{m_2}\right)^2(2-2\cosh\theta+\theta\sinh\theta)\Big]\\ \times\Big[\sinh^3\theta-\frac{1}{8}\frac{m_2}{m_1}(\sinh 4\theta-4\theta)+\frac{\alpha}{2\pi}\frac{5}{12}\left(\frac{m_1}{m_2}\right)^2(\theta\cosh\theta\\ -\sinh\theta)\Big]^{-1}\end{aligned} \tag{10a}$$

when $\theta < 3$, whereas for $\theta \ll 1$ we get

$$a_2(\theta)=-0.056\,\theta. \tag{10b}$$

Without allowance for electromagnetic corrections, $a_0(\theta)=\theta/4$ when $\theta \ll 1$.

For the electron polarization vector we obtain in the interval $0 \le \theta \lesssim 3$

$$\xi_2=-\mathbf{n}_2\frac{(3-2\varepsilon)\tanh\theta+\alpha g(\theta)/2\pi-\xi_1\mathbf{n}_2[(2\varepsilon-1)(\cosh\theta-1)/\cosh\theta+\alpha l(\theta)/2\pi]}{3-2\varepsilon+\alpha f(\theta)/2\pi-\xi_1\mathbf{n}_2[(2\varepsilon-1)\tanh\theta+\alpha h(\theta)/2\pi]}-\xi_1\frac{2\varepsilon^{-1}(1-\varepsilon)m_2/m_1+\alpha m(\theta)/2\pi}{3-2\varepsilon+\alpha f(\theta)/2\pi-\xi_1\mathbf{n}_2[(2\varepsilon-1)\tanh\theta+\alpha h(\theta)/2\pi]}. \tag{11}$$

(Without allowance for the corrections, $\xi_2 = -\mathbf{v}_2$, where $\mathbf{v}_2$ is the electron velocity. We use the system of units with $\hbar = c = 1$.)

From (11) we obtain with $\xi_1 = 0$

$$\xi_2=-\mathbf{n}_2(1-\Delta),$$

$$\Delta=\left[(3-2\varepsilon)(1-\tanh\theta)+\frac{\alpha}{2\pi}\left(\frac{m_1}{m_2}\right)^2\cdot\frac{5}{6}\frac{1+\theta-\theta\coth\theta}{\sinh 2\theta}\right]\times\left[3-2\varepsilon+\frac{\alpha}{2\pi}f(\theta)\right]^{-1}.$$

In the nonrelativistic case

$$\xi_2=-\mathbf{n}_2\cdot 0.42\,\theta, \qquad \theta\ll 1.$$

For the interval $1 \lesssim \theta \lesssim 3$

$$\begin{aligned}\xi_2=-\mathbf{n}_2\Big\{3-2\varepsilon+\frac{\alpha}{2\pi}\frac{5}{3}\varepsilon^{-2}(\ln\varepsilon+\omega-1)-\xi_1\mathbf{n}_2\Big[2\varepsilon-1\\ +\frac{\alpha}{2\pi}\frac{1}{3}\varepsilon^{-2}(\ln\varepsilon+\omega-2)\Big]\Big\}\Big\{3-2\varepsilon+\frac{\alpha}{2\pi}\frac{5}{3}\varepsilon^{-2}(\ln\varepsilon+\omega)\\ -\xi_1\mathbf{n}_2\Big[2\varepsilon-1+\frac{\alpha}{2\pi}\frac{1}{3}\varepsilon^{-2}(\ln\varepsilon+\omega-1)\Big]\Big\}^{-1},\end{aligned}$$

$$\Delta=\frac{\alpha}{2\pi}\frac{5}{3}\varepsilon^{-2}\Big/\left[3-2\varepsilon+\frac{\alpha}{2\pi}\frac{5}{3}\varepsilon^{-2}(\ln\varepsilon+\omega)\right].$$

The values of the functions f, h, Δ, r_i, s_i, and m are listed in the table and are shown in the diagram.

3. Integrating (2) over d^3p_2, we obtain the following values for the spectrum of radiation probability and the Stokes parameters ξ_γ of the photons in internal bremsstrahlung, at $m_1/m_2 \gg 1$:

Correction functions $f(\epsilon)$ and $h(\epsilon)$ at the start of the spectrum ($\theta = 0$ for $\epsilon = 0.00966$)

ε	$\alpha(2\pi)^{-1}f(\varepsilon)$	$\alpha(2\pi)^{-1}h(\varepsilon)$
0,00966	20,2	0
0,01	19,5	0,35
0,02	7,5	0,61
0,05	1,9	0,22
0,08	0,97	0,11
0,1	0,69	0,078

$$\tau_0 \frac{dw}{dt} = \frac{\alpha}{6\pi}(1-\varkappa)\, d\varkappa \frac{d\Omega_\gamma}{4\pi}\{a(\varkappa) - \xi_1 \mathbf{n}_\gamma b(\varkappa)$$

$$- \xi_2 \mathbf{n}_2 c(\varkappa) + (\xi_1 \mathbf{n}_\gamma)(\xi_2 \mathbf{n}_2) d(\varkappa)\} \cdot \tfrac{1}{2}(1 + \xi_d \xi_\gamma);$$

$$a(\varkappa) = M(\varkappa)(3/\varkappa - 2(1-\varkappa)^2) - \tfrac{1}{12}(1-\varkappa)(22 - 13\varkappa),$$

$$b(x) = M(\varkappa)(1/\varkappa + 2\varkappa^2) - \tfrac{1}{12}\varkappa^{-1}(1-\varkappa)(4 + 10\varkappa + 13\varkappa^2),$$

$$c(\varkappa) = M(\varkappa)(3/\varkappa - 2(1-\varkappa)^2) + \tfrac{1}{12}(59\varkappa^2 - 109\varkappa - 22),$$

$$d(\varkappa) = M(\varkappa)(1/\varkappa + 2\varkappa^2) - \tfrac{1}{12}\varkappa^{-1}(59\varkappa^3 + 3\varkappa^2 + 6\varkappa + 4);$$

$$M(\varkappa) = 2\omega + \ln(1-\varkappa) - \tfrac{17}{6}, \quad \varkappa = \frac{2\varepsilon_\gamma}{m_1}, \quad \omega = \ln\frac{m_1}{m_2},$$

$$\xi_{\gamma i} = f_i / r \qquad (i = 1, 2), \qquad \xi_{\gamma 3} = f_3 / r - 1,$$

$$r = \tfrac{1}{3}\varkappa^{-1}\{a(\varkappa) - \xi_1 \mathbf{n}_\gamma b(\varkappa) - \xi_2 \mathbf{n}_2 c(\varkappa) + (\xi_1 \mathbf{n}_\gamma)(\xi_2 \mathbf{n}_2) d(\varkappa)\},$$

$$f_1 = 0, \; f_2 = \tfrac{1}{3}\varkappa^{-1}\{M(\varkappa)(\varkappa^2 + \varkappa - 5) + \tfrac{1}{12}(1-\varkappa)(32 - 5\varkappa)$$

$$+ \xi_1 \mathbf{n}_\gamma [M(\varkappa)(\varkappa^2 + \varkappa + 1) - \tfrac{1}{12}(1-\varkappa)(4 + 5\varkappa)]$$

$$- \xi_2 \mathbf{n}_2 [M(\varkappa)(\varkappa^2 + \varkappa - 5) + \tfrac{1}{12}(32 + 107\varkappa - 67\varkappa^2)]$$

$$- (\xi_1 \mathbf{n}_\gamma)(\xi_2 \mathbf{n}_2)[M(\varkappa)(\varkappa^2 + \varkappa + 1) - \tfrac{1}{12}(4 + \varkappa + 67\varkappa^2)]\},$$

$$f_3 = M(\varkappa)(2-\varkappa) + \tfrac{1}{12}(\varkappa - 1) - \xi_1 \mathbf{n}_\gamma [M(\varkappa)\varkappa + \tfrac{1}{12}(1-\varkappa)]$$

$$- \xi_2 \mathbf{n}_2 [M(\varkappa)(2-\varkappa) + \tfrac{1}{12}(25\varkappa - 49)]$$

$$+ (\xi_1 \mathbf{n}_\gamma)(\xi_2 \mathbf{n}_2)[M(\varkappa)\varkappa + \tfrac{1}{12}(1 - 25\varkappa)].$$

The function $a(\kappa)$ was obtained by Kinoshita and Sirlin.[5]

In conclusion, I thank Prof. V. B. Beresteskiĭ for guidance of this work and to Prof. A. O. Vaĭsenberg for continuous interest in the investigation and for a discussion in the results.

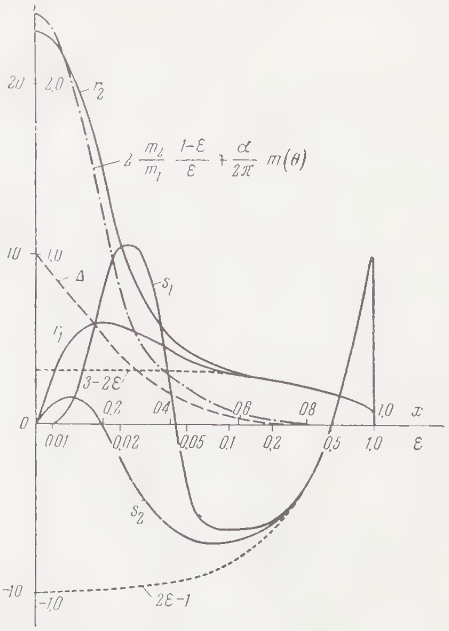

Functions that determine the polarization of the electron. For the sake of convenience, the argument is given in two forms: ε and $x = \theta/\ln(m_1/m_2)$, where $(m_1/m_2)\varepsilon = 2\cosh\theta$. The left-hand set of ordinates is for the functions $3 - 2\varepsilon$, r_1 and r_2; the right-hand scale is for all others.

---

[1] T. Kinoshita and A. Sirlin, Phys. Rev. **113**, 1652 (1959).

[2] V. P. Kuznetsov, JETP **37**, 1102 (1959), Soviet Phys. JETP **10**, 989 (1960).

[3] M. Gell-Mann and R. Feynman, Phys. Rev. 109, 193 (1958).

[4] T. Kinoshita and A. Sirlin, Phys. Rev. Lett. **2**, 177 (1959).

[5] T. Kinoshita and A. Sirlin, Phys. Rev. **107**, 638 (1957).

Translated by J. G. Adashko
314

SOVIET PHYSICS JETP VOLUME 12, NUMBER 6 JUNE, 1961

THERMODYNAMICS OF TURBULENT SYSTEMS

V. G. NEVZGLYADOV

Leningrad State University

Submitted to JETP editor July 6, 1960

J. Exptl. Theoret. Phys. (U.S.S.R.) **39**, 1727-1733 (December, 1960)

Some consequences of the second law of thermodynamics for single-component turbulent systems are derived. It is shown that the second law must be generalized in order to be applicable to turbulent systems. This is done by means of the concept of "turbulent-thermal entropy."

1. AVERAGING OF THE EQUATIONS OF THERMODYNAMICS

1. The thermodynamic equations of irreversible processes are applicable also to those systems in which the medium moves in turbulent fashion. The equation for the change in the specific entropy s, namely $Tds = du + pdv$, is applicable for all single component systems for which the deviator* of the stress tensor does not depend on the strain tensor (in general, it depends on the tensor of the strain velocity) — the so-called "simple systems." The changes must be considered as substantial, i.e., referring them to unit time, we get

$$T\frac{ds}{dt} = \frac{du}{dt} - \frac{p}{\rho^2}\frac{d\rho}{dt}, \qquad \rho = \frac{1}{v}, \tag{1.1}$$

where $d/dt = \partial/\partial t + v_k \partial/\partial x_k$ (the double subscript indicates summation). Making use of the continuity equation

$$\frac{\partial\rho}{\partial t} + \frac{\partial}{\partial x_k}(\rho v_k) = 0 \tag{1.2}$$

and the thermodynamic equation for the energy

$$\rho\frac{du}{dt} = -\operatorname{div}\mathbf{j} + p_{ik}\frac{\partial v_i}{\partial x_k} \tag{1.3}$$

(which are valid for multi-component systems also), we get from (1.1)

$$T\rho\frac{ds}{dt} = -\operatorname{div}\mathbf{j} + P_{ik}\frac{\partial v_i}{\partial x_k}. \tag{1.4}$$

j is the thermal flux density; P_{ik} is the deviator of the stress tensor:

$$P_{ik} = p\delta_{ik} + p_{ik}, \qquad p = -\tfrac{1}{3}(p_{11} + p_{22} + p_{33}). \tag{1.5}$$

Since for each continuous function $f(x_1, x_2, x_3, t)$ (scalar or tensor) the equation

$$\rho\frac{df}{dt} = \frac{\partial}{\partial t}(\rho f) + \frac{\partial}{\partial x_k}(\rho f v_k), \tag{1.6}$$

is identically valid, Eq. (1.4) can be transformed to the well-known equation for the continuity of the entropy:

$$\frac{\partial s_v}{\partial t} + \operatorname{div}\mathbf{Q} = \vartheta, \qquad s_v = \rho s. \tag{1.7}$$

Here s_V is the entropy per unit volume, Q is the density of entropy flux

$$\mathbf{Q} = s_v\mathbf{v} + T^{-1}\mathbf{j}; \tag{1.8}$$

ϑ is the rate of generation of entropy per unit volume of the medium:

$$\vartheta = \vartheta_1 + \vartheta_2, \quad \vartheta_1 = \mathbf{j}\nabla\frac{1}{T}, \qquad \vartheta_2 = \frac{P_{ik}}{T}\frac{\partial v_i}{\partial x_k}. \tag{1.9}$$

The second law requires $\vartheta > 0$, while the inequalities

$$\vartheta_1 > 0, \qquad \vartheta_2 > 0 \tag{1.10}$$

are separately valid.

2. In the case of turbulent motion, the derived equations must be averaged. Carrying out the averaging in the sense of Reynolds, we obtain from (1.2)

$$\partial\bar{\rho}/\partial t + \partial\,\overline{(\rho v_k)}/\partial x_k = 0. \tag{1.11}$$

We introduce two fields of mean velocities. We introduce the first in the usual fashion

$$\bar{v}_i = \frac{1}{t_1}\int\limits_{-t_1/2}^{+t_1/2} v_i(x_1, x_2, x_3, t + \tau)\,d\tau \tag{1.12}$$

(or similarly, by integration over the volume). In this case the field of pulsating velocities v_i' is determined by the equality

$$v_i' = v_i - \bar{v}_i, \tag{1.13}$$

and (1.11) takes the form

---

*The deviator of a tensor t_{ik} is the difference between this tensor and its isotropic part:

$$t_{ik}^{\text{dev}} \equiv t_{ik} - \tfrac{1}{3}(t_{11} + t_{22} + t_{33})\delta_{ik}.$$

$$\frac{\partial\bar{\rho}}{\partial t}+\frac{\partial}{\partial x_k}(\bar{\rho}\bar{v}_k+l_k)=0, \qquad l_k\equiv\overline{\rho v'_k}. \tag{1.14}$$

The flux density of the momentum is the sum of two vectors, the flux density of the mean momentum $\rho \mathbf{v}$ and the flux density of the pulsating momentum $\mathbf{l}$, for which one can write down the equation of motion in the usual fashion:

$$\mathbf{l}=-\alpha\nabla\bar{\rho}, \tag{1.15}$$

where α is a positive coefficient which depends on the turbulent energy. We introduce the second velocity field $\tilde{v}_i$, following Hesselsberg[1] (it was also employed by Blackadar[2]), by forming the mean, weighted according to the density:

$$\tilde{v}_i=\overline{\rho v_i}/\bar{\rho}. \tag{1.16}$$

The continuity equation (1.11) now takes the form

$$\frac{\partial\bar{\rho}}{\partial t}=\frac{\partial}{\partial x_k}(\bar{\rho}\tilde{v}_k)=0. \tag{1.17}$$

The two velocity fields are connected by the relation

$$\tilde{v}_i=\bar{v}_i+l_i/\bar{\rho}=\bar{v}_i-(\alpha/\bar{\rho})\,\partial\bar{\rho}/\partial x_i. \tag{1.18}$$

One field is expressed in terms of the other and the gradient of the mean density $\bar{\rho}$. However, α is a function of the turbulent energy E_t, which has a different definition depending on the form of averaging taken. In the first case,

$$\bar{\rho}E_t=\frac{1}{2}\overline{\rho v^2}-\frac{1}{2}\bar{\rho}\bar{v}^2, \qquad \bar{v}^2=\bar{v}_i\bar{v}_i, \tag{1.19}$$

and in the second

$$\bar{\rho}\tilde{E}_t=\tfrac{1}{2}\overline{\rho v^2}-\tfrac{1}{2}\bar{\rho}\tilde{v}^2, \qquad \tilde{v}^2=\tilde{v}_i\tilde{v}_i. \tag{1.20}$$

We then find the connection

$$\tilde{E}_t=E_t-(\bar{\rho})^{-1}[\bar{v}_il_i+\tfrac{1}{2}l^2]. \tag{1.21}$$

The averaged equations of hydrodynamics and thermodynamics will include both velocity fields; if for the function $\alpha(E_t)$ we neglect the difference between E_t and $\tilde{E}_t$, taking $\alpha(E_t)\approx\alpha(\tilde{E}_t)$, then Eq. (1.18) (with accuracy up to the sign) expresses one field symmetrically in terms of the other. Correspondingly, there are two fields of pulsating velocities: that defined by (1.13) and

$$v''_i=v_i-\tilde{v}_i=v'_i-l_i/\bar{\rho}, \tag{1.22}$$

where

$$\overline{v'_i}=0, \qquad \overline{v''_i}=-l_i/\bar{\rho}, \qquad \overline{\rho v''_i}=0. \tag{1.23}$$

For an incompressible liquid, the difference between the two velocity fields vanishes and $\bar{v}_i = \tilde{v}_i$.

3. Averaging of the equations of motion leads to a much simpler expression if we use the field $\tilde{v}_i$:

$$\bar{\rho}\frac{\tilde{D}\tilde{v}_i}{Dt}=\bar{\rho}f_i+\frac{\partial}{\partial x_k}(\bar{p}_{ik}+T_{ik}), \tag{1.24}$$

where

$$T_{ik}=-\overline{\rho v''_iv''_k}, \qquad \tilde{D}/Dt=\partial/\partial t+\tilde{v}_k\partial/\partial x_k. \tag{1.25}$$

However, the velocity field $\bar{v}_i$ also appears here explicitly in the tensor $\bar{p}_{ik}$ which is substantial in the boundary layer and close to it.

We obtain the following equation for the turbulent energy $\tilde{E}_t$:

$$\bar{\rho}\frac{\tilde{D}}{Dt}\tilde{E}_t=-\frac{\partial I_k}{\partial x_k}+T_{ik}\frac{\partial\tilde{v}_i}{\partial x_k}-\overline{p_{ik}\frac{\partial v''_i}{\partial x_k}}+\frac{\partial}{\partial x_k}\overline{(p_{ik}v''_i)},$$

$$I_k=\tfrac{1}{2}\overline{\rho v''_iv''_iv''_k}. \tag{1.26}$$

Averaging of Eq. (1.3) leads to the following equation:

$$\bar{\rho}\frac{\tilde{D}\tilde{u}}{Dt}=-\frac{\partial}{\partial x_k}(\bar{j}_k+J_k)+\bar{p}_{ik}\frac{\partial\tilde{v}_i}{\partial x_k}+\overline{p_{ik}\frac{\partial v''_i}{\partial x_k}}; \quad J_k=\overline{\rho uv''_k}. \tag{1.27}$$

Closure of the system of six equations (1.14), (1.24), (1.26) and (1.27) was carried out by the author[3] by the construction of the corresponding equations of state upon neglect of quantities containing l_k. As basic quantities, the following six were used:

$$\bar{v}_i,\ \bar{p},\ \bar{T},\ E_t; \tag{1.28}$$

all others were expressed in terms of these and their derivatives; the second law was not used in this case.

2. CONSEQUENCES OF THE SECOND LAW FOR TURBULENT FLOWS

Use of the second law yields additional information on the character of the equations of state; however, in this case it is shown that the quantities (1.28) are not sufficient for describing the turbulent state. Two others are also necessary $\overline{T'^2}$ and $\overline{\rho'^2}$, where $T' = T - \bar{T}$, $\rho' = \rho - \bar{\rho}$.

We carry out averaging of the equation (1.7):

$$\frac{\partial\bar{s}_v}{\partial t}+\frac{\partial\bar{Q}_k}{\partial x_k}=\bar{\vartheta}_1+\bar{\vartheta}_2, \tag{2.1}$$

$$\bar{Q}_k=\bar{s}_v\tilde{v}_k+\overline{s_vv''_k}+\overline{(T^{-1}j_k)}, \qquad \vartheta_1=\overline{j_k\frac{\partial}{\partial x_k}\left(\frac{1}{T}\right)},$$

$$\vartheta_2=\overline{\frac{P_{ik}}{T}\frac{\partial v_i}{\partial x_k}}. \tag{2.2}$$

Setting $\mathbf{j} = -\kappa\nabla T$, and making use of the expansion

$$\frac{1}{T}\approx\frac{1}{\bar{T}}\left(1-\frac{T'}{\bar{T}}+\frac{T'^2}{T^2}\right),$$

we obtain

$$\bar{Q}_k=\bar{s}_v\tilde{v}-\beta\frac{\partial s_v}{\partial x_k}+\frac{\bar{j}_k}{\bar{T}}\left(1+\frac{\overline{T'^2}}{\bar{T}^2}\right)+\frac{\varkappa}{2\bar{T}^2}\frac{\partial}{\partial x_k}\overline{T'^2}. \tag{2.3}$$

Here the equations of state are also satisfied

$$\overline{s_v v_k''} = -\beta \partial \bar{s}_v / \partial x_k. \tag{2.4}$$

Discarding terms of third order in T', we obtain

$$\bar{\vartheta}_1 \approx \frac{\varkappa}{\bar{T}^2}\left\{(\nabla \bar{T})^2\left(1+3\,\frac{\overline{T'^2}}{\bar{T}^2}\right)+\overline{(\nabla T')^2}-\frac{2}{\bar{T}}\left(\nabla \bar{T},\ \nabla \overline{T'^2}\right)\right\}. \tag{2.5}$$

Finally,

$$\bar{\vartheta}_2 = \frac{\eta}{\bar{T}}\left[\Phi_0+\left(1+\frac{\overline{T'^2}}{\bar{T}^2}\right)\Phi_1+\Psi\right], \tag{2.6}$$

$$\Phi_0 = \frac{1}{2}\sum_{i,k}\overline{\left(\frac{\partial v_i'}{\partial x_k}+\frac{\partial v_k'}{\partial x_i}\right)^2}-\frac{2}{3}\,\overline{\operatorname{div}^2 \mathbf{v}'},$$

$$\Phi_1 = \frac{1}{2}\sum_{i,k}\left(\frac{\partial \bar{v}_i}{\partial x_k}+\frac{\partial \bar{v}_k}{\partial x_i}\right)^2-\frac{2}{3}\operatorname{div}^2 \bar{\mathbf{v}}, \tag{2.7}$$

$$\Psi = 2\left(A_{ik}+B_{ik}\right)\frac{\partial \bar{v}_i}{\partial x_k}-\frac{4}{3}(A+B)\operatorname{div}\bar{\mathbf{v}}+C+D, \tag{2.8}$$

where

$$A_{ik} = -\overline{\frac{T'}{\bar{T}}\left(\frac{\partial v_i'}{\partial x_k}+\frac{\partial v_k'}{\partial x_i}\right)}, \qquad B_{ik} = \overline{\frac{T'^2}{\bar{T}^2}\left(\frac{\partial v_1'}{\partial x_k}+\frac{\partial v_k'}{\partial x_i}\right)}, \tag{2.9}$$

$$A = -(\bar{T})^{-1}\,\overline{T'\operatorname{div}\mathbf{v}'}, \qquad B = (\bar{T})^{-2}\,\overline{T'^2\operatorname{div}\mathbf{v}'};$$

$$C = \frac{1}{2\bar{T}}\sum_{i,k}\overline{T'\left(\frac{\partial v_i'}{\partial x_k}+\frac{\partial v_k'}{\partial x_i}\right)^2}-\frac{2}{3\bar{T}}\,\overline{T'\operatorname{div}^2\mathbf{v}'}; \tag{2.10}$$

$$D = \frac{1}{2\bar{T}^2}\sum_{i,k}\overline{T'^2\left(\frac{\partial v_i'}{\partial x_k}+\frac{\partial v_k'}{\partial x_i}\right)^2}-\frac{2}{3\bar{T}^2}\,\overline{T'^2\operatorname{div}^2\mathbf{v}'}. \tag{2.11}$$

Considering $\bar{s}_V$ as the characteristic of the turbulent state of the system, we note that it depends not only on $\bar{T}$, $\bar{\rho}$, but also on $\overline{T'^2}$ and $\overline{\rho'^2}$; in fact, $\bar{s}_V = \overline{\rho s} + \overline{\rho' s'}$. Noting that $s(T, \rho) = s(\bar{T} + T', \bar{\rho} + \rho')$, and carrying out the expansion in a Taylor series, we get, after averaging,

$$\bar{s} = s(\bar{T},\ \bar{\rho}) + \frac{1}{2\bar{T}^2}\left[\bar{T}\,\frac{\partial c_v}{\partial T}-c_v\right]\overline{T'^2} + \frac{1}{2}\frac{\partial^2 s}{\partial \rho^2}\,\overline{\rho'^2}+\frac{\partial^2 s}{\partial \rho\partial T}\,\overline{\rho' T'}. \tag{2.12}$$

(For a perfect gas $\partial^2 s/\partial\rho\partial T = 0$ and $\partial^2 s/\partial\rho^2 = R/M\bar{\rho}^{-2}$.) We shall obtain a similar expression for $\bar{u}$. The quantities $\overline{T'^2}$ and $\overline{\rho'^2}$ cannot be expressed in terms of the fundamental quantities (1.28), but are themselves fundamental characteristics and it is necessary to derive equations for them. We shall obtain an equation for $\overline{\rho'^2}$ by averaging Eq. (1.2), which is first multiplied by ρ':

$$\frac{1}{2}\frac{\partial}{\partial t}\overline{\rho'^2}+\operatorname{div}\left(\overline{\rho'^2}\tilde{\mathbf{v}}+\overline{\rho'^2\mathbf{v}''}\right)=\frac{1}{2}\left(\tilde{\mathbf{v}},\ \nabla\overline{\rho'^2}\right) + \bar{\rho}\,\overline{(\mathbf{v}'',\ \nabla\rho')}+\frac{1}{2}\overline{(\mathbf{v}'',\ \nabla\rho'^2)}. \tag{2.13}$$

Similarly, multiplying Eq. (1.3) by $T' = T - \bar{T}$ and averaging, we obtain:

$$\frac{1}{2}c_v\frac{\partial}{\partial t}\rho\overline{T'^2} = -c_v\left[\overline{\rho' T'}\,\frac{\partial \bar{T}}{\partial t}+\overline{\rho T' v_k}\,\frac{\partial \bar{T}}{\partial x_k}+\frac{1}{2}\frac{\partial}{\partial x_k}\left(\tilde{v}_k\rho\overline{T'^2} + \overline{\rho T'^2 v_k''}\right)\right]+\frac{1}{2}\varkappa\Delta\overline{T'^2}-\varkappa\overline{(\nabla T')^2}-\overline{p T'\operatorname{div}\mathbf{v}} - \eta\bar{T}\left[2A_{ik}\,\frac{\partial \bar{v}_i}{\partial x_k}-\frac{4}{3}A\operatorname{div}\bar{\mathbf{v}}+C\right]+\overline{T'q}, \tag{2.14}$$

$$q = -\rho\left(\partial u/\partial\rho\right)_T d\rho/dt.$$

Keeping the principal terms in Eq. (2.13) and (2.14), it is possible to express them in terms of the fundamental quantities (1.28) and in terms of $\overline{\rho'^2}$ and $\overline{T'^2}$ by means of the equation of state. For example,

$$\overline{\rho'^2\mathbf{v}''} = -\beta\nabla\overline{\rho'^2}; \qquad \overline{\rho T'^2\mathbf{v}''} = -\gamma\nabla\overline{T'^2}. \tag{2.15}$$

Thus, from the eight equations (1.17), (1.24), (1.26), (1.27), (2.13), and (2.14), we can construct a closed system for finding the eight quantities — the six of (1.28), $\overline{\rho'^2}$ and $\overline{T'^2}$.

The second law leads to Eq. (2.1) for turbulent flows and to the inequalities

$$\bar{\vartheta}_1 > 0, \qquad \bar{\vartheta}_2 > 0, \tag{2.16}$$

which are obtained by averaging the inequalities (1.10). The inequalities (2.16) give some evidence on the equations of state and the validity of their derivation.

The quantity $\overline{T'^2}$ is small in comparison with $\bar{T}^2$. Its change, however, and also $\overline{(\nabla T')^2}$, can be significant in the boundary layer. The physical quantity $\overline{\rho'^2}$ should play a role in the account of scattering of radio waves in a turbulent atmosphere. If the turbulent flow of the gas is close to the critical state, then $\overline{\rho'^2}$ becomes important.

If Eq. (2.12) is substituted in (2.1), then we obtain an equation for $s(\bar{T}, \bar{\rho})$ and it is possible to compare it with Eq. (2.14) of Blackadar.[2] For the function s_m, introduced by Blackadar, we can write $s_m = s(\tilde{u}, \bar{\rho}) \approx s(\bar{T}, \bar{\rho})$. Here Eq. (2.1) is not identical with Eq. (2.4) of Blackadar, even in the principal terms. The vector of the entropy flux density $\mathbf{Q}$ and the $\mathbf{Q}_m$ of Blackadar corresponding to it do not coincide:

$$\bar{\mathbf{Q}} - \mathbf{Q}_m \approx \overline{\rho s\mathbf{v}''} - \overline{\rho h\mathbf{v}''}\tilde{T}^{-1} \tag{2.17}$$

(h is the specific enthalpy). Nor does $\bar{\vartheta}$ correspond to $\sigma(s_m)$ of Blackadar.

3. GENERALIZATION OF THE SECOND LAW TO TURBULENT PHENOMENA

The mean value of the entropy $\overline{s}$ as a characteristic of the turbulent state cannot describe its important peculiarities, because it does not depend upon the turbulent energy $\widetilde{E}_t$. Thus the consequences of the second law obtained above are not sufficient, and there is a definite need for its generalization. There is also a definite basis for the generalization of the second law to turbulent phenomena, the same that makes it possible to give a definite meaning to the operation of averaging in the sense of Reynolds, namely the instability of the motion described by the hydrodynamical equations.

The first averaging (molecular) is the reason for the possibility of introduction of the entropy s, and the second averaging (phenomenological, after Reynolds) is the reason for the existence of a certain new function S_e — "the turbulent entropy" per unit mass — as a function which is independent of s.

We shall base the generalization on the following circumstances.

1. The entropy S_e of the turbulent system is a function of its turbulent "internal" state, i.e., a function of the quantities

$$\widetilde{u},\ \overline{\rho},\ \overline{\rho'^2},\ \overline{T'^2},\ \widetilde{E}_t \tag{3.1}$$

(for a one-component system), which do not include $\widetilde{v}_i$. The function S_e may be independent of some of the quantities of (3.1), but depends in an essential manner on $\widetilde{E}_t$ — the second internal energy of the turbulent system (the first is $\widetilde{u}$).

2. In the equation of continuity,

$$\partial(\overline{\rho}S_e)/\partial t + \operatorname{div}\mathbf{Q}_e = \vartheta_e \tag{3.2}$$

the rate of production of turbulent-thermal entropy per unit volume, ϑ_e, is always a positive quantity:

$$\vartheta_e > 0. \tag{3.3}$$

This inequality is a generalization of the second law to turbulent systems.

3. In the formulation of the explicit form of Eq. (3.2), it is necessary to make use of the basic relation (1.1) by carrying out its generalization.

One generalization that satisfies this requirement is to replace the internal energy u by the total internal energy $\widetilde{u} + \widetilde{E}_t$, the pressure p by the total pressure of the turbulent system $\overline{p} + \Pi$, and the temperature by a new integrating divisor, "the generalized temperature" T_e. Thus we define S_e by the differential relation

$$\delta S_e = T_e^{-1}\{\delta(\widetilde{u} + \widetilde{E}_t) - (\overline{p} + \Pi)\,\delta\overline{\rho}/\overline{\rho}^2\}, \tag{3.4}$$

where Π is the turbulent pressure:

$$\Pi = -\tfrac{1}{3}(T_{11} + T_{22} + T_{33}) = \tfrac{2}{3}\overline{\rho}\,\widetilde{E}_t, \tag{3.5}$$

T_e is a function of the turbulent state, i.e., of the variables (3.1); if the two variables $\overline{\rho}$ and $(\widetilde{u} + \widetilde{E}_t)$ are independent the integrating divisor T_e exists as a function of these variables; moreover, it can depend both on the parameters and on the remaining independent variables of (3.1). After choosing of the form of T_e from the relation (3.4), we can find S_e with accuracy up to an additive constant.

We construct an explicit expression for (3.2). Equation (3.4) will be regarded as the substantial change per unit mass moving with mean speed $\widetilde{v}_i$. Referring this change to unit time, we obtain

$$\frac{\widetilde{D}S_e}{Dt} = \frac{1}{T_e}\left\{\frac{\widetilde{D}}{Dt}(\widetilde{u} + \widetilde{E}_t) - \frac{(\Pi + \overline{p})}{\overline{\rho}^2}\frac{\widetilde{D}\overline{\rho}}{Dt}\right\}. \tag{3.6}$$

Making use of Eqs. (1.17), (1.26), and (1.27), we transform (3.6) to the form (3.2). In this case we obtain the flux density of the turbulent-thermal entropy

$$(\mathbf{Q}_e)_k = \overline{\rho}S_e\widetilde{v}_k + T_e^{-1}(\overline{j}_k + J_k + I_k - \overline{p_{ik}v_i''}) \tag{3.7}$$

and the rate of its production

$$\vartheta_e = (\overline{j}_k + J_k + I_k - \overline{p_{ik}v_i''})\frac{\partial}{\partial x_k}\left(\frac{1}{T_e}\right) + T_e^{-1}(\hat{T}_{ik} + \overline{P}_{ik})\frac{\partial\widetilde{v}_i}{\partial x_k}; \tag{3.8}$$

the deviator is defined as $\hat{T}_{ik} \equiv T_{ik} + \Pi\delta_{ik}$. Consideration of the particular cases make it possible to divide inequality (3.3) into two separate relations:

$$(\overline{j}_k + J_k + I_k - \overline{p_{ik}v_i''})\frac{\partial}{\partial x_k}\left(\frac{1}{T_e}\right) > 0, \tag{3.9}$$

$$(\hat{T}_{ik} + P_{ik})\,\partial\widetilde{v}_i/\partial x_k > 0. \tag{3.10}$$

It follows directly from (3.10) that

$$\hat{T}_{ik}\partial\widetilde{v}_i/\partial x_k > 0, \tag{3.11}$$

while consideration of the concrete cases makes it possible to obtain two other inequalities from (2.9):

$$I_k\frac{\partial}{\partial x_k}\left(\frac{1}{T_e}\right) > 0, \tag{3.12}$$

$$(J_k - \overline{p_{ik}v_i''})\frac{\partial}{\partial x_k}\left(\frac{1}{T_e}\right) > 0. \tag{3.13}$$

We note that $J_k - \overline{p_{ik}v_i''} = \overline{\rho h v_k''} - \overline{P_{ik}v_i''}$ where $h = u + p/\rho$ is the specific enthalpy.

In the generalization of the second law proposed by Blackadar,[2] the function S_e is introduced by the definition

$$\widetilde{E}_t\delta S_E = \delta\widetilde{E}_t - \Pi\delta\overline{\rho}/\overline{\rho}^2. \tag{3.14}$$

However, in formulating Eq. (3.2) for this case, we do not obtain the inequality (3.3), because the turbulent energy is continuously dissipated, being converted into thermal energy.

---

[1] H. T. Hesselsberg, Beitr. Phys. f. Atmos., **12**, 141 (1925).

[2] A. K. Blackadar, J. Meteorology, **12**, 165 (1955).

[3] V. G. Nevzglyadov, Doklady Akad. Nauk SSSR **58**, 547 (1947); Vestnik, Leningrad State University No. 3, 3 (1948).

Translated by R. T. Beyer
315

μ^- MESON DECAY FROM THE K ORBIT

M. V. TERENT'EV

Submitted to JETP editor July 8, 1960

J. Exptl. Theoret. Phys. (U.S.S.R.) 39, 1734-1736 (December, 1960)

The decay $\mu^- \to e^- + \nu + \bar{\nu}$ is considered theoretically for the case when the meson is in a bound state in the K orbit of the atom. The spectra of the decay electrons are calculated for several elements and the μ^- meson lifetime as a function of Z is determined. The calculations are carried out with an accuracy up to linear terms in the parameter Z/137.

A number of experimental papers[1,2] have been devoted to the measurement of the probability of the decay $\mu^- \to e^- + \nu + \bar{\nu}$ for the case when the meson is in a bound state in an atom. It was found that the decay probability $\lambda(\xi)$ (where $\xi = Z/137$, Z is the atomic number) increases initially, but then begins to decrease rapidly with growing ξ; for $\xi \gtrsim 0.22$ it becomes smaller than λ_0, where λ_0 is the decay probability of the free μ meson.

The theoretical determination of the function $\lambda(\xi)$ with an accuracy up to linear terms in ξ was attempted by, for example, Überall[3] (here references to earlier work can also be found). The calculation was based on the assumption that the μ meson is bound in the K orbit of an atom with a point-like nucleus. It was found that the function $\lambda(\xi)$ decreases monotonically with increasing ξ, which is in contradiction with the experimental data.

We have taken into account the finite dimensions of the nucleus. The expression for the spectrum of the electrons produced in the decay of the μ meson, including all effects which give a contribution to the terms of order ξ^0 and ξ^1, has the form

$$dW = \frac{w_0}{\pi}(\Phi_1 + \xi\Phi_2)\,dy,$$

$$w_0 = 16\lambda_0(3-4y)\,y^2, \qquad \lambda_0 = G^2\mu^5/192\pi^3,$$

$$\Phi_1 = \frac{\pi}{2} + \tan^{-1}\frac{1-2y}{\tilde{\xi}} + \frac{\tilde{\xi}(1-2y)}{X} + \frac{2\tilde{\xi}^2(1-2y)}{3X^2} - \frac{2\tilde{\xi}^5}{3X^2},$$

$$\Phi_2 = \left(\tan^{-1}\frac{1-2y}{\xi^2}\right)^2 - \frac{\pi^2}{4} + \frac{2\xi(1-2y)+\xi^2}{X_0} + \frac{2}{3}\xi^2\frac{2\xi(1-2y)-\xi^2}{X_0^2},$$

$$X = \left(2y-1+\frac{\tilde{\xi}^2}{2}\right)^2 - \tilde{\xi}^2,$$

$$X_0 = (2y-1)^2 + \xi^2, \quad \xi = \quad -0.306\xi^2\mu R, \qquad (1)$$

where $y = \epsilon/\mu$, ϵ is the energy of the electron, μ is the mass of the meson, G is the weak coupling constant, and R is the radius of the nucleus.

In the calculation we have used the interaction

$$U_{\mathrm{int}} = G(\bar{\psi}_e\gamma_\tau(1+\gamma_5)\psi_{\tilde{\nu}})(\bar{\psi}_\nu\gamma^\tau(1+\gamma_5)\psi_\mu)/\sqrt{2}.$$

The accuracy of the expression for Φ_1 can be improved without further complication of the formulas.

We have considered the model of a nucleus with uniform charge distribution, where the nuclear radius is $R = 1.2 \times 10^{-13}A^{1/3}$, with A the atomic weight. The wave functions of the μ meson were chosen in the following form:

$$\psi_\mu(r) = \psi_\mu^{(0)}(r) + \psi_\mu^{(1)}(r),$$

$$\psi_\mu^{(0)} = Cu(0)\begin{cases} 1 - a(r/R)^{3/2} & r < R \\ w\exp[b(1-r/R)] & r > R, \end{cases}$$

$$\psi_\mu^{(1)} = C\frac{i}{2}\xi\gamma_0\boldsymbol{\gamma}\frac{\mathbf{r}}{r}e^{-\mu\xi r}u(0);$$

$$\gamma_0 = \begin{pmatrix} 1 & 0 \\ 0 & -1 \end{pmatrix}, \qquad \boldsymbol{\gamma} = \begin{pmatrix} 0 & \sigma \\ -\sigma & 0 \end{pmatrix}.$$

Here $\psi_\mu^{(1)}$ is a relativistic correction, γ_0 and γ are Dirac matrices, u(0) is the spinor function, and C is a normalization coefficient. The parameters a, b, and $w = 1 - a$ are functions of the quantity $t = \xi\mu R$. Tables of these parameters are given in the paper of Pustovalov.[4]

It appeared in the course of the calculations that the region $r < R$ gives no contribution to the spectrum in our approximation, while the effect of the finite dimensions of the nucleus consists in the replacement $\xi \to \xi' = \xi - 0.306\xi t$.

Allowance for the finite dimensions of the nucleus in the consideration of the interaction of the electron with the nucleus leads to the replacement of the quantity ξk^{-2}, which corresponds to the external field line in the Feynman graph of Fig. 1, by the expression $k^{-2}\xi\cos kR + \varphi(k)/k$, where k is the momentum transferred from the external field to the electron, and the function $\varphi(k)$ is related to the actual shape of the charge distribution in the nucleus, with $\varphi(k) \to 0$ for $k \to 0$. The region of small k ($k \lesssim \xi\mu$) plays the

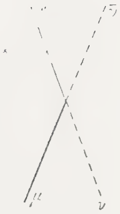

FIG. 1

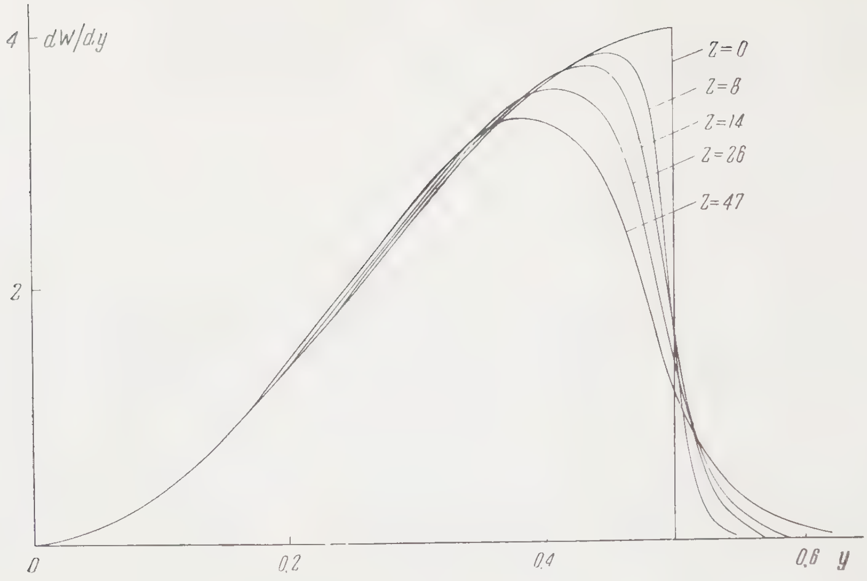

FIG. 2

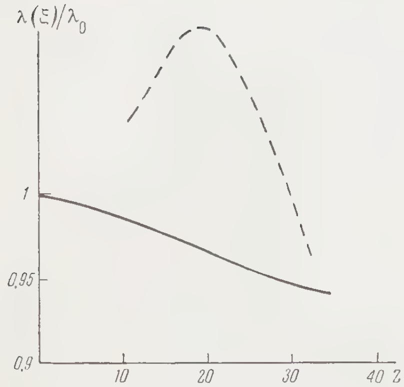

FIG. 3

most important role in the calculation of the integrals to be considered, so that we can disregard, in our approximation, the finite dimensions of the nucleus in this region. Then the contribution from the graph of Fig. 1 to the spectrum is given by the function Φ_2. It is easily seen that the finite dimensions of the nucleus do not lead to the appearance of linear terms in the probability of the μ decay, but affects only the terms $\sim \xi^3$. As we have learned recently, the same result was found by Überall.[5]

We show in Fig. 2 the behavior of the function dW/dy and in Fig. 3 the behavior of the function $\lambda(\xi)$ obtained by numerical integration of expression (1). (The dotted line represents the experimental curve.)

There is little hope that the inclusion of the terms $\sim \xi^2$ in the spectrum will remove the disagreement between theory and experiment. Indeed, let us consider the expression $\rho = \lambda(\xi) - \lambda_0$. We write $\rho = \rho^{(0)} + \rho^{(1)} + \ldots$, where $\rho^{(i)}$ denotes the part of the function ρ coming from the corrections $n\xi^i$ to the spectrum. Integrating the expression (1) we see that $\rho^{(1)}/\rho^{(2)} \approx 0.2$ ($Z \sim 20$); to fit the experimental curve we must require $\rho^{(2)}/\rho^{(1)} \approx 25$; $\rho^{(2)}/\rho^{(0)} \approx 5$, i.e., the effects of higher order in ξ must dominate. Strictly speaking, this possibility cannot be excluded, since we do not know the coefficients of the terms proportional to ξ^2 in the spectrum; however, without any physical reasons to sustain it, this case seems to be wholly unimaginable. Thus, if we reject this possibility, we are not able to interpret the experimental data by assuming that the decay of the μ meson proceeds from the K orbit and including the effects discussed by Überall[3] and in the present paper.

In conclusion I regard it my obligation to express my gratitude to V. B. Berestetskiĭ, A. O. Vaĭsenberg, and L. B. Okun' for constant interest in this work.

---

[1] Sens, Lundy, Swanson, Telegdi, and Yovanovich, Phys. Rev. Letters **1**, 102 (1958).

[2] Barret, Holmstrom, and Keuffel, Phys. Rev. **113**, 661 (1959).

[3] H. Überall, Nuovo cimento **15**, 163 (1960).

[4] G. Pustovalov, JETP **36**, 1806 (1959), Soviet Phys. JETP **9**, 1288 (1959).

[5] H. Überall, Bull. Am. Phys. Soc., ser. **11**, Nr. 5, 256 (1960).

Translated by R. Lipperheide

SOVIET PHYSICS JETP VOLUME 12, NUMBER 6 JUNE, 1961

CROSS SECTIONS FOR RADIATIVE CAPTURE OF NEUTRONS BY HEAVY NUCLEI

P. É. NEMIROVSKIĬ

Submitted to JETP editor July 9, 1960

J. Exptl. Theoret. Phys. (U.S.S.R.) 39, 1737-1743 (December, 1960)

It is shown that even at low energies (beginning at 1 kev) p-wave neutrons are important in radiative capture by heavy nuclei. At energies of 0.1 — 1.0 Mev, neutrons with $l = 1, 2, 3$ dominate the capture cross section. The optical model gives satisfactory agreement with the experiments. In the absence of inelastic scattering the radiative capture cross section becomes constant at energies greater than 0.3 Mev; it increases somewhat at higher energies, owing to the increasing level density. If there is inelastic scattering of neutrons with low l-values, the cross section is nearly proportional to E^{-1}.

1. The radiative capture of low-energy neutrons by heavy nuclei is a resonant process which proceeds predominantly through compound nucleus formation. However, it has been shown[1,2] that direct capture is also possible in heavy nuclei, particularly if it leaves the final nucleus in its ground state. Only for magic nuclei is the direct capture a significant fraction of the total radiative capture. At higher energies, many levels fall within the resolution of the neutron beam, and only average radiative capture cross sections can be measured. At still higher energies (where inelastic scattering is the dominant process) the resonances merge and the average capture cross section is the true capture cross section. It should be noted that at energies of 10 Mev direct capture may predominate.

This paper is devoted to the calculation of the average cross section. The radiative capture cross section for neutrons with orbital angular momentum l near a resonance with total angular momentum $\mathbf{J} = \mathbf{l} + \mathbf{s}$ (where $\mathbf{s} = \mathbf{i} \pm \boldsymbol{\sigma}$, with $\mathbf{i}$ the spin of the target nucleus and $\boldsymbol{\sigma}$ the neutron spin) is

$$\sigma_r^{(lJ)} = \sum_s (2l+1)\,\pi\bar{\lambda}^2 g_{lJs}\,\frac{\Gamma_n^{ls}\Gamma_r}{(E_0-E)^2+\Gamma^2/4}, \qquad (1)$$

where g_{lJs}, the statistical factor, is

$$g_{lJs} = (2J+1)/(2i+1)(2\sigma+1)(2l+1);$$

Γ_n^{ls}, the neutron width, may be non-zero if $|l - s| \leq J \leq l + s$; in the absence of inelastic scattering $\Gamma = \sum_{ls} \Gamma_n^{ls} + \Gamma^r$. Averaging (1), we obtain the well-known expression

$$\sigma_r^{(l)} = \sum_s (2l+1)\,2\pi^2\bar{\lambda}^2 g_{lJs}\,\frac{\overline{\Gamma_n^l\Gamma_r}}{\Gamma}\,\frac{1}{D}, \qquad (2)$$

where D is the average level spacing.

Equation (2) has two factors. The first, $\overline{\Gamma}_n/D = f$, is given by the optical model. The second factor is

$$F = \frac{\overline{\Gamma_n\Gamma_r}}{\Gamma}\,\frac{1}{\overline{\Gamma}_n}. \qquad (3)$$

If a level is formed by neutrons with a single l-value, then

$$F = \frac{\overline{\Gamma_n\Gamma_r}}{\Gamma_n+\Gamma_r}\,\frac{1}{\overline{\Gamma}_n}. \qquad (3a)$$

Thus, to calculate F, it is necessary to determine Γ_r, $D = \overline{\Gamma}_n/f$, and the distribution of neutron widths.

2. Γ_r and D can be determined from thermal-neutron experiments. The level density, D, is determined experimentally, as a rule, only for neutrons with $l = 0$. Only for Al^{28} are there data[3] for neutrons with other orbital angular momenta. To find the dependence of D on l it is necessary to make some assumptions about the dependence of D on the spin and parity of the compound-nucleus levels.

We assume that D does not depend on the parity of the level. For excitation energies of the order of the neutron binding energy, this assumption is reasonable.

The dependence of the level density on spin is given by

$$\rho(E_0, J) = \rho(E_0)\,\frac{2J+1}{(2c\tau)^{1/2}}\exp\left\{-\frac{(J+1/2)^2}{2c\tau}\right\}. \qquad (4)$$

In the statistical theory, a formula can be derived in which $\rho(E_0, J)$ is proportional to $(2J + 1)^2$. Such a formula is correct for spherical nuclei. Small deviations from spherical symmetry remove the degeneracy in the internal axis of the nucleus. For large excitation, only magic nuclei are spherical; other nuclei have non-degenerate internal axes.

Hibdon[3] compared (4) with experimental data on Al^{28} and obtained good agreement. If his results are fitted to the distribution

$$\rho(J) = A(2J+1)^2 \exp\{-(J+{}^1/_2)^2/2c\tau\}, \tag{5}$$

it is not possible to fit both J = 0 and J = 1. In reference 4 level densities were measured in W^{183}. D was found to be 46 ev for J = 0 and 18 ev for J = 1, in agreement with (4). Moreover, it was shown that the strength function for s-wave neutrons is independent of J. Thus, experiment corroborates (4).

Let us consider the quantity F for slow neutrons with $l = 0$. Then (3a) should be used. In nuclei far from magic, radiative capture proceeds with the neutrons making transitions into a large number of different states, making the number of reaction channels large in this case. Therefore, the radiative width is the sum of a large number of widths, one for each channel, and thus does not change much from one level to the next. The dependence of the radiative width on J can be estimated by using a formula given in Blatt and Weisskopf:[5]

$$\Gamma_r \sim \int (E_0 - E)^3 \sum_{J'} \frac{D_J(E_0)}{D_{J'}(E)}\, dE. \tag{6}$$

Here the capture γ rays are assumed to be dipole. If the exponential factor in (4) is neglected (this is accurate enough for small J), then the sum over J′ in (6), and therefore also the radiative width, does not depend on J. The exponential decrease of the level density, which is more rapid for the final-state energy, leads to a slow decrease in the radiative width with increasing J.

In those cases where the radiative widths in a nucleus have been measured for levels with varying $J(i \pm \sigma)$, they have been the same within the experimental accuracy. In our calculations, we neglect the weak dependence of Γ_r on J in Eqs. (6) and (4). For fixed J, Γ_r is taken to be constant. Then the radiative width can be taken outside the averaging in (3a).

The average $\overline{\Gamma_n/(\Gamma_n + \Gamma_r)}$ can be obtained if the distribution of neutron widths is given. If the averaging interval is small compared to the neutron energy, then the distribution of neutron widths is identical with the distribution of reduced neutron widths $\Gamma_n/E^{1/2}$, since $E^{1/2}$ may be considered constant. For heavy nuclei and energies greater than 1 kev, the averaging interval may be taken to be less than the neutron energy.

For the reduced widths, Porter and Thomas[6] give the distribution

$$f(x) = (2\pi\overline{\Gamma}_n x)^{-1/2} \exp\{-x/2\overline{\Gamma}_n\}. \tag{7}$$

This distribution, however, is not the only one which agrees with experiment. In some nuclei, a large number of small neutron widths is observed, but the statistics are not sufficiently good. The simpler exponential distribution

$$f(x) = \exp(-x/\overline{\Gamma}_n)/\overline{\Gamma}_n \tag{8}$$

is also not in disagreement with experiments.

It is easy to calculate the quantity

$$\alpha = \overline{\frac{\overline{\Gamma}_n}{\Gamma_n + \Gamma_r}} \Bigg/ \frac{\overline{\Gamma}_n}{\overline{\Gamma}_n + \Gamma_r}. \tag{9}$$

For the distribution (8) we have

$$\int_0^\infty \frac{f(x)}{1 + \Gamma_r/x}\, dx = 1 + \frac{\Gamma_n}{\overline{\Gamma}_n} \exp\left(\frac{\Gamma_r}{\overline{\Gamma}_n}\right) \mathrm{Ei}\left(-\frac{\Gamma_r}{\Gamma_n}\right).$$

For the distribution (7) this integral must be calculated numerically. In Table I, the second row gives α calculated from (8), the third row α as calculated from (7), as a function of $\Gamma_r/\overline{\Gamma}_n$. The difference between the distributions is not greater than 16%. Thus, the difference in the radiative cross section calculated from the two distributions will be of the order of 10%, and the energy dependence of the cross section is nearly independent of the assumptions about the distribution of widths.

For very small energies, where d-wave capture can be neglected, the results of Table I correctly describe the average for $l = 0$. For $l = 1$ Table I applies only to even-even nuclei; for odd nuclei the channel spin can take on two values, and the calculation is more complicated.

For $l > 0$, we shall consider also the spin-orbit interaction. Then, for each l, there are different strength functions for the two different values, $j = l \pm 1/2$, of the total angular momentum of the neutron. If the resonant level with spin J can be formed by capture of neutrons with both values of j, the average radiative capture cross section is given by

$$\sigma_r = \pi\lambda^2 \sum_J \frac{2J+1}{2(2i+1)} \sum_{j=|J-i|}^{J+i} \sum_\pi \frac{\overline{\Gamma_n^{j\pi J}\Gamma_r^J}}{D^J\Gamma_J}. \tag{10}$$

Here π is the parity of the level capturing the neutron. The statistical factor is independent of j and π and the expression to be averaged is

$$\sum_j \Gamma_n^{j\pi J}\Gamma_r^J \Big/ \Big(\sum_j \Gamma_n^{j\pi J} + \Gamma_r^J\Big). \tag{11}$$

TABLE I

$\Gamma_r/\overline{\Gamma}_n$	0.01	0.02	0.05	0.1	0.2	0,5	1,0	2,0	10	20
α_{exp}	0,969	0,952	0,916	0.880	0,842	0.808	0,809	0,830	0.90	0.96
$\alpha_{\text{p.t.}}$	0.894	0.858	0.795	0.747	0.712	0,679	0,679	0.725	0.869	0.922

If the distributions of neutron widths are independent, the averaging reduces to the calculation of multiple integrals in which each independent width is a variable of integration. α increases with the number of averagings. On the other hand, if the neutron widths are related to each other by constant ratios, we obtain α from Table I by replacing $\sum \Gamma_n^{j\pi J}$ by Γ_n^J. The two cases differ by not more than 10%. We use the second assumption and the results of Table I.

3. The usual formula for the level density is

$$\rho = c \exp(a\sqrt{E}). \tag{12}$$

However, in particular energy intervals, the dependence may be

$$\rho = c' \exp(a'E). \tag{13}$$

But, if the energy variation is within a narrow interval $\Delta E \ll E$ ($\Delta E \sim 1$ Mev for $E \sim 7$ Mev), then the level density always follows the law

$$\rho = \rho_0 \exp(b\Delta E). \tag{14}$$

The level density in heavy nuclei is well known for two energies: in the interval from the ground state to excitations of 1.5 — 2 Mev, and near the neutron binding energy (from slow neutron reaction data).

The radiative capture cross section is proportional to $\rho\Gamma_r/(f + \rho\Gamma_r)$. ρ varies more slowly with energy in (12) than in (13), but Γ_r increases; with (13) Γ_r is constant. When E_{exc} is equal to the binding energy of about 7 Mev, the value of the constant is such that the variation of σ_r with energy is roughly the same for (12) as for (13). The difference can be as large as 20% for $\Delta E \sim 1$ Mev.

4. Inelastic scattering strongly affects the radiative capture cross section. At the inelastic threshold σ_r changes sharply, since there is a jump in its first or higher derivative (depending on the difference in orbital angular momentum of the ground and excited states). The change is in the factor Γ_r/Γ, since Γ now contains the inelastic width Γ_n^{in} along with the elastic widths.

The quantity $f_{in}^{lj} = \Gamma_n^{lj\,in}/D$ can be calculated from the optical model for neutrons escaping with orbital angular momentum l and total angular momentum j. It is given by the coefficient for absorption of neutrons of energy E_1 by the nucleus in the state with excitation $E_0 - E_1$. Here we assume that the optical potential in an excited state of the nucleus is identical with the optical potential in the ground state. Then

$$f_{\text{in}}^{lj} = \frac{1}{2\pi}\{1 - |\eta_{E_1}^{lj}|^2\}. \tag{15}$$

In the calculations, the quantity

$$[\overline{\Gamma_n\Gamma_r}/(\Gamma_n^{H} + \Gamma_n^{J} + \Gamma_r)]\,[\overline{\Gamma}_n\,\overline{\Gamma}_r/\overline{\Gamma}]^{-1} \tag{16}$$

plays an essential role. Since it is natural to consider the elastic and inelastic widths as independent, (16) is calculated by a double integration over the distribution of widths.

5. Recently many measurements of radiative capture cross sections have appeared. However, they are not very accurate. Nevertheless, general regularities can be traced in the data from one group of measurements. In our method of calculation, we need to know the parameters for slow neutrons, the level density near the ground state of the compound nucleus, and the absorption coefficients for the various values of l, j. Thus, our method is applicable only to spherical nuclei, since there are no data on η^{lj} for $l \neq 0$ in non-spherical nuclei.

The calculation is most accurate for nuclei with high level densities; for this reason we have considered odd Z nuclei, in particular the nuclei In^{115}, Au^{197}, Ag^{109}. For In^{115} a spherical model is satisfactory, since in this nucleus Z differs by only one from a magic number. For Au^{197} and Ag^{109}, a spherical model of the nucleus may be somewhat worse. In all three nuclei, the positions of the excited states are well known up to 0.5 — 0.6 Mev (Table II).

The quantities η^{lj} were calculated from an optical potential with diffuse edge and spin-orbit interaction.[7] The results of the calculation and comparison with experimental results[8] for all three nuclei are shown in the figures. In indium, the experiments measure the cross section for formation of one of the isomers. The ratio of the cross sections for formation of the two isomers has been measured by Hughes at E = 1 Mev to be $\sigma(In^{116}, J = 1)/\sigma(In^{116}, J = 4) = 0.5$. We have used this ratio for all energies. In the calculations, the exponential distribution for the neutron widths was

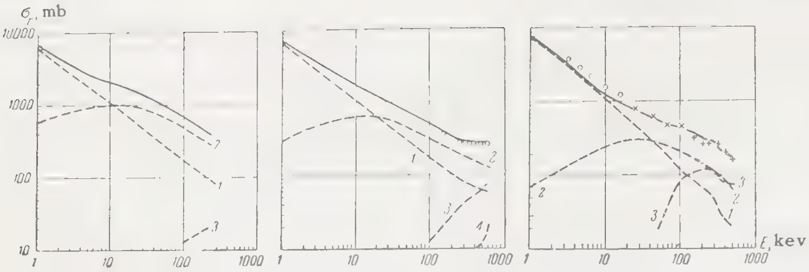

Ag^{109} In^{115} Au^{197}

Radiative capture cross sections. The dashed curves refer to partial waves. The numbers on the curves indicate the value of $l + 1$. The solid curve gives the total cross section. The experimental points are: o – from reference 9; +, × – from reference 8.

TABLE II

Nucleus	Ag^{109}	In^{115}	Au^{197}
Spin and parity of target nucleus	$1/2^-$	$9/2^+$	$3/2^+$
Γ_r, 10^{-3} ev, for $E_n \sim 0$	140	80	125
D, ev, for compound nucleus with $J = j + 1/2$ for $E_n \sim 0$	21.5	17.4	29.7
D, kev, for compound nucleus, E = 1 Mev	25	25	20
Excited states of target nucleus, Mev			
first	0.088 $7/2^+$	0.335 $1/2^-$	0.077 $1/2^+$
second	0.31 $3/2^-$	0.595	0.268 $3/2^+$
third	0.41 $5/2$		0.279 $5/2^+$
fourth			0.41 $11/2^-$

used. The Thomas-Porter distribution gives cross sections which are smaller by 10 – 15%, but the energy dependence is the same, and agreement with experiment is no worse. For energies from 1 to 100 kev, the cross sections for all three nuclei are essentially the same. In Ag, where p-wave neutrons are important, the capture falls as $E^{-1/2}$, and in Au it falls as $E^{-0.6}$. However, at 0.1 Mev the contributions of the individual orbital angular momenta are different: p-waves contribute 50% in Au and 75% in Ag; d-waves contribute 20% in Au, 2% in Ag. At higher energies the cross sections begin to differ significantly. The indium spin-½ level is excited only by capture or emission of neutrons with $l = 2$ or 3. The presence of this level does not significantly affect the radiative capture cross section; starting at 0.4 Mev the radiative capture cross section becomes constant, and at about 0.6 Mev even increases somewhat. The latter behavior is a consequence of the increase in the level density, which compensates the decrease in the cross section for formation of the compound nucleus. In Au^{197}, the cross section falls as $E^{-1/2}$ in the interval 0.1 – 0.25 Mev, but the increase in inelastic scattering around 0.3 Mev leads to a sharp drop in the cross section, with a subsequent return to $E^{-1/2}$ at about 0.5 Mev. Similar behavior is observed in Ag^{109}. Good agreement with experiment is also obtained for I^{127}. For even-even nuclei, there are almost no data on level densities in the resonance region (except in U^{238} and Th^{232}). Therefore, one can try to determine the level spacing from the radiative capture cross section at 0.1 Mev (if the radiative width is known). In Mo^{100}, a value of D of 2 kev is obtained for s levels. With such a level density, and with D = 50 kev for an excitation of 1 Mev in Mo^{101}, the cross section is found to be nearly constant in the interval 0.1 – 0.5 Mev, in agreement with experiment.

Recently F. L. Shapiro[9] and colleagues investigated radiative capture in Ag and Au in the interval 1 – 20 kev. In Ag, the observed dependence of the cross section on energy agrees well with our calculations, but in Au the theory leads to a somewhat sharper fall-off in the cross section than is observed. In a recent paper,[10] Mossin-Kotin, Margolis, and Troubetskoy have also investigated σ_r. Notwithstanding their use of an essentially different method, the results they obtain are close to ours.

---

[1] A. V. Shutko and D. F. Zaretskiĭ, JETP **29**, 834 (1955), Soviet Phys. JETP **2**, 714 (1956).

[2] D. F. Zaretskiĭ, JETP **37**, 1084 (1959), Soviet Phys. JETP **10**, 772 (1959).

[3] C. Hibdon, Phys. Rev. **114**, 179 (1959).

[4] Waters, Evans, Kinsey, and Williams, Nucl. Phys. **12**, 563 (1959).

[5] Blatt and Weisskopf, Theoretical Nuclear Physics, Wiley 1952, p. 649.

[6] K. G. Thomas and C. C. Porter, Phys. Rev. **104**, 483 (1956).

[7] P. E. Nemirovskiĭ, Ядерные реакции при малых и средних энергиях (Nuclear Reactions at Low and Medium Energies), U.S.S.R. Acad. Sci. 1958.

[8] Атлас нейтронных сечений (Atlas of Neutron Cross Sections) 2nd ed., Atomizdat 1959.

[9] Isakov, Popov, and Shapiro, JETP **38**, 989 (1960), Soviet Phys. JETP **11**, 712 (1960).

[10] Mossin-Kotin, Margolis, and Troubetskoy, Phys. Rev. **116**, 937 (1959).

Translated by M. Bolsterli
317

SOVIET PHYSICS JETP VOLUME 12, NUMBER 6 JUNE, 1961

SYMMETRY OF THE SOLUTIONS OBTAINED IN DETERMINING THE SINGULARITIES OF FEYNMAN DIAGRAMS BY LANDAU'S METHOD

A. Z. PATASHINSKIĬ

Siberian Division, Academy of Sciences, U.S.S.R.

Submitted to JETP editor July 9, 1960

J. Exptl. Theoret. Phys. (U.S.S.R.) **39**, 1744-1746 (December 1960)

It is proved that for some diagrams the solutions obtained by Landau's method for determining the position of the singularities are symmetric.

In finding the position of the singularities of Feynman diagrams by Landau's method[1] considerable simplification results for symmetric diagrams, provided the premise is accepted that the solutions for the angles and the parameters α exhibit a symmetry. The diagram should be symmetric under transformations which leave unchanged the invariants characterizing the location of the singularity. For the four-point function, clearly, only rotations through the angle π and reflections are possible.

The symmetry assumption is related to the question of uniqueness of the solution with respect to α for prescribed values of the external invariants in the Landau system of equations

$$\Sigma\alpha_i q_i = 0, \tag{1}$$

$$\alpha_i > 0, \qquad q_i^2 - m_i^2 = 0. \tag{2}$$

Equation (1), together with conservation laws at each vertex, determines the internal vectors q as linear combinations of the external vectors p with coefficients that depend on α. From (2) we obtain a system of l equations

$$P_l[\alpha_k,\ (p_s p_m)] = 0 \quad (i,\ k = 1,\ \ldots,\ l;\ s,\ m = 1, 2, 3), \tag{3}$$

where l is the number of internal lines in the diagram and P_l is a polynomial homogeneous in α. For the case of a symmetric diagram, under a transformation with respect to which the diagram is symmetric the system (3) is transformed into itself. If there exists a solution which is not symmetric with respect to α then there also exists another solution in which the parameters α are interchanged. If on the other hand for the given values of the external parameters the system of equations (3) has a unique solution, then that solution is symmetric. The symmetries of α and of the angles of the diagram are in a one to one correspondence.

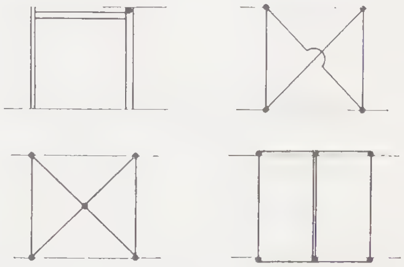

FIG. 1

There exist for symmetric diagrams nonsymmetric solutions of the system (3), but all such solutions that we were able to find failed to satisfy the requirement that the α be positive. We were not able to prove the symmetry assertion for the general case, and therefore it is necessary to verify its validity for every individual case anew.

For a number of diagrams it can be shown that the requirement that the α be positive leads to symmetry. In particular, this could be done for those $\pi\pi$-scattering diagrams with asymptotes $16 \times 16\mu^2$, whose singularities were determined by Kolkunov et al.[2] (Fig. 1). We will show how this can be done on the example of the diagram shown in Fig. 2.

We set the masses of all lines equal to unity. From the equation $\alpha_2 q_2 + \alpha_7 q_7 - \alpha_6 q_6 = 0$, and the analogous equations for other contours, we obtain for $\mu_{ik} = q_i \cdot q_k$ in terms of the α:

$$\mu_{27} = (\alpha_6^2 - \alpha_2^2 - \alpha_7^2)/2\alpha_2\alpha_7,$$

$$\mu_{26} = -(\alpha_7^2 - \alpha_2^2 - \alpha_6^2)/2\alpha_2\alpha_6, \ldots \tag{4}$$

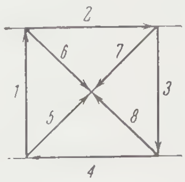

FIG. 2

From the equality

$$\alpha_1 q_1 + \alpha_2 q_2 = \alpha_5 q_5 - \alpha_7 q_7,$$

we obtain by squaring both sides

$$\alpha_1^2 + \alpha_2^2 + 2\alpha_1\alpha_2\mu_{12} = \alpha_5^2 + \alpha_7^2 - 2\alpha_5\alpha_7\mu_{57}. \qquad (5)$$

Making use of the conservation laws at the appropriate vertices we can express μ_{12} and μ_{57} in terms of the angles given by Eq. (4):

$$\mu_{12} = 1 + \mu_{26} - \mu_{16}, \qquad \mu_{57} = -1 - \mu_{56} - \mu_{67}.$$

After substituting into Eq. (5) and expressing all angles in terms of the α we obtain as a result of some simple manipulations

$$(\alpha_1 + \alpha_2 - \alpha_5 - \alpha_7)[\alpha_1 + \alpha_2 + \alpha_5 + \alpha_7 + (\alpha_1 + \alpha_5)(\alpha_2 + \alpha_7)/\alpha_6 + \alpha_6] = 0.$$

As a consequence of the positive nature of the α the expression in the square brackets cannot vanish and so we deduce that

$$\alpha_1 + \alpha_2 = \alpha_5 + \alpha_7.$$

The consideration of contours obtained from the one used by us by a rotation about the central vertex by $\pi/2$, etc., yields

$$\alpha_2 + \alpha_3 = \alpha_6 + \alpha_8, \qquad \alpha_3 + \alpha_4 = \alpha_5 + \alpha_7,$$
$$\alpha_4 + \alpha_1 = \alpha_6 + \alpha_8.$$

It follows from these four relations that

$$\alpha_1 = \alpha_3, \qquad \alpha_2 = \alpha_4, \qquad \alpha_5 + \alpha_7 = \alpha_6 + \alpha_8.$$

Let us take these equalities into account in Eq. (4). The conservation law at the central vertex gives:

$$1 + \mu_{67} = 1 + \mu_{58}, \qquad -1 + \mu_{56} = -1 + \mu_{78}.$$

Upon substituting into these expressions the angles from Eq. (4) we obtain

$$[\alpha_2^2 - (\alpha_6 - \alpha_7)^2](1/\alpha_6\alpha_7 - 1/\alpha_5\alpha_8) = 0,$$
$$[\alpha_1^2 - (\alpha_6 - \alpha_5)^2](1/\alpha_5\alpha_6 - 1/\alpha_7\alpha_8) = 0.$$

It is not hard to show that the requirements that the α be positive leads to the relations

$$\alpha_5\alpha_6 = \alpha_7\alpha_8, \qquad \alpha_6\alpha_7 = \alpha_5\alpha_8,$$

hence

$$\alpha_5 = \alpha_6 = \alpha_7 = \alpha_8.$$

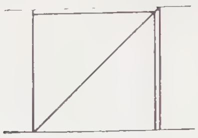
FIG. 3

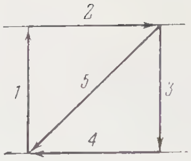

FIG. 4

We note that had we required the α to be non-negative we would have also obtained the solution corresponding to the non-symmetric diagram, Fig. 3, which arises on reduction starting from one of the lines that enter the central vertex.

The symmetry of the remaining $\pi\pi$ diagrams can be proved in an analogous manner. The symmetry of the diagram shown in Fig. 4 may be deduced somewhat differently.

To this end we set $\alpha_5 = 1$. The condition $\alpha > 0$ makes it possible to express uniquely α_2 in terms of α_1, and α_4 in terms of α_3:

$$\alpha_2 = -\alpha_1/2 + Z_1, \qquad \alpha_4 = -\alpha_3/2 + Z_3,$$

where

$$Z_1 = \sqrt{1 - 3\alpha_1^2/4} \qquad Z_3 = \sqrt{1 - 3\alpha_3^2/4}.$$

Squaring both sides of the equation

$$\alpha_1 q_1 + \alpha_2 q_2 = -(\alpha_3 q_3 + \alpha_4 q_4),$$

and expressing all angles in terms of α_1 and α_3, we obtain after some regrouping of terms

$$(\alpha_1 - \alpha_3)\left[\frac{5}{2}(\alpha_1 + \alpha_3) + \frac{3}{4}\alpha_1\alpha_3 + 2 + Z_1Z_3 + Z_3\left(1 + \frac{\alpha_1}{2}\right) + Z_1\left(1 + \frac{\alpha_3}{2}\right)\right] + Z_3\alpha_1(1 + \alpha_1) - Z_1\alpha_3(1 + \alpha_3) = 0.$$

For $0 < \alpha_1, \alpha_3 < 1$ the expression on the left side can vanish only if $\alpha_1 = \alpha_3$.

The author is grateful to V. V. Sudakov for interest in this work and advice.

---

[1] L. D. Landau, JETP **37**, 62 (1959), Soviet Phys. JETP **10**, 45 (1960).

[2] Kolkunov, Okun', Rudik, and Sudakov, JETP **39**, 340 (1960), Soviet Phys. JETP **12**, 242 (1961).

Translated by A. M. Bincer
318

SOVIET PHYSICS JETP VOLUME 12, NUMBER 6 JUNE, 1961

ON THE DETERMINATION OF THE SIGN OF THE MASS DIFFERENCE OF K_1^0 *AND* K_2^0 *MESONS*

S. G. MATINYAN

Physics Institute, Academy of Sciences, Georgian S.S.S.R.

Submitted to JETP editor July 9, 1960

J. Exptl. Theoret. Phys. (U.S.S.R.) 39, 1747-1755 (December, 1960)

The experiment proposed by Kobzarev and Okun'[1] for determining the sign of the mass difference Δm of K_1^0 and K_2^0 mesons is discussed with a view to taking into account the finite thickness of the plates through which the K_2^0-meson beam passes. A modification of this experiment which should lead to an increased K_1^0-meson yield from the plates is suggested. Other methods of determining the sign of Δm are also discussed.

1. Kobzarev and Okun' recently proposed[1] an experimental method for determining the sign of the mass difference $\Delta m = m_1 - m_2$ of K_1^0 and K_2^0 mesons, which are the oscillating odd and even components, respectively, of the K^0 and $\overline{K}^0$ mesons:

$$K^0 = (K_1^0 + K_2^0)/\sqrt{2}, \qquad \overline{K}^0 = (K_1^0 - K_2^0)/\sqrt{2}.$$

The experiment suggested in reference 1 is based on the idea of using interference phenomena occurring during the passage of a K_2^0-meson beam through two plates of different nuclear properties. Owing to the difference in the interactions of the strongly interacting components of the K_2^0 wave in the transmitted undeflected beam, there arises K_1^0 waves with a non-zero phase difference $\Delta\varphi$. The decisive role is played by the difference in the scattering properties of the plates, which results in a difference in the forward scattering amplitudes of the K^0 and $\overline{K}^0$ waves in the plates. This non-zero phase difference between the two coherent states also makes it possible to determine the sign of Δm.

A diagram of the proposed experiment is shown schematically in Fig. 1.

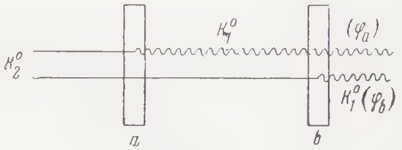

FIG. 1

Kobzarev and Okun'[1] considered this phenomenon for the case of thin plates, which give a small K_1^0-meson yield to the right of plate b for a given number of incident K_1^0 mesons.

On the other hand, it is obvious that for a given K_2^0-meson beam one can choose the thickness of a plate of given material so as to obtain the maximum K_1^0-meson yield from it. This is connected with the opposite effects resulting from the thickness factor as regards the "regeneration" and "survival" of K_1^0 mesons in the plate.

In fact, it can be shown (see below) that the dependence of the number of K_1^0 mesons emerging from the plate on its thickness $x = vt$ (v is the K^0-meson velocity, which is assumed to be constant during the passage of the beam through the plate; t is the time of flight) is fundamentally given by the expression

$$1 - 2\cos(\Delta m t/\gamma)e^{-t/2\gamma\tau_1} + e^{-t/\gamma\tau_1}, \tag{1}$$

where τ_1 is the lifetime of the K_1^0 meson, $\gamma = 1/\sqrt{1 - v^2}$ ($\hbar = c = 1$). This expression has a maximum at values of x considerably exceeding the K_1^0 range relative to its decay $l = \gamma\tau_1\nu$. For example, for a meson kinetic energy of the order of 40 Mev, it is a maximum at $x \approx 3$ cm and $l = 1.2$ cm.

The thickness of the first plate a can thus be chosen to be the "optimum" from the viewpoint of the K_1^0-meson yield. Of course, the thickness of the second plate b should then be comparable to that of plate a.

In connection with the discussion above, there is the problem of considering the experiment proposed in reference 1 with a view to taking into account the finite thickness of the plates. Here, the question naturally arises as to whether the increase in thickness of the plates leads to a fundamental decrease in the oscillation effect and thus reduces the possibility of distinguishing between the signs of Δm.

It will be shown below, however, that if we increase the K_1-meson yield by making the plate thicker, we are able at the same time to determine the sign of Δm (at least, for large enough $\Delta\varphi$). In this respect, the situation is no worse than in the limiting case of thin plates.

Moreover, the consideration of plates of finite thickness makes it possible to propose a modification of the experiment so as to increase the intensity of K_1^0 mesons and provide the possibility of determining the sign of Δm in the case of values of $\Delta\varphi$ smaller than in the originally proposed experiment. (Of course, it is still necessary to have information as regards the sign of $\Delta\varphi$.)

We shall now consider the problem.

2. Let $\alpha_1(t)$ and $\alpha_2(t)$ be the amplitudes of the K_1^0 and K_2^0 components of the K^0 beam at the time t. The time variation of these amplitudes as the K^0 beam passes through a substance is determined by the following equations:[2]

$$\frac{d\alpha_1}{dt} = \left[-i\omega_1 - \frac{1}{2\gamma\tau_1} + ikv\frac{n+\bar{n}}{2}\right]\alpha_1 + ikv\frac{n-\bar{n}}{2}\alpha_2,$$
$$\frac{d\alpha_2}{dt} = \left[-i\omega_2 - \frac{1}{2\gamma\tau_2} + ikv\frac{n+\bar{n}}{2}\right]\alpha_2 + ikv\frac{n-\bar{n}}{2}\alpha_1. \quad (2)$$

Here $\omega_{1,2} = (k^2 + m_{1,2}^2)^{1/2}$, τ_2 is the lifetime of K_2^0 mesons (hereafter, for simplicity, we shall set $\tau_2 = \infty$), k is the K^0-meson momentum, $n(\bar{n})$ is the index of refraction of the $K^0(\bar{K}^0)$ wave in the substance.

If we introduce into the considerations the forward coherent scattering amplitude of the $K^0(\bar{K}^0)$ mesons $f(0)[\bar{f}(0)]$, then we can write

$$n = 1 + 2\pi k^{-2}Nf(0), \qquad \bar{n} = 1 + 2\pi k^{-2}N\bar{f}(0), \quad (3)$$

where N is the number of atoms per cm^3 of substance.

From Eq. (2) it is seen that the "regeneration" effect is determined by the terms with $n - \bar{n}$, i.e., by the difference in the complex forward-scattering amplitudes of the K^0 and $\bar{K}^0$ waves. As a good approximation, we can take

$$vk\left|\frac{n-\bar{n}}{2}\right| \ll 1/2\gamma\tau_1. \quad (4)$$

This inequality reflects the fact that the K_1^0-meson decays predominate over the "regeneration" effects in the substance.

If we neglect $f(0)$ in comparison with $\bar{f}(0)$, then inequality (4) reduces to the condition

$$2\pi m^{-1}N(\bar{\sigma}/4\pi)^{1/2} \ll 10^{10}, \quad (4')$$

which is always well satisfied.* Here $\bar{\sigma}$ is the total interaction cross section of $\bar{K}^0$ mesons with nuclei of the substance and m is the K^0-meson mass.

In this approximation, the solution of Eqs. (2) for the given initial conditions $\alpha_1(T)$ and $\alpha_2(T)$ has the form

$$\alpha_1(t) = [\alpha_1(T) - R\alpha_2(T)]\exp\{-\lambda^{(+)}(t-T)\}$$
$$+ R\alpha_2(T)\exp\{-\lambda^{(-)}(t-T)\},$$
$$\alpha_2(t) = -R\alpha_1(T)\exp\{-\lambda^{(+)}(t-T)\} + [\alpha_2(T)$$
$$+ R\alpha_1(T)]\exp\{-\lambda^{(-)}(t-T)\}. \quad (5)$$

In (5) we introduce the notation

$$R = \frac{ivk(n-\bar{n})/2}{i\Delta m/\gamma + 1/2\gamma\tau_1}; \qquad |R| \ll 1,$$

$$\lambda^{(+)} = i\omega_1 + 1/2\gamma\tau_1 - ivk(n+\bar{n})/2,$$
$$\lambda^{(-)} = i\omega_2 - ivk(n+\bar{n})/2.$$

In writing the solution (5), we have neglected, in accordance with the condition (4), the terms with R^2, which we shall also do in what follows.

If at the time $t = T = 0$ a beam of K_2^0 mesons $[\alpha_1(0) = 0$ and $\alpha_2(0) = 1]$ is incident on plate a of thickness $x_a = vt_a$, then a wave propagating along the direction of the primary K_2^0 beam will fall on plate b of thickness $x_b = vt_b$ placed at a distance of $x_0 = vt_0$ from the first plate; the amplitudes of the K_1^0 and K_2^0 waves of this beam will be equal respectively to

$$\alpha_1(t_a + t_0) = R_a(\exp\{-\lambda_a^{(-)}t_a\}$$
$$- \exp\{-\lambda_a^{(+)}t_a\})\exp\{-(i\omega_1 + 1/2\gamma\tau_1)t_0\},$$
$$\alpha_2(t_a + t_0) = \exp\{-\lambda_a^{(-)}t_a\}e^{-i\omega_2 t_0}. \quad (6)$$

Taking these α_i (i = 1, 2) as the initial conditions for plate b in (5), we find the amplitudes of the K_1^0 and K_2^0 waves in the unscattered beam emerging from plate b:*

$$\alpha_1(t_a + t_0 + t_b) = R_a(\exp\{-\lambda_a^{(-)}t_a\}$$
$$- \exp\{-\lambda_a^{(+)}t_a\})\exp\{-\lambda_b^{(+)}t_b\}\exp\{-[i\omega_1$$
$$+ 1/2\gamma\tau_1]t_1\} + R_b(\exp\{-\lambda_b^{(-)}t_b\}$$
$$- \exp\{-\lambda_b^{(+)}t_b\})\exp\{-\lambda_a^{(+)}t_a\}e^{-i\omega_2 t_0},$$
$$\alpha_2(t_a + t_0 + t_b) = \exp\{-\lambda_a^{(-)}t_a - \lambda_b^{(-)}t_b\}e^{-i\omega_2 t_0}. \quad (7)$$

We introduce the notation

$$\frac{1}{2}k(n_a - \bar{n}_a) = r_a e^{i\varphi_a}, \quad (8)$$

where, according to (3)

$$r_a = \pi N_a k^{-1}([\mathrm{Im}(f_a(0) - \bar{f}_a(0))]^2 + [\mathrm{Re}(f_a(0) - \bar{f}_a(0))]^2)^{1/2}, \quad (9)$$

---

*Thus, for example, in the case of copper (if we take $\bar{\sigma} \approx 10^{-24}$ cm^2) the left-hand side of (4′) is equal to 1.7×10^8.

*From (6) and (7) it follows that the discarding of the terms with R^2 in our problem reduces to the neglecting of the phenomenon of the production of K_2^0 mesons from K_1^0 mesons, which is natural.

$$\tan\varphi_a = \mathrm{Im}\,[f_a(0) - \bar{f}_a(0)]\,/\,\mathrm{Re}\,[f_a(0) - \bar{f}_a(0)]. \qquad (10)$$

Similar notation is introduced for plate b. (We note that the $r_{a,b}$ introduced here differ from the corresponding quantities in reference 1 in that they refer to a unit length of substance.)

With this notation we obtain, after some calculation, the following formula for the number of K_1^0 mesons N_1 (per incident K_2^0 meson) traveling forward to the right of plate b:

$$N_1 = \exp\left\{-\frac{v}{2}\left[N_a(\sigma_a + \bar{\sigma}_a)\,t_a + N_b(\sigma_b + \bar{\sigma}_b)\,t_b\right]\right\}$$
$$\times \left\{r_a^2 P(t_a)\exp\left[-\frac{t_0 + t_b}{\gamma\tau_1}\right]\right.$$
$$+ r_b^2 P(t_b) + 2r_a r_b\left[C(t_a, t_b)\cos\left(\Delta\varphi - \frac{\Delta m}{\gamma}(t_0 + t_b)\right)\right.$$
$$\left.\left. - S(t_a, t_b)\sin\left(\Delta\varphi - \frac{\Delta m}{\gamma}(t_0 + t_b)\right)\right]\exp\left[-\frac{(t_0 + t_b)}{2\gamma\tau_1}\right]\right\}, \qquad (11)$$

where $\sigma_i(\bar{\sigma}_i)$ is the total cross section for the interaction of K_0 ($\bar{K}_0$) mesons with the nuclei of plate i ($i = a, b$), $\Delta\varphi = \varphi_a - \varphi_b$.

In (11) we have introduced the following notation:

$$P(t) = \left[1 - 2\cos\left(\frac{\Delta m}{\gamma}t\right)\exp\left\{-\frac{t}{2\gamma\tau_1}\right\}\right.$$
$$\left. + \exp\left\{-\frac{t}{\gamma\tau_1}\right\}\right]\left[\left(\frac{\Delta m}{\gamma v}\right)^2 + \left(\frac{1}{2\gamma\tau_1 v}\right)^2\right]^{-1},$$
$$C(t_a, t_b) = \left[1 - \cos\left(\frac{\Delta m}{\gamma}t_a\right)e^{-t_a/2\gamma\tau_1} - \cos\left(\frac{\Delta m}{\gamma}t_b\right)e^{-t_b/2\gamma\tau_1}\right.$$
$$\left. - \cos\left(\frac{\Delta m}{\gamma}(t_a + t_b)\right)\exp\left\{-\frac{t_a + t_b}{2\gamma\tau_1}\right\}\right]\left[\left(\frac{\Delta m}{\gamma v}\right)^2\right.$$
$$\left. + \left(\frac{1}{2\gamma\tau_1 v}\right)^2\right]^{-1},$$
$$S(t_a, t_b) = \left[\sin\left(\frac{\Delta m}{\gamma}t_a\right)\exp\left\{-\frac{t_a}{2\gamma\tau_1}\right\}\right.$$
$$- \sin\left(\frac{\Delta m}{\gamma}t_b\right)\exp\left\{-\frac{t_b}{2\gamma\tau_1}\right\}$$
$$\left. - \sin\left(\frac{\Delta m}{\gamma}(t_a - t_b)\right)\exp\left\{-\frac{t_a + t_b}{2\gamma\tau_1}\right\}\right]\left[\left(\frac{\Delta m}{\gamma v}\right)^2\right.$$
$$\left. + \left(\frac{1}{2\gamma\tau_1 v}\right)^2\right]^{-1}. \qquad (12)$$

The meaning of the terms in formula (11) is clear. Thus, for example, the presence of the factor $P(t_a)$ in a product with r_a^2 is connected with the oscillation of the odd K_2^0 mesons into the even K_1^0 mesons and the decay of the latter inside plate a. The occurrence of the maximum for this factor also makes it possible to choose the "optimum" thicknesses of the plates.

The exponential expression following r_a^2 characterizes the decrease in K_1^0 mesons between the plates and in the second plate due to decays. The term with r_b^2 has a similar meaning. The presence of the common exponential factor in (11) is connected with the attenuation of the beam due to the interactions of K^0 and $\bar{K}^0$ mesons with the substance and is determined by the imaginary part of the scattering amplitudes at the angle zero. This factor varies weakly with the plate thickness.

Formula (11), which takes into account the finite thickness of the plates, has the property that the thickness of the second plate $x_b = vt_b$ enters (11) on an equal basis with the distance between plates $x_0 = vt_0$. This allows us to obtain information on the sign of Δm both by studying the dependence of N_1 on x_0 for fixed plate thicknesses and by observing the variation of N_1 as a function of the thickness of the second plate x_b ("optimum") and x_0 (which can be taken equal to zero).

We thus have another way of performing an experiment to determine the sign of Δm: We place plates a and b flat against each other and vary the thickness of plate b with plate a at the "optimum" thickness.

In connection with formula (11) one should note the following. Formula (11) gives the number of K_1^0 mesons in the beam which have traversed the plates without deflection as a function of x_a, x_0, x_b, Δm, and $\Delta\varphi$. The corresponding wave is the result of the coherent superposition of waves scattered at a zero angle on nuclei of the substance situated along the incident beam.

Apart from such a "coherent" mechanism leading to the "regeneration" of K_1^0 mesons in the undeflected beam, one can employ a high-energy K_1^0 beam to obtain a second mechanism associated with the different diffraction scattering of the K^0 and $\bar{K}^0$ waves on the individual nuclei of a substance; this mechanism is incoherent in nature. The number of K_1^0 mesons "regenerated" by means of diffraction scattering does not disclose the oscillations associated with the mass difference Δm and has an angular distribution characteristic of diffraction, which makes it possible to distinguish between these two mechanisms.

Moreover, the increase in thickness of the plates [within the limits in which the "coherent mechanism" is important; see formula (1)] is also advantageous from this viewpoint. It makes it possible to increase the value of the difference between the number of K_1^0 mesons from the "coherent" mechanism and from zero-angle diffraction.[3]

Before going on to the analysis of the obtained formula with a view to choosing the most convenient experimental conditions, we shall introduce the limiting values of the functions P, C, and S in the case of small thicknesses t_a and t_b:

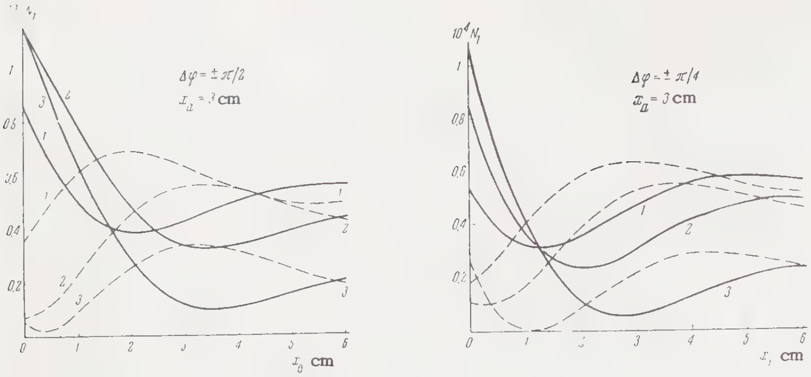

FIG. 2. Dependence of N_1 on the distance between plates x_0. Curves 1, 2, and 3 correspond to thicknesses x_b of the second plate equal to 3, 2, and 1 cm, respectively.

$$P(t_i) \simeq v^2 t_i^2 = x_i^2 \qquad (i = a,\ b),$$

$$C(t_a,\ t_b) \simeq v^2 t_a t_b = x_a x_b, \qquad S(t_a,\ t_b) \simeq 0, \qquad (13,$$

so that (11) passes over into formula (12) of reference 1, derived under the assumption of very small thicknesses.

3. We now go on to the analysis of formula (11). First of all, it is obvious that (11) does not change if we change the signs of $\Delta\varphi$ and Δm simultaneously, so that the knowledge of the sign of $\Delta\varphi$ is a necessary prerequisite for carrying out the experiment. If the sign of $\Delta\varphi$ is known, the sign of Δm can be determined in experiments of either type discussed in Sec. 2. Increasing the thickness of the plates leads to an essential increase in the K_1^0-meson yield, which preserves the possibility of determining the sign of Δm.

In order to obtain graphically the dependence of N_1 on the parameters x_a, x_0, x_b and $\Delta\varphi$, we take into account the material of the plates and take the value of $|\Delta m|$ equal to 10^{10} sec^{-1} (see reference 3). By way of example, we take the K^0-meson kinetic energy equal to 40 Mev.* We choose copper as the material of plate a and graphite as that of plate b. Since we wish only to show that it is, in principle, possible to measure the sign of Δm, we neglect in $r_{a,b}$ the amplitude $f(0)$ in comparison with $\bar{f}(0)$. Then

$$r_{a,\,b} = \pi N_{a,\,b} k^{-1} (\bar{\sigma}_{a,\,b} / 4\pi)^{1/2}.$$

For $\bar{\sigma}_{a,b}$, we take the expression $\pi r_0^2 A_{a,b}^{2/3}$ ($r_0 = 1.4 \times 10^{-13}$ cm). The data above was used for the graphical analysis of formula (11).

Figures 2 and 3 show the variation of N_1 for $\Delta\varphi = \pm\pi/2$, $\pm\pi/4$, and $\pm\pi/8$ as a function of the distance between plates x_0 at the "optimum" plate thickness $x_a = 3$ cm and $x_b = 1$, 2, and 3 cm.

In these figures (and in those that follow), the solid curves correspond to the same signs of Δm and $\Delta\varphi$, the dotted curves correspond to the opposite signs of Δm and $\Delta\varphi$.

Taking the value of 2 cm for x_a — somewhat below the optimum — with the remaining parameters fixed, we obtain similar curves with somewhat smaller ordinates. Those curves are not shown here to save space.

Figures 4 and 5 show for comparison the corresponding curves calculated from formula (12) of reference 1 for the same values of r_a, r_b, and $|\Delta m|$. We took the values $x_a = 0.2$, 0.3, and 0.4 cm and $x_b = 0.2$ cm.

From comparison of these figures with Figs. 2 and 3, it is seen that by taking thick plates we have for $\Delta\varphi = \pm\pi/2$ and $\pm\pi/4$ a gain in the K_1^0-meson yield of approximately 5 — 10 times that given by formula (12) in the article of Kobzarev and Okun'.[1] As an example, we point out that for $x_a = 3$ cm, $x_b = 3$ cm, and $\Delta\varphi = \pm\pi/2$ it is necessary to have (depending on the sign of $\Delta m/\Delta\varphi$) approximately 15,000 and 26,000 K_2^0 mesons to obtain the experimental point when $x_0 = 2$ cm.

Figures 2 and 3 show that the use of thick plates does not essentially diminish the oscillation effect, since for $\Delta\varphi = \pm\pi/2$ and $\pm\pi/4$ the sign of the mass difference Δm can be determined. As a criterion for the possibility of distinguishing between the curves, we can take, for example, the difference in the ordinates of the curves for various x_0. If $\Delta\varphi = \pm\pi/8$, then it is difficult to distinguish between curves with opposite signs of Δm in the case of either thick or thin plates.

On the other hand, the following important circumstance leads to a sharp distinction between the groups of curves of Figs. 2, 3 and Figs. 4,5. In the case of plates of finite size, the curves with opposite signs of Δm are most sharply distinguished for $x_0 = 0$, while for the curves of Figs. 4 and 5, this point should not be considered in gen-

---

*The increase in energy of the beam leads to an increase in the "optimum" plate thickness, owing to the increase in the decay length l.

FIG. 3. Dependence of N_1 on x_0. 1 – x_b = 3; 2 – x_b = 2; 3 – x_b = 1 cm.

FIG. 4. Dependence of N_1 on x_0 for the limiting case of thin plates calculated from formula (12) of reference 1. Curves 1, 2, and 3 correspond to thicknesses x_0 of the first plate equal to 0.4, 0.3, and 0.2 cm, respectively.

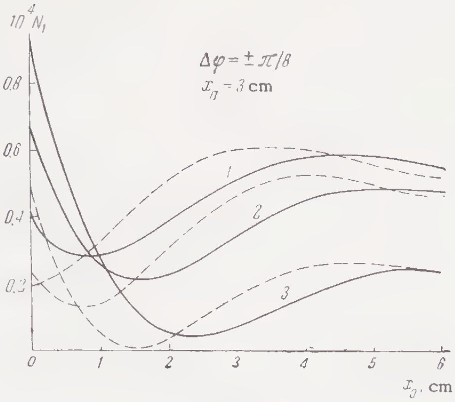

FIG. 3

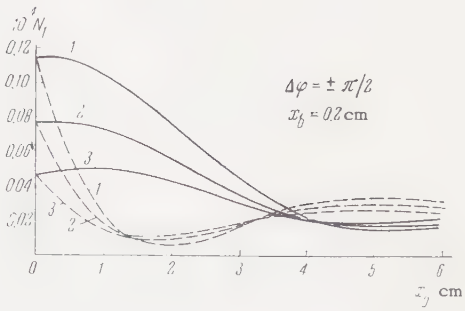

FIG. 4

eral, since a condition for the derivation of formula (12) in reference 1 is x_a, $x_b \ll x_0$.

The use of thick plates thus allows one to carry out an experimental determination of the sign of Δm with the combination of plates when the thickness of plate a is chosen to be the "optimum" one and the thickness of plate b is varied. Then, as seen from the curves of the dependence of N_1 on x_b for $x_0 = 0$ in Fig. 6, favorable conditions are created for distinguishing the sign of Δm even for a phase difference $\Delta\varphi$ equal to $\pm\pi/8$. It is particularly significant that, in this variant of the experiment, the curves corresponding to different signs of $\Delta m/\Delta\varphi$ have a qualitatively different dependence on x_b.

We note that the second variant of the experiment in the case of thin plates would correspond to a fixed finite x_0 (for example x_0 = 1.5 cm) with a variation of the thickness of the thin plate b. There would then be a monotonic increase in N_1 with x_b for both signs of Δm, and the difference in the two corresponding curves would occur only in the value of the ordinates (negligible for $\Delta\varphi = \pm\pi/8$), where, as seen from the curves of Figs. 4 and 5, the K_1^0-meson yield would be small.

The analysis presented thus leads to the conclusion that the most favorable conditions for carrying out the experiment on the determination of the sign of Δm (for a known sign of $\Delta\varphi$) occurs in the case of thick plates placed flat against one another. Of course, in experimenting with thick plates, one should keep in mind the possibility that the undesirable neutron background may increase.

4. We shall consider other possible methods of determining the sign of Δm. They are connected with the change in the number of K^0 and $\overline{K}^0$ mesons after the K_2^0-meson beam traverses the substance.

We shall find the number of K^0 and $\overline{K}^0$ mesons traveling forward after the initially pure K_2^0 beam passes through a plate of thickness $x = vt$ at a distance $x_0 = vt_0$ from the plate. This number will be determined by the relations

$$N_{K^0} = \tfrac{1}{2}\,|\alpha_1(t+t_0) + \alpha_2(t+t_0)|^2,$$

$$N_{\overline{K}^0} = \tfrac{1}{2}\,|\alpha_1(t+t_0) - \alpha_2(t+t_0)|^2, \qquad (14)$$

where α_1 and α_2 are given by formulas (6).

Using the same approximation employed previously, we obtain

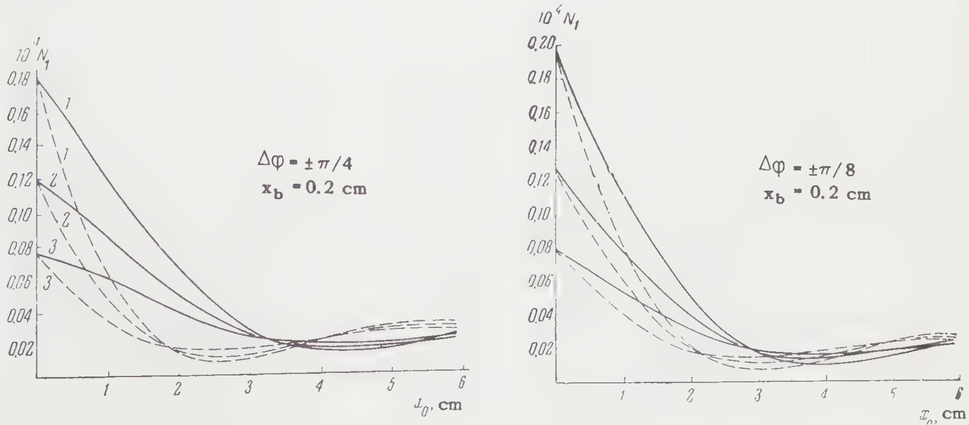

FIG. 5. Dependence of N_1 on x_0 for the case of thin plates. 1 – x_a = 0.4; 2 – x_a = 0.3; 3 – x_a = 0.2 cm.

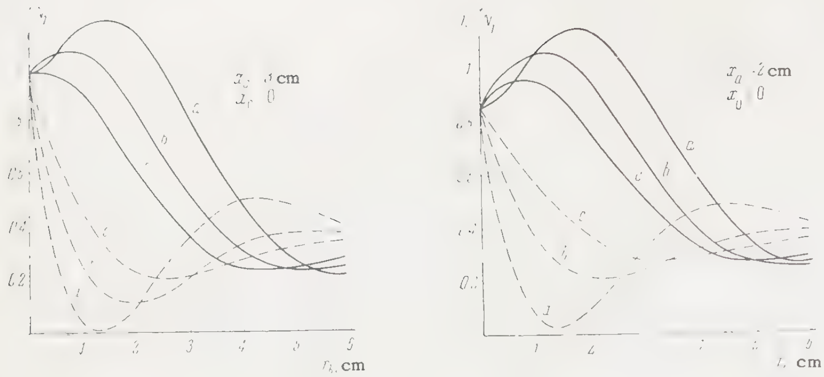

FIG. 6. Dependence of N_1 on the thickness x_b of the second plate placed flat against the first. Curves a, b, and c correspond to values of $\Delta\varphi$ equal respectively to ± $\pi/2$, ±$\pi/4$, and ±$\pi/8$.

$$\begin{pmatrix} N_{K^0} \\ N_{\overline{K}^0} \end{pmatrix} = \exp\left\{-\frac{v}{2}N(\sigma+\bar{\sigma})t\right\} \times\left\{\frac{1}{2}\mp re^{-t_0/2\gamma\tau_1}\left[\sigma(t)\sin\left(\varphi-\frac{\Delta m}{\gamma}t_0\right) - \varkappa(t)\cos\left(\varphi-\frac{\Delta m}{\gamma}t_0\right)\right]\right\}, \qquad (15)$$

where

$$\sigma(t)=\left[\frac{1}{2\gamma\tau_1 v}\left(1-e^{-t/2\gamma\tau_1}\cos\frac{\Delta mt}{\gamma}\right)+\frac{\Delta m}{\gamma v}e^{-t/2\gamma\tau_1}\sin\frac{\Delta mt}{\gamma}\right] \times\left[\left(\frac{\Delta m}{\gamma v}\right)^2+\left(\frac{1}{2\gamma\tau_1 v}\right)^2\right]^{-1},$$

$$\varkappa(t)=\left[\frac{\Delta m}{\gamma v}\left(1-\cos\frac{\Delta mt}{\gamma}e^{-t/2\gamma\tau_1}\right)-\frac{1}{2\gamma\tau_1 v}e^{-t/2\gamma\tau_1}\sin\frac{\Delta mt}{\gamma}\right] \times\left[\left(\frac{\Delta m}{\gamma v}\right)^2+\left(\frac{1}{2\gamma\tau_1 v}\right)^2\right]^{-1}. \qquad (16)$$

One of the methods of determining the sign of Δm involves the study of the number of hyperons produced in a second plate of small thickness, placed at a distance x_0 from the first, as a function of x_0. This number is proportional to the quantity $N_{\overline{K}_0}$ from (15). In the limiting case of small plate thicknesses $\sigma(t) \approx x$ and $\kappa(t) \approx 0$, which leads to formula (14) of reference 1.

Another method of determining the sign of Δm connected with the result (15) involves the study of the lepton decays K^0_{e3} and $K^0_{\mu 3}$ in the direction of the incident beam as a function of the distance x_0 to the plate through which the pure K^0_2 beam passed.

It is known (see, for example, reference 4 that the decays $K^0 \rightarrow \pi^- + e^+(\mu^+) + \nu$ and $\overline{K}^0 \rightarrow \pi^+ + e^-(\mu^-) + \bar{\nu}$ are allowed and the decays $K^0 \rightarrow \pi^+ + e^-(\mu^-) + \bar{\nu}$ and $\overline{K}^0 \rightarrow \pi^- + e^+(\mu^-) + \nu$ are forbidden by the rule $\Delta Q/\Delta S = 1$, where S is the strangeness and Q is the charge of the strongly-interacting particles. By the CPT theorem, the allowed decays take place with a total inverse lifetime Γ_l. Therefore the ratio of the number of lepton decays per second at a distance of x_0 to the right of the plate to the initial number of mesons in the beam to $\Gamma_l N_{K^0}$ for decays into a π^- meson and leptons and $\Gamma_l N_{\overline{K}^0}$ for decays into a π^+ meson and leptons.

A general shortcoming of the methods considered in this section is the smallness of the oscillating term in comparison with the basic term and the need for very large statistics for the study of the rare lepton decays. An increase in the thickness of the first plate to the optimum value leads to an increase in the amplitude of oscillation.

In conclusion, the author expresses his deep gratitude to I. Yu. Kobzarev, L. B. Okun', and B. Pontecorvo for valuable advice and discussion of the results, to Z. Sh. Mandzhavidze, N. N. Roĭnishvili, G. R. Khutsishvili, and G. E. Chikovani for interest in this work and for valuable discussions.

The author is sincerely indebted to G. I. Lebedevich and also to D. M. Kotlyarevskiĭ and A. N. Mestvirishvili for carrying out the numerical calculations.

---

[1] I. Yu. Kobzarev and L. B. Okun', JETP **39**, 605 (1960), Soviet Phys. JETP **12**, 426 (1961).

[2] M. L. Good, Phys. Rev. **106**, 591 (1957) and **110**, 550 (1958).

[3] Muller, Birge, Fowler, Good, Hirsch, Matsen, Oswald, Powell, and White, Phys. Rev. Letters **4**, 418 (1960).

[4] Okubo, Marshak, Sudarshan, Teutsch, and Weinberg, Phys. Rev. **112**, 665 (1958).

Translated by E. Marquit
319

PHOTODISINTEGRATION OF He^4 AT HIGH ENERGIES

R. I. DZHIBUTI and A. V. TAGVIASHVILI

Tbilisi State University

Submitted to JETP editor July 18, 1960

J. Exptl. Theoret. Phys. (U.S.S.R.) 39, 1756-1759 (December, 1960)

The two-particle model was used to find the angular distributions and total cross sections for photo-nucleons produced in the reactions $He^4(\gamma p)H^3$ and $He^4(\gamma n)He^3$. The results are compared with experimental data.

1. Analysis of photonuclear reactions shows that for γ-ray energies less than the threshold for π-meson production there is only a small probability that individual photonucleons be produced by disintegration of a quasi-deuteron. This result is especially valid for light nuclei, since in these the small number of nucleons makes it unlikely that the partner of a photonucleon will be trapped by collisions within the nucleus. On the other hand, experimentally there is a large yield of individual nucleons in photonuclear reactions. For example, in the disintegration of α particles by γ rays of maximum energy 170 Mev, it is observed that the yield of photoneutrons is 95% of the yield of photoprotons, while the yield of nucleon pairs is only 19% of the total.[1] These facts imply that there is some mechanism for the interaction of γ rays with light nuclei other than the quasi-deuteron mechanism.

In this connection it is interesting to consider the photodisintegration of the He^4 nucleus by high-energy γ rays from the point of view of direct interactions.

He^4 is an interesting nucleus to study for at least two reasons: first, there is a large amount of reliable experimental data available, and second, in some sense α particle nucleon groupings apparently exist in light nuclei, and these must play a part in radiative transitions of light nuclei. A detailed understanding of the photodisintegration of He^4 will then contribute to an understanding of the interaction between light nuclei and γ rays.

Theoretical calculations of the photodisintegration of helium near giant resonance[2-4] have used various He^4 wave functions. These calculations have not been satisfactory, since it has not been possible to choose parameters in the wave function so as to fit simultaneously the radius of the nucleus, its binding energy, the position of the maximum in the cross section, and the magnitude of the maximum. Gunn and Irving[3] have made calculations in the energy region above the giant resonance; these also are not satisfactory, since the calculated total cross section decreases with energy more slowly than does the observed one.

Barton and Smith[5] have carried out experiments on the photodisintegration of He and Li by γ quanta of higher energies (150 to 280 Mev); their results were in satisfactory agreement with the quasi-deuteron theory of the nuclear photoeffect. This model is apparently applicable to He^4 for energies greater than the threshold for π-meson production. There are no calculations of the photodisintegration of helium for photon energies between the giant resonance and the threshold for meson production.

The existing experimental data on the photodisintegration of He^4 in this energy range indicate, first, that the probability for emission of a photo-nucleon drops exponentially with increasing γ-ray energy, second, that the angular distribution of photo-protons is asymmetric, with most protons being emitted forward, and third, that the angular distribution of photoneutrons is essentially isotropic.

These facts suggest that in He^4 the photon can knock out a nucleon directly. The He^4 nucleus can be represented by a two particle model, with the photonucleon moving in a field due to the residual nucleus, He^3 or H^3. If collective motions of the whole nucleus were important in the ejection of a nucleon, then it would not be very likely that the residual nucleus would be left in an unexcited state. This suggests that the photodisintegration of He^4 be viewed as a two particle process.

The purpose of this paper is to consider the reactions $He^4(\gamma p)$ and $He^4(\gamma n)$ at high energies (but not exceeding the threshold for π meson production), and to do this from the point of view of the two-particle model. Since the dipole approximation is not adequate at high energies, we calculate the photodisintegration in a general way, without expanding the vector potential of the electromagnetic field in multipoles.

2. The differential cross section for the process in question can be written in the form

$$d\sigma = 2\pi\hbar^{-1}c^{-1}\,|H'|^2\,\rho(E)\,d\Omega, \tag{1}$$

where

$$|H'|^2 = \frac{2\pi\hbar c^2}{\omega}\,\frac{1}{2J+1}\sum_{m_J=-J}^{J}\sum_{\sigma}|I^{\sigma}_{J,\,m_J}|^2,$$

$$\rho(E) = \frac{(1-1/A)\,Mp}{8\pi^3\hbar^3}, \tag{2}$$

$$I^{\sigma}_{J,\,m_J} = \sum_{S}\int \Phi^{*}_{\sigma}(\mathbf{r})\,V\,\Psi_{J,\,m_J}(\mathbf{r})\,d\mathbf{r}. \tag{3}$$

Here we have

$$V = \sum_{i}^{4} W_i, \qquad \Phi_\sigma(\mathbf{r}) = \begin{cases} \alpha e^{i\mathbf{kr}}, & \sigma_z = 1/2 \\ \beta e^{i\mathbf{kr}}, & \sigma_z = -1/2 \end{cases},$$

where J is the total angular momentum of the photonucleon in the original nucleus, m_J is its projection on the z axis, **k** is the wave vector of the photonucleon in the center-of-mass system, M and p are the mass and momentum of the photonucleon, and A is the mass number of the target nucleus.

Since the photonucleon in He^4 is in an S state, the potential V must include interactions between: (1) the charge of the final nucleus and the vector potential of the γ ray, W_1; (2) the magnetic moment of the final nucleus and the magnetic field of the wave, W_2; (3) the charge of the photonucleon and the vector potential of the γ ray, W_3; and (4), the magnetic moment of the photonucleon and the magnetic field of the γ ray, W_4.

Equation (3) neglects the interaction of the photonucleon with the residual nucleus in the final state. This is justified by the work of Bransden, Douglas, and Robertson,[4] who studied the photodisintegration of the α particle at low energies. These authors used the scattering phase shifts of reference 6 to take into account the proton-triton interaction in the final state. They found that the interaction has a negligible effect on the form of the total cross section curve at low energies, while at energies greater than 30 Mev, the two curves, with and without the interaction, practically coincide.

The initial state wave functions are

$$\Psi_{1/2,\,1/2} = \alpha R(r)\,Y_0^0, \qquad \Psi_{1/2,\,-1/2} = \beta R(r)\,Y_0^0,$$

$$R(r) = 2\pi^{-1/4}\gamma^{3/2}\exp\left[-\tfrac{1}{2}(\gamma r)^2\right],$$

where the parameter γ is equal to $8 \times 10^{12}\ \mathrm{cm}^{-1}$, according to Mayer and Jensen.[7]

Our initial and final states are not orthogonal to one another, but the error this contributes is of the same order of magnitude as the error involved in neglecting the interaction in the final state.

The result of the computation is that the differential cross section of the photodisintegration of He^4 is

$$\begin{aligned} \frac{d\sigma}{d\Omega} = {} & \frac{3\pi^{1/2}e^2k^3}{2c\gamma^3M\omega}\exp\left[-\frac{k^2}{\gamma^2}-\frac{\omega^2}{16\gamma^2c^2}\right]\left\{\left[\delta\exp\left(-\frac{\omega^2}{4c^2\gamma^2}+\frac{\omega k}{c\gamma^2}\cos\theta\right)\right.\right. \\ & \left.-\frac{\eta}{3}\right]^2\exp\left[-\frac{\omega k}{2c\gamma^2}\cos\theta\right]\sin^2\theta+\frac{\mu^2_{n,\,p}\omega^2}{2c^2k^2}\exp\left[\frac{\omega^2}{16\gamma^2c^2}\right] \\ & \times\left(\exp\left[-\frac{\omega^2}{32\gamma^2c^2}-\frac{\omega k}{4c\gamma^2}\cos\theta\right]\right. \\ & \left.\left.-\exp\left[-\frac{9\omega^2}{32c^2\gamma^2}+\frac{3\omega k}{4\gamma^2c}\cos\theta\right]\right)^2\right\}, \end{aligned} \tag{4}$$

where

$$k = \left\{\frac{3M}{2\hbar^2}\left[\hbar\omega-\varepsilon-\frac{1}{8Mc^2}(\hbar\omega)^2\right]\right\}^{1/2}. \tag{5}$$

In these equations, ϵ is the binding energy of the photonucleon, $\eta = 1$ or 2 and $\delta = 1$ or 0, depending on whether a proton or neutron is ejected, while $\mu_{n,p}$ is the magnetic moment of the neutron or proton in nuclear magnetons.

Upon integrating (4) over the angles, we obtain the following expression for the total cross section:

$$\begin{aligned} \sigma = {} & \frac{12\pi^{3/2}e^2}{\gamma M}\left(\frac{k}{\omega}\right)^2\exp\left[-\frac{k^2}{\gamma^2}-\frac{\omega^2}{16\gamma^2c^2}\right] \\ & \times\left\{\frac{4c\gamma^2\delta}{9\omega k}\exp\left[-\frac{\omega^2}{2c^2\gamma^2}\right]\left(\cosh\frac{3\omega k}{2c\gamma^2}-\frac{2c\gamma^2}{3\omega k}\sinh\frac{3\omega k}{2c\gamma^2}\right)\right. \\ & +\frac{4c\gamma^2}{\omega k}\left(\frac{\eta^2}{9}-\frac{2\eta\delta}{3}\exp\left[-\frac{\omega^2}{4c^2\gamma^2}\right]\right) \\ & \times\left(\cosh\frac{\omega k}{2c\gamma^2}-\frac{2c\gamma^2}{\omega k}\sinh\frac{\omega k}{2c\gamma^2}\right) \\ & +\frac{\mu^2_{n,\,p}\omega^2}{2c^2k^2}\exp\left[\frac{\omega^2}{16\gamma^2c^2}\right]\left(\exp\left[-\frac{\omega^2}{16\gamma^2c^2}\right]\sinh\frac{\omega k}{2c\gamma^2}\right. \\ & -2\exp\left[-\frac{5\omega^2}{16\gamma^2c^2}\right]\sinh\frac{\omega k}{2c\gamma^2} \\ & \left.\left.+\frac{1}{3}\exp\left[-\frac{9\omega^2}{16c^2\gamma^2}\right]\sinh\frac{3\omega k}{2c\gamma^2}\right)\right\}. \end{aligned} \tag{6}$$

3. Figures 1 – 4 show the results of numerical calculations. In Figs. 1 and 2, the solid curves show the theoretical angular distributions of photoprotons and photoneutrons for γ quanta having energy 80 Mev, while the dots show experimental data obtained by Gorbunov and Spiridonov.[1] From formula (4) it is easy to see that as the γ-ray energy is increased, the maximum in the angular distribution shifts toward lower angles. This is in accord with the experimental data.[1]

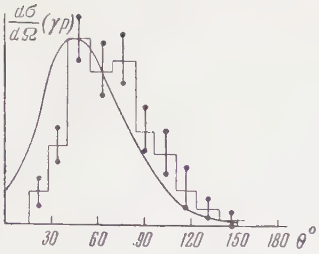

FIG. 1. Angular distribution of protons (center-of-mass system) arising from the reaction He$^4(\gamma p)$H^3 for γ rays with energy $\hbar\omega = 80$ Mev.

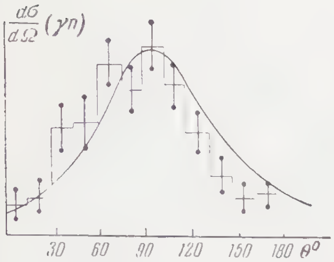

FIG. 2. Angular distribution (center-of-mass system) of neutrons from the reaction He$^4(\gamma n)$He^3 for γ-ray energy = 80 Mev.

Figures 3 and 4 show the calculated total cross sections (solid curves) and experimental data (dots)[1] for the reactions He$^4(\gamma p)$ and He$^4(\gamma n)$.

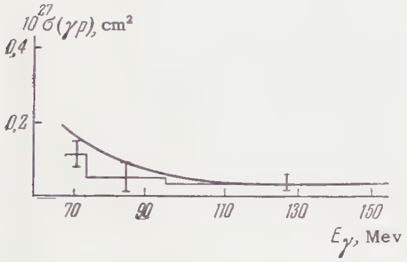

FIG. 3. The total cross section of the reaction He$^4(\gamma p)$H^3 as a function of the γ-ray energy.

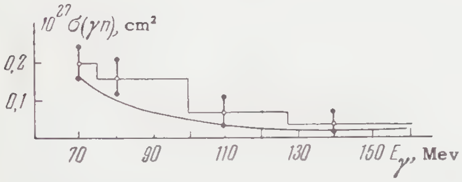

FIG. 4. Total cross section of the reaction He$^4(\gamma n)$He^3 as a function of the γ-ray energy.

From these figures it is clear that $\sigma(\gamma n)/\sigma(\gamma p) \approx 1$. This agrees with the experimental data of Gorbunov and Spiridonov,[1] and can be explained as follows: For photoprotons, there is an interference term between the interaction of the γ ray with, on the one hand, the charge of the proton, and, on the other hand, the charge of the triton. This interference decreases the proton yield. There is no such term for photoneutrons. Hence, even though the neutron is uncharged, there are as many neutrons coming out as protons.

From Figs. 1 — 4 it appears that there is good agreement between theory and experiment in the energy range 70 to 150 Mev. Below 70 Mev, the agreement gets worse, which reflects the inadequacy of the two-particle model at energies near the giant resonance. This may be connected with the anomalously large binding energy of the last nucleon in the α particle.

For γ ray energies greater than 150 Mev, the quasi-deuteron mechanism is dominant, as has been shown by Barton and Smith.[5]

We should like to thank Prof. V. I. Mamasakhlisov for his constant interest and valuable discussions.

---

[1] A. I. Gorbunov and V. M. Spiridonov, JETP **33**, 21 (1957), Soviet Phys. JETP **6**, 16 (1958).

[2] B. H. Flowers and F. Mandl, Proc. Roy. Soc. (London) **A206**, 131 (1951).

[3] J. C. Gunn and J. Irving, Phil. Mag. **42**, 1353 (1951).

[4] Bransden, Douglas, and Robertson, Phil. Mag. **2**, 1211 (1957).

[5] M. Q. Barton and J. H. Smith, Phys. Rev. **110**, 1143 (1958).

[6] Bransden, Robertson, and Swan, Proc. Phys. Soc. (London) **A69**, 877 (1956).

[7] M. Goeppert Mayer and J. H. D. Jensen, Elementary Theory of Nuclear Shell Structure, Wiley, N.Y., 1955 (p. 236).

Translated by R. Krotkov
320

SOVIET PHYSICS JETP VOLUME 12, NUMBER 6 JUNE, 1961

INELASTIC SCATTERING OF HIGH-ENERGY ELECTRONS BY NUCLEI

A. G. SITENKO and V. N. GUR'EV

Physico-Technical Institute, Academy of Sciences, Ukrainian S.S.R.

Submitted to JETP editor July 18, 1960

J. Exptl. Theoret. Phys. (U.S.S.R.) **39**, 1760-1765 (December, 1960)

The inelastic scattering of fast electrons by nuclei is treated for cases in which the scattering is accompanied by the ejection of nucleons from the nucleus. The differential cross section for the process is expressed in terms of the correlation function for the nucleons that is caused by two-particle interactions. The correlation function obtained from an analysis of the data on the capture of neutrons by protons colliding with nuclei is used to calculate an energy spectrum of the electrons, which agrees with the experimental data.

1. Collisions of high-energy electrons with nuclei can lead to inelastic scattering as well as to elastic scattering. By studying the elastic scattering one can obtain information about the dimensions of nuclei, about the nucleon density distribution inside the nucleus, and also about other characteristics of the nucleus in the ground state.[1] The study of the inelastic scattering of electrons gives important information about the dynamical properties of nuclei.

Inelastic scatterings can be divided into two types. First, it is possible for the inelastic scattering of an electron to be accompanied by the transition of the nucleus into an excited state that corresponds to a discrete energy level. The study of such a process gives information about the energy levels of the nucleus and about their widths and other characteristics.[1] Second, there is a possible inelastic process, sometimes called electrodisintegration of the nucleus, in which the scattered electron knocks a nucleon (proton or neutron) out of the nucleus.

By the study of this type of inelastic scattering one can get direct information about the momentum distribution of nucleons in the nucleus, which depends on the spatial correlation between the nucleons in the nucleus. The securing of such information is important for the further development of theoretical ideas about the structure of the nucleus, particularly about the nature of the two-particle interaction between nucleons, and also about effects on this interaction of the surrounding nucleons inside the nucleus.

The present paper is devoted to the study of inelastic electron scattering accompanied by the ejection of a nucleon from the nucleus.

2. Let us consider the electromagnetic interaction of a fast electron with an individual proton of the nucleus. Treating the proton as a nonrelativistic particle, we can write the energy of this interaction in the form

$$V(\mathbf{r}) = e\varphi - \frac{e}{2M}(\mathbf{pA} + \mathbf{Ap}) - \frac{e}{2M}(1+\varkappa)\,\boldsymbol{\sigma}\mathbf{H} + \frac{e}{8M^2}(1+2\varkappa)\,\boldsymbol{\sigma}([\mathbf{p}\times\mathbf{E}] - [\mathbf{E}\times\mathbf{p}]) - \frac{e}{8M^2}(1+2\varkappa)\operatorname{div}\mathbf{E}, \tag{1}$$

where φ and **A** are the Møller potentials,

$$\varphi = -\frac{4\pi e}{q^2 - \Delta E^2}(\bar{u}'\beta u)\,e^{i\mathbf{qr}}, \quad \mathbf{A} = -\frac{4\pi i e}{q^2 - \Delta E^2}(\bar{u}'\gamma u)\,e^{i\mathbf{qr}}, \tag{2}$$

and the fields **E** and **H** are connected with these potentials by the relations

$$\mathbf{E} = -\operatorname{grad}\varphi + i\Delta E\mathbf{A}, \qquad \mathbf{H} = \operatorname{curl}\mathbf{A},$$

$\mathbf{q} = \mathbf{k} - \mathbf{k}'$ and $\Delta E = E - E'$ are the momentum and energy transferred to the proton by the electron; **p** and σ are the momentum and spin operators of the proton; and e, M, and κ are the charge, mass, and anomalous magnetic moment of the proton (we are setting $\hbar = c = 1$).

By using perturbation theory, it is not hard to find the probability for ejection of a proton from the nucleus by the electron. If we denote the momentum of the ejected proton by **K**, perturbation theory gives for the cross section for this process the expression

$$d\sigma = 2\pi\sum|H'_{if}|^2\,\delta(\Delta E + \varepsilon_{if} - E_p)\frac{d\mathbf{k}'}{(2\pi)^3}\frac{d\mathbf{K}}{(2\pi)^3}, \tag{3}$$

where H'_{if} is the matrix element of the interaction energy,

$$H' = \sum_{j=1}^{Z} V(\mathbf{r}_j),$$

$$V(\mathbf{r}_j) = -\frac{4\pi e^2}{q^2 - \Delta E^2}\,\bar{u}'\left\{\left(1 - \frac{q^2 - \Delta E^2}{8M^2}(1+2\varkappa)\right)\beta + \frac{i}{2M}\left(\mathbf{q} + 2i\nabla_j + i(1+\varkappa)[\mathbf{q}\times\boldsymbol{\sigma}_j]\right)\gamma\right\}u e^{i\mathbf{qr}_j}; \tag{4}$$

ϵ_{if} is the change of the energy of the nucleus, and E_p is the kinetic energy of the liberated proton.

When we include the effects of the correlations between pairs of particles that appear at small distances, the wave function of a system of Z protons and N neutrons can be written in the form

$$\Psi(Z, N) = \sum_P (-1)^P P \frac{1}{\sqrt{Z!}} \prod_{j=1}^{Z} \psi_{\alpha_j}(\mathbf{r}_j) \frac{1}{\sqrt{N!}}$$
$$\times \prod_{k=1}^{N} \psi_{\beta_k}(\mathbf{r}_k) \prod_{j<j'} f_{\alpha_j\alpha_{j'}}(\mathbf{r}_j - \mathbf{r}_{j'})$$
$$\times \prod_{k<k'} f_{\beta_k\beta_{k'}}(\mathbf{r}_k - \mathbf{r}_{k'}) \prod_{jk} f_{\alpha_j\beta_k}(\mathbf{r}_j - \mathbf{r}_k), \qquad (5)$$

where $\psi_\alpha(\mathbf{r})$ and $\psi_\beta(\mathbf{r})$ are the one-particle functions for proton and neutron and $f_{\alpha\beta}(\mathbf{r})$ is the correlation function between particles that are in the states α and β. In Eq. (5) the summation is taken over all permutations P of identical particles. The function (5) is assumed normalized to unity.

As the wave function of the final state we take

$$\Psi_f(Z, N) = \frac{1}{\sqrt{Z}} \sum_{j=1}^{Z} \psi_{\mathbf{K}}(\mathbf{r}_j)\, \Phi_f(\mathbf{r}_1, \ldots, \mathbf{r}_{j-1}, \mathbf{r}_{j+1}, \ldots, \mathbf{r}_Z; N),$$

where $\psi_{\mathbf{K}}(\mathbf{r})$ is the wave function of the ejected proton with the momentum $\mathbf{K}$ and the function $\Phi_f(\mathbf{r}_1, \ldots; N)$ is chosen so that

$$\Phi_f(\mathbf{r}_2, \ldots, \mathbf{r}_Z; N) = \Psi_f(Z-1, N).$$

Replacing the quantity ϵ_{if} in Eq. (3) by an average value $\overline{\epsilon}_{if}$ that is of the order of magnitude of the binding energy s_p of a proton, and using the completeness of the functions $\Psi_f(Z-1, N)$, we can perform without difficulty the summing over the final states of the residual nucleus that is indicated in Eq. (3),

$$\sum_f |H'_{if}|^2 = Z \int d\tau^{Z-1} d\tau^N \left| \int d\mathbf{r}_1 \psi^*_{\mathbf{K}}(\mathbf{r}_1) V(\mathbf{r}_1) \Psi_i(Z, N) \right|^2. \qquad (6)$$

If for the proton with the radius vector $\mathbf{r}_1$ we take into account only pair correlations with other particles, we can perform the integration in Eq. (6) over the coordinate space of $A-2$ particles. As the result of this integration we get

$$\sum_f |H'_{if}|^2 = \sum_{\alpha\beta} \int d\mathbf{r}_2 \left| \int d\mathbf{r}_1 \psi^*_{\mathbf{K}}(\mathbf{r}_1) V(\mathbf{r}_1) \psi_{\alpha\beta}(\mathbf{r}_1, \mathbf{r}_2) \right|^2, \qquad (7)$$

where

$$\psi_{\alpha\beta}(\mathbf{r}_1, \mathbf{r}_2) \equiv \psi_\alpha(\mathbf{r}_1) \psi_\beta(\mathbf{r}_2) f_{\alpha\beta}(\mathbf{r}_1 - \mathbf{r}_2). \qquad (8)$$

In the case of a high-energy incident electron, for which the momentum of the ejected proton is sufficiently large, we can set

$$\psi_{\mathbf{K}}(\mathbf{r}) = e^{i\mathbf{K}\mathbf{r}}.$$

In this case the cross section (3) can be put in the form

$$d\sigma = \frac{4e^4}{(q^2 - \Delta E^2)^2} Z(A-1)$$
$$\times S g(\mathbf{q} - \mathbf{K})\, \delta(\Delta E - s_p - E_p)\, d\mathbf{k}' d\mathbf{K}, \qquad (9)$$

where

$$g(\mathbf{q} - \mathbf{K}) = \frac{1}{Z(A-1)} \sum_{\alpha\beta} \frac{1}{(2\pi)^3} \int d\mathbf{r}_2 \left| \int d\mathbf{r}_1 e^{i(\mathbf{q}-\mathbf{K})\mathbf{r}_1} \psi_{\alpha\beta}(\mathbf{r}_1, \mathbf{r}_2) \right|^2, \qquad (10)$$

$$S = \frac{1}{2} \sum \Big| \bar{u}' \Big\{ \Big(1 - \frac{q^2 - \Delta E^2}{8M^2}(1 + 2\varkappa)\Big) \beta$$
$$+ \frac{i}{2M} (\mathbf{q} - 2\mathbf{K} + i(1 + \varkappa)[\mathbf{q} \times \boldsymbol{\sigma}])\, \boldsymbol{\gamma} \Big\} u \Big|^2. \qquad (11)$$

The summation in Eq. (11) is taken over the various initial and final spin states of the electron.

The function $g(\mathbf{q} - \mathbf{K})$ has a sharp maximum for $\mathbf{q} = \mathbf{K}$, i.e., when the momentum of the ejected proton is equal to the change of momentum of the electron. Setting $\mathbf{q} = \mathbf{K}$ in Eq. (11) and carrying out the summation over the spin states of the electron, we find

$$S \approx \Big\{ 1 - \frac{s_p}{M} + \frac{q^2}{4M^2} \Big[2(1 + \varkappa)^2 \tan^2\frac{\vartheta}{2} + \varkappa^2 - 2 \Big] \Big\} \cos^2\frac{\vartheta}{2},$$

where ϑ is the angle through which the electron is scattered. Also performing the integration over the proton energy in Eq. (9) by using the δ function, we finally get the following formula for the cross section for inelastic scattering of the electron accompanied by the ejection of a proton from the nucleus:

$$d\sigma = \frac{e^4 \cos^2(\vartheta/2)}{4E^2 \sin^4(\vartheta/2)} \Big\{ 1 - \frac{s_p}{M} + \frac{q^2}{4M^2} \Big[2(1 + \varkappa)^2 \tan^2\frac{\vartheta}{2} + \varkappa^2 \Big] \Big\}$$
$$\times Z(A-1)\, g(\mathbf{q} - \mathbf{K})\, MK dE' do' do,$$
$$K^2/2M = \Delta E - s_p. \qquad (12)$$

In the case of scattering of an electron by a free proton ($s_p = 0$) we have instead of $Z(A-1)\, g(\mathbf{q} - \mathbf{K})$ the function $\delta(\mathbf{q} - \mathbf{K})$, and Eq. (12) goes over into the Rosenbluth formula

$$d\sigma = \sigma_p(\vartheta)\, do',$$
$$\sigma_p(\vartheta) = e^4 \cos^2\frac{\vartheta}{2} \Big\{ 1 + \frac{q^2}{4M^2} \Big[2(1 + \varkappa)^2 \tan^2\frac{\vartheta}{2} + \varkappa^2 \Big] \Big\} \Big/ 4E^2$$
$$\times \sin^4\frac{\vartheta}{2} \Big(1 + \frac{2E}{M} \sin^2\frac{\vartheta}{2} \Big). \qquad (13)$$

The function $g(\mathbf{q} - \mathbf{K})$ that appears in the cross section (12) characterizes the distribution of relative momenta $\mathbf{q} - \mathbf{K}$ of the nucleon pairs in the nucleus. This function will also be involved in the cross sections for other direct high-energy processes in collisions with nuclei (for example, in the cross section for the nuclear photoelectric effect at high energies,[2,3] in the cross section for capture of a neutron from a nucleus by a high-energy proton,[2,4] and so on). Therefore the cross section for the scattering of an electron together with the ejection of a nucleon from the nucleus can be directly related to the cross sections for these processes.

3. We can calculate the function $g(\mathbf{q}-\mathbf{K})$, which depends on the two-particle correlations between the nucleons, by taking as the one-particle functions the plane waves

$$\psi_\alpha(\mathbf{r}) = \Omega^{-1/2} e^{i\mathbf{p}_\alpha \mathbf{r}}$$

(Ω is the volume of the nucleus). Corresponding to the ground state of the nucleus we then have values of the nucleon momentum from 0 to a limiting momentum p_F. This choice of the one-particle functions means that we are neglecting Coulomb and surface effects in the nucleus. Analogous assumptions are ordinarily made in the theory of nuclear matter,[5,6] and also in the treatment of other processes in the high energy region (photoelectric effect, pick-up, and so on).

By introducing the radius vector of the center of mass of two nucleons, $\mathbf{R} = (\mathbf{r}_1 + \mathbf{r}_2)/2$, and the relative-position vector of the two nucleons, $\mathbf{r} = \mathbf{r}_1 - \mathbf{r}_2$, we can put the wave function (8) of two nucleons, in the approximation we have adopted, in the form

$$\psi_{\mathbf{p}_1\mathbf{p}_2}(\mathbf{r}_1, \mathbf{r}_2) = \Omega^{-1/2} e^{i\mathbf{P}\mathbf{R}} \varphi_{\mathbf{p}}(\mathbf{r}), \qquad \varphi_{\mathbf{p}}(\mathbf{r}) = \Omega^{-1/2} e^{i\mathbf{p}\mathbf{r}} f(r), \quad (14)$$

where $\mathbf{P} = \mathbf{p}_1 + \mathbf{p}_2$ is the momentum of the center of mass and $\mathbf{p} = (\mathbf{p}_1 - \mathbf{p}_2)/2$ the relative momentum, and $\varphi_{\mathbf{p}}$ is the wave function of the relative motion of the two nucleons in the nucleus.

Using Eq. (14), we have

$$g(\mathbf{q} - \mathbf{K}) = \mathop{\mathrm{S}}_{\mathbf{p},\mathbf{P}} \frac{1}{(2\pi)^3} \left| \int d\mathbf{r}\, e^{i(\mathbf{q}-\mathbf{K}+\mathbf{P}/2)\mathbf{r}} \varphi\ (\mathbf{r}) \right|^2, \quad (15)$$

where S denotes averaging over all allowed values of the momenta $\mathbf{p}$ and $\mathbf{P}$.

Assuming that the interaction between nucleons occurs only in the S state and that the interaction is characterized by the presence of a repulsive core of radius r_c, we can use for the wave function $\varphi_{\mathbf{p}}(\mathbf{r})$ the Brueckner function[5]

$$\varphi_{\mathbf{p}}(\mathbf{r}) = \begin{cases} 0, & r < r_c \\ \dfrac{1}{\sqrt{\Omega}} \left(\dfrac{\sin pr}{pr} - \dfrac{\sin pr_c}{pr} e^{-\lambda(r-r_c)} \right), & r > r_c, \end{cases} \quad (16)$$

where $\lambda^2 = 2p_F^2/5$; this function leads to the correct value of the binding energy per nucleon for heavy nuclei. By the use of this function it is not hard to get for $p_F r_c \ll 1$ the following expression for the distribution $g(\kappa)$:

$$g(\varkappa) = \frac{2r_c^2}{\pi\Omega} \left\{ \frac{1}{\varkappa^2} \left(\cos \varkappa r_c - \frac{\sin \varkappa r_c}{\varkappa r_c} \right) - \frac{\varkappa^{-1}\lambda \sin \varkappa r_c + \cos \varkappa r_c}{\lambda^2 + \varkappa^2} \right\}^2,$$
$$\varkappa = \mathbf{q} - \mathbf{K}. \quad (17)$$

For small values of κ $(\kappa r_c \ll 1)$ we have from Eq. (17)

$$g(\varkappa) = 2r_c^2/\pi\Omega\, (\lambda^2 + \varkappa^2)^2.$$

This distribution agrees with the Chew-Goldberger distribution[4]

$$g_{\text{C-G}}(\varkappa) = \alpha/\pi^2 (\alpha^2 + \varkappa^2)^2. \quad (18)$$

Figure 1 shows the distribution $g(\kappa)$, normalized to unity at $\kappa = 0$. Curve 1 corresponds to the empirical formula

$$g(\varkappa) = \pi^{-3/2} \alpha^{-3} \exp(-\varkappa^2/\alpha^2), \qquad \alpha^2/2M = 14\,\text{Mev} \quad (19)$$

obtained from an analysis of the experimental data on the capture of neutrons from C^{12} nuclei by fast protons.[7] Curve 2 corresponds to the Chew-Goldberger distribution (18) for $\alpha^2/2M = 18$ Mev. Curves 3 and 4 correspond to the distribution (17) for $p_F = 1.48 \times 10^{13}$ cm^{-1} and the respective values 0.4×10^{-13} cm and 0.6×10^{-13} cm for the radius of the repulsive core.

Equation (17), like the Chew-Goldberger formula, gives probabilities that are too large for large values of the relative momenta of nucleons in the nucleus. It must be noted, however, that the empirical distribution (19) drawn in Fig. 1 corresponds to the nucleus C^{12}, to which the Fermi-gas model does not apply very well.

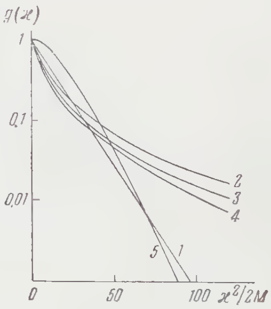

FIG. 1

The distribution $g(\kappa)$ for C^{12} can be calculated on the basis of the shell model. Using oscillator wave functions for nucleons in S and P states

$$\psi_{00}(\mathbf{r}) = (\nu/\sqrt{\pi})^{3/2} e^{-\nu^2 r^2/2},$$
$$\psi_{1m}(\mathbf{r}) = (8\nu^5/3\sqrt{\pi})^{1/2} r e^{-\nu^2 r^2/2} Y_{1m}(\theta, \varphi)$$

and neglecting the correlations between nucleons, we get

$$g(\varkappa) = \tfrac{1}{3} (\nu\sqrt{\pi})^{-3} (1 + \tfrac{4}{3} \varkappa^2/\nu^2) \exp(-\varkappa^2/\nu^2). \quad (20)$$

The parameter ν that appears in the oscillator functions can be related to the value of the nuclear radius.[8] Taking as the radius of the C^{12} nucleus

$R = 3.07 \times 10^{-13}$ cm, we find $\nu^2/2M = 5$ Mev. This value of ν leads, however, to too rapid a decrease of $g(\kappa)$ with increasing κ.

Inclusion of the correlation between the nucleons does not lead to much change of the dependence of g on κ. This may be due to the illegitimacy of replacing the wave function $\psi_{\mathbf{K}}(\mathbf{r})$ of the liberated nucleon by a plane wave in the case of the oscillator potential.

A distribution close to that found from experiment can be obtained from Eq. (20) by choosing larger values for ν. Curve 5 in Fig. 1 corresponds to Eq. (20) with $\nu^2/2M = 9.1$ Mev. (This value of ν leads, however, to too small a value for the radius of the nucleus.)

4. If we use the empirical momentum distribution of the nucleon pairs, obtained on the basis of a study of the pick-up reaction at high energies, Eq. (19), then we can obtain the energy and angle distribution of the electrons from the inelastic scattering in explicit form. Substituting Eq. (19) in Eq. (12) and carrying out the integration over the angles of emergence of the proton, we find

$$d\sigma(\vartheta, E') = (A-1)\{Z\sigma_p(\vartheta) + N\sigma_n(\vartheta)\}\left(1 + \frac{2E}{M}\sin^2\frac{\vartheta}{2}\right)\frac{M}{\sqrt{\pi}\alpha q} \times \{\exp[-(q-K)^2/\alpha^2] - \exp[-(q+K)^2/\alpha^2]\}\,dE'\,do', \tag{21}$$

where $\sigma_p(\vartheta)$ and $\sigma_n(\vartheta)$ are the cross sections for scattering of the electron by a free proton and a free neutron.

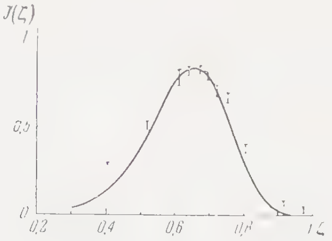

FIG. 2

Figure 2 shows the energy distribution of the inelastically scattered electrons from scattering of 400 Mev electrons by C^{12} nuclei, for the scattering angle $\vartheta = 90°$. The experimental data are taken from the paper of Ehrenberg and Hofstadter.[9] As can be seen, the calculated spectrum of the electrons agrees well with the experimental spectrum ($\xi = E'/E$; $s_p = 16$ Mev).

We express our gratitude to A. I. Akhiezer for a discussion of the results of this paper.

---

[1] R. Hofstadter, Revs. Modern Phys. **28**, 214 (1956).

[2] Brueckner, Eden, and Francis, Phys. Rev. **98**, 1445 (1955).

[3] J. S. Levinger, Phys. Rev. **84**, 43 (1951).

[4] G. Chew and M. Goldberger, Phys. Rev. **77**, 470 (1950).

[5] K. Brueckner and J. Gammel, Phys. Rev. **109**, 1023 (1958).

[6] Gomes, Walecka, and Weisskopf, Ann. Phys. **3**, 241 (1958).

[7] W. Selove, Phys. Rev. **101**, 231 (1956).

[8] W. Heisenberg, Nuclear Physics (Russian Translation), IIL.

[9] H. Ehrenberg and R. Hofstadter, Phys. Rev. **110**, 544 (1958).

Translated by W. H. Furry
321

SOVIET PHYSICS JETP VOLUME 12, NUMBER 6 JUNE, 1961

THE FORM FACTOR FOR $K_{\mu 3}$ *AND* K_{e3} *DECAY*

Ya. B. ZEL'DOVICH

Submitted to JETP editor July 20, 1960

J. Exptl. Theoret. Phys. (U.S.S.R.) **39**, 1766-1769 (December, 1960)

A hypothesis is proposed according to which the K-meson and pion 4-velocities enter symmetrically the expression for the matrix element of the interaction between K mesons or pions and the lepton current (on which $K_{\mu 3}$ and K_{e3} decay depend).

THE decay of a K meson into a pion and two leptons can be thought of as the result of weak four-fermion interaction with $\Delta S = 1$. In this case the decay goes through intermediate states of a baryon-antibaryon pair. The K-meson and pion momenta, p_K and p_π, are small compared with the baryon masses M_B. One can therefore assume that the decisive quantities are the K-meson and pion velocities. We note that in the K-meson rest system the pion velocity may attain 0.87 c.

For the mathematical formulation, we introduce the four-velocity u, with $u^2 = -1$ (we assume $c = 1$).

The matrix element of the process is, as usual,

$$M = \sum V_\alpha \bar{\psi}_{\mu,e} \gamma_\alpha (1 + \gamma_5) \psi_\nu .$$

The proposed hypothesis leads to an expression for the vector current

$$V_\alpha = \varphi(-u_K u_\pi)\,[u_{K\alpha} + u_{\pi\alpha}]. \qquad (1)$$

The form factor φ depends on the invariant product of velocities $-u_K u_\pi$.*

The K meson and pion velocities enter in (1) symmetrically. Such an expression does not contradict the commonly accepted and most general[1] expression

$$V_\alpha = f_1(k^2)\,p_{K\alpha} + f_2(k^2)\,p_{\pi\alpha}, \qquad k = p_K - p_\pi . \qquad (2)$$

Actually, we have

$$u_{K\alpha} = p_{K\alpha}/m_K, \qquad u_{\pi\alpha} = p_{\pi\alpha}/m_\pi,$$

$$k^2 = (p_K - p_\pi)^2 = -m_K^2 - m_\pi^2 - 2(p_K p_\pi)$$

$$= -m_K^2 - m_\pi^2 + 2m_K m_\pi(-u_K u_\pi).$$

Compared with the general expression (2), the proposed expression (1) fixes the ratio of the two functions f_1 and f_2:

$$m_K f_1(k^2) = m_\pi f_2(k^2) = \varphi(-u_K u_\pi) = \varphi\left(\frac{m_K^2 + m_\pi^2 + k^2}{2m_K m_\pi}\right). \qquad (3)$$

In addition, it is often assumed that the expansion of f_1 and f_2 is in powers of k^2/M_B^2, so that in practice f_1 and f_2 can be considered constant. From our point of view the dimensionless argument of the function $(-u_K u_\pi)$ changes from 1 to 2, and there are no grounds for assuming that φ is constant.

We note that the assumption that the divergence of the current vector vanishes[2,3] leads to essentially different conclusions: in the notation of formula (2), the result of Weinberg, Marshak et al. is of the form

$$\operatorname{div} V = (p_K - p_\pi)(f_1 p_K + f_2 p_\pi)$$

$$= (p_K^2 - p_K p_\pi) f_1 - (p_K p_\pi - p_\pi^2) f_2 = 0, \qquad (4)$$

$$f_1/f_2 = (p_\pi^2 - p_K p_\pi)/(p_K^2 - p_K p_\pi)$$

$$= [m_\pi^2 - m_K m_\pi(-u_K u_\pi)]/[m_K^2 - m_\pi m_K(-u_K u_\pi)]. \qquad (5)$$

If the pion is at rest (with respect to the K meson) we have $-u_K u_\pi = 1$, so that $f_1/f_2 = -m_\pi/m_K$, i.e., a value equal but opposite to that implied by formula (2).

The authors of references 2 and 3 set the divergence of the vector current equal to zero by analogy with the vector interaction in the usual β decay, without change of strangeness. Actually, the properties of the vector current in the β decay follow by analogy from the electromagnetic interaction.[4-6] In particular, the electromagnetic interaction of pions is obviously given by the expression $j_\alpha A_\alpha$ where A_α is the 4-potential of the electromagnetic field, and the current j_α is given by the formula

$$j_\alpha = \frac{e}{2im}\left(\overset{*}{\pi}_1 \tau_3 \frac{\partial \pi_2}{\partial x_\alpha} - \frac{\partial \overset{*}{\pi}_\alpha}{\partial x_\alpha} \tau_3 \pi_\alpha\right), \qquad (6)$$

which can be written in the form

$$j = \frac{e\tau_3}{2m}(p_1 + p_2) = \frac{e\tau_3}{2}(u_1 + u_2). \qquad (7)$$

---

*We note that in the K-meson rest system the invariant $u_K u_\pi$ is equal to the ratio of the total pion energy to its rest mass.

The β decay of a charged pion with production of a neutral pion, which can be denoted by π_{e3}, was first considered by Zel'dovich.[7] The matrix element of this process is naturally obtained from the expression for the electromagnetic process by a rotation in isotopic space:[*]

$$V = \text{const}\cdot\tau_+(p_1 + p_2) = \text{const}\cdot\tau_+(p_{\pi^+} + p_{\pi^0}) \approx \text{const}\cdot\tau_+(u_{\pi^0} + u_{\pi^+}). \quad (8)$$

The divergence of the vector current is

$$\operatorname{div} V \sim (p_{\pi^+} - p_{\pi^0})(p_{\pi^+} + p_{\pi^0}) = p_{\pi^+}^2 - p_{\pi^0}^2 = m_{\pi^0}^2 - m_{\pi^+}^2. \quad (9)$$

It vanishes only in the approximation in which the masses of the charged and neutral pion are equal, i.e., in the isotopic-invariance approximation. It is known, for example, that the corrections for electromagnetic interaction violate the condition div V = 0 and change the vector-interaction constant.

The application of the condition div V = 0 by the method proposed in references 2 and 3, with simultaneous allowance for the inequality of the π^+ and π^0 masses, would lead to an utterly incorrect expression for the vector current for π_{e3}, and would completely destroy the entire present-day theory of β interaction.

Thus, the proposal of Marshak and his coworkers that the divergence of V vanishes, which leads to different signs of f_1 and f_2, can actually not be based on an analogy with the usual β decay ($\Delta S = 0$).

On the basis of a definite assumption on the magnitude of div V, and also on the assumption that f_1 and f_2 depend weakly on k^2, Gandel'man[8] drew the conclusion that $f_1 = f_2$, and connected this constant with the probability of the $\Lambda \to p + e^- + \nu$ decay.

In the case of π_{e3} decay, the masses of the π^+ and π^0 mesons are close to each other, and therefore one cannot distinguish between the equalities $f_1 = f_2$ and $f_1/m_{\pi^+} = f_2/m_{\pi^0}$, i.e., one cannot distinguish between an expression of the type obtained by Gandel'man, $\varphi_1(k^2)(p_1 + p_2)$, and our expression $\varphi_2(-u_1u_2)(u_1 + u_2)$.[*]

Considering the diagram of

$$K^+ \to p + \bar{\Lambda} \to p + \bar{p} + e^+ + \nu \to \pi^0 + e^+ + \nu$$

in the perturbation theory after Feynman, we obviously obtain an expression in which the momenta p_K and p_π enter symmetrically, i.e., an expression of the form given by Gandel'man.

The form of the expression proposed in this note, wherein the velocities u_K and u_π (and not their momenta) enter symmetrically, is based on the ideas of Fermi, Yang, Sakata, and Markov. We imagine the K^+ meson as a bound system ("nucleus") of a baryon and antibaryon $p\bar{\Lambda}$, and the π^0 as a superposition $(p\bar{p} - n\bar{n})/\sqrt{2}$. The mass defects of these two systems are extremely large ($2M_N - m_\pi = 2 \times 931 - 138 = 1724$ Mev, $M_N + M_\Lambda - m_K = 931 + 1106 - 494 = 1543$ Mev), and are close to each other. The effective radius of such a system is of the order of the nucleon Compton wavelength $\hbar/M_N c$. We seek a matrix element of the vector operator V which transforms Λ into p. If a π^0 is at rest relative to a K^+, then $V_4 = 1/\sqrt{2}$ and $\mathbf{V} = 0$, since the spatial wave functions of the K^+ and π^0 are similar.[†] In the decay $K^0 \to \pi^- + e^+ + \nu$ we obtain a matrix element equal to $V_4 = 1$. However, experimentally one can observe the K_{e3} decay of the long-lived K_2^0 only; two modes of decay are possible in this case: $\pi^- + e^+ + \nu$, and $\pi^+ + e^- + \bar{\nu}$, for each of which separately the matrix element $V_4 = 1/\sqrt{2}$ for a $\pi^\pm$ at rest.

If the π^0 moves relative to K^+, then the wave function of the π^0 is multiplied by $e^{i\mathbf{p}\cdot\mathbf{x}}$; however, when $p_\pi \ll M_N c$ this is unimportant. Simultaneously there occurs a velocity (not momentum) dependent Lorentz transformation of the spinor wave functions of the two fermions of which the π^0 consists. It is this transformation that determines the dependence of V on the relative motion of the K meson and pion.

Problems concerning experimentally observable effects of our hypothesis in K_{e3} and $K_{\mu 3}$ decay, the best means for differentiating between our conclusions and those of Gandel'man, and the experimental determination of the function $\varphi(-u_K u_\pi)$ will be considered separately.

---

[*] We note in particular that in comparing mesons of different masses, for example a pion triplet and a K-meson doublet, equal coefficients in the interaction with the electromagnetic field are obtained if we write the matrix element of the transition from one one-meson state to another in terms of the 4-velocity, and not in terms of the 4-momentum.

In precisely the same way, for the conservation of the vector β constant, the matrix elements of the one-meson transitions $\pi^+ \to \pi^0 + e^+ + \nu$, $\pi^0 \to \pi^- + e^+ + \nu$, $K^+ \to K^0 + e^+ + \nu$, and $K^- \to \bar{K}^0 + e^+ + \nu$ have an equal constant for the τ_+ operator only when V is expressed in terms of u, and not in terms of p.

[*] The form factors $\varphi_1(k^2)$ or $\varphi_2(-u_1u_2)$ can be found by investigating the electromagnetic interaction of charged pions with virtual quanta (with $k^2 \neq 0$), i.e., in processes of pion scattering by an electron or in the peripheral electromagnetic process of knocking out a pion by an electron, $p + e^- = n + \pi^+ + e^-$.

[†] We note that for π_{e3} the matrix element is $V_4 = \sqrt{2}$, corresponding to unity isospin of the pion. Physically one can say that the transformation $\pi^+ \to p\bar{n} \to \pi^0 = (p\bar{p} - n\bar{n})/\sqrt{2}$ can proceed either via $p \to n + e^+ + \nu$ or via $\bar{n} \to \bar{p} + e^+ + \nu$. Their contributions are additive.

I take this opportunity to express my gratitude for discussions to B. L. Ioffe, L. B. Okun', I. Ya. Pomeranchuk and particularly to G. M. Gandel'man who supplied the manuscript of his work.[8]

---

[1] L. B. Okun', Usp. Fiz. Nauk **68**, 449 (1959), Ann. Revs. Nuc. Sci. Vol. 9, p. 61.

[2] Weinberg, Marshak, Okubo, Sudarshan, and Teutsch, Phys. Rev. Lett. **1**, 25 (1958).

[3] R. E. Marshak and S. Okubo, Nuovo cimento **16**, 333 (1960).

[4] S. S. Gershteĭn and Ya. B. Zel'dovich, JETP **29**, (1955), Soviet Phys. JETP **2**, 576 (1956).

[5] M. Gell-Mann and R. P. Feynman, Phys. Rev. **109**, 193 (1958).

[6] B. L. Ioffe, JETP **34**, 1343 (1958), Soviet Phys. JETP **7**, 927 (1958).

[7] Ya. B. Zel'dovich, Doklady Akad. Nauk SSSR **97**, 421 (1954).

[8] G. M. Gandel'man, JETP (in press).

Translated by Z. Barnea
322

SOVIET PHYSICS JETP VOLUME 12, NUMBER 6 JUNE, 1961

BREMSSTRAHLUNG OF SLOW ELECTRONS DECELERATED BY NEUTRAL ATOMS

O. B. FIRSOV and M. I. CHIBISOV

Submitted to JETP editor July 20, 1960

J. Exptl. Theoret. Phys. (U.S.S.R.) **39**, 1770-1776 (December, 1960)

The bremsstrahlung cross section for slow ($E_{el} < 3$ ev) electrons colliding with neutral atoms is expressed in terms of the cross section for elastic scattering of electrons on atoms. The absorption coefficient of the radiation is determined. The range of gas temperatures and pressures in which collisions between the electrons and atoms yield the largest contribution to the radiation is indicated.

1. INTRODUCTION

THE intensity of radiation of a system going from state a into state b is given by the following formula (see reference 1)

$$S = \frac{4e^2}{3c^3}\left|\sum_i \mathbf{r}_i\right|^2_{ab}\nu^4 = \frac{4e^2}{3c^3}\left|\sum_i \ddot{\mathbf{r}}_i\right|^2_{ab} = \frac{4e^2}{3c^3}\left|\sum_i \frac{\nabla_i U}{m_i}\right|^2_{ab}, \qquad (1)$$

where the summation over i is over all particles of the system; ν is the cyclic frequency of the radiated electron, $\hbar\nu = E_a - E_b$, where E_a and E_b are the energies of the initial and final states of the system; U is the potential energy of the system.

For an atom together with an incoming electron we have

$$U = -\sum_{i=0}^{Z}\frac{Ze^2}{|\mathbf{r}_i|} + \frac{1}{2}\sum_{i=0}^{Z}\sum_{k=0}^{Z}{}' \frac{e^2}{|\mathbf{r}_i - \mathbf{r}_k|} \qquad (2)$$

($\mathbf{r}_0$ is the radius vector of the incoming electron) and therefore

$$\sum_i \nabla_i U = \sum_{i=0}^{Z} Ze^2\mathbf{r}_i/r_i^3, \qquad (3)$$

since the sum of the internal forces in a system of Z + 1 electrons is equal to zero. Consequently, the last expression in (1) is made up of only forces that act between the nucleus and each electron.

The product of the wave functions $\Psi_a\Psi_b$ of the system is symmetrical with respect to interchange of coordinates and spins of any pair of electrons. After summing over the spins (for a specified total spin of the system), the product becomes symmetrical with respect to the interchange of the electron coordinates only. Therefore all the terms of the sum in (1) are equal to each other and

$$S = \frac{4e^2}{3c^3}\nu^4\left|\int \rho_{ab}\mathbf{r}_0 d\mathbf{r}_0\right|^2 = \frac{4Z^2e^6}{3m^2c^3}\left|\int \rho_{ab}\frac{\mathbf{r}_0 d\mathbf{r}_0}{r_0^3}\right|^2, \qquad (4)$$

where ρ_{ab} is a function of $\mathbf{r}_0$ only, defined as

$$\rho_{ab}(\mathbf{r}_0) = (Z+1)\int\sum \Psi_b^*\Psi_a d\tau_1\ldots d\tau_Z \qquad (5)$$

Here the summation is over all Z + 1 spins of the electrons (for a specified system spin), and the integration is only over the Z spatial variables. At large values of r_0, the function of the system should go into the product of the wave function of the atom χ by the wave function of the free electron φ, while ρ_{ab} should go into the product $\varphi_a(\tau_0)\varphi_b(\tau_0)$ (here φ_a and φ_b are approximately plane waves). At small values of r_0, the value of ρ_{ab} is determined by the Schrödinger equations with potential (2), the solution of which is practically impossible. It is therefore more advantageous to calculate in formula (4) the matrix element of the dipole moment, which, as will be shown below, is determined by the behavior of ρ_{ab} outside the atom. The calculation of the matrix element of acceleration (or ∇U) calls for exact knowledge of the Schrödinger equation with potential (2).

Nedelsky[2] and Biberman and Romanov[3] calculate $\langle\ddot{\mathbf{r}}\rangle_{ab}$, not for expression (2) but for the interaction between the electron and the static field — the screening by the nuclear field. This means that the fact that the slow electron greatly perturbs the atoms is disregarded, as is the fact that in this case radiation from the atomic electrons is present in addition to radiation from the incoming electron. (Furthermore, in reference 3 the wave functions of the incoming and scattered electrons are taken in the Born approximation).

We shall show that, at least in the classical theory, the radiation is due essentially to the atom when the incoming electron is at distances on the order of the dimensions of the atoms.

2. CLASSICAL ESTIMATE OF THE RADIATION OF THE ELECTRON AND THE ATOM

In the first approximation the perturbation of the atom by a slow electron manifests itself in the polarization of the atom. Let the coefficient of polarizability be α. If the natural period of the oscillations of the atomic dipole ($\sim 10^{-16}$ sec) is much less than the time of flight of the electron past the atom (i.e., $v_{el} < 10^8$ cm/sec, or $E_{el} < 3$ ev), then the change in the dipole is adiabatic and amounts to

$$\mathrm{d} = \alpha \mathrm{E} = \alpha e \mathrm{r}/\mathrm{r}^3,$$

where $\mathbf{r}$ is the radius vector of the incoming electron in a system bound to the nucleus. For simplicity we confine ourselves to a frontal collision, when

$$\mathrm{d} = \alpha e/r^2, \qquad \ddot{\mathrm{d}} = -2e\alpha\ddot{r}/r^3 + 6\alpha e\dot{r}^2/r^4.$$

The energy of interaction of the electron with the induced dipole is $U = \alpha e^2/2r^4$, and therefore the energy conservation law yields (assuming the radiated energy to be small)

$$m\dot{r}^2/2 - \alpha e^2/2r^4 = \varepsilon_0,$$

where ϵ_0 is the kinetic energy of the electron at $r = \infty$. Taking account also of the fact that $m\ddot{r} = -\nabla U$, we obtain

$$-\ddot{d}/e\ddot{r} = 5\alpha/r^3 + 6\varepsilon_0 r/e^2.$$

This ratio increases both as $r \rightarrow \infty$ and as $r \rightarrow 0$, and passes through a minimum at $r_{min} = (5\alpha e^2/2\epsilon_0)^{1/4}$. Since α is $\sim 10^{-24}$ cm^3 for most substances, we have, $r_{min} \sim 3 \times 10^{-8}$ cm when $\epsilon_0 \sim 10^{-12}$ erg, and

$$|\ddot{d}/e\ddot{r}|_{r=r_{min}} = (4\varepsilon_0/e^2)(5\alpha e^2/\varepsilon_0)^{1/4} = (4\varepsilon_0/e^2)\, r_{min},$$

i.e., this ratio remains on the order of several units even at the minimum. Thus, when r is on the order of several atomic radii the main radiation is produced by the induced atomic dipole. The case of non-frontal collisions does not affect the results in principle.

This shows that in principle we cannot obtain correct results by treating the radiation of a slow electron on an atom as a single-particle problem through the use of a certain statistical field in lieu of the atom in the calculation of $\langle \ddot{\mathbf{r}} \rangle_{ab}$, if the field is determined in the absence of the electron.

3. CALCULATION OF $\langle \mathbf{r} \rangle_{ab}$.

As already indicated, for large values of r we have

$$\rho_{ab}(\mathbf{r}) = \varphi_a(\mathbf{r})\, \overset{*}{\varphi}_b(\mathbf{r}), \tag{6}$$

where φ_a and φ_b are the solutions of the "free" Schrödinger equation. Their expansion in spherical harmonics has the form

$$\varphi_a = e^{i\mathbf{k}_a\mathbf{r}} = \sum_{l_a=0}^{\infty} (-i)^{l_a}(2l_a + 1) P_{l_a}(\cos\theta_a) f_{l_a}(k_a r) \tag{7}$$

(with similar expressions for φ_b). Here $\mathbf{k}_a$ and $\mathbf{k}_b$ are the wave vectors of the incoming and scattered electrons; θ_a is the angle between $\mathbf{k}_a$ and $\mathbf{r}$; θ_b is the angle between $\mathbf{k}_b$ and $\mathbf{r}$. The quantities ρ_{ab} and $\langle \mathbf{r} \rangle_{ab}$ are expressed in terms of the scattering phase shifts, and consequently, the exact interaction between the electron and the atom will be represented by the phase shifts. At small incoming-electron energies we can neglect all phases except δ_0, and δ_0 itself can be expressed in terms of the elastic-scattering cross section

$$\sigma_p(k) = 4\pi k^{-2} \sin^2 \delta_0(k). \tag{8}$$

We furthermore have

$$|\langle \mathbf{r} \rangle_{ab}|^2 = |\langle z \rangle_{ab}|^2 + |\langle (x - iy) \rangle_{ab}|^2,$$

where x, y, z are Cartesian coordinates, with the z axis directed along $\mathbf{k}_a$ and the x axis in the plane of the vectors $\mathbf{k}_a$ and $\mathbf{k}_b$. Straightforward but cumbersome integration of the expressions, which contain three Legendre polynomials, followed by integration over the angle between $\mathbf{k}_a$ and $\mathbf{k}_b$, yields

$$\begin{aligned}\int |\langle \mathbf{r} \rangle_{ab}|^2 d\Omega_{k_b} = 64\pi^3 \sum_{l=0}^{\infty} \Big\{ \frac{1}{2l+1} \Big| l \int f_{l-1}(k_a r) f_l(k_b r) r^3 dr \\ - (l+1) \int f_{l+1}(k_a r) f_l(k_b r) r^3 dr \Big|^2 \\ + \frac{(l+1)(l+2)}{2l+3} \Big| \int [f_l(k_a r) + f_{l+2}(k_a r)] f_{l+1}(k_b r) r^3 dr \Big|^2 \Big\}.\end{aligned} \tag{9}$$

In this entire sum only the first term, $l = 0$, is of significance, since electrons with momenta $l \geq 2$ are far away from the atom at low energies, and do not interact with it in practice. In expansion (7) we put

$$f_0(kr) = \frac{\sin(kr + \delta_0)}{kr} \qquad (l = 0);$$

$$f_l(kr) = \left(\frac{r}{k}\right)^l \left(\frac{1}{r}\frac{d}{dr}\right)^l \frac{\sin(kr)}{kr} \qquad (l > 0),$$

since $\delta_1 \ll \delta_0$, and obtain finally

$$\begin{aligned}&\int |\langle \mathbf{r} \rangle_{ab}|^2 d\Omega_{k_b} \\ &= \frac{64\pi^3}{k_a^2 k_b^2} \Big\{ \Big| \int_0^{\infty} \sin(k_a r + \delta_0) \Big[\cos(k_b r) - \frac{\sin(k_b r)}{k_b r}\Big] r dr \Big|^2 \\ &+ \Big| \int_0^{\infty} \sin k_b r + \delta_0) \Big[\cos(k_a r) - \frac{\sin(k_a r)}{k_a r}\Big] r dr \Big|^2 \Big\}.\end{aligned} \tag{10}$$

To calculate these integrals we normalize $\varphi_{a,b}$

not to $\delta(k_{a,b} - k)$, but to the wave packet, i.e., by the condition

$$\int_0^\infty dr \left| \int_{k-\Delta k/2}^{k+\Delta k/2} A e^{ikr} dk \right|^2 = 1. \qquad (11)$$

With such a normalization there appears in the integrands of (10) a factor $(\alpha r)^{-2} \sin^2 \alpha r$, where $\alpha = \Delta k/2 \ll k$, which makes the integrals convergent.

Simple integration yields

$$\int \left| \langle \mathbf{r} \rangle_{ab} \right|^2 d\Omega_{k_b} = \frac{64\pi^2 \left[k_a^2 \sigma_p(k_b) + k_b^2 \sigma_p(k_a)\right]}{(k_a^2 - k_b^2)^4}, \qquad (12)$$

where $\sin^2 \delta_0$ is expressed in terms of $\sigma_p(k)$ according to (8). The integrals contained in (10) and taken over the region $0 < r < a$ yield $a^2/2$, even if the wave functions are replaced by unity. Comparing this with the minimum value of the integral over the region $0 < r < \infty$, namely

$$2k_a^2 \sin \delta_0 / (k_a^2 - k_b^2)^2 \approx k_a^{-1} \sqrt{\sigma_p / \pi}$$

we obtain for $\sigma_p(k) \approx (6 \times 10^{-9}\ \text{cm})^2$, the condition under which the integrals (12) are determined by the outer region

$$k_a < (4\sigma / \pi a^4)^{1/2},$$

i.e., $k_a < 5 \times 10^7$, if we put $a = 1.3 \times 10^{-8}$ cm, which corresponds to an incoming electron of 1 ev energy. Since this is an overestimate, we can assume that (12) is applicable up to 3 ev in all cases.

Strictly speaking, the integral over the region $0 < r < a$ must be calculated not with plane waves, but with ρ_{ab}. It can be shown, that $\rho_{ab} \geq \sqrt{\rho_{aa}\rho_{bb}}$ where ρ_{aa} and ρ_{bb} determine the probability of the electron coordinate. Therefore ρ_{ab} can hardly be much greater inside the atom than outside, with the exception of the case when a quasistable system is made up by the electron and the atom. But even in such a case, if the lifetime of this system exceeds the time of flight of the electron through the atomic region by not more than two orders of magnitude, the estimate of the integral remains valid in the region $0 < r < a$.

An analogous expression for the bremsstrahlung in terms of scattering was obtained by Shmushkevich[4] for a collision between a neutron and a proton.

4. INTENSITY OF GAS RADIATION

To obtain the intensity of radiation by a single electron per atom in the frequency interval $d\nu$, it is necessary to multiply (4) by the density of the final states of the electron $(2\pi)^{-3} k_b^2 dk_b d\Omega_{k_b}$, and express k_b by means of

$$\hbar^2 (k_a^2 - k_b^2) / 2m = \hbar\nu.$$

Substituting then (12) in (4) we obtain the spectrum of radiation of an electron per atom in a cubic centimeter

$$dS = 4.5 \cdot 10^{-3} \frac{\sigma_p(0)}{c^2} \left(\frac{E}{m}\right)^{3/2} \sqrt{1 - \frac{\hbar\nu}{E}} \left(2 - \frac{\hbar\nu}{E}\right) d(\hbar\nu). \qquad (13)$$

To obtain the spectrum radiated by a unit volume of gas, it is necessary to integrate (13) over the energy spectrum of the electron and to multiply by the atom density n_{at}. For a Maxwellian electron spectrum we obtain

$$dS(\hbar\nu, \Theta) = 5 \cdot 10^{-3} \frac{\sigma_p(0)\, n_e n_{at}}{c^2 m^{3/2}} \Theta^{3/2} \left[4 + 3\frac{\hbar\nu}{\Theta}\right] e^{-\hbar\nu/\Theta} d(\hbar\nu). \qquad (14)$$

Integrating this expression over $\hbar\nu$ within the limits $0 < \hbar\nu < \infty$, we obtain the total energy lost per unit volume of gas,

$$S(\Theta) = 35 \cdot 10^{-3} \frac{\sigma_p(0)}{c^2 m^{3/2}} n_e n_{at} \Theta^{5/2}. \qquad (15)$$

In all these formulas all the quantities are in the cgs esu, while Θ and E are the temperature of the gas and the electron energy in ergs. In addition, we assume $\sigma_p(k_a) = \sigma_p(k_b) = \sigma_p(0)$, since $\sigma_p \approx$ const for small k. If σ_p changes strongly in the region $k \sim \Theta$, then the formulas given give only the order of magnitude.

Let us give also the expression for the radiation cross section

$$\frac{d\sigma_{\mathbf{rad}}}{d(\hbar\nu)} = 3.1 \cdot 10^{-3} \frac{\sigma_p(0)}{mc^2} \frac{\sqrt{1 - \hbar\nu / E}\,(2 - \hbar\nu / E)}{\hbar\nu / E}. \qquad (16)$$

We see from the formulas that the dependence on the type of substance is expressed through $\sigma_p(0)$. Since the elastic scattering cross section $\sigma_p(0)$ is not correlated with Z^2 (Z is the atomic number of the substance), the radiation does not increase as Z^2 (unlike the results obtained by Biberman and Romanov[3]).

5. COEFFICIENT OF ABSORPTION OF RADIATION

To determine the absorption of radiation by means of free-free transitions of the electrons in the field of the atoms, we introduce a coefficient of absorption $a(\nu, k_b)$, equal to the probability per second of absorption of energy of frequency ν by a single electron contained in one cm^3 of gas, and we use the statistical principle of detailed balancing. Let the radiation be in equilibrium with the gas, and then

$$n_e f(k_a)\,dk_a \cdot n_{\mathbf{at}} \frac{\hbar k_a}{m} \frac{d\sigma}{d\nu} (1 + \bar{n}_\nu)\,d\nu$$

$$= n_e f(k_b)\,dk_b \cdot \bar{n}_\nu \frac{\nu^2 d\nu}{\pi^2 c^3} a(\nu, k_b), \tag{17}$$

where $\bar{n}_\nu$ are the occupation numbers of the photon gas, $n_e f(k)\,dk$ is the distribution of the electrons of the gas over k, and $d\sigma/d\nu$ is the cross section of bremsstrahlung as defined above.

Since

$$f(k_a)\,dk_a / f(k_b)\,dk_b = (k_a / k_b)\,e^{-\hbar\nu/\Theta},$$

and in thermal equilibrium

$$\bar{n}_\nu = [e^{\hbar\nu/\Theta} - 1]^{-1},$$

we have

$$a(\nu, k_b) = \frac{\hbar k_a^2}{m k_b} n_{\mathbf{at}} \frac{\pi^2 c^3}{\nu^2} \frac{d\sigma}{d\nu}. \tag{18}$$

Substituting $d\sigma/d\nu$, we obtain after a simple transformation

$$a(\hbar\nu, E) = 5.8 \frac{e^2 \sigma_p(0)}{m} \left(\frac{\hbar}{m}\right)^2 n_{\mathbf{at}} \left(\frac{m}{E}\right)^{3/2} \frac{\sqrt{1 + \hbar\nu / E}\,(2 + \hbar\nu/E)}{(\hbar\nu / E)^3}. \tag{19}$$

Averaging this expression over the spectrum of the electrons, we obtain the coefficient of absorption of radiation by a unit volume of gas

$$A(\hbar\nu) = \frac{46 e^2 \sigma_p(0)}{m} \sqrt{\frac{\hbar}{m}}\, n_e n_{\mathbf{at}} \left(\frac{\Theta}{\hbar}\right)^{-3/2} \left(\frac{\Theta}{\hbar\nu}\right)^{3/2}$$

$$\times \left[1 + \frac{3}{2}\frac{\Theta}{\hbar\nu} + \frac{27}{2}\left(\frac{\Theta}{\hbar\nu}\right)^{3/2}\right]. \tag{20}$$

All the quantities in these formulas are, as before, in the cgs esu system.

It is seen from (20) that the absorption increases strongly with decreasing radiation frequency. However, our calculations are not correct for long waves. We have assumed that the electron interacts with one definite atom. For this it is necessary that the dimensions of the group of waves of the electron be less than the average distance between atoms $\Delta r < R$, which corresponds to a momentum uncertainty $\Delta k \sim 1/R$. Therefore, for photons with energy less than $\Delta E_{el} = \hbar^2 k \Delta k/m$, all the formulas obtained are incorrect. From this we obtain the long-wave limit of applicability of the theory: $\lambda < 2\pi c m R/\hbar k$. When $n = 10^{19}$ and $k = 10^8$, we obtain $\lambda < 10^{-3}$ cm. Emission of photons with longer wavelengths should be determined by the interaction between the electrons and all the atoms.

The mean free path of the photon is evidently

$$\Lambda_\nu = c / A(\hbar\nu). \tag{21}$$

When $\Theta = 1$ ev, $\hbar\nu = 1$ ev ($\lambda = 1\mu$), and $n_e n_{at} = 10^{28}$, we have $\Lambda_\nu = 10^4$ km.

6. COMPARISON WITH RADIATION ON IONS

Babikov,[5] using the results obtained by Sommerfeld and Maue,[6] determined the radiation of slow electrons on ions. According to his calculations, the spectrum and the total intensity of radiation emitted per second from one cubic centimeter of gas are respectively

$$dS_i = \frac{10^3}{(137)^2} \frac{e^4}{\Theta^2 c^2} \frac{n_e n_i}{m^{3/2}} \Theta^{3/2} e^{-\hbar\nu/\Theta} d(\hbar\nu),$$

$$S_i = \frac{10^3}{(137)^2} \frac{e^4}{\Theta^2 c^2} \frac{n_e n_i}{m^{3/2}} \Theta^{5/2}.$$

Comparing this with (14) and (15), we get

$$dS_i / dS_{\mathbf{at}} = 11 e^4 n_i / \Theta^2 \sigma_p(0)\,[4 + 3\hbar\nu / \Theta]\, n_{\mathbf{at}}$$

$$= 2.2 \cdot 10^3 n_i / \Theta^2 \sigma_p(0)\,[4 + 3\hbar\nu / \Theta]\, n_{\mathbf{at}},$$

$$S_i / S_{\mathbf{at}} = 1.5 e^4 n_i / \sigma_p(0)\,\Theta^2 n_{\mathbf{at}} = 300 n_i / \Theta^2 \sigma_p(0)\, n_{\mathbf{at}},$$

if Θ is the temperature in electron volts, and $\sigma_p(0)$ is in units of 10^{-16} cm^2. The ratio n_i/n_{at} can be obtained by the Saha formula, which determines the degree of thermal ionization of gas as a function of the temperature

$$\frac{n_i}{n_{\mathbf{at}}} = \sqrt{\frac{2g_i}{g_{\mathbf{at}}}} \left(\frac{m}{2\pi}\right)^{3/4} \hbar^{-3/2} \frac{\Theta^{3/4}}{\sqrt{n}} e^{-\varepsilon_i/2\Theta} = 5 \cdot 10^{10} \frac{\Theta^{3/4}}{\sqrt{n}} e^{-\varepsilon_i/2\Theta},$$

where ϵ_i is the ionization potential; Θ does not change substantially if the ratio of the statistical weights of the ion and the atom, g_i/g_{at}, is set equal to unity. If $S_i/S_{at} \sim 1$, then the total density is $n \approx n_{at}$ and

$$\frac{S_i}{S_{\mathbf{at}}} = \frac{1.5 \cdot 10^{13}}{\sigma_p(0)} \frac{\Theta^{-5/4}}{\sqrt{n_{\mathbf{at}}}} e^{-\varepsilon_i/2\Theta}. \tag{22}$$

Thus, putting $S_i/S_{at} = 1$, we get

$$\frac{n_{\mathbf{at}} \sigma_p^2(0)}{2.2 \cdot 10^{26}} = \Theta^{-5/2} e^{-\varepsilon_i/\Theta} \equiv f(\Theta); \tag{23}$$

This function is plotted in the figure for $\epsilon_i = 13.5$ ev. It is obvious that at the points above the curve the radiation is determined by the ions,

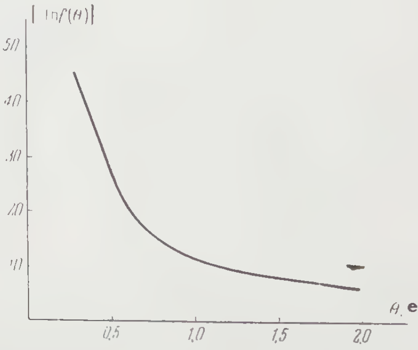

and below that by the atoms. Thus, for $n = 10^{19}$ and $\sigma_p(0) = 10^{-16}$ cm^2, we get $\Theta = 0.7$ ev.

Thus, for temperatures below 7 or 8 × 10^3 deg K, in the pressure range $10^{-5} - 10^3$ mm Hg, the radiation of the gas is determined by collisions between the electrons and the atoms.

---

[1] W. Heitler, The quantum Theory of Radiation, Oxford, 1954, Chapter V, Section 17.

[2] L. Nedelsky, Phys. Rev. **42**, 641 (1932).

[3] L. M. Biberman and V. Romanov, Оптика и спектроскопия (Optics and Spectroscopy) **3**, 646 (1957).

[4] I. M. Shmushkevich, JETP **19**, 431 (1959).

[5] M. Babikov, Сб. Физика плазмы и проблемы управляемых термоядерных реакций (Plasma Physics and Problems of Controllable Thermonuclear Reactions) Vol. 2, Academy of Sciences Press, p. 226.

[6] A. Sommerfeld and A. Maue, Ann. Physik **23**, 589 (1935).

Translated by J. G. Adashko
323

SOVIET PHYSICS JETP VOLUME 12, NUMBER 6 JUNE, 1961

PRODUCTION OF NEGATIVE-TEMPERATURE STATES BY ELECTRON EXCITATION IN A GAS MIXTURE

N. G. BASOV and O. N. KROKHIN

P. N. Lebedev Physics Institute, Academy of Sciences, USSR

Submitted to JETP editor, July 22, 1960

J. Exptl. Theoret. Phys. (U.S.S.R.) 39, 1777-1780 (December, 1960).

The conditions for the production of negative-temperature states by electron-beam excitation in a mixture of two gases with identical energy levels are considered.

A number of authors have considered methods of obtaining negative-temperature states in gases. Sanders[1] and Javan[2] have studied the gas discharge while Rautian and Sobel'man[3] have investigated a method based on the interaction between monochromatic radiation and a binary gas mixture.

A number of papers[4-6] have also reported on experimental investigations of the radiation from a discharge in a mixture of two gases with close-lying atomic energy levels. Ferkhman and Frish[5] have studied a discharge in a mixture of mercury and sodium vapors. It would appear that negative temperatures were produced between excited sodium levels in this work.

Ablekov, Pesin, and Fabelinskiĭ[6] have observed directly the amplification of electromagnetic radiation transmitted through a discharge chamber and have shown that collisions of the second kind between atoms play an important role in the production of a negative temperature.

A theoretical analysis of a discharge in a two-component mixture has been given by Javan.[2] This author has noted that if there are two close-lying atomic energy levels in the two gases it is possible for excitation energy to be transferred from atoms of one gas to the other; this process can cause a substantial change in the atomic distribution over excited states. In the present paper we shall consider the conditions for which negative temperatures can be produced in a gaseous discharge in a binary gas mixture with identical atomic energy levels.

It is well known that the mean kinetic energy of the electrons in a gaseous discharge is considerably greater than the mean kinetic energy of the atoms because the atoms are cooled by the walls of the discharge chamber. If we assume a Maxwellian velocity distribution (electron temperature T_e and atomic temperature T_a), the following relation holds: $T_e \gg T_a$.

If the lifetime of the excited atomic state is affected only by collisions of the second kind between electrons and atoms, the number of excited atoms is given by the Boltzmann formula, in which the temperature is the electron temperature T_e

$$N_i = N_0 \exp\{-\varepsilon_i/kT_e\}, \tag{1}$$

where ϵ_i is the excitation energy and N_0 is the number of atoms in the ground state.

However, the number of excited atoms in the discharge is in fact appreciably smaller for two reasons. 1) Collisions between atoms result in the conversion of atomic excitation energy into kinetic energy of atoms. This process causes a reduction in the atomic excitation temperature T, (the inverse process is also taken into account) so that the T satisfies the inequality $T_e > T > T_a$. 2) Atoms make transitions from higher energy levels to lower energy levels by radiation processes. As a rule, the second mechanism is of greater importance since it is characterized by shorter transition times.

As a result of the relaxation processes noted above, the atomic distribution over excited states is considerably different from that given in Eq. (1) and cannot be given by some temperature T. We shall use the concept of a temperature below, however, keeping in mind that it refers only to the two levels being considered.

We consider two gases a and b, with two identical excited levels $\epsilon_i^a = \epsilon_i^b$. In accordance with the considerations given above, in the absence of any interaction between the atoms in the two gases, these levels will be characterized by temperatures $T_i^a < T_e$ and $T_i^b < T_e$, where, in general $T_i^a \neq T_i^b$. However, for two identical levels the interaction cross section may reasonably be expected to be of resonance nature so that the transfer of excitation from a atoms to b atoms (and the inverse process) will be strong. This interaction between levels ϵ_i^a and ϵ_i^b leads to an equalization of the temperatures of these levels. In particular, if initially $T_i^a < T_i^b$, as a result of the process indicated above, the level ϵ_i^a will be excited to a temperature $T_i^{a'} > T_i^a$. Under these conditions we can expect the production of a negative temperature between the level ϵ_i^a and some level $\epsilon_k^a < \epsilon_i^a$, whose temperatures satisfy the condition $T_k^a < (\epsilon_i^a / \epsilon_k^a) T_i^{a'}$.

We now consider in greater detail the conditions required for the production of a negative temperature in a two-gas mixture. The analysis is simplest for the case in which the lifetime of an atom in level i is much smaller than the transition time from state i to state k.

The time rate of change in the density of the a atoms in an excited level of energy ϵ_i^a is

$$\frac{dN_i^a}{dt} = -N_i^a\left(\frac{1}{\theta_{i0}} + \frac{1}{\tau_{i0}} + \frac{1}{t_{ab}}\right) + N_0^a\left(\frac{1}{\theta_{0i}} + \frac{1}{t_{ba}}\right), \quad (2)$$

where $1/\theta_{0i} = n\overline{\sigma_{0i}v}$ is the probability for electronic excitation of the atom in collisions of the first kind; $1/\theta_{i0} = n\overline{\sigma_{i0}v}$ is the probability for a transition to the ground state in collisions of the second kind with electrons; $1/\tau_{i0}$ is the total probability for transition of the atom from level i (due to all possible relaxation processes except for collisions of the second kind with electrons); $1/t_{ab} = N_0^b\overline{\sigma_{ab}v}$ is the probability for transfer of excitation from an a atom to a b atom; $1/t_{ba} = N_i^b\overline{\sigma_{ba}v}$ is the probability for the inverse process; σ is the cross section for a given process; v is the relative velocity of the particles in collisions; n, N_i, and N_0 are the densities of electrons and atoms in excited states and in the ground states respectively ($\epsilon_0 = 0$). The bar above the expression σv denotes an average over the kinetic energy distribution of the particles. For a Maxwellian electron distribution we have

$$\theta_{i0} / \theta_{0i} = \exp\{-\varepsilon_i / kT_e\}. \quad (3)$$

In Eq. (2) we have neglected processes associated with radiative transitions from higher states and excitation resulting from interatomic collisions.

The number of particles N_k^a in the level ϵ_k^a is found by an equation similar to (2), with account taken of the fact that $1/t_{ab} = 1/t_{ba} = 0$.

In the stationary state dN/dt = 0; to have a negative temperature between the levels ϵ_i^a and ϵ_k^a we require, in view of (3),

$$\frac{(1 + \theta_{k0} / \tau_{k0})(1 + (\theta_{i0} / t_{ba}) \exp\{\varepsilon_i^a / kT_e\})}{1 + \theta_{i0} / \tau_{i0} + (\theta_{i0} / t_{ba}) N_0^b / N_i^b} > \exp\left\{\frac{\varepsilon_i^a - \varepsilon_k^a}{kT_e}\right\}. \quad (4)$$

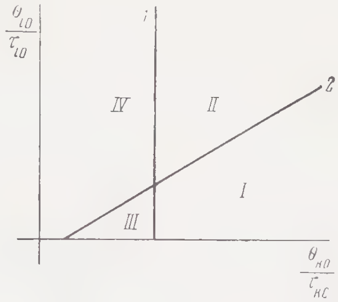
$\frac{\theta_{i0}}{\tau_{i0}}$
1
IV
II
2
I
III
$\frac{\theta_{k0}}{\tau_{k0}}$

It should be noted that (4) depends on both the ratio of the densities of excited atoms and ground-state atoms in gas b and, what is more important, on the absolute density of gas b. The ratio N_i^b/N_0^b can be determined from equations similar to (2); however, this ratio and the density of gas b may be considered as external parameters upon which the inequality in (4) depends. We write the latter in the form

$$\frac{\theta_{i0}}{t_{ba}} \gtrless \exp\left\{-\frac{\varepsilon_i^a}{kT_e}\right\} \frac{\exp\{(\varepsilon_i^a - \varepsilon_k^a) / kT_e\}(1 + \theta_{i0} / \tau_{i0}) - (1 + \theta_{k0} / \tau_{k0})}{1 + \theta_{k0} / \tau_{k0} - (N_0^b / N_i^b) \exp\{-\varepsilon_k^a / kT_e\}}. \quad (5)$$

Here, the symbols > and < refer to the cases in which the denominator of the right hand side is positive or negative respectively.

The inequality in (5) has different meaning in different regions of the variables θ_{i0}/τ_{i0} and θ_{k0}/τ_{k0}, depending on the sign of the right-hand (cf. the figure). We may consider the regions I, II, III and IV in the plane of the variables θ_{i0}/τ_{i0} and θ_{k0}/τ_{k0} which are formed by the two lines

$$1)\quad \frac{\theta_{k0}}{\tau_{k0}} = \frac{N_0^b}{N_i^b} \exp\left\{-\frac{\varepsilon_k^a}{kT_e}\right\} - 1,$$

$$2)\quad \frac{\theta_{i0}}{\tau_{i0}} = \frac{\theta_{k0} / \tau_{k0} + 1 - \exp\{-(\varepsilon_i^a - \varepsilon_k^a)/kT_e\}}{\exp\{(\varepsilon_i^a - \varepsilon_k^a) / kT_e\}}.$$

In region I a negative temperature is produced in gas a even in the absence of gas b because of the favorable ratio for the probabilities of excitation and transition to the ground state in gas a (as in the case considered by Javan[2]). In this case, however, the absence of gas b increases the ratio N_i^a/N_k^a, that is to say, the absolute value of the negative temperature between levels ϵ_i^a and ϵ_k^a is reduced.

In region II a negative temperature is produced because of the presence of gas b; the inequality in (5) gives the condition on the absolute density of excited atoms of gas b.

In region III, the addition of gas b worsens the conditions for the production of a negative temperature. This result follows because the temperature associated with the excitation of level ϵ_i^b in gas b is lower than the temperature for level ϵ_i^a in gas a so that the presence of gas b reduces N_i^a, the number of excited a atoms.

In region IV a negative temperature cannot be produced in gas a.

It would appear that the conditions considered here for the production of a negative temperature have been satisfied in the experiments cited above.[4-6]

---

[1] J. H. Sanders, Phys. Rev. Letters **3**, 86 (1959).

[2] A. Javan, Phys. Rev. Letters **3**, 87 (1959).

[3] S. G. Rautian and I. I. Sobel'man, JETP **39**, 217 (1960), Soviet Phys. JETP **12**, 156 (1961).

[4] F. A. Butaeva and V. A. Fabrikant, "Исследования по экспериментальной и теоретической физике" памяти Г. С. Ландсберга (Research in Experimental and Theoretical Physics, Volume dedicated to the Memory of G. S. Landsberg) Academy of Sciences USSR Press, 1959.

[5] A. Ferkhman and S. Frish, Sow. Phys. **9**, 466 (1936).

[6] Ablekov, Pesin, and Fabelinskiĭ, JETP **39**, 892 (1960), Soviet Phys. JETP **12**, 618 (1961).

Translated by H. Lashinsky
324

SOVIET PHYSICS JETP VOLUME 12, NUMBER 6 JUNE, 1961

CONTRIBUTION TO THE THEORY OF SUPERCONDUCTING ALLOYS WITH PARAMAGNETIC IMPURITIES

A. A. ABRIKOSOV and L. P. GOR'KOV

Institute for Physics Problems, Academy of Sciences, U.S.S.R.

Submitted to JETP editor July 25, 1960

J. Exptl. Theoret. Phys. (U.S.S.R.) **39**, 1781-1796 (December, 1960)

We show in the framework of superconductivity theory that the transition temperature T_c is lowered in comparison with that of a pure metal when paramagnetic impurities are introduced into a superconductor. We have determined the dependence of T_c on the impurity concentration. Superconductivity vanishes at a certain critical concentration. We have made a detailed study of the thermodynamic and magnetic properties of superconducting alloys in the concentration range close to critical. We have found that in that range there is no exponential term in the expression for the heat capacity as $T \rightarrow 0$. The concentration dependence of the gap in the energy spectrum of such a system is determined. It is shown that the gap disappears at a concentration $n' \approx 0.9\, n_{cr}$, while at higher concentrations the energy spectrum of the system is continuous.

A large number of recent papers are devoted to a study of the influence of paramagnetic impurities on the transition of a metal into a superconducting state. It was observed in experiments by Matthias et al.[1] that rare earth impurities in lanthanum in the range of concentrations of about 1% appreciably lower the superconducting transition temperature. Herring[2] and also Suhl and Matthias[3] have in this connection expressed the hypothesis that the occurrence of this effect might be explained on the basis of an exchange interaction between the conduction electrons and the impurity atoms. A little later Matthias et al.[4] found also that a small amount of ferromagnetic impurities in titanium can lead to an increase of its superconducting transition temperature.

The present paper is devoted to a study of this problem on the basis of a microscopic superconductivity theory. It is well known that the mechanism responsible for superconductivity is the formation of bound electron pairs in a singlet state. The exchange interaction between electrons and spinning impurity atoms leads to nonconservation of the electron spin, which may affect the formation of Cooper pairs. It is most probable that the spin of the impurity should inhibit the appearance of the superconducting correlation, i.e., cause a decrease in T_c. The rigorous calculation given in the following confirms this supposition.

It is well known that the transition temperature of superconductors with nonmagnetic impurities remains practically unchanged in the region of low concentrations, and this was also shown in a paper by the present authors.[5] The significant change in T_c is in such cases caused by the influence of the foreign atoms on the basic lattice. One can neglect this effect in the low-concentration region in comparison with the change in the electromagnetic properties of the alloy, which are completely due to the scattering of the electrons by impurity atoms. After the metal has changed into the superconducting state, there arises a specific interelectron correlation which acts at distances of the order of $\xi_0 = \hbar v/2\pi T_c$; these distances have the physical meaning of the average dimensions of a Cooper pair. The scattering of the electrons by the impurities decreases this correlation, restricting it at sufficiently high concentrations to distances of the order of the mean free path.

In the present paper we shall assume that there is a term due to exchange in the interaction between an electron and an impurity atom

$$\hat{v}(\mathbf{r}) = u_1(\mathbf{r}) + u_2(\mathbf{r})(\mathbf{S}\hat{\sigma}), \tag{1}$$

where $\mathbf{S}$ is the moment of the impurity atom and $\hat{\sigma}$ are the electron spin matrices. The Hamiltonian of the interaction between the electrons and the impurity atoms is in the second quantization representation of the form

$$H_{int} = (\psi^+ \hat{V} \psi) = (\psi^+ \sum_a \hat{v}(\mathbf{r} - \mathbf{r}_a)\, \psi).$$

1. THE DEPENDENCE OF THE TRANSITION TEMPERATURE ON THE IMPURITY CONCENTRATION

We consider first the problem of the dependence of the transition temperature on the impurity concentration. To do this we note that one can describe a superconductor by means of two Green's functions $\mathfrak{G}(x, x')$ and $\mathfrak{F}^+(x, x')$ as was shown by one of the authors.[6] In the thermodynamic approach the equations for the Fourier components of these functions are of the form

$$\begin{gathered}(i\omega_n + \nabla^2/2m + \mu)\hat{\mathfrak{G}}_\omega(\mathbf{r}, \mathbf{r}') - \hat{V}\hat{\mathfrak{G}}_\omega(\mathbf{r}, \mathbf{r}') \\ + \hat{\Delta}(\mathbf{r})\hat{\mathfrak{F}}^+_\omega(\mathbf{r}, \mathbf{r}') = \delta(\mathbf{r} - \mathbf{r}'), \\ (i\omega_n - \nabla^2/2m - \mu)\hat{\mathfrak{F}}^+_\omega(\mathbf{r}, \mathbf{r}') + \hat{V}^t\hat{\mathfrak{F}}^+_\omega(\mathbf{r}, \mathbf{r}') \\ + \hat{\Delta}^*(\mathbf{r})\hat{\mathfrak{G}}_\omega(\mathbf{r}, \mathbf{r}') = 0, \\ V^t_{\alpha\beta} = \hat{V}_{\beta\alpha}, \qquad \omega_n = (2n+1)\pi T. \end{gathered} \tag{2}$$

We used the fact that in the constant field of the impurities the functions $\mathfrak{G}$ and $\mathfrak{F}^+$ will be functions of the difference between the "time" variables $\tau = \tau_1 - \tau_2$ only, and we have performed a Fourier transformation with respect to this difference. In particular,

$$\hat{\Delta}(\mathbf{r}) = |g| T \sum_\omega \hat{\mathfrak{F}}_\omega(\mathbf{r}, \mathbf{r}). \tag{3}$$

Unlike reference 7, we have written Eqs. (2) in matrix form as far as the spin variables are concerned, and the product $\hat{V}\hat{\mathfrak{G}}$, for instance, indicates a matrix product. Since $\hat{\Delta}(\mathbf{r})$ and $\hat{\Delta}^*(\mathbf{r})$ are expressed in terms of averages over $\psi\psi$ or $\psi^+\psi^+$ in one point,

$$\hat{\Delta}_{\alpha\beta}(\mathbf{r}) = \langle\psi_\alpha(x)\psi_\beta(x)\rangle, \quad \Delta^*_{\alpha\beta}(\mathbf{r}) = \langle\psi^+_\alpha(x)\psi^+_\beta(x)\rangle, \tag{4}$$

it is clear that the relation

$$\Delta_{\alpha\beta}(\mathbf{r}) = -\Delta_{\beta\alpha}(\mathbf{r}), \tag{5}$$

and also

$$\Delta^*_{\alpha\beta}(\mathbf{r}) = -\Delta^*_{\beta\alpha}(\mathbf{r}) \tag{6}$$

are always valid. When the metal is in its normal state with $T > T_c$, Eqs. (2) do not possess solutions with non-vanishing $\mathfrak{F}^+$ and Δ. The temperature T_c, at which the transition into the superconducting phase occurs, is determined by the fact that at $T = T_c$ there exist for the first time solutions of Eqs. (2) with non-vanishing, though arbitrary small, $\mathfrak{F}^+$ (and Δ). Retaining in (2) only the terms which are linear in $\mathfrak{F}^+$ (and Δ) we get

$$\begin{gathered}(i\omega_n + \nabla^2/2m + \mu)\hat{\mathfrak{G}}'(\mathbf{r}, \mathbf{r}') - \hat{V}(\mathbf{r})\hat{\mathfrak{G}}'_\omega(\mathbf{r}, \mathbf{r}') = \delta(\mathbf{r} - \mathbf{r}'), \\ (i\omega_n - \nabla^2/2m - \mu)\hat{\mathfrak{F}}^+_\omega(\mathbf{r}, \mathbf{r}') + \hat{V}^t(\mathbf{r})\hat{\mathfrak{F}}^+_\omega(\mathbf{r}, \mathbf{r}') \\ + \hat{\Delta}^*(\mathbf{r})\hat{\mathfrak{G}}'_\omega(\mathbf{r}, \mathbf{r}') = 0. \end{gathered} \tag{7}$$

The first of these equations determines the Green's function $\mathfrak{G}'_\omega(\mathbf{r}, \mathbf{r}')$ of the normal metal when there are impurity atoms present. One checks easily that the Green's function $\mathfrak{G}'_\omega(\mathbf{r}, \mathbf{r}')$, on the other hand, also satisfies the equation

$$(i\omega_n + \nabla'^2/2m + \mu)\hat{\mathfrak{G}}'_\omega(\mathbf{r}, \mathbf{r}') - \hat{\mathfrak{G}}'_\omega(\mathbf{r}, \mathbf{r}')\hat{V}(\mathbf{r}') = \delta(\mathbf{r} - \mathbf{r}'),$$

where the prime on the ∇^2 indicates that the differentiation is with respect to the coordinates $\mathbf{r}'$ in $\mathfrak{G}'_\omega(\mathbf{r}, \mathbf{r}')$. Comparing this last equation with the second of Eqs. (7) we find that $\mathfrak{F}^+_\omega(\mathbf{r}, \mathbf{r}')$ can be expressed in terms of Δ^* as follows

$$(\hat{\mathfrak{F}}^+_\omega(\mathbf{r}, \mathbf{r}'))_{\alpha\beta} = \int \mathfrak{G}'_{-\omega\gamma\alpha}(\mathrm{s}, \mathbf{r})\Delta^*_{\gamma\lambda}(\mathrm{s})\mathfrak{G}'_{\omega\lambda\beta}(\mathrm{s}, \mathbf{r}')\, d^3\mathrm{s}. \tag{8}$$

Substituting this expression into (3) we get an equation for the function $\hat{\Delta}^*(\mathbf{r})$. The temperature at which this equation has for the first time a non-vanishing solution is just the transition temperature T_c which interests us:

$$\Delta^*_{\alpha\beta}(\mathbf{r}) = |g| T \sum_\omega \int \mathfrak{G}'_{-\omega\gamma\alpha}(\mathrm{s}, \mathbf{r})\Delta^*_{\gamma\lambda}(\mathrm{s})\mathfrak{G}'_{\omega\lambda\beta}(\mathrm{s}, \mathbf{r})\, d^3\mathrm{s}. \tag{9}$$

We must average this equation over the positions of the impurity atoms. We developed in reference 5 a method which enabled us to perform such an averaging (see also reference 7). If on the diagrams for the Green's functions or for the other quantities we designate the scattering by an impurity atom by a cross, we see easily that to each such cross there corresponds a factor $v(\mathbf{q})e^{i\mathbf{q}\cdot\mathbf{r}_a}$ where $\mathbf{q}$ is the momentum transferred and $\mathbf{r}_a$ the position of the impurity atom.* The average over $\mathbf{r}_a$ vanishes when $\mathbf{q} \neq 0$ unless this diagram contains at least one scattering at $\mathbf{r}_a$ with $\mathbf{q}' = -\mathbf{q}$. In the latter case the result of the averaging will be

$$n|v(\mathbf{q})|^2, \tag{10}$$

where n is the number of impurity atoms per unit volume. It thus turns out that the averaging over the impurity-atom positions can be put in the form of a special diagram technique, by joining two identical atoms on the diagram with a dotted line, and this corresponds to a factor (10) in the matrix elements.

When taking the average of Eq. (9) one can independently take the average of $\Delta^*(\mathbf{s})$ and of the product of the two Green's functions on the right-hand side. One can directly check that this is correct. It can, however, also be seen from the fact that $\Delta^*(\mathbf{s})$, which is a constant when there

---

*We use here the Born approximation for the scattering of the electrons by an impurity atom. The physical results are independent of this approximation and we can therefore replace everywhere the Fourier component of the impurity potential by the corresponding scattering amplitude.

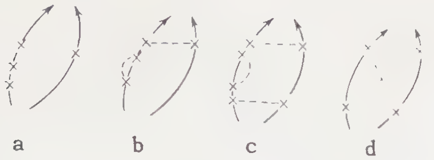

FIG. 1

are no impurities, is only changed near the impurity atoms while $\mathfrak{G}_\omega(\mathbf{r}, \mathbf{s})$ is a fast oscillating function. The result is

$$\overline{\Delta^*_{\alpha\beta}} = |g| T \sum_\omega \int \overline{\Delta^*_{\gamma\lambda}}\, \overline{\mathfrak{G}'_{-\omega\gamma\alpha}(\mathrm{s}, \mathrm{r})\, \mathfrak{G}'_{\omega\lambda\beta}(\mathrm{s}, \mathrm{r})}\, d^3\mathrm{s}. \tag{11}$$

The product of the two Green's functions $\mathfrak{G}'$ in (11) is depicted in Fig. 1a. The averaging over the impurity positions leads to the diagrams of Figs. 1b, c, and d. In this case, however, the dotted line no longer corresponds to a factor (10), but to a factor

$$n v_{\alpha\beta}(\mathbf{q})\, v_{\gamma\lambda}(-\mathbf{q}),$$

since the electron — impurity interaction contains, according to (1), an exchange part.

Apart from averaging over the impurity-atom coordinates, we must still average over the orientation of their spins. We assume that the spins are oriented arbitrarily relative to the lattice and that there is no correlation whatever between them. Therefore

$$\overline{\mathrm{S}} = 0; \qquad \overline{S_i S_k} = \tfrac{1}{3} S(S+1)\, \delta_{ik}.$$

We shall discuss later on the basis of such an assumption. Assuming that the averaging sign in (11) includes also an average over the orientation of the spins of all impurity atoms, we shall let each dotted line in Fig. 1 correspond to a factor

$$n\left(|u_1(\mathbf{q})|^2 + \tfrac{1}{3} S(S+1)\, |u_2(\mathbf{q})|^2\, \sigma_{\alpha\beta}\sigma_{\gamma\lambda}\right). \tag{12}$$

It was shown in reference 5 that diagrams such as the ones of Fig. 1d, which contain intersections of dotted lines, and also any diagrams in which a dotted line includes a vertex with a momentum transfer of an electron line of the order of p_0, give a small contribution $\sim 1/p_0 l$, where l is the mean free path, and can therefore be discarded. Dotted lines such as the ones of Fig. 1b which join two crosses on the same electron line give a contribution to the averaged Green's function $\mathfrak{G}'_\omega(\mathbf{r}, \mathbf{r}')$ [we bear in mind that here $\mathfrak{G}'_\omega(\mathbf{r}, \mathbf{r}')$ refers to the normal metal]. One can easily check that in complete analogy with the result of reference 5 the sum of all such diagrams leads to the Green's function

$$\overline{\mathfrak{G}'_\omega(\mathbf{r}, \mathbf{r}')} = \widetilde{\mathfrak{G}}_\omega(\mathbf{r} - \mathbf{r}') = \mathfrak{G}_\omega(\mathbf{r} - \mathbf{r}') \exp\left(-|\mathbf{r} - \mathbf{r}'|/2l_1\right), \tag{13}$$

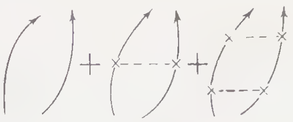

FIG. 2

where $\mathfrak{G}_\omega(\mathbf{r} - \mathbf{r}')$ is the Green's function of the normal metal when there are no impurity atoms. The Fourier components of the function

$$\widetilde{\mathfrak{G}}_\omega(\mathbf{r} - \mathbf{r}') = (2\pi)^{-3} \int \widetilde{\mathfrak{G}}_\omega(\mathbf{p})\, e^{i\mathbf{p}(\mathbf{r} - \mathbf{r}')}\, d^3\mathbf{p}$$

are equal to

$$\widetilde{\mathfrak{G}}_\omega(\mathbf{p}) = [i\omega\eta_1 - \xi]^{-1}, \tag{14}$$

where

$$\eta_1 = 1 + 1/2\tau_1|\omega|, \qquad \xi = v(p - p_0), \qquad v = p_0/m,$$
$$\frac{1}{\tau_1} = \frac{nmp_0}{(2\pi)^2} \int \left\{ |u_1(\mathbf{q})|^2 + |u_2(\mathbf{q})|^2 \frac{1}{3} S(S+1) \right\} do, \quad l_1 = v\tau_1.$$

The evaluation of the average of the product of the two Green's functions in (11) can thus be reduced to a summation of the "ladder" diagrams depicted in Fig. 2. In those diagrams the averaged electron Green's functions (13) and (14) occur as electron lines.

It follows from (5) and (6) that $\Delta^*_{\alpha\beta}$ is of the form

$$\Delta^*_{\alpha\beta} = \Delta^* g_{\alpha\beta}, \qquad g_{\alpha\beta} = \begin{pmatrix} 0 & 1 \\ -1 & 0 \end{pmatrix}_{\alpha\beta}, \tag{15}$$

where $g_{\alpha\beta}$ is the covariant metric tensor in spinor algebra.[8] We can now cancel the constant Δ^* in (11). We introduce the symbol $K_{\omega\alpha\beta}(\mathrm{p}_1, \mathrm{p}_2)$ for the Fourier component of the expression

$$\overline{\mathfrak{G}_{-\omega\gamma\alpha}(\mathrm{s}, \mathrm{r})\, g_{\gamma\lambda}\, \mathfrak{G}_{\omega\lambda\beta}(\mathrm{s}, \mathrm{r}')}$$
$$= (2\pi)^{-6} \int K_{\omega\alpha\beta}(\mathbf{p}_1, \mathbf{p}_2) \exp\{i\mathbf{p}_1(\mathrm{s} - \mathrm{r})$$
$$+ i\mathbf{p}_2(\mathrm{s} - \mathrm{r}')\}\, d^3\mathbf{p}_1 d^3\mathbf{p}_2. \tag{16}$$

The sum of all diagrams of Fig. 2 can be obtained by solving the following obvious integral equation

$$K_{\omega\alpha\beta}(\mathbf{p}_1, \mathbf{p}_2) = \widetilde{\mathfrak{G}}_\omega(\mathbf{p}_1)\, \widetilde{\mathfrak{G}}_{-\omega}(\mathbf{p}_2) \Big[g_{\alpha\beta} + \frac{n}{(2\pi)^3} \int \Big[|u_1|^2$$
$$+ \frac{1}{3} S(S+1)\, |u_2|^2 (\sigma_{\lambda\alpha}\sigma_{\rho\beta}) \Big] K_{\lambda\rho\omega}(\mathbf{p}'_1, \mathbf{p}'_2)\, d^3\mathbf{p}' \Big],$$
$$\mathbf{p}_1 - \mathbf{p}'_1 = \mathbf{p}'_2 - \mathbf{p}_2. \tag{17}$$

It is clear from this that $K_{\omega\alpha\beta}$ is proportional to $g_{\alpha\beta}$. One verifies easily by using spinor algebra that

$$\hat{g}^{-1} \hat{\sigma}^t \hat{g} = -\hat{\sigma}. \tag{18}$$

If $K_{\omega\alpha\beta}(\mathrm{p}_1, \mathrm{p}_2) = K_\omega(\mathrm{p}_1, \mathrm{p}_2)\, g_{\alpha\beta}$, we have thus

$$K_\omega(\mathbf{p}_1, \mathbf{p}_2) = \widetilde{\mathfrak{G}}_\omega(\mathbf{p}_1)\, \widetilde{\mathfrak{G}}_{-\omega}(\mathbf{p}_2) \Big[1 + \frac{n}{(2\pi)^3} \int \Big[|u_1|^2$$
$$- \frac{S(S+1)}{4} |u_2|^2 \Big] K_\omega(\mathbf{p}'_1, \mathbf{p}'_2)\, d^3\mathbf{p}' \Big]. \tag{19}$$

We are, according to (11), interested in the values for $\mathbf{p}_1 = -\mathbf{p}_2$. Substituting Eq. (14) for $\widetilde{\mathfrak{G}}_\omega(\mathbf{p})$ into (19) and denoting the integral on the right-hand side of this expression by L_ω we find

$$K_\omega(\mathbf{p}, \mathbf{q}-\mathbf{p}) = \widetilde{\mathfrak{G}}_\omega(\mathbf{p})\, \widetilde{\mathfrak{G}}_{-\omega}(\mathbf{q}-\mathbf{p})\, [1 + L_\omega]. \qquad (20)$$

For L_ω we get the following expression

$$L_\omega = \frac{1}{2\tau_2\omega\eta_1}\left[1 - \frac{1}{2\tau_2\omega\eta_1}\right]^{-1} = \frac{1}{2\tau_2\omega\eta_s}, \qquad (21)$$

where

$$\frac{1}{\tau_2} = \frac{nmp_0}{(2\pi)^2}\int\left[|u_1|^2 - \frac{1}{4}S(S+1)|u_2|^2\right]do,$$

$$\eta_s = 1 + 1/\tau_s|\omega|; \qquad 1/\tau_s = 1/2\tau_1 - 1/2\tau_2 > 0.$$

Substituting the expression for L_ω into (20) and then substituting $K_\omega(\mathbf{p}_1, \mathbf{p}_2)$ into the kernel of Eq. (11) we get, if we use (21), the following relation

$$1 = \frac{|g|T_c}{(2\pi)^3}\sum_\omega\int\frac{\eta_1/\eta_s}{\omega^2\eta_1^2 + \xi^2}\,d^3\mathbf{p}; \qquad \omega_n = (2n+1)\pi T_c.$$

The sum and the integral over $d^3\mathbf{p}$ in this expression diverge for large ω and ξ. In the papers by Bardeen, Cooper, and Schrieffer[9] and Bogolyubov[10] this divergence was removed by cutting off the electron energies at $|\xi| = \omega_D$. It is convenient to subtract from the right-hand side of the relation which we have obtained the term that does not contain τ. The remaining difference can be integrated over ξ. Putting $1/|g| = (mp_0/2\pi^2)\ln(2\omega_D\gamma/\pi T_{c0})$, where T_{c0} is the transition temperature of the pure superconductor, we get

$$\frac{1}{2}\ln\frac{T_{c0}}{T_c} = \frac{1}{\pi T_c\tau_s}\sum_{n>0}\frac{1}{(2n+1)(2n+1+1/\tau_s\pi T_c)}.$$

We can express the expression on the right-hand side in terms of $\psi(x)$, the derivative of the logarithm of the Γ-function

$$\ln\frac{T_{c0}}{T_c} = \psi\left(\frac{1}{2} + \frac{\rho}{2}\right) - \psi\left(\frac{1}{2}\right), \qquad (22)$$

where $\rho = 1/\pi\tau_s T_c$. The shift in T_c is thus connected only with the exchange part of the interaction and depends on the parameter $1/\tau_s > 0$. Introducing f_+ and f_-, the scattering amplitudes of an electron with total angular momentum $S + 1/2$ and $S - 1/2$, we can express $1/\tau_s$ in the form

$$\frac{1}{\tau_s} = \frac{nmp_0}{2\pi^2}\frac{S(S+1)}{(2S+1)^2}\int|f_+ - f_-|^2\,do.$$

If $\rho \ll 1$, i.e., if the impurity concentration is low, we have

$$T_c = T_{c0} - \pi/4\tau_s. \qquad (23)$$

At low impurity concentrations the transition temperature decreases proportionally to the concentration.

If $\rho \gg 1$, i.e., if $T_c/T_{c0} \ll 1$, we have

$$T_c^2 = (6/\pi^2\tau_s^2)\ln(\pi T_{c0}\tau_s/2\gamma). \qquad (24)$$

At a certain critical concentration which is determined by the condition

$$\tau_{s\,\mathrm{cr}} = 2\gamma/\pi T_{c0}, \qquad (25)$$

superconductivity vanishes at all temperatures in a system with paramagnetic impurities. The "critical mean free path" $l_{s\,\mathrm{cr}} = v\tau_{s\,\mathrm{cr}} \sim 10^{-4}$ cm. One should, however, bear in mind that the magnitude of the exchange interaction u_2 in (1) is always less than the non-exchange part so that the value of l_s is roughly two orders of magnitude longer than the mean free path which is determined, say, by the conductivity of the normal metal. Thus, $l_s \sim 10^{-4}$ cm corresponds to $l \sim 10^{-6}$ cm, or, an impurity concentration of about 1%.

The experimental data of Matthias, Suhl, and Corenzwit[1] indicate apparently the linear dependence of the change in the critical temperature of a solution of gadolinium in lanthanum. If we use the slope of their straight line to construct the theoretical dependence according to Eqs. (23) and (22), the disagreement with the experimental data is nowhere more than 10%. One must regard such an agreement as good. At the same time there exists another paper by the same authors[4] in which they report that for titanium with several ferromagnetic elements as impurities the transition temperature increases with increasing number of impurity atoms at comparatively low concentrations (1 – 5%). This result is in direct contradiction with the results obtained in the foregoing. The reason for this is not clear at the present time. Of course, one must note the well-known difficulties of experiments with alloys particularly in connection with the poor solubility of elements of the iron type in titanium.* Moreover, the concentrations used in reference 4 were of the order of several percent.

Generally speaking, the theory given in the foregoing contained an expansion in terms of the order a/l, where a is the interatomic distance and l the mean free path, and it should therefore be valid at sufficiently low concentrations when the presence of impurity atoms should lead solely to the scattering of the conduction electrons. It is possible that the increase in T_c observed in reference 4 is a secondary effect caused by different interactions between the impurity atoms which are important at the concentrations studied. In any case, the actual nature of the impurity atoms was inessential for our consideration.

---

*The authors are grateful to A. I. Shal'nikov for drawing their attention to this fact.

Let us now consider in more detail the possibility of averaging over the orientation of the spin of a separate atom. There have appeared recently a number of papers[1,11] in which the existence of "impurity" ferromagnetism was detected in a number of alloys and, in particular, it was asserted in reference 11 that in some cases it was possible that there existed simultaneously superconductivity and ferromagnetism caused by paramagnetic impurities. If, indeed, some ferromagnetic ordering of spins were possible, the averaging over the spin orientation which was used by us should be completely unfounded. In that case it would, in general, not be possible to consider the spins on separate impurity atoms to be independent. In the framework of the model considered here, however, we see no positive basis whatever for such an ordering at low impurity concentrations.

Ruderman and Kittel[12] have considered the interaction between two paramagnetic atoms caused in a metal by the exchange of conduction electrons. The fact that the long-range part of this interaction oscillates over distances of the order of atomic distances, is typical of this interaction. At low concentrations, where the distances between the impurity atoms are sufficiently large, this interaction will thus vanish on the average for all atoms and, even if it leads to a ferromagnetic transition, this will occur with an exponentially small Curie temperature.* As far as the direct dipole interaction between impurities is concerned, this is also too small.

On these grounds, our averaging over the spins is fully valid for low concentrations. Apparently, this is precisely the situation with the experiments by Matthias et al.[1] from which one can see that for low concentrations the dependence of the ferromagnetic transition temperature on the concentration is not at all linear. The crossing of the ferromagnetic and the superconducting transition temperatures of an alloy, which was observed in reference 11, occurred when the concentration of one of the components was about 6%. Such a concentration is no longer low and all that has been said in the foregoing is inapplicable to it. As far as the nature of impurity ferromagnetism is concerned for such a system, it is probable that this is caused by the above-mentioned exchange interaction between impurities, which is due to the conduction electrons.

We must draw attention to the fact that order-of-magnitude estimates of all the quantities lead, as was shown in the foregoing, to the conclusion that the whole phenomenon breaks up in the concentration range on the order of 1%. The magnitude of the interval in which T_c changes with the impurity concentration as determined from our theory depends thus strongly on the nature of the effect studied or, to be more precise, on the magnitude of the exchange interaction u_2 in (1). The larger u_2, the faster will the T_c corresponding to the superconducting transition decrease and the lower the concentration that corresponds to the critical value $\tau_{s\,cr}$ of (25). It follows in any case from (23) that for low concentrations T_c must decrease linearly with increasing concentration. As we have said already, the fact that this was not observed in reference 11 shows that it is necessary to study those alloys at even lower concentrations.

2. THE THERMODYNAMIC AND ELECTROMAGNETIC PROPERTIES OF ALLOYS NEAR THE CRITICAL CONCENTRATION

We now turn to a study of the properties of alloys with paramagnetic impurities. Of most interest will be the results obtained in the concentration range where the temperature of the superconducting transition is small compared with T_{c0} of a pure superconductor, i.e., when $\tau_s \approx \tau_{s\,cr}$. In that range the quantities Δ and $\mathfrak{F}^+$ are small ($\Delta\tau_{s\,cr} \ll 1$). We write Eqs. (2) in yet another form, including in them an additional magnetic field

$$\left\{i\omega_n + \frac{1}{2m}\left(\frac{\partial}{\partial \mathbf{r}} - ie\mathbf{A}\right)^2 + \mu\right\}\hat{\mathfrak{G}}_\omega(\mathbf{r},\mathbf{r}') - \hat{V}\hat{\mathfrak{G}}_\omega(\mathbf{r},\mathbf{r}')$$
$$+ \hat{\Delta}(\mathbf{r})\hat{\mathfrak{F}}^+_\omega(\mathbf{r},\mathbf{r}') = \delta(\mathbf{r}-\mathbf{r}'),$$
$$\left\{i\omega_n - \frac{1}{2m}\left(\frac{\partial}{\partial \mathbf{r}} + ie\mathbf{A}\right)^2 - \mu\right\}\hat{\mathfrak{F}}^+_\omega(\mathbf{r},\mathbf{r}') + \hat{V}^t\hat{\mathfrak{F}}^+_\omega(\mathbf{r},\mathbf{r}')$$
$$+ \hat{\Delta}^*(\mathbf{r})\hat{\mathfrak{G}}_\omega(\mathbf{r},\mathbf{r}') = 0. \tag{26}$$

In the region under consideration we can expand Eqs. (26) in terms of the quantity Δ. The corresponding calculations are similar to the derivation, by one of the authors,[7] of the equations of the Ginzburg-Landau theory[14] near T_c for superconducting alloys.

Introducing the Green's function $\mathfrak{G}'_\omega(\mathbf{r},\mathbf{r}')$ of the normal metal, which satisfies the equation

$$\left\{i\omega_n + \frac{1}{2m}\left(\frac{\partial}{\partial \mathbf{r}} - ie\mathbf{A}\right)^2 + \mu\right\}\hat{\mathfrak{G}}'_\omega(\mathbf{r},\mathbf{r}') - \hat{V}\hat{\mathfrak{G}}'_\omega(\mathbf{r},\mathbf{r}')$$
$$= \delta(\mathbf{r}-\mathbf{r}'),$$

---

*We feel in this connection that the attempt by Brout[13] to explain impurity ferromagnetism by a model where the Hamiltonian contains a constant term proportional to $\Sigma S_i S_k$, where S_i are the spins of the impurity atoms, is incorrect.

we can use it to write for $\mathfrak{F}^{+}_{\omega}$ and $\mathfrak{G}_{\omega}$ up to terms of the third and second order in $|\Delta|$ respectively

$$\mathfrak{F}^{+}_{\omega\alpha\beta}(\mathbf{r}, \mathbf{r}') = \int \mathfrak{G}'_{-\omega\lambda\alpha}(\mathbf{s}, \mathbf{r})\, \Delta^{*}_{\lambda\nu}(\mathbf{s})\, \mathfrak{G}'_{\omega\nu\beta}(\mathbf{s}, \mathbf{r}')\, d^3\mathbf{s}$$
$$- \iiint \mathfrak{G}'_{-\omega\lambda\alpha}(\mathbf{s}, \mathbf{r})\, \Delta^{*}_{\lambda\nu}(\mathbf{s})\, \mathfrak{G}'_{\omega\nu k}(\mathbf{s}, \mathbf{l})\, \Delta_{ki}(\mathbf{l})\, \mathfrak{G}'_{-\omega\varkappa i}(\mathbf{m}, \mathbf{l})$$
$$\times \Delta^{*}_{\varkappa\nu}(\mathbf{m})\, \mathfrak{G}'_{\omega\nu\beta}(\mathbf{m}, \mathbf{r}')\, d^3\mathbf{m}\, d^3\mathbf{l}\, d^3\mathbf{s},$$

$$\mathfrak{G}_{\omega\alpha\beta}(\mathbf{r}, \mathbf{r}') = \mathfrak{G}'_{\omega\alpha\beta}(\mathbf{r}, \mathbf{r}') - \iint \mathfrak{G}'_{\alpha k}(r, l)\, \Delta_{ki}(\mathbf{l})\, \mathfrak{G}'_{-\omega\varkappa i}$$
$$\times (\mathbf{m}, \mathbf{l})\, \Delta^{*}_{\varkappa\rho}(\mathbf{m})\, \mathfrak{G}'_{\omega\rho\beta}(\mathbf{m}, \mathbf{r}')\, d^3\mathbf{m}\, d^3\mathbf{l}. \tag{27}$$

Substituting Eq. (27) for $\mathfrak{F}^{+}$ into (3) we get an equation to determine $\hat{\Delta}^{*}(\mathbf{r})$

$$\Delta^{*}_{\alpha\beta}(\mathbf{r}) = |g|\, T \sum_{\omega} \Big\{ \int \mathfrak{G}'_{-\omega\lambda\alpha}(\mathbf{s}, \mathbf{r})\, \Delta^{*}_{\lambda\nu}(\mathbf{s})\, \mathfrak{G}'_{\omega\nu\beta}(\mathbf{s}, \mathbf{r})\, d^3\mathbf{s}$$
$$- \iiint \mathfrak{G}'_{-\omega\lambda\alpha}(\mathbf{s}, \mathbf{r})\, \Delta^{*}_{\lambda\nu}(\mathbf{s})\, \mathfrak{G}'_{\omega\nu k}(\mathbf{s}, \mathbf{l})\, \Delta_{ki}(\mathbf{l})\, \mathfrak{G}'_{-\omega\varkappa i}(\mathbf{m}, \mathbf{l})$$
$$\times \Delta^{*}_{\varkappa\nu}(\mathbf{m})\, \mathfrak{G}'_{\omega\nu\beta}(\mathbf{m}, \mathbf{r})\, d^3\mathbf{m}\, d^3\mathbf{l}\, d^3\mathbf{s} \Big\}. \tag{28}$$

As far as the dependence of the Green's function $\mathfrak{G}'_{\omega\alpha\beta}(\mathbf{s}, \mathbf{r})$ on the magnetic field is concerned, it was established in reference 7 that since the screening radius of the electron in a magnetic field is large compared with the mean free path, one can write it in the form

$$\mathfrak{G}'_{\omega\alpha\beta}(\mathbf{s}, \mathbf{r}) = \exp\{iec^{-1}(\mathbf{A}, \mathbf{s} - \mathbf{r})\}\, \mathfrak{G}^{0}_{\omega\alpha\beta}(\mathbf{s}, \mathbf{r}), \tag{29}$$

where $\mathfrak{G}^{0}_{\omega\alpha\beta}(\mathbf{s}, \mathbf{r})$ is the Green's function of the normal electrons when there is no field. The concentration range $n \sim n_{cr}$ is characterized, as we have seen, by the quantities $1/\tau_s \sim T_{c0}$. As has been stated above, the magnitude of the exchange interaction is appreciably less than the non-exchange part in (1). The normal mean free path l is thus in that case appreciably less than the correlation parameter $\xi \sim \hbar v/2\pi T_{c0}$.

It is natural to assume that under those conditions a localized situation occurs, i.e., that the function $\Delta(\mathbf{r})$ and the field $A(\mathbf{r})$ change over distances which are larger than the characteristic distances in the integrals of Eq. (28). For this reason we can in the third-order term neglect the dependence of $\Delta(\mathbf{r})$ on the coordinates and that of the functions $\mathfrak{G}'$ on the field, as is confirmed by the final result, and in the second term we can as far as this dependence is concerned expand in a Taylor series about the point $\mathbf{r}$, limiting ourselves to terms of the second order in $|\mathbf{r} - \mathbf{s}|$. Using (29) we get as a result

$$\frac{1}{|g|}\Delta^{*}(\mathbf{r})\, g_{\alpha\beta} = \Delta^{*}(\mathbf{r})\, Q^{(2)}_{\alpha\beta}$$
$$+ \frac{1}{6}\Big(\frac{\partial}{\partial \mathbf{r}} + 2ie\mathbf{A}(\mathbf{r})\Big)\Delta^{*}(\mathbf{r})\, Q^{(2)}_{\alpha\beta} + B_{\alpha\beta}|\Delta(\mathbf{r})|^2 \Delta^{*}(\mathbf{r});$$
$$Q^{(1)}_{\alpha\beta} = T \sum_{\omega} \int \overline{\mathfrak{G}^{0}_{-\omega\lambda\alpha}(\mathbf{s}, \mathbf{r})\, \hat{g}_{\lambda\nu}\, \mathfrak{G}^{0}_{\omega\nu\beta}(\mathbf{s}, \mathbf{r})}\, d^3\mathbf{s}, \tag{30}$$

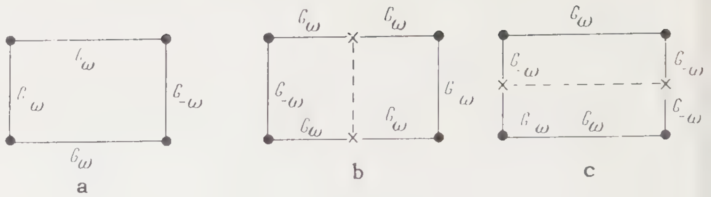

FIG. 3

$$Q^{(2)}_{\alpha\beta} = T \sum_{\omega} \int |\mathbf{r} - \mathbf{s}|^2\, \overline{\mathfrak{G}^{0}_{-\omega\lambda\alpha}(\mathbf{s}, \mathbf{r})\, g_{\lambda\nu}\, \mathfrak{G}^{0}_{\omega\nu\beta}(\mathbf{s}, \mathbf{r})}\, d^3\mathbf{s}, \quad B_{\alpha\beta} = T$$
$$\times \sum_{\omega} \iiint \overline{\mathfrak{G}^{0}_{-\omega\lambda\alpha}(\mathbf{s}, \mathbf{r})\, g_{\lambda\nu}\, \mathfrak{G}^{0}_{\omega\nu k}(\mathbf{s}, \mathbf{l})\, g_{ki}\, \mathfrak{G}^{0}_{-\omega\varkappa i}(\mathbf{m}, \mathbf{l})\, g_{k\nu}\, \mathfrak{G}^{0}_{\omega\nu\beta}(\mathbf{m}, \mathbf{r})}$$
$$\times d^3\mathbf{m}\, d^3\mathbf{l}\, d^3\mathbf{s}. \tag{31}$$

As before, the bar indicates averaging over the impurity atom positions and over the orientation of their spins. The first two coefficients $Q^{(1)}_{\alpha\beta}$ and $Q^{(2)}_{\alpha\beta}$ can easily be connected with the kernel $K_{\omega\alpha\beta}(\mathbf{p}_1, \mathbf{p}_2)$ of (16). Indeed, we have

$$Q^{(1)}_{\alpha\beta} = \frac{T}{(2\pi)^3} \sum_{\omega} \int K_{\omega\alpha\beta}(\mathbf{p}, -\mathbf{p})\, d^3\mathbf{p},$$

$$Q^{(2)}_{\alpha\beta} = -\frac{T}{(2\pi)^3} \sum_{\omega} \int \Big[\frac{\partial^2}{\partial q_i^2} K_{\omega\alpha\beta}(\mathbf{p}, \mathbf{q} - \mathbf{p})\Big]_{\mathbf{q}=0} d^3\mathbf{p}.$$

To find them we must thus solve Eqs. (19) and (20) up to terms of second order in q.

The product of four $\mathfrak{G}$-functions in B is schematically depicted in Fig. 3a. It follows from (20) and (21) that we average over the impurity atom positions first by replacing the lines in Fig. 3a by averaged Green's functions $\tilde{\mathfrak{G}}_{\omega}(\mathbf{p})$, and by replacing unity in the vertex by the ratio η_1/η_s. Moreover, the averaging gives rise to the two new diagrams of Figs. 3b and c, in which a dotted line joins two Green's functions with the same frequency. One verifies easily that all other diagrams are either equal to zero, (because all the poles lie in one half-plane) when integrating over $\xi = v(p - p_0)$ or contain intersecting dotted lines and their contribution can be neglected for the reasons given at the start of this paper. The actual determination of the coefficients $Q^{(1)}$, $Q^{(2)}$, and B requires elementary, but somewhat cumbersome algebraic calculations which we shall omit here.

As in (18), it is extremely essential to maintain the correct order of the spinor indices in the calculations. If we assume that in (1) the exchange part of the interaction is small compared with the non-exchange part, we get the final form of Eq. (30) in the temperature range $T \ll T_{c0}$ and range of concentrations $|n - n_{cr}| \ll n_{cr}$

$$\left\{\pi^2 (T^2 - T_c^2) + \frac{|\Delta|^2}{2}\right\} \Delta^* + 2 \left(\frac{\partial}{\partial \mathbf{r}} + 2ie\mathbf{A}\right)^2 \Delta^* v^2 \frac{\tau_{tr}}{\tau_s} = 0, \tag{32}$$

where τ_{tr} is the "transport" collision time, which enters in the conductivity of the normal metal

$$\sigma = Ne^2\tau_{tr}/m.$$

In the approximation considered we have

$$\frac{1}{\tau_{tr}} = \frac{nmp_0}{(2\pi)^2}\int |u_1|^2 (1 - \cos\theta)\, do.$$

When there is no field

$$\Delta^2 = 2\pi^2 (T_c^2 - T^2). \tag{33}$$

To determine the thermodynamic characteristics of the system we use the well-known formula for the variation of the thermodynamic potential

$$\delta\Omega / \delta g = g^{-1} \langle H_{int}\rangle.$$

We get from this[15]

$$\Omega_s - \Omega_n = \int_0^{|g|} \delta (1/|g|)\, \Delta^2. \tag{34}$$

Using the relation $\delta(1/|g|) = -(mp_0/2\pi^2)\delta T_{c0}/T_{c0}$ and Eq. (32) we get

$$F_s - F_n = -\frac{mp_0}{2\pi^2}\frac{\tau_s^2\Delta^4}{24} = -\frac{mp_0}{2\pi^2}\frac{\tau_s^2\pi^4}{6}(T_c^2 - T^2)^2. \tag{35}$$

The critical field, defined in the usual way, is equal to

$$H_c = \frac{2\gamma}{T_{c0}}\sqrt{\frac{2mp_0\pi}{3}}\left(1 - \frac{T^2}{T_c^2}\right) = H_{c0}\left(1 - \frac{T^2}{T_c^2}\right).$$

We find from (35) the ratio of the heat capacity in the superconducting phase to the heat capacity in the normal phase at $T = T_c$

$$\begin{aligned} C_s(T)/C_n(T_c) &= T/T_c - (\pi^2\tau_s^2/T_c)(T_c^2 T - 3T^3) \\ &= T/T_c - 12.4\,(T_c/T_{c0})^2 (T/T_c - 3T^3/T_c^3). \end{aligned} \tag{36}$$

When there is a field one must add to Eq. (34) the equation of the electrodynamics of superconductors. To do this one must substitute in the definition of the electromagnetic current

$$\mathbf{j}(\mathbf{r}) = \left\{\frac{ie}{m}(\nabla_r - \nabla_{r'})\,\mathfrak{G}(x, x') + \frac{2e^2\mathbf{A}(\mathbf{r})}{mc}\,\mathfrak{G}(x, x')\right\}_{\mathbf{r}=\mathbf{r}',\, t'=t+0}$$

the expression (27) for the Green's function. We shall not dwell on the calculations since they are, apart from the existence of spin at the impurities, similar to the calculations in reference 7. Performing the averaging and restricting ourselves to the first non-vanishing terms in **A** and Δ, we get

$$\mathbf{j} = \left\{\frac{ie}{m}\left(\Delta\frac{\partial\Delta^*}{\partial\mathbf{r}} - \Delta^*\frac{\partial\Delta}{\partial\mathbf{r}}\right) - \frac{4e^2}{mc}\mathbf{A}|\Delta|^2\right\}\frac{N\tau_s\tau_{tr}}{2\pi^2}. \tag{37}$$

Equations (32) and (37) together have the same form as the set of equations in the phenomenological Ginzburg-Landau theory.[14] The origin of the doubled elementary charge in these equations has a distinct physical meaning. It is related to the existence of pair correlations in present-day superconductivity theory.

In contrast to the case of pure superconductors, and also to the case of non-magnetic impurities,[7,15] these equations are applicable here in the whole temperature range of the superconducting phase. The temperature dependence enters into the different characteristics of the system through the factor $1 - T^2/T_c^2$ in Eq. (32). In particular, we get for the penetration depth of a weak magnetic field in superconductors

$$\begin{aligned} \delta &= \left[\frac{16\pi^3 Ne^2\tau_s\tau_{tr}T_c^2}{mc^2}\left(1 - \frac{T^2}{T_c^2}\right)\right]^{-1/2} \\ &= \frac{c}{4\pi T_c}\left[\frac{2\sigma\gamma}{T_{c0}}\left(1 - \frac{T^2}{T_c^2}\right)\right]^{-1/2}. \end{aligned} \tag{38}$$

For Eqs. (32) and (37) we can construct one dimensionless constant

$$\varkappa = 2\sqrt{2}eH\delta^2/\hbar c = ec\,(\pi\gamma)^{1/2}/4\sigma,$$

where γ is the coefficient in the linear law for the electronic part of the heat capacity of the normal metal. It is worth noting that as in reference 7 κ depends only on the parameters of the normal metal, while the dependence on τ_s disappears.

The most interesting result is that there is no exponential term in the heat capacity (36) as $T \to 0$. This indicates that there is no gap in the spectrum of such superconductors. This conclusion is confirmed also by the absence of a threshold in the absorption of electromagnetic radiation at $T = 0$. We can, namely, obtain by a method which we have used before[5] the following expression for the dielectric constant of paramagnetic alloys

$$\varepsilon(\omega) = -c^2/\omega^2\delta^2 + 4\pi i\sigma/\omega. \tag{39}$$

We study this problem now in more detail.

3. THE DEPENDENCE OF THE GAP IN THE SPECTRUM AT T = 0 ON THE IMPURITY CONCENTRATION AND THE HEAT CAPACITY AT LOW TEMPERATURES

Migdal and Galitskiĭ[16] have shown that when $\omega > 0$ the imaginary part of the Fourier component of the electron Green's function

$$G(x, x') = -i\langle T(\psi(x), \psi^+(x'))\rangle$$

can at absolute zero be written in the form

$$\operatorname{Im} G_\omega(\mathbf{p}) = \sum_n \rho_n(\mathbf{p})\,\delta(\omega - \omega_{n0}), \quad (\omega > 0),$$

where $\rho_n(\mathbf{p})$ is some real spectral function, and

$\omega_{n0} = E_n - E_0$ is the difference in energy between the n-th excited state and the ground state of the system. When there are impurities present the system has no single-particle spectrum, which is determined from the poles of the function $G_\omega(p)$. All the same, however, if the first excited state is separated from the ground state by a gap, the magnitude of the gap is determined by the value of the frequency ω at which the Green's function has a non-vanishing imaginary part for the first time.

One can show in the case of a superconductor that the same holds for the function $iF_\omega(p)$, where $F_\omega(p)$ is the Fourier component of $F^+(x, x') = \langle T(\psi^+(x), \psi^+(x'))\rangle$, or for the function $iF^+_{R\omega}(p)$, which is the Fourier component of the so-called retarded anticommutator of the two ψ^+ (the two functions are the same at $T = 0$ for $\omega > 0$). Bearing in mind the further calculation of the heat capacity, we consider the function $F^+_{R\omega}(p)$. Its characteristic property is its direct connection with the temperature-dependent function $\mathfrak{F}^+_{\omega_n}(p)$. Using methods similar to the ones used in reference 17, one can show that in the upper half-plane $iF^+_{R\omega}(p)$ is an analytic function that coincides with $\mathfrak{F}^+_{\omega_n}(p)$ in the points $\omega_n = i\pi T(2n + 1)$ (when $n > 0$). We have solved the equations for the temperature-dependent Green's functions in the limiting case where Δ and $\mathfrak{F}^+$ were small. These equations can be obtained in the general case by the same method as was used by us for the case of normal superconductors.[5] A new aspect is here the occurrence of two relaxation times τ_1 and τ_2 and the dependence of the quantity $\Delta^* = |g|\,\mathfrak{F}^+(x, x)$ on the concentration of the paramagnetic impurities. The functions $\mathfrak{G}_{\omega_n}$ and $\mathfrak{F}^+_{\omega_n}$ obtained in this way are of the form

$$\mathfrak{G}_{\omega_n}(\mathbf{p}) = -\frac{\widetilde{\omega}_n + \xi}{\widetilde{\omega}_n^2 + \xi^2 + \widetilde{\Delta}_n^2}, \qquad \mathfrak{F}^+_{\omega_n}(\mathbf{p}) = \frac{\widetilde{\Delta}_n}{\widetilde{\omega}_n^2 + \xi^2 + \widetilde{\Delta}_n^2}, \tag{40}$$

where

$$\widetilde{\omega}_n = \omega_n + \frac{1}{2\tau_1}\frac{u_n}{\sqrt{u_n^2+1}}, \qquad \widetilde{\Delta}_n = \Delta + \frac{1}{2\tau_2}\frac{1}{\sqrt{u_n^2+1}}, \tag{41}$$

$$u_n = \frac{\widetilde{\omega}_n}{\widetilde{\Delta}_n}, \qquad \frac{\omega_n}{\Delta} = u_n\left(1 - \frac{1}{\tau_s\Delta}\frac{1}{\sqrt{u_n^2+1}}\right). \tag{42}$$

One can obtain similar equations using the technique applicable at absolute zero. We can determine the function $F^+_{R\omega}(p)$ which interests us as follows. If we formally replace ω_n by $-i\omega$ and at the same time $\widetilde{\omega}_n$ by $-i\widetilde{\omega}$, u_n by $-iu$, and $\widetilde{\Delta}_n$ by $\widetilde{\Delta}$ we get for u the following equation

$$\frac{\omega}{\Delta} = u\left(1 - \frac{1}{\tau_s\Delta}\frac{1}{\sqrt{1-u^2}}\right). \tag{42'}$$

The radical must be defined here as the analytical continuation of the positive square root $+\sqrt{1-u^2}$ for real u and $|u| < 1$ in the upper half-plane of the variable u. (One can verify that this definition is correct by comparing these formulae with the results obtained by the usual technique at the absolute zero.)

In actual fact we need for the following not the whole of the function $F^+_{R\omega}(p)$ but only some of its properties. It follows from Eq. (42′) that when $\tau_s\Delta > 1$ and when ω is sufficiently small there exists a real solution for u, with $|u| < 1$. The connection with the limiting case $1/\tau_s \to 0$ shows that in our case we must also choose just that solution. Studying the right-hand side of (42′) one sees easily that it has a maximum for

$$u_0 = [1 - (1/\tau_s\Delta)^{2/3}]^{1/2},$$
$$\omega_0 = \Delta[1 - (1/\tau_s\Delta)^{2/3}]^{3/2}; \tag{43}$$

and that therefore all solutions of Eq. (42′) are complex when $\omega > \omega_0$.

Since we must take the real solution of Eq. (42′) when ω is small, it follows that u becomes complex and $F_{R\omega}(p)$ acquires thereby an imaginary part when $\omega > \omega_0$. The quantity ω_0 thus determines the size of the gap. When the concentration is increased, the value of ω_0 diminishes and tends to zero when $1/\tau_s\Delta = 1$. The magnitude of Δ is thus not at all equal to the gap in the energy spectrum for paramagnetic alloys.

We find now the dependence of Δ on the impurity concentration. The definition of $\Delta^* = |g|\,\mathfrak{F}^+(x, x)$ yields the equation

$$\Delta = \frac{|g|T}{(2\pi)^3}\sum_n \int \frac{d^3\mathbf{p}\,\widetilde{\Delta}_n}{\widetilde{\omega}_n^2 + \xi^2 + \widetilde{\Delta}_n^2}. \tag{44}$$

Since we are interested in the case $T = 0$, we can change from summation over n to integration, using the formula

$$T\sum_n \to (2\pi)^{-1}\int d\Omega.$$

After this it is convenient to add and subtract under the integral sign the expression $\Delta_0/(\Omega^2 + \xi^2 + \Delta_0^2)$ (Δ_0 is the value of Δ for $T = 0$). The result is

$$\Delta_0 \ln\frac{\Delta_0}{\Delta_{00}} = \int_0^\infty d\Omega\left\{\frac{1}{\sqrt{u^2+1}} - \frac{1}{\sqrt{\Omega^2/\Delta_0^2+1}}\right\}$$

(Δ_{00} is the value of Δ_0 for a pure superconductor). It is convenient to use Eq. (42) and change in this integral the integration over $d\Omega$ to one over du. The result is

$$\ln\frac{\Delta_0}{\Delta_{00}} = -\frac{\pi}{4\tau_s\Delta_{00}}, \qquad \frac{1}{\tau_s\Delta_0} < 1;$$

$$\ln\frac{\Delta_0}{\Delta_{00}} = -\ln\left[\frac{1+\sqrt{1-(\tau_s\Delta_0)^2}}{\tau_s\Delta_0}\right] + \frac{1}{2}\sqrt{1-(\tau_s\Delta_0)^2} - \frac{1}{2\tau_s\Delta_0}\arcsin\tau_s\Delta_0,$$

$$\frac{1}{\tau_s\Delta_0} > 1. \tag{45}$$

We have $1/\tau_{s\,cr} = \pi T_{c0}/2\gamma = \Delta_{00}/2$. When $\tau_s\Delta_0 = 1$ we have $\Delta_0 = e^{-\pi/4}\Delta_{00}$. From this it is clear that there is some value of the concentration which is lower than the critical one for which the gap in the energy spectrum (43) vanishes

$$n' = 2e^{-\pi/4}n_{cr} \approx 0.91\, n_{cr}. \tag{46}$$

The fact that there exists a superconductor without a gap needs some explanations. We started from Eqs. (2) in our derivation. The possibility of describing a superconductor by such a set of equations for the functions $\mathfrak{G}$ and $\mathfrak{F}^+$ is based upon the hypothesis that several pair formations of electrons show a Bose condensation.[6] In a pure superconductor such formations are Cooper pairs, which are condensed in a state with total momentum equal to zero [$\mathfrak{F}^+(x, x')$ depends only on the difference between the coordinates]. Since the number of such pairs in an infinitely large system is arbitrarily large, the creation or annihilation of such a pair would not change the ground state of the system. This fact is indeed reflected in the existence of non-vanishing averages

$$\mathfrak{F}^+(x-x') = \langle T(\psi^+(x), \psi^+(x'))\rangle.$$

We have shown that when n is larger than the n' given by (46) the functions $\mathfrak{F}^+$ are non-vanishing and finite, which confirms the validity of the assumption of a Bose condensation; the change in the gap in the spectrum (46) shows, however, that we are dealing here with a more complicated situation than in the case of a pure superconductor. There remains something obscure in the overall picture.

It is of interest to trace how the vanishing of the gap with increasing impurity concentration affects the temperature dependence of the electronic heat capacity in the range $T \ll T_c$. We first transform somewhat Eq. (34) for the thermodynamic potential. We subtract from (34) the analogous equation for a metal in which a different value for the coupling constant has been taken, $|g_1| > |g|$. This leads to

$$\Omega_s - \Omega_{s1} = -\int_{|g|}^{|g_1|} \delta\left(\frac{1}{|g|}\right)\Delta^2.$$

We use the equation for the gap, which we write in the form

$$\Delta = \frac{|g|\, mp_0}{2\pi^2} f_T(\Delta), \tag{47}$$

and we change from an integral over $|g|$ to one over Δ. Clearly

$$\Omega_s - \Omega_{s1} = -\frac{mp_0}{2\pi^2}\int_{\Delta}^{\Delta_1} [f_T'(y)\,y - f_T(y)]\,dy.$$

We now subtract from this relation its value for T = 0.

We assume that $\Delta_1(0) \gg \Delta(0)$. In that case $\Omega_{s1}(T) - \Omega_{s1}(0) \to 0$. We get thus

$$\Omega_s(T) - \Omega_s(0) = -\frac{mp_0}{2\pi^2}\left\{\int_{\Delta}^{\Delta_1}[f_T'(y)\,y - f_T(y)]\,dy - \int_{\Delta_0}^{\Delta_1}[f_0'(y)\,y - f_0(y)]\,dy\right\}_{\Delta_1\to\infty},$$

where $\Delta_0 \equiv \Delta(0)$ and the $f_0(y)$ are the values of the corresponding functions at T = 0. At low temperatures we can write

$$f_T(\Delta) = f_0(\Delta) + \delta f_T(\Delta), \qquad \Delta = \Delta_0 + \delta\Delta(T);$$

the additional temperature-dependent terms are small compared with the values at absolute zero. Using Eq. (47) we can express $\delta\Delta(T)$ in terms of $\delta f_T(\Delta)$:

$$\delta\Delta(T) = \Delta_0\delta f_T(\Delta)/(f_0 - f_0'\Delta_0).$$

Substituting this into the equation for the thermodynamic potential we find

$$\Omega_s(T) - \Omega_s(0) = \frac{mp_0}{\pi^2}\int_{\Delta_0}^{\infty}\delta f_T(y)\,dy. \tag{48}$$

It is thus sufficient for us to find merely the temperature-dependent addition to the right-hand side of Eq. (44) for Δ.

We start with the simplest case $\tau_s\Delta_0 < 1$. We note that the expression under the summation sign in (44) is symmetric with respect to a change in the sign of n. As before we go over from a summation to an integration but we now take into account a correction term using the well-known formula

$$T\sum_{n>0}\varphi(\omega_n) \to \frac{1}{2\pi}\left\{\int_0^{\infty}\varphi(\Omega)\,d\Omega - \frac{\pi^2T^2}{6}[\varphi'(\infty) - \varphi'(0)]\right\}.$$

The first term here is temperature-independent and the correction is proportional to T^2. After the necessary calculations we get

$$\delta f_T(\Delta) = -\pi^2T^2\tau_s/6\sqrt{(1/\tau_s\Delta)^2 - 1}.$$

When substituting this into (48) we must take into account (vide infra) that the region where $\delta f \sim T^2$

extends only to $\Delta = 1/\tau_s$ and furthermore that this function depends exponentially on T, i.e., it tends to zero, even when we take terms in T^2 into account. The integral over Δ must thus only be taken up to that limit. As a result we get for the heat capacity

$$C_s = \tfrac{1}{3} m p_0 \sqrt{1 - (\tau_s \Delta_0)^2}\, T. \tag{49}$$

When $\Delta_0 \tau_s \ll 1$ this formula is the same as (36) in the limit $T \ll T_c$.

In the case $\Delta_0 \tau_s > 1$ the method given here can not be applied, since it yields only an extra term which is quadratic in T in the thermodynamic potential and which is not present here. If we were to apply this method to the case we are now considering, we would only get the result that there is no such extra term. This is not surprising, since the presence of a gap in the energy spectrum compels us to assume that when $\Delta_0 \tau_s > 1$ the extra term will be exponential. Because of this we shall apply another method.

If in Eq. (44) we change to a summation over positive n only, we can replace this sum by a contour integral. The right-hand side of Eq. (44) will be of the form

$$-\frac{1}{2\pi i} \int_C d\omega \tanh \frac{\omega}{2T} \int_{-\omega_D}^{\omega_D} d\xi \frac{m p_0}{2\pi^2} \mathfrak{F}(-i\omega, \xi).$$

The contour of integration is given in Fig. 4. We now distort the contour and take it along the real axis. This is possible since it was shown that the integral over ω can be considered to be the integral of the function $iF_{R\omega}(\mathbf{p})$ which is analytical in the upper half-plane. For real ω which are such that $|\omega| < \omega_0$ this function is real and symmetric with respect to replacing ω by $-\omega$. From this it follows that the real part of $iF_{R\omega}(\mathbf{p})$ on the real axis is symmetric with respect to a change in sign in ω while its imaginary part is antisymmetric. All that remains of this integral is therefore

$$\frac{1}{\pi} \operatorname{Im} \left\{ \int_0^{\infty} d\omega \tanh \frac{\omega}{2T} \int_{-\omega_D}^{\omega_D} \frac{m p_0}{2\pi^2} d\xi \frac{\widetilde{\Delta}}{-\widetilde{\omega}^2 + \xi^2 + \widetilde{\Delta}^2} \right\}.$$

From the foregoing it follows that the imaginary part of the function $iF_{R\omega}(\mathbf{p})$ appears only starting with $\omega = \omega_0$. If $T \ll \omega_0$ we can thus replace $\tanh \omega/2T$ by $1 - e^{-\omega/T}$. The term 1 gives a contribution to $f_T(\Delta)$ which is independent of the temperature. $\delta f_T(\Delta)$ is thus determined by substituting $-2e^{-\omega/T}$ for $\tanh \omega/2T$. The integral over ξ and ω is then formally convergent and we can first integrate over ξ. In this way we find

$$\delta f_T(\Delta) = -2 \int_{\omega_0}^{\infty} e^{-\omega/T} \operatorname{Im} \left[\frac{1}{\sqrt{1 - u^2}} \right] d\omega.$$

The $\sqrt{1 - u^2}$ under the integral sign must be defined, as a function of ω, as the analytical continuation of its real positive value with a cut $\omega < \omega_0$ through the upper half-plane. Because of the presence of an exponential factor the most essential part of the integral will come from the neighborhood of the point ω_0. Expanding Eq. (42′) in a power series in $u - u_0$ and taking the definition of $\sqrt{1 - u^2}$ for $\omega > \omega_0$ into account, we get

$$\operatorname{Im} \left[\frac{1}{\sqrt{1 - u^2}} \right] = \sqrt{\omega - \omega_0} \left(\frac{3\Delta_0}{2} \right)^{-1/2} \left[1 - \left(\frac{1}{\tau_s \Delta_0} \right)^{2/3} \right]^{1/4} (\Delta_0 \tau_s)^{2/3}.$$

Substituting this into the integral for $\delta f_T(\Delta)$ we find

$$\delta f_T(\Delta) = -\sqrt{\frac{2\pi}{3}}\, T^{3/2} \tau_s^{1/2} [(\Delta_0 \tau_s)^{2/3} - 1]^{1/4} e^{-\omega_0/T}.$$

Substituting this expression into (48) and integrating over Δ we can find the temperature dependent extra term in the thermodynamic potential. We get for the heat capacity

$$C_s(T) = \left(\frac{m p_0}{\pi^2} \right) \sqrt{\frac{2\pi}{3}}\, \tau_s^{2/3} \Delta_0^{1/3} [\Delta_0^{2/3} - \tau_s^{-2/3}]^{11/4} \exp \left\{ -\frac{1}{T} [\Delta_0^{2/3} - \tau_s^{-2/3}]^{3/2} \right\}. \tag{50}$$

One sees easily that this formula does not go over into the formula for the pure superconductor in the limit as $\tau_s \to \infty$. This is connected with the fact that the possibility of expanding Eq. (42′) in powers of $u - u_0$ imposes a restriction on the region of applicability of Eq. (50). The latter is obtained when one estimates the next term of such an expansion. This gives

$$T \ll \Delta_0^{1/3} \tau_s^{-2/3}.$$

At low concentrations this condition is stronger than the condition $T \ll \Delta_0$ which is necessary to separate off the exponential region of the heat capacity. The connection between Eq. (50) and the equation for a pure superconductor could be obtained by considering the case $\tau_s \Delta_0 \gg 1$, $T \ll \Delta_0$, but we shall not perform here the appropriate calculations as we are interested in the basic influence of the vanishing of the gap in the spectrum on the heat capacity.

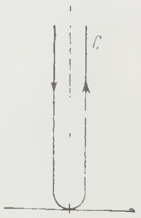

FIG. 4

It follows from Eq. (50) that when the impurity concentration increases the absolute magnitude of the exponent decreases while it does not vanish at $\Delta_0 \tau_S = 1$. In the point $\Delta_0 = 1/\tau_S$ itself, where the exponential and the linear dependence come together one finds from calculating it that $C_S \sim T^{4/3}$. In view of the fact that this single point is not of great interest we shall not give the corresponding calculations or write out the coefficients.

In conclusion we express our gratitude to Academician L. D. Landau for many useful discussions of this paper.

---

[1] Matthias, Suhl, and Corenzwit, Phys. Rev. Letters **1**, 92 (1958).

[2] C. Herring, Physica **24**, S 184 (1958).

[3] H. Suhl and B. T. Matthias, Phys. Rev. **114**, 977 (1959).

[4] Matthias, Compton, Suhl, and Corenzwit, Phys. Rev. **115**, 1597 (1959).

[5] A. A. Abrikosov and L. P. Gor'kov, JETP **35**, 1558 (1958), Soviet Phys. JETP **8**, 1090 (1959); JETP **36**, 319 (1959), Soviet Phys. JETP **9**, 220 (1959).

[6] L. P. Gor'kov, JETP **34**, 735 (1958), Soviet Phys. JETP **7**, 505 (1958).

[7] L. P. Gor'kov, JETP **37**, 1407 (1959), Soviet Phys. JETP **10**, 998 (1960).

[8] L. D. Landau and E. M. Lifshitz, Quantum Mechanics, Pergamon Press, London, 1958, Sec. 54.

[9] Bardeen, Cooper, and Schrieffer, Phys. Rev. **108**, 1175 (1957).

[10] N. N. Bogolyubov, JETP **34**, 58 (1958), Soviet Phys. JETP **7**, 41 (1958).

[11] Matthias, Suhl, and Corenzwit, Phys. Rev. Letters **1**, 449 (1958).

[12] M. A. Ruderman and C. Kittel, Phys. Rev. **96**, 99 (1954).

[13] R. Brout, Phys. Rev. **115**, 824 (1959).

[14] V. L. Ginzburg and L. D. Landau, JETP **20**, 1064 (1950).

[15] L. P. Gor'kov, JETP **36**, 1918 (1959), Soviet Phys. JETP **9**, 1364 (1959).

[16] A. B. Migdal and V. M. Galitskiĭ, JETP **34**, 139 (1958), Soviet Phys. JETP **7**, 96 (1958).

[17] Abrikosov, Gor'kov, and Dzyaloshinskiĭ, JETP **36**, 900 (1959), Soviet Phys. JETP **9**, 636 (1959).

Translated by D. ter Haar
325

SOVIET PHYSICS JETP VOLUME 12, NUMBER 6 JUNE, 1961

SOME PROPERTIES OF STRONGLY COMPRESSED MATTER. I

A. A. ABRIKOSOV

Institute of Physics Problems, Academy of Sciences, U.S.S.R.

Submitted to JETP editor July 26, 1960

J. Exptl. Theoret. Phys. (U.S.S.R.) **39**, 1797-1805 (December, 1960)

The ground-state energy of matter at very high densities is calculated. In contrast to the assumptions made in references 1 — 3, it is shown that the ions form a crystal lattice. The moduli of elasticity and the oscillation spectrum of the lattice are determined. The destruction of the lattice at extremely high densities is discussed. The electron-ion correlation energy is calculated.

GELL-MANN and Brueckner[1] and also Sawada[2] have considered the ground-state energy of highly compressed electron gas, accurate to terms containing the zeroth power of interatomic distance (logarithm and constant). In addition, Gell-Mann[3] determined the rate of excitation on the Fermi boundary (or, what is the same, the coefficient in the linear expression for the specific heat) accurate to terms of order $(V/N)^{1/3}e^2m/\hbar^2$ compared with the ground state.

The model used in references 1 — 3, however, differs substantially from real matter in that it is assumed to contain not ions, but a certain positive charge distributed in space with uniform density. The disadvantage of this model is quite obvious when the ions form a lattice. However, it differs appreciably from the Gell-Mann and Brueckner model also when the substance is a liquid.

The present investigation is devoted to a study of the properties of strongly compressed matter (single element) at $T = 0$ under the assumption that the nuclei form a crystal lattice.

1. LATTICE BINDING ENERGY

We first introduce the following notation. All the energies and the distances will be expressed in the final formulas in atomic units, equal to $e^4m/\hbar^2 = 2$ Ry for the energy and $\hbar^2/e^2m$ for the distances. The atomic volume, expressed in these units, will be designated by the letter v. In all the calculations we assume $v \ll 1$, but at the same time so large that the electrons can be considered nonrelativistic. We shall establish more accurate criteria later on. The energy of the ground state will be referred to one atom.

In the case $v \ll 1$, the greatest contribution to the ground-state energy is made by the kinetic energy of the electrons, the value of which is

$$E^{(0)} = \frac{2V}{N}\int\frac{\mathbf{p}^2}{2m}\frac{d^3\mathbf{p}}{(2\pi\hbar)^3} = \frac{V}{N}\frac{p_0^5}{10\pi^2 m\hbar^3} \quad (p_0/\hbar = (3\pi^2 ZN/V)^{1/3}),$$

where N is the number of atoms in the lattice, p_0 is the limiting Fermi momentum. In atomic units we have

$$E^{(0)} = \frac{3Z}{10}\left(\frac{3\pi^2 Z}{v}\right)^{2/3} = 2{,}87\,\frac{Z^{5/3}}{v^{2/3}}, \tag{1.1}$$

where Z is the atomic number.

The next in order of magnitude is the value of the Coulomb energy (see reference 4). It comprises the energy of interaction between the ions themselves, between ions and electrons, and between electrons themselves, the latter including both the direct and the exchange energies. The ion-ion interaction energy is

$$E_{ii}^{(1)} = \frac{Z^2e^2}{2N}\sum_{n\neq m}\frac{1}{|\mathbf{R}_n-\mathbf{R}_m|} = \frac{Z^2e^2}{2}\sum_{\mathbf{R}\neq 0}\frac{1}{R},$$

where the last sum is taken over the coordinates of all the ions, with exception of the one ion chosen as the reference. The energy of interaction between the electrons and ions is of the form

$$E_{ie}^{(1)} = -\frac{Z^2e^2}{V}\sum_n\int dV\,\frac{1}{|\mathbf{r}-\mathbf{R}_n|} = -Z^2e^2\,\frac{N}{V}\int\frac{dV}{r}.$$

The non-exchange electron interaction yields

$$E_{ee,\,d}^{(1)} = \frac{Z^2e^2}{2}\,\frac{N}{V}\int\frac{dV}{r}.$$

Each of the foregoing three energies diverges by itself, but their sum is the convergent expression

$$E_1^{(1)} = \frac{Z^2e^2}{2}\left(\sum_{\mathbf{R}\neq 0}\frac{1}{R} - \frac{N}{V}\int\frac{dV}{r}\right), \tag{1.2}$$

which must be considered as the limit of the expression calculated for a finite volume.

The exchange energy of the electrons has been calculated many times, and its value is

$$E_2^{(1)} = -\frac{Ve^2}{N} \int\limits_{|\mathbf{p}_1|<p_0} \frac{d^3\mathbf{p}_1}{(2\pi\hbar)^3} \int\limits_{|\mathbf{p}_2|<p_0} \frac{d^3\mathbf{p}_2}{(2\pi\hbar)^3} \frac{4\pi\hbar^2}{|\mathbf{p}_1-\mathbf{p}_2|^2} = -\frac{Ve^2p_0^4}{4\pi^3N\hbar^4}. \tag{1.3}$$

The energy (1.2) is due exclusively to the formation of the lattice. Calculation shows that this energy, at least for the most symmetrical structures, is negative. This means that the lattice is certainly produced.

The energy $E_1^{(1)}$, taken with the minus sign, determines the binding energy of the lattice. It is interesting to note that it contains Z as a factor. This means that all elements have perfectly identical lattices at sufficiently large pressures. The binding energy of such a lattice should be maximum.

For practical calculation of the binding energy, it is most convenient to start with the Fourier transformation. This yields

$$-E_1^{(1)} = \frac{4\pi Z^2e^2}{2} \lim_{P\to\infty} \Bigg(\int\limits_{|\mathbf{k}|<P} \frac{d^3\mathbf{k}}{(2\pi)^3} \frac{1}{\mathbf{k}^2} - \frac{N}{V} \sum_{0<|\mathbf{K}|<P} \frac{1}{\mathbf{K}^2} \Bigg), \tag{1.4}$$

where the sum is taken over the non-vanishing reciprocal-lattice vectors. This expression converges more rapidly than (1.2).

The lattice with the greatest binding energy should, in all probability, be among one of the most symmetrical types, cubic volume-centered, cubic-face-centered, or hexagonal of the "close-packed" type. In the latter case the ratio of the fundamental period along the hexagonal axis to the perpendicular one is not governed by symmetry considerations, and should be obtained from the maximum binding energy condition. Unfortunately, the energies of different lattices can be calculated only with limited accuracy, and since the difference between them amounts to merely several percent, the question of the choice of the most stable lattice remains unsolved. We shall consider henceforth only cubic lattices. In the case, however, when accurate calculation leads to preference of the hexagonal configuration, suitable changes can be readily made in the results that follow.

Expressing the exchange energy (1.3) in atomic units, and adding it to the binding energy (1.4), we obtain

$$E^{(1)} = -v^{-1/3}(0.74\, Z^{4/3} + 1.3\, Z^2). \tag{1.5}$$

Comparing (1.5) with (1.1) we can obtain a more accurate criterion for the applicability of the expansion in powers of $v^{1/3}$, namely

$$v^{1/3} \ll 2Z^{-1/3}. \tag{1.6}$$

According to (1.1), this corresponds to pressures greater than 10^8 atm. We give here a criterion for the applicability of the nonrelativistic approximation. From the condition* $p_0/m \ll c$ we get

$$v^{1/3} \gg 0.02\, Z^{1/3}. \tag{1.7}$$

2. ELASTIC MODULI

Going over to a study of the elastic moduli, we note first the appreciable difference between the bulk compressibility and the shear moduli. The compressibility is determined essentially by the electrons, the kinetic energy of which makes the main contribution to the total energy. The shear moduli, on the other hand, are determined by the Coulomb interaction of the nuclei, i.e., they are of the order $v^{1/3}$ relative to the bulk compressibility.

Differentiating twice with respect to the volume the expressions for the kinetic energy of the electrons, we obtain the bulk compressibility

$$K = V\frac{\partial^2 E}{\partial V^2} = \frac{\pi^{4/3}\hbar^2}{3^{1/3}m}\left(\frac{ZN}{V}\right)^{5/3}. \tag{2.1}$$

To calculate the shear moduli let us consider the change in the lattice energy accompanying small atomic displacements that are almost homogeneous in space $(a\,|\partial \mathbf{u}/\partial x| \ll |\mathbf{u}| \ll a$, $\mathbf{u}$ is the displacement of the atom and a is the lattice period). During the course of the calculation we assume the displacements to be purely in shear, i.e., we put $\operatorname{div}\mathbf{u} = 0$. The potential energy of the lattice ions

$$\frac{Z^2e^2}{2}\sum_{i\neq k}\frac{1}{|\mathbf{R}_i-\mathbf{R}_k|} - Z^2e^2\frac{N}{V}\int dV \sum_{\mathbf{R}_i}\frac{1}{|\mathbf{r}-\mathbf{R}_i|},$$

expanded in powers of the small ion displacements, is of the form

$$\frac{Z^2e^2}{4}\sum_{i\neq k}\left[\frac{3(\mathbf{R}_{ik}(\mathbf{u}_i-\mathbf{u}_k))^2}{R_{ik}^5} - \frac{(\mathbf{u}_i-\mathbf{u}_k)^2}{R_{ik}^3}\right]. \tag{2.2}$$

In spite of the fact that the displacements of the neighboring atoms differ little from each other, we cannot make in this expression a substitution of the form $u_i - u_k \to R_{ik,\alpha}\,\partial u/\partial x_\alpha$, for in this case we obtain divergent sums over R_{ik}. It is easy to show, however, that the divergence of these sums can be eliminated by subtracting the terms containing $\operatorname{div}\mathbf{u}$, i.e., the terms that vanish in accordance with our assumption. Let us consider the expression

---

*The condition that the relativistic correction be small is of the form $v^{2/3} \gg 10^{-4}Z^{2/3}$ for the energy and $v^{2/3} \gg 2\times10^{-4}Z^{2/3}$ for the pressure.

$$-\frac{Z^2e^2}{2}\left(\frac{N}{V}\right)^2\int dV\,dV'\,\frac{\operatorname{div}\mathbf{u}(\mathbf{r})\operatorname{div}\mathbf{u}(\mathbf{r}')}{|\mathbf{r}-\mathbf{r}'|}. \qquad (2.3)$$

Integrating twice by parts and discarding the surface integral, which is of no interest, we get

$$\frac{Z^2e^2}{2}\left(\frac{N}{V}\right)^2\int dV\,dV'\,u_\alpha(\mathbf{r})\,u_\beta(\mathbf{r}')\left[\frac{\delta_{\alpha\beta}}{|\mathbf{r}-\mathbf{r}'|^3}\right.$$
$$\left.-\frac{3(\mathbf{r}-\mathbf{r}')_\alpha(\mathbf{r}-\mathbf{r}')_\beta}{|\mathbf{r}-\mathbf{r}'|^5}\right]$$
$$=\frac{Z^2e^2}{4}\left(\frac{N}{V}\right)\int dV\,dV'\left[\frac{3(\mathbf{u}(\mathbf{r})-\mathbf{u}(\mathbf{r}'),\ \mathbf{r}-\mathbf{r}')^2}{|\mathbf{r}-\mathbf{r}'|^5}\right.$$
$$\left.-\frac{(\mathbf{u}(\mathbf{r})-\mathbf{u}(\mathbf{r}'))^2}{|\mathbf{r}-\mathbf{r}'|^3}\right].$$

After subtracting this expression from (2.2) we can now make the substitution

$$u_\alpha(\mathbf{R}_i)-u_\alpha(\mathbf{R}_k)=R_\beta\partial u_\alpha/\partial x_\beta,$$

where $R_\beta = R_{ik\,\beta}$, and go from summation over $i \neq k$ in (2.2) to integration over dV and summation over R. The value of the energy is found to be (in the case of one of the cubic lattices)

$$\frac{Z^2e^2}{4}\,\frac{N}{V}\left[3\int dV\,\frac{\partial u_\alpha}{\partial x_\beta}\,\frac{\partial u_\gamma}{\partial x_\delta}\left(\sum_R\frac{R_\alpha R_\beta R_\gamma R_\delta}{R^5}-\frac{N}{V}\int\frac{r_\alpha r_\beta r_\gamma r_\delta}{r^5}\,dV\right)\right.$$
$$\left.-\frac{1}{3}\int dV\left(\frac{\partial u_\alpha}{\partial x_\beta}\right)^2\left(\sum_R\frac{1}{R}-\frac{N}{V}\int\frac{dV}{r}\right)\right].$$

For the sake of symmetry, we add to the integral $\int dV(\partial u_\alpha/\partial x_\beta)^2$ the expression $\int(\partial u_\alpha/\partial x_\beta)(\partial u_\beta/\partial x_\alpha)\,dV$, which, accurate to a surface integral, is equal to $\int(\operatorname{div}\mathbf{u})^2dV = 0$. The energy will then contain only the combination $u_{\alpha\beta} = \frac{1}{2}(\partial u_\alpha/\partial x_\beta + \partial u_\beta/\partial x_\alpha)$. Writing this in the form $\lambda'_{\alpha\beta\gamma\delta}u_{\alpha\beta}u_{\gamma\delta}$, we obtain

$$\lambda'_{\alpha\beta\gamma\delta}=\frac{Z^2e^2}{4}\,\frac{N}{V}\left[3\left(\sum_{\mathbf{R}}\frac{R_\alpha R_\beta R_\gamma R_\delta}{R^5}-\frac{N}{V}\int\frac{r_\alpha r_\beta r_\gamma r_\delta}{r^5}\,dV\right)\right.$$
$$\left.-\frac{1}{3}(\delta_{\alpha\gamma}\delta_{\beta\delta}+\delta_{\alpha\delta}\delta_{\beta\gamma})\left(\sum_{\mathbf{R}}\frac{1}{R}-\frac{N}{V}\int\frac{dV}{r}\right)\right]. \qquad (2.4)$$

Finally, it is necessary to discard the "longitudinal" part in the tensor $\lambda'_{\alpha\beta\gamma\delta}$. For this we break it up into parts

$$\lambda'_{\alpha\beta\gamma\delta}=\Lambda\delta_{\alpha\beta}\delta_{\gamma\delta}+\lambda_{\alpha\beta\gamma\delta},$$

where $\lambda_{\alpha\alpha\gamma\delta} = 0$.

The "transverse" tensor $\lambda_{\alpha\beta\gamma\delta}$ differs from the expression written above for $\lambda'_{\alpha\beta\gamma\delta}$ in that the bracket with the δ symbols contains also the term $\frac{1}{3}\delta_{\alpha\beta}\delta_{\gamma\delta}$. The expression for the "transverse" part of the density of potential energy of the ions then assumes the form

$$4\lambda_{xyxy}(u_{xy}^2+u_{xz}^2+u_{yz}^2)+\lambda_{xxxx}(u_{xx}^2+u_{yy}^2+u_{zz}^2$$
$$-u_{xx}u_{yy}-u_{yy}u_{zz}-u_{zz}u_{xx}). \qquad (2.5)$$

Making the Fourier transformation, we obtain for the shear moduli the expression

$$\lambda_{xxxx}=8\pi Z^2e^2\,\frac{N}{V}\lim_{P\to\infty}\left[\frac{1}{45}\int\limits_{|\mathbf{k}|<P}\frac{d^3\mathbf{k}}{\mathbf{k}^2}\right.$$
$$\left.-\frac{N}{V}\sum_{0<|\mathbf{K}|<P}\left(\frac{2}{9\mathbf{K}^2}-\frac{K_x^4}{\mathbf{K}^6}\right)\right],$$
$$\lambda_{xyxy}=4\pi Z^2e^2\,\frac{N}{V}\lim_{P\to\infty}\left[\frac{1}{30}\int\frac{d^3k}{\mathbf{k}^2}\right.$$
$$\left.-\frac{N}{V}\sum_{0<|\mathbf{K}|<P}{}'\left(\frac{K_x^4}{\mathbf{K}^6}-\frac{1}{6\mathbf{K}^2}\right)\right], \qquad (2.6)$$

where the sums are again taken over the reciprocal-lattice vectors.

The coefficients λ are approximately the same for a body-centered and face-centered cubic lattice, equal to

$$\lambda_{xxxx}\approx 0, \qquad \lambda_{xyxy}\approx 0.16\,Z^2e^2(N/V)^{4/3}. \qquad (2.7)$$

As to the coefficient λ_{xxxx}, we can merely state that it does not exceed $0.1\,\lambda_{xyxy}$. The low computation accuracy does not allow us to make a more rigorous estimate.

3. SPECTRUM OF OSCILLATIONS

The great difference between the modulus of compression and the shear moduli brings about very curious features in the oscillation spectrum. It is readily understood that one of the branches of the spectrum in the vicinity of long waves, $\lambda \gg a$, will correspond to oscillations with almost completely longitudinal polarization (the deviation from longitudinal is of higher order in $v^{1/3}$). By virtue of the orthogonality of the natural oscillations, the remaining two branches will be almost completely transverse. The corresponding velocities of sound are determined by shear moduli and, consequently, are much smaller than the velocity of propagation of the longitudinal oscillations, which is determined by the compressibility.

Let us proceed now to a more detailed analysis of the spectrum. The rate of propagation of longitudinal sound is obtained from formula (2.1)

$$c_l=\sqrt{\frac{K}{M}}=\frac{\pi^{2/3}Z^{5/6}(N/V)^{1/3}}{3^{1/6}(mM)^{1/2}}. \qquad (3.1)$$

It is easy to see, however, that the linear dispersion law $\omega_l = c_l k$ is true only for the longest waves, namely when $\lambda \gg \rho_D$, where ρ_D is the Debye radius. In the case when $\lambda \leq \rho_D$, the change in the electron density begins to lag the change in the ion density; the frequency of the oscillations begins to determine more and more by the Coulomb interaction of the ions, and thus, dispersion of the longitudinal oscillations sets in.

To determine the complete dependence $\omega_l(\mathbf{k})$ for the case $\lambda \gg a$ we can proceed as follows.

Taking it into consideration that $\omega_l \gg \omega_t$, we can, in first approximation, disregard the shear moduli completely. This means that only longitudinal oscillations remain, i.e., oscillations connected with the change in the charge density. We can therefore, in the same approximation, replace the forces acting on a given ion displaced from equilibrium by a certain effective electric field. In view of the fact that the matter is electrically neutral in the absence of oscillations, the potential of the electric field φ satisfies the equation

$$\Delta\varphi = -4\pi(\delta\rho_e + \delta\rho_i).$$

The change in the electron charge density, obtained by applying the Debye theory to the Fermi gas (see reference 5), has the form

$$\delta\rho_e = -e^2\varphi \frac{\partial(N_e V)}{\partial\mu} = -\frac{e^2}{\pi^2} p_0 m\varphi.$$

The change in the charge density of the ions is

$$\delta\rho_i = -ZeV^{-1}N \operatorname{div} \mathbf{u}(\mathbf{r}).$$

Thus we have

$$\Delta\varphi - \varkappa^2\varphi = 4\pi ZeV^{-1}N \operatorname{div} \mathbf{u}(\mathbf{r}), \tag{3.2}$$

where $\kappa = 1/\rho_D = \sqrt{4e^2 p_0 m/\pi}$.

The equation for the ion oscillations will be

$$M\frac{N}{V}\frac{\partial^2\mathbf{u}}{\partial t^2} = -Ze\frac{N}{V}\nabla\varphi. \tag{3.3}$$

Assuming that φ and $\mathbf{u}$ depend on the coordinates and on the time as $\exp\{i(\mathbf{k}\cdot\mathbf{r} - \omega t)\}$, we obtain

$$\omega_l = \left(\frac{4\pi Z^2e^2N}{MV}\,\frac{k^2}{k^2+\varkappa^2}\right)^{1/2}. \tag{3.4}$$

When $k \ll \kappa$ the expression (3.4) becomes $\omega_l = c_l k$, and when $k \gg \kappa$, ω_l tends to the constant limit

$$\omega_0 = (4\pi Z^2e^2N/MV)^{1/2}. \tag{3.5}$$

The remaining (transverse) branches of the vibrational spectrum do not experience dispersion when $k \sim 1/\rho_D$. This follows at least from the fact that the differences between the sums and the integrals in Eq. (2.4) for the shear moduli converge over distances on the order of the lattice period and are not affected by the Debye screening. The transverse oscillations have a linear dispersion law $\omega_{1,2} = c_{t\,1,2}k$. The velocities of sound $c_{t\,1,2}$ can be determined from the shear moduli (2.7) (see reference 6). Obviously, $c_t \sim (V\lambda/NM)^{1/2} \sim (Zv)^{1/6}c_l$.

In the region of short waves, i.e., when k approaches values on the order of π/a, where a is the lattice constant, all the frequencies are of the order of ω_0 (3.5). Therefore the foregoing method of calculation, which is based on the separation of the longitudinal and transverse oscillations, can no longer be used here. To obtain the oscillation spectrum in this case it is necessary to solve the general problem, and obviously, except in a few special directions, the oscillations will in general be neither purely longitudinal nor transverse.

4. POSSIBILITY OF DESTRUCTION OF THE LATTICE AT HIGH COMPRESSION

The type of lattice-vibration spectrum obtained in the preceding section leads to an interesting consequence. Let us estimate the zero-point oscillation energy

$$E_v = \frac{\hbar}{2N}\sum_{\mathbf{k},\,s}\omega(\mathbf{k},\ s), \tag{4.1}$$

where $S = 1, 2, 3$ denotes the numbers of the natural oscillations, while the summation over $\mathbf{k}$ is confined to the unit cell of the reciprocal lattice. It is easy to see that the values of $|\mathbf{k}|$ of order of the upper limit, i.e., of order π/a, are significant in the integral with respect to $\mathbf{k}$. Here we obtain (in atomic units)

$$E_v \sim Z\sqrt{m/M}\,v^{-1/2}. \tag{4.2}$$

Comparing this with (1.5) we note that at sufficiently small volumes the positive zero-point oscillation energy exceeds the negative Coulomb energy, and this leads to a destruction of the crystal lattice.

It is of interest to determine the transition point more accurately. This is difficult because of the complications involved in the accurate calculation of the spectrum, and we shall use the following estimate. We know that there exist in nature two transitions from a solid to a liquid state under the influence of the zero-point oscillations. These are the transitions of the helium isotopes He^4 and He^3. One can assume that in transitions of this type the amplitude of the zero-point oscillations is always a fixed portion of the interatomic distance $a_V = Qa$. We know that $a_V = \sqrt{\hbar/M\omega}$. Since the values of the wave vector near the upper limit are significant in this case, the frequency will be of order c/a, where the "velocity of sound" c is chosen to be the combination $c = c_t(1 + c_t/2c_l)^{-1}$. Regarding the constant Q as universal, we obtain the conditions

$$Aca = \text{const} = (Aca)_{He^4},$$

where A is the atomic weight.

The elastic moduli of solid helium are unknown. We therefore make use of the fact that for most solids the Poisson coefficient σ is close to 0.35. This enables us to express c_{He^4} in terms of the compressibility. For lack of other data, we use the value 4×10^{-3} atm^{-1} (reference 7), obtained by taking the derivative along the melting curve in the vicinity of 30 atm. This is apparently justified because, in any case for liquid helium, the temperature expansion in the low-temperature region is practically zero. Thus, we obtain $c \approx 170$ m/sec. Putting $a_{He^4} = 3 \times 10^8$ (see reference 7), we get

$$Aca = 2 \cdot 10^{-3}. \tag{4.3}$$

For a strongly compressed lattice, $c \approx c_t$. But since the velocity c_t is highly anisotropic, we take for c a certain average, which can be calculated from the longitudinal velocity of sound, but only with the "lattice" part $-1.3\, Z^2 v^{-1/3}$ of the energy $E^{(1)}$ [see (1.5)]. Thus, we get

$$c \approx 0{,}76 \frac{Ze}{\sqrt{M}} \left(\frac{N}{V}\right)^{1/6}.$$

From this we obtain with the aid of (4.3)

$$a \sim 5 \cdot 10^{-11}/Z^2 A \text{ cm}. \tag{4.4}$$

The corresponding expression for the specific volume assumes the following form in atomic units

$$v \sim 10^{-6} Z^{-6} A^{-3}. \tag{4.5}$$

Comparison of (4.4) and (1.7) shows that at so strong a compression the relativistic effects in the motion of electrons become appreciable. This leads to no changes whatever in formula (4.4), since the zero-point oscillation amplitude is independent of the electron spectrum in the approximation considered here. It is seen from (4.4) that the interatomic distances at the transition point are greater than the nuclear dimensions only for the lightest elements, hydrogen and helium. Thus, such a transition can take place only in these two elements.

5. SECOND-ORDER CORRECTIONS TO THE GROUND-STATE ENERGY

Gell-Mann and Brueckner[1] determined the corrections, of zero degree (in v), to the ground-state energy, for a model with a diffuse positive ion charge. As we have seen earlier, the presence of an ion lattice leads to additional energy terms. In first order, this is the ion binding energy (we assume the zero-point oscillation energy to be small). We now consider the additions introduced by the ion lattice to the terms of zero degree in the volume.

For this purpose we must determine the energy of interaction between the electrons and the ions in the second order of perturbation theory or, in other words, the electron-correlation energy. Considering that the matrix element of the interaction energy of a given electron with all the ions is of the form

$$(V_{ei})_{\mathbf{p}+\hbar\mathbf{q}/2,\ \mathbf{p}-\hbar\mathbf{q}/2} = -Ze^2 \frac{4\pi}{\mathbf{q}^2} \frac{N}{V} \sum_{\mathbf{K}} \delta_{\mathbf{q},\mathbf{K}}, \tag{5.1}$$

where $\mathbf{K}$ is the reciprocal lattice vector, we obtain the energy per atom

$$E_{ei}^{(2)} = 2\,(4\pi)^2 Z^2 e^4 \frac{N}{V} \sum_{|\mathbf{K}|>0} \frac{1}{K^4} \int \frac{d^3\mathbf{p}}{(2\pi\hbar)^3} \frac{2m}{\left(\mathbf{p} - \frac{\hbar\mathbf{K}}{2}\right)^2 - \left(p + \frac{\hbar\mathbf{K}}{2}\right)^2}, \tag{5.2}$$

where the summation is over all the vectors of the reciprocal lattice, and the integration is over the domain

$$|\mathbf{p} - \hbar\mathbf{K}/2| < p_0, \qquad |\mathbf{p} + \hbar\mathbf{K}/2| > p_0.$$

Let us call attention to the fact that the expression is not divergent, unlike the term due to the electron-electron correlation,[1] and therefore needs no correction by allowance for the next approximations.

Carrying out the integration over $d^3\mathbf{p}$ and going to atomic units, we obtain (for cubic lattices)

$$E_{ei}^{(2)} = -\frac{Z^2 \nu}{\pi^3} \sum_{|\mathbf{q}|>0} \frac{1}{q^5} \left(\frac{4\alpha^2 - q^2}{4} \ln \left| \frac{2\alpha + q}{2\alpha - q} \right| + q\alpha \right), \tag{5.3}$$

where q is the modulus of the reciprocal-lattice vector in units $2\pi/a$, a is the edge of the cube, $\nu = a^3/v$, i.e., $\nu = 1$, 2, and 4 for the primitive, body-centered, and face-centered lattice, respectively, and $\alpha = (2\pi)^{-1} (3\pi^2 Z \nu)^{1/3}$.

The limiting values of (5.3) for large and small α are

$$E_{ei}^{(2)} = \begin{cases} -\nu^2 Z^3 \pi^{-4} \sum\limits_{|\mathbf{q}|>0} q^{-6} \approx -0{,}073\, Z^3, & \alpha \ll 1 \\ -3^{1/3} \nu^{4/3} Z^{7/3} \pi^{-10/3} \sum\limits_{|\mathbf{q}|>0} q^{-4} \approx -0{,}4\, Z^{7/3}, & \alpha \gg 1. \end{cases} \tag{5.4}$$

The case $\alpha \ll 1$, naturally, is not realized; we give here the corresponding formula only to explain the character of the function. The numerical values pertain to the body-centered and face-centered cubic lattices.

The energy of the electron-electron correlation is in this case the same as in the model with the diffuse positive charge. The value obtained by Gell-Mann and Brueckner[1] can be written in the form

$$E_{ee}^{(2)} = Z\,[0{,}0104 \ln (v/Z) - 0{,}1108]. \tag{5.5}$$

Expressions (5.4) and (5.5) yield all the energy corrections of order v^0.

As noted earlier, the calculation of the zero-point oscillation energy is difficult. It is therefore natural to inquire under what conditions will not only $E^{(1)}$ but also $E^{(2)}$ be greater than the zero-point oscillation energy. A comparison of (5.4) and (4.2) shows that this will take place when

$$v \gg m/MZ^{8/3}.$$

We see that under these conditions the parameter of the energy expansion, $v^{1/3}$, still remains small.

In conclusion I take this opportunity to thank Academician L. D. Landau for a discussion of the work.

---

[1] M. Gell-Mann and K. A. Brueckner, Phys. Rev. **106**, 364 (1957).

[2] K. Savada, Phys. Rev. **106**, 372 (1957).

[3] M. Gell-Mann, Phys. Rev. **106**, 369 (1957).

[4] A. A. Abrikosov, Астрономический журнал (Astronomy Journal) **31**, 112 (1954).

[5] L. D. Landau and E. M. Lifshitz, Статистическая физика (Statistical Physics), Gostekhizdat, 1951, p. 249.

[6] L. D. Landau and E. M. Lifshitz, Механика сплошных сред (Mechanics of Continuous Media), Gostekhizdat, 1953, p. 743.

[7] W. Keesom, Helium, Elsevier, Amsterdam, 1942.

Translated by J. G. Adashko
326

SOVIET PHYSICS JETP VOLUME 12, NUMBER 6 JUNE, 1961

THE ANGULAR DISTRIBUTION AND POLARIZATION OF THE NEUTRONS THAT ARE EMITTED IN μ CAPTURE IN CERTAIN LIGHT NUCLEI

M. K. AKIMOVA, L. D. BLOKHINTSEV, and É. I. DOLINSKIĬ

Institute of Nuclear Physics, Moscow State University

Submitted to JETP editor July 29, 1960

J. Exptl. Theoret. Phys. (U.S.S.R.) **39**, 1806-1817 (December, 1960)

The energy spectra, angular distributions, and polarizations are calculated for the neutrons produced in the direct process of μ capture in the nuclei C^{12}, Ne^{20}, Si^{28}, and S^{32}. The calculations are made on the basis of an effective Hamiltonian for μ capture that takes into account first-order (v/c) effects for the nucleons, including "weak magnetism" and the effective pseudoscalar interaction. The state of the protons in the nucleus is described by the nuclear shell model with jj coupling; the interaction of the emerging neutron with the nucleus is taken into account by the use of the optical model. The results are compared with the experimental data.

THE study of the angular distribution and polarization of the neutrons emitted from nuclei in the μ capture reaction process $\mu^- + P \rightarrow N + \nu$ is one possible way of establishing the type of coupling and the magnitude of the constant for the weak interaction between μ mesons and nucleons.[1,2] Formulas for the angular distribution and polarization of the neutrons, calculated in nonrelativistic approximation for the Fermi and Gamow-Teller types of interaction and in first approximation in v_N/c (v_N is the speed of the nucleons) for the pseudoscalar type of four-fermion interaction, have been published in earlier papers.[3,4] The formulas were obtained by using the nuclear shell model with jj coupling to describe the protons bound in the nucleus and the optical model to take into account the interaction between the emerging neutron and the nucleus. These papers[3,4] also give the results of numerical calculations for μ capture in the nuclei O^{16} and Ca^{40}.

1. BASIC ASSUMPTIONS AND FORMULAS

In the present paper we shall take as the basis for the calculations the assumption of the theory of the universal Fermi interaction, that the interaction of "bare" fermions is described by the V and A types of four-fermion coupling.[5,6] Starting from this assumption and including all relativistic terms of first order in v_N/c, we have the following expression for the effective Hamiltonian H_{eff} that describes the process of μ capture[7] ($\hbar = c = 1$):

$$H_{\mathbf{eff}} = \frac{1}{2}(1-\boldsymbol{\sigma}\boldsymbol{\nu})\sum_{i=1}^{A}\tau_i^{(-)}\Big[g_V^{(\mu)}\Big(1+\frac{E_\nu}{2M}\Big) + \Big(g_A^{(\mu)} - g_V^{(\mu)}\mu\frac{E_\nu}{2M}\Big)\boldsymbol{\sigma}\boldsymbol{\sigma}_i + (g_P^{(\mu)} - g_A^{(\mu)} - g_V^{(\mu)}\mu)\frac{E_\nu}{2M}\boldsymbol{\sigma}_i\boldsymbol{\nu} + g_V^{(\mu)}\frac{\boldsymbol{\sigma}\hat{\mathbf{p}}_i}{M} + g_A^{(\mu)}\frac{\boldsymbol{\sigma}_i\hat{\mathbf{p}}_i}{M}\Big]\delta(\mathbf{r}-\mathbf{r}_i). \qquad (1)$$

In Eq. (1) we have used the following notation: operators that have the index i act on nucleons, and those without the index i on leptons; $\tau_i^{(-)}$ is the well known isotopic operator; $\boldsymbol{\sigma}$ and $\boldsymbol{\sigma}_i$ are Pauli matrices; $\boldsymbol{\nu}$ is the unit vector in the direction of emission of the neutrino, and E_ν is the energy of the neutrino; M is the mass of the nucleon, and $\hat{\mathbf{p}}_i = -i\hbar\nabla_i$ is the momentum operator of the i-th nucleon; $g_V^{(\mu)}$ and $g_A^{(\mu)}$ are the coupling constants of the vector and axial-vector interactions for μ capture, and $g_P^{(\mu)}$ is the effective coupling constant for the pseudoscalar interaction caused by the presence of virtual π mesons.

It is assumed that the neutrino emitted in μ capture is polarized antiparallel to its direction of motion.

In the theory of the universal Fermi interaction with conserved vector current[5,8] we have the following estimates[7] for the quantities $g_V^{(\mu)}$ and μ:

$$g_V^{(\mu)} = 0{,}972\ g_V^{(\beta)}, \qquad \mu = 1 + \mu_P - \mu_N = 4.71, \qquad (2)$$

where $g_V^{(\mu)}$ is the Fermi coupling constant for the β decay of nucleons, and μ_P and μ_N are the anomalous magnetic moments of proton and neutron in units of the nuclear magneton. For the quantities $g_A^{(\mu)}$ and $g_P^{(\mu)}$ we have the relations[9]

$$g_A^{(\mu)} = 0.999\ g_A^{(\beta)}, \qquad g_P^{(\mu)} = 8 g_A^{(\beta)}, \tag{3}$$

where $g_A^{(\beta)}$ is the Gamow-Teller coupling constant for the β decay of nucleons.

The formulas given below do not include contributions from the last two terms in the effective Hamiltonian, which contain derivatives of the nucleon wave functions. It is obvious that the order of magnitude of the matrix elements of the operators $\hat{p}_i/Mc$ is $\hbar/McR$, where R is the radius of the nucleus, so that for the nuclei considered here ($R \sim 4 \times 10^{-13}$ cm) the omitted contributions amount to about 5 percent. There are contributions of this same order of magnitude from the other relativistic corrections to the nonrelativistic matrix elements for the vector and axial-vector interactions that remain in Eq. (1) if we set $g_P^{(\mu)} = 0$ and $\mu = 1$.

Numerical estimates show, however, that relativistic corrections of this kind change the values of the μ-capture probability and the asymmetry coefficient in the angular distribution of the neutrons calculated in the nonrelativistic approximation by not more than 10 percent, and have practically no effect on the value of the longitudinal polarization of the neutrons. At the same time, as will be seen later, the expected large values of $g_P^{(\mu)}$ and μ have the result that the relativistic terms proportional to $g_P^{(\mu)}E_\nu/2M$ and $\mu E_\nu/2M$ decidedly alter the value of the asymmetry coefficient in the angular distribution of the neutrons. Therefore it can be expected that omission from Eq. (1) of the terms that contain derivatives of nucleon wave functions will lead to errors that do not exceed a few percent.

Using the Hamiltonian (1) and Eq. (9) of reference 3, we get the following expression for the probability of emission of a neutron from the nucleus with kinetic energy in the interval (E_N, $E_N + dE_N$) and direction in the solid angle $d\Omega_N$ at the angle θ with the direction of polarization of the μ^- meson:

$$dW(E_N, \theta) = G^{(\mu)2} W_0(E_N)\, [I(E_N) + P_\mu K_1(E_N)\cos\theta]\, dE_N d\Omega_N/4\pi, \tag{4}$$

$$I(E_N) = (1 + 3\lambda^2) + 2[1 + 2\lambda\mu - \lambda^2(\varkappa - 1)]\,\gamma_1(E_N) + [2\mu^2 + \lambda^2(\varkappa - 1)^2 + 1]\,\gamma_2(E_N), \tag{5}$$

$$K_1(E_N) = -\{(-1 + \lambda^2)\,\beta_0(E_N) + 2[-1 + 2\lambda\mu + \lambda^2(\varkappa - 1)]\,\beta_1(E_N)\gamma_1(E_N) + [2\mu^2 - \lambda^2(\varkappa - 1)^2 - 1]\,\beta_2(E_N)\gamma_2(E_N)\}, \tag{6}$$

where

$$G^{(\mu)} = g_V^{(\mu)} \cdot 10^{49}\ \mathrm{erg}^{-1}\ \mathrm{cm}^{-3},$$

$$\lambda = -g_A^{(\mu)}/g_V^{(\mu)}, \qquad \varkappa = g_P^{(\mu)}/g_A^{(\mu)},$$

and P_μ is the degree of polarization of the μ^- meson in the K orbit of the mesic atom at the instant of capture. The kinetic energy of the neutron is measured in megavolts. Here and in what follows, notations not defined are the same as those used in reference 3.

We recall (for details see reference 3) that all the formulas considered in the present paper are for neutrons from the direct process, which are emitted from the nucleus immediately after the absorption of the μ^- meson, and thus with omission of the stage of the compound nucleus. In Eq. (4) and the formulas given later for the angular distribution and polarization of the neutrons no account is taken of effects of the hyperfine structure of the mesic atomic levels, which should be taken into account in the treatment of μ capture in a nucleus with a nonzero spin that is due in any part to protons (for details see references 3, 10, and 11).

Using Eq. (4), we can write the angular distribution of the neutrons emitted from the nucleus in the capture of polarized μ^- mesons in the following form:

$$q(E_N, \theta) = 1 + P_\mu \alpha_1(E_N)\cos\theta, \tag{7}$$

$$\alpha_1(E_N) = K_1(E_N)/I(E_N). \tag{8}$$

Recalling the results of a previous paper by one of the writers[4] [Eq. (6c)], we get the following expression for the longitudinal polarization of the neutrons emitted on the absorption of unpolarized μ^- mesons:

$$P_N^{\parallel}(E_N) = L_1(E_N)/I(E_N), \tag{9}$$

$$L_1(E_N) = -2\{\lambda(\lambda + 1)\,\beta_0(E_N) + \lambda[2(\mu + 1) - \varkappa]\,\beta_1(E_N)\gamma_1(E_N) + [\mu^2 - \lambda(\varkappa - 1)]\,\beta_2(E_N)\gamma_2(E_N)\}. \tag{10}$$

Equation (9) also describes the longitudinal polarization of the neutrons emitted at an angle $\theta = \pm\pi/2$ in the capture of polarized μ^- mesons.

Equations (4), (7), and (9) are for neutrons with the fixed energy E_N. If we integrate over the neutron energy E_N, we get formulas of entirely analogous forms with the functions $W_0(E_N)$, $\beta(E_N)$, and $\gamma_k(E_N)$ replaced by the corresponding constants $\widetilde{W}_0$, $\widetilde{\beta}_k$, and $\widetilde{\gamma}_k$.

2. NUMERICAL CALCULATIONS

The numerical calculation of the coefficients W_0, β_k, γ_k that appear in Eqs. (4), (7), and (9)

TABLE I

Nucleus	$10^{13}r_0$, cm	U_N, Mev	U_P, Mev	Energy levels of protons in nucleus, Mev				α
				1s	1p	1d	2s	
C^{12}	1.45	42	40.7	28.4	16.0*	—	—	0.0777
Ne^{20}	1.45	42	49.6	39.9	30.0	—	12.70*	0.154
Si^{28}	1.45	42	36,6	28.9	21.2	11.56*	—	0.240
S^{32}	1.45	42	35.7	28.7	21,4	12.5	8,85*	0,287

*Data on energy of removal of protons taken from reference 12.

TABLE II

Nucleus	ζ	$10^3\widetilde{W}_0$, sec^{-1}	$\widetilde{\beta}^0$	$10\widetilde{\gamma}_1$	$10^2\widetilde{\gamma}_2$	Ratios of probabilities of μ capture in the individual shells				Ratios of specific probabilities (per proton) of μ capture in the individual shells				Total probability of direct process, $10^3\widetilde{W}$ in sec^{-1}	$\widetilde{W}/W_{exp}$, %
						1s	1p	1d	2s	1s	1p	1d	2s		
1	2	3	4	5	6			7				8		9	10
C^{12}	0	4.70	0.174	0.438	0,192	1	20.9	—	—	1	10.5	—	—	5.40	12.3
	−0.10	2,71	0,416	0.434	0.189	1	32,9	—	—	1	16,5	—	—	3.10	7.0
	−0.15	2.35	0,500	0.434	0,189	1	34.4	—	—	1	17.2	—	—	2,69	6,1
Ne^{20}	0	83.9	0.388	0.440	0.195	1	215	—	1200	1	71.7	—	1200	96.3	—
	−0.10	41.0	0.578	0.441	0.196	1	141	—	871	1	47.0	—	871	47.0	—
	−0.15	32,1	0,641	0.441	0.196	1	105	—	673	1	35.0	—	673	36.8	—
Si^{28}	0	187	0.045	0.457	0.209	1	188	1730	—	1	62.7	577	—	214	27.5
	−0.10	45,7	0.366	0.451	0.204	1	111	831	—	1	37.0	277	—	52,6	6.8
	−0,15	37,4	0.441	0.451	0.204	1	78.2	590	—	1	26.1	197	—	43.1	5.5
S^{32}	0	216	0.273	0.463	0.215	1	58,8	890	982	1	19.6	297	982	250	18.0
	−0.10	113	0.515	0.465	0.217	1	58.2	632	961	1	19.4	211	961	130	9.4
	−0.15	93.2	0.590	0.465	0.217	1	50,5	483	752	1	16,8	161	752	108	7.8
Ne^{20}	p. w.	467	0.183	0.355	0.128	1	2.52	—	0,68	1	0.42	—	0.34	526	—

has been carried out on the "Strela" computer of the Moscow State University for the nuclei C^{12}, Ne^{20}, Si^{28}, and S^{32}, on the following assumptions:

1. The state of the protons in the nucleus was described by the nuclear shell model with jj coupling; the spin-orbit splitting of the proton levels was neglected. The potential for the shell model was taken in the form of a rectangular well of radius $R = r_0A^{1/3}$ (A is the mass number).

2. The interaction $V_N(r)$ of the neutron with the nucleus was described by a complex rectangular well

$$V_N(r) = \begin{cases} -U_N(1+i\zeta), & r < R \\ 0, & r > R \end{cases} \qquad (11)$$

with the same radius R as for the protons. The calculations were made for three values of ζ: $\zeta = 0$ (there is no absorption of neutrons in the nucleus), $\zeta = -0.10$, and $\zeta = -0.15$.

Unlike references 3 and 4, the present work takes into account the coordinate dependence of the wave function ψ_μ of the μ^- meson in the K orbit; ψ_μ was taken to be the solution of the Schrödinger equation in the Coulomb field of a point charge Ze:

$$\psi_\mu = \sqrt{\alpha^3/\pi}\,e^{-\alpha r}, \qquad \alpha = Zm_\mu e^2/\hbar^2, \qquad (12)$$

where m_μ is the mass of the μ meson. The parameters used for the proton and neutron potentials, and also the values of α, are shown in Table I.

The results of the calculations are shown in Table II and in Figs. 1 and 2. The quantity $\widetilde{W}_0$ shown in column 3 of Table II is the value obtained by integrating the quantity $W_0(E_N)$ over the energy of the emitted neutron. $W_0(E_N)$ as a function of the kinetic energy E_N of the neutron is shown in Fig. 1, from which we see that $W_0(E_N)$ reaches a maximum at $E_N \sim 5-10$ Mev and decreases sharply for $E_N \gtrsim 20$ Mev. The calculations show that to accuracy $1-3$ percent

$$\gamma_1(E_N) = E_\nu^{\text{out}}/2Mc^2, \qquad \gamma_2(E_N) = [\gamma_1(E_N)]^2,$$

where $E_\nu^{\text{out}} = m_\mu c^2 - \epsilon_p^{\text{out}} - E_N$ is the energy of the neutrino emitted together with a neutron of energy E_N in the absorption of the μ^- meson by a proton of the outer shell of the nucleus, which had a binding energy ϵ_p^{out}.

Since for any reasonable choice of the quantities λ, μ, and κ the terms proportional to $\gamma_1(E_N)$ and $\gamma_2(E_N)$ in the formula for $I(E_N)$, Eq. (5), are small in comparison with the constant term independent of E_N, and furthermore in the energy range $E_N \lesssim 20$ Mev the fractional changes of

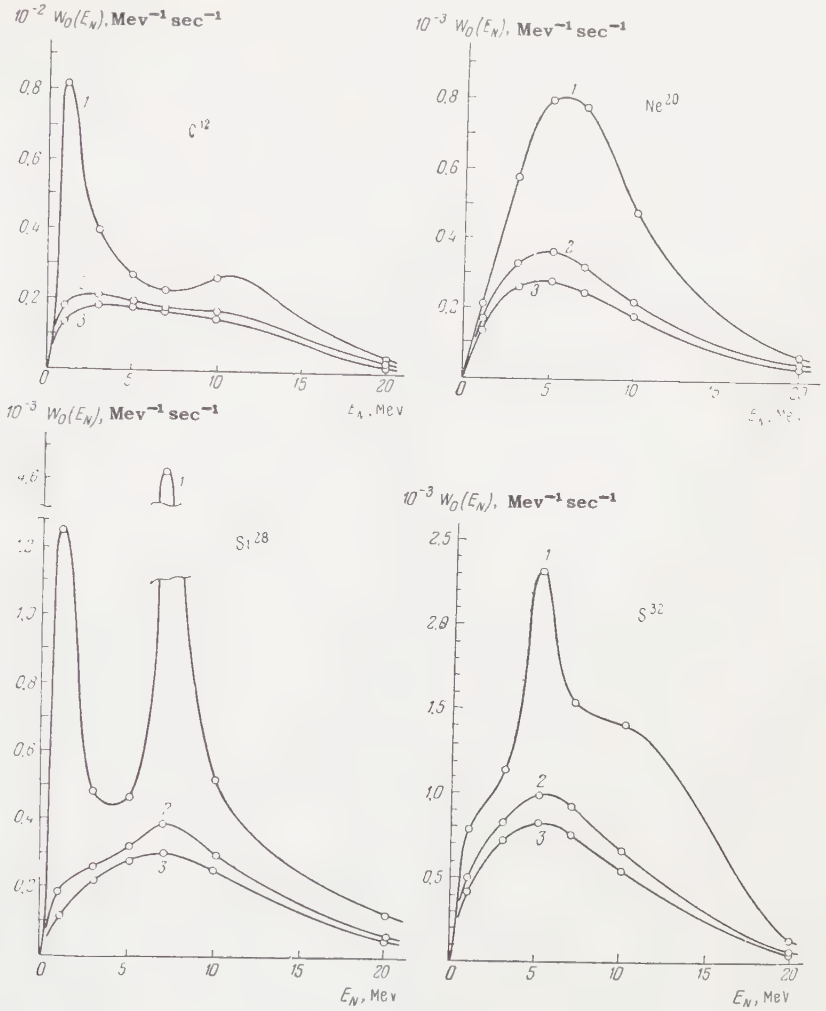

FIG. 1. Dependence of the quantity $W_0(E_N)$ on the neutron energy E_N for the nuclei C^{12}, Ne^{20}, Si^{28}, S^{32}. Curves 1, 2, and 3 are for the respective cases $\zeta = 0$, $\zeta = -0.10$, and $\zeta = -0.15$.

$\gamma_1(E_N)$ and $\gamma_2(E_N)$ do not exceed 20 percent and 40 percent, respectively, the curves for $W_0(E_N)$ describe the shape of the neutron energy spectrum with good accuracy.

It follows from Table II and Fig. 1 that inclusion of the absorption of the neutron in the nucleus ($\zeta \neq 0$) decidedly diminishes the probability of the direct process and smooths out the energy spectrum of the neutrons. The calculations show that the quantities β_1 and β_2 differ from β_0 by not more than 1 — 2 percent. Therefore the functions $K_1(E_N)$ and $L_1(E_N)$ [Eqs. (6) and (10)] can be represented to good accuracy by the formulas

$$K_1(E_N) = \beta_0(E_N) K(E_N), \tag{13}$$

$$L_1(E_N) = \beta_0(E_N) L(E_N), \tag{14}$$

$$K(E_N) = -\{(-1+\lambda^2) + 2[-1+2\lambda\mu+\lambda^2(\varkappa-1)]\gamma_1(E_N) + [2\mu^2-\lambda^2(\varkappa-1)^2-1]\gamma_2(E_N)\}, \tag{15}$$

$$L(E_N) = -2\{\lambda(\lambda+1) + \lambda[2(\mu+1)-\varkappa]\gamma_1(E_N) + [\mu^2-\lambda(\varkappa-1)]\gamma_2(E_N)\}. \tag{16}$$

Thus the formulas for the angular distribution and the longitudinal polarization of the neutrons take the forms

$$q(E_N, \theta) = 1 + P_\mu \beta_0(E_N)\alpha(E_N)\cos\theta, \tag{17}$$

$$P_N^{\parallel}(E_N) = \beta_0(E_N) P^{\parallel}(E_N), \tag{18}$$

$$\alpha(E_N) = K(E_N)/I(E_N), \qquad P^{\parallel}(E_N) = L(E_N)/I(E_N). \tag{19}$$

Equations of analogous forms hold for the quantities averaged over the neutron energy, $\widetilde{q}(\theta)$ and $\widetilde{P}_N^{\parallel}$.

We note that when we make the substitutions $\gamma_1(E_N) \to \gamma_H = 0.053$ and $\gamma_2(E_N) \to \gamma_H^2 = 0.0028$ the quantities $\alpha(E_N)$ and $P^{\parallel}(E_N)$ go over into the angular-asymmetry coefficient α_H and the longitudinal polarization $P_H^{\parallel}$ of the neutrons produced by μ capture in mesic hydrogen, as calculated with neglect of effects of the hyperfine structure of the mesic atom.

The dependences of the quantities $\alpha(E_N)$ and $P^{\parallel}(E_N)$ on E_N are weak,* so that in the neutron energy range $E_N \leq 20$ Mev they can to good accuracy be replaced by their average values $\widetilde{\alpha}$ and $\widetilde{P}^{\parallel}$. The energy dependence of the angular-asym-

---

*For example, for $\lambda = 1.25$, $\mu = 4.71$, $\kappa = 8$ the difference between $\alpha(E_N)$ and $\widetilde{\alpha}$ does not exceed 5 to 10 percent, and $P^{\parallel}(E_N)$ is practically identical with $\widetilde{P}^{\parallel}$.

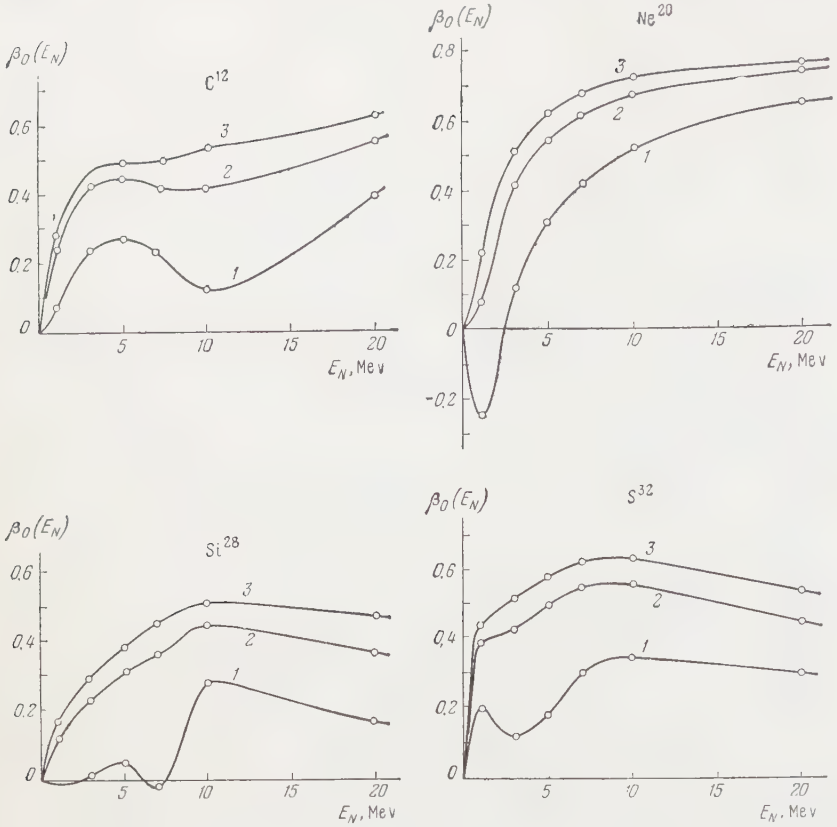

FIG. 2. Dependence of the quantity $\beta_0(E_N)$ on the neutron energy E_N for the nuclei C^{12}, Ne^{20}, Si^{28}, S^{32}. The curves 1, 2, 3 are for the cases $\zeta = 0$, $\zeta = -0.10$, and $\zeta = -0.15$.

metry coefficient and the longitudinal polarization of the neutrons is thus determined by the quantity $\beta_0(E_N)$. As has been shown in reference 13, the quantity $\beta_0(E_N)$, which takes into account the influence of the nucleus on the angular distribution and polarization of the neutrons, has a simple physical meaning, namely

$$\beta_0(E_N) = -\int f(E_N, \vartheta)\cos\vartheta\, d\Omega, \qquad \int f(E_N, \vartheta)\, d\Omega = 1, \tag{20}$$

where $f(E_N, \vartheta)$ is the neutron-neutrino angular correlation function, which depends on the angle ϑ between the directions of emission of the neutron and neutrino and the neutron energy E_N. For μ capture in mesic hydrogen $f = (2\pi)^{-1}\delta(1 + \cos\vartheta)$ and $\beta_0 = 1$; in the case of a nucleus "localized at a point" $f = 1/4\pi$ and $\beta_0 = 0$. For an unlimited nucleus, described by the Fermi-gas model, in virtue of the law of conservation of momentum and the Pauli principle we always have $\cos\vartheta < 0$, and consequently $\beta_0 > 0$. For a real nucleus $0 \le |\beta_0| \le 1$.

For a concrete nucleus the absolute value and sign of β_0 are determined by two factors: the character of the momentum distribution of the protons in the nucleus and the form of the interaction between the emerging neutron and the nucleus. A comparison of the results of calculations made with neglect of the interaction between the neutron and the nucleus (see below) and of calculations with various values of the imaginary part of the optical potential shows that both of these factors are important. Furthermore it follows from an analysis of the results of calculations in the Born approximation for the neutron that proton momentum distributions that fall off monotonically with increasing momentum lead to positive values of $\beta_0(E_N)$, but nonmonotonic distributions can lead to values $\beta_0(E_N) < 0$. The quantities $\tilde{\beta}_0$ and $\beta_0(E_N)$ are shown in column 4 of Table II and in Fig. 2.

Comparing the values of β_0 for different values of the coefficient ζ, we see that inclusion of the absorption of the neutron in the nucleus $(\zeta \neq 0)$ makes a considerable increase in the angular asymmetry and longitudinal polarization of the neutrons. This fact can be explained qualitatively in the following way. Using quasi-classical arguments, we can say that an increase of the imaginary part of the complex potential leads to a relative increase of the probability of emission of a neutron with a large "impact parameter" and to a decrease of the probability for a small "impact parameter." Because of this the contribution from s neutrons, which are always emitted isotropically from the nucleus, is decreased in comparison with the contributions of p, d, ... neutrons, which of course causes an increase of the asymmetry of the angular distribution. From analogous considerations we can also understand the increase of the longitudinal polarization of the neutrons with increase of ξ.

It must be noted that in the optical model for describing the scattering of neutrons the quantity ξ is a function of the neutron energy E_N; according to reference 14, as E_N varies from 3 to 20 Mev the quantity ξ changes from about $+0.05$ to about $+0.20$. Therefore the values $\xi = -(0.10-0.15)$ are reasonable average values in the energy range we are considering.* It can be expected that inclusion of the energy dependence of ξ would not cause much change in the results obtained in this paper, especially since, as can be seen from Table II and Figs. 1 and 2, the results of the calculations for the two different nonvanishing values of ξ are very close together. Clearly more detailed calculations using an energy-dependent parameter ξ would make sense only after the accumulation of sufficient experimental information.

In columns 7 and 8 of Table II we present the ratios of the probabilities for direct emission of neutrons in μ capture from the individual nuclear shells. These results show that it is practically only the outer shells of the nucleus that contribute to the probability of the process in question. The last two columns of Table II give the total probabilities $\widetilde{W}$ of the direct μ-capture process and the ratios $\widetilde{W}/W_{exp}$, where W_{exp} is the total experimental probability of μ capture in the nuclei considered.† The quantity $\widetilde{W}$ is given by the formula‡

$$\widetilde{W} = G^{(\mu)2}\widetilde{W}_0\widetilde{I}, \tag{21}$$

where $\widetilde{I}$ is obtained from $I(E_N)$ by replacing $\gamma_k(E_N)$ by $\widetilde{\gamma}_k$. We see from these results that the probability of μ capture with direct emission of a neutron, for $\xi = 0$, is $\sim 5-10$ percent of the total probability of μ capture. In order to get the fraction of the total number of neutrons emitted on μ capture that are neutrons from the direct process, one must divide the values of $\widetilde{W}/W_{exp}$ given in Table II by the average number of neutrons emitted per μ-capture act.

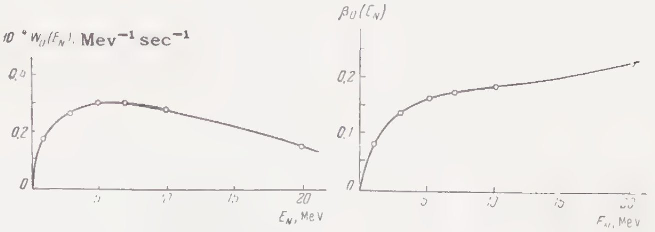

FIG. 3. Values of $W_0(E_N)$ and $\beta_0(E_N)$ as functions of the neutron energy E_N, calculated for the nucleus Ne^{20} by using the Born approximation for the neutron.

Control calculations for the nucleus Ne^{20} have shown that inclusion of the radial dependence of the wave function of the μ^- meson in the K orbit changes the coefficient β_0 by not more than $2-3$ percent, while the probability of the direct process is decreased by $20-25$ percent. For heavier nuclei the decrease of the probability must be even larger.

To determine the influence of the interaction between the neutron and the nucleus on the effects under consideration, numerical calculations have been made for the nucleus Ne^{20}, by the use of the Born approximation for the emitted neutron, i.e., by taking the wave function of the neutron to be a plane wave (p.w.). The results of this calculation are shown in the last row of Table II and in Fig. 3. They differ sharply from the results obtained for Ne^{20} when the interaction of the neutron with the nucleus is taken into account (see Table II and the corresponding curves in Figs. 1 and 2). Inclusion of the nuclear interaction of the neutron leads to a decrease of the probability of the process by several fold, a relative increase of the number of neutrons with smaller energies, and a considerable increase of the asymmetry coefficient and of the longitudinal polarization of the neutrons. Moreover, in the Born approximation the contributions of the various shells to the probability of the direct process in μ capture are comparable, and the probability of the direct process is much larger than the total experimental probability for absorption of μ^- mesons by Ne^{20} nuclei. Thus in treating the phenomena discussed in this paper it is necessary to take into account the interaction between the emitted neutron and the nucleus.

TABLE III

μ	$\varkappa$	α_H	$P_H^{\parallel}$	$\widetilde{\alpha}$	W
4.71	8	—0.45	—0.99	—0.41	1.0
1	8	—0.33	—0.99	—0.30	0.8
4.71	0	—0.23	—0.99	—0.21	1.2
1	0	—0.09	—0.99	—0.09	1.0
nonrelativistic approximation		—0.10	—0.99	—0.10	0.9

---

*As was pointed out in reference 3, in the case of production of neutrons the sign of ζ must be negative.

†The values of W_{exp} are taken from a paper by Sens.[15]

‡The calculations of $\widetilde{W}$ were made with the values of the constants that are most reasonable according to present ideas about μ capture:

$$G^{(\mu)} = 1{,}37, \qquad \lambda = 1{,}25, \qquad \mu = 4{,}71, \qquad \varkappa = 8.$$

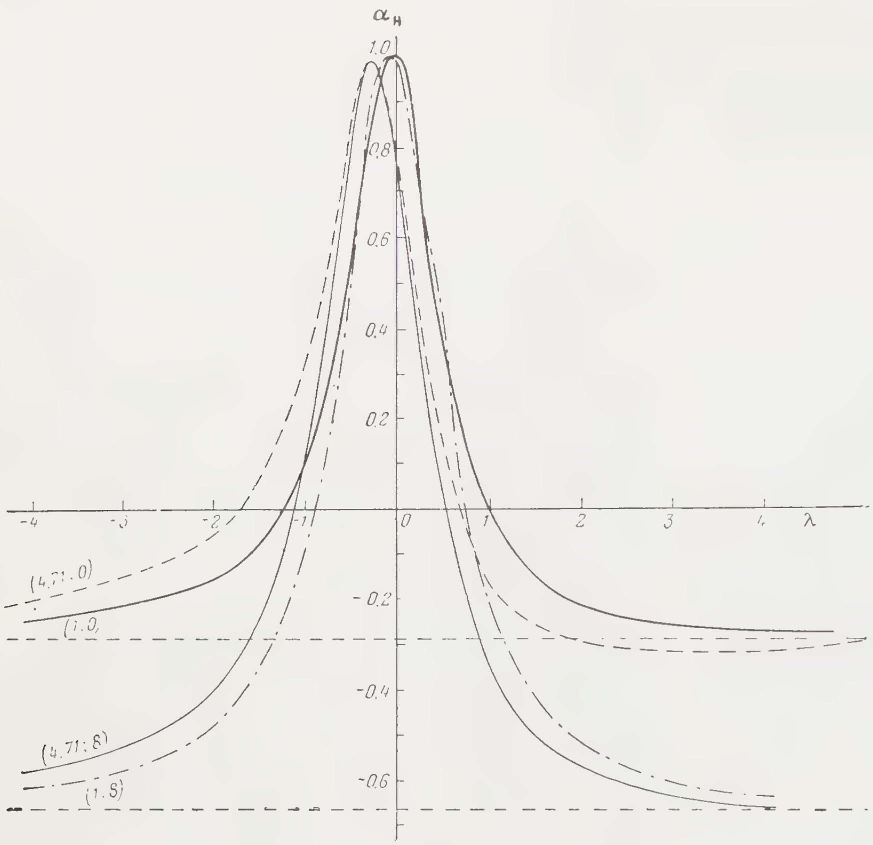

FIG. 4. Dependence of values of α_H on $\lambda = -g_A^{(\mu)}/g_V^{(\mu)}$. The first number in parentheses near a curve is the value of μ, and the second is the value of κ.

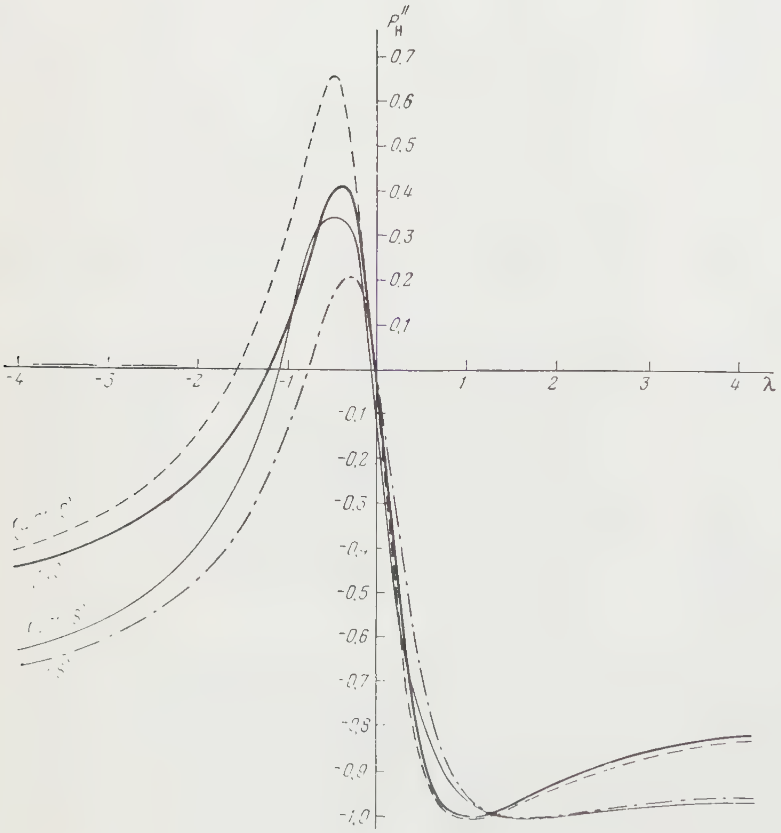

FIG. 5. Dependence of $P_H^{\parallel}$ on λ. The notation is the same as in Fig. 4.

3. COMPARISON WITH EXPERIMENT

The quantities α and $P^{||}$ [Eqs. (17), (18)] depend on the constants λ, μ, and κ contained in the Hamiltonian of the weak interaction between μ mesons and nucleons. Table III shows the values of the mesic-hydrogen asymmetry coefficient α_H and polarization $P^{||}_H$ for $\lambda = 1.25$ and four different combinations of values of μ and κ. For comparison we show also the values of α_H and $P^{||}_H$ obtained with the nonrelativistic approximation for the nucleons.

The value of λ for μ capture is not known exactly, but from experiments[16] on μ capture in C^{12} we can draw the conclusion that $|\lambda\mu\text{ capture}/\lambda\beta\text{ decay}| \approx 1$, and the experiments of the Telegdi group[17] show that $\lambda > 0$. Therefore the value of λ used for Table III was the value for β decay: $\lambda = 1.25$. The quantity α_H does not differ from the asymmetry coefficient $\widetilde{\alpha}$, averaged over the neutron energy, for the nuclei considered here by more than 10 percent, and $P^{||}_H$ and $\widetilde{P}^{||}_H$ agree to within about 1 percent. The values of $\widetilde{\alpha}$ and $\widetilde{P}^{||}$ remain practically unchanged from nucleus to nucleus, since the values of $\widetilde{\gamma}_k$ are almost the same for the various nuclei (see Table II). As an example we show in the next to last column of Table III the values of $\widetilde{\alpha}$ for the nucleus S^{32}. The last column gives in relative units the total probabilities of μ capture with direct neutron emission.

The data shown in Table III show that for $\lambda = 1.25$ the angular asymmetry coefficient of the neutrons depends fairly strongly on the presence or absence of the effective pseudoscalar coupling and the weak-magnetism term in the Hamiltonian for the interaction between μ mesons and nucleons. At the same time the longitudinal polarization of the neutrons remains constant in all of the cases considered, and the total probability of the direct process does not change by more than 20 percent.

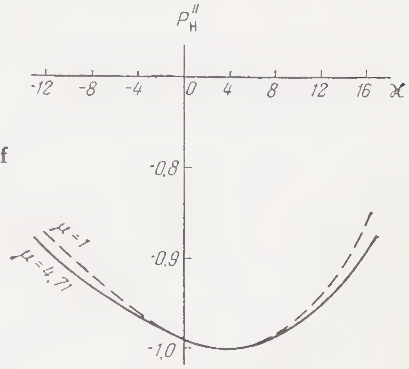

FIG. 7. Dependence of $P^{''}_H$ on κ. The asymptotic value is $P^{''}_H(\infty) = 0$.

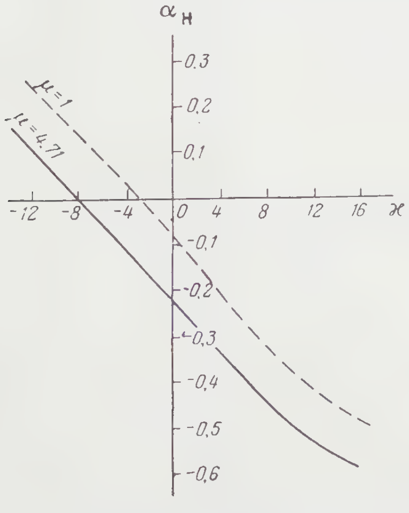

FIG. 6. Dependence of the quantity α_H on $\kappa = g_P^{(\mu)}/g_A^{(\mu)}$ for $\lambda = 1.25$ and two values of μ. The asymptotic value is $\alpha_H(\infty) = 1$.

Figures 4 and 5 show α_H and $P^{||}_H$ as functions of λ for $\mu = 1$ and 4.71 and $\kappa = 0$ and 8. The dependence of α_H and $P^{||}_H$ on κ for $\lambda = 1.25$ and these same values of μ is shown in Figs. 6 and 7. As can be seen from Figs. 5 and 7, $P^{||}_H \approx 1$ for $0.75 \lesssim \lambda \lesssim 2$ for all reasonable values of μ and κ. Because of this it is possible to get values of $\widetilde{\beta}_0$ directly by measuring the longitudinal polarization of the neutron, $\widetilde{P}^{||}_N = \widetilde{\beta}_0\widetilde{P}^{||} = \widetilde{\beta}_0 P^{||}_H$. Comparison of values so obtained with the calculated values of $\widetilde{\beta}_0$ will make it possible to judge the applicability of the model we have adopted and the correctness of the choice of the parameters. Knowing $\widetilde{\beta}_0$, one can use the experimental value of the asymmetry, $a = P_\mu\widetilde{\beta}_0\widetilde{\alpha}$, to determine $\widetilde{\alpha}$ and obtain information about the quantities λ, μ, and κ.

When the possibility of absorption of the neutron in the nuclear matter is taken into account ($\zeta \neq 0$), one finds for the nuclei considered in this paper $\widetilde{\beta} \approx 0.4 - 0.6$. Therefore it is to be expected that the longitudinal polarization of the neutrons will be $\widetilde{P}^{||}_N \approx 0.4 - 0.6$. If we use for P_μ the values obtained by Ignatenko and others[18] ($P_\mu \approx 0.15 - 0.20$), then in the case that is most probable from the point of view of the present theory ($\lambda = 1.25$, $\mu = 4.71$, $\kappa = 8$) we get for the total angular asymmetry coefficient a the value $a \approx -(0.03 - 0.05)$. For other values of μ and κ (see Table III) there will be correspondingly smaller values of a.

At present there are two papers on measurements of the asymmetry of the angular distribution of the neutrons emitted from nuclei in μ capture (there have been no experiments so far on the polarization of the neutrons from μ capture). Astbury and others[19] have studied the anisotropy of the neutrons emitted in μ capture by S^{32}. The experimentally observed angular distribution of the neutrons is of the form $1 + P_{\mu}\widetilde{\beta}_0\widetilde{\alpha}\Phi \cos\theta$, where the factor Φ allows for the presence of an isotropic background of evaporated neutrons. For the quantity $\widetilde{\beta}_0\widetilde{\alpha}\Phi$ the authors give the value $\widetilde{\beta}_0\widetilde{\alpha}\Phi = -0.30 \pm 0.12$. Since $\Phi \leq 1$, this number is an upper limit for $\widetilde{\beta}_0\widetilde{\alpha}$.

According to Table II we have for the nucleus S^{32} with $\zeta \neq 0$ the value $\widetilde{\beta}_0 \approx 0.5 - 0.6$, so that according to our calculations the upper limit for $\widetilde{\alpha}$ is $\widetilde{\alpha}_{\max} \approx -(0.5 - 0.6) \pm 0.2$. Of the cases shown in Table III the one that comes closest to this upper limit is that with $\mu = 4.71$ and $\kappa = 8$. For all the other cases in Table III the theoretical values of $\widetilde{\alpha}$ differ from the average value of the upper limit by more than the experimental error. A crude calculation of the quantity Φ $(\Phi \sim 0.7)$[19] leads the authors to the estimate $\widetilde{\beta}_0\widetilde{\alpha} \sim -0.4$, which is also closest to the value of $\widetilde{\alpha}$ predicted by the theory of the universal Fermi interaction with conserved vector current when one includes an effective pseudoscalar interaction with coupling constant $g_P^{(\mu)} = 8g_A^{(\mu)}$.

Baker and Rubbia[20] have measured the asymmetry in the angular distribution of the neutrons with energy $E_N > 5.5$ Mev emitted in μ capture in magnesium. The value found for $\widetilde{\beta}_0\widetilde{\alpha}$ is $+0.15 \pm 0.11$, which differs both in magnitude and in sign from the results of Astbury and others[19] and the expected theoretical values. Although we have not made numerical calculations for μ capture in magnesium, it is to be expected that the coefficients β_0 and γ_k for Mg^{24} are close to the corresponding values for Si^{28}, since these nuclei are very similar in structure and the binding energies of the outer protons are almost identical. Therefore it is hard to explain the results of Baker and Rubbia from the point of view of present ideas about μ capture.

In conclusion we express our sincere gratitude to Professor I. S. Shapiro for a discussion of this work.

---

[1] Shapiro, Dolinskiĭ, and Blokhintsev, Doklady Akad. Nauk SSSR **116**, 946 (1957), Soviet Phys.-Doklady **2**, 475 (1958); Nuclear Phys. **4**, 273 (1957).

[2] B. L. Ioffe, JETP **33**, 308 (1957), Soviet Phys. JETP **6**, 240 (1957). H. Überall, Nuovo cimento **6**, 583 (1957). Huang, Yang, and Lee, Phys. Rev. **108**, 1340 (1957). L. Wolfenstein, Nuovo cimento **7**, 706 (1958).

[3] É. I. Dolinskiĭ and L. D. Blokhintsev, JETP **35**, 1488 (1958), Soviet Phys. JETP **8**, 1040 (1959); Nuclear Phys. **10**, 527 (1959).

[4] L. D. Blokhintsev, JETP **36**, 258 (1959), Soviet Phys. JETP **9**, 175 (1959).

[5] R. P. Feynman and M. Gell-Mann, Phys. Rev. **109**, 193 (1958).

[6] E. C. G. Sudarshan and R. E. Marshak, Phys. Rev. **109**, 1860 (1958).

[7] A. Fujii and H. Primakoff, Nuovo cimento **12**, 327 (1959).

[8] M. Gell-Mann, Phys. Rev. **111**, 362 (1958).

[9] M. L. Goldberger and S. B. Treiman, Phys. Rev. **111**, 354 (1958).

[10] É. I. Dolinskiĭ, JETP **36**, 1179 (1959), Soviet Phys. JETP **9**, 838 (1959).

[11] I. M. Shmushkevich, JETP **36**, 953 (1959), Soviet Phys. JETP **9**, 673 (1959).

[12] N. Feather, Advances in Physics **2**, 141 (1953).

[13] É. I. Dolinskiĭ, Dissertation, Joint Institute for Nuclear Research, 1959.

[14] Kawai, Nagasaki, Soga, Terasawa, Ui, and Wada, Progr. Theoret. Phys. **18**, 66 (1957).

[15] J. C. Sens, Phys. Rev. **113**, 679 (1959).

[16] Argo, Harrison, Cruse, and McGuire, Phys. Rev. **114**, 626 (1959).

[17] V. L. Telegdi, Phys. Rev. Letters **3**, 59 (1959).

[18] Ignatenko, Egorov, Khalupa, and Chultém, JETP **35**, 1131 (1958), Soviet Phys. JETP **8**, 792 (1959).

[19] Astbury, Blair, Hussain, Kemp, Muirhead, and Voss, Phys. Rev. Letters **3**, 476 (1959).

[20] W. F. Baker and C. Rubbia, Phys. Rev. Letters **3**, 179 (1959).

Translated by W. H. Furry
327

SOVIET PHYSICS JETP VOLUME 12, NUMBER 6 JUNE, 1961

APPLICATION OF THE MANDELSTAM METHOD TO THE COMPUTATION OF SCATTERING AMPLITUDES WITH ANOMALOUS SINGULARITIES

V. A. FRANKE

Leningrad Institute For Labor Welfare

Submitted to JETP editor July 29, 1960

J. Exptl. Theoret. Phys. (U.S.S.R.) **39**, 1818-1828 (December, 1960)

Mandelstam's method for the calculation of the scattering amplitude[1] is extended to the case of two interacting neutral scalar fields describing particles with masses m and M subject to the condition $m\sqrt{3} > M > m\sqrt{2}$. The anomalous singularities of the amplitude which appear as a consequence of the indicated relation between the masses are taken into account. Conditions for the extension of the method of the present paper to more complicated cases are indicated.

1. INTRODUCTION

MANDELSTAM'S method of calculation of the scattering amplitude[1] appears to be very promising at the present time. It is interesting to extend it to the case where the amplitude has anomalous singularities. This is connected with two difficulties. First, the Mandelstam representation of the scattering amplitude must be generalized. Second, the unitarity conditions do not determine the discontinuities of the scattering amplitude along the cuts coming from the anomalous singularities. The first difficulty can be overcome with comparative ease if the anomalous singularities are of the simplest kind. In the present paper we consider just this case on the example of two interacting scalar fields. Methods for dealing with the second difficulty have been pointed out in the papers of Mandelstam[2] and Cutkosky.[3]

We shall use the method of Cutkosky,[3] in which the expressions for the discontinuities along the above-mentioned cuts are obtained from an analogy with perturbation theory. As a result, we obtain certain integral equations that are solved by expanding in powers of the coupling constant. This is equivalent to summing a certain class of Feynman graphs. This class includes the same graphs that are accounted for in the Mandelstam method in the absence of anomalous singularities.[4] It can be easily seen from the subsequent considerations under what conditions the results obtained can be extended to more complicated cases.

2. MANDELSTAM-TYPE REPRESENTATION FOR THE SCATTERING AMPLITUDE

Let us consider a system of two neutral scalar fields describing particles with masses M and m. We shall denote these particles by the letters a and b, and represent them in the graphs by means of straight and wavy lines. In order that the scattering amplitude have anomalous singularities, we subject the masses of the particles to the condition

$$M > m\sqrt{2}. \quad (1)$$

On the other hand, the method explained below is applicable only if

$$m\sqrt{3} > M. \quad (2)$$

To simplify the derivations, we assume that the even more restrictive condition

$$2m \sin 50^\circ > M \quad (3)$$

is fulfilled. The meaning of inequalities (2) and (3) will be explained below.

The following reactions can take place in this system:

$$a + a \rightleftarrows a + a, \quad (I)$$
$$a + a \rightleftarrows a + b, \quad (II)$$
$$a + a \rightleftarrows b + b, \quad (III)$$
$$a + b \rightleftarrows b + b, \quad (IV)$$
$$b + b \rightleftarrows b + b. \quad (V)$$

The other possible reactions are obtained from (I) to (V) by interchanging the initial and final states of the particles.

We can easily see from a consideration of the graphs of perturbation theory[5,6] that only the amplitudes of the processes (I) to (III) contain anomalous singularities under the conditions (1) and (3). These singularities correspond to the graphs shown in Fig. 1 and to graphs obtained from the former by interchanging the single external particles. It is evident that the graphs obtained from those mentioned above by replacing the vertices by arbitrary graphs also contain anomalous singularities. Graphs of this type will be called derivative graphs.

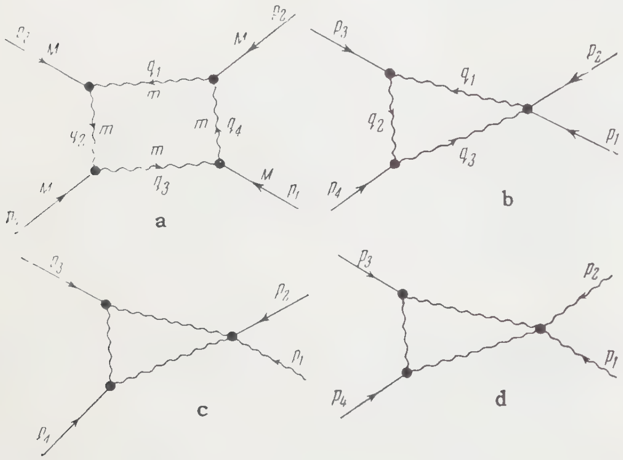

FIG. 1

We shall make the basic assumption that only the graphs enumerated above contain anomalous singularities.* The correctness of this assumption can be easily verified for all graphs of the "triangular" and "quadrangular" type.† It can also be justified for other graphs of the simplest type (in particular, for the graphs shown in Figs. 5 and 6, see below). This assumption plays the same role as the assumption of the validity of the Mandelstam representation in the case when the simplest graphs do not contain anomalous singularities.

It is known that the Mandelstam representation for the amplitude can be preserved in the presence of singularities in the graphs of Fig. 1 b, c, and d and their derivatives, if the lower limits of integration are changed.[7] We shall call the resulting representation a Mandelstam-type representation. The only singularities not accounted for by this representation are the proper singularity* of the graph of Fig. 1 a and the corresponding singularities of its derivative graphs. These singularities appear only in the scattering amplitude of process (I). Using the results of Cutkosky,[3] we can separate out of this amplitude the term which contains these singularities, and calculate it exactly. It is easy to do the latter by estimating the magnitude of the discontinuity along the cut coming from the proper singularity of the graph of Fig. 1 a. Each of its derivative graphs gives a contribution to this discontinuity. According to the results of Cutkosky, this contribution is equal to†

$$F^{(4)}_{iklm} = -i\int d^4q_1 \Gamma_i(q_3, q_4)\Gamma_k(q_4, q_1) \times \Gamma_l(q_1, q_2)\Gamma_m(q_2, q_3)\prod_{r=1}^{4}\delta(q_r^2 - m^2), \tag{4}$$

where $\Gamma_i(q_j, q_k)$ are the contributions to the corresponding vertex parts from the graphs substituted for the vertices in the graph of Fig. 1.

The internal momenta q_r in formula (4) must be expressed in terms of the external momenta p_i and the momentum q_1 with the help of the conservation laws.

Here and in what follows we assume that the solution of the system of equations $q_r^2 - m^2 = 0$ (in terms of the components of the vector q_1) gives a contribution to integrals of the type (4) also in the case when the roots of this system are complex. In this case we must regard expression (4) as the analytic continuation of a similar integral in terms of the masses of the particles from the region where the corresponding roots are real and satisfy the conditions $q_1^2 > 0$, $q_{10} > 0$. The roots satisfying the inequalities $q_1^2 > 0$, $q_{10} < 0$ are not taken into account.

The total magnitude of the discontinuity along the cut is obtained by summing expressions of the type (4) for all derivative graphs formed from the graph of Fig. 1 a. This magnitude is evidently also given by formula (4) if each of the functions Γ_i is replaced by the full vertex part Γ. Since the arguments of the functions Γ in the integral (4) always correspond to the physical values of the masses of the particles, we can set

$$\Gamma = \gamma_{12}, \tag{5}$$

where γ_{12} is the renormalized constant of the coupling of a single particle a with two particles b.* This leads to the following formula for the total discontinuity along the cut:

---

*We shall call anomalous all those singularities which are not taken care of by the Mandelstam representation with the usual limits of integration.

†The class of graphs of the "triangular" and "quadrangular" type also contains those graphs in which one or several sides consist of an arbitrary number of parallel lines (e.g., the graph of Fig. 2b below).

*A singularity is called the proper singularity of a given graph if it does not appear in the graphs obtained from the former by the addition of arbitrary vertices.

†The scattering amplitude is normalized in the same way as in reference 1.

$$F^{(4)} = -i\gamma_{12}^4 \int d^4 q_1 \prod_{r=1}^{4} \delta(q_r^2 - m^2). \tag{6}$$

Thus the discontinuity is determined only by the graph of Fig. 1a with the renormalized coupling constant. The contribution of this graph as well as of the two others that are obtained from the former by interchanging the external particles can be calculated exactly. Let us denote the sum of these three contributions by a. Then the quantity $A^{I} - a$, where A^{I} is the scattering amplitude of the process (I), fulfills the requirements of the Mandelstam-type representation.†

We note that, if we disregard condition (3) while keeping condition (2), a similar subtraction must be made for the process (II). This is due to the circumstance that the graph shown in Fig. 2 a introduces a proper anomalous singularity. If we also discard condition (2), anomalous singularities from the graph of Fig. 2 b will appear, which cannot be separated by the described method.

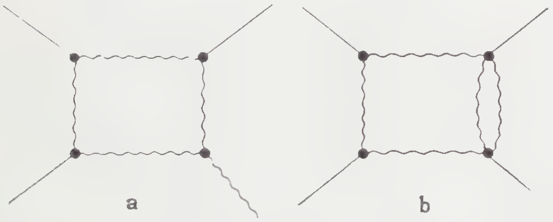
a b

FIG. 2

Returning to the case where condition (3) is satisfied, we can write for the amplitude of the process (I) the Mandelstam-type representation

$$A^{I}(s_1, s_2, s_3) = a(s_1, s_2, s_3) + \sum_{i=1}^{3} \frac{\gamma_{21}^2}{m^2 - s_i} + \sum_{i=1}^{3} \frac{\gamma_{30}^2}{M^2 - s_i}$$
$$+ \frac{1}{\pi} \sum_{\substack{i,k \\ =1,2;2,3;\,3,1}} \int_{s_0}^{\infty}\int_{s_0}^{\infty} \frac{A_{ik}^{I}(\sigma, \sigma')\, d\sigma\, d\sigma'}{(\sigma - s)(\sigma' - s_k)}. \tag{7}$$

Here the A_{ik}^{I} are certain spectral functions which satisfy $A_{ki}^{I}(\sigma, \sigma') = A_{ik}^{I}(\sigma', \sigma)$; γ_{21} and γ_{30} are the renormalized constants of the coupling of two particles a with a single particle b and of three particles a among themselves. The variables s_i are given by

$$s_1 = (p_1 + p_2)^2, \qquad s_2 = (p_1 + p_4)^2,$$
$$s_3 = (p_1 + p_3)^2, \tag{8}$$

where the p_i are the momenta of the interacting particles (see Fig. 1 a). The quantities s_i are connected through the relation

$$s_1 + s_2 + s_3 = 4M^2. \tag{9}$$

The integration limit s_0 in (7) is determined by the anomalous threshold of the graph of Fig. 1 b, and is equal to

$$s_0 = M^2(4m^2 - M^2)/m^2. \tag{10}$$

Here and in the following, we shall, for simplicity, not carry out the subtractions necessary for the convergence of the integrals in formulas of the type (7). These subtractions can be performed in the usual way. We note that all functions A_{ik}^{I} are equal to each other by virtue of the symmetry conditions.

Formulas of the type (7) without the term a can also be written down for the amplitudes of the processes (II) to (V). Here the usual Mandelstam representation is valid for the processes (IV) and (V).

3. INTEGRAL EQUATIONS FOR THE SPECTRAL FUNCTIONS

In the following we shall require functions that are defined by

$$A_i^{(l)}(s_i, s_j) = A_i^{(l)}(s_i, s_j, s_k) = A_i^{(l)}(s_i, s_j, 4M^2 - s_i - s_j)$$
$$= \frac{1}{\pi} \int_{s_0^{(l)}}^{\infty} \left[\frac{A_{ij}^{(l)}(s_i, \sigma)}{\sigma - s_j} + \frac{A_{ik}^{(l)}(s_i, \sigma)}{\sigma - s_k}\right] d\sigma. \tag{11}$$

The values of the indices i, j, k are obtained by cyclic permutation of the numbers 1, 2, 3; the index l takes on the values (I) to (V) which denote the type of reaction. For the reactions (II) to (V) the quantities $2iA_i^{(l)}$ are equal to the discontinuities of the amplitude on the cuts in the planes of the variables s_i. The functions $2iA_i^{I}$ are equal to the corresponding discontinuities of the quantity $A^{I} - a$.

For the derivation of the integral equations we must express the functions $A_i^{(l)}$ in terms of the amplitudes of the different processes. We shall consider these expressions only for the discontinuities of the amplitude A^{I}. The relations for the other amplitudes will have an analogous form with a number of simplifications due to the absence of the term $a(s_1, s_2, s_3)$. Let us consider first of all the discontinuity along the cut in the s_1 plane from s_0 to $4m^2$. We note that only two graphs have a proper singularity at $s_1 = s_0$: the graph shown in

---

*Here and in the following we use coupling constants defined in such a way that the coefficient of the interaction term in the Hamiltonian is equal to $\gamma_{ik}/i!k!$, where i and k are the numbers of identical operators in this term.

†We note that the derivative graphs of the graph of Fig. 1a do not contain proper singularities, as can be easily verified by the Landau method.[6]

Fig. 1 b and the graph obtained from the former by the interchange of particles $p_1 \rightleftarrows p_3$, $p_2 \rightleftarrows p_4$. All graphs derived from these two graphs give a contribution to the discontinuity along the cut coming from this singularity. According to the results of Cutkosky,[3] the contribution from any graph derived from the graph of Fig. 1 a is equal to

$$F_{ikl}^{(3)} = -\frac{1}{2\pi}\int d^4q_1\Gamma_i(q_1, q_2)\,\Gamma_k(q_2, q_3)$$
$$\times B_l(q_1, q_3, p_1)\prod_{r=1}^{3}\delta(q_r^2 - m^2). \qquad (12)$$

Here the Γ_i have the same meaning as in (4), and B_l is the contribution to the vertex part connecting four particles from the graph substituted in the graph of Fig. 1 b in place of the corresponding vertex. We regard the internal momenta q_i as being expressed in terms of the external momenta p_i and the momentum q_1 with the help of the conservation laws.

Repeating the considerations leading to formula (4) and noting that the total vertex part B connecting four particles is equal to the scattering amplitude A^{III} for values of the arguments corresponding to the masses of the real particles, we obtain the equation

$$A_1^{I}(s_1, s_2, s_3) + a_1(s_1, s_2, s_3)$$
$$= \frac{i\gamma_{12}^2}{4\pi}\Big[\int d^4q_1 A^{III}(s_1, s_2'', s_3')\prod_{i=1}^{3}\delta(q_i^2 - m^2)$$
$$+\int d^4q_1 A^{III*}(s_1, s_2', s_3')\prod_{i=1}^{3}\delta(q_i^2 - m^2)\Big]. \qquad (13)$$

Here

$$s_2' = (p_4 - q_3)^2, \qquad s_3' = (p_4 + q_1)^2,$$
$$s_2'' = (p_1 + q_3)^2, \qquad s_3'' = (p_1 - q_1)^2;$$

$2ia_1$ is the discontinuity of the quantity $a(s_1, s_2, s_3)$ along the cut in the s_1 plane. The quantity s_1 lies between the limits s_0 and $4m^2$. The second term on the right-hand side of (13) comes from the graph obtained from the graph of Fig. 1 b by interchanging the particles. By following the path of the cuts we can verify that the complex conjugate value of A^{III} must be used in this term. This has been accounted for in formula (13).

Using a representation of the type (7) for the amplitude A^{III} and the relation (11), we can write this amplitude in the form

$$A^{III}(s_1, s_2, s_3) = \sum_{i=1}^{3}\frac{\gamma_{12}^2}{m^2 - s_i} + \sum_{i=1}^{3}\frac{\gamma_{21}^2}{M^2 - s_i}$$
$$+\frac{1}{\pi}\int_{4m^2}^{\infty}\Big[\frac{A_2^{III}(\sigma, s_1)}{\sigma - s_2} + \frac{A_3^{III}(\sigma, s_1)}{\sigma - s_3}\Big]d\sigma. \qquad (14)$$

Let us substitute this result in (13) and let us consider the various terms of the resulting expression. The terms coming from the poles of A^{III} in the variable s_1 give a contribution only to the subtraction terms, which we do not write down explicitly. The poles of A^{III} at $s_2' = m^2$, $s_3' = m^2$, and $s_2'' = m^2$, $s_3'' = m^2$ give rise to a term which cancels the term $a_1(s_1, s_2, s_3)$, as can be easily verified. As a result we obtain the formula

$$A_1^{I}(s_1, s_2, s_3) = 2\gamma_{12}^2\gamma_{21}^2[\varphi(s_1, s_2;\ M^2) + \varphi(s_1, s_3;\ M^2)]$$
$$+\frac{\gamma_{12}^2}{\pi}\int_{4m^2}^{\infty}\Big[(A_2^{III}(\sigma, s_1) + A_2^{III*}(\sigma, s_1))\,\varphi(s_1, s_2; \sigma)$$
$$+(A_3^{III}(\sigma, s_1) + A_3^{III*}(\sigma, s_1))\varphi(s_1, s_3; \sigma)\Big]d\sigma, \qquad (15)$$

where

$$\varphi(s_1, s_2; \sigma) = -\frac{i}{4\pi}$$
$$\times\int d^4q_1\frac{\delta(q_1^2 - m^2)\,\delta[(q_1 + p_3)^2 - m^2]\,\delta[(q_1 + p_3 + p_4)^2 - m^2]}{(q_1 - p_2)^2 - \sigma} \qquad (16)$$

The function $2i\varphi$ is equal to the discontinuity of the Feynman integral corresponding to the graph of Fig. 3 along the cut coming from the singularity at $s_1 = s_0$. One of the masses of the internal particles in this integral is equal to $\sqrt{\sigma}$. As has been shown by Cutkosky,[3] the function φ has a singularity which coincides with the proper singularity of the graph in Fig. 3. The discontinuity of the function $2i\varphi$ along the cut coming from this singularity is the same as the discontinuity of the above-mentioned Feynman integral and is equal to

$$-4f(s_1, s_2; \sigma, m^2) = -i\int d^4q_1\delta(q_1^2 - m^2)\,\delta[(q_1 + p_3)^2 - m^2]$$
$$\times\,\delta[(q_1 + p_3 + p_4)^2 - m^2]\,\delta[(q_1 - p_2)^2 - \sigma]. \qquad (17)$$

An explicit expression for the function f was obtained in references 1 and 3.

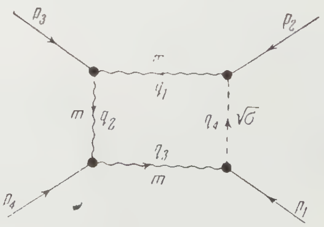

FIG. 3

The singularities of the graph of Fig. 3 are shown in Fig. 4. The region in which the function f is different from zero is shaded (simple and double shading). For comparison, the boundary of the corresponding region in the case when there are no anomalous thresholds is indicated in the

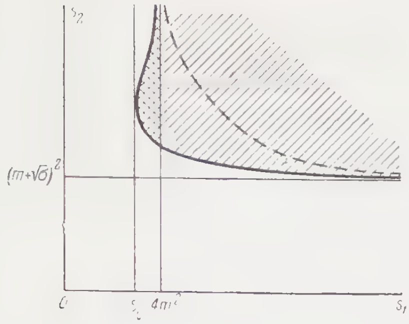

FIG. 4

same figure by a dotted line. It should be emphasized that the graph of Fig. 3 has no singularities which violate the Mandelstam-type representation, since owing to condition (2)

$$\sqrt{\sigma} \geqslant s_0 > M. \tag{18}$$

The singularities of the graph of Fig. 3 have been analyzed in detail in the paper by Tarsky.[7]

On the basis of the preceding considerations we can write

$$\varphi(s_1, s_2; \sigma) = \frac{1}{\pi} \int\limits_{\sigma_1'(s_1)}^{\sigma_2'(s_1)} \frac{f(s_1, \sigma'; \sigma, m^2)}{\sigma' - s_2}\, d\sigma', \tag{19}$$

where the integration goes over the region in which the function f is different from zero (doubly shaded region in Fig. 4).

Substituting (19) in (15), we find, for $s_0 < s_1 < 4m^2$

$$A_1^{\mathrm{I}}(s_1, s_2, s_3) = \frac{1}{\pi} \int\limits_{\sigma_1'(s_1)}^{\sigma_2'(s_1)} d\sigma' \left[\frac{Q_{21}^{(a)}(\sigma', s_1)}{\sigma' - s_2} + \frac{Q_{31}^{(a)}(\sigma', s_1)}{\sigma' - s_3}\right], \tag{20}$$

$$Q_{21}^{(a)}(\sigma', s_1) = Q_{31}^{(a)}(\sigma', s_1) = 2\gamma_{12}^2\gamma_{21}^2 f(s_1, \sigma'; M^2, m^2)$$
$$+ \frac{\gamma_{12}^2}{2\pi} \int\limits_{4m^2}^{\infty} [A_2^{\mathrm{III}}(\sigma, s_1) + A_2^{\mathrm{III}*}(\sigma, s_1)$$
$$+ A_3^{\mathrm{III}}(\sigma, s_1) + A_3^{\mathrm{III}*}(\sigma, s_1)]\, f(s_1, \sigma'; \sigma, m^2)\, d\sigma. \tag{21}$$

By virtue of the symmetry conditions, $A_2^{\mathrm{III}}(\sigma, s_1) = A_3^{\mathrm{III}}(\sigma, s_1)$. This has been used in the derivation of formulas (20) and (21).

Comparing (20) with (11), we conclude that for $s_0 < s_1 < 4m^2$

$$A_{21}^{\mathrm{I}}(s_2, s_1) = Q_{21}^{(a)}(s_2, s_1), \qquad A_{31}^{\mathrm{I}}(s_3, s_1) = Q_{31}^{(a)}(s_3, s_1). \tag{22}$$

Let us now turn to the discontinuity of the amplitude A^{I} along the cut in the s_1 plane from $4m^2$ to ∞, which is determined by the unitarity condition. As usual, we shall consider in this relation only intermediate states with two particles and that part of the contribution from the remaining intermediate states which is necessary to satisfy the conditions of crossing symmetry.[4] In this case we have, for $4m^2 < s_1 < \infty$,

$$A_1^{\mathrm{I}}(s_1, s_2, s_3) = C_1^{\mathrm{I}}(s_1, s_2, s_3) + D_1^{\mathrm{I}}(s_1, s_2, s_3), \tag{23}$$

$$C_1^{\mathrm{I}}(s_1, s_2, s_3) = \xi_1^{\mathrm{I}}(s_1) \int A'^{\mathrm{I}*}(s_1, s_2', s_3')\, A'^{\mathrm{I}}(s_1, s_2'', s_3'')\, \frac{dn}{4\pi}$$
$$+ \xi_1^{\mathrm{II}}(s_1) \int A^{\mathrm{II}*}(s_1, s_2', s_3')\, A^{\mathrm{II}}(s_1, s_2'', s_3'')\, \frac{dn}{4\pi}$$
$$+ \xi_1^{\mathrm{III}}(s_1) \int A^{\mathrm{III}*}(s_1, s_2', s_3')\, A^{\mathrm{III}}(s_1, s_2'', s_3'')\, \frac{dn}{4\pi}$$
$$- a_1(s_1, s_2, s_3) + \Delta'_1(s_1, s_2, s_3), \tag{24}$$

$$D_1^{\mathrm{I}}(s_1, s_2, s_3) = \xi_1^{\mathrm{I}}(s_1) \int [a^*(s_1, s_2', s_3')\, a(s_1, s_2'', s_3'')$$
$$+ a^*(s_1, s_2', s_3')\, A'^{\mathrm{I}}(s_1, s_2'', s_3'')$$
$$+ A'^{\mathrm{I}*}(s_1, s_2', s_3')\, a(\text{[illegible]} \tag{25}$$

Here

$$A'^{\mathrm{I}} = A^{\mathrm{I}} - a, \quad s_2' = (p_4 - q_3)^2, \quad s_3' = (p_4 + q_1^2),$$
$$s_2'' = (p_1 + q_3)^2, \quad s_3'' = (p_1 - q_1)^2,$$

q_1 and q_3 are the momenta of the particles in the intermediate state; dn is a surface element of the unit sphere in the space of the momenta $\mathbf{q}_1$ in the center-of-mass system, $\Delta'(s_1, s_2, s_3)$ and $\Delta''(s_1, s_2, s_3)$ are the included parts of the contribution of intermediate states with more than two particles.

The quantities $\xi_1^{(l)}(s_1)$ are equal to

$$\xi_1^{(l)}(s_1) = \sqrt{(s_1 - s_+^{(l)})(s_1 - s_-^{(l)})}/16\pi\nu^{(l)} s_1, \tag{26}$$

where

$$\nu^{\mathrm{I}} = \nu^{\mathrm{III}} = 2, \qquad \nu^{\mathrm{II}} = 1, \qquad s_-^{\mathrm{I}} = s_-^{\mathrm{III}} = 0,$$
$$s_-^{\mathrm{II}} = (M - m)^2, \quad s_+^{\mathrm{I}} = 4M^2, \quad s_+^{\mathrm{II}} = (M + m)^2, \quad s_+^{\mathrm{III}} = 4m^2.$$

Expression (24) for C_1^{I} can be transformed in the same way as in the case when there are no anomalous thresholds.[1-4] We shall consider only the third term of this expression, subtracting from it the quantity $a_1(s_1, s_2, s_3)$. After this subtraction the contribution of this term to the spectral function A_{21}^{I} is equal to*

$$Q_{21}^{\mathrm{III}}(s_2, s_1) = 2\gamma_{12}^2\gamma_{21}^2 f(s_1, s_2; M^2, m^2) + \gamma_{30}^2 f(s_1, s_2; M^2, M^2)$$
$$+ \frac{\gamma_{12}^2}{2\pi} \int\limits_{4m^2}^{\infty} d\sigma\, [A_2^{\mathrm{III}}(\sigma, s_1) + A_2^{\mathrm{III}*}(\sigma, s_1)$$

---

*Our function f is related to the function Γ_1 used by Ter-Martirosyan[4] by

$$f(s_1, s_2; \sigma', \sigma'') = \frac{1}{16\pi}\, \Gamma_1(\sigma', \sigma''; s_2, s_1).$$

The amplitude A^{I} in our work differs from the amplitude used in reference 4 by the factor $(1/32)\pi$.

$$+ A_3^{\mathrm{III}}(\sigma, s_1) + A_3^{\mathrm{III}*}(\sigma, s_1)]\, f(s_1, s_2; \sigma, m^2)$$

$$+ \frac{\gamma_{30}^2}{2\pi} \int_{4m^2}^{\infty} d\sigma\, [A_2^{\mathrm{III}}(\sigma, s_1) + A_2^{\mathrm{III}*}(\sigma, s_1) + A_3^{\mathrm{III}}(\sigma, s_1)$$

$$+ A_3^{\mathrm{III}*}(\sigma, s_1)]\, f(s_1, s_2; \sigma, M^2)$$

$$+ \frac{1}{2\pi^2} \int_{4m^2}^{\infty} \int_{4m^2}^{\infty} d\sigma' d\sigma''\, [A_2^{\mathrm{III}*}(\sigma', s_1)\, A_2^{\mathrm{II}\sim}(\sigma'', s_1)$$

$$+ A_3^{\mathrm{III}*}(\sigma', s_1)\, A_3^{\mathrm{III}}(\sigma'', s_1)]\, f(s_1, s_2; \sigma', \sigma''). \qquad (27)$$

Comparing (27) and (20), we easily see that (21) is the analytic continuation of (27) into the region $s_0 < s_1 < 4m^2$. Here we must take account of the fact that in this region only the terms containing $f(s_1, s_2; M^2, m^2)$ and $f(s_1, s_2; \sigma, m^2)$ are different from zero. Thus the discontinuity of the function $A^{\mathrm{I}} - a$ on the cut from s_0 to $4m^2$ in the s_1 plane is treated correctly if we continue expression (27) into the region where the corresponding functions f are different from zero. The same result can apparently be obtained by analytic continuation in the particle masses of the corresponding relations derived under the assumption that there are no anomalous thresholds. This procedure has been pointed out in the paper by Mandelstam.[2] The result does not depend on the specific model that we have chosen. It holds in all cases involving anomalous thresholds connected with graphs of the triangular type (Fig. 1 b, c, d), while the proper singularities of the graphs of quadrangular type are excluded.

Returning to the consideration of the spectral function A_{21}^{I}, we note that the expression (27) must be supplemented by terms deriving from the unitarity condition for the second channel (where s_2 is the energy).* The common contribution to the spectral function from the third term of (24) and the analogous term entering in the unitarity condition for the second channel, is equal to

$$W_{21}^{\mathrm{III}}(s_2, s_1) = Q_{21}^{\mathrm{III}}(s_2, s_1) + Q_{12}^{\mathrm{III}}(s_1, s_2)$$

$$- \gamma_{30} f(s_1, s_2; M^2, M^2), \qquad (28)$$

where $Q_{12}^{\mathrm{III}}(s_1, s_2)$ is obtained from the unitarity condition for the second channel in the same way as (27) is obtained from (24). By virtue of the symmetry conditions

$$Q_{12}^{\mathrm{III}}(\sigma', \sigma'') = Q_{21}^{\mathrm{III}}(\sigma', \sigma''). \qquad (29)$$

In a similar way, but without the complications connected with the anomalous thresholds, we can find the quantities $W_{ik}^{\mathrm{I}}(s_i, s_k)$ and $W_{ik}^{\mathrm{II}}(s_i, s_k)$, which represent the contributions of the first and second terms of expressions of the type (24) to the spectral function A_{ik}^{I}. The total contribution of the quantity $C_1^{\mathrm{I}}(s_1, s_2, s_3)$ to the spectral function is given by the formula

$$C_{ik}^{\mathrm{I}}(s_i, s_k) = \sum_{l=\mathrm{I}}^{\mathrm{III}} W_{ik}^{(l)}(s_i, s_k). \qquad (30)$$

Let us now consider the function $D_1^{\mathrm{I}}(s_1, s_2, s_3)$, which is given by formula (25). In correspondence with (7) and (11), we write $A'^{\mathrm{I}}(s_1, s_2, s_3)$ in the form

$$A'^{\mathrm{I}}(s_1, s_2, s_3) = \sum_{i=1}^{3} \frac{\gamma_{21}^2}{m^2 - s_i} + \sum_{i=1}^{3} \frac{\gamma_{30}^2}{M^2 - s_i}$$

$$+ \frac{1}{\pi} \int_{s_0}^{\infty} \left[\frac{A_2^{\mathrm{I}}(\sigma, s_1)}{\sigma - s_2} + \frac{A_3^{\mathrm{I}}(\sigma, s_1)}{\sigma - s_3} \right] d\sigma. \qquad (31)$$

Let us substitute this expression in (25). Under the integral sign we have

$$\xi_1(s_1) \frac{dn}{4\pi} = \frac{d^4 q_1}{16\pi} \delta(q_1^2 - M^2)\, \delta(q_3^2 - M^2), \qquad (32)$$

where q_1 and q_3 are the momenta of the intermediate particles. As in the derivation of formula (15), the poles at $s_1 = m^2$ and $s_1 = M^2$ in the amplitude A'^{I} give a contribution only to the subtraction terms, which we do not write down explicitly. As a result we obtain the formula

$$D_1^{\mathrm{I}}(s_1, s_2, s_3) = \varphi_2(s_1, s_2, s_3)$$

$$+ \gamma_{21}^2 [\varphi_1^*(s_1, s_2, s_3; m^2) + \varphi_1(s_1, s_2, s_3; m^2)]$$

$$+ \gamma_{30}^2 [\varphi_1^*(s_1, s_2, s_3; M^2) + \varphi_1(s_1, s_2, s_3; M^2)]$$

$$+ \frac{1}{\pi} \int_{s_0}^{\infty} d\sigma\, \{[A_2^{\mathrm{I}}(\sigma, s_1) + A_3^{\mathrm{I}}(\sigma, s_1)]\, \varphi_1^*(s_1, s_2, s_3; \sigma)$$

$$+ [A_2^{\mathrm{I}*}(\sigma, s_1) + A_3^{\mathrm{I}*}(\sigma, s_1)]\, \varphi_1(s_1, s_2, s_3; \sigma)\}$$

$$+ \Delta_1''(s_1, s_2, s_3); \qquad (33)$$

$$\varphi_1(s_1, s_2, s_3; \sigma) = \frac{1}{8\pi^2} \int \frac{a(s_1, s_2'', s_3'')\, \delta(q_1^2 - M^2)\, \delta(q_3^2 - M^2)}{\sigma - s_2''} d^4 q_1, \qquad (34)$$

$$\varphi_2(s_1, s_2, s_3) = \frac{1}{16\pi^2} \int a^*(s_1, s_2', s_3')\, a(s_1, s_2'', s_3'')\, \delta$$

$$\times (q_1^2 - M^2)\, \delta(q_3^2 - M^2)\, d^4 q_1. \qquad (35)$$

Here we have used the same notation as in formulas (23) to (25).

As pointed out earlier, the quantity a represents the sum of three Feynman integrals. These integrals correspond to the graph of Fig. 1 a and two others which are obtained from the former by interchanging the external particles. Taking this

---

*In formula (24) the corresponding terms are included in the quantity $\Delta_1'(s_1, s_2, s_3)$. The problem of accounting for these terms has been discussed in detail by Ter-Martirosyan.[4]

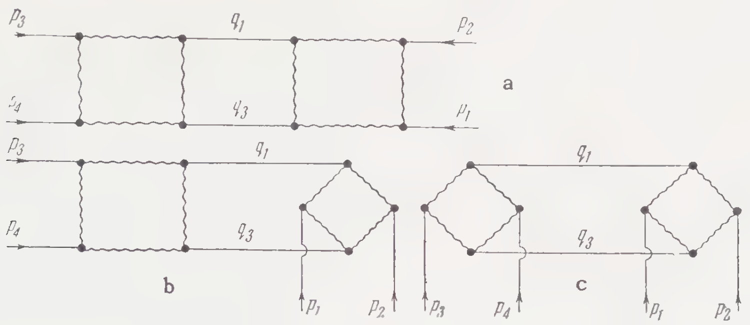

FIG. 5

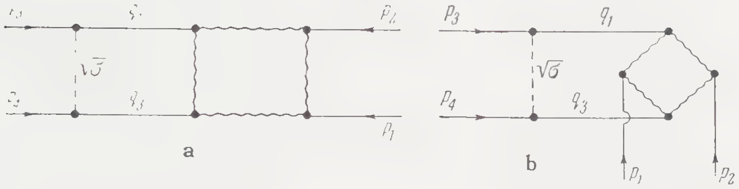

FIG. 6

into account and using the results of Cutkosky,[3] we readily conclude that the function $2i\varphi_2(s_1, s_2, s_3)$ is equal to the sum of the discontinuities of a number of Feynman integrals on the cut coming from the singularity at $s_1 = 4M^2$. Five graphs give a contribution to this sum: the three graphs shown in Fig. 5 a, b, and c and the two graphs obtained from the graphs of Fig. 5 a and b by interchanging the external particles. Analogously, the function $2i\varphi_2(s_1, s_2, s_3; \sigma)$ is equal to the sum of the discontinuities of three Feynman integrals along the cut coming from the singularity at $s_1 = 4M^2$. These integrals correspond to the graphs shown in Fig. 6 a and b and the graph obtained from the graph of Fig. 6 a by interchanging the external particles. The dotted line in this figure represents a particle with the mass $\sqrt{\sigma}$, where $\sqrt{\sigma} > m$.

By the method proposed in the paper of Landau[6] we can verify that, in accordance with our initial assumption, the graphs of Figs. 5 a, b, c and 6 a, b do not contain singularities that are not accounted for by a Mandelstam-type representation. We can therefore write down such a representation for the above-mentioned Feynman integrals. According to the results of Cutkosky,[3] on the other hand, all singularities of the functions φ_1 and φ_2 are simultaneously singularities of any one of the above-mentioned Feynman integrals and lie in the region $s_1 \geq 4M^2$. The discontinuities of the functions $2i\varphi_1$ and $2i\varphi_2$ along the cuts coming from these discontinuities are equal to the sums of the discontinuities of the corresponding Feynman integrals.

Repeating the general considerations leading from formula (7) to the equalities (11) and (31), we readily conclude that the functions φ_1 and φ_2 can be represented in the form

$$\varphi_1(s_1, s_2, s_3; \sigma) = \frac{1}{\pi} \int\limits_{(2m+\sqrt{\sigma})^2}^{\infty} \left[\frac{f_{12}^{(1)}(s_1, \sigma', \sigma)}{\sigma' - s_2} + \frac{f_{13}^{(1)}(s_1, \sigma', \sigma)}{\sigma' - s_3}\right] d\sigma', \quad (36)$$

$$\varphi_2(s_1, s_2, s_3) = \frac{1}{\pi} \int\limits_{16m^2}^{\infty} \left[\frac{f_{12}^{(2)}(s_1, \sigma')}{\sigma' - s_2} + \frac{f_{13}^{(2)}(s_1, \sigma')}{\sigma'' - s_3}\right] d\sigma'. \quad (37)$$

Since $f_{ik}^{(1)}$ and $f_{ik}^{(2)}$ are expressed in terms of the discontinuities of definite Feynman integrals, they can be computed without any principal difficulties (in any case, by numerical methods).

Substitution of (36) and (37) in (33) leads to the equality

$$D_1^{\mathrm{I}}(s_1, s_2, s_3) = \frac{1}{\pi} \int\limits_{\sigma_0'(s_1)}^{\infty} d\sigma' \left[\frac{V_{21}(\sigma', s_1)}{\sigma' - s_2} + \frac{V_{31}(\sigma', s_1)}{\sigma' - \sigma_3}\right] + \Delta_1''(s_1, s_2, s_3), \quad (38)$$

$$\begin{aligned} V_{i1}(s_i, s_1) &= f_{1i}^{(2)}(s_1, s_i) + \gamma_{21}^2 [f_{1i}^{(1)*}(s_1, s_i; m^2) + f_{1i}^{(1)}(s_1, s_i; m^2)] + \gamma_{30}^2 [f_{1i}^{(1)*}(s_1, s_i; M^2) \\ &+ f_{1i}^{(1)}(s_1, s_i; M^2)] \\ &+ \frac{1}{\pi} \int\limits_{s_0}^{\infty} d\sigma [(A_2^{\mathrm{I}}(\sigma, s_1) + A_3^{\mathrm{I}}(\sigma, s_1)) f_{1i}^{(1)*}(s_1, s_i; \sigma) \\ &- (A_2^{\mathrm{I}*}(\sigma, s_1) + A_3^{\mathrm{I}*}(\sigma, s_1)) f_{1i}^{(1)}(s_1, s_i; \sigma)] \end{aligned} \quad (39)$$

where $i = 2, 3$.

The functions $V_{i1}(s_i, s_1)$ are different from zero only for $s_i > 9m^2$, $s_1 > 4M^2$. If we add to expression (38) the terms obtained from the unitarity conditions for the other channels, we find that the contribution from $D_1^I(s_1, s_2, s_3)$ to the spectral function $A_{21}^I(s_2, s_1)$ is equal to

$$D_{21}^I = V_{21}(s_2, s_1) + V_{12}(s_1, s_2), \tag{40}$$

where V_{12} is obtained from the unitarity conditions for the second channel in a similar way as in the case of V_{21} (s_2 is the energy). By virtue of the symmetry of our problem

$$V_{21}(\sigma', \sigma'') = V_{12}(\sigma', \sigma''). \tag{41}$$

The total value of the spectral function A_{21}^I is, according to (30) and (40), equal to

$$A_{21}^I(s_2, s_1) = \sum_{l=1}^{III} W_{21}^{(l)} + D_{21}^I(s_2, s_1), \tag{42}$$

where $W_{12}^{(l)}$ and D_{21}^I are defined by (28) and (40). Similar expressions can be found for all spectral functions of each of the five scattering amplitudes. Together, these expressions form a complete system of integral equations for all these functions.

In conclusion we note that for the extension of this method to any more complicated cases it is necessary and sufficient that all graphs of the type of Fig. 2 b (quadrangles with sides consisting of several parallel lines) have no singularities which cannot be dealt with by a Mandelstam-type representation. All anomalous singularities of graphs of the quadrangular type with sides consisting of a single line can be separated out of the amplitude and be accounted for in the manner described above.

---

[1] S. Mandelstam, Phys. Rev. **112**, 1344 (1958).

[2] S. Mandelstam, Phys. Rev. Lett. **4**, 84 (1960).

[3] R. E. Cutkosky, J. Math. Phys., in press.

[4] K. Ter-Martirosyan, JETP **39**, 827 (1960), Soviet Phys. JETP **12**, 575 (1961).

[5] Karplus, Sommerfield, and Wichman, Phys. Rev. **111**, 1187 (1958) and **114**, 375 (1959).

[6] L. D. Landau, JETP **37**, 62 (1959), Soviet Phys. JETP **10**, 45 (1960).

[7] J. Tarsky, J. Math. Phys., in press.

Translated by R. Lipperheide
328

SOVIET PHYSICS JETP VOLUME 12, NUMBER 6 JUNE, 1961

POLARIZATION PHENOMENA IN THE COMPTON EFFECT

G. V. FROLOV

Radium Institute, Academy of Sciences, U.S.S.R.

Submitted to JETP editor July, 1960

J. Exptl. Theoret. Phys. (U.S.S.R.) **39**, 1829-1836 (December, 1960)

Expressions for all coefficients characterizing polarization phenomena in the Compton effect have been derived in terms of form factors that enter in the scattering amplitude. Relations derived from the invariance of the scattering amplitude under time inversion and also from crossing symmetry are established between these coefficients. The relations derived have a relativistically invariant form. The results obtained are employed to compute the polarization of recoil electrons produced in the scattering of unpolarized photons on unpolarized electrons.

INTRODUCTION

A study of the polarization in the Compton effect makes it possible to determine experimentally the scattering amplitude or to compare with experiment the amplitude calculated, for example, with the aid of the dispersion relations. For this purpose it is necessary to express various quantities, which characterize the polarization phenomena, in terms of the form factors that enter in the scattering amplitude. These quantities will henceforth be called polarization coefficients; they are defined by the formulas in (6).

Expressions for the simplest polarization coefficients (a, l_λ and c^i in our notation) in terms of the form factors were obtained by Lapidus[1] and Lapidus and Chou Kuang-Chao,[2] who used non-covariant notation. It was also shown that in scattering of unpolarized particles the expressions for polarization of the nucleons and photons in the final state coincide with the expressions for the contribution made to the cross section by the polarization of the corresponding particles in the initial state, this being a consequence of the invariance under time inversion (T invariance). In the non-covariant form, the question of the connection between the polarization phenomena, which follows from the T-invariance, was investigated in general form by Shirokov[3] and by Belen'kiĭ et al.[4]

In Sec. 1 of the present paper we obtain in a relativistically-covariant form all the relations, resulting from T invariance, between the polarization coefficients for the Compton effect, including those obtained earlier in reference 1. We also investigate the relations that follow from the crossing symmetry and charge conjugation. In Sec. 2 we obtain expressions, in terms of the form factors that enter into the scattering amplitude, for all the polarization coefficients, some of which were known before.[1,2] In Sec. 3 the formulas obtained are used to calculate the polarization of the recoil electrons in scattering of unpolarized photons by unpolarized electrons.

1. CONNECTION BETWEEN POLARIZATION PHENOMENA

The matrix element of the Compton effect on the nucleon will be written in the form

$$S_{if} = e'_\mu e_\nu \bar{u}(p') S_{\mu\nu} u(p).$$

Here and henceforth we shall use the following notation: e_μ — polarization vector; k — photon momentum; p — momentum; E — energy; M — nucleon mass. The primes denote the final state. The polarization of the nucleons is characterized by the density matrix[5] ρ_N:

$$\rho_N = {}^1\!/_2 (1 + \Sigma Z)\, \eta^{(+)}(p);$$

$$\Sigma Z = \Sigma_\mu Z_\mu, \qquad \Sigma_\mu = i\gamma_5\gamma_\mu, \qquad \eta^{(+)}(p) = \frac{M - i\hat{p}}{2E}\gamma_4,$$

where Z_μ is the 4-vector of nucleon polarization and $\eta^{(+)}$ is the operator of projection on a state with positive energy.

The polarization of the photons is described by the following density matrix[5]

$$\rho_\gamma = {}^1\!/_2 (1 + \xi\tau),$$

where ξ^i are Stokes parameters and τ^i are Pauli matrices.

The polarization matrix of the density of the final state has the form

$$(\rho_f)_{\mu\alpha}$$

$$= \frac{(M-i\hat{p}')\,S_{\mu\nu}\,(1+\xi\tau)_{\nu\beta}\,(1+\Sigma Z)\,(M-i\hat{p})\,\bar{S}_{\beta\alpha}\,(M-i\hat{p}')\gamma_4}{2E'\,\mathrm{Sp}\,\{S_{\mu\nu}\,(1+\xi\tau)_{\nu\beta}\,(1+\Sigma Z)\,(M-i\hat{p})\,\bar{S}_{\beta\mu}\,(M-i\hat{p}')\}}; \qquad (1)$$

here $\bar{S}_{\beta\alpha} = \gamma_4 S^{+}_{\alpha\beta}\gamma_4$.

It will prove to be more convenient to rewrite (1) in a more symmetric form, using the equalities

$$(M-i\hat{p})^2 = 2M\,(M-i\hat{p}),$$

$$(1+\Sigma Z)\,(M-i\hat{p}) = (M-i\hat{p})\,(1+\Sigma Z).$$

We then obtain the following quantities for the various polarization phenomena: the differential cross section

$$d\sigma/d\Omega \sim R = \mathrm{Sp}\,\{(M-i\hat{p}')\,S_{\mu\nu}\,(1+\xi\tau)_{\nu\beta}\,(M-i\hat{p})$$
$$\times(1+\Sigma Z)\,(M-i\hat{p})\,\bar{S}_{\beta\mu}\,(M-i\hat{p}')\}; \qquad (2)$$

the polarization of the scattered photons

$$\xi'^{j} R = \tau^{j}_{\alpha\mu}\,\mathrm{Sp}\,\{(M-i\hat{p}')\,S_{\mu\nu}\,(1+\xi\tau)_{\nu\beta}\,(M-i\hat{p})$$
$$\times(1+\Sigma Z)\,(M-i\hat{p})\,\bar{S}_{\beta\alpha}\,(M-i\hat{p}')\}; \qquad (3)$$

the polarization of the recoil nucleons

$$Z'_{\lambda} R = \mathrm{Sp}\,\{\Sigma_{\lambda}\,(M-i\hat{p}')\,S_{\mu\nu}\,(1+\xi\tau)_{\nu\beta}\,(M-i\hat{p})$$
$$\times(1+\Sigma Z)\,(M-i\hat{p})\,\bar{S}_{\beta\mu}\,(M-i\hat{p}')\}; \qquad (4)$$

and the polarization correlation

$$Q'^{j}_{\lambda} R = \tau^{j}_{\alpha\mu}\,\mathrm{Sp}\,\{\Sigma_{\lambda}\,(M-i\hat{p}')\,S_{\mu\nu}\,(1+\xi\tau)_{\nu\beta}\,(M-i\hat{p})$$
$$\times(1+\Sigma Z)\,(M-i\hat{p})\,\bar{S}_{\beta\alpha}\,(M-i\hat{p}')\}. \qquad (5)$$

Let us rewrite (2) — (5) by introducing several polarization coefficients:

$$\begin{aligned}
R &= a + c^{i}\xi^{i} + b_{\varkappa}Z_{\varkappa} + d^{i}_{\varkappa}\xi^{i}Z_{\varkappa},\\
\xi'^{j} R &= f^{j} + h^{ji}\xi^{i} + g^{j}_{\varkappa}Z_{\varkappa} + t^{ji}_{\varkappa}\xi^{i}Z_{\varkappa},\\
Z'_{\lambda} R &= l_{\lambda} + m^{i}_{\lambda}\xi^{i} + n_{\lambda\varkappa}Z_{\varkappa} + q^{i}_{\lambda\varkappa}\xi^{i}Z_{\varkappa},\\
Q'^{j}_{\lambda} R &= u^{j}_{\lambda} + v^{ji}_{\lambda}\xi^{i} + x^{j}_{\lambda\varkappa}Z_{\varkappa} + y^{ji}_{\lambda\varkappa}\xi^{i}Z_{\varkappa}.
\end{aligned} \qquad (6)$$

The formulas that determine these coefficients follow from (2) — (5). The experiments by which these coefficients are measured are also clear. In order to obtain the relations between the polarization coefficients we make use of the invariance of the scattering amplitude. Inasmuch as the time-inversion operation is equivalent in the case of the Compton effect to the product of the crossing-symmetry and the charge-conjugation transformations,[6] we shall henceforth take T invariance to mean the invariance of the scattering amplitude with respect to the product of these two transformations. We therefore have[6]

$$\begin{aligned}
S_{\mu\nu}\,(p,\ p',\ k,\ k') &= S_{\nu\mu}\,(p,\ p' -k',\ -k),\\
\bar{S}_{\beta\alpha}\,(p,\ p',\ k,\ k') &= \bar{S}_{\alpha\beta}\,(p,\ p',\ -k',\ -k);
\end{aligned} \qquad (7)$$

$$\begin{aligned}
S_{\mu\nu}\,(p,\ p',\ k,\ k') &= CS^{t}_{\mu\nu}\,(-p',\ -p,\ k,\ k')\,C^{-1},\\
\bar{S}_{\beta\alpha}\,(p,\ p',\ k,\ k') &= C\bar{S}^{t}_{\beta\alpha}\,(-p',\ -p,\ k,\ k')\,C^{-1};
\end{aligned} \qquad (8)$$

$$\begin{aligned}
S_{\mu\nu}\,(p,\ p',\ k,\ k') &= CS^{t}_{\nu\mu}\,(-p',\ -p,\ -k',\ -k)\,C^{-1},\\
\bar{S}_{\beta\alpha}\,(p,\ p',\ k,\ k') &= C\bar{S}^{t}_{\alpha\beta}\,(-p',\ -p,\ -k',\ -k)\,C^{-1}.
\end{aligned} \qquad (9)$$

The superscript t denotes transposition over the spinor indices, and C is the charge-conjugation matrix. Inserting (9) in the explicit expressions for the polarization coefficients, we obtain the relations between them due to the T invariance

$$\begin{gathered}
a = \tilde{\bar{a}}, \qquad b_{\varkappa} = \tilde{\bar{l}}_{\varkappa}, \qquad c^{i} = \pm\tilde{\bar{f}}^{i}, \qquad g^{i}_{\varkappa} = \pm\tilde{\bar{m}}^{i}_{\varkappa},\\
d^{i}_{\varkappa} = \pm\tilde{\bar{u}}^{i}_{\varkappa}, \qquad h^{ij} = \pm\tilde{\bar{h}}^{ji}, \qquad n_{\lambda\varkappa} = \tilde{\bar{n}}_{\varkappa\lambda},\\
t^{ij}_{\varkappa} = \pm\tilde{\bar{v}}^{ji}_{\varkappa}, \qquad x^{i}_{\lambda\varkappa} = \pm\tilde{\bar{q}}^{i}_{\varkappa\lambda}, \qquad y^{ji}_{\lambda\varkappa} = \pm\tilde{\bar{y}}^{ij}_{\varkappa\lambda}.
\end{gathered} \qquad (10)$$

Here

$$\tilde{\bar{\beta}}(p,\ p',\ k,\ k') = \beta(-p',\ -p,\ -k',\ -k),$$

where β is any polarization coefficient. The plus sign corresponds to an even multiple of two among the Latin indices pertaining to photon polarization, while the minus sign corresponds to an odd number. It is seen that T invariance relates the coefficients that are symmetrical with respect to the principal diagonal in (6).

With the aid of (7) or (8) we obtain

$$\begin{gathered}
a = \tilde{a}, \qquad b_{\varkappa} = \tilde{b}_{\varkappa}, \qquad l_{\varkappa} = \tilde{l}_{\varkappa}, \qquad c^{i} = \bar{c}^{i},\\
f^{i} = \bar{f}^{i}, \qquad h^{ij} = \bar{h}^{ij}, \qquad n_{\lambda\varkappa} = \tilde{n}_{\lambda\varkappa}, \qquad t^{ij}_{\varkappa} = \pm\tilde{t}^{ji}_{\varkappa},\\
v^{ij}_{\varkappa} = \pm\tilde{v}^{ji}_{\varkappa}, \qquad x^{i}_{\lambda\varkappa} = \bar{x}^{i}_{\varkappa\lambda}, \qquad q^{i}_{\lambda\varkappa} = \bar{q}^{i}_{\varkappa\lambda}, \qquad y^{ij}_{\lambda\varkappa} = \bar{y}^{ij}_{\varkappa\lambda};
\end{gathered} \qquad (11)$$

$$m^{i}_{\varkappa} = \pm\tilde{u}^{i}_{\varkappa}, \qquad d^{i}_{\varkappa} = \pm\tilde{g}^{i}_{\varkappa}, \qquad (12)$$

where

$$\tilde{\beta}(p,\ p',\ k,\ k') = \beta(p,\ p',\ -k',\ -k),$$
$$\bar{\beta}(p,\ p',\ k,\ k') = \beta(-p',\ -p,\ k,\ k');$$

β is any polarization coefficient. The sign rule is the same as in (10).

In most cases the crossing symmetry and the charge conjugation yield relations between coefficients which are already related through T invariance. Therefore the relations between the coefficients obtained with the aid of crossing or charge symmetry, are equivalent to additional limitations imposed on the coefficients. Formulas (11) are written in a form that highlights this fact. The novelty compared with (10) lies in relations (12), which have, however, a different character than (10). By virtue of the conservation laws, the scattering is characterized by two invariants, κ_1 and κ_2

$$M^2\varkappa_1 = 2pk = 2p'k', \qquad M^2\varkappa_2 = -2p'k = -2pk'.$$

The invariants do not change under the substitutions $k \rightleftarrows -k'$ and $p \rightleftarrows -p'$, whereas the substitutions $k \rightleftarrows -k'$ or $p \rightleftarrows -p'$ results in an interchange $\kappa_1 \rightleftarrows \kappa_2$. Consequently the equations in (12) relate, for example, g^i_κ and d^i_κ whenever the arguments of one of these quantities are in the non-physical region

2. FORMULAS FOR THE POLARIZATION COEFFICIENTS

Considerations of T invariance and gauge invariance cause the most general expression for $S_{\mu\nu}$ to have the following form:[6]

$$\begin{aligned} S_{\mu\nu} = {} & A_1\frac{P_\mu P_\nu}{P^2} + A_2\frac{P_\mu P_\nu}{P^2}\frac{i\hat{K}}{M} + A_3\frac{N_\mu N_\nu}{N^2} + A_4\frac{N_\mu N_\nu}{N^2}\frac{i\hat{K}}{M} \\ & + \frac{A_5}{2P^2K^2}(P_\mu N_\nu - N_\mu P_\nu)\, i\gamma_5 - \frac{A_6}{2P^2K^2}(P_\mu N_\nu + N_\mu P_\nu)\frac{\gamma_5\hat{K}}{M}. \end{aligned} \tag{13}$$

Here the form factors A_i are functions of the invariants κ_1 and κ_2 only;

$$K_\mu = {}^1/_2\,(k_\mu + k'_\mu), \qquad Q_\mu = k_\mu - k'_\mu,$$
$$P_\mu = {}^1/_2\,(p_\mu + p'_\mu) - \frac{(p+p')\,K}{2K^2}K_\mu,$$
$$N_\mu = i\varepsilon_{\mu\nu\rho\sigma}P_\nu K_\rho Q_\sigma.$$

The vectors K, P, Q, and N form an orthogonal system. The unit photon-polarization vectors are chosen as follows:

$$\mathbf{e}_1 = \mathbf{e}'_1 = [\mathbf{k}\times\mathbf{k}']/|[\mathbf{k}\times\mathbf{k}']|, \qquad \mathbf{e}_2 = [\mathbf{k}\times\mathbf{e}_1]/|\mathbf{k}|,$$
$$\mathbf{e}'_2 = [\mathbf{k}'\times\mathbf{e}_1{}']/|\mathbf{k}'|. \tag{14}$$

With the unit vectors so chosen, the Stokes parameter ξ^2 is related to the probability of circular polarization of the photon, while the parameters ξ^1 and ξ^3 are connected with the probabilities of linear polarization along axes that make an angle of 45° (reference 5). Substituting (13) in (2) — (5) and using definitions (6), we obtain explicit expressions for the polarization coefficients in terms of the form factors:

$$\begin{aligned} a = {} & \alpha_1(|A_1|^2 + |A_3|^2) - 2\alpha_2|A_5|^2 - \varkappa_1\varkappa_2(|A_2|^2 + |A_4|^2) \\ & + 2\alpha_4|A_6|^2 + 2\alpha_3\,\mathrm{Re}\,(A_1A_2^* + A_3A_4^*), \end{aligned}$$

$$c^1 = c^2 = h^{13} = h^{31} = h^{32} = h^{23} = 0,$$

$$\begin{aligned} c^3 = {} & \alpha_1(|A_3|^2 - |A_1|^2) - \varkappa_1\varkappa_2(|A_4|^2 - |A_2|^2) \\ & - 2\alpha_3\,\mathrm{Re}\,(A_1A_2^* - A_3A_4^*), \end{aligned}$$

$$\begin{aligned} h^{11} = {} & -2\{\alpha_1\,\mathrm{Re}\,A_1A_3^* - \varkappa_1\varkappa_2\,\mathrm{Re}\,A_2A_4^* + \alpha_2|A_5|^2 \\ & + \alpha_4|A_6|^2 + \alpha_3\,\mathrm{Re}\,(A_1A_4^* + A_2A_3^*)\}, \end{aligned}$$

$$h^{12} = 2\,\mathrm{Im}\,\{\alpha_1A_1A_3^* - \varkappa_1\varkappa_2A_2A_4^* + \alpha_3(A_1A_4^* + A_2A_3^*)\},$$

$$b_\lambda = t^{33}_\lambda = 4N_\lambda\,\mathrm{Im}\,(A_1A_2^* + A_3A_4^*)/M^3,$$

$$\begin{aligned} d^1_\lambda = {} & F_\lambda\,\mathrm{Im}\,\{4(A_3A_5^* - A_1A_5^*) + \alpha_2(A_2A_6^* + A_4A_6^*) \\ & - \alpha_3(A_2A_5^* - A_4A_5^* + A_1A_6^* + A_3A_6^*)\} \\ & - 2G_\lambda\,\mathrm{Im}\,\{\alpha_1(A_1A_6^* + A_3A_6^*) - \alpha_2(A_2A_5^* - A_4A_5^*) \\ & + \alpha_3(A_2A_6^* + A_4A_6^*)\}, \end{aligned}$$

$$\begin{aligned} d^2_\lambda = {} & F_\lambda\,\mathrm{Re}\,\{\alpha_2(A_2A_6^* - A_4A_6^*) - 4(A_1A_5^* + A_3A_5^*) \\ & - \alpha_3(A_2A_5^* + A_4A_5^* + A_1A_6^* - A_3A_6^*)\} \\ & - 2G_\lambda\,\mathrm{Re}\,\{\alpha_1(A_1A_6^* - A_3A_6^*) - \alpha_2(A_2A_5^* + A_4A_5^*) \\ & + \alpha_3(A_2A_6^* - A_4A_6^*)\}, \end{aligned}$$

$$d^3_\lambda = 4N_\lambda\,\mathrm{Im}\,\{A_3A_4^* - A_1A_2^* + 2A_5A_6^*)/M^3,$$

$$t^{11}_\lambda = t^{22}_\lambda = -4N_\lambda\,\mathrm{Im}\,\{A_1A_4^* + A_3A_2^*)/M^3,$$

$$t^{12}_\lambda = 4N_\lambda\,\mathrm{Re}\,(A_2A_3^* - A_1A_4^* + 2A_5A_6^*)/M^3,$$

$$\begin{aligned} t^{13}_\lambda = {} & F_\lambda\,\mathrm{Im}\,\{4(A_1A_5^* + A_3A_5^*) + \alpha_2(A_2A_6^* - A_4A_6^*) \\ & + \alpha_3(A_2A_5^* + A_4A_5^* - A_1A_6^* + A_3A_6^*)\} \\ & - 2G_\lambda\,\mathrm{Im}\,\{\alpha_1(A_1A_6^* - A_3A_6^*) + \alpha_2(A_2A_5^* + A_4A_5^*) \\ & + \alpha_3(A_2A_6^* - A_4A_6^*)\}, \end{aligned}$$

$$\begin{aligned} t^{23}_\lambda = {} & F_\lambda\,\mathrm{Re}\,\{4(A_3A_5^* - A_1A_5^*) - \alpha_2(A_2A_6^* + A_4A_6^*) \\ & + \alpha_3(A_4A_5^* - A_2A_5^* + A_1A_6^* + A_3A_6^*)\} \\ & + 2G_\lambda\,\mathrm{Re}\,\{\alpha_1(A_1A_6^* + A_3A_6^*) \\ & - \alpha_2(A_4A_5^* - A_2A_5^*) + \alpha_3(A_2A_6^* + A_4A_6^*)\}, \end{aligned}$$

$$\begin{aligned} q^1_{\lambda\varkappa} = {} & \mathrm{Re}\,\{T_{\lambda\varkappa}(A_1A_5^* - A_3A_5^*) + B_{\lambda\varkappa}(A_4A_5^* - A_2A_5^*) \\ & + C_{\lambda\varkappa}(A_1A_6^* + A_3A_6^*) - D_{\lambda\varkappa}(A_2A_6^* + A_4A_6^*)\}, \end{aligned}$$

$$\begin{aligned} q^2_{\lambda\varkappa} = {} & \mathrm{Im}\,\{B_{\lambda\varkappa}(A_2A_5^* + A_4A_5^*) - T_{\lambda\varkappa}(A_1A_5^* + A_3A_5^*) \\ & + C_{\lambda\varkappa}(A_3A_6^* - A_1A_6^*) + D_{\lambda\varkappa}(A_2A_6^* - A_4A_6^*)\}, \end{aligned}$$

$$\begin{aligned} q^3_{\lambda\varkappa} = {} & I_{\lambda\varkappa}[\alpha_1(|A_3|^2 - |A_1|^2) - \varkappa_1\varkappa_2(|A_4|^2 - |A_2|^2) \\ & - 2\alpha_3\,\mathrm{Re}\,(A_1A_2^* - A_3A_4^*)] + 2H_\lambda G_\varkappa\alpha_2(|A_4|^2 - |A_2|^2) \\ & + H_\lambda F_\varkappa[4\mathrm{Re}\,(A_1A_2^* - A_3A_4^* + 2A_5A_6^*) \\ & - \alpha_3(|A_4|^2 - |A_2|^2)] + L_\lambda G_\varkappa[4\mathrm{Re}\,(A_1A_2^* - A_3A_4^* - 2A_5A_6^*) \\ & - \alpha_3(|A_4|^2 - A_2|^2)] + 2M^2L_\lambda F_\varkappa[|A_3|^2 - |A_1|^2 \\ & - \alpha_3\,\mathrm{Re}\,(A_1A_2^* - A_3A_4^*) - \alpha_5(|A_4|^2 - |A_2|^2)]/(pp'), \end{aligned}$$

$$\begin{aligned} n_{\lambda\varkappa} = {} & I_{\lambda\varkappa}[\alpha_1(|A_1|^2 + |A_3|^2) + 2\alpha_2|A_5|^2 - 2\alpha_4|A_6|^2 \\ & - \varkappa_1\varkappa_2(|A_2|^2 + |A_4|^2) + 2\alpha_3\,\mathrm{Re}\,(A_1A_2^* + A_3A_4^*)] \\ & + 2H_\lambda G_\varkappa[\alpha_2(|A_2|^2 + |A_4|^2) + 2\alpha_1|A_6|^2] \\ & - (H_\lambda F_\varkappa + L_\lambda G_\varkappa)[4\mathrm{Re}\,(A_1A_2^* + A_3A_4^*) + \alpha_3(|A_2|^2 + |A_4|^2 \\ & - 2|A_6|^2)] + 2M^2L_\lambda F_\varkappa[|A_1|^2 + |A_3|^2 + 2|A_5|^2 \\ & + \alpha_3\,\mathrm{Re}\,(A_1A_2^* + A_3A_4^*) \\ & - \alpha_5(|A_2|^2 + |A_4|^2) - \alpha_6|A_6|^2]/(pp'), \end{aligned}$$

$$\begin{aligned} y^{12}_{\lambda\varkappa} = {} & 2\mathrm{Im}\,\{I_{\lambda\varkappa}[\alpha_1A_1A_3^* - \varkappa_1\varkappa_2A_2A_4^* + \alpha_3(A_1A_4^* + A_2A_3^*)] \\ & + 2H_\lambda G_\varkappa\alpha_2A_2A_4^* - H_\lambda F_\varkappa[2(A_1A_4^* + A_2A_3^* + 2A_5A_6^*) \\ & + \alpha_3A_2A_4^*] - L_\lambda G_\varkappa[2(A_1A_4^* + A_2A_3^* - 2A_5A_6^*) + \alpha_3A_2A_4^*] \\ & + M^2L_\lambda F_\varkappa[2A_1A_3^* + \alpha_3(A_1A_4^* + A_2A_3^*) - 2\alpha_5A_2A_4^*]/(pp'), \end{aligned}$$

$$y^{13}_{\lambda\varkappa} = \mathrm{Re}\,\{B_{\lambda\varkappa}\,(A_2A_5^* + A_4A_5^*) - T_{\lambda\varkappa}\,(A_1A_5^* + A_3A_5^*)$$
$$+ C_{\lambda\varkappa}\,(A_1A_6^* - A_3A_6^*) - D_{\lambda\varkappa}\,(A_2A_6^* - A_4A_6^*)\},$$
$$y^{23}_{\lambda\varkappa} = \mathrm{Im}\,\{T_{\lambda\varkappa}\,(A_3A_5^* - A_1A_5^*) + B_{\lambda\varkappa}\,(A_2A_5^* - A_4A_5^*)$$
$$+ C_{\lambda\varkappa}\,(A_1A_6^* + A_3A_6^*) - D_{\lambda\varkappa}\,(A_2A_6^* + A_4A_6^*)\},$$
$$y^{11}_{\lambda\varkappa} = 2\,\{I_{\lambda\varkappa}\,[\alpha_2\,|A_5|^2 - \alpha_1\,\mathrm{Re}\,A_1A_3^* + \varkappa_1\varkappa_2\,\mathrm{Re}\,A_2A_4^*$$
$$+ \alpha_4\,|A_6|^2 - \alpha_3\,\mathrm{Re}\,(A_1A_4^* + A_2A_3^*)]$$
$$+ (H_\lambda F_\varkappa + L_\lambda G_\varkappa)\,[2\mathrm{Re}\,(A_1A_4^* + A_2A_3^*)$$
$$+ \alpha_3\,(\mathrm{Re}\,A_2A_4^* - |A_6|^2)] - 2H_\lambda G_\varkappa\,[\alpha_1\,|A_6|^2 + \alpha_2\,\mathrm{Re}\,A_2A_4^*]$$
$$+ M^2L_\lambda F_\varkappa\,[2\,|A_5|^2 - 2\mathrm{Re}\,A_1A_3^* - \alpha_3\,\mathrm{Re}\,(A_1A_4^* + A_2A_3^*)$$
$$+ 2\alpha_5\,\mathrm{Re}\,A_2A_4^* + \alpha_6\,|A_6|^2]/(pp'). \qquad (15)$$

The differences between h^{22} and h^{11}, h^{33} and a, $y^{22}_{\lambda\kappa}$ and $y^{11}_{\lambda\kappa}$, and $y^{3}_{\lambda\kappa}$ and $n_{\lambda\kappa}$ are due to the difference in sign between the terms with $|A_5|^2$ and $|A_6|^2$.

The following notation is used:

$$\alpha_1 = 4 - \varkappa_1 - \varkappa_2, \qquad \alpha_2 = \varkappa_1 + \varkappa_2, \qquad \alpha_3 = \varkappa_1 - \varkappa_2,$$
$$\alpha_4 = \varkappa_1 + \varkappa_2 - \varkappa_1\varkappa_2, \quad \alpha_5 = [2\,(\varkappa_1 + \varkappa_2) - (\varkappa_1 - \varkappa_2)^2]/8,$$
$$\alpha_6 = [2\,(\varkappa_1 + \varkappa_2) + (\varkappa_1 - \varkappa_2)^2]/4,$$
$$L_\lambda = \left(p_\lambda + \frac{(pp')}{M^2}\,p'_\lambda\right) \Big/ M, \qquad F_\varkappa = \left(p'_\varkappa + \frac{(pp')}{M^2}\,p_\varkappa\right) \Big/ M,$$
$$H_\lambda = \left(K_\lambda + \frac{(Kp')}{M^2}\,p'_\lambda\right) \Big/ M, \qquad G_\varkappa = \left(K_\varkappa + \frac{(Kp)}{M^2}\,p_\varkappa\right) \Big/ M,$$
$$I_{\lambda\varkappa} = \delta_{\lambda\varkappa} - p_\lambda p'_\varkappa/(pp'), \qquad T_{\lambda\varkappa} = 4i\varepsilon_{\lambda\varkappa\mu\sigma}\,p_\sigma p'_\mu/M^2,$$
$$B_{\lambda\varkappa} = 4\,[i\varepsilon_{\lambda\varkappa\mu\sigma}K_\sigma Q_\mu + N_\varkappa p'_\lambda/M^2 - N_\lambda p_\varkappa/M^2]/M^2,$$
$$C_{\lambda\varkappa} = 4\,[(N_\varkappa p'_\lambda + N_\lambda p_\varkappa)/M^2 - i\varepsilon_{\lambda\varkappa\mu\sigma}K_\sigma\,(p_\mu + p'_\mu)]/M^2,$$
$$D_{\lambda\varkappa} = [4\,(N_\varkappa K_\lambda + N_\lambda K_\varkappa)/M^2$$
$$+ i\,(\varkappa_1 - \varkappa_2)\,\varepsilon_{\lambda\varkappa\mu\sigma}K_\sigma\,(p_\mu + p'_\mu)]/M^2. \qquad (16)$$

We note that the following equalities hold:

$$Lp' = Hp' = Fp = Gp = 0,$$
$$I_{\lambda\varkappa}p_\varkappa = I_{\lambda\varkappa}p'_\lambda = T_{\lambda\varkappa}p_\varkappa = T_{\lambda\varkappa}p'_\lambda = B_{\lambda\varkappa}p_\varkappa$$
$$= B_{\lambda\varkappa}p'_\lambda = C_{\lambda\varkappa}p_\varkappa = C_{\lambda\varkappa}p'_\lambda = D_{\lambda\varkappa}p_\varkappa = D_{\lambda\varkappa}p'_\lambda = 0. \qquad (17)$$

It follows from (6) and (7) that $p'Z' = p'Q'^{j} = 0$.

The formulas for the remaining coefficients can be obtained from (15) with the aid of relations (10) and (12).

Let us derive expressions that show the behavior of the quantities contained in (15), for different substitutions of the momenta. The substitution $k \rightleftarrows -k'$ yields

$$L_\lambda \leftrightarrows L_\lambda, \qquad F_\varkappa \leftrightarrows F_\varkappa, \qquad H_\lambda \leftrightarrows -H_\lambda, \quad G_\varkappa \rightleftarrows -G_\varkappa,$$
$$I_{\lambda\varkappa} \rightleftarrows I_{\lambda\varkappa}, \qquad T_{\lambda\varkappa} \rightleftarrows T_{\lambda\varkappa}, \qquad B_{\lambda\varkappa} \leftrightarrows -B_{\lambda\varkappa}, \quad C_{\lambda\varkappa} \leftrightarrows -C_{\lambda\varkappa},$$
$$D_{\lambda\varkappa} \rightleftarrows D_{\lambda\varkappa}, \qquad A_i \leftrightarrows A_i\,(i = 1, 3, 5, 6), \quad A_i \rightleftarrows -A_i\,(i = 2, 4). \qquad (18)$$

From the substitutions $k \rightleftarrows -k'$ and $p \rightleftarrows -p'$ we get

$$H_\lambda \leftrightarrows -G_\lambda, \quad L_\lambda \leftrightarrows -F_\lambda, \qquad I_{\lambda\varkappa} \leftrightarrows I_{\varkappa\lambda}, \qquad T_{\lambda\varkappa} \leftrightarrows T_{\varkappa\lambda},$$
$$B_{\lambda\varkappa} \leftrightarrows B_{\varkappa\lambda}, \quad C_{\lambda\varkappa} \rightleftarrows -C_{\varkappa\lambda}, \quad D_{\lambda\varkappa} \leftrightarrows -D_{\varkappa\lambda}, \qquad A_i \leftrightarrows A_i. \qquad (19)$$

We see from (15) that the expression for any polarization coefficient β has the form

$$\beta = \sum_n \mu_n\varphi_n$$

where μ_n is a known tensor quantity and φ_n is a definite bilinear combination of the form factors A_i. Knowing β, we can readily determine all the φ_n, by taking various projections. This also determines the quantity $\overset{\approx}{\beta}_n$

$$\overset{\approx}{\beta}_n = \sum_n \overset{\approx}{\mu}_n\,\overset{\approx}{\varphi}_n = \sum_n \overset{\approx}{\mu}_n\varphi_n,$$

inasmuch as $\overset{\approx}{\mu}_n$ is obtained from μ_n with the aid of (19). Experiments on the determination of quantities which are connected by relation (10) are not independent. In particular, some of the relations (10) are merely equalities, namely

$$b_\varkappa = l_\varkappa, \qquad c^i = \pm f^i, \qquad h^{ij} = \pm h^{ji}, \qquad g^3_\varkappa = m^3_\varkappa,$$
$$d^3_\lambda = u^3_\lambda, \qquad t^{ij}_\varkappa = \pm v^{ji}_\varkappa \qquad (ij = 11, 22, 33, 12). \qquad (20)$$

The sign rule is the same as in (10). The first two equalities were derived earlier.[1] The coefficient connected with the β by means of relation (12) has the form

$$\tilde{\beta} = \sum_n \tilde{\mu}_n\tilde{\varphi}_n.$$

With the aid of (18) we can express $\overset{\approx}{\varphi}_n$ in terms of the form factors A_i with arguments lying in the physical region. However, $\tilde{\varphi}_n$ is a combination of form factors different from φ_n. Therefore relations (12) make it possible to obtain, for example, g^i_κ from a known value of d^i_κ, but for this purpose it is necessary to have an analytical expression for d^i_κ. With the aid of (18) and (19) we can readily verify that formulas (15) satisfy the conditions imposed by relations (11).

3. APPLICATION TO THE COMPTON EFFECT ON AN ELECTRON

Equations (15) were derived under most general assumptions regarding the scattering amplitude. Therefore, if the amplitude is known in some approximation, it is sufficient to recast it in form (13) and determine A_i, and then the polarization coefficients can be directly obtained from (15).

For the Compton effect on an electron, all the polarization coefficients were calculated in the first non-vanishing approximation by Lipps and Tolhoek.[7] By using the equations derived in the present article it is possible to calculate the polarization effect in the next higher approximation and find the radiative corrections for the existing expressions. In addition, certain polarization effects appear in the second approximation for the first time.

In fact, as can be seen from (15), some polarization effects are determined by imaginary parts of expressions of the type $A_iA_j^*$, whereas in the first approximation all the A_i are real. The expressions obtained for A_i in the second approximation with the aid of the paper of Brown and Feynman[8] are very cumbersome. We cite therefore only the simplest result — the expression for b_λ, which characterizes the polarization of the recoil electrons, and also the azimuthal asymmetry in the scattering of unpolarized photons by polarized electrons ($b_\lambda = 0$ in the first approximation):

$$b_\lambda = \frac{\pi N_\lambda}{m^3(\varkappa_1\varkappa_2 - \varkappa_1 - \varkappa_2)} \Big\{ \ln(1-\varkappa_1)\Big[1 + \frac{\varkappa_2}{\varkappa_1} - \frac{4}{\varkappa_1} - \frac{3}{\varkappa_2} - \frac{\varkappa_2}{\varkappa_1^2} + 8\frac{\varkappa_1}{\varkappa_2} - 3\frac{\varkappa_1^2}{\varkappa_2}\Big] - \frac{4y}{\sinh 2y}\Big[\frac{3\varkappa_1}{2}\Big(1 + \frac{\varkappa_1}{\varkappa_2}\Big) - 7\frac{\varkappa_1}{\varkappa_2} - \frac{\varkappa_2}{\varkappa_1} - 1 + 6\Big(\frac{1}{\varkappa_1} + \frac{1}{\varkappa_2}\Big)\Big] - \frac{2P^2}{m^2(\varkappa_1 - 1)}\Big[4\Big(\frac{\varkappa_1}{\varkappa_2} + \frac{\varkappa_2}{\varkappa_1}\Big) - 3\Big(1 + \frac{\varkappa_2}{\varkappa_1^2} + \frac{1}{\varkappa_2}\Big) + \frac{2}{\varkappa_1} - \frac{1}{2(\varkappa_1 - 1)}\Big(\frac{\varkappa_1}{\varkappa_2} + \frac{\varkappa_2}{\varkappa_1}\Big)\Big]\Big\}. \tag{21}$$

The coefficient b_λ is normalized to make

$$\frac{d\sigma}{d\Omega} = \left(\frac{d\sigma}{d\Omega}\right)_0 \left(1 - \frac{\alpha}{\pi}\frac{U_1}{U_0} + \frac{\alpha}{\pi}\frac{Z_\lambda b_\lambda}{U_0}\right);$$

m is the electron mass, $(d\sigma/d\Omega)_0$ is the first-approximation cross section averaged over the polarizations, and the symbols for y, U_0, and U_1 are the same as in Sec. 52 of the book by Akhiezer and Berestetskiĭ.[5]

The complete results of the second-approximation calculations of the polarization effects in the Compton effect on an electron and in pair annihilation will be published separately.

The author is grateful to I. M. Shmushkevich for continuous interest in this work.

---

[1] L. I. Lapidus, JETP **34**, 922 (1958), Soviet Phys. JETP **7**, 638 (1958).

[2] L. I. Lapidus and Chou Kuang-Chao, JETP **38**, 201 (1960), Soviet Phys. JETP **11**, 147 (1960).

[3] M. I. Shirokov, JETP **33**, 975 (1957), Soviet Phys. JETP **6**, 748 (1958).

[4] Bilen'kiĭ, Lapidus, Puzikov, and Ryndin, JETP **35**, 959 (1958), Soviet Phys. JETP **8**, 669 (1959).

[5] A. I. Akhiezer and V. B. Berestetskiĭ, Квантовая электродинамика (Quantum Electrodynamics), 2d. Ed. Fizmatgiz, 1959.

[6] R. E. Prange, Phys. Rev. **110**, 240 (1958).

[7] F. P. Lipps and H. A. Tolhoek, Physica **20**, 85, 224 (1959).

[8] L. Brown and R. Feynman, Phys. Rev. **85**, 231 (1952).

Translated by J. G. Adashko
329

SOVIET PHYSICS JETP VOLUME 12, NUMBER 6 JUNE, 1961

EMISSION OF ELECTROMAGNETIC RADIATION IN COLLISIONS OF PARTICLES WITH SIMILAR VALUES OF e/m

E. I. MALKOV and I. M. SHMUSHKEVICH

Leningrad Physico-Technical Institute, Academy of Sciences, U.S.S.R.

Submitted to JETP editor July 30, 1960

J. Exptl. Theoret. Phys. (U.S.S.R.) **39**, 1837-1846 (December, 1960)

We calculate the differential cross section for bremsstrahlung in the collision of charged particles with equal or similar e/m values, for which quadrupole radiation predominates. We obtain formulas for the distributions in angle and energy and for the polarization, taking into account the quadrupole and dipole terms and their interference. The calculation is a classical one, which is valid for low frequencies and for sufficiently low energies of the colliding particles.

1. The bremsstrahlung emitted in electron-electron collisions has been studied theoretically by several authors,[1] who used the Born approximation; therefore their results, even for the nonrelativistic case, are valid only for particle velocities high enough to satisfy the well known condition

$$e_1 e_2/\hbar v \ll 1. \qquad (1.1)$$

In the opposite limiting case and for $v \ll c$, the calculations must be performed using the exact Coulomb wave functions. The results obtained are, from the practical point of view, a somewhat unwieldy series; the only exception to this drawback is found in the case of dipole radiation.[2]

In electron-electron collisions, as well as in general when particles with equal e/m values collide, the radiation given off is essentially of a quadrupole nature. In particular, for instance, in experiments[3] on Coulomb excitation of nuclei by multiply charged ions, the incident and target particles have about equal values of Z/A. This occurs, for example, when Mg_{12}^{24} or C_6^{12} is bombarded by Ne_{10}^{20} nuclei,[3] or in general in the collision of not very heavy nuclei, for which $Z/A \approx 1/2$. In these experiments the velocities are such as to lead to the condition that

$$Z_1 Z_2 e^2/\hbar v \gg 1, \qquad (1.2)$$

under which the Born approximation is invalid. If, however, one is interested in the emission of quanta whose energy is low compared to the nuclear kinetic energy E, i.e., such that

$$\hbar\omega \ll E = \mu v^2/2 \qquad (1.3)$$

(where μ is the reduced mass of the colliding particles, and v is their relative velocity) and if, further, (1.2) is fulfilled, the intensity of radiation and cross section can be calculated classically. This is done by first finding the particle trajectories neglecting the radiation reaction, and then finding the radiation arising from motion along the already determined trajectory. Such calculations for dipole radiation were carried out partially in the old works of Kramers and Wentzel.[4] Landau and Lifshitz[5] have given a complete treatment of the classical dipole case. In the present work we use the same classical method to study quadrupole emission, which is of fundamental importance in the cases mentioned above.

Bearing in mind that the e/m values of colliding nuclei, although very similar, may not be equal, we shall include not only the electric quadrupole, but also the electric dipole radiation, and therefore also their interference. In no case does magnetic dipole radiation occur. In our calculations the particle velocities are treated as nonrelativistic.

2. In our approximation, that is with the inclusion of dipole and quadrupole terms only, the Fourier transform $\mathbf{H}(\omega)$ of the magnetic radiation field is given by[5]

$$\mathbf{H}(\omega) = \frac{1}{c^2 R_0}\left\{[\ddot{\mathbf{d}}(\omega) \times \mathbf{n}] + \frac{1}{6c}[\dddot{\mathbf{D}}(\omega) \times \mathbf{n}]\right\}. \qquad (2.1)$$

Here $\mathbf{n}$ is the unit vector in the direction of propagation, $\dddot{D}_\alpha(\omega) = \dddot{D}_{\alpha\beta}(\omega) n_\beta$, and $\ddot{d}_\alpha(\omega)$ and $\dddot{D}_{\alpha\beta}(\omega)$ are the Fourier transforms of the corresponding time derivatives of the components of the dipole and quadrupole moments,

$$\mathbf{H}(\omega) = \frac{1}{2\pi}\int_{-\infty}^{+\infty} \mathbf{H} e^{i\omega t}\, dt, \ldots \qquad (2.2)$$

Using (2.1), we find that the energy $d\mathscr{E}_\omega$ radiated in an element of solid angle do and a frequency interval $d\omega$ is given by

$$d\mathscr{E}_\omega = \frac{d\omega do}{c^3}\Big\{\ddot{d}_\alpha(\omega)\,\ddot{d}^*_\alpha(\omega) - \ddot{d}_\alpha(\omega)\,\ddot{d}^*_\beta(\omega)\,n_\alpha n_\beta$$
$$+\frac{1}{3c}\,\mathrm{Re}\,[\ddot{d}^*_\alpha(\omega)\,\dddot{D}_{\alpha\beta}(\omega)\,n_\beta - \ddot{d}^*_\alpha(\omega)\,\dddot{D}_{\beta\gamma}(\omega)\,n_\alpha n_\beta n_\gamma]$$
$$+\frac{1}{36c^2}\,[\dddot{D}_{\alpha\beta}(\omega)\,\dddot{D}^*_{\alpha\gamma}(\omega)\,n_\beta n_\gamma$$
$$-\dddot{D}_{\alpha\beta}(\omega)\,\dddot{D}^*_{\gamma\delta}(\omega)\,n_\alpha n_\beta n_\gamma n_\delta]\Big\}. \qquad (2.3)$$

All the following calculations will be performed in the center-of-mass (c.m.) system of the colliding particles. In this system the dipole and quadrupole moments are given by

$$d_\alpha = \mu\,(e_1/m_1 - e_2/m_2)\,x_\alpha,$$

$$D_{\alpha\beta} = \mu^2\,(e_1/m_1^2 + e_2/m_2^2)\,(3x_\alpha x_\beta - r^2\delta_{\alpha\beta}), \qquad (2.4)$$

where m_1, m_2, e_1, and e_2 are the masses and charges of the colliding particles, $\mu = m_1m_2/(m_1 + m_2)$, and the x_α are the components of the radius vector **r** from particle 2 to particle 1.

Let ρ be the impact parameter of our trajectory, and let φ be the angle between the plane of this trajectory and the xy plane. We choose our coordinate system so that the x axis is along the relative velocity vector of the particles, and we denote the unit vector in this direction by **j**. Then the differential cross section is given by

$$d\sigma = (d\mathscr{E}_\omega/\hbar\omega)\,\rho d\rho d\varphi. \qquad (2.5)$$

In order to integrate this cross section over all impact parameters, we first average (2.3) over φ. This averaging is most easily accomplished by a method which we shall explain through the following example.

In addition to our unprimed xyz coordinate system, let us introduce a new xy′z′ coordinate system whose xy′ plane is that of our trajectory. Then the primed and unprimed components of the $\dddot{D}_{\alpha\beta}(\omega)\,\dddot{D}^*_{\gamma\delta}(\omega)$ tensor are related by

$$\dddot{D}_{\alpha\beta}(\omega)\,\dddot{D}^*_{\gamma\delta}(\omega) = a_{\alpha\mu}a_{\beta\nu}a_{\gamma\rho}a_{\delta\lambda}\,\dddot{D}'_{\mu\nu}(\omega)\,\dddot{D}'^*_{\rho\lambda}(\omega), \qquad (2.6)$$

where the $a_{\alpha\mu}$ are the elements of the matrix for rotation through an angle φ about the x axis. Since our problem has a unique preferred direction characterized by the **j** vector, averaging over φ gives a tensor which, when one takes account of the symmetry of the $\dddot{D}_{\alpha\beta}(\omega)$ tensor, must be of the form

$$\overline{\ddot{D}_{\alpha\beta}(\omega)\,\dddot{D}^*_{\gamma\delta}(\omega)} = C_1\delta_{\alpha\beta}\delta_{\gamma\delta} + C_2(\delta_{\alpha\gamma}\delta_{\beta\delta} + \delta_{\alpha\delta}\delta_{\beta\gamma})$$
$$+ C_3(j_\alpha j_\beta\delta_{\gamma\delta} + j_\gamma j_\delta\delta_{\alpha\beta})\;C_4(j_\alpha j_\gamma\delta_{\beta\delta} + j_\beta j_\delta\delta_{\alpha\gamma}$$
$$+ j_\alpha j_\delta\delta_{\beta\gamma} + j_\beta j_\gamma\delta_{\alpha\delta}) + C_5 j_\alpha j_\beta j_\gamma j_\delta. \qquad (2.7)$$

The C_i are invariants which, according to (2.6) are bilinear functions of $\dddot{D}_{\alpha\beta}(\omega)$ and $\dddot{D}'^*_{\gamma\delta}(\omega)$. It is possible to construct just three such invariants out of these quantities and the vector **j**, namely

$$|\dddot{D}'|^2 = \dddot{D}'_{\alpha\beta}(\omega)\,\dddot{D}'^*_{\alpha\beta}(\omega), \qquad |\dddot{D}'j|^2 = \dddot{D}'_{\alpha\beta}(\omega)\,\dddot{D}'^*_{\alpha\gamma}(\omega)\,j_\beta j_\gamma,$$
$$|j\dddot{D}'j|^2 = \dddot{D}'_{\alpha\beta}(\omega)\,\dddot{D}'^*_{\gamma\delta}(\omega)\,j_\alpha j_\beta j_\gamma j_\delta. \qquad (2.8)$$

Hence we may write

$$C_i = C_i^{(1)}|\dddot{D}'|^2 + C_i^{(2)}|\dddot{D}'j|^2 + C_i^{(3)}|j\dddot{D}'j|^2, \qquad (2.9)$$

where $C_i^{(1)}$, $C_i^{(2)}$, and $C_i^{(3)}$ are numbers easily found by giving specific values to the indices α, β, γ, and δ and integrating (2.6) over φ.

After some rather lengthy algebraic manipulations we arrive at the following formula for the cross section averaged over φ:

$$\overline{d\sigma} = \frac{do\,d\omega}{\hbar\omega c^3}\,2\pi\rho d\rho\Big\{\Big[\frac{2}{3}|\ddot{d}'|^2 + \Big(\frac{1}{3}|\ddot{d}'|^2 - |\ddot{d}'j|^2\Big)P_2(\cos\vartheta)\Big]$$
$$+\frac{1}{3c}\,\mathrm{Re}\Big[\frac{3}{5}(\ddot{d}'^*\dddot{D}'j)\,P_1(\cos\vartheta)$$
$$+\Big(\frac{2}{5}(\ddot{d}'^*\dddot{D}'j) - (j\dddot{D}'j)(\ddot{d}'^*j)\Big)P_3(\cos\vartheta)\Big]$$
$$+\frac{1}{36c^2}\Big[\frac{1}{5}|\dddot{D}'|^2 - \frac{1}{7}(|\dddot{D}'|^2 - 3|\dddot{D}'j|^2)\,P_2(\cos\vartheta)$$
$$+\Big(-\frac{2}{35}|\dddot{D}'|^2 + \frac{4}{7}|\dddot{D}'j|^2 - |j\dddot{D}'j|^2\Big)P_4(\cos\vartheta)\Big]\Big\}, \qquad (2.10)$$

where ϑ is the angle between **n** and **j**, and

$$(\ddot{d}'^*\dddot{D}'j) = \ddot{d}'^*_\alpha(\omega)\,\dddot{D}'_{\alpha\beta}(\omega)\,j_\beta, \qquad (j\dddot{D}'j) = \dddot{D}'_{\alpha\beta}(\omega)\,j_\alpha j_\beta,$$
$$(\ddot{d}'^*j) = \ddot{d}'^*_\alpha(\omega)\,j_\alpha, \qquad |\ddot{d}'|^2 = \ddot{d}'_\alpha(\omega)\,\ddot{d}'^*_\alpha(\omega).$$

As is well known, for a Coulomb interaction the particle trajectories are hyperbolas. The Fourier transforms of the dipole and quadrupole moments are most easily calculated in an x″y″z′ coordinate system such that the x″y″ plane coincides with the x′y′ plane (i.e., the trajectory plane) but such that the x″ axis lies along the symmetry axis of the hyperbola. In this coordinate system the parametric equations for the time-dependence of the relative coordinates are of the form (assuming the particles to have charges of the same sign)

$$x = a(\varepsilon + \cosh\xi), \qquad y = a\sqrt{\varepsilon^2 - 1}\,\sinh\xi,$$
$$r = a(\varepsilon\cosh\xi + 1), \qquad t = \omega_0^{-1}(\varepsilon\sinh\xi + \xi)$$
$$(-\infty < \xi < \infty). \qquad (2.11)$$

Here $a = e_1e_2/2E$, $\omega_0 = (e_1e_2/\mu a^3)^{1/2}$, and ϵ is the eccentricity of the orbit, which is given in terms of the impact parameter by the relation (the notation is that of Landau and Lifshitz[5])

$$\varepsilon = \sqrt{1 + \rho^2/a^2}. \qquad (2.12)$$

(In the x″y″z″ coordinate system the components of j are $j_x = -1/\epsilon$, $j_y = -\sqrt{1 - 1/\epsilon^2}$, and $j_z = 0$.)

Appendix I gives an example of the calculation of $\ddot{d}_\beta$ and $\dddot{D}_{\alpha\beta}$.

After inserting $\ddot{d}_\beta(\omega)$ and $\dddot{D}_{\alpha\beta}(\omega)$ into (2.10), we must integrate over ρ. To do this we change variables from ρ to ϵ, noting that according to (2.12) $\rho d\rho = a^2 \epsilon d\epsilon$ and that the integration over ϵ is from 1 to ∞. Then three types of integrals occur in our calculation. They are ($\nu = \omega/\omega_0$)

$$J_1 = \int_1^\infty K_{i\nu}(\nu\varepsilon) K'_{i\nu}(\nu\varepsilon) \varepsilon^n d\varepsilon,$$

$$J_2 = \int_1^\infty K'^2_{i\nu}(\nu\varepsilon) \varepsilon^n d\varepsilon, \quad J_3 = \int_1^\infty K^2_{i\nu}(\nu\varepsilon) \varepsilon^n d\varepsilon, \tag{2.13}$$

where $K_{i\nu}(x)$ is a Macdonald function.

In Appendix II these integrals are calculated for the relevant values of n. The result for the cross section integrated over ρ and φ is

$$\sigma(\omega, \mathbf{n}) \ddot{d}o \ddot{d}\omega$$
$$= \frac{do}{4\pi} \frac{d\omega}{\omega} \frac{e_1^2 e_2^2}{\hbar c^3 v^2} \left\{ \left(\frac{e_1}{m_1} - \frac{e_2}{m_2} \right)^2 [g_1^{(0)} + g_1^{(2)} P_2(\cos\vartheta)] \right.$$
$$+ \mu^2 \left(\frac{e_1}{m_1^2} + \frac{e_2}{m_2^2} \right)^2 \frac{v^2}{c^2} [g_2^{(0)} + g_2^{(2)} P_2(\cos\vartheta) + g_2^{(4)}$$
$$P_4(\cos\vartheta)] + \mu \left(\frac{e_1}{m_1^2} + \frac{e_2}{m_2^2} \right) \left(\frac{e_1}{m_1} - \frac{e_2}{m_2} \right)$$
$$\left. \frac{v}{c} [g_{12}^{(1)} P_1(\cos\vartheta) + g_{12}^{(3)} P_3(\cos\vartheta) \right\}]. \tag{2.14}$$

Here

$$g_1^{(0)} = -\frac{16}{3} \nu e^{-\pi\nu} K_{i\nu}(\nu) K'_{i\nu}(\nu),$$

$$g_1^{(2)} = \nu e^{-\pi\nu} \left[\frac{16}{3} K_{i\nu}(\nu) K'_{i\nu}(\nu) + 8\nu K^2_{i\nu}(\nu) \frac{d}{d\nu} \frac{K'_{i\nu}(\nu)}{K_{i\nu}\nu)} \right],$$

$$g_2^{(0)} = \nu e^{-\pi\nu} \left[\frac{16}{3} \nu K'^2_{i\nu}(\nu) - \frac{16}{5} K_{i\nu}(\nu) K'_{i\nu}(\nu) \right],$$

$$g_2^{(2)} = \nu e^{-\pi\nu} \left[\frac{32}{21} \nu K'^2_{i\nu}(\nu) - \frac{16}{7} K_{i\nu}(\nu) K'_{i\nu}(\nu) \right.$$
$$\left. - \frac{8}{7} \nu K^2_{i\nu}(\nu) \frac{d}{d\nu} \frac{K'_{i\nu}(\nu)}{K_{i\nu}(\nu)} \right],$$

$$g_2^{(4)} = \nu e^{-\pi\nu} \left[-\frac{32}{21} \nu K'^2_{i\nu}(\nu) + \left(\frac{80}{3} \nu^2 + \frac{192}{35} \right) K_{i\nu}(\nu) K'_{i\nu}(\nu) \right.$$
$$\left. - \frac{32}{3} \nu K^2_{i\nu}(\nu) + \left(80\nu^3 + \frac{64}{7} \nu \right) K^2_{i\nu}(\nu) \frac{d}{d\nu} \frac{K'_{i\nu}\nu)}{K_{i\nu}(\nu)} \right],$$

$$g_{12}^{(1)} = \nu e^{-\pi\nu} \left[\frac{64}{5} K_{i\nu}(\nu) K'_{i\nu}(\nu) + \frac{16}{5} \nu K^2_{i\nu}(\nu) \frac{d}{d\nu} \frac{K'_{i\nu}(\nu)}{K_{i\nu}(\nu)} \right],$$

$$g_{12}^{(3)} = \nu e^{-\pi\nu} \left[-\frac{64}{5} K_{i\nu}(\nu) K'_{i\nu}(\nu) - \frac{96}{5} \nu K^2_{i\nu}(\nu) \frac{d}{d\nu} \frac{K'_{i\nu}(\nu)}{K_{i\nu}(\nu)} \right). \tag{2.15}$$

Integrating (2.14) over do and denoting the result by $\sigma(\omega) d\omega$, we obtain

$$\sigma(\omega) d\omega = \frac{e_1^2 e_2^2}{\hbar c^3 v^2} \left\{ \left(\frac{e_1}{m_1} - \frac{e_2}{m_2} \right)^2 g_1^{(0)} \right.$$
$$\left. + \mu^2 \left(\frac{e_1}{m_1^2} + \frac{e_2}{m_2^2} \right)^2 \frac{v^2}{c^2} g_2^{(0)} \right\} \frac{d\omega}{\omega}. \tag{2.16}$$

The effective radiation $\kappa(\omega, \mathbf{n}) d\omega do$ is defined by[5]

$$\varkappa(\omega, \mathbf{n}) do d\omega = \hbar\omega\sigma(\omega, \mathbf{n}) do d\omega.$$

Inserting (2.14) and integrating over ω (see Appendix III), we obtain

$$\varkappa(\mathbf{n}) do = do \int \varkappa(\omega, n) d\omega = \frac{do}{4\pi} \frac{8\pi\mu v e_1 e_2}{9c^3} \left\{ \left(\frac{e_1}{m_1} - \frac{e_2}{m_2} \right)^2 \right.$$
$$+ \frac{\mu^2 v^2}{c^2} \left(\frac{e_1}{m_1^2} + \frac{e_2}{m_2^2} \right)^2 \left[1 + \frac{2}{5} P_2(\cos\vartheta) \right]$$
$$\left. - \frac{2\mu v}{c} \left(\frac{e_1}{m_1} - \frac{e_2}{m_2} \right) \left(\frac{e_1}{m_1^2} + \frac{e_2}{m_2^2} \right) P_1(\cos\vartheta) \right\}. \tag{2.17}$$

Let us now consider the two limiting cases of low and high frequencies, $\omega \ll \omega_0$ and $\omega \gg \omega_0$. If

$$\nu = \omega / \omega_0 \ll 1$$

(for which $K_{i\nu}(\nu) \approx K_0(\nu) \approx \ln(2/\gamma\nu)$, where $\gamma = e^C = 1.781$, and C is Euler's constant), we may use (2.14) and (2.15) to obtain

$$\sigma(\omega, \mathbf{n}) do d\omega = \frac{do}{4\pi} \frac{d\omega}{\omega} \frac{e_1^2 e_2^2}{\hbar c^3 v^2} \left\{ \left(\frac{e_1}{m_1} - \frac{e_2}{m_2} \right)^2 \left[\frac{16}{3} \ln \frac{2}{\gamma\nu} \right. \right.$$
$$\left. + \left(\frac{8}{3} \ln \frac{2}{\gamma\nu} - 1 \right) P_2(\cos\vartheta) \right] + \mu^2 \left(\frac{e_1}{m_1^2} + \frac{e_2}{m_2^2} \right)^2$$
$$\times \frac{v^2}{c^2} \left[\frac{16}{5} \left(\ln \frac{2}{\gamma\nu} + \frac{5}{3} \right) + \frac{8}{7} \left(\ln \frac{2}{\gamma\nu} + \frac{7}{3} \right) P_2(\cos\vartheta) \right.$$
$$\left. + \left(\frac{128}{35} \ln \frac{2}{\gamma\nu} - \frac{32}{3} \right) P_4(\cos\vartheta) \right] - \mu \left(\frac{e_1}{m_1^2} + \frac{e_2}{m_2^2} \right)$$
$$\times \left(\frac{e_1}{m_1} - \frac{e_2}{m_2} \right) \frac{v}{c} \left[\frac{48}{5} \left(\ln \frac{2}{\gamma\nu} + \frac{1}{3} \right) P_1(\cos\vartheta) \right.$$
$$\left. \left. + \frac{32}{5} \left(\ln \frac{2}{\gamma\nu} - 3 \right) P_3(\cos\vartheta) \right] \right\}. \tag{2.18}$$

From (2.14) and (2.16) — (2.18) it follows, for instance, that if Mg_{12}^{24} or C_6^{12} nuclei are bombarded by those of Ne_{10}^{20}, the quadrupole radiation becomes more intense than the dipole for $v/c > 5 \times 10^{-3}$ and $v/c > 1.2 \times 10^{-3}$, respectively. In the laboratory coordinate system (in which the Mg and C nuclei are at rest) this corresponds to Ne nuclei of energies greater than 0.25 Mev and 0.015 Mev, respectively.

For high frequencies such that

$$\nu = \omega / \omega_0 \gg 1$$

[but such that $\omega \ll E/\hbar$; see Eq. (1.3)], we use the asymptotic formula[6]

$$K_{i\nu}(\nu) \sim e^{-\pi\nu/2} \left[\frac{\Gamma(1/3)}{2\sqrt{3}(\nu/6)^{1/3}} - \frac{\Gamma(2/3)}{840\sqrt{3}(\nu/6)^{5/3}} + O\left(\frac{1}{\nu^{7/3}} \right) \right]. \tag{2.19}$$

Inserting this into (2.14) and (2.15) we arrive at

$$\sigma(\omega, \mathbf{n})\, do\, d\omega = \frac{do}{4\pi}\frac{d\omega}{\omega}\frac{e_1^2 e_2^2}{\hbar c^3 v^2} e^{-2\pi\nu}\left\{\frac{16\pi}{3\sqrt{3}}\left(\frac{e_1}{m_1}-\frac{e_2}{m_2}\right)^2 \right.$$
$$\times\left[1+\frac{1}{2}P_2(\cos\vartheta)\right]+\mu^2\left(\frac{e_1}{m_1^2}+\frac{e_2}{m_2^2}\right)^2\frac{v^2}{c^2}$$
$$\times\frac{\Gamma^2(2/3)\ 8\cdot 6^{1/3}}{3}\nu^{1/3}\left[1+\frac{2}{7}P_2(\cos\vartheta)\right]+\mu\left(\frac{e_1}{m_1^2}+\frac{e_2}{m_2^2}\right)$$
$$\times\left(\frac{e_1}{m_1}-\frac{e_2}{m_2}\right)\frac{v}{c}\left[-\frac{176\pi}{15\sqrt{3}}P_1(\cos\vartheta)\right.$$
$$\left.\left.+\frac{32}{5\sqrt{3}}P_3(\cos\vartheta)\right]\right\}. \tag{2.20}$$

3. When we include the dipole and quadrupole terms, the Fourier transform of the electric radiation field becomes

$$\mathbf{E}(\omega) = \frac{1}{c^2 R_0}\left[\left[\ddot{\mathbf{d}}(\omega)+\frac{1}{6c}\dddot{\mathbf{D}}(\omega)\times\mathbf{n}\right]\times\mathbf{n}\right]. \tag{3.1}$$

Let $\mathbf{e}_\perp$ and $\mathbf{e}_\parallel$ be unit vectors perpendicular to each other and to $\mathbf{n}$ and such that

$$\mathbf{e}_\perp = [\mathbf{n}\times\mathbf{j}]/|[\mathbf{n}\times\mathbf{j}]|, \qquad \mathbf{e}_\parallel = [\mathbf{n}\times\mathbf{e}_\perp]. \tag{3.2}$$

Let $E_1(\omega)$ and $E_2(\omega)$ be the components of $\mathbf{E}(\omega)$ along the two directions defined by these unit vectors, and let us define the polarization density matrix $P_{\mu\nu}$ by

$$P_{\mu\nu} = \overline{AE_\mu(\omega)E_\nu^*(\omega)}. \tag{3.3}$$

Here μ and ν take on the values 1 and 2, and the bar denotes averaging over the parameters ρ and φ of the incident particle (as usual, the constant A is determined by the normalization condition Sp P = 1).

It is easily shown that as a result of averaging over φ alone, $P_{12} = P_{21} = 0$. This means that in our case the radiation in any direction $\mathbf{n}$ is a superposition of two incoherent waves polarized along $\mathbf{e}_\perp$ and $\mathbf{e}_\parallel$. In analogy with (2.14), we therefore define the cross sections $\sigma_\perp(\omega, \mathbf{n})\,d\omega do$ and $\sigma_\parallel(\omega, \mathbf{n})\,d\omega do$ corresponding, respectively, to radiation polarized in these two directions.

Proceeding by methods similar to those of the previous section, we obtain

$$\sigma_\perp(\omega, \mathbf{n})\,d\omega do = \frac{do}{4\pi}\frac{d\omega}{\omega}\frac{e_1^2e_2^2}{\hbar c^3 v^2}\left\{\left(\frac{e_1}{m_1}-\frac{e_2}{m_2}\right)^2 g_{1\perp}^{(0)}+\mu\frac{v}{c}\left(\frac{e_1}{m_1^2}+\frac{e_2}{m_2^2}\right)\left(\frac{e_1}{m_1}-\frac{e_2}{m_2}\right)g_{12\perp}^{(1)}P_1(\cos\vartheta)\right.$$
$$\left.+\mu^2\left(\frac{e_1}{m_1^2}+\frac{e_2}{m_2^2}\right)\frac{v^2}{c^2}\left[g_{2\perp}^{(0)}+g_{2\perp}^{(2)}P_2(\cos\vartheta)\right]\right\};$$
$$g_{1\perp}^{(0)} = 4\nu^2e^{-\pi\nu}K_{i\nu}^2(\nu)\frac{d}{d\nu}\frac{K_{i\nu}'(\nu)}{K_{i\nu}(\nu)}, \qquad g_{12\perp}^{(1)} = -8\nu^2e^{-\pi\nu}K_{i\nu}^2(\nu)\frac{d}{d\nu}\frac{K_{i\nu}'(\nu)}{K_{i\nu}(\nu)},$$
$$g_{2\perp}^{(0)} = \nu^2e^{-\pi\nu}\left[\frac{8}{9}K_{i\nu}'^2(\nu)+\frac{10}{9}\nu K_{i\nu}(\nu)K_{i\nu}'(\nu)-\frac{4}{9}K_{i\nu}^2(\nu)+\left(\frac{10}{3}\nu^2+\frac{2}{3}\right)K_{i\nu}^2(\nu)\frac{d}{d\nu}\frac{K_{i\nu}'(\nu)}{K_{i\nu}(\nu)}\right],$$
$$g_{2\perp}^{(2)} = \nu^2e^{-\pi\nu}\left[\frac{4}{9}K_{i\nu}'^2(\nu)+\frac{50}{9}\nu K_{i\nu}(\nu)K_{i\nu}'(\nu)-\frac{20}{9}K_{i\nu}^2(\nu)+\left(\frac{50}{3}\nu^2+\frac{4}{3}\right)K_{i\nu}^2\frac{d}{d\nu}\frac{K_{i\nu}'(\nu)}{K_{i\nu}(\nu)}\right]. \tag{3.4}$$

We express our gratitude to I. Kh. Lemberg and A. P. Grinberg, who demonstrated to us the value of the calculations here presented.

APPENDIX I

We show how the Fourier transforms (2.2) are calculated, using $\dddot{D}_{xx}(\omega)$ as an example. We first perform a change of variables from t to ξ according to (2.11) in the integral expression (2.2) for $\dddot{D}_{xx}(\omega)$; we remark that ξ varies from $-\infty$ to $+\infty$. Further, we displace the contour of integration in the complex ξ plane upward by an amount $\pi/2$, and integrate twice by parts, obtaining

$$\dddot{D}_{xx}(\omega) = -\frac{\omega^2}{2\pi}e^{-\pi\omega/2\omega_0}\int_{-\infty}^{+\infty}\exp\left\{-\frac{\omega}{\omega_0}(\cosh\eta - i\eta)\right\}$$
$$\times\frac{d}{d\eta}D_{xx}\left(\eta+\frac{i\pi}{2}\right)d\eta, \tag{I.1}$$

where $\eta = \xi - i\pi/2$. According to (2.4) and (2.11) we have

$$D_{xx}\left(\eta+\frac{i\pi}{2}\right) = \mu^2a^2\left(\frac{e_1}{m_1^2}+\frac{e_2}{m_2^2}\right)[(\varepsilon^2-3)\sinh^2\eta$$
$$+4i\varepsilon\sinh\eta+(3\varepsilon^2-1)]. \tag{I.2}$$

We insert (I.2) into (I.1) and write out the hyperbolic functions as sums of exponentials. Then using the integral representation[6]

$$K_\nu(z) = \frac{1}{2}\int_{-\infty}^{+\infty}\exp\{-z\cosh\eta+\nu\eta\}\,d\eta \tag{I.3}$$

for the Macdonald function, as well as the recurrence relation

$$zK_\nu'(z)+\nu K_\nu(z) = -zK_{\nu-1}(z),$$
$$zK_\nu'(z)-\nu K_\nu(z) = -zK_{\nu+1}(z), \tag{I.4}$$

we obtain

$$\dddot{D}''_{xx}(\omega) = \frac{2i}{\pi}\left(\frac{e_1}{m_1^2} + \frac{e_2}{m_2^2}\right) 2\mu E\nu e^{-\pi\nu/2}$$

$$\left[3\frac{\varepsilon^2 - 1}{\varepsilon}\nu K'_{i\nu}(\nu\varepsilon) - \frac{\varepsilon^2 - 3}{\varepsilon^2} K_{i\nu}(\nu\varepsilon)\right] \qquad \text{(I.5)}$$

The other components of $\dddot{D}_{\alpha\beta}(\omega)$ and of $\ddot{d}_{\alpha}(\omega)$ are calculated similarly.

APPENDIX II

Integration by parts reduces J_1 and J_2 to integrals of the type J_3:

$$\int_1^\infty K_{i\nu}(\nu\varepsilon) K'_{i\nu}(\nu\varepsilon)\,\varepsilon^n\,d\varepsilon = -\frac{1}{2\nu}K_{i\nu}^2(\nu) - \frac{n}{2\nu}\int_1^\infty K_{i\nu}^2(\nu\varepsilon)\,\varepsilon^{n-1}\,d\varepsilon,$$

$$\int_1^\infty K'^2_{i\nu}(\nu\varepsilon)\,\varepsilon^n\,d\varepsilon = -\frac{1}{\nu}K_{i\nu}(\nu)K'_{i\nu}(\nu) + \frac{n-1}{2\nu^2}K_{i\nu}^2(\nu)$$

$$-\int_1^\infty K_{i\nu}^2(\nu)\left[\varepsilon^n - \left(1 + \frac{(n-1)^2}{2\nu^2}\right)\varepsilon^{n-2}\right]d\varepsilon. \qquad \text{(II.1)}$$

In these integrals n takes on odd values from − 7 to + 3. The necessary integration can be performed with the aid of Schafheitlin's reduction formula[6]

$$(n+2)\int^z z^{n+2} Z_\mu^2(z)\,dz$$

$$= (n+1)\{\mu^2 - \tfrac{1}{4}(n+1)^2\}\int^z z^n Z_\mu^2(z)\,dz$$

$$+ \tfrac{1}{2}[z^{n+1}\{zZ'_\mu(z) - \tfrac{1}{2}(n+1)Z_\mu(z)\}^2$$

$$+ z^{n+1}\{z^2 - \mu^2 + \tfrac{1}{4}(n+1)^2\}Z_\mu^2(z)], \qquad \text{(II.2)}$$

where $Z_\mu(z)$ may be any cylindrical function.

Writing $Z_\mu(z) = H_{i\nu}^{(1)}(i\nu\epsilon) = (2/\pi i)e^{\pi\nu/2}K_{i\nu}(\nu\epsilon)$, we obtain

$$(n+2)\nu^2\int_1^\infty \varepsilon^{n+2}K_{i\nu}^2(\nu\varepsilon)\,d\varepsilon$$

$$= (n+1)[\nu^2 + \tfrac{1}{4}(n+1)^2]\int_1^\infty \varepsilon^n K_{i\nu}^2(\nu\varepsilon)\,d\varepsilon$$

$$+ \tfrac{1}{2}[\nu^2 K'^2_{i\nu}(\nu) - (n+1)\nu K_{i\nu}(\nu)K'_{i\nu}(\nu)$$

$$+ \tfrac{1}{2}(n+1)^2 K_{i\nu}^2(\nu)]. \qquad \text{(II.3)}$$

With the aid of this formula all of our integrals can be expressed in terms of integrals with n = 1 and n = − 1. Those with n = 1 can be expressed simply in terms of $K_{i\nu}(\nu)$ by means of (II.2), and those with n = − 1 represent a special case of Lommel's integral[7]

$$\int_1^\infty [K_n(\lambda x)]^2\frac{dx}{x} = \frac{\lambda}{2n}\left\{K'_n(\lambda)\frac{\partial}{\partial n}K_n(\lambda) - K_n(\lambda)\frac{\partial}{\partial n}K'_n(\lambda)\right\}. \qquad \text{(II.4)}$$

In our case $n = i\nu$, $\lambda = \nu$, and $x = \epsilon$. The final results, in which derivatives with respect to the index of the Macdonald function are written in terms of the derivatives with respect to the argument and the total derivative with respect to ν, are the following

$$\int_1^\infty K_{i\nu}^2(\nu\varepsilon)\,\varepsilon\,d\varepsilon = \frac{1}{2}K'^2_{i\nu}(\nu),$$

$$\int_1^\infty K_{i\nu}^2(\nu\varepsilon)\,\varepsilon^3\,d\varepsilon = \left(\frac{1}{2} + \frac{1}{3\nu^2}\right)K'^2_{i\nu}(\nu) - \frac{1}{3\nu}K_{i\nu}(\nu)K'_{i\nu}(\nu)$$

$$+ \frac{1}{3\nu^2}K_{i\nu}^2(\nu),$$

$$\int_1^\infty K_{i\nu}^2(\nu\varepsilon)\,\varepsilon^{-1}\,d\varepsilon = \frac{1}{2}K_{i\nu}^2(\nu)\frac{d}{d\nu}\frac{K'_{i\nu}(\nu)}{K_{i\nu}(\nu)}$$

$$+ \frac{1}{2}K'^2_{i\nu}(\nu) + \frac{1}{2\nu}K_{i\nu}(\nu)K'_{i\nu}(\nu),$$

$$\int_1^\infty K_{i\nu}^2(\nu\varepsilon)\,\varepsilon^{-3}\,d\varepsilon = \frac{1}{4(\nu^2+1)}\left[\nu^2 K_{i\nu}^2(\nu)\frac{d}{d\nu}\frac{K'_{i\nu}(\nu)}{K_{i\nu}(\nu)} + 2\nu^2 K'^2_{i\nu}(\nu)\right.$$

$$\left. + 3\nu K_{i\nu}(\nu)K'_{i\nu}(\nu) + 2K_{i\nu}^2(\nu)\right],$$

$$\int_1^\infty K_{i\nu}^2(\nu\varepsilon)\,\varepsilon^{-5}\,d\varepsilon = \frac{1}{16(\nu^2+1)(\nu^2+4)}\left[(8\nu^4 + 2\nu^2)K'^2_{i\nu}(\nu)\right.$$

$$+ (17\nu^3 + 8\nu)K_{i\nu}(\nu)K'_{i\nu}(\nu) + (22\nu^2 + 16)K_{i\nu}^2(\nu)$$

$$\left. + 3\nu^4 K_{i\nu}^2(\nu)\frac{d}{d\nu}\frac{K'_{i\nu}(\nu)}{K_{i\nu}(\nu)}\right],$$

$$\int_1^\infty K_{i\nu}^2(\nu\varepsilon)\,\varepsilon^{-7}\,d\varepsilon$$

$$= \frac{1}{96(\nu^2+1)(\nu^2+4)(\nu^2+9)}\left[(48\nu^6 + 50\nu^4 + 32\nu^2)K'^2_{i\nu}(\nu)\right.$$

$$+ (133\nu^5 + 280\nu^3 + 192\nu)K_{i\nu}(\nu)K'_{i\nu}(\nu)$$

$$+ (254\nu^4 + 800\nu^2 + 576)K_{i\nu}^2(\nu)$$

$$\left. + 15\nu^6 K_{i\nu}^2\frac{d}{d\nu}\frac{K'_{i\nu}(\nu)}{K_{i\nu}(\nu)}\right]. \qquad \text{(II.5)}$$

APPENDIX III

Let us turn to one of the integrals occurring in the calculation of the effective radiation $\kappa(\mathbf{n})$, namely

$$J = \int_0^\infty e^{-\pi\nu}\nu K_{i\nu}(\nu)K'_{i\nu}(\nu)\,d\nu. \qquad \text{(III.1)}$$

Using the integral representation

$$K_\lambda(z) = \tfrac{1}{2}e^{-i\pi\lambda/2}\int_{-\infty}^{+\infty}\exp\{-iz\sinh t - \lambda t\}\,dt,$$

$$z > 0, -1 < \operatorname{Re}\nu < 1, \qquad \text{(III.2)}$$

of the Macdonald function,[6] we have

$$K_{i\nu}(\nu)e^{-\pi\nu/2} = \frac{1}{2}\int_{-\infty}^{+\infty} \exp\{-i\nu(\sinh t + t)\}\, at,$$

$$K'_{i\nu}(\nu)e^{-\pi\nu/2} = -\frac{i}{2}\int_{-\infty}^{+\infty} \exp\{-i\nu(\sinh\tau + \tau)\}\sinh\tau d\tau. \tag{III.3}$$

We now insert (III.3) into (III.1) and, making use of the symmetry of the integrand so obtained, extend the integral over ν from $-\infty$ to $+\infty$. We then obtain

$$J = -\frac{i}{8}\int_{-\infty}^{+\infty}\nu d\nu \iint_{-\infty}^{+\infty} \exp\{-i\nu(\sinh t + \sinh\tau + t + \tau)\}\sinh\tau\, dt\, d\tau = \frac{1}{8}\frac{d}{dx}\int_{-\infty}^{+\infty} d\nu \iint_{-\infty}^{+\infty} \exp\{-i\nu(\sinh t + \sinh\tau + t + \tau + x)\}\sinh\tau\, dt\, d\tau\Big|_{x=0}. \tag{III.4}$$

Changing the order of integration and recalling the integral representation

$$\delta(\nu) = \frac{1}{2\pi}\int_{-\infty}^{+\infty} e^{i\nu x}dx,$$

of the δ-function, we arrive at

$$J = \frac{\pi}{4}\frac{d}{d\nu}\iint_{-\infty}^{+\infty} \sinh\tau\,\delta(\sinh t + \sinh\tau + t + \tau + x)\, dt\, d\tau\Big|_{x=0}. \tag{III.5}$$

For given x and τ, the argument of the δ-function has a single root t_0 on the real axis, and this root is simple. For small values of x this root is easily expressed in powers of x, namely

$$t_0 = -\tau - \frac{x}{\cosh\tau + 1} + \frac{x^2}{2(\cosh\tau + 1)^3} + \cdots \tag{III.6}$$

Hence

$$\delta(\sinh t + \sinh\tau + t + \tau + x) = \frac{\delta[t + \tau + x/(1 + \cosh\tau) + \cdots]}{\cosh[\tau + x/(1 + \cosh\tau) + \cdots] + 1}. \tag{III.7}$$

Inserting (III.7) into (III.5), we obtain

$$J = \frac{\pi}{4}\int_{-\infty}^{+\infty}\sinh\tau\, d\tau \frac{d}{dx}\left\{1 + \cosh\left[\tau + \frac{x}{1 + \cosh\tau}\right]\right\}^{-1}\Big|_{x=0} = -\frac{\pi}{2}\int_0^{\infty}\frac{\sinh^2\tau\, d\tau}{(\cosh\tau + 1)^3} = -\frac{\pi}{6}. \tag{III.8}$$

Similar methods may be used to calculate the other integrals which occur, namely

$$\int_0^{\infty} e^{-\pi\nu}\nu^2 K'^2_{i\nu}(\nu)\, d\nu = \frac{\pi}{15}, \qquad \int_0^{\infty} e^{-\pi\nu}\nu^2 K^2_{i\nu}(\nu)\, d\nu = \frac{\pi}{105},$$

$$\int_0^{\infty} e^{-\pi\nu}\nu^2\left(K_{i\nu}(\nu)\frac{d}{d\nu}K'_{i\nu}(\nu) - K'_{i\nu}(\nu)\frac{d}{d\nu}K_{i\nu}(\nu)\right)d\nu = \frac{\pi}{9},$$

$$\int_0^{\infty} e^{-\pi\nu}\nu^3 K_{i\nu}(\nu)K'_{i\nu}(\nu)\, d\nu = -\frac{2\pi}{315},$$

$$\int_0^{\infty} e^{-\pi\nu}\nu^4\left(K_{i\nu}(\nu)\frac{d}{d\nu}K'_{i\nu}(\nu) - K'_{i\nu}(\nu)\frac{d}{d\nu}K_{i\nu}(\nu)\right)d\nu = \frac{16\pi}{4725}. \tag{III.9}$$

In these calculations, higher powers of x must be maintained in the expansion (III.6).

---

[1] E. M. Lifshitz, JETP **18**, 562 (1948); B. K. Fedyushin, JETP **22**, 140 (1952).

[2] A. Sommerfeld, Atombau and Spektrallinien, F. Vieweg, 1939.

[3] Alkhazov, Grinberg, Lemberg, Rozhdestvenskiĭ, JETP **36**, 322 (1959), Soviet Phys. JETP **9**, 222 (1959); Alkhazov, Grinberg, Grokhina, Lemberg, Izv. Akad. Nauk SSSR, Ser. Fiz. **23**, 223 (1959), Columbia Tech. Transl. p. 215; Alkhazov, Grinberg, Gusinskii, Erokhina, and Lemberg, JETP **35**, 1056 (1958), Soviet Phys. JETP **8**, 737 (1959).

[4] H. A. Kramers, Phil. Mag. **46**, 836 (1923); G. Wentzel, Z. Physik **27**, 257 (1924).

[5] L. D. Landau and E. M. Lifshitz, Теория поля (The Classical Theory of Fields) Gostekhizdat 1960. [3d Ed.].

[6] G. N. Watson, A Treatise on the Theory of Bessel Functions, Cambridge 1944.

[7] Gray, Mathews, and MacRobert, A Treatise on Bessel Functions and their Applications to Physics, Macmillan 1931.

Translated by E. J. Saletan
330

SOVIET PHYSICS JETP VOLUME 12, NUMBER 6 JUNE, 1961

SOME ENERGY RELATIONS OBTAINED WITH ALLOWANCE FOR PARITY NONCONSERVATION IN μ– e DECAY

V. S. BEREZINSKIĬ and G. T. ZATSEPIN

P. N. Lebedev Physics Institute, Academy of Sciences, U.S.S.R.

Submitted to JETP editor August 12, 1960

J. Exptl. Theoret. Phys. (U.S.S.R.) **39**, 1847-1849 (December, 1960)

The portion of the energy transferred to the electrons in μ-e or π-μ-e decay is calculated with allowance for the nonconservation of parity in μ-e decay.

1. We shall determine the fraction of the energy transferred to the electron component in the decay of a fully or partially polarized μ-meson beam.

The energy of the decay electron in the laboratory system is given by

$$E_e = \gamma (E_{ec} + \beta p_{ec} \cos \theta_{\mu e}), \tag{1}$$

where γ is the Lorentz factor of the muon, β its velocity, E_{ec} and p_{ec} the energy and momentum of the electron in the rest system of the muon, and $\theta_{\mu e}$ the momentum of the electron in the rest system of the muon and the direction of motion of the muon in the laboratory system. Here, as also in the following we employ the system of units with $c = 1$.

Until the discovery of parity nonconservation it was assumed that the average momentum vector of the electron in the rest system of the muon vanishes, and therefore averaging (1) yields

$$\overline{E}_e = \gamma \overline{E}_{ec}.$$

Furthermore, assuming $\overline{E}_{ec} = m_\mu/3$, we obtain $\overline{E}_e = E_\mu/3$, where m_μ is the rest mass of the muon, and E_μ is the energy of the muon in the laboratory system. In fact, in the decay of a resting muon the electron carries away an average momentum of

$$\overline{p}_{ec} = 0.05\, m_\mu, \tag{2}$$

directed along the spin of the μ^+ meson for a positron, and in the direction opposite to that of the spin of the μ^- meson for an electron; this follows from the angular and momentum distribution of the electrons given by the formula of Lee and Young:

$$dN / N = 2x^2 [3 - 2x + \lambda (2x - 1) \cos \theta]\, dx\, d\Omega, \tag{3}$$

where $x = p/p_{\max}$, p is the momentum of the electron, $p_{\max} = E_{\max} = m_\mu/2$ (accurate to $m_e^2/2m_\mu$) m_e is the electron mass, λ is a constant determined by the relation of the variants of the theory ($\lambda = +1$ for the decay of a μ^+ meson, $\lambda = -1$ for the decay of a μ^- meson), and θ is the angle between the momentum of the electron and the spin of the muon.

From (3) we find in the rest system of the muon the average energy of the electron $\overline{E}_{ec}$, and the average fraction of the energy of the muon $K_{e\mu c}$ carried away by the electron:

$$\overline{E}_{ec} = (^7/_{20})\, m_\mu, \qquad K_{e\mu c} = \overline{E}_{ec}/m_\mu = {^7/_{20}}. \tag{4}$$

For a beam of fully polarized muons we find these quantities in the laboratory system from (1), (2), and (4), making use of the fact that for fully polarized muons $\theta_{\mu e} = \theta$ or $\theta_{\mu e} = \pi - \theta$:

$$K_{\mu e} = \overline{E}_e / \gamma m_\mu = (\overline{E}_{ec} + \beta \overline{p_{ec} \cos \theta_{\mu e}}) / m_\mu = 0.35\, (1 \pm {^1/_7}\, \beta).$$

We choose the plus sign for a μ^+ meson polarized in the direction of motion; the sign changes when we go over from μ^+-meson decay to μ^--meson decay, and also when the polarization is reversed.

This leads to a simple rule of signs for completely polarized muons (the polarization vector of which lies along the straight line of their motion), produced in the π^+-meson decay, since in the rest system of the pions the polarization of the muons also changes sign when the meson charge changes sign. From this, independently of the sign of the meson charge, we obtain

$$K_{e\mu} = 0.35\, (1 - {^1/_7}\, \beta), \tag{5}$$

if the neutrino (antineutrino) from the pion decay moves in a direction opposite to the muon (in the rest system of the pion this is always so), and

$$K_{e\mu} = 0.35\, (1 + {^1/_7}\, \beta), \tag{6}$$

if the neutrino (antineutrino) moves in the same direction as the muon. For $\beta = 1$ from (6) we obtain $K_{e\mu} = 0.40$.

In the most general case, when the beam of muons is partly polarized and the vector of the average polarization makes an angle α with the vector momentum of the muons, analogous reasoning yields

$$K_{e\mu} = 0.35\,(1 \pm {}^1/_7\,\eta\beta\cos\alpha), \tag{7}$$

where η is the polarization; the plus sign refers to μ^+ mesons, and the minus sign to μ^- mesons.

For cosmic rays at sea level $|\eta| = 0.3$ and $\alpha = 0$ for muons of both signs, and the sign in the parenthesis of expression (7) is minus. For the case when $\beta = 1$ this yields $K_{e\mu} = 0.337$, which differs very little from the commonly accepted value $K_{e\mu} = 1/3$. In the case of unpolarized mesons $(\eta = 0)$, or $\alpha = \pi/2$ we would have $K_{e\mu} = 0.35$.

2. We determine next the average fraction of the energy transferred in the decay of $\pi^\pm$ mesons in vacuum to the electron component. Initially we shall consider the pion rest system. The decay muons in this system are fully polarized along the radius vector of the direction of their emission in such a way that the average vector momentum of the decay electrons of the muon is directed opposite to its momentum. The energy transferred to the electrons is, therefore, equal to

$$E_{e\pi} = \gamma\,(\overline{E}_{ec} - \beta\overline{p}_{ec}), \tag{8}$$

where $\gamma = (m_\pi^2 + m_\mu^2)/2m_\pi m_\mu$, $\beta = (m_\pi^2 - m_\mu^2)/(m_\pi^2 + m_\mu^2)$ is the Lorentz factor, and the velocity of the muon in the rest system of the pion; $\overline{E}_{ec} = 0.35\ m_\mu$ and $\overline{p}_{ec} = 0.05\ m_\mu$ is the average energy and the average momentum of the electrons in the rest system of the muon. Hence we obtain

$$K_{e\pi} = E_{e\pi}/m_\pi = 0.15 + 0.2\,m_\mu^2/m_\pi^2,$$

which yields $K_{e\pi} = 0.2646$. On going over from a rest system of the pion to the laboratory system of coordinates nothing is changed, since the average vector momentum of the electrons in the pion system vanishes.

Analogous calculations for the case of $K_{\mu 2}$ decay yield $K_{eK} = 0.159$. In the calculations we used mass values $m_\pi = 273.2\ m_e$, $m_\mu = 206.7\ m_e$, and $m_K = 966.5\ m_e$.

If the decay processes take place not in vacuum but in some medium, then the precise values of the corresponding quantities are considerably more difficult to obtain, since the energy losses of the muons prior to decay depend on their initial energy, which is in turn related to their polarization.

Translated by Z. Barnea
331

SOVIET PHYSICS JETP VOLUME 12, NUMBER 6 JUNE, 1961

Letters to the Editor

EXPERIMENTAL DETERMINATION OF THE POLARON MASS IN CUPROUS OXIDE

N. I. KRIVKO and N. M. REĬNOV

Leningrad Physico-Technical Institute, Academy of Sciences, U.S.S.R.

Submitted to JETP editor July 12, 1960

J. Exptl. Theoret. Phys. (U.S.S.R.) **39**, 1850 (December, 1960)

SUPPLEMENTING the previously described[1] experiments on the determination of the effective masses of the polarons in polycrystalline cuprous oxide, we performed analogous experiments on single crystals.

The [111] plane of the single crystal of cuprous oxide made an angle of 10° with the direction of the external magnetic field.

With the single crystal illuminated with white light we obtained at 4.2°K the dependence of the absorption of high-frequency energy on the magnetic field shown in the figure. It is seen that in strong magnetic fields there are two moderate maxima, corresponding to effective masses $M_1 = 5.8\,m_0$ and $M_2 = 6.6\,m_0$, as calculated from the relation $\omega = eH/Mc$. In accordance with the arguments advanced earlier,[1] we assume that in strong magnetic fields the absorption maxima are due to polaron states.

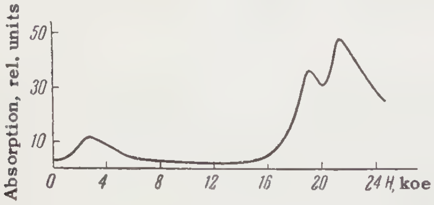

The authors are grateful to A. I. Gubanov for a discussion of the results.

---

[1] Gubanov, Krivko, and Reĭnov, JETP **38**, 341 (1960), Soviet Physics JETP **11**, 247 (1960).

Translated by J. G. Adashko
332

PRODUCTION OF CHARGED MESONS BY 245-Mev NEGATIVE PIONS ON HYDROGEN

Yu. A. BATUSOV, S. A. BUNYATOV, V. M. SIDOROV, and V. A. YARBA

Joint Institute for Nuclear Research

Submitted to JETP editor October 1, 1960

J. Exptl. Theoret. Phys. (U.S.S.R.) **39**, 1850-1852 (December, 1960)

WE report here preliminary results obtained in an investigation of the reaction

$$\pi^- + p \rightarrow \pi^+ + \pi^- + n \qquad (1)$$

at a primary meson energy 245 ± 15 Mev. The experiment was performed with the synchrocyclotron of the Nuclear Problems Laboratory of the Joint Institute for Nuclear Research, using emulsion chambers. The method of scanning for meson-production events and the selection criteria have been described earlier.[1]

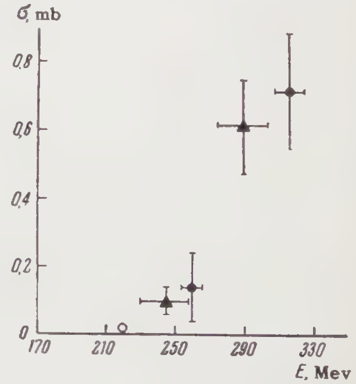

FIG. 1. Energy dependence of the total cross section of the reaction $\pi^- + p \rightarrow \pi^+ + \pi^- + n$ near threshold.

A total of 32 events were registered. The cross section of the reaction (1) at an energy 245 ± 15 Mev was found to be 0.10 ± 0.04 mb. Figure 1 shows the experimental data[1,2,3] on the total cross sections of reaction (1) as functions of the energy of the incident pion. On approaching threshold (172 Mev), the cross section falls off rapidly, but remains nevertheless greater than the theoretical values[4] obtained with the Chew-Low static model, which assumes a direct interaction between the incoming pion and the nucleon. To explain the dependence of the meson-production cross section on the energy, Rodberg[5] proposed that the cross section is due entirely to the interaction of the incoming pion directly with the meson of the "coat" of the nucleon. However, there are no indications that such an assumption is valid at energies close to threshold. An interpretation of meson production by mesons near threshold was

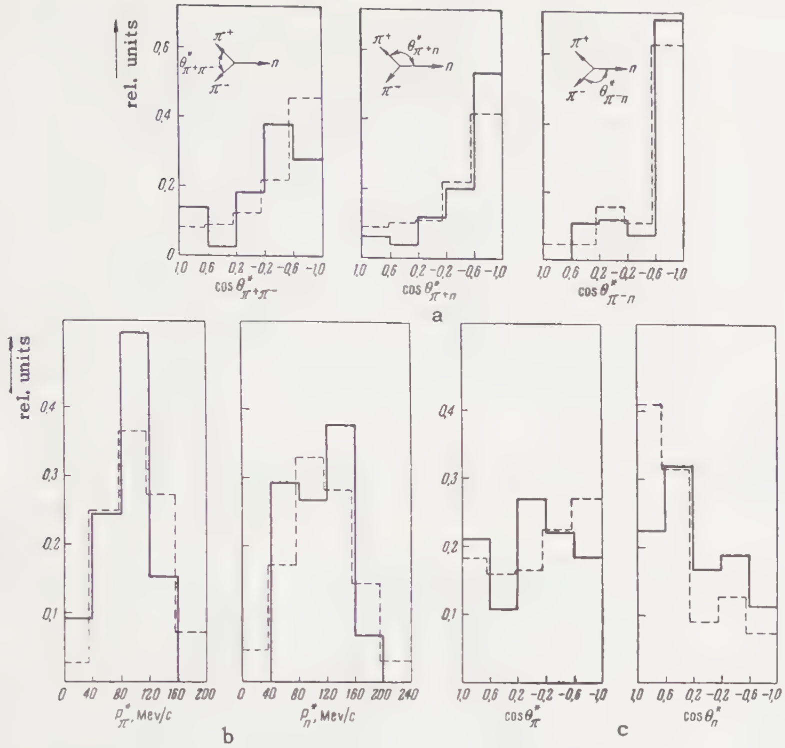

FIG. 2. Momentum and angular distributions of secondary particles for the reaction $\pi^- + p \rightarrow \pi^+ + \pi^- + n$ in the c.m.s. Solid line – at 245 Mev (32 events), dashed line – at 290 Mev (250 events[8]). a – distribution of angles between secondary particles, b – momentum distributions, c – angular distributions relative to the direction of the primary meson.

given by Ansel'm and Gribov,[6] who showed that the energy dependence of the cross section is brought about by the interaction between particles in the final state, and is determined essentially by the amplitudes of the charge exchanges $\pi^+ + \pi^- \rightarrow \pi^0 + \pi^0$ and $\pi^+ + n \rightarrow \pi^0 + p$. This makes it possible to obtain the amplitude of charge exchange of a pion on a pion by determining the dependence of the cross section on the energy of the incident pion. However, this calls for more detailed and more exact data on the total cross sections of the meson-production reactions near threshold than are available at the present time.

Another method of obtaining the pion-pion charge-exchange cross section from the relative momenta and angular distributions of the secondary particles from reaction (1), at an incoming-pion energy of 290 Mev, was obtained in reference 7, where the advisability of performing the experiment at a lower energy was noted. Figure 2 shows the momentum and angular distributions of the secondary particles in the c.m.s. at a pion energy of 245 Mev, compared with the data obtained at 290 Mev.[8] The corresponding values of the average particle scattering angles in the c.m.s. are:

	245 **Mev**	290 **Mev**
$\bar\theta^*_{\pi^+\pi^-}$, **deg**	103 ± 7	116,7 ± 2,4
$\bar\theta^*_{\pi^+n}$, **deg**	125 ± 7	113,4 ± 2,5
$\bar\theta^*_{\pi^-n}$, **deg**	131 ± 5	129,3 ± 2,4

It is evident from the foregoing and from Fig. 2 that the angular distributions of the secondary particles (in the c.m.s.) do not change significantly as the energy is reduced from 290 to 245 Mev.

A detailed reduction of the experimental data obtained at 245 Mev will be made with larger statistical material, in order to determine the pion-pion charge-exchange amplitude at zero energy.

The authors are grateful to V. P. Dzhelepov and L. I. Lapidus for interest and attention to the work.

---

[1] Batusov, Bogachev, Bunyatov, Sidorov, and Yarba, Doklady Akad. Nauk SSSR **133**, 52 (1960), Soviet Phys.-Doklady **5**, 731 (1961).

[2] Perkins, Caris, Kenney, and Perez-Mendez, Phys. Rev. **118**, 1364 (1960).

[3] Deahl, Derrick, Fetkovich, Fields, and Yodh, Bull. Amer. Phys. Soc. **5**, 71 (1960).

[4] J. Franklin, Phys. Rev. **105**, 1101 (1957); L. Rodberg, Phys. Rev. **106**, 1090 (1957); E. Kazes, Phys. Rev. **107**, 1131 (1957).

[5] L. Rodberg, Phys. Rev. Lett. **3**, 58 (1959).

[6] A. A. Ansel'm and V. N. Gribov, JETP **37**, 501 (1959), Soviet Phys. JETP **10**, 354 (1960).

[7] Batusov, Bunyatov, Sidorov, and Yarba, JETP **39**, 506 (1960), Soviet Phys. JETP **12**, 354 (1961).

[8] Batusov, Bunyatov, Sidorov, and Yarba, JETP **40**, 460 (1961), Soviet Phys. JETP, in press.

Translated by J. G. Adashko
333

THE CRYSTAL STRUCTURE OF SOLID HYDROGEN DEUTERIDE

R. F. BULATOVA, V. S. KOGAN, and
B. G. LAZAREV

Submitted to JETP editor October 1, 1960

J. Exptl. Theoret. Phys. (U.S.S.R.) **39**, 1853
(December, 1960)

As we previously reported,[1,2] hydrogen and deuterium have a tetragonal body-centered lattice with the values of c/a different by a factor of more than two: 0.82 for H_2 and 1.73 for D_2.* The heaviest isotope of hydrogen — tritium — has the same structure as deuterium. It seemed of interest to examine the structure of the fourth in this isotopic series — hydrogen deuteride.

Gaseous hydrogen deuteride was obtained by electrolysis of a 50% mixture of heavy water in ordinary water. The mixture then passed through a non-regenerative rectification column working at liquid hydrogen temperature, to obtain pure HD.† The helium cryostat for low temperature x-ray diffraction photography, previously described,[1] was used for examining the crystal structure. As in the case of deuterium and tritium, only one line (here at an angle of 19°) appears in the diffraction pattern obtained from solid HD specimens. The calculation from the patterns showed that the hydrogen deuteride lattice belongs to the same group — C_4^5 (body-centered tetragonal lattice) as the deuterium and tritium lattices. The density of solid hydrogen deuteride calculated from the parameters obtained ($a = 3.39$ A, $c = 5.86$ A, $c/a = 1.73$) comes out as 0.146 g/cm^3, which is in good agreement with the value of 0.143 g/cm^3 at 4.2°K found by extrapolation of the literature value[5] of 0.137 g/cm^3 at 16.6°K. Thus, while c/a remains constant in the series hydrogen deuteride, deuterium, tritium, the value of the lattice parameters decreases monotonically (the values of a are, respectively, 3.39, 3.35 and 3.30 A). We should point out that a similar trend has been found in the solid neon isotopes, with a possible explanation in the difference of zero-point energy.[6]

---

*From the x-ray structure analysis data, a hexagonal structure with axial ratio $c/a = 1.73$ could be ascribed to hydrogen equally as well as the tetragonal structure indicated above; however, investigations carried out by other methods[3,4] indicate that the tetragonal structure is evidently to be preferred.

†The column will be described in a separate communication.

---

[1] Kogan, Lazarev, and Bulatova, JETP **37**, 678 (1959), Soviet Phys. JETP **10**, 485 (1960).

[2] Kogan, Lazarev, and Bulatova, JETP **34**, 238 (1958), Soviet Phys. JETP **7**, 165 (1958).

[3] A. A. Galkin and I. V. Matyash, JETP **37**, 1831 (1959), Soviet Phys. JETP **10**, 1292 (1960).

[4] S. S. Dukhin, JETP **37**, 1486 (1959), Soviet Phys. JETP **10**, 1054 (1960).

[5] Woolley, Scott, and Brickwedde, J. Res. Nat. Bureau Stand. **41**, 379 (1948).

[6] Kogan, Lazarev, and Bulatova, JETP **40**, 29 (1961), Soviet Phys. JETP **13**, in press.

Translated by R. Berman
334

CONCERNING PARITY NONCONSERVATION IN STRONG INTERACTIONS WITH PARTICIPATION OF STRANGE PARTICLES

WANG KANG-CH'ANG, WANG TS'U-CHIENG,
V. I. VEKSLER, I. VRANA, TING TA-TS'AO,
V. G. IVANOV, KIM HI YING, E. N. KLADNITSKAYA, A. A. KUZNETSOV, NGUYEN DINH TY,
A. V. NIKITIN, M. I. SOLOV'EV, T. KHOFMOKL',
and CH'ENG LING-YEN

Joint Institute for Nuclear Research

Submitted to JETP editor September 1, 1960

J. Exptl. Theoret. Phys. (U.S.S.R.) **39**, 1854-1856
(December, 1960)

Following the discovery of parity nonconservation in weak interactions, the question of the status of this law in strong interaction has been under frequent discussion by various authors. Solov'ev[1,2] discussed the possibility of verifying this law. It follows from his papers that the longitudinal polarization of a Λ^0 hyperon generated in nuclear collisions would be evidence of parity nonconservation in strong interactions, provided the Λ^0 hyperon has no preferred direction. Several experiments were performed on the detection of longitudinal polarization of hyperons. These experiments were performed with primaries near zero[3,4] or medium energies[5-7] and the momentum of the generated strange particles was less than or about 300 — 500 Mev/c in the c.m.s. No longitudinal polarization of the hyperons was observed. An analysis of these data leads to the conclusion that to answer the posed question the experiments must be carried out at high energy and must involve interactions not with nuclei but with nucleons, for the former make interpretation of the phenomenon difficult.

For this purpose we analyzed the angular symmetries in the decays of Λ^0 generated in π^-p collisions at 7 — 8 Bev energy.[8] The preliminary results are reported in this letter. In the 14,000 photographs obtained with a beam of 6.8-Bev π^- mesons we found 84 Λ^0 and 9 V^0, which can also be classed as Λ^0 and K^0, while the 20,000 photographs with ~ 8 Bev/c incident π^- mesons contained 91 Λ^0 and 24 Λ^0 or K^0. The Λ^0 admixture formed on the quasi-free protons amounts to 20 percent,[8] while the Λ^0 produced by Σ^0 decay make up a very small fraction.*

All 208 events were broken up into four momentum intervals (see Table I).

TABLE I

p_{Λ^0}, Mev/c	No. of Λ^0	No. of Λ^0 or K^0	Systematic omissions in scanning
<400	3	0	
400—800	50	1	6
800—1200	54	3	
>1200	68	29	
Total	175	33	6

The Λ^0 hyperons can be easily identified in principle by the kinematics of the decay and ionization of the decay products only up to a momentum of 1200 Mev/c. In some cases the identification of the Λ^0 is made difficult by the conditions of the experiment (decay geometry, luminosity). For this reason, four unresolved cases remained in the region below 1200 Mev/c. In the region above 1200 Mev/c we have found 29 V^0 which can be classed, in accordance with their kinematics, as either Λ^0 or K^0. Measurements of the ionization of the positive decay products likewise do not permit identification of the Λ^0 in this case. In addition to the difficulty of identification at high energies, systematic omissions in scanning are possible if the π^- meson from the decay of the Λ^0 has a momentum ≤ 50 Mev/c (range approximately 7 mm). The fraction of these events was estimated from the spectrum of the observed Λ^0 and amounted to not more than 3.5% (assuming that the angles of emission of the proton in the rest frame of the Λ^0 are distributed isotropically). In our statistics this corresponds to 6 events. The main contribution of these events is in the interval from 500 to 1000 Mev/c for p_{Λ^0}.

The asymmetry in the Λ^0 decays was investigated in the coordinate system shown in the figure: x — direction $[p_{\pi^-} \times p_{\Lambda^0}]$, normal to the plane of Λ^0 production, y — direction p_{Λ^0} of emission of the Λ^0, z — direction $p_{\Lambda^0} \times [p_{\pi^-} \times p_{\Lambda^0}]$ perpendicular to the xy plane. The angles between p_p^* and the xyz axes are denoted ξ^*, θ_+^*, and φ^*, respectively. The asymmetry in the distribution of the angle ξ^* is the up-down asymmetry (asymmetry coefficient $\alpha\overline{P}_3$), that in the distribution of the angle θ_+^* is the forward-backward asymmetry $(\alpha\overline{P}_1)$, while that in the distribution of φ^* is the right-left asymmetry.

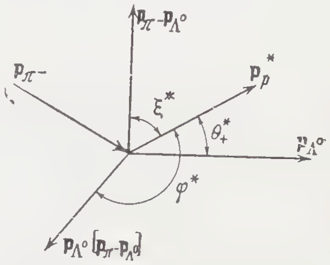
$p_{\pi^-} \cdot p_{\Lambda^0}$
p_{π^-}
p_p^*
ξ^*
θ_+^*
p_{Λ^0}
φ^*
$p_{\Lambda^0}[p_{\pi^-} \cdot p_{\Lambda^0}]$

The asymmetry coefficient $\alpha\overline{P}_1$ is calculated from the formula

$$\alpha\overline{P}_1 = \frac{3}{N}\sum_{i=1}^{N}\cos\theta_i^* \pm \sqrt{3\,[1-(\alpha\overline{P})^2]/N},$$

where α is the asymmetry coefficient of the completely polarized $\Lambda^0\,(\overline{P} = 1)$, $\overline{P}_1$ is the average polarization of the Λ^0, and θ^* is the angle between the proton from the Λ^0 decay and the direction of motion of the Λ^0. The coefficients $\alpha\overline{P}_2$ and $\alpha\overline{P}_3$ are calculated similarly.

The result of our analysis, with allowance for the possible omissions, is presented in Table II. The figures in the parenthesis stand for additional

TABLE II

p_{Λ^0}	N	$\alpha\overline{P}_1$	$\alpha\overline{P}_2$	$\alpha\overline{P}_{,}$
$400 < p_{\Lambda^0} \leqslant 1200$	104 104 + (4) 104 + (4) + (6)	—0.58 ± 0.15 —0.50 ± 0.15 —0.37 ± 0.15	0.00 ± 0.17 0.06 ± 0.16	0.03 ± 0.17 0.07 ± 0.16
$p_{\Lambda^0} > 1200$	68 68 + (29)	—0.66 ± 0.19 —0.09 ± 0.17	0.14 ± 0.21 0.06 ± 0.17	0.24 ± 0.21 0.21 ± 0.17
All p_{Λ^0}	172 172 + (33) 172 + (33) + (6)	—0.61 ± 0.12 —0.31 ± 0.12 —0.24 ± 0.12	0.05 ± 0.13 0.00 ± 0.12	0.11 ± 0.13 0.12 ± 0.12

unresolved and omitted events. The value $\alpha\overline{P}_1 = -0.37 \pm 0.15$ for cases with $400 < p_{\Lambda^0} \leq 1200$ Mev/c and $\alpha\overline{P}_1 = -0.24 \pm 0.12$ for all cases are lower limits, and therefore we classed all unresolved cases as Λ^0, it being known that some of these, but not many, are K^0.

We investigated the possible systematic errors in the data reduction, for example systematic errors in the particle momenta, and in the angles, which could lead to errors in the determination of θ^*, and the like. We found no such errors.

We note that the average c.m.s. momentum of the Λ^0, for the group of events in the momentum range 400 — 1200 Mev/c (in the laboratory system) is 1100 Mev/c, and approximately 600 Mev/c for the group with > 1200 Mev/c in the laboratory system. It is possible that the value of $\alpha\overline{P}_1$ depends on the c.m.s. momentum of the Λ^0. Naturally, more study is needed here.

No right-left (in φ^*) or up-down asymmetry (in ξ^*) was observed, within the limits of statistical errors. The presence of forward-backward asymmetry is an important result, in connection with parity nonconservation in strong interactions with production of strange particles. It is possible that the result obtained is nonetheless the consequence of poor statistics, since we processed only about 200 Λ^0. The work is now being continued.

***Material presented at the Tenth International Conference on the Physics of High-Energy Particles, 1960.**

---

[1] V. G. Solov'ev, Preprint R-147, Joint Inst. Nucl. Res., 1958.

[2] V. G. Solov'ev, Doklady Akad. Nauk SSSR **129**, 68 (1959), Soviet Phys.-Doklady **4**, 1255 (1960).

[3] Leitner, Nordin, Rosenfeld, Solmitz, and Tripp, Phys. Rev. Lett. **3**, 238 (1959).

[4] Block, Brucker, Gasaroli, Kikuchi, Meltzer, Revzner, Schlein, Strand, Cohn, Harth, Leitner, Minguzzi-Ranzi, Lonari, and Puppi, Preprint.

[5] Lander, Rowell, and White, Phys. Rev. Lett. **3**, 236 (1959).

[6] Crawford, Cresti, Good, Solmitz, and Stevenson, Phys. Rev. Lett. **1**, 209 (1958).

[7] Crawford, Cresti, Good, Solmitz, and Stevenson, Phys. Rev. Lett. **2**, 11 (1959).

[8] Wang, Wang, Veksler, Vrana, Ting, Ivanov, Kladnitskaya, Kuznetsov, Nguyen, Nikitin, Solov'ev, and Ch'eng, JETP **40**, 464 (1961), Soviet Phys. JETP, in press.

Translated by J. G. Adashko
335

SMALL BINDING ENERGIES IN QUANTUM FIELD THEORY

L. D. LANDAU

Institute for Physics Problems, Academy of Sciences, U.S.S.R.

Submitted to JETP editor October 21, 1960

J. Exptl. Theoret. Phys. (U.S.S.R.) **39**, 1856-1857 (December, 1960)

THE recent trend in quantum field theory has been to consider not Hamiltonians but only the unitarity relation and analyticity properties of diagrams, expressing the local nature of the interaction. It is true that one has not succeeded as yet in writing down the complete equations for such a theory; however, one might hope that such equations would represent, in essence, a new theory, basically different from a discussion of interaction processes.

Occasionally the thought has been expressed that such a theory would only constitute a "framework," i.e., that it would allow the introduction of all kinds of particles with all kinds of relations among them. The purpose of this note is to show that for loosely bound (but strongly interacting) particles there arises in such a theory a direct relation between the coupling constant and the binding energy of the particles.

Let us denote by the letter c a particle which, when given a comparatively small amount of energy, can decay into two particles a and b. Obviously

$$M_c = M_a + M_b - \varepsilon, \tag{1}$$

where ϵ is the binding energy. These conditions, as is well known, are satisfied by the deuteron. It is true that it is customary to treat the deuteron as a composite particle, "consisting" of a proton and neutron. In reality, however, the concepts of "elementary" and "composite" lose their meaning in relativistic quantum field theory and the assertion that the deuteron is a "composite" particle differs only quantitatively from the assertion that mesons "consist" of nucleons and antinucleons. Only the assumption that all particles under consideration interact strongly is relevant.

For simplicity let us suppose that all particles have zero spin. It is understood that the particle c has even parity relative to the particles a and b (s-state!). Let us denote by the letter g the full vertex part for the transition a + b → c. We look now at the amplitude for the mutual scattering of particles a and b. This amplitude has a pole term, associated with the virtual production of the particle c, equal to

$$(g^2/8\pi)/(M_a+M_b)\,[(p_a+p_b)^2-M_c^2]. \qquad (2)$$

Replacing $(p_a+p_b)^2$ by $(M_a+M_b+E)^2$, where E is the energy in the barycentric frame after subtraction of the rest energy, expressing M_c in terms of Eq. (1), and assuming that E and ϵ are small, we find

$$(g^2/16\pi)/(M_a+M_b)^2\,(E+\varepsilon). \qquad (3)$$

Let us compare this expression with the well known expression for the resonant scattering amplitude for not too high energies. The latter is given by

$$\sqrt{{}^1\!/_2\,(1/M_a+1/M_b)}\,/\,[\sqrt{\varepsilon}+i\sqrt{E}\,]. \qquad (4)$$

It is obvious that the expression $1/(\sqrt{\epsilon}+i\sqrt{E})$ evaluated at the point $E=-\epsilon$ is equal to $2\sqrt{\epsilon}$. One may therefore assert that

$$g^2/16\pi\,(M_a+M_b)^2=\sqrt{2\,(1/M_a+1/M_b)\,\varepsilon}\,.$$

Finally we obtain

$$\varepsilon=(g^4/512\pi^2)\,M_aM_b/(M_a+M_b)^5. \qquad (5)$$

This is the desired formula which expresses the binding energy, assuming it is small, in terms of the corresponding coupling constant.

It should be noted that analogous relations were already encountered by Faĭnberg and Fradkin[1] in writing dispersion relations for nucleon scattering.

It seems to me that it would be of interest to derive this formula directly from unitarity and analyticity properties of the amplitudes.

---

[1] V. Faĭnberg and E. Fradkin, Doklady Akad. Nauk SSSR **109**, 507 (1956), Soviet Phys.-Doklady **1**, 455 (1957).

Translated by A. M. Bincer
336

SOVIET PHYSICS JETP VOLUME 12, NUMBER 6 JUNE, 1961

Author Index to Volume 12

References with L are Letters to the Editor

Ablekov, V. K., M. S. Pesin, and I. L. Fabelinskiĭ. The Realization of a Medium with Negative Absorption Coefficient — 618L.

Abrikosov, A. A. Some Properties of Strongly Compressed Matter. I — 1254.

— and L. P. Gor'kov. Contribution to the Theory of Superconducting Alloys with Paramagnetic Impurities — 1243.

— and L. P. Gor'kov. On the Problem of the Knight Shift in Superconductors — 337.

Adamovich, M. I., N. M. Panova, V. M. Popova, and F. R. Yagudina. Ratio of Cross Sections for Positive and Negative Photomeson Production on Beryllium — 1103.

Akhiezer, I. A. and S. V. Peletminskiĭ. Theory of the Magnetic Properties of a Nonideal Fermi Gas at Low Temperatures — 913.

Akhmatov, A. P., P. I. Blinov, V. F. Bolotin, A. V. Borodin, P. P. Gavrin, E. K. Zavoĭskiĭ, I. A. Kovan, M. N. Oganov, B. I. Patrushev, E. V. Piskarev, V. D. Rusanov, G. E. Smolkin, A. R. Striganov, D. A. Frank-Kamenetskiĭ, P. A. Cheremnykh, and R. V. Chikin. Magneto-Acoustic Resonance in a Plasma — 376.

Akimova, M. K., L. D. Blokhintsev, and É. I. Dolinskiĭ. The Polarization and Angular Distribution of Neutrons Emitted in μ Capture from Some Light Nuclei — 1260.

Aleksandrov, B. N., B. I. Verkin, and I. V. Svechkarev. Temperature Dependence of the Magnetic Susceptibility of Indium, Lead, and Tin Crystals — 25.

Alekseev, N. V., K. I. Zherebtsova, V. F. Litvin, and Yu. A. Nemilov. Investigation of Stripping Reactions on C^{12}, O^{16}, and Si^{28} — 1049.

Alekseevskiĭ, N. E., Yu. P. Gaĭdukov, I. M. Lifshitz, and V. G. Peschanskiĭ. Fermi Surface of Tin — 837.

Aleksin, V. G. and V. I. Yashin. Investigation of the Stability of a Plasma by a Generalized Energy Principle — 572.

Alikhanov, A. I., G. P. Eliseev, and V. A. Lyubimov. Longitudinal Polarization of β Electrons from Au^{198} — 414.

Alikhanov, R. A. Antiferromagnetism of $CoCO_3$ — 1028.

Al'tshuler, L. V., L. V. Kuleshova, and M. N. Pavlovskiĭ. The Dynamic Compressibility, Equation of State, and Electrical Conductivity of Sodium Chloride at High Pressures — 10.

Amaglobeli, N. S., Yu. M. Kazarinov, S. N. Sokolov, and I. N. Silin. Determination of the Pion-Nucleon Coupling Constant from the Elastic np Scattering Differential Cross Sections — 657.

Amatuni, A. Ts. and N. A. Korkhmazyan. Transition Radiation in the Case of a Diffuse Boundary Between Two Media — 703.

Amus'ya, M. Ya. On the Ground States of Atomic Nuclei. I. — 449.

Andreev, V. V. and A. M. Kosevich. Quantum Oscillations of the Thermal Conductivity Coefficient of an Electron Gas in a Magnetic Field — 517.

Andronikashvili, É. L. and N. N. Roĭnishvili Transverse Momentum Component of Strange Particles Produced in Penetrating Cosmic-ray Showers — 192.

Anisovich, V. V. A Resonance Model for the $\pi + N \to \pi + \pi + N$ Reaction at Meson Energies of 300 — 400 Mev — 71.

— A Resonance Model for the Reactions $N + \pi \to N + \pi + \pi$ and $\gamma + N \to N + \pi + \pi$ — 946.

Apalin, V. F. (see Spivak, P. E.) — 1027L.

Artamonova, K. P., L. V. Gustova, Yu. N. Podkopaev, and O. V. Chubinskiĭ. The γ Spectrum of Na^{24} in the 2.5 — 5.5 Mev Energy Range — 1109.

Artemov, K. P. and N. A. Vlasov. Charged Products from the Reactions $He^4 + d$ (20 Mev) — 1124.

Askar'yan, G. A. Electromagnetic Radiation from Electron Diffusion — 151L.

Assovskaya, A. S. and N. S. Ivanova. Production of Nuclear Fragments in Nuclear Emulsions by 80-Mev Mesons — 1051.

Avvakumov, V. I., N. S. Garif'yanov, and E. I. Semenova. Electron Paramagnetic Resonance and Paramagnetic Relaxation in Liquid and Supercooled Ti^{+++} Salt Solutions — 847.

Azbel', M. Ya. A New Resonance Effect in Metals at High Frequencies — 283.

— On the Possibility of Determining the Correlation Function for Fermi Fluids in Metals — 793.

— Quantum Oscillations of Thermodynamic Quantities for an Arbitrary Fermi Surface — 608.

— Quasiclassical Quantization Near Singular Classical Trajectories — 891.

— and É. A. Kaner. Experimental Investigation of Cyclotron Resonance in Metals — 58.

Azimov, S. A., K. T. Teshabaev, L. P. Chernova, G. M. Chernov, and V. M. Chudakov. Angular Distribution of Shower Particles Produced in Nuclear Interactions Between Fast Nucleons and Heavy Nuclei of Photographic Emulsions — 1068.

Babushkina, N. A. (see Kikoin, I. K.) — 816L.

Baĭer, V. N. and I. B. Khriplovich. A Scheme of Weak Interactions with Neutral Currents — 959.

Baĭkov, I. S. Polarization of Internal Conversion Electrons Emitted After β Decay of Oriented Nuclei — 439.

Balats, M. Ya., L. N. Kondrat'ev, L. G. Landsberg, P. I. Lebedev, B. V. Obukhov, and B. Pontecorvo. Intensity of Nonradiative Transitions in Mu-Mesic Atoms — 813L.

Baldin, A. M. On the Role of the Nonphysical Region in the Dispersion Relations for the Photoproduction of π Mesons — 800L.

— and S. F. Semenko. On the Theory of the Optical Anisotropy of Atomic Nuclei — 306.

Bannik, B. P. and V. G. Grishin. Interference Between Coulomb and Nuclear Scattering at High Energies — 69.

Barbashov, B. M. and G. V. Efimov. A Method of Solution of Field-Theoretical Problems Involving a Static

Nucleon — 316.

Barmin, V. V., V. P. Kanavets, and B. V. Morozov. Polarization of Cosmic Ray μ^+ Mesons — 683.

—, Yu. S. Krestnikov, I. I. Pershin, V. P. Rumyantseva, Ya. Ya. Shalamov, and V. A. Shebanov. Freon Bubble Chamber Observations on the Asymmetry in the Decay of Λ^0 Hyperons Produced by 2.8 Bev/c π^- Mesons — 857.

Bar'yakhtar, V. G. and S. V. Maleev. Scattering of Slow Neutrons in Ferrites and Antiferromagnets — 995.

— and S. V. Peletminskiĭ. Contribution to the Theory of Relaxation of the Magnetic Moment in Ferromagnetic Substances — 457.

— and G. I. Urushadze. The Scattering of Spin Waves and Phonons by Impurities in Ferromagnetic Dielectrics — 251.

Basov, N. G. and O. N. Krokhin. Conditions for Electron Excitation of Negative Temperature States in a Gas Mixture — 1240.

—, O. N. Krokhin, and Yu. M. Popov. Possibility of Using Indirect Transitions to Obtain a Negative Temperature in Semiconductors — 1033L.

Batusov, Yu. A., S. A. Bunyatov, V. M. Sidorov, and V. A. Yarba. Determination of the Charge-exchange Cross Section for Pion-pion Collision from the Analysis of the $\pi^- + p \rightarrow \pi^- + \pi^+ + n$ Reaction at 290 Mev — 354L.

—, S. A. Bunyatov, V. M. Sidorov, and V. A. Yarba. Production of Charged Mesons by 245-Mev π^- Mesons on Hydrogen — 1290L.

Bekarevich, I. L. and I. M. Khalatnikov. Theory of the Kapitza Thermal Discontinuity at the Boundary Between Liquid He^3 and a Solid Body — 1187.

Belov, K. P. and A. V. Ped'ko. Anomalies in the Temperature Dependence of the Coercive Force in Garnet Ferrites of the Rare Earth Elements in the Vicinity of the Compensation Point — 666.

—, L. A. Malevskaya, and V. I. Sokolov. Resonance and Magnetic Properties of Garnet-type Yttrium Ferrite at Low Temperatures — 1074.

—, M. A. Zaĭtseva, and A. M. Kadomtseva. Magnetic Properties of Orthoferrites of Lanthanum and Praseodymium with Partial Replacement of Fe^{3+} Ions by Al^{3+} Ions — 799L.

Belyaev, S. T. On the Nature of the First Excited States of Even-even Spherical Nuclei — 968.

Belyakov, V. A., Wang Shu-Fen, V. V. Glagolev, N. Dalkhazhav, R. M. Lebedev, N. N. Mel'nikova, V. A. Nikitin, V. Petrzhilka, V. A. Sviridov, M. Suk, and K. D. Tolstov. Inelastic Interactions of 7 Bev Negative Pions and Nucleons — 650.

Berestetskiĭ, V. B. Anomalous Magnetic Moments of the Muon and Electron — 993.

— and I. Ya. Pomeranchuk. Asymptotic Behavior of Cross Sections at High Energies — 752.

— and E. D. Zhizhin. Photoproduction of π Mesons on Nucleons in Peripheral Collisions — 295.

Berezinskiĭ, V. S. and G. T. Zatsepin. Some Energy Relations Deduced by Taking into Account Parity Nonconservation in $\mu - e$ Decay — 1288.

Bezuglyĭ, P. A. and A. A. Galkin. The Anisotropy of the Energy Gap in Tin in the Basal Plane of the Crystal — 810L.

—, A. A. Galkin, and A. P. Korolyuk. Investigation of the Anisotropy of the Energy Gap in Superconducting Tin — 4.

Biberman, L. M. and B. A. Veklenko. Generalized Reciprocity Principle — 64.

Bil'dyukevich, A. L., V. M. Vinokurov, M. M. Zaripov, Yu. E. Pol'skiĭ, V. G. Stepanov, G. K. Chirkin, and L. Ya. Shekun. Electron Paramagnetic Resonance in Andalusite — 1078.

Blinov, P. I. (see Akhmatov, A. P.) — 376.

Blokhintsev, D. Note on the Optical Theorem — 802L.

Blokhintsev, L. D. (see Akimova, M. K.) — 1259.

— (see Shapiro, I. S.) — 775.

Bogdankevich, O. V., L. E. Lazareva, and A. M. Moiseev. Inelastic Scattering of Photons on Rh^{103} Nuclei — 853.

Bogolyubov, N. N., D. N. Zubarev, and Yu. A. Tserkovnikov. An Asymptotically Exact Solution for the Model Hamiltonian of the Theory of Superconductivity — 88.

Bolotin, V. F. (see Akhmatov, A. P.) — 376.

Boos, É. G. Analysis of Nuclear Interactions of Nucleons with $E \geq 10^{11}$ ev in Photographic Emulsions — 433.

Borodin, A. V. (see Akhmatov, A. P.) — 376.

Borovik-Romanov, A. S. and V. I. Ozhogin. Weak Ferromagnetism in an Antiferromagnetic $CoCO_3$ Single Crystal — 18.

Borovikov, A. V. (see Rusinov, L. I.) — 1064.

Brandt, N. B. and N. I. Ginzburg. Superconductivity of Crystalline Modifications of Bismuth — 1082.

— and M. V. Razumeenko. On the Effect of Impurities on the Energy Spectrum of Electrons in Bismuth — 198.

Braun, M. A. On the Normalization Constants of the State Vectors in Field Theory — 514.

— and Yu. V. Novozhilov. Some Properties of Dressed Particle Operators in Field Theory — 919.

— and L. V. Prokhorov. Properties of the Scattering Amplitude Conditioned by the Unitarity Condition — 1146.

Brodskiĭ, A. M. Effect of Weak Interactions on the Electromagnetic Properties of Fermions — 229.

Bryukhanov, V. A. (see Delyagin, N. N.) — 159L.

— (see Delyagin, N. N.) — 619L.

Buishvili, L. L., G. R. Khutsishvili, and O. D. Cheĭshvili. Magnetic Relaxation in Ferromagnetic Metals — 507.

Bukat, G. M. Calculation of l-Forbidden Transition Probabilities — 1198.

Bulaevskiĭ, L. N., V. M. Faĭn, and G. I. Freĭdman. Instability of Uniform Precession of Magnetization — 361L.

Bulatova, R. F., V. S. Kogan, and B. G. Lazarev. Crystal Structure of Solid Deutero-Hydrogen — 1291L.

Bunyatov, S. A. (see Batusov, Yu. A.) — 354L.

— (see Batusov, Yu. A.) — 1290L.

Burmistrov, V. R. and V. P. Radchenko. Two-Cascade Transition in the Nd^{144} Nucleus Accompanying the Capture of Thermal Neutrons — 411.

Bushmanov, V. K. Hydrodynamic Stability of a Liquid Layer on a Vertical Wall — 873.

Buslaev, V. S. Dispersion Relations in Nonrelativistic Scattering Theory in which Account is Made for Spin-Orbit Interaction — 990.

Bychkov, Yu. A. Influence of Impurities on the De Haas-Van Alphen Effect — 971.

— Quantum Theory of the Electrical Conductivity of Metals in Strong Magnetic Fields — 483.
Bykov, V. P. (see Kapitza, S. P.) — 693.
Chaĭka, M. P. (see Kaliteevskiĭ, N. I.) — 661.
Charakhch'yan, A. N., V. F. Tulinov, and T. N. Charakhch'yan. Cosmic Rays from the Sun — 179.
Charakhch'yan, T. N. (see Charakhch'yan, A. N.) — 179.
Cheĭshvili, O. D. (see Buishvili, L. L.) — 507.
Cheng Lin-Yang (see Wang Kang-Ch'ang) — 1291L.
Cheng P'u-Ying (see Dzhanelidze, L. P.) — 863.
Cheremnykh, P. A. (see Akhmatov, A. P.) — 376.
Chernov, G. M. (see Azimov, S. A.) — 1068.
Chernova, L. P. (see Azimov, S. A.) — 1068.
Chibisov, M. I. (see Firsov, O. B.) — 1235.
Chikin, R. V. (see Akhmatov, A. P.) — 376.
Chilashvili, G. A. (see Vashakidze, I. Sh.) — 278.
— (see Vashakidze, I. Sh.) — 466.
Chirkin, G. K. (see Bil'dyukevich, A. L.) — 1078.
Chirkov, A. K. and A. A. Kokin. On the Shape of the Electron Resonance Line in a Particle System Possessing an Anisotropic g-Factor — 964.
Chou Kuang-Chao. On the Pseudovector Current and Lepton Decays of Baryons and Mesons — 492.
— (see Ho Tso-Hsiu) — 1032L.
— (see Lapidus, L. I.) — 82.
— (see Lapidus, L. I.) — 735.
— (see Lapidus, L. I.) — 898.
— (see Lapidus, L. I.) — 258.
Chubinskiĭ, O. V. (see Artamonova, K. P.) — 1109.
Chudakov, V. M. (see Azimov, S. A.) — 1068.
Chuev, V. I. (see Vlasov, N. A.) — 1020L.
— (see Vlasov, N. A.) — 1127.
— (see Vlasov, N. A.) — 1129.
Chuvilo, I. V. (see Ivanovskaya, I. A.) — 31.
Ciulli, S. (see Fischer, J.) — 941.
Dalkhazhav, N. (see Belyakov, V. A.) — 650.
— (see Wang Shu-Fen) — 663.
Deĭgen, M. F. and V. Ya. Zevin. Spin-lattice Relaxation of Local Electron Centers in Nonmetallic Crystals — 785.
Delyagin, N. N., V. S. Shpinel', V. A. Bryukhanov, and B. Zvenglinskiĭ. Hyperfine Structure of Gamma Rays Produced by Quadrupole Interaction in a Crystal Lattice — 159L.
—, V. S. Shpinel', V. A. Bryukhanov, and B. Zvenglinskiĭ. Nuclear Zeeman Effect in Sn^{119} — 619L.
Demidov, B. A. and S. D. Fanchenko. Observation of Charged Relativistic Particles in a Luminescent Chamber — 46.
Dmitriev, I. S. (see Nikolaev, B. S.) — 627.
Dmitriev, V. N., L. V. Drapchinskiĭ, K. A. Petrzhak, and Yu. F. Romanov. Energy Distribution of the Fragments of Triple U^{235} Fission — 390.
Dneprovskiĭ, I. S., L. Német, and L. K. Peker. Decay of Er^{161} — 8.
Dnestrovskiĭ, Yu. N. and D. P. Kostomarov. Electromagnetic Waves in Half-space Filled with a Plasma — 587.
Dokuchaev, V. P. On the Growth of Magnetohydrodynamic Waves in a Plasma Stream Moving through an Ionized Gas — 292.
Dolinskiĭ, É. I. (see Akimova, M. K.) — 1259.
Dovzhenko, O. I. Calculation of Transition Effects at Various Distances from the Electron-Photon Shower Axis — 1178.
— (see Emel'yanov, A. A.) — 567.
Drapchinskiĭ, L. V. (see Dmitriev, V. N.) — 390.
Dremin, I. M. Peripheral Interactions between π Mesons and Nucleons at High Energies — 94.
Dulkova, L. S. Polarization of Deuterons Elastically Scattered on Helium — 701.
Dykhne, A. M. and V. L. Pokrovskiĭ. Change of the Adiabatic Invariant of a Particle in a Magnetic Field. I — 264.
— (see Pokrovskiĭ, V. L.) — 503.
Dzhanelidze, L. P., D. K. Kopylova, Yu. B. Korolevich, N. I. Kostanashvili, K. V. Mandritskaya, N. I. Petukhova, M. I. Podgoretskiĭ, D. Tuvdendorzh, O. A. Shakhulashvili, and Cheng P'u-Ying. Production of Charged Hyperons by 9 Bev Protons Interacting with Photographic Emulsion Nuclei — 671.
Dzhibuti, R. I. and A. V. Tagviashvili. Photodisintegration of the He^4 Nucleus at High Energies — 1225.
Dzyub, I. P. Contribution to the Theory of Exciton States in Semiconductors — 429.
Efimov, G. V. (see Barbashov, B. M.) — 316.
Efremov, A. V., V. A. Meshcheryakov, and D. V. Shirkov. Pion-Nucleon Scattering at Low Energies I. — 308.
—, V. A. Meshcheryakov, and D. V. Shirkov. Pion-Nucleon Scattering at Low Energies, II — 766.
Egorov, G. A. and Yu. V. Yablokov. Paramagnetic Resonance in a Quasi-Single Crystal of CrCl$_3$ — 190.
Éliashberg, G. M. Temperature Green's Function for Electrons in a Superconductor — 1000.
Eliseev, G. P. (see Alikhanov, A. I.) — 414.
Emel'yanov, A. A. and O. I. Dovzhenko. Lateral Distribution of High Energy Nuclear-active Particles in the Core of Extensive Atmospheric Showers — 567.
Épshteĭn, É. M. (see Guliev, N. A.) — 304.
Érnst, B. M. (see Lomsadze, Yu. M.) — 803L.
Fabelinskiĭ, I. L. (see Ablekov, V. K.) — 618L.
Faddeev, L. D. Scattering Theory for a Three-particle System — 1014.
Faĭn, V. M. (see Bulaevskiĭ, L. N.) — 361L.
— (see Ginzburg, V. L.) — 923.
Fakidov, I. G. (see Gaĭdukov, L. G.) — 636.
— (see Krasovskiĭ, V. P.) — 170.
Fanchenko, S. D. (see Demidov, B. A.) — 46.
Fateeva, L. N. (see Nikolaev, V. S.) — 627.
Fedorov, F. I. (see Moroz, L. G.) — 209.
Fesenko, A. I. (see Ivanov, Yu. M.) — 1037.
Fikhtengol'tz, I. G. On the Coordinate Conditions in Einstein's Theory of Gravitation — 564.
Filippov, A. I. (see Kozodaev, M. S.) — 644.
Filov, R. A. (see Ostroumov, V. I.) — 77.
Firsov, O. B. and M. I. Chibisov. Bremsstrahlung of Slow Electrons Decelerated by Neutral Atoms — 1235.
— (see Mordvinov, Yu. P.) — 301.
Fischer, J. and S. Ciulli. Recurrent Construction of Angular Operators, II. – 941.
Fogel', Ya. M., A. G. Koval', Yu. Z. Levchenko, and A. F. Khodyachikh. Composition of the Ions Produced During the Ionization of Gases by Negative Ions — 384.
—, V. F. Kozlov, and G. N. Polyakova. Double Charge Exchange of Alkali Metal Ions — 826

Fradkin, É. E. (see Kaliteevskiĭ, N. I.) — 661.

Frank-Kamenetskiĭ, D. A. Natural Oscillations of a Bound Plasma — 469.

— (see Akhmatov, A. P.) — 376.

— (see Patrushev, B. I.) — 1045.

— (see Rysanov, V. D.) — 1041.

Franke, V. A. Application of Mandelstam's Method to a Computation of the Scattering Amplitude with Anomalous Singularities — 1268.

Freĭdman, G. I. (see Bulaevskiĭ, L. N.) — 361L.

Friedlander, E. M. Investigation of Azimuthal Effects in Meson Showers Produced by 9-Bev Protons — 669.

Frolov, G. V. Polarization Phenomena in the Compton Effect. — 1276.

Gaĭdukov, L. G., N. P. Grazhdankina, and I. G. Fakidov. Investigation of the Temperature Dependence of the Spontaneous Magnetization of Chromium Telluride — 636.

Gaĭdukov, Yu. P. (see Alekseevskiĭ, N. E.) — 837.

Galitskiĭ, V. M. On the Problem of Pairing with Non-Zero Angular Momenta — 806L.

Galkin, A. A., É. A. Kaner, and A. P. Korolyuk. Investigation of Ultrasonic Absorption by a Metal in a Magnetic Field — 1055

— (see Bezuglyĭ, P. A.) — 810L.

— (see Bezuglyĭ, P. A.) — 4.

Gantmakher, V. F. and Yu. V. Sharvin. Non-monotonic Dependence of the Surface Impedance of Tin on the Magnetic Field at 1.9 Megacycles — 358L.

— (see Sharvin, Yu. V.) — 866.

Gaponov, A. V. Instability of a System of Excited Oscillators with Respect to Electromagnetic Perturbations — 232.

Garibyan, G. M. Phenomenological Quantum Electrodynamics in the Case of Two Media — 1138.

— Radiation of a Particle Moving across the Interface of Two Media with Account of Multiple Scattering — 237.

Garif'yanov, N. S. (see Avvakumov, V. I.) — 847.

Garkusha, V. I. (see Rusanov, V. D.) — 1041.

Gavrin, P. P. (see Akhmatov, A. P.) — 376.

Gazazyan, A. D. (see Ter-Mikaelyan, M. L.) — 1183.

Geĭlikman, B. T. and V. Z. Kresin. On Thermomagnetic Effects in Superconductors — 352.

Gel'fer, G. (see Vovchenko, V. G.) — 1084.

Gerasimova, N. M. Energy Fluctuations in the Interaction Between High Energy Particles — 758.

Gershteĭn, S. S. On the Probability of Meson Capture in Different Meso-Atomic Levels — 815L.

Gershuni, G. Z. On a Certain Mechanism of Absorption of Ultrasound in Paramagnetic Metals in a Magnetic Field — 256.

Geshkenbeĭn, B. V. (see Valuev, B. N.) — 728.

Ginzburg, N. I. (see Brandt, N. B.) — 1082.

Ginzburg, V. L. and V. M. Faĭn. Contribution to the Theory of Ferro- and Antiferromagnetism — 923.

— and A. P. Levanyuk. Raman Scattering of Light near Second-Order Phase-Transition Points — 138.

Giterman, M. Sh. (see Voronel', A. V.) — 809L.

Glagolev, V. L., A. M. Morozov, and P. A. Yampol'skiĭ. On Reactions Involving the Formation of the Pb^{205m} Isomer — 1131.

Glagolev, V. V. (see Belyakov, V. A.) — 650.

Gofman, Yu. V. and O. F. Nemets. Elastic Scattering of Deuterons by Nuclei — 1035.

Gol'danskiĭ, V. I. Limits of Stability and Proton and Two-proton Radioactivity of Neutron-Deficient Isotopes of Light Nuclei — 348.

— and V. M. Maksimenko. The Hypothesis of the Neutral ρ^0 Meson in the Light of Data on Antiproton Annihilation — 584.

—, O. A. Karpukhin, and G. G. Petrov. Observation of Positronium Reactions in Aqueous Solutions — 1026L.

Gor'kov, L. P. (see Abrikosov, A. A.) — 1243.

— (see Abrikosov, A. A.) — 337.

Gorshkov, V. G. Account of the Nuclear Coulomb Field in Processes Involving the Interaction Between Electrons and an Electromagnetic Field — 983.

— (see Krutov, V. A.) — 417.

Goryunov, N. N. and G. T. Zatsepin. Observation of μ-meson Bursts in a Set of Ionization Chambers — 195.

Govorov, A. M. (see Li Ga Youn) — 163.

Gramenitskiĭ, I. M. (see Wang Shu-Fen) — 663.

Grashin, A. F. and Yu. P. Nikitin. On the Nucleon-nucleon Potential — 498.

Grazhdankina, N. P. (see Gaĭdukov, L. G.) — 636.

Grechukhin, D. P. The Possibility of Experimental Verification of the Nonaxial Rotator Model by Studying the Effect of the Medium on the Angular Correlation of a Gamma Quantum Cascade — 957.

Grigor'ev, V. I. (see Vavilov, B. T.) — 554.

Grin', Yu. T. Effect of Pair Correlation of Nucleons on the Probabilities of Electromagnetic Transitions in the Nucleus — 100.

Grishin, V. G. (see Bannik, B. P.) — 69.

— (see Wang Shu-Fen) — 663.

Guliev, N. A. and É. M. Épshteĭn. Bremsstrahlung from a Distributed Proton — 304.

Gur'ev, V. N. (see Sitenko, A. G.) — 1128.

Gurevich, A. V. On the Theory of Runaway Electrons — 904.

Gustova, L. V. (see Artamonova, K. P.) — 1109.

Gvozdev, V. S. (see Rusinov, L. I.) — 1064.

Ho Tso-Hsiu and Chou Kuang-Chao. Pion-Pion Resonance in p State — 1032L.

— (see Hsien Ting-Ch'ang) — 1165.

Hsien Ting-Ch'ang, Ho Tso-Hsiu, and W. Zöllner. Low-Energy $\pi\pi$ Scattering Integral Equations — 1165.

Ignatenko, V. A. (see Kirenskiĭ, L. V.) — 881.

Igosheva, T. N. (see Kikoin, I. K.) — 816L.

Ilescu, E. (see Vasilevskiĭ, I. M.) — 616L.

Ioffe, M. S., R. I. Sobolev, V. G. Tel'kovskiĭ, and E. E. Yushmanov. Investigation of Magnetic Mirror Confinement of a Plasma. I. — 1117.

Ivanenko, I. P. (see Vernov, S. N.) — 356L.

Ivanov, V. G. (see Wang Kang-Ch'ang) — 1292L.

Ivanov, Yu. M. and A. I. Fesenko. Investigation of μ^+-Meson Depolarization in a Nuclear Emulsion — 1037.

Ivanova, N. S. (see Assovskaya, A. S.) — 1051.

Ivanovskaya, I. A., E. V. Kuznetsov, É. I. Mal'tsev, A. Prokesh, G. M. Stashkov, and I. V. Chuvilo. A Possible Neutral Cascade Meson Decay — 31.

Kadomtseva, A. M. (see Belov, K. P.) — 799L.

Kaganov, M. I. Excitation of Standing Spin Waves in a Film — 114.

— and V. M. Tsukernik. Theory of Non-resonance Absorption of an Oscillating Magnetic Field by a Ferromagnetic Dielectric — 362L.
Kaganskiĭ, M. G. (see Vasilenko, S. S.) — 672.
Kaipov, D. K. and Yu. K. Shubnyĭ. Effect of Collisions of Recoil Nuclei on the Cross Section for Resonance Scattering of Gamma Rays by Ni^{60} — 615L.
Kalinin, S. P. (see Vlasov, N. A.) — 1020L.
— (see Vlasov, N. A.) — 1127.
— (see Vlasov, N. A.) — 1129.
Kaliteevskiĭ, N. I., É. E. Fradkin, and M. P. Chaĭka. Quadrupole Moments of Odd Barium Isotopes — 661.
Kalyush, A. V. (see Yakovlev, V. A.) — 219.
Kaminskiĭ, D. L. (see Vasilenko, S. S.) — 672.
Kanavets, V. P. (see Barmin, V. V.) — 683.
Kaner, É. A. Theory of Absorption of Ultrasound by Metals in a Strong Magnetic Field, II — 747.
— (see Azbel’, M. Ya.) — 58.
— (see Galkin, A. A.) — 1055.
Kapitza, S. P. Radiation from a Charge Moving in an Inhomogeneous Medium — 954.
—, V. P. Bykov, and V. N. Melekhin. A High Current Microtron — 693.
Kaplan, I. G. On the Diamagnetism of a System of Interacting Particles — 733.
Karadzhev, K. V. and V. I. Man’ko. Polarization of Protons Scattered from O^{16} — 294.
Karnaukhov, V. A. and N. I. Tarantin. On the Possibility of Proton Decay of Nuclei — 771.
Karpman, V. I. The Microscopic Theory of the Fermi Liquid — 133.
Karpukhin, O. A. (see Gol’danskiĭ, V. I.) — 1026L.
Kazarinov, Yu. M. (see Amaglobeli, N. S.) — 657.
Kazarnovskiĭ, M. V. and A. V. Stepanov. Elastic Resonance Scattering of Slow Neutrons in Crystals — 723.
Kessel’, A. R. Effect of Pulsed Acoustic Resonance Action on a Nuclear Spin System — 604.
Khabibullin, B. M. Inelastic Magnetic Scattering of Slow Neutrons on Phonons — 714.
Khaĭkin, M. S. Concerning Cyclotron Resonance in Tin — 359L.
— Oscillator Dependence of the Surface Resistance of a Metal on a Weak Magnetic Field — 152L.
— Paramagnetic Resonance in Single-Crystal Tin — 623L.
Khalatnikov, I. M. (see Bekarevich, I. L.) — 1187.
— (see Lifshitz, E. M.) — 108.
— (see Lifshitz, E. M.) — 558.
Khalfin, L. A. A Fundamental Method for Measuring Time — 353L.
— On the Influence of the Inelastic Processes on the Elastic Scattering in the Vicinity of the Thresholds of the Inelastic Reaction Modes — 709.
Khalkin, V. A. (see Wang Yung-Yü) — 166.
— (see Wang Yung-Yü) — 370.
Khazov, Yu. L. (see Rusinov, L. I.) — 1064.
Khoduleva, Z. K. (see Nakhutin, I. E.) — 687.
Khodyachikh, A. F. (see Fogel’ Ya. M.) — 384.
Khofmokl’, T. (see Wang Kang-Ch’ang) — 1292L.
Khriplovich, I. B. (see Baĭer, V. N.) — 959.
Khristiansen, G. B. (see Vernov, S. N.) — 356L.
Khudaverdyan, A. G. (see Vartapetyan, G. A.) — 16.
Khutsishvili, G. R. (see Buishvili, L. L.) — 507.
Kikoin, I. K. and S. D. Lazarev. Anisotropy of Even Photomagnetic Effect in n-Germanium at Low Temperatures — 1022L.
—, N. A. Babushkina, and T. N. Igosheva. Magnetic Change in Resistivity of Ferromagnets above the Curie Point — 816L.
Kim Hi Ying (see Wang Kang-Ch’ang) — 1291L.
Kirenskiĭ, L. V., V. A. Ignachenko, and A. M. Radichev. Behavior of Domain Structure under the Action of Elastic Stresses — 881.
Kladnitskaya, E. N. (see Wang Kang-Ch’ang) — 1291L.
Klyucharev, A. P. (see Val’ter, A. K.) — 807L.
Kobzarev, I. Yu. and L. B. Okun’. Signs of Constants of Strong Interactions — 150L.
— and L. B. Okun’. Which is the Heavier, the K$_1^0$ Meson or K$_2^0$ Meson? — 426.
Kogan, A. V., V. D. Kul’kov, L. P. Nikitin, N. M. Reĭnov, I. A. Sokolov, and M. F. Stel’makh. Polarization of Sc^{46} Nuclei in Iron — 34.
Kogan, V. S. (see Bulatova, R. F.) — 1291L.
Kokin, A. A. (see Chirkov, A. K.) — 964.
Koksharova, S. F. (see Vasilenko, S. S.) — 672.
Kolesnikov, N. N. (see Voronkov, V. V.) — 136.
Kolganova, É. D. (see Vaĭsenberg, A. O.) — 834.
Kolkunov, V. A., L. B. Okun’, A. P. Rudik, and V. V. Sudakov. Location of the Nearest Singularities of the $\pi\pi$-scattering Amplitude — 242.
Komar, A. P. (see Vorob’ev, A. A.) — 50.
Kompaneets, A. S. On the Bond in the C^{12} — C^{12} Nuclear Molecule — 1196.
Kondrat’ev, L. N. (see Balats, M. Ya.) — 813.
Konstantinov, O. V. and V. I. Perel’. A Diagram Technique for Evaluating Transport Quantities — 142.
— and V. I. Perel’. Collisions of Particles in a High Temperature Plasma — 597.
Kopaleĭshvili, T. I. (see Vashakidze, I. Sh.) — 278.
— (see Vashakidze, I. Sh.) — 466.
Kopylov, G. I. A Method of Calculation of the Statistical Weights and Distributions in Multiple Production Theories — 761.
— Concerning the Paper “Evaluation of Phase Integrals in the Covariant Formulation of the Theory of Multiple Production of Particles” by L. G. Yakovlev — 150L.
Kopylova, D. K. (see Dzhanelidze, L. P.) — 863.
Korkhmazyan, N. A. (see Amatuni, A. Ts.) — 703.
Kornfel’d, M. I. and V. V. Lemanov. Nuclear Magnetic Resonance in Plastically Deformed Rock Salt — 188.
— and V. V. Lemanov. Quadrupole Effects in Nuclear Magnetic Resonance in NaNO$_3$ — AgNO$_3$ Mixed Crystals — 38.
Korolev, V. A. (see Vorob’ev, A. A.) — 50.
Korolevich, Yu. B. (see Dzhanelidze, L. P.) — 863.
Korolyuk, A. P. (see Bezuglyĭ, P. A.) — 4.
— (see Galkin, A. A.) — 1055.
Kosevich, A. M. (see Andreev, V. V.) — 517.
Kostanashvili, N. I. (see Dzhanelidze, L. P.) — 863.
Kostomarov, D. P. (see Dnestrovskiĭ, Yu. N.) — 587.
Koval’, A. G. (see Fogel’, Ya. M.) — 384.
Kovan, I. A. (see Akhmatov, A. P.) — 376.
— (see Patrushev, B. I.) — 1045.
— (see Rusanov, V. D.) — 1041.

Kovrizhnykh, L. M. Shock Waves in Relativistic Magnetohydrodynamics — 725.
Kozlov, V. F. (see Fogel', Ya. M.) — 826.
Kozodaev, M. S., M. M. Kulyukin, R. M. Sulyaev, A. I. Filippov, and Yu. A. Shcherbakov. Angular and Momentum Distribution of Residual Nuclei Produced in the Inelastic Scattering of Fast Pions and Protons on Helium — 644.
Krasovskiĭ, V. P. and I. G. Fakidov. Magnetocaloric Effect in the Low-temperature Range of Transformation of Magnetite — 170.
Kresin, V. Z. (see Geĭlikman, B. T.) — 352.
Krestnikov, Yu. S. (see Barmin, V. V.) — 857.
Krivko, N. I. and N. M. Reĭnov. Experimental Determination of Polaron Mass in Cuprous Oxide — 1289L.
Krokhin, O. N. (see Basov, N. G.) — 1240.
— (see Basov, N. G.) — 1033L.
Krutov, V. A. and V. G. Gorshkov. Higher Born Approximation in Pair Conversion — 417.
Kuks, I. M. (see Zhdanov, A. P.) — 819.
Kul'chitskiĭ, L. A. and V. Presperin. Fast Photoneutrons from Some Elements — 696.
Kuleshova, L. V. (see Al'tshuler, L. V.) — 10.
Kulikov, G. V. (see Vernov, S. N.) — 356L.
Kul'kov, V. D. (see Kogan, A. V.) — 34.
Kulyukin, M. M. (see Kozodaev, M. S.) — 644.
Kuo Ch'i-Ting and B. S. Ratner. Investigation of the (γ, p) Reaction on the Sn^{120} Isotope — 1098.
Kutikov, I. E. (see Spivak, P. E.) — 1027L.
Kuz'min, V. A. (see Zatsepin, G. T.) — 1171.
Kuznetsov, A. A. (see Wang Kang-Ch'ang) — 1292L.
Kuznetsov, A. S. (see Vovchenko, V. G.) — 1084.
Kuznetsov, E. V. (see Ivanovskaya, I. A.) — 31.
Kuznetsov, V. P. Internal Bremsstrahlung and Electromagnetic Corrections to $\mu - e$-decay — 1202.
Kuznetsov, V. V. (see Wang Yung-Yü) — 166.
— (see Wang Yung-Yü) — 370.
Kuznetsova, M. Ya. (see Wang Yung-Yü) — 166.
— (see Wang Yung-Yü) — 370.
Landau, L. D. Low Binding Energies in Quantum Field Theory — 1293L.
Landsberg, L. G. (see Balats, M. Ya.) — 813L.
Lapidus, L. I. and Chou Kuang-Chao. Dispersion Relations and Analysis of the Energy Dependence of Cross Sections near Thresholds of New Reactions — 82.
— and Chou Kuang-Chao. Elastic Scattering of γ Quanta by Nuclei — 735.
— and Chou Kuang-Chao. Elastic Scattering of γ-Rays on Deuterons below the Pion-Production Threshold — 898.
— and Chou Kuang-Chao. Inelastic Final-state Interactions and Near-threshold Singularities — 258.
Lazarev, B. G., E. E. Semenenko, and A. I. Sudovtsov. Polymorphic Transitions of Lithium, Sodium, and Potassium in Films Condensed on a Cold Substrate — 811L.
— (see Bulatova, R. F.) — 1292L.
Lazarev, S. D. (see Kikoin, I. K.) — 1022L.
Lazareva, L. I. (see Bogdankevich, O. V.) — 853.
Lebedev, P. I. (see Balats, M. Ya.) — 813L.
Lebedev, R. M. (see Belyakov, V. A.) — 650.
— (see Wang Shu-Fen) — 663.
Lemanov, V. V. Second-order Quadrupole Effects in Sodium Nitrate — 187.
— (see Kornfel'd, M. I.) — 188.
— (see Kornfel'd, M. I.) — 38.
Lend'el, V. I. (see Lomsadze, Yu. M.) — 803L.
Levanyuk, A. P. (see Ginzburg, V. L.) — 138.
Levchenko, Yu. Z. (see Fogel', Ya. M.) — 384.
Li Ga Youn, G. M. Osetinskiĭ, N. Sodnom, A. M. Govorov, I. V. Sizov, and V. I. Salatskiĭ. Investigation of the $He^3 + H^3$ Reaction — 163.
Lifshitz, E. M. and I. M. Khalatnikov. On the Singularities of Cosmological Solutions of the Gravitational Equations. I. — 108.
— and I. M. Khalatnikov. On the Singularities of Cosmological Solutions of the Gravitational Equations, II — 558.
Lifshitz, I. M. (see Alekseevskiĭ, N. E.) — 837.
Liperovskiĭ, V. A. On the Anisotropy in the Propagation of Longitudinal Electroacoustic Oscillations in a Drifting Plasma — 951.
Litvin, V. F. (see Alekseev, N. V.) — 1049.
Lobov, G. A. Polarization of Internal Conversion Electrons and Positrons Emitted After β decay of the Nucleus — 479.
Lomsadze, Yu. M., V. I. Lend'el, and B. M. Érnst. High-Energy Behavior of the Total Cross Section for π-p Scattering — 803L.
Luk'yanov, V. K. Rotational State Energies of Nonaxial Nuclei with $J = 10$ and $J = 12$ — 731.
Lutsik, V. A. (see Val'ter, A. K.) — 807L.
Lyubimov, V. A. (see Alikhanov, A. I.) — 414.
Lyul'ka, V. A. π^--Mesic Decay of the ${}_\Lambda H^3$ Hypernucleus — 56.
— Energy and Angular Distributions from Decays of Hypernuclei — 331.
Maksimenko, V. M. and I. L. Rozental'. On Covariant Statistical Theories of Multiple Particle Production — 527.
— (see Gol'danskiĭ, V. I.) — 584.
Maleev, S. V. On the Use of the Mössbauer Effect for Studying Localized Oscillations of Atoms in Solids — 617L.
— (see Bar'yakhtar, V. G.) — 995.
Malevskaya, L. A. (see Belov, K. P.) — 1074.
Malkiél', G. S. On Slow and Fast Neutron Capture Processes in the Theory of Origin of Elements — 1143.
Malkov, E. I. and I. M. Shmushkevich. Electromagnetic Radiation Emitted in the Collisions Between Charged Particles with Close Specific Charge e/m Values — 1281.
Mal'tsev, É. I. (see Ivanovskaya, I. A.) — 31.
Mal'tsev, V. M. and Yu. D. Prokoshkin. On Secondary Processes in the Production of π Mesons on Nuclei — 1134.
Mamaladze, Yu. G. On Mutual Friction in Helium II — 595.
Mamasakhlisov, V. I. (see Vashakidze, I. Sh.) — 466.
Mandritskaya, K. V. (see Dzhanelidze, L. P.) — 863.
Man'ko, V. I. (see Karadzhev, K. V.) — 294.
Marutyan, N. A., K. A. Matevosyan, and R. T. Toshyan. Interaction of 5×10^{12} ev Nucleons with Photographic Emulsion Nuclei — 689.

Matevosyan, K. A. (see Marutyan, N. A.) — 689.
Matinyan, S. G. On the Determination of the Sign of the Mass Difference of K_1^0 and K_2^0 Mesons — 1219.
Mekhedov, V. N. (see Wang Yung Yü) — 370.
Melekhin, V. N. (see Kapitza, S. P.) — 693.
Mel'nikova, N. N. (see Belyakov, V. A.) — 650.
Mentkovskiĭ, Yu. L. On Perturbation Theory for Large Quantum Systems — 225.
Meshcheryakov, M. G. (see Vovchenko, V. G.) — 1084.
Meshcheryakov, V. A. (see Efremov, A. V.) — 308.
— (see Efremov, A. V.) — 766.
Mikaélyan, L. A. (see Spivak, P. E.) — 404.
— (see Spivak, P. E.) — 1027L.
Moiseev, A. M. (see Bogdankevich, O. V.) — 853.
Mordvinov, Yu. P. and O. B. Firsov. Dependence of the Inelastic Collision Cross Sections of Atoms and Ions on Velocity in the Case of Pseudo-intersection of the Levels — 301.
Moroz, L. G. On Electromagnetic Scattering of Spin ½ Particles — 416.
— and F. I. Fedorov. The Scattering Matrix with the Pauli Interaction Taken into Account — 209.
Morozov, A. M., V. V. Remaev, and P. A. Yampol'skiĭ. Five New Millisecond Isomers Produced by 19.2 Mev Protons — 674.
— (see Glagolev, V. L.) — 1131.
Morozov, B. V. (see Barmin, V. V.) — 683.
Musicař, Č. The Vavilov-Cerenkov Effect in Uniaxial Crystals — 117.
Nakhutin, I. E., V. V. Ovechkin, D. V. Ochkin, A. S. Polyakov, and S. K. Khoduleva. Production of the Radioactive Isotope Kr^{85} and Measurement of its γ Radiation — 687.
Nemét, L. (see Dneprovskiĭ, I. S.) — 8.
Nemets, O. F. (see Gofman, Yu. V.) — 1035.
— (see Zaika, N. I.) — 1.
Nemilov, Yu. A. (see Alekseev, N. V.) — 1049.
Nemirovskiĭ, P. E. Cross Sections for Radiative Capture of Neutrons by Heavy Nuclei — 1213.
Neudachin, V. G., V. G. Shevchenko, and N. P. Yudin. The Position of the Giant Resonance in the Dipole Absorption of Gamma Quanta by Atomic Nuclei — 79.
Nevzglyadov, V. G. Thermodynamics of Turbulent Systems — 1206.
Nguyen Dinh Ty (see Wang Kang-Ch'ang) — 1292L.
Nikishov, A. I. Radiative Corrections to the Scattering of μ Mesons on Electrons — 529.
Nikitin, A. V. (see Wang Kang-Ch'ang) — 1292L.
Nikitin, L. P. (see Kogan, A. V.) — 34.
Nikitin, V. A. (see Belyakov, V. A.) — 650.
Nikitin, Yu. P. (see Grashin, A. F.) — 498.
Nikolaev, V. S., I. S. Dmitriev, L. N. Fateeva, and Ya. A. Teplova. Investigation of the Equilibrium Charge Distribution in a Fast Ion Beam — 627.
Nikol'skiĭ, S. I. and A. A. Pomanskiĭ. Calculation of Averaged Characteristics of Extensive Atmospheric Cosmic Ray Showers — 934.
— and Yu. A. Smorodin. Interpretation of Experimental Data on the Spectrum of Electron-Photon Cascades with Energy 10^{12} ev in the Upper Layers of the Atmosphere — 804L.
Nomofilov, A. A. (see Wang Shu-Fen) — 663.
Nosov, V. G. Theory of Alpha Decay of Nonspherical Nuclei — 102.
— Determination of the Deformation of α-Active Nuclei and Their Quadrupolarization on Basis of the α-Particle Energy and Angular Distributions — 1159.
Novozhilov, Yu. V. (see Braun, M. A.) — 727.
Obukhov, B. V. (see Balats, M. Ya.) — 813L.
Ochkin, D. V. (see Nakhutin, I. E.) — 687.
Oganov, M. N. (see Akhmatov, A. P.) — 376.
Ogloblin, A. A. (see Vlasov, N. A.) — 1020L.
— (see Vlasov, N. A.) — 1127.
— (see Vlasov, N. A.) — 1129.
Okonov, É. O. Annihilation of an Antiproton-Proton System — 738.
—, N. I. Petrov, A. M. Rozanova, and V. A. Rusakov. Four-Pronged Decay of the Long Lived K^0 Meson — 48.
— (see Shirokov, M. I.) — 204.
Okun', L. B. Properties of the Axial Vector Interaction and the Decay $\Sigma \rightarrow \Lambda + e + \nu$ — 154L.
— and A. P. Rudik. The Decay $\Sigma^0 \rightarrow \Lambda^0 + 2\gamma$ and the Magnetic Moment of the Σ^0 Hyperon — 268.
— and A. P. Rudik. On the Decays $K^+ \rightarrow \pi + e^+ + e^-$ and $K^+ \rightarrow \pi^+ + \mu^+ + \mu^-$ — 422.
— (see Kobzarev, I. Yu.) — 150L.
— (see Kobzarev, I. Yu.) — 426.
— (see Kolkunov, V. A.) — 242.
Oraevskiĭ, V. N. On Resonance Photon-photon Scattering — 730.
Orlenko, B. F. (see Pasechnik, M. V.) — 634.
Osetinskiĭ, G. M. (see Li Ga Youn) — 163.
Osovets, S. M. Dynamic Stabilization of a Plasma Ring — 221.
Ostroumov, V. I., N. A. Perfilov, and R. A. Filov. Energy Spectrum of Cascade Alpha Particles in Photographic Emulsion Stars Produced by High-Energy Protons — 77.
Ovechkin, V. V. (see Nakhutin, I. E.) — 687.
Ozhogin, V. I. (see Borovik-Romanov, A. S.) — 18.
Pafomov, V. E. Radiation Emitted by a Charged Particle Passing through a Plate — 97.
Panova, N. M. (see Adamovich, M. I.) — 1103.
Pasechnik, M. V., N. N. Pucherov, B. F. Orlenko, and V. S. Prokopenko. Polarization of 6.8 Mev Protons Scattered on Carbon — 634.
Patashinskiĭ, A. Z. On Symmetry of the Solutions Obtained in Determining the Singularities of Feynman Diagrams by Landau's Method — 1217.
Patrushev, B. I., V. D. Rusanov, I. A. Kovan, V. V. Savichev, and D. A. Frank-Kamenetskiĭ. Gyrotropic Properties of a Plasma During Propagation of an Extraordinary Wave — 1045.
— (see Akhmatov, A. P.) — 376.
— (see Rusanov, V. D.) — 1041.
Pavlov, K. B. Some Properties of Stationary Flows in Magnetic Gas Dynamics — 216.
Pavlovskiĭ, M. N. (see Al'tshuler, L. V.) — 10.
Ped'ko, A. V. (see Belov, K. P.) — 666.
Peker, L. K. (see Dneprovskiĭ, I. S.) — 8.
Peletminskiĭ, S. V. (see Akhiezer, I. A.) — 913.
— (see Bar'yakhtar, V. G.) — 457.
Perel', V. I. (see Konstantinov, O. V.) — 142.
— (see Konstantinov, O. V.) — 597.

— (see Konstantinov, O. V.) — 597.
Perelomov, A. M. (see Zel'dovich, Ya. B.) — 777.
Perfilov, N. A. (see Ostroumov, V. I.) — 77.
Pershin, I. I. (see Barmin, V. V.— 857.
Peschanskiĭ, B. G. (see Alekseevskiĭ, N. E.) — 837.
Pesin, M. S. (see Ablekov, V. K.) — 618L.
Petrov, G. G. (see Gol'danskiĭ, V. I.) — 1026L.
Petrov, N. I. (see Okonov, É. O.) — 48.
Petrzhak, K. A. (see Dmitriev, V. N.) — 390.
Petrzhilka, V. (see Belyakov, V. A.) — 650.
Petukhova, N. I. (see Dzhanelidze, L. P.) — 863.
Piskarev, E. V. (see Akhmatov, A. P.) — 376.
Pitaevskiĭ, L. P. The Problem of the Form of the Spectrum of Elementary Excitations of Liquid Helium. II — 155L.
— Electric Forces in a Transparent Dispersive Medium — 1008.
Plyutto, A. A. Acceleration of Positive Ions in an Expanding Vacuum Spark Plasma — 1106.
— (see Dzhanelidze, L. P.) — 863.
— (see Wang Shu-Fen) — 663.
— (see Zastavenko, L. G.) — 711.
— and I. I. Roĭzen. On the Radiation of a Nucleus in the Presence of Unexcited Nuclei of the Same Type — 1023L.
Podkopaev, Yu. N. (see Artamonova, K. P.) — 1109.
Pokrovskiĭ, V. L. and A. M. Dykhne. Decay of Acoustic Excitations in Crystals — 503.
— (see Dykhne, A. M.) — 264.
Polovin, R. V. Contribution to the Theory of Simple Magnetohydrodynamic Waves — 326.
— On the Flow of a Plasma into Vacuum in the Presence of a Magnetic Field — 461.
— On the Motion of Shock Waves Along a Magnetic Field — 699.
Pol'skiĭ, Yu. E. (see Bil'dyukevich, A. L.) — 1078.
Polyakov, A. S. (see Nakhutin, I. E.) — 687.
Polyakova, G. N. (see Fogel', Ya. M.) — 826.
Pomanskiĭ, A. A. (see Nikol'skiĭ, S. I.) — 934.
Pomeranchuk, I. Ya. (see Berestetskiĭ, V. B.) — 752.
Pontecorvo, B. Experiments with Neutrinos Emitted by Mesons — 812L
— (see Balats, M. Ya.) — 813L.
Popov, Yu. M. (see Basov, N. G.) — 1033L.
Popova, V. M. (see Adamovich, M. I.) — 1103.
Porsev, G. D. (see Rusinov, L. I.) — 1064.
Presperin, V. (see Kul'chitskiĭ, L. A.) — 696.
Prokesh, A. (see Ivanovskaya, I. A.) — 31.
Prokhorov, A. M. (see Zverev, G. M.) — 41.
— (see Zverev, G. M.) — 160L.
— (see Zverev, G. M.) — 382.
Prokhorov, L. V. (see Braun, M. A.) — 1146.
Prokof'ev, A. N. (see Velyukhov, G. E.) — 395.
Prokopenko, V. S.(see Pasechnik, M. V.) — 634.
Prokoshin, Yu. D. (see Mal'tsev, V. M.) — 1134.
Ptukha, T. P. The Determination of the Coefficients of Diffusion and of Heat Conductivity of Weak Solution of He^3 in Helium II — 621L.
Pucherov, N. N. (see Pasechnik, M. V.) — 634.
Radchenko, V. P. (see Burmistrov, V. R.) — 411.
Ratner, B. S. (see Kuo Ch'i-Ting) — 1098.
Rautian, S. G. and I. I. Sobel'man. Negative Absorption in Metal Vapors — 156L.
Razumeenko, M. V. (see Brandt, N. B.) — 198.
Reĭnov, N. M. (see Kogan, A. V.) — 34.
— (see Krivko, N. I.) — 1289L.
Remaev, V. V. (see Morozov, A. M.) — 674.
Rodichev, A. M. (see Kirenskiĭ, L. V.) — 881.
Roĭnshvili, N. N. (see Andronikashvili, É. L.) — 192.
Roĭzen, I. I. (see Podgoretskiĭ, M. I.) — 1023L.
Romanov, A. M. Excited States of the Si^{30} Nucleus — 1072.
Romanov, Yu. A. Decay of a Plasmon at Absolute Zero — 464.
Romanov, Yu. F. (see Dmitriev, V. N.) — 390.
Rostovskiĭ, V. S. Electric Monopole Transitions in the Theory of Nonaxial Nuclei — 592.
Rozanova, A. M. (see Okonov, É. O.) — 48.
Rozental', I. L. (see Maksimenko, V. M.) — 527.
Rudik, A. P. (see Kolkunov, V. A.) — 242.
— (see Okun', L. B.) — 268.
— (see Okun', L. B.) — 422,
Rumyantseva, V. P. (see Barmin, V. V.) — 857.
Rusakov, V. A. (see Okonov, É. O.) — 48.
Rusanov, V. D., B. I. Patrushev, I. A. Kovan, V. I. Garkusha, and D. A. Frank-Kamenetskiĭ. Investigation of Magneto-acoustic Resonance in a Plasma with Aid of Double Electric Probes — 1041.
— (see Akhmatov, A. P.) — 376.
— (see Patrushev, B. I.) — 1045.
Rusinov, L. I., A. V. Borovikov, V. S. Gvozdev, G. D. Porsev, S. L. Sakharov, and Yu. L. Khazov. Investigation of the Decay Scheme of Dy^{166} — 1064.
Rus'kin, V. I. (see Usik, P. A.) — 1200.
Ruuge, E. K. (see Teplov, I. B.) — 640.
Sagdeev, R. Z. and V. D. Shafranov. On the Instability of a Plasma with an Anisotropic Distribution of Velocities in a Magnetic Field — 130.
Sakharov, S. L. (see Rusinov, L. I.) — 1064.
Salatskiĭ, V. I. (see Li Ga Youn) — 163.
Samoĭlov, I. M. and A. A. Sokolov. On Azimuthal Instabilities of Circulating Currents — 185.
Savichev, V. V. (see Patrushev, B. I.) — 1045.
Semenenko, E. E. (see Lazarev, B. G.) — 811L.
Semenko, S. F. (See Baldin, A. M.) — 306.
Semenova, E. I. (see Avvakumov, V. I.) — 847.
Shabalin, E. P. Spectra of K_{e4} and $K_{\mu 4}$ Decays — 245.
Shafranov, V. D. (see Sagdeev, R. Z.) — 130.
Shakhbazyan, V. A. On the Infrared Catastrophe in Scalar Quantum Electrodynamics — 340.
Shakhulashvili, O. A. (see Dzhanelidze, L. P.) — 863.
Shalamov, Ya. Ya. and V. A. Shebanov. Production of π^0 Mesons in Collisions between 2.8 Bev/c π^- Mesons and Protons — 859.
— (see Barmin, V. V.) — 857.
Shapiro, I. S. and L. D. Blokhintsev. Capture of Mesons by the O^{16} Nucleus — 775.
Sharvin, Yu. V. and V. F. Gantmakher. Dependence of the Depth of Penetration of a Magnetic Field in a Superconductor on the Magnetic Field Strength — 866.
— (see Gantmakher, V. F.) — 358L.
Shavtvalov, L. Ya. (see Vasil'ev, S. S.) — 851.
Shcherbakov, Yu. A. (see Kozodaev, M. S.) — 644.
Shebanov, V. A. (see Barmin, V. V.) — 857.

— (see Shalamov, Ya. Ya.) — 859.
Shekun, L. Ya. (see Bil'dyukevich, A. L.) — 1078.
Shevchenko, O. P. (see Teplov, I. B.) — 640.
Shevchenko, V. G. (see Neudachin, V. G.) — 79.
Shirkov, D. V. (see Efremov, A. V.) — 308.
— (see Efremov, A. V.) — 766.
Shirokov, M. I. On a Relativistic General Theory of Reactions — 445.
— and E. O. Okonov. The Spatial and Charge Parities and Two-Meson Annihilation of the Proton-antiproton System — 204.
Shiryaeva, O. I. (see Shur, Ya. S.) — 1111.
Shklyarevskiĭ, G. M. Theory of Photonuclear Reaction on Light Nuclei Involving the Emission of Deuterons — 717.
Shmidt, V. V. On the Effect of Interelectron Interaction in Metals on the Fine Structure of the X-ray Spectra — 886.
Shmushkevich, I. M. (see Malkov, E. I.) — 1281.
Shpinel', V. S. (see Delyagin, N. N.) — 159L.
— (see Delyagin, N. N.) — 619L.
Shubnyĭ, Yu. K. (see Kaipov, D. K.) — 615L.
Shur, Ya. S. and O. I. Shiryaeva. Ferromagnetic Resonance in Iron Silicon Crystals and its Relation to the Domain Structure — 1111.
— and I. E. Startseva. Temperature Hysteresis of the Domain Structure in Iron Silicon Crystals — 397.
Sidorov, V. M. (see Batusov, Yu. A.) — 354L.
— (see Batusov, Yu. A.) — 1290L.
Silin, I. N. (see Amaglobeli, N. S.) — 657.
Simonov, Yu. A. and K. A. Ter-Martirosyan. Semianalytical Solution of Equations of the Chew-Mandelstam Type — 1003.
Sirotina, E. P. and S. I. Syrovat-skiĭ. The Structure of Low Intensity Shock Waves in Magnetohydrodynamics — 521.
Sitenko, A. G. and V. N. Gur'ev. Inelastic Scattering of High-Energy Electrons on Nuclei — 1128.
Sitnikov, K. P. Investigation of Paramagnetic Relaxation in Magnetically Dilute Systems — 365.
Sizov, I. V. (see Li Ga Youn) — 163.
Skirda, N. V. (see Zhdanov, A. P.) — 819.
Smirnit-skiĭ, V. A. (see Vaĭsenberg, A. O.) — 175.
— (see Vaĭsenberg, A. O.) — 834.
Smolkin, G. E. (see Akhmatov, A. P.) — 376.
Smorodin, Yu. A. (see Nikol'skiĭ, S. I.) — 804L.
Sobolev, R. I. (see Ioffe, M. S.) — 1117.
Sobel'man, I. I. (see Rautian, S. G.) — 156L.
— (see Vaĭnshteĭn, L. A.) — 536.
Sodnom, N. (see Li Ga Youn) — 163.
Sokolov, A. A. (see Samoĭlov, I. M.) — 185.
Sokolov, I. A. (see Kogan, A. V.) — 34.
Sokolov, S. N. (see Amaglobeli, N. S.) — 657.
Sokolov, V. I. (see Belov, K. P.) — 1074.
Solov'ev, M. I. (see Wang Kang Ch'ang) — 1291.
Spivak, P. E. and L. A. Mikaélyan. Longitudinal Polarization of β Electrons — 404.
—, L. A. Mikaélyan, I. E. Kutikov, and V. F. Apalin. Asymmetry in Double Mott Scattering and Absolute Values of Longitudinal Polarization of β Particles — 1027L.
Starodubtsev, S. V. (see Velyukhov, G. E.) — 395.
Startseva, I. E. (see Shur, Ya. S.) — 397.
Stashkov, G. M. (see Ivanovskaya, I. A.) — 31.
Stel'makh, M. F. (see Kogan, A. V.) — 34.
Stepanov, A. V. (see Kazarnovskiĭ, M. V.) — 723.
Stepanov, V. G. (see Bil'dyukevich, A. L.) — 1078.
— (see Vinokurov, V. M.) — 1081.
Stratonovich, R. L. Fluctuation Thermodynamics of Nonequilibrium Processes — 1150.
Strel'tsov, V. N. (see Wang Shu-Fen) — 663.
Striganov, A. R. (see Akhmatov, A. P.) — 376.
Strutinskiĭ, V. M. Angular Distribution of Fission Fragments Produced by Low Energy Neutrons — 546.
Sudakov, V. V. (see Kolkunov, V. A.) — 242.
Sudovtsov, A. I. (see Lazarev, B. G.) — 811L.
Suk, M. (see Belyakov, V. A.) — 650.
Sulyaev, R. M. (see Kozodaev, M. S.) — 644.
Svechkarev, I. V. (see Aleksandrov, B. N.) — 25.
Sviridov, V. A. (see Belyakov, V. A.) — 650.
Svirskiĭ, M. S. (see Vonsovskiĭ, S. V.) — 272.
Svyatkovskiĭ, V. (see Vovchenko, V. G.) — 1084.
Syrovat-skiĭ, S. I. (see Sirotina, E. P.) — 521.
Tagviashvili, A. V. (see Dzhibuti, R. I.) — 1225.
Tarantin, N. I. (see Karnaukhov, V. A.) — 771.
Tel'kovskiĭ, V. G. (see Ioffe, M. S.) — 1117.
Teplov, I. B., O. P. Shevchenko, and E. K. Ruuge. Angular Distribution of α Particles from the $F^{19}(p,\alpha)O^{16}$ Reaction — 640.
Teplova, Ya. A. (see Nikolaev, V. S.) — 627.
Teodorovich, É. V. Pion-pion Interaction and the Electromagnetic Structure of the Nucleon in the Static Theory — 334.
Ter-Martirosyan, K. A. Equations for the Mandelstam Spectral Representation Functions — 575.
— (see Simonov, Yu. A.) — 1003.
Ter-Mikaelyan, M. L. and A. D. Gazazyan. Resonance Effects of Radiation in a Laminar Medium — 1183.
Terent'ev, M. V. Mu-Meson Decay from the K Orbit — 1211.
Ternovskiĭ, F. F. Effect of Multiple Scattering on the Proper Field of a Fast Charged Particle — 344.
— On the Theory of Radiative Processes in Piecewise Homogeneous Media — 123.
Teshabaev, K. T. (see Azimov, S. A.) — 1068.
Timofeev, A. V. Build up of Ion Acoustic Vibrations in an Anisotropic Plasma — 281.
Ting Ta-Ts'ao (see Wang Kang-Ch'ang) — 1292L.
Tietz, T. Electron Scattering in the Thomas-Fermi Model — 940.
Tkalich, V. S. Finite-Amplitude Waves in a Multi-Component Conducting Medium — 52.
Tolstov, K. D. (see Belyakov, V. A.) — 650.
Toshyan, R. T. (see Marutyan, N. A.) — 689.
Tserineo, M. A. (see Zaika, N. I.) — 1.
Tserkovnikov, Yu. A. (see Bogolyubov, N. N.) — 88.
Tsukernik, V. M. (see Kaganov, M. I.) — 362L.
Tulinov, V. F. (see Charakhch'yan, A. N.) — 179.
Tuvdendorzh, D. (see Dzhanelidze, L. P.) — 863.
Tyapkin, A. A. (see Vasilevskiĭ, I. M.) — 616L.
Urushadze, G. I. Relaxation of the Magnetic Moment in an Antiferromagnetic Dielectric — 476.
— (see Bar'yakhtar, V. G.) — 251.
Usik, P. A. and V. I. Rus'kin. On a Particular Case of

Peripheral Interactions Between High Energy Nucleons — 1200.

Vaĭnshteĭn, L. A. and I. I. Sobel'man. Deduction of the Radial Equations of the Theory of Collisions Between Electrons and Atoms — 536.

Vaĭsenberg, A. O. and V. A. Smirnit-skiĭ. Asymmetry of $\pi^+ \to \mu^+ \to e^+$ Decay in a Magnetic Field — 175.

—, E. D. Kolganova, and V. A. Smitnit-skiĭ. A Study of Asymmetry in the Decay of Negative μ Mesons in a Nuclear Emulsion — 834.

Val'ter, A. K., I. I. Zalyubovskiĭ, A. P. Klyucharev, and V. A. Lutsik. A New Method to Identify Gamma Radiation from $(p, p'\gamma)$, (p, γ), and $(p, n\gamma)$ Reactions — 807L.

Valuev, B. N. and B. V. Geshkenbeĭn. Determination of the Relative Parity of Σ^0 and Λ Particles from the Reaction $\Sigma^0 \to \Lambda + e^+ + e^-$ — 728.

Vanyashin, V. S. Second-order Equations for Spinor Fields — 240.

Varshalovich, D. A. Probabilities of Rotational Gamma Transitions of Type E2 and Quadrupole Moments of Deformed Nuclei with K = 1 and ½ — 324.

Vartapetyan, G. A. and A. G. Khudaverdyan. On the Level Scheme of Ta^{181} — 16.

Vashakidze, I. Sh., T. I. Kopaleĭshvili, and G. A. Chilashvili. Investigation of the (n, p) Reaction in Li^6 — 278.

—, T. I. Kopaleĭshvili, V. I. Mamasakhlisov, and G. A. Chilashvili. Resonance Scattering of γ Quanta on the Li^7 Nucleus — 466.

Vasilenko, S. S., M. G. Kaganskiĭ, D. L. Kaminskiĭ, and S. F. Koksharova. On the Production of Mono-energetic Positrons in the Decay of Eu^{152} — 672.

Vasil'ev, S. S. and L. Ya. Shavtvalov. The Spectrum of Si^{27} — 851.

Vasilevskiĭ, I. M., V. V. Vishnyakov, E. Ilescu, and A. A. Tyapkin. Coefficient of Spin Correlation in pp Scattering at 310 Mev and 90° in the C.M.S. — 616L.

Vavilov, B. T. and V. I. Grigor'ev. Relation Between the Matrices of Various Transitions and Multiple Processes — 554.

Veklenko, B. A. (see Biberman, L. M.) — 64.

Veksler, V. I. (see Wang Kang-Ch'ang) — 1291L.

Velyukhov, G. E., A. N. Prokof'ev, and S. V. Starodubtsev. Capture by F^{19}, P^{31}, and S^{32} Nuclei — 395.

Verkin, B. I. (see Aleksandrov, B. N.) — 25.

Vernov, S. N., I. P. Ivanenko, G. V. Kulikov, and G. B. Khristiansen. The Nature of the Particle Beams in the Core of Extensive Air Showers — 356L.

Vinokurov, V. M., M. M. Zaripov, and V. G. Stepanov. Paramagnetic Resonance of Mn^{2+} in Dolomite and Magnesite — 1081.

— (see Bil'dyukevich, A. L.) — 1078.

Vinternitts, P. Scattering Matrix of Nucleons Scattered on a Target of Spin 1 — 1025L.

Visky, T. (see Wang Shu-Fen) — 663.

Vishnyakov, V. V. (see Vasilevskiĭ, I. M.) — 616L.

Vladimirskiĭ, V. V. Magnetic Mirrors, Channels, and Bottles for Cold Neutrons — 740.

Vlasov, N. A., S. P. Kalinin, A. A. Ogloblin, and V. I. Chuev. The (α, t) Reaction on Li^7, Be^9, and Na^{23} — 1020L.

—, S. P. Kalinin, A. A. Ogloblin, and V. I. Chuev. The (d, t) Reaction on Zirconium Isotopes — 1127.

—, S. P. Kalinin, A. A. Ogloblin, and V. I. Chuev. The Reaction $B^{11}(d, t)B^{10}$ — 1129.

— (see Artemov, K. P.) — 1124.

Vonsovskiĭ, S. V. and M. S. Svirskiĭ. On the Superconductivity of a Ferromagnetic with a Weak Exchange Interaction — 272.

Vorob'ev, A. A., A. P. Komar, and V. A. Korolev. Measurement of the Energy of Alpha Particles from Some Emitters — 50.

Voronel', A. V. and M. Sh. Giterman. The Hydrostatic Effect Near the Critical Point of a Liquid — 809L.

Voronkov, V. V. and N. N. Kolesnikov. Electronic Levels of Atoms of Super-Heavy Elements — 136.

Vovchenko, V. G., G. Gel'fer, A. S. Kuznetsov, M. G. Meshcheryakov, and V. Svyatkovskiĭ. Effect of Nuclear Binding of Nucleons on the Shape of the Meson Energy Spectra — 1084.

Vrana, I. (see Wang Kang-Ch'ang) — 1292L.

Wang Kang-Ch'ang, Wang Ts'u-Chieng, V. I. Veksler, I. Vrana, Ting Ta-Ts'ao, V. G. Ivanov, Kim Hi-Ying, E. N. Kladnitskaya, A. A. Kuznetsov, Nguyen Dinh Ty, A. V. Nikitin, M. I. Solov'ev, T. Khofmokl', and Ch'eng Ling-Yen. Concerning Parity Nonconservation in Strong Interactions with Participation of Strange Particles — 1292L.

Wang Ts'u-Chieng (see Wang Kang-Ch'ang) — 1291L.

Wang Shu-Fen, T. Visky, I. M. Gramenitskiĭ, V. G. Grishin, N. Dalkhazhav, R. M. Lebedev, A. A. Nomofilov, M. I. Podgoretskiĭ, and V. N. Strel'tsov. Inelastic Interactions Between 9-Bev Protons and Nucleons — 663.

— (see Belyakov, V. A.) — 650.

Wang Yung-Yü, V. V. Kuznetsov, M. Ya. Kuznetsova, and V. A. Khalkin. Investigation of Secondary (α, xn) Reactions in Bismuth — 166.

—, V. V. Kuznetsov, M. Ya. Kuznetsova, V. N. Mekhedov, and V. A. Khalkin. Investigation of Secondary Capture of Lithium Nuclei by Lead — 370.

Yablokov, Yu. V. (see Egorov, G. A.) — 190.

Yagudina, F. R. (see Adamovich, M. I.) — 1103.

Yakovlev, R. M. (see Zhdanov, A. P.) — 819.

Yakovlev, V. A. and A. V. Kalyush. Excitation Spectrum of a System of Electrons and Ions Situated in a Homogeneous Magnetic Field — 219.

Yampol'skiĭ, P. A. (see Glagolev, V. L.) — 1131.

— (see Morozov, A. M.) — 674.

Yarba, V. A. (see Batusov, Yu. A.) — 354L.

— (see Batusov, Yu. A.) — 1289L.

Yashin, V. I. (see Aleksin, V. F.) — 572.

Yudin, N. P. (see Neudachin, V. G.) — 79.

Yushmanov, E. E. (see Ioffe, M. S.) — 1117.

Zaika, N. I., O. F. Nemets, and M. A. Tserineo. Angular Distribution of Protons from the $C^{12}(dp)C^{13}$ Reaction with 5—13 Mev Deuterons — 1.

Zaĭtsev, A. A. Application of the Laplace Transform for Calculation of the Partition Function — 878.

Zaĭtseva, M. A. (see Belov, K. P.) — 799L.

Zalyubovskiĭ, I. I. (see Val'ter, A. K.) — 807L.

Zaripov, M. M. (see Bil'dyukevich, A. L.) — 1078.

— (see Vinokurov, V. M.) — 1081.

Zastavenko, L. G. and M. I. Podgoretskiĭ. Effect of External Fields on the Angular Correlations and Resonance Processes During Quantum Transitions — 711.

Zatsepin, G. T. and V. A. Kuz'min. Angular Distributions of High-Energy μ Mesons in the Atmosphere and their Production Mechanism — 1171.

— (see Berezinskiĭ, V. S.) — 1288.

— (see Goryunov, N. N.) — 195.

Zavaritskiĭ, N. V. Measurement of the Anisotropy of the Thermal Conductivity of Zinc and Cadmium in the Superconducting State — 831.

— Thermal Conductivity of High Purity Thallium and Tin — 1093.

Zavoĭskiĭ, E. K. (see Akhmatov, A. P.) — 376.

Zel'dovich, Ya. B. Contribution to the Theory of Unstable States — 542.

— Dipole Moment of Unstable Elementary Particles — 1030L.

— Form Factor for $K_{\mu 3}$ amd K_{e3} Decay — 1232.

— and A. M. Perelomov. Effect of Weak Interaction on the Electromagnetic Properties of Particles — 777.

Zevin, V. Ya. (see Deĭgen, M. F.) — 785.

Zhdanov, A. P., I. M. Kuks, N. V. Skirda, and F. M. Yakovlev. Multiple Production of Particles in the Interaction of Nucleons with $> 10^{11}$ ev in Photographic Emulsion Nuclei — 819.

Zherebtsova, K. I. (see Alekseev, N. V.) — 1049.

Zhizhin, E. D. Behavior of the Total Cross Section for the Photoproduction of π Mesons at High Energies — 158L.

— (see Berestetskiĭ, V. B.) — 295.

Zöllner, W. (see Hsien Ting-Ch'ang) — 1165.

Zubarev, D. N. (see Bogolyubov, N. N.) — 88.

Zvenglinskiĭ, B. (see Delyagin, N. N.) — 159L.

— (see Delyagin, N. N.) — 619L.

Zverev, G. M. and A. M. Prokhorov. Electron Paramagnetic Resonance and Spin-lattice Relaxation of Co^{2+} in Corundum — 41.

— and A. M. Prokhorov. Electron Paramagnetic Resonance of Vanadium in Rutile — 160L.

— and A. M. Prokhorov. Cross Spin Relaxation in the Hyperfine Structure of the Electron Paramagnetic Resonance of Co^{2+} in Corundum — 382.

Analytic Subject Index to Volume 12

References with L are Letters to the Editor. Items are listed under the following categories:

Accelerators (Theory and Construction)
Astrophysics
Atomic Levels
Collisions, Atomic (Theory)
Cosmic Radiation
Crystalline Lattice
Elementary Particle Interactions (Experiment)
Fission, Nuclear
Gravitation
Helium, Liquid
Hydrodynamics
Ions, Ionization
Isotopes
Magnetic Properties of Matter
Magnetic Resonance, Magnetic Relaxation
Magnetohydrodynamics
Metals (Electronic Properties, Elastic Properties)
Methods and Instruments
Multiple Production of Particles
Mu Mesons
Nuclear Reactions and Scattering at High Energy (Experiment)
Nuclear Reactions and Scattering at Medium and Low Energies (Experiment)
Nuclear Reactions, Disintegrations, Scattering (Theory)
Nuclear Reactions on Multiply Charged Ions
Nuclear Spectra (α, β, γ) (Experiment)
Nuclear Structure (Theory)
Photonuclear Reactions
Phase Transformations
Plasma (Theory)
Plasma, Gas-Discharge (Experiment)
Polarization, Nuclear
Positrons
Pressures, High
Quantum Electrodynamics
Quantum Field Theory, Theory of Strong Interactions
Quantum Mechanics (Various Problems)
Radiation, Electromagnetic
Scattering (General Theory)
Scattering in Crystals
Scattering of Electrons and Gamma Quanta
Semiconductors
Statistical Physics (General Problems)
Strange Particles
Superconductivity
Weak Interactions
X Rays

Accelerators (Theory and Construction)
A High Current Microtron. S. P. Kapitza, V. P. Bykov, and V. N. Melekhin — 693.
On Azimuthal Instabilities of Circulating Currents. I. M. Samoĭlov and A. A. Sokolov — 185.
Astrophysics
On Slow and Fast Neutron Capture Processes in the Theory of Origin of Elements. G. S. Malkiél' — 1143.
Atomic Levels
Electronic Levels of Atoms of Super-Heavy Elements. V. V. Voronkov and N. N. Kolesnikov — 136.
Collisions, Atomic (Theory)
Bremsstrahlung of Slow Electrons Decelerated by Neutral Atoms. O. B. Firsov and M. I. Chibisov — 1235.
Deduction of the Radial Equations of the Theory of Collisions Between Electrons and Atoms. L. A. Vaĭnshteĭn and I. I. Sobel'man — 536.
Dependence of the Inelastic Collision Cross Sections of Atoms and Ions on Velocity in the Case of Pseudo-intersection of the Levels. Yu. P. Mordvinov and O. B. Firsov — 301.
Cosmic Radiation
Angular Distributions of High Energy μ Mesons in the Atmosphere and their Production Mechanism. G. T. Zatsepin and V. A. Kuz'min — 1171.
Calculation of Averaged Characteristics of Extensive Atmospheric Cosmic Ray Showers. S. I. Nikol'skiĭ and A. A. Pomanskiĭ — 934.
Calculation of Transition Effects at Various Distances from the Electron-Photon Shower Axis. O. I. Dovzhenko — 1178.
Cosmic Rays from the Sun. A. N. Charakhch'yan, V. F. Tulinov, and T. N. Charakhch'yan — 179.
Investigation of Azimuthal Effects in Meson Showers Produced by 9 Bev Protons. E. M. Friedlander — 669.
Lateral Distribution of High Energy Nuclear-active Particles in the Core of Extensive Atmospheric Showers. A. A. Emel'yanov and O. I. Dovzhenko — 567.
Polarization of Cosmic Ray μ^+ Mesons. V. V. Barmin, V. P. Kanavets, and B. V. Morozov — 683.
The Nature of the Particle Beams in the Core of Extensive Air Showers. S. N. Vernov, I. P. Ivanenko, G. V. Kulikov, and G. B. Khristiansen — 356L.
Transverse Momentum Component of Strange Particles Produced in Penetrating Cosmic-ray Showers. É. L. Andronikashvili and N. N. Roĭnishvili — 192.
Interpretation of Experimental Data on the Spectrum of Electron-Photon Cascades with Energy 10^{12} ev in the Upper Layers of the Atmosphere. S. I. Nikol'skiĭ and Yu. A. Smorodin — 804L.
Crystalline Lattice
Decay of Acoustic Excitation in Crystals. V. L. Pokrovskiĭ and A. M. Dykhne — 503.
On the Use of the Mössbauer Effect for Studying Localized Oscillations of Atoms in Solids.

S. V. Maleev — 617L.
Crystal Structure of Solid Deutero-Hydrogen. R. F. Bulatova, V. S. Kogan, and B. G. Lazarev — 1292L.

Elementary Particle Interactions (Experiment)
Determination of the Charge-Exchange Cross Section for Pion-pion Collision from the Analysis of the $\pi^- + p \rightarrow \pi^- + \pi^+ + n$ Reaction at 290 Mev. Yu. A. Batusov, S. A. Bunyatov, V. M. Sidorov, and V. A. Yarba — 354L.
Determination of the Pion-Nucleon Coupling Constant from the n-p Elastic Scattering Differential Cross Sections. N. S. Amaglobeli, Yu. M. Kazarinov, S. N. Sokolov, and I. N. Silin — 657.
Effect of Nuclear Binding of Nucleons on the Shape of the Meson Energy Spectra. V. G. Vovchenko, G. Gel'fer, A. S. Kuznetsov, M. G. Meshcheryakov, and V. Svyatkovskiĭ — 1084.
Inelastic Interactions Between 9 Bev Protons and Nucleons. Wang Shu-Fen, T. Visky, I. M. Gramenitskiĭ, N. Dalkhazhav, R. M. Lebedev, A. A. Nomofilov, M. I. Podgoretskiĭ, and V. N. Strel'tsov — 663.
Inelastic Interactions Between 7 Bev π^- Mesons and Nucleons. V. A. Belyakov, Wang Shu-Fen, V. V. Glagolev, N. Dalkhazhav, R. M. Lebedev, N. N. Mel'nikova, V. A. Nikitin, V. Petrzhilka, V. A. Sviridov, M. Suk, and K. D. Tolstov — 650.
Production of π^0 Mesons in Collisions Between 2.8 Bev/c π^- Mesons and Protons. Ya. Ya. Shalamov and V. A. Shebanov — 859.
Coefficient of Spin Correlation in pp Scattering at 310 Mev and 90° in the C.M.S. I. M. Vasilevskiĭ, V. V. Vishnyakov, E. Ilescu, and A. A. Tyapkin — 616L.
Production of Charged Mesons by 245-Mev π^- Mesons on Hydrogen. Yu. A. Batusov, S. A. Bunyatov, V. M. Sidorov, and V. A. Yarba — 1290L.

Fission, Nuclear
Angular Distribution of Fission Fragments Produced by Low Energy Neutrons. V. M. Strutinskiĭ — 546.
Energy Distribution of the Fragments of Triple U^{235} Fission. V. N. Dmitriev, L. V. Drapchinskiĭ, K. A. Petrzhak, and Yu. F. Romanov — 390.

Gravitation
On the Coordinate Conditions in Einstein's Theory of Gravitation. I. G. Fikhtengol'tz — 564.
On the Singularities of Cosmological Solutions of the Gravitational Equations. I. E. M. Lifshitz and I. M. Khalatnikov — 108.
On the Singularities of Cosmological Solutions of the Gravitational Equations. II. E. M. Lifshitz and I. M. Khalatnikov — 558.

Helium, Liquid
On Mutual Friction in Helium II. Yu. G. Mamaladze — 595.
The Microscopic Theory of the Fermi Liquid. V. I. Karpman — 133.
The Problem of the Form of the Spectrum of Elementary Excitations of Liquid Helium. II. L. P. Pitaevskiĭ — 155L.
Theory of the Kapitza Thermal Discontinuity at the Boundary Between Liquid He^3 and a Solid Body. I. L. Bekarevich and I. M. Khalatnikov — 1187.
The Determination of the Coefficients of Diffusion and of Heat Conductivity of Weak Solution of He^3 in Helium II. T. P. Ptukha — 621L.

Hydrodynamics
Hydrodynamic Stability of a Liquid Layer on a Vertical Wall. V. K. Bushmanov — 873.
Thermodynamics of Turbulent Systems. V. G. Nevzglyadov — 1206.

Ions, Ionization
Composition of the Ions Produced During the Ionization of Gases by Negative Ions. Ya. M. Fogel', A. G. Koval', Yu. Z. Levchenko, and A. F. Khodyachikh — 384.
Double Charge Exchange of Alkali Metal Ions. Ya. M. Fogel', V. F. Kozlov, and G. N. Polyakova — 826.
Investigation of the Equilibrium Charge Distribution in a Fast Ion Beam. V. S. Nikolaev, I. S. Dmitriev, L. N. Fateeva, and Ya. A. Teplova — 627.

Isotopes
Limits of Stability and Proton and Two-proton Radioactivity of Neutron-deficient Isotopes of Light Nuclei. V. I. Gol'danskiĭ — 348.
On the Possibility of Proton Decay of Nuclei. V. A. Karnaukhov and N. I. Tarantin — 771.
Production of the Radioactive Isotope Kr^{85} and Measurement of its γ Radiation. I. E. Nakhutin, V. V. Ovechkin, D. V. Ochkin, A. S. Polyakov, and S. K. Khoduleva — 687.

Magnetic Properties of Matter
Anomalies in the Temperature Dependence of the Coersive Force in Garnet Ferrites of the Rare Earth Elements in the Vicinity of the Compensation Point. K. P. Belov and A. V. Ped'ko — 666.
Behavior of Domain Structure Under the Action of Elastic Stresses. L. V. Kirenskiĭ, V. A. Ignachenko, and A. M. Radichev — 881.
Contribution to the Theory of Ferro- and Antiferromagnetism. V. L. Ginzburg and V. M. Faĭn — 923.
Excitation of Standing Spin Waves in a Film. M. I. Kaganov — 114.
Influence of Impurities on the De-Haas—Van Alphen Effect. Yu. A. Bychkov — 971.
Instability of Uniform Precession of Magnetization. L. N. Bulaevskiĭ, V. M. Faĭn, and G. I. Freĭdman — 361L.
Investigation of the Temperature Dependence of the Spontaneous Magnetization of Chromium Telluride. L. G. Gaĭdukov, N. P. Grazhdankina, and I. G. Fakidov — 636.
Magnetocaloric Effect in the Low-temperature Range of Transformation of Magnetite. V. P. Krasovskiĭ and I. G. Fakidov — 170.
On the Diamagnetism of a System of Interacting Particles. I. G. Kaplan — 733.
Resonance and Magnetic Properties of Garnet-type Yttrium Ferrite at Low Temperatures. K. P. Belov — 1074.
Temperature Dependence of the Magnetic Susceptibility of Indium, Lead, and Tin Crystals. B. N. Aleksandrov, B. I. Verkin, and I. V. Svechkarev — 25.
Temperature Hysteresis of the Domain Structure in Iron Silicon Crystals. Ya. S. Shur

and I. E. Startseva — 397.
The Scattering of Spin Waves and Phonons by Impurities in Ferromagnetic Dielectrics. V. G. Bar'yakhtar and G. I. Urushadze — 251.
Theory of the Magnetic Properties of a Nonideal Fermi Gas at Low Temperatures. I. A. Akhiezer and S. V. Peletminskiĭ — 913.
Theory of the Non-resonance Absorption of an Oscillating Magnetic Field by a Ferromagnetic Dielectric. M. I. Kaganov and V. M. Tsukernik — 362L.
Weak Ferromagnetism in an Antiferromagnetic $CoCO_3$ Single Crystal. A. S. Borovik-Romanov and V. I. Ozhogin — 18.
Antiferromagnetism of $CoCO_3$. R. A. Alikhanov — 1028L.
Magnetic Properties of Orthoferrites of Lanthanum and Praseodymium with Partial Replacement of Fe^{3+} Ions by Al^{3+} Ions. K. P. Belov, M. A. Zaĭtseva, and A. M. Kadomtseva — 799L.

Magnetic Resonance, Magnetic Relaxation (see also Polarization of Nuclei)
Contribution to the Theory of Relaxation of the Magnetic Moment in Ferromagnetic Substances. V. G. Bar'yakhtar and S. V. Peletminskiĭ — 457.
Cross Spin Relaxation in the Hyperfine Structure of the Electron Paramagnetic Resonance of Co^{2+} in Corundum. G. M. Zverev and A. M. Prokhorov — 382.
Electron Paramagnetic Resonance and Paramagnetic Relaxation in Liquid and Supercooled Ti^{+++} Salt Solutions. V. I. Avvakumov, N. S. Garif'yanov, and E. I. Semenova — 847.
Electron Paramagnetic Resonance and Spin-lattice Relaxation of Co^{2+} in Corundum. G. M. Zverev and A. M. Prokhorov — 41.
Electron Paramagnetic Resonance in Andalusite. A. L. Bil'dyukevich, V. M. Vinokurov, M. M. Zaripov, Yu. E. Pol'skiĭ, V. G. Stepanov, G. K. Chirkin, and L. Ya. Shekun — 1078.
Electron Paramagnetic Resonance of Vanadium in Rutile. G. M. Zverev and A. M. Prokhorov — 160L.
Ferromagnetic Resonance in Iron Silicon Crystals and its Relation to the Domain Structure. Ya. S. Shur and O. I. Shiryaeva — 1111.
Investigation of Paramagnetic Relaxation in Magnetically Dilute Systems. K. P. Sitnikov — 365.
Magnetic Relaxation in Ferromagnetic Metals. L. L. Buishvili, G. R. Khutsishvili, and O. D. Cheĭshvili — 507.
On the Shape of the Electron Resonance Line in a Particle System Possessing an Anisotropic g-Factor. A. K. Chirkov and A. A. Kokin — 964.
Paramagnetic Resonance in a Quasi-single Crystal of $CrCl_3$. G. A. Egorov and Yu. V. Yablokov — 190.
Paramagnetic Resonance of Mn^{2+} in Dolomite and Magnesite. V. M. Vinokurov, M. M. Zaripov, and V. G. Stepanov — 1081.
Relaxation of the Magnetic Moment in an Antiferromagnetic Dielectric. G. I. Urushadze — 476.
Spin-lattice Relaxation of Local Electron Centers in Nonmetallic Crystals. M. F. Deĭgen and V. Ya. Zevin — 785.
Paramagnetic Resonance in Single-Crystal Tin. M. S. Khaĭkin — 623L.

Magnetohydrodynamics
Contribution to the Theory of Simple Magnetohydrodynamic Waves. R. V. Polovin — 326.
On the Flow of a Plasma into a Vacuum in the Presence of a Magnetic Field. R. V. Polovin — 461.
On the Motion of Shock Waves Along a Magnetic Field. R. V. Polovin — 699.
Shock Waves in Relativistic Magnetohydrodynamics. L. M. Kovrizhnykh — 725.
Some Properties of Stationary Flows in Magnetic Gas Dynamics. K. B. Pavlov — 216.
The Structure of Low Intensity Shock Waves in Magnetohydrodynamics. E. P. Sirotina and S. I. Syrovat-skiĭ — 521.

Metals (Electronic Properties, Elastic Properties)
A New Resonance Effect in Metals at High Frequencies. M. Ya. Azbel' — 283.
Concerning Cyclotron Resonance in Tin. M. S. Khaĭkin — 359L.
Decay of a Plasmon at Absolute Zero. Yu. A. Romanov — 464.
Excitation Spectrum of a System of Electrons and Ions Situated in a Homogeneous Magnetic Field. V. A. Yakovlev and A. V. Kalyush — 219.
Experimental Investigation of Cyclotron Resonance in Metals. M. Ya. Azbel' and É. A. Kaner — 58.
Fermi Surface of Tin. N. E. Alekseevskiĭ, Yu. P. Gaĭdukov, I. M. Lifshitz, and V. G. Peschanskiĭ — 837.
Investigation of Ultrasonic Absorption by a Metal in a Magnetic Field. A. A. Galkin, É. A. Kaner, and A. P. Korolyuk — 1055.
Non-monotonic Dependence of the Surface Impedance of Tin on the Magnetic Field at 1.9 Megacycles. V. F. Gantmakher and Yu. V. Sharvin — 358L.
On a Certain Mechanism of Absorption of Ultrasound in Paramagnetic Metals in a Magnetic Field. G. Z. Gershuni — 256.
On the Effect of Impurities on the Energy Spectrum of Electrons in Bismuth. N. B. Brandt and M. V. Razumeenko — 198.
On the Possibility of Determining the Correlation Function for Fermi Fluids in Metals. M. Ya. Azbel' — 793.
Oscillator Dependence of the Surface Resistance of a Metal on a Weak Magnetic Field. M. S. Khaĭkin — 152L.
Quantum Oscillations of the Thermal Conductivity Coefficient of an Electron Gas in a Magnetic Field. V. V. Andreev and A. M. Kosevich — 517.
Quantum Oscillations of Thermodynamic Quantities for an Arbitrary Fermi Surface — 608.
Quantum Theory of the Electrical Conductivity of Metals in Strong Magnetic Fields. Yu. A. Bychkov — 483.
Quasiclassical Quantization Near Singular Classical Trajectories. M. Ya. Azbel' — 891.
Theory of Absorption of Ultrasound by Metals in a Strong Magnetic Field II. É. A. Kaner — 747.
Thermal Conductivity of High Purity Thallium and Tin. N. V. Zavaritskiĭ — 1093.

Magnetic Change in Resistivity of Ferromagnets Above the Curie Point. I. K. Kikoin, N. A. Babushkina, and T. N. Igosheva — 816L.

Methods and Instruments

A Fundamental Method for Measuring Time. L. A. Khalfin — 353L.

Magnetic Mirrors, Channels, and Bottles for Cold Neutrons. V. V. Vladimirskiĭ — 740.

Observation of Charged Relativistic Particles in a Luminescent Chamber. B. A. Demidov and S. D. Fanchenko — 46.

A New Method to Identify Gamma Radiation from (p, p′ γ), (p, γ), and (p, nγ) Reactions. A. K. Val'ter, I. I. Zalyubovskiĭ, A. P. Klyucharev, and V. A. Lutsik — 807L.

Multiple Production of Particles (see also Cosmic Radiation)

A Method of Calculation of the Statistical Weights and Distributions in Multiple Production Theories. G. I. Kopylov — 761.

Analysis of Nuclear interactions of Nucleons with $E \geq 10^{11}$ ev in Photographic Emulsions. É. G. Boos — 433.

Angular Distribution of Shower Particles Produced in Nuclear Interactions Between Fast Nucleons and Heavy Nuclei of Photographic Emulsions. S. A. Azimov, K. T. Teshabaev, L. P. Chernova, G. M. Chernov, and V. M. Chudakov — 1068.

Concerning the Paper "Evaluation of Phase Integrals in the Covariant Formulation of the Theory of Multiple Production of Particles" by L. G. Yakovlev. G. I. Kopylov — 150L.

Energy Fluctuations in the Interaction Between High Energy Particles. N. M. Gerasimova — 758.

Multiple Production of Particles in the Interaction of Nucleons with $\geq 10^{11}$ ev in Photographic and Photographic Emulsion Nuclei. A. P. Zhdanov, I. M. Kuks, N. V. Skirda, and F. M. Yakovlev — 819.

On a Particular Case of Peripheral Interactions Between High Energy Nucleons. P. A. Usik and V. I. Rus'kin — 1200.

On Covariant Statistical Theories of Multiple Particle Production. V. M. Maksimenko and I. L. Rozental' — 527.

Relation Between the Matrices of Various Transitions and Multiple Processes. B. T. Vavilov and V. I. Grigor'ev — 554.

Mu Mesons (see also Cosmic Rays; Weak Interactions)

A Study of Asymmetry in the Decay of Negative μ Mesons in a Nuclear Emulsion. A. O. Vaĭsenberg, É. D. Kolganova, and V. A. Smirnit-skiĭ — 834.

Investigation of μ^+-Meson Depolarization in a Nuclear Emulsion. Yu. M. Ivanov and A. I. Fesenko — 1037.

Mu-Meson Decay from the K-Orbit. M. V. Terent'ev — 1211.

Observation of μ-Meson Bursts in a Set of Ionization Chambers. N. N. Goryunov and G. T. Zatsepin — 195.

Radiative Corrections to the Scattering of μ Mesons on Electrons. A. I. Nikishov — 529.

Intensity of Nonradiative Transitions in Mu-Mesic Atoms. M. Ya. Balats, L. N. Kondrat'ev, L. G. Landsberg, P. I. Lebedev, B. V. Obukhov, and B. Pontecorvo — 812L.

On the Probability of Meson Capture in Different Meso-Atomic Levels. S. S. Gershteĭn — 815L.

Nuclear Reactions and Scattering at High Energy (Experiment)

Angular and Momentum Distribution of Residual Nuclei Produced in the Inelastic Scattering of Fast π Mesons and Protons on Helium. M. S. Kozodaev, M. M. Kulyukin, R. M. Sulyaev, A. I. Filippov, and Yu. A. Shcherbakov — 644.

Interaction of 5×10^{12} ev Nucleons with Photographic Emulsion Nuclei. N. A. Marutyan, K. A. Matevosyan, and R. T. Toshyan — 689.

Investigation of Secondary (α, xn) Reactions in Bismuth. Wang Yung-Yü, V. V. Kuznetsov, M. Ya. Kuznetsova, and V. A. Khalkin — 166.

Polarization of 6.8-Mev Protons Scattered on Carbon. M. V. Pasechnik, N. N. Pucherov, B. F. Orlenko, and V. S. Prokopenko — 634.

Production of Charged Hyperons by 9-Bev Protons Interacting with Photographic Emulsion Nuclei. L. P. Dzhanelidze, D. K. Kopylova, Yu. B. Korolevich, N. I. Kostanashvili, K. V. Mandritskaya, N. I. Petukhova, M. I. Podgoretskiĭ, D. Tuvdendorzh, O. A. Shakhulashvili, and Cheng P'u-Ying — 863.

Nuclear Reactions and Scattering at Medium and Low Energies (Experiment)

Angular Distribution of α Particles Produced in the Reaction $F^{19}(p, \alpha)O^{16}$. I. B. Teplov, O. P. Shevchenko, and E. K. Ruuge — 640.

Angular Distribution of Protons from the $C^{12}(d, p)C^{13}$ Reaction with 5 — 13 Mev Deuterons. N. I. Zaika, O. F. Nemets, and M. A. Tserineo — 1.

Capture by F^{19}, P^{31}, and S^{32} Nuclei. G. E. Velyukhov, A. N. Prokof'ev, and S. V. Starodubtsev — 395.

Charged Products from the Reactions $He^4 + d$ (20 Mev). K. P. Artemov and N. A. Vlasov — 1124.

Elastic Scattering of Deuterons by Nuclei. Yu. V. Gofman and O. F. Nemets — 1035.

Excited States of the Si^{30} Nucleus. A. M. Romanov — 1072.

Five New Millisecond Isomers Produced by 19.2-Mev Protons. A. M. Morozov, V. V. Remaev, and P. A. Yampol'skiĭ — 674.

Investigation of Stripping Reactions on C^{12}, O^{16}, and Si^{28}. N. V. Alekseev, K. I. Zherebtsova, V. F. Litvin, and Yu. A. Nemilov — 1049.

Investigation of the $He^3 + He^3$ Reaction. Li Ga Youn, G. M. Osetinskiĭ, N. Sodnom, A. M. Gavorov, I. V. Sizov, and V. I. Salatskiĭ — 163.

Production of Nuclear Fragments in Nuclear Emulsions by 80-Mev Mesons. A. S. Assovskaya and N. S. Ivanova — 1051.

The (d, t) Reaction on Zirconium Isotopes. N. A. Vlasov, S. P. Kalinin, A. A. Ogloblin, and V. I. Chuev — 1127.

The Reaction $B^{11}(d, t)B^{10}$. N. A. Vlasov, S. P. Kalinin, A. A. Ogloblin, and V. I. Chuev — 1129.

The (α, t) Reaction on Li^7, Be^9, and Na^{23}. N. A. Vlasov, S. P. Kalinin, A. A. Ogloblin, and V. I. Chuev — 1020L.

Nuclear Reactions, Disintegrations, Scattering (Theory)
Cross Sections for Radiative Capture of Neutrons by Heavy Nuclei. P. E. Nemirovskiĭ — 1213.
Dispersion Relations and Analysis of the Energy Dependence of Cross Sections near Thresholds of New Reactions. L. I. Lapidus and Chou Kuang-Chao — 82.
Energy Spectrum of Cascade Alpha Particles in Photographic Emulsion Stars Produced by High-Energy Protons. V. I. Ostroumov, N. A. Perfilov, and R. A. Filov — 77.
Inelastic Final-state Interactions and Near-threshold Singularities. L. I. Lapidus and Chou Kuang-Chao — 258.
Interference between Coulomb and Nuclear Scattering at High Energies. B. P. Bannik and V. G. Grishin — 69.
Investigation of the (n, p) Reaction in Li^6. I. Sh. Vashakidze, T. I. Kopaleĭshvili, and G. A. Chilashvili — 278.
A Relativistic General Theory of Reactions. M. I. Shirokov — 445.
On the Bond in the C^{12} — C^{12} Nuclear Molecule. A. S. Kompaneets — 1196.
On the Influence of the Inelastic Processes on the Elastic Scattering in the Vicinity of the Thresholds of the Inelastic Reaction Modes. L. A. Khalfin — 709.
Polarization of Deuterons Elastically Scattered on Helium. L. S. Dulkova — 701.
Polarization of Protons Scattered from O^{16}. K. V. Karadzhev and V. I. Man'ko — 294.
Theory of Alpha Decay of Nonspherical Nuclei. V. G. Nosov — 102.
Nuclear Reactions on Multiply Charged Ions
Secondary Capture of Lithium Nuclei by Lead. Wang Yung-Yu, V. V. Kuznetsov, M. Ya. Kuznetsova, V. N. Mekhedov, and V. A. Khalkin — 370.
Nuclear Spectra (α, β, γ) (Experiment)
Decay of Er^{161}. I. S. Dneprovskiĭ, L. Német, and L. K. Peker — 8.
Hyperfine Structure of Gamma Rays Produced by Quadrupole Interaction in a Crystal Lattice. N. N. Delyagin, V. S. Shpinel', V. A. Bryukhanov, and B. Zvenglinskiĭ — 159L.
Investigation of the Decay Scheme of Dy^{166}. L. I. Rusinov, A. V. Borovikov, V. S. Gvozdev, G. D. Porsov, S. L. Sakharov, and Yu. L. Khazov — 1064.
Measurement of the Energy of Alpha Particles from Some Emitters. A. A. Vorob'ev, A. P. Komar, and V. A. Korolev — 50.
Nuclear Zeeman Effect in Sn^{119}. N. N. Delyagin, V. S. Shpinel', V. A. Bryukhanov, and B. Zvenglinskiĭ — 619L.
On Reactions Involving the Formation of Pb^{205m} Isomer. V. L. Glagolev, A. M. Morozov, and P. A. Yampol'skiĭ — 1131.
On the Level Scheme of Ta^{181}. G. A. Vartapetyan and A. G. Khudaverdyan — 16.
On the Production of Monoenergetic Positrons in the Decay of Eu^{152}. S. S. Vasilenko, M. G. Kaganskiĭ, and S. F. Kiksharova — 672.
The γ Spectrum of Na^{24} in the 2.5 — 5.5 Mev Energy Range. K. P. Artamonova, L. V. Gustova, Yu. N. Podkopaev, and O. V. Chubinskiĭ — 1109.
The β^+ Spectrum of Si^{27}. S. S. Vasil'ev and L. Ya. Shavtvalov — 851.
Two-Cascade Gamma Transition in the Nd^{144} Nucleus Accompanying the Capture of Thermal Neutrons. V. R. Burmistrov,and V. P. Radchenko — 411.
Nuclear Structure (Theory)
Determination of the Deformation of α-Active Nuclei and their Quadrupolarization on Basis of the α-Particle Energy and Angular Distributions. V. G. Nosov — 1159.
Effect of Pair Correlation of Nucleons on the Probabilities of Electromagnetic Transitions in the Nucleus. Yu. T. Grin' — 100.
Electric Monopole Transitions in the Theory of Nonaxial Nuclei. V. S. Rostovskiĭ — 592.
On the Ground States of Atomic Nuclei. M. Ya. Amus'ya — 449.
On the Nature of the First Excited States of Even-even Spherical Nuclei. S. T. Belyaev — 968.
On the Theory of the Optical Anisotropy of Atomic Nuclei. A. M. Baldin and S. F. Semenko — 306.
Probabilities of Rotational Gamma Transitions of Type E2 and Quadrupole Moments of Deformed Nuclei with K = 1 and ½. D. A. Varshalovich — 324.
Quadrupole Moments of Odd Barium Isotopes. N. I. Kaliteevskiĭ, É. E. Fradkin, and M. P. Chaĭka — 661.
Rotational State Energies of Nonaxial Nuclei with J = 10 and J = 12. V. K. Luk'yanov — 731.
The Possibility of Experimental Verification of the Nonaxial Rotator Model by Studying the Effect of the Medium on the Angular Correlation of a Gamma Quantum Cascade. D. P. Grechukhin — 957.
On the Problem of Pairing with Non-Zero Angular Momenta. V. M. Galitskiĭ — 806L.
Photonuclear Reactions
Behavior of the Total Cross Section for the Photoproduction of π Mesons at High Energies. E. D. Zhizhin — 158L.
Fast Photoneutrons from Some Elements. L. A. Kul'chitskiĭ and V. Presperin — 696.
Investigation of the (γ, p) Reaction on the Sn^{120} Isotope. Kuo Ch'i-Ting and B. S. Ratner — 1098.
Photodisintegration of the He^4 Nucleus at High Energies. R. I. Dzhibuti and A. V. Tagviashvili — 1225.
Photoproduction of π Mesons on Nucleons in Peripheral Collisions. V. B. Berestetskiĭ and E. D. Zhizhin — 295.
Ratio of Cross Sections for Positive and Negative Photomeson Production on Beryllium. M. I. Adamovich, N. M. Panova, V. M. Popova, and F. R. Yagudina — 1103.
The Position of the Giant Resonance in the Dipole Absorption of Gamma Quanta by Atomic Nuclei. V. G. Neudachin, V. G. Shevchenko, and N. P. Yudin — 79.
Theory of Photonuclear Reaction on Light Nuclei Involving the Emission of Deuterons. G. M. Shklyarevskiĭ — 717.
On the Role of the Nonphysical Region in the Dispersion Relations for the Photoproduction of π Mesons. A. M. Baldin — 800L.

Phase Transformations

The Hydrostatic Effect Near the Critical Point of a Liquid. A. V. Voronel' and M. Sh. Giterman — 809L.

Polymorphic Transformations of Lithium, Sodium, and Potassium in Films Condensed on a Cold Substrate. B. G. Lazarev, E. E. Semenenko, and A. I. Sudovtsov — 811L.

Plasma (Theory)

Build up of Ion Acoustic Vibrations in an Anisotropic Plasma. A. V. Timofeev — 281.

Collisions of Particles in a High Temperature Plasma. O. V. Konstantinov and V. I. Perel' — 597.

Dynamic Stabilization of a Plasma Ring. S. M. Osovets — 221.

Electromagnetic Waves in Half-Space Filled with a Plasma. Yu. N. Dnestrovskiĭ and D. P. Kostomarov — 587.

Finite-Amplitude Waves in a Multi-component Conducting Medium. V. S. Tkalich — 52.

Investigation of the Stability of a Plasma by a Generalized Energy Principle. V. G. Aleksin and V. I. Yashin — 572.

On the Anisotropy in the Propagation of Longitudinal Electroacoustic Oscillations in a Drifting Plasma. V. A. Liperovskiĭ — 951.

On the Growth of Magnetohydrodynamic Waves in a Plasma Stream Moving through an Ionized Gas. V. P. Dokuchaev — 292.

On the Instability of a Plasma with an Anisotropic Distribution of Velocities in a Magnetic Field. R. Z. Sagdeev and V. D. Shafranov — 130.

On the Theory of Runaway Electrons. A. V. Gurevich — 904.

Natural Oscillations of a Bound Plasma. D. A. Frank-Kamenetskiĭ — 469.

Plasma, Gas-Discharge (Experiment)

Acceleration of Positive Ions in an Expanding Vacuum Spark Plasma. A. A. Plyutto — 1106.

Conditions for Electron Excitation of Negative Temperature States in a Gas Mixture. N. G. Basov and O. N. Krokhin — 1240.

Gyrotropic Properties of a Plasma During Propagation of an Extraordinary Wave. B. I. Patrushev, V. D. Rusanov, I. A. Kovan, V. V. Savichev, and D. A. Frank-Kamenetskiĭ — 1045.

Investigation of Magnetic Mirror Confinement of a Plasma, I. M. S. Ioffe, R. I. Sobolev, V. G. Tel'kovskiĭ, and E. E. Yushmanov — 1117.

Investigation of Magneto-acoustic Resonance in a Plasma with Aid of Double Electric Probes. V. D. Rusanov, B. I. Patrushev, I. A. Kovan, V. I. Garkusha, and D. A. Frank-Kamenetskiĭ — 1041.

Magneto-acoustic Resonance in a Plasma. A. P. Akhmatov, P. I. Blinov, V. F. Bolotin, A. V. Borodin, P. P. Gavrin, E. K. Zavoĭskiĭ, I. A. Kovan, M. N. Oganov, B. I. Patrushev, E. V. Piskarev, V. D. Rusanov, G. E. Smolkin, A. R. Striganov, D. A. Frank-Kamenetskiĭ, P. A. Cheremnykh, and R. V. Chikin — 376.

The Realization of a Medium with Negative Absorption Coefficient. V. K. Ablekov, M. S. Pesin, and I. L. Fabelinskiĭ — 618L.

Polarization, Nuclear

Effect of Pulsed Acoustic Resonance Action on a Nuclear Spin System. A. R. Kessel' — 604.

Nuclear Magnetic Resonance in Plastically Deformed Rock Salt. M. I. Kornfel'd and V. V. Lemanov — 188.

Polarization of Sc^{46} Nuclei in Iron. A. V. Kogan, V. D. Kul'kov, L. P. Nikitin, N. M. Reĭnov, I. A. Sokolov, and M. F. Stel'makh — 34.

Quadrupole Effects in Nuclear Magnetic Resonance in $NaNO_3$ — $AgNO_3$ Mixed Crystals. M. I. Kornfel'd and V. V. Lemanov — 38.

Second-order Quadrupole Effects in Sodium Nitrate. V. V. Lemanov — 187.

Positrons

Observation of Positronium Reactions in Aqueous Solutions. V. I. Gol'danskiĭ, O. A. Karpukhin, and G. G. Petrov — 1026L.

Pressures, High

Some Properties of Strongly Compressed Matter, I. A. A. Abrikosov — 1254.

The Dynamic Compressibility, Equation of State, and Electrical Conductivity of Sodium Chloride at High Pressures. L. V. Al'tshuler, L. V. Kuleshova, and M. N. Pavlovskiĭ — 10.

Quantum Electrodynamics

Account of the Nuclear Coulomb Field in Processes Involving the Interaction between Electrons and an Electromagnetic Field. V. G. Gorshkov — 983.

Anomalous Magnetic Moments of the Muon and Electron. V. B. Berestetskiĭ — 993.

Bremsstrahlung from a Distributed Proton. N. A. Guliev and E. M. Épshteĭn — 304.

Change of the Adiabatic Invariant of a Particle in a Magnetic Field. I. A. M. Dykhne and V. L. Pokrovskiĭ — 264.

Effect of Multiple Scattering on the Proper Field of a Fast Charged Particle. F. F. Ternovskiĭ — 344.

Higher Born Approximation in Pair Conversion. V. A. Krutov and V. G. Gorshkov — 417.

On the Infrared Catastrophe in Scalar Quantum Electrodynamics. V. A. Shakhbazyan — 340.

Phenomenological Quantum Electrodynamics in the Case of Two Media. G. M. Garibyan — 1138.

Quantum Field Theory; Theory of Strong Interactions

A Method of Solution of Field-Theoretical Problems Involving a Static Nucleon. B. M. Barbashov and G. V. Efimov — 316.

A Resonance Model for the $\pi + N \rightarrow \pi + \pi + N$ Reaction at Meson Energies of 300 — 400 Mev. V. V. Anisovich — 71.

A Resonance Model for the $N + \pi \rightarrow N + \pi + \pi$ and $\gamma + N \rightarrow N + \pi + \pi$ Reactions. V. V. Anisovich — 946.

Annihilation of an Antiproton-Proton System. É. O. Okonov — 738.

Application of Mandelstam's Method to a Computation of the Scattering Amplitude with Anomalous Singularities. V. A. Franke — 1269.

Asymptotic Behavior of Cross Sections at High Energies. V. B. Berestetskiĭ and I. Ya. Pomeranchuk — 752.

Equations for the Mandelstam Spectral Representation Functions. K. A. Ter-Martirosyan — 575.

Location of the Nearest Singularities of the $\pi\pi$-Scattering Amplitude. V. A. Kolkunov, L. B. Okun', A. P. Rudik, and V. V. Sudakov — 242.
Low Energy $\pi\pi$ Scattering Integral Equations. Hsien Ting-Ch'ang, Ho Tso-Hsiu, and W. Zöllner — 1165.
On Secondary Processes in the Production of π Mesons on Nuclei. V. M. Mal'tsev and Yu. D. Prokoshkin — 1134.
On Symmetry of the Solutions Obtained in Determining the Singularities of Feynman Diagrams by Landau's Method. A. Z. Patashinskiĭ — 1217.
On the Normalization Constants of the State Vectors in Field Theory. M. A. Braun — 514.
On the Nucleon-nucleon Potential. A. F. Grashin and Yu. P. Nikitin — 498.
Peripheral Interactions between π Mesons and Nucleons at High Energies. I. M. Dremin — 94.
Pion-Nucleon Scattering at Low Energies. I. A. V. Efremov, V. A. Meshcheryakov, and D. V. Shirkov — 308.
Pion-Nucleon Scattering at Low Energies, II. A. V. Efremov, V. A. Meshcheryakov, and D. V. Shirkov — 766.
Pion-pion Interaction and the Electromagnetic Structure of the Nucleon in the Static Theory. E. V. Teodorovich — 334.
Semi-analytical Solution of Equations of the Chew-Mandelstam Type. Yu. A. Simonov and K. A. Ter-Martirosyan — 1003.
Signs of Constants of Strong Interactions. I. Yu. Kobzarev and L. B. Okun' — 150L.
Some Properties of Dressed Particle Operators in Field Theory. M. A. Braun and Yu. V. Novoshilov — 919.
The Hypothesis of the Neutral ρ^0 Meson in the Light of Data on Antiproton Annihilation. V. I. Gol'danskiĭ and V. M. Maksimenko — 584.
The Spatial and Charge Parities and Two-meson Annihilation of the Proton-antiproton System. M. I. Shirokov and É. O. Okonov — 204.
High-Energy Behavior of the Total Cross Section for π-p Scattering. Yu. M. Lomsadze, V. I. Lend'el, and B. M. Érnst — 803L.
Pion-Pion Resonance in p State. Ho Tso-Hsiu and Chou Kuang-Chao — 1032L.

Quantum Mechanics (Various Problems)
On the Theory of Unstable States. Ya. B. Zel'dovich — 776.
Second-order Equations for Spinor Fields. V. S. Vanyashin — 240.

Radiation, Electromagnetic
Electric Forces in a Transparent Dispersive Medium. L. P. Pitaevskiĭ — 1008.
Electromagnetic Radiation Emitted in the Collisions Between Charged Particles with Close Specific Charge e/m Values. E. I. Malkov and I. M. Shmushkevich — 1282.
Electromagnetic Radiation from Electron Diffusion. G. A. Askar'yan — 151L.
Generalized Reciprocity Principle. L. M. Biberman and B. A. Veklenko — 64.
Instability of a System of Excited Oscillators with Respect to Electromagnetic Perturbations. A. V. Gaponov — 232.
Negative Absorption in Metal Vapors. S. G. Rautian and I. I. Sobel'man — 156L.
On the Theory of Radiative Processes in Piecewise Homogeneous Media. F. F. Ternovskiĭ — 123.
Raman Scattering of Light near Second-Order Phase-Transition Points. V. L. Ginzburg and A. P. Levanyuk — 138.
Radiation Emitted by a Charged Particle Passing through a Plate. V. E. Pafomov — 97.
Radiation from a Charge Moving in an Inhomogeneous Medium. S. P. Kapitza — 954.
Radiation of a Particle Moving across the Interface of Two Media with Account of Multiple Scattering. G. M. Garibyan — 237.
Resonance Effects of Radiation in a Laminar Medium. M. L. Ter-Mikaelyan and A. D. Gazazyan — 1183.
The Vavilov-Cerenkov Effect in Uniaxial Crystals. Č. Musicař — 117.
Transition Radiation in the Case of a Diffuse Boundary Between Two Media. A. Ts. Amatuni and N. A. Korkhmazyan — 703.
On the Radiation of a Nucleus in the Presence of Unexcited Nuclei of the Same Type. M. I. Podgoretskiĭ and I. I. Roĭzen — 1023L.

Scattering (General Theory)
Dispersion Relations in Nonrelativistic Scattering Theory in which Account is Made for Spin-orbit Interaction. V. S. Buslaev — 990.
Effect of External Fields on the Angular Correlations and Resonance Processes During Quantum Transitions. L. G. Zastavenko and M. I. Podgoretskiĭ — 711.
On Electromagnetic Scattering of Particles of Spin ½. L. G. Moroz — 416.
Properties of the Scattering Amplitude Conditioned by the Unitarity Condition. M. A. Braun and L. V. Prokhorov — 1146.
Recurrent Construction of Angular Operators. III. J. Fischer and S. Ciulli — 941.
Scattering Theory for a Three-particle System. L. D. Faddeev — 1014.
The Scattering Matrix with the Pauli Interaction Taken into Account. L. G. Moroz and F. I. Fedorov — 209.
Scattering Matrix of Nucleons Scattered on a Target of Spin 1. P. Vinternitts — 1025L.
Note on the Optical Theorem. D. Blokhintsev — 802L.

Scattering in Crystals
Elastic Resonance Scattering of Slow Neutrons in Crystals. M. V. Kazarnovskiĭ and A. V. Stepanov — 723.
Inelastic Magnetic Scattering of Slow Neutrons on Phonons. B. M. Khabibullin — 714.
Scattering of Slow Neutrons in Ferrites and Antiferromagnets. V. G. Bar'yakhtar and S. V. Maleev — 995.

Scattering of Electrons and Gamma Quanta
Elastic Scattering of γ Quanta by Nuclei. L. I. Lapidus and Chou Kuang-Chao — 735.
Elastic Scattering of γ Quanta on Deuterons below the Threshold for Pion Production. L. I. Lapidus and Chou Kuang-Chao — 898.
Electron Scattering in the Thomas-Fermi Model.

T. Tietz — 940.
Inelastic Scattering of High Energy Electrons on Nuclei. A. G. Sitenko and V. N. Gur'ev — 1128.
Inelastic Scattering of Photons on Rh^{103} Nuclei. O. V. Bogdankevich, L. E. Lazareva, and A. M. Moiseev — 853.
On Resonance Photon-photon Scattering. V. N. Oraevskiĭ — 730.
Polarization Phenomena in the Compton Effect. G. V. Frolov — 1276.
Resonance Scattering of γ Quanta on the Li^7 Nucleus. I. Sh. Vashakidze, T. I. Kopaleĭshvili, V. I. Mamasakhlisov, and G. A. Chilashvili — 466.
Effect of Collisions of Recoil Nuclei on the Cross Section for Resonance Scattering of Gamma Rays by Ni^{60}. D. K. Kaipov and Yu. K. Shubnyĭ — 615L.

Semiconductors
Contribution to the Theory of Exciton States in Semiconductors. I. P. Dzyub — 429.
Anisotropy of Even Photomagnetic Effect in n-Germanium at Low Temperatures. I. K. Kikoin and S. D. Lazarev — 1022L.
Possibility of Using Indirect Transitions to Obtain a Negative Temperature in Semiconductors. N. G. Basov, O. N. Krokhin, and Yu. M. Popov — 1033L.
Experimental Determination of Polaron Mass in Cuprous Oxide. N. I. Krivko and N. M. Reĭnov — 1290L.

Statistical Physics (General Problems)
A Diagram Technique for Evaluating Transport Quantities. O. V. Konstantinov and V. I. Perel' — 142.
Application of the Laplace Transform for Calculation of the Partition Function. A. A. Zaĭtsev — 878.
Fluctuation Thermodynamics of Nonequilibrium Processes. R. L. Stratonovich — 1150.
On Perturbation Theory for Large Quantum Systems. Yu. L. Mentkovskiĭ — 225.

Strange Particles
A Possible Neutral Cascade Meson Decay. I. A. Ivanovskaya, E. V. Kuznetsov, É. I. Mal'tsev, A. Prokesh, G. M. Stashkov, and I. V. Chuvilo — 31.
Determination of the Relative Parity of Σ^0 and Λ Particles from the Reaction $\Sigma^0 \rightarrow \Lambda + e^+ + e^-$. B. N. Valuev and B. V. Geshkenbeĭn — 728.
Energy and Angular Distributions from Decays of Hypernuclei. V. A. Lyul'ka — 331.
Form Factor for $K_{\mu 3}$ and K_{e3} Decay. Ya. B. Zel'dovich. — 1232.
Four-Pronged Decay of the Long Lived K^0 Meson. É. O. Okonov, N. I. Petrov, A. M. Rozanova, and V. A. Rusakov — 48.
Freon Bubble Chamber Observations on the Asymmetry in the Decay of Λ^0 Hyperons Produced by 2.8 Bev/c π^- Mesons. V. V. Barmin, Yu. S. Krestnikov, I. I. Pershin, V. P. Rumyantseva, Ya. Ya. Shalamov, and V. A. Shebanov — 857.
On the Decays $K^+ \rightarrow \pi^+ + e^+ + e^-$ and $K^+ \rightarrow \pi^+ + \mu^+ + \mu^-$. L. B. Okun' and A. P. Rudik — 422.
On the Determination of the Sign of the Mass Difference of K_1^0 and K_2^0 Mesons. S. G. Matinyan — 1219.
π^--Mesic Decay of the $_\Lambda H^3$ Hypernucleus. V. A. Lyul'ka — 56.
Properties of the Axial Vector Interaction and the Decay $\Sigma \rightarrow \Lambda + e + \nu$. L. B. Okun' — 154L.
Spectra of K_{e4} and $K_{\mu 4}$ Decays. E. P. Shabalin — 245.
The Decay $\Sigma^0 \rightarrow \Lambda^0 + 2\gamma$ and the Magnetic Moment of the Σ^0 Hyperon. L. B. Okun' and A. P. Rudik — 268.
Which is the Heavier, the K_1^0 Meson or K_2^0 Meson? I. Yu. Kobzarev and L. B. Okun' — 426.
Concerning Parity Nonconservation in Strong Interactions with Strange Particles Participating. Wang Kang-Ch'ang, Wang Ts'u-Chieng, V. I. Veksler, I. Vrana, Ting Ta-Ts'ao, V. G. Ivanov, Kim Hi Ying, E. N. Kladnitskaya, A. A. Kuznetsov, Nguyen Dinh Ty, A. V. Nikitin, M. I. Solov'ev, T. Khofmokl', and Ch'eng Ling-Yen — 1292L.

Superconductivity
An Asymptotically Exact Solution for the Model Hamiltonian of the Theory of Superconductivity. N. N. Bogolyubov, D. N. Zubarev, and Yu. A. Tserkovnikov — 88.
Contribution to the Theory of Superconducting Alloys with Paramagnetic Impurities. A. A. Abrikosov and L. P. Gor'kov — 1243.
Dependence of the Depth of Penetration of a Magnetic Field in a Superconductor on the Magnetic Field Strength — 866.
Investigation of the Anisotropy of the Energy Gap in Superconducting Tin. P. A. Bezuglyĭ, A. A. Galkin, and A. P. Korolyuk — 4.
Measurement of the Anisotropy of the Thermal Conductivity of Zinc and Cadmium in the Superconducting State. N. V. Zavaritskiĭ — 831.
On the Problem of the Knight Shift in Superconductors. A. A. Abrikosov and L. P. Gor'kov — 337.
On the Superconductivity of a Ferromagnet with a Weak Exchange Interaction. S. V. Vonsovskiĭ and M. S. Svirskiĭ — 272.
On the Thermomagnetic Effects in Superconductors. B. T. Geĭlikman and V. Z. Kresin — 352.
Superconductivity of Crystalline Modifications of Bismuth. N. B. Brandt and N. I. Ginzburg — 1082.
Temperature Green's Function for Electrons in a Superconductor. G. M. Éliashberg — 1000.
The Anisotropy of the Energy Gap in Tin in the Basal Plane of the Crystal. P. A. Bezuglyĭ and A. A. Galkin — 810L.

Weak Interactions
A Scheme of Weak Interactions with Neutral Currents. V. N. Baĭer and I. B. Khriplovich — 959.
Asymmetry of $\pi^+ - \mu^+ - e^+$ Decay in a Magnetic Field. A. O. Vaĭsenberg and V. A. Smirnit-skiĭ — 175.
Calculation of l-Forbidden Transition Probabilities. G. M. Bukat — 1198.
Capture of Mesons by the O^{16} Nucleus. I. S. Shapiro and L. D. Blokhintsev — 775.
Effect of Weak Interactions on the Electromagnetic Properties of Fermions. A. M. Brodskiĭ — 229.
Effect of Weak Interaction on the Electromagnetic Properties of Particles. Ya. B. Zel'dovich and A. M. Perelomov — 777.
Internal Bremsstrahlung and Electromagnetic Corrections to $\mu - e$ Decay. V. P. Kuznetsov — 1202.

Longitudinal Polarization of β Electrons. P. E. Spivak and L. A. Mikaélyan — 404.

Longitudinal Polarization of β Electrons from Au^{198}. A. I. Alikhanov, G. P. Eliseev, and V. A. Lyubimov — 414.

On the Pseudovector Current and Lepton Decays of Baryons and Mesons. Chou Kuang-Chao — 492.

Polarization of Internal Conversion Electrons Emitted After β Decay of Oriented Nuclei. I. S. Baikov — 439.

Polarization of Internal Conversion Electrons and Positrons Emitted After β Decay of the Nucleus. G. A. Lobov — 479.

Some Energy Relations Deduced by Taking into Account Parity Nonconservation in $\mu - e$ Decay. V. S. Berezinskiĭ and G. T. Zatsepin — 1288.

The Polarization and Angular Distribution of Neutrons Emitted in μ Capture from Some Light Nuclei. M. K. Akhimova, L. D. Blokhintsev, and É. I. Dolinskiĭ — 1259.

Experiments with Neutrinos Emitted by Mesons. B. Pontecorvo — 812L.

Dipole Moment of Unstable Elementary Particles. Ya. B. Zel'dovich — 1030L.

Asymmetry in Double Mott Scattering and Absolute Values of Longitudinal Polarization of β Electrons. P. E. Spivak, L. A. Mikaélyan, I. E. Kutikov, and V. F. Apalin — 1037L.

Low Binding Energies in Quantum Field Theory. L. D. Landau — 1294L.

X Rays

On the Effect of Interelectron Interaction in Metals on the Fine Structure of the X-Ray Spectra. V. V. Shmidt — 886.

Errata

Volume	No.	Author	page	col.	line	Reads	Should read
10	5	Bogachev et al.	872	1	21	± 0.3 cm	± 0.7 cm
11	6	Gol'danskii et al.	1229	r	Eq. (13)	$\frac{1}{4\pi^2}\ \frac{h}{Mc}$	$\frac{1}{4\pi^2}\ \frac{h}{Mc}$
			1331	r	4	$\dots + \frac{1}{4} + \frac{\gamma_a}{2}$	$\dots + \frac{1}{4}\cos \quad + \frac{\lambda}{2}$
12	2	Moroz and Fedorov	210	1	Eq. (7)	$\dots \frac{\sin k_0 x_0}{k_0} e^{i\mathbf{kx}} d^3k,$	$\dots \frac{ik_0\delta(k^2)}{\lvert k_0 \rvert} e^{ikx}\, d^4k.$
			212	1	Eq. (39)	$\dots = 4\pi\hbar c \dots$	$\dots = -4\pi\hbar c \dots$
			212-3	r-1	Eqs. (44) and (39)	$\dots + \frac{1}{2} iel\, \nabla_k \psi_4(x) \dots$	$\dots + \frac{1}{2} iel \nabla_k \psi_4''(x) \dots$
			213	r	Eq. (51), line 2	$\dots \frac{iel}{2} \int \nabla_m \psi_4(x) \dots$	$\dots \frac{iel}{2} \int \nabla_m \psi_4''(x) \dots$
			213	r	Eq. (53)	$\dots e^{-ik_0\lvert x_0 - x_0' \rvert} e^{i\mathbf{k}(\mathbf{x}-\mathbf{x}')} \frac{d^3k}{k_0}.$	$\dots e^{ik(x-x')} \frac{d^4k}{2\pi i(k^2 - i\varepsilon)}$
12	3	Nikishov	530	1	Eq. (10)	—	$\mu^{(2)} = \frac{1}{2\beta_2\zeta} \ln\left[\frac{y_1 - 1}{y_1 + 1} \cdot \frac{-y_2 - 1}{-y_2 + 1}\right]$
			533	r	Fig. 4	The dashed curve of Fig. 4 has been incorrectly calculated (corrections to μ^+ scattering on electrons). Its value ranges from − 6 to − 8.	
12	1	Anisovich	72, 75		Eqs. (4a), (4b), (11)	$\sigma(\pi^+ + p \rightarrow n + \pi^+ + \pi^+)$	$2\sigma(\pi^+ + p \rightarrow n + \pi^+ + \pi^+)$
	5	"	948		Eq. (6)	$\sigma(\pi^- + p \rightarrow n + \pi^0 + \pi^0)$	$2\sigma(\pi^- + p \rightarrow n + \pi^0 + \pi^0).$